



Unité U1296 : Radiations

Défense, Santé, Environnement

Lyon & Brétigny-sur-Orge, France

# PORTFOLIO of the Unit

**Inserm**

La science pour la santé  
From science to health





## **UP Fundamental Radiobiology**

- Final report about the PIA2 INDIRA Project
- Le Reun et al IJMS 2022

## **UP Defense**

- Restier-Verlet et al., Biomolecules 2023 (about radioprotection)
- IMRIS Workshop

## **UP Health**

- Le Reun et al., Cancers 2023 (about Cynerknife radiotherapy)

## **UP Environment and Space**

- Duboeuf et al. Eur J Cancer 2024
- Giampiccolo et al., Environ Int 2024
- Restier-Verlet et al. IJMS 2021 (new paradigm for space biology)
- Restier-Verlet et al., in prep

## **POPS**

- A paper about the COVID-19 pandemic
- A Lecture about AIDS
- A Présentation of the new MASTER
- The Final report of the HSS Part of the INDIRA project (in French)

## **UP Valorization**

- Berthel et al., Cells 2023 about diagnosis of Alzheimer's disease

## **UP Teaching and Dissemination**

- 5 short movies about the radiation pioneers of Lyon

## **The tree of the major projects of the Unit**



# **UP Fundamental Radiobiology**





# PROJET INDIRA



## SUMMARY

The INDIRA project aims to better understand the concept of individual radiosensitivity and to measure its frequency in the general population. The two major deliverables of this project were: objective 1: the development of predictive tests for individual radiosensitivity; objective 2: the estimation of radiosensitive subpopulations in the general population. Launched in October 2013 when research on individual radiosensitivity was not very developed, the INDIRA initiative was and still constitutes today a pioneering approach. This subject is now one of the concerns of the ASN (seminar of December 2013 then decision of February 2019), of the EDF (main theme of calls for projects since 2014) of the CIPR (working group in January 2015 then 2019 then TG111 in 2024) and finally of EURATOM (dedicated calls for tenders from 2016 to 2020 then of the PIANOFORTE project).

The project resulted in 3 major advances: 1) a general mechanistic model of the individual response to radiation based on the transit of the ATM protein (RIANS model) valid for a very wide spectrum of doses and radiosensitivities; 2) an original multiparametric genomic approach characterizing radiosensitive patients predictive of specific post-radiotherapy reactions (Team 2); 3) An estimate of the radiosensitive subpopulation in the general population of 23%, consistent with other work developed within the framework of this same project and which justifies the questions which led, more than 10 years ago, to the construction of this project.

Objective 1 can be considered outdated today since the predictive tests developed are the most sensitive in the literature and the RIANS model allows for a quantitative link to be established between clinical, cellular and molecular biomarkers of radiation response, which other tests do not. In addition, specific biomarkers of accelerated aging (perinuclear ATM coronas) and cancer predisposition (combined plasmid and proliferation tests) broaden the applications and perspectives of the project to other fields of radiobiology. In parallel, the achievements of Team 2 with its integrative genomic approach also point towards a specific description of individual radiosensitivity with the functional identification of a VIM-AS1 biomarker, identified in the global signature of 20 lncRNAs of radiosensitive individuals. This biomarker is involved in the development of fibrosis, a pathology that constitutes a major radiation-induced complication

As for objective 2, it can also be considered as exceeded since an estimate of sensitive sub-populations could finally be carried out (despite all the delays that occurred throughout the project) with, in parallel, a study of human and social sciences on the same healthy donors: it is a new vision of clinical studies which opens with an approach which is deliberately intended to be multidisciplinary. In addition, the progress made in the knowledge of the radiosensitivity of certain genetic diseases also helps us to better estimate the populations at risk, so that the data from the INDIRA project concerns the widest range of individual responses to radiation.

Finally, the topics addressed in the two successive refinancings have enabled the project to be advantageously completed. First of all, the scope of validity of the RIANS model, already extended to low doses of radiation (less than 0.5 Gy) now extends beyond 4 Gy, giving a new vision to acute radiation syndrome where the ATM protein would be involved. Finally, the first data comparing the responses to radiation of different tissues (eye, heart, skin, breast, bone, ovary, prostate, intestine, brain) initiate a future major study which would consist of defining equivalences like those currently refining the Sievert system.

More than 10 years after the launch of the INDIRA project, we can affirm that it now embodies an innovative, more comprehensive, and integrative vision of individual responses to radiation.

We thank the General Investment Commission and the ANR for their financial support.





# PROJET INDIRA



## ACTIVITY 01 – GOVERNANCE

**PURPOSE:** The purpose of this work package was to ensure project governance and ensure that the objectives were achieved.

**SYNTHESIS :** Governance took place at the pace of joint meetings, particularly those organized before the submission of the annual activity report and the interactions imposed by the tasks (organization of samples for Team 4 (SAMU) and samples for Team 5 (CLB)). However, it was mainly between Teams 1 and 2, which were responsible for “experimental” tasks, that regular interaction was established (see the list of meetings at the end of the chapter).

During the INDIRA project, 3 essential decisions had to be taken by the governance:

- **2014-2016: COPENIC Collection:** The successive delays linked to the implementation of samples from healthy volunteers of the Paris SAMU (cohort and INDIRA collection) forced us to work on cells from the COPENIC collection of Team 1 (collection of skin fibroblasts from patients treated by radiotherapy or suffering from well-characterized genetic syndromes and showing a broad spectrum of radiosensitivity, see activity 02). This action allowed Teams 1 and 2 to continue their research on predictive tests without any real delay since the cells from the COPENIC collection were already available. Note that Team 3 did not wish to continue its research on a large number of these cells (see below). The Steering Committee was informed of this temporary change of study collection. In hindsight, while objective 2 (estimating the importance of radiosensitive subpopulations) required the INDIRA cohort and collection, the choice to work on the COPENIC collection to achieve objective 1 (determining one or more of the most robust and rapid predictive tests for radiosensitivity) was beneficial.

- **2018 – 2020: Team 3 activity:** The attitude of Team 3 managers towards the milestones to be met (particularly for activity reports) made real cooperation and emulation difficult, if not impossible. Early in the project, we noted that Team 3 was not participating in the discussions common to the “experimental science” Teams, Teams 1, 2 and 3. This situation could only get worse because Team 3, which was originally competent in biodosimetry (estimating the absorbed dose of radiation by considering the irradiated individual as radioresistant – “we determine the dose without knowing the status of the irradiated individual”) did not ultimately change its approach to develop predictive radiosensitivity tests (we determine the status of the irradiated individual from radiobiological data for which the dose is known). In addition, the planned task (activity 03) of Team 3 differed from those of Teams 1 and 2 by the nature of the



tissue sampled: lymphocytes or hair follicles. The use of several dozen COPERNIC fibroblasts could have less document the Team 3 method (see Activity 05). Unfortunately, the application of Team 3's method to lymphocytes was limited to a biodosimetry validation and its application to hair follicles proved to be a failure. In 2018, Team 3 informed us that it had completed its objectives while the intercomparison of the different tests (Activity 06) was a task that it also had to carry out, like the application of its method on the INDIRA cohort. Thus, such an abandonment during the project required scientific and financial justification as well as the redistribution of the balance left by Team 3. By the Convention which governs the project and which gave it the possibility of redistributing funds in this type of situation, the coordinator therefore decided to reinforce the tasks of the 1st and 2nd contributions. Thus, in addition to having Team 1 carry out the test intercomparison task (Activity 05) which was normally assigned to Team 3, the coordinator decided to pay:

- one-third of the balance left by Team 3 (i.e., €9,000) for the "Low Doses" task of the first funding round, adding a study on the validity of the RIANS model for very high doses of radiation (see activity 08-1), a task that was completed by Team 1 in the last 6 months of the project.

- one-third of the balance left by Team 3 (i.e., €9,000) for the "Humanities and Social Sciences" task of the first funding round (see activity 08-2) for the organization of a seminar on the legal aspects of taking individual radiosensitivity into account, a task that was to be completed by Team 1 in the last 6 months of the project (or even later).

- one third of the balance left by Team 3 (i.e. 9 kEuros) for the benefit of the task "differences in radiosensitivity between tissues" of the 2nd contribution (activity 09) to add additional tissues to the study including the ovary, a task which was completed by Team 1 in the last 6 months of the project.

**- last half of 2024: Team 1 premises:** A final decision from the governance concerned Team 1, previously based at the Léon-Bérard Center (CLB). During 2024, strong pressure was put on Team 1 by the CLB Research Department to find another location in Lyon. Although this action had been planned for a long time, solutions were not yet available and additional efforts were therefore mobilized to find a workplace for Team 1. Under these conditions, a seminar (see above) planned and organized by Team 1 was very difficult. The coordinator therefore decided to allocate the last third of the balance left by Team 3 (i.e. 9 kEuros) no longer to the organization of the seminar but to reinforce the "Radiosensitivity, Radiosusceptibility" task of the 1st contribution by adding a study on accelerated aging (Radiodegeneration) to advantageously complete this task (see Activity 08-2).

**In conclusion, the decisions taken by the governance and the coordinator have enabled not only all the project objectives to be achieved but also some to be exceeded. We nevertheless regret the attitude of Team 3, which has not truly integrated itself into the scientific project and the approach defined from the beginning of the project by the founding institutions.**



**Table 1** : Les acteurs du projet

<b>Responsable scientifique et technique du projet</b>	
<b>Equipe coordinatrice</b>	U1296 Inserm
<b>Nom, Prénom</b>	FORAY Nicolas
<b>Téléphone</b>	0426556794
<b>Courriel</b>	Nicolas.foray@inserm.fr

<b>TABLEAU RECAPITULATIF DES PARTENAIRES DU PROJET (hors coordinateur)</b>	
Partenaire n°1	<i>LGRK/IRCM/DSV/CEA</i>
Titre, Prénom, nom du RST	Dr Michèle MARTIN
Courriel	<a href="mailto:Michele.martin@cea.fr">Michele.martin@cea.fr</a>
Etablissement gestionnaire	CEA DSV

Partenaire n°2	<i>LCE/IRCM/DSV/CEA</i>
Titre, Prénom, nom du RST	Dr Sylvie CHEVILLARD
Courriel	<a href="mailto:Sylvie.chevillard@cea.fr">Sylvie.chevillard@cea.fr</a>
Etablissement gestionnaire	CEA DSV

Partenaire n°3	<i>SAMU 75</i>
Titre, Prénom, nom du RST	Dr Caroline TELION
Courriel	<a href="mailto:caroline.telion@nck.aphp.fr">caroline.telion@nck.aphp.fr</a>
Etablissement gestionnaire	AP-HP

Partenaire n°4	<i>Centre Léon-Bérard (CLB)</i>
Titre, Prénom, nom du RST	Pr Jean-Yves BLAY
Courriel	<a href="mailto:Jean-yves.blay@lyon.unicancer.fr">Jean-yves.blay@lyon.unicancer.fr</a>
Etablissement gestionnaire	CLB





# PROJET INDIRA



## ACTIVITY 02 – CELL COLLECTIONS

**PURPOSE:** The aim of this workpackage was to provide biological material (in this case skin fibroblasts) to, on the one hand, develop predictive radiosensitivity tests (objective 1) and, on the other hand, an assessment of radiosensitive subpopulations. While Team 1's COPENIC collection already existed before the start of the project, the establishment of the collection and the organization of the clinical study of the INDIRA cohort (composed of healthy donors from the Paris SAMU) is a task assigned to Team 4.

**SUMMARY:** Since 2004, Team 1 has collected skin fibroblasts from patients treated with radiotherapy for their cancer and who have shown various radiosensitivity reactions. In 2004, the COPENIC network of radiotherapists brought together approximately thirty radiotherapists. In 2014, the COPENIC network doubled. In 2024, it tripled. Each week, the Team 1 laboratory receives at least 1 to 2 skin biopsies for a request for radiosensitivity expertise. In addition to this collection, which has become one of the largest collections of human cells with different radiosensitivity, Team 1 has accumulated skin fibroblasts from patients suffering from well-characterized genetic syndromes associated with radiosensitivity, radiosusceptibility, and/or radiodegeneration. To avoid confusion, these latter fibroblasts constitute the CELLINE sub-collection. The two collections COPENIC and CELLINE were made available to Teams 2 and 3 to compensate for delays in implementing the INDIRA collection. In hindsight, the use of the COPENIC collection and the CELLINE sub-collection enabled Teams 1 and 2 to successfully achieve Objective 1. Unfortunately, Team 3 did not wish to benefit from the entire collection (see Activity 01 – Governance). In addition to the publications from the INDIRA collection to achieve Objective 1, the direct characterization of the COPENIC collection was the subject of three publications (1-3).

Concerning the INDIRA collection and cohort, it was finally in 2023 that 30 skin samples were taken by Team 4. The radiobiological study of skin fibroblasts was carried out in full by Team 1 and 7 lines out of 30 showed a delay in ATM transit (group II, moderate radiosensitivity), which represents 23.3% of apparently healthy individuals being radiosensitive (see activity 03): objective 2 was therefore achieved. However, given the scale of the analysis, no publication has been submitted to date: the submission of a publication summarizing the achievements of the INDIRA project as well as the figures of the final estimate is planned before the end of 2024.



**CONCLUSIONS:** The COPERNIC collection of Team 1 enabled major progress in achieving objective 1 and the INDIRA collection, although late, enabled objective 2 to be achieved before the end of the project.

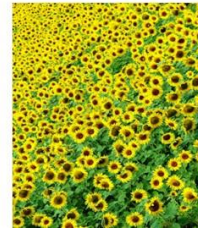
#### **PUBLICATIONS DIRECTLY RELATED TO THIS ACTIVITY**

1. A. Granzotto *et al.*, Influence of Nucleoshuttling of the ATM Protein in the Healthy Tissues Response to Radiation Therapy: Toward a Molecular Classification of Human Radiosensitivity. *International journal of radiation oncology, biology, physics* **94**, 450-460 (2016).
2. E. Le Reun *et al.*, Quantitative correlations between radiosensitivity biomarkers show that the ATM protein kinase is strongly involved in the radiotoxicities observed after radiotherapy. *International journal of molecular sciences* **23**, (2022).
3. L. Sonzogni *et al.*, Prediction of radiotherapy toxicity: 20 years of COPERNIC radiosensitivity diagnosis procedure. *Cancer radiotherapie : journal de la Societe francaise de radiotherapie oncologique*, (2024).





# PROJET INDIRA



## ACTIVITY 03 –PREDICTIVE ASSAYS – Team 1

**PURPOSE:** The goal of this workpackage was to develop predictive radiosensitivity tests for Team 1 (objective 1).

**SUMMARY:** After irradiation, phosphorylation of the histone variant H2AX ( $\gamma$ H2AX) by the ATM protein kinase is known to be the first step in the recognition of DNA double-strand breaks (DSBs) that precedes their repair (1). From the aforementioned COPERNIC collection, Team 1 had noticed that many cell lines showed fewer  $\gamma$ H2AX foci than expected after 2 Gy followed by 10 min post-irradiation using the anti- $\gamma$ H2AX immunofluorescence technique (each  $\gamma$ H2AX foci should correspond to a DSB and after a dose of 2 Gy,  $40 \times 2 = 80$  DSBs are expected (based on 40 DSBs per Gy per fibroblast). This result could not be considered as a decrease in the number of DSBs induced by radiation but rather in the number of DSBs recognized by ATM. We therefore hypothesized that the ATM protein was more abundant in the cytoplasm than in the nucleus and that irradiation produced monomerization of ATM dimers before they diffused into the nucleus: the radiation-induced ATM nucleoshuttling model was born (RIANS model) (1).

Thus, the RIANS model can be described as follows: in the absence of stress, ATM molecules appear as dimers. After irradiation, ATM dimers monomerize proportionally to the dose: the cell has its own dosimeter! ATM monomers diffuse into the nucleus to trigger DSB repair. Any delay in this radiation-induced ATM nucleoshuttling (RIANS) leads to adverse toxicity reactions, cancers, or accelerated aging diseases (1). The delay in RIANS is caused by the interaction between ATM protein monomers and certain overexpressed cytoplasmic proteins called X proteins, specific to each individual, tissue or syndrome. ATM-X-protein complexes formed in the cytoplasm reduce the flux of ATM monomers diffusing into the nucleus. In 2016, we demonstrated that the more DSBs ATM recognized in the nucleus, the more complete their repair, the less severe the post-radiotherapy reaction and the lower its clinical severity grade, the CTCAE grade (2, 3). For the first time, a molecular test could predict the severity of radiosensitivity reactions by linking clinical radiosensitivity (CTCAE grade), cellular radiosensitivity (clonogenic survival at 2 Gy) and molecular radiosensitivity (maximal ATM activity) (4). Based on the RIANS model, 3 radiosensitivity groups were defined (5):

- **Group I:** ATM transit is rapid, and all DSBs are recognized and repaired. Individuals in Group I are radioresistant and at low risk of cancer or degenerative diseases. After radiotherapy, they exhibit CTCAE grade 0 to 1 reactions.



- **Group II:** ATM transit is delayed by overexpression of cytoplasmic X proteins, and not all DSBs are repaired. Clinically, individuals in Group II exhibit moderate but significant radiosensitivity and are at high risk of cancer or degenerative diseases. After radiotherapy, they may exhibit CTCAE grade 1 to 4 reactions.

- **Group III:** Regardless of ATM transit, mutations in ATM or its direct partners can cause ATM activity to be virtually nonexistent: a vast majority of DSBs are neither recognized nor repaired. Group III individuals are generally children suffering from syndromes associated with hyperradiosensitivity, a very high risk of cancer (e.g., AT) or neurodegenerative diseases (e.g., progeria). Radiotherapy is systematically fatal for them (CTCAE grade 5).

As a predictor of radiosensitivity, the model was able, for the first time, to predict post-radiotherapy reactions with the best current robustness (6-9). But far beyond that, the RIANS model has made it possible to:

- Provide a new biological interpretation of the linear-quadratic model, a true flagship formula in radiobiology linking dose and effect (10-15)
- Explain the radiosensitivity associated with many genetic diseases (16-26)
- Develop a new approach to radioprotection (27)
- Provide a biological interpretation of the specific effects at low doses (28-30)
- Provide a new interpretation of the relationship between biological efficacy and linear energy transfer (31)

**CONCLUSIONS:** The COPENIC collection of Team 1 has made it possible to establish the ATM protein transit model (RIANS model) on a very solid basis with a wide range of maximum radiosensitivity. For this activity, the achievement of objective 1 and the development of a predictive test have been largely exceeded because it is an interpretation model, or even a paradigm, which has been proposed.

#### MAIN PUBLICATIONS DIRECTLY RELATED TO THIS ACTIVITY

1. E. Berthel, N. Foray, M. L. Ferlazzo, The Nucleoshuttling of the ATM Protein: A Unified Model to Describe the Individual Response to High- and Low-Dose of Radiation? *Cancers* **11**, (2019).
2. A. Granzotto *et al.*, Influence of Nucleoshuttling of the ATM Protein in the Healthy Tissues Response to Radiation Therapy: Toward a Molecular Classification of Human Radiosensitivity. *International journal of radiation oncology, biology, physics* **94**, 450-460 (2016).
3. L. Sonzogni *et al.*, Prediction of radiotherapy toxicity: 20 years of COPENIC radiosensitivity diagnosis procedure. *Cancer radiotherapie : journal de la Societe francaise de radiotherapie oncologique*, (2024).
4. E. Le Reun *et al.*, Quantitative correlations between radiosensitivity biomarkers show that the ATM protein kinase is strongly involved in the radiotoxicities observed after radiotherapy. *International journal of molecular sciences* **23**, (2022).



5. N. Foray, M. Bourguignon, N. Hamada, Individual response to ionizing radiation. *Mutation Research Review* **770**, 369-386 (2016).
6. A. Granzotto *et al.*, Individual susceptibility to radiosensitivity and to genomic instability: its impact on low doses phenomena. *Health physics* **100**, 282 (2011).
7. S. Pereira *et al.*, Fast and binary assay for predicting radiosensitivity based on the nucleoshuttling of ATM protein: development, validation and performances. *International journal of radiation oncology, biology, physics* **100**, 353-360 (2018).
8. S. Pereira *et al.*, The time is coming to compare radiosensitivity predictive assays by their scientific relevance and statistical performances. *International Journal of Radiation Oncology Biology and Physics* **101**, 491-492 (2018).
9. G. Vogin *et al.*, The Phosphorylated ATM Immunofluorescence Assay: A High-performance Radiosensitivity Assay to Predict Postradiation Therapy Overreactions. *International journal of radiation oncology, biology, physics* **101**, 690-693 (2018).
10. L. Bodgi *et al.*, [The enigma of the biological interpretation of the linear-quadratic model finally resolved? A summary for non-mathematicians]. *Cancer radiotherapie : journal de la Societe francaise de radiotherapie oncologique* **20**, 314-321 (2016).
11. L. Bodgi *et al.*, Mathematical models of radiation action on living cells: From the target theory to the modern approaches. A historical and critical review. *Journal of theoretical biology* **394**, 93-101 (2016).
12. L. Bodgi, N. Foray, The nucleo-shuttling of the ATM protein as a basis for a novel theory of radiation response: resolution of the linear-quadratic model. *International journal of radiation biology* **92**, 117-131 (2016).
13. L. Bodgi, N. Foray *Effets biologiques des radiations ionisantes. Une théorie basée sur le transit cyto-nucléaire de la protéine ATM. Applications à la radiothérapie* (Editions universitaires européennes, Sarrebruck, Allemagne, 2016).
14. L. Bodgi *et al.*, A single formula to describe radiation-induced protein relocalization: towards a mathematical definition of individual radiosensitivity. *Journal of theoretical biology* **333**, 135-145 (2013).
15. L. Bodgi, L. Pujo-Menjouet, A. Bouchet, M. Bourguignon, N. Foray, Seventy Years of Dose-response Models: From the Target Theory to the Use of Big Databases Involving Cell Survival and DNA Repair. *Radiation research* **202**, 130-142 (2024).
16. M. L. Ferlazzo, N. Foray, Huntington Disease: A Disease of DNA Methylation or DNA Breaks? *The American journal of pathology* **186**, 1750-1753 (2016).
17. M. L. Ferlazzo *et al.*, Mutations of the Huntington's Disease Protein Impact on the ATM-Dependent Signaling and Repair Pathways of the Radiation-Induced DNA Double-Strand Breaks: Corrective Effect of Statins and Bisphosphonates. *Molecular neurobiology* **49**, 1200-1211 (2014).
18. M. L. Ferlazzo *et al.*, Radiobiological characterization of tuberous sclerosis: A delay in the nucleo-shuttling of ATM may be responsible for radiosensitivity. *Molecular neurobiology* **55**, (2017).
19. I. Moulay Lakhdar *et al.*, Fibroblasts from Retinoblastoma Patients Show Radiosensitivity Linked to Abnormal Localization of the ATM Protein. *Curr Eye Res*, 1-12 (2020).
20. J. M. Bachelet *et al.*, Radiobiological characterization of skin fibroblasts from a young patient suffering from the Immunodeficiency Centromeric instability Facial anomalies type 1 (ICF1) syndrome. *Archives of Medical and Clinical Case Reports* **in press**, (2022).
21. J. T. Bachelet *et al.*, First Radiobiological Characterization of Skin and Bone Cells from A Patient Suffering from the PI3KCA-Related Overgrowth Spectrum (PROS) Syndrome. *Archives of Medical and Clinical Case Reports* **4**, 1052-1066 (2020).
22. J. T. Bachelet *et al.*, First radiobiological characterization of the McCune-Albright syndrome: influence of the ATM protein and effect of statins + bisphosphonates treatment. *International journal of radiation biology* **97**, 317-328 (2021).



23. J. Al-Choboq *et al.*, Usher Syndrome Belongs to the Genetic Diseases Associated with Radiosensitivity: Influence of the ATM Protein Kinase. *International journal of molecular sciences* **23**, (2022).
24. J. Al-Choboq *et al.*, Molecular and Cellular Responses to Ionization Radiation in Untransformed Fibroblasts from the Rothmund–Thomson Syndrome: Influence of the Nucleo-Shuttling of the ATM Protein Kinase. *Radiation* **3**, 21-38 (2023).
25. L. El Nache, J. Al-Choboq, M. Bourguignon, N. Foray, Response of Fibroblasts from Menkes' and Wilson's Copper Metabolism-Related Disorders to Ionizing Radiation: Influence of the Nucleo-Shuttling of the ATM Protein Kinase. *Biomolecules* **13**, (2023).
26. P. Combemale *et al.*, Individual Response to Radiation of Individuals with Neurofibromatosis Type I: Role of the ATM Protein and Influence of Statins and Bisphosphonates. *Molecular neurobiology* **59**, 556-573 (2022).
27. J. Restier-Verlet *et al.*, Molecular Influence of the ATM Protein in the Treatment of Human Cells with Different Radioprotective Drugs: Comparisons between Antioxidative and Pro-Episkevic Strategies. *Biomolecules* **13**, (2023).
28. C. Devic, M. L. Ferlazzo, E. Berthel, N. Foray, Influence of Individual Radiosensitivity on the Hormesis Phenomenon: Toward a Mechanistic Explanation Based on the Nucleoshuttling of ATM Protein. *Dose-response : a publication of International Hormesis Society* **18**, 1559325820913784 (2020).
29. C. Devic, M. L. Ferlazzo, N. Foray, Influence of Individual Radiosensitivity on the Adaptive Response Phenomenon: Toward a Mechanistic Explanation Based on the Nucleo-Shuttling of ATM Protein. *Dose-response : a publication of International Hormesis Society* **16**, 1-11 (2018).
30. C. Devic *et al.*, Le phénomène d'hypersensibilité aux faibles doses : une énigme de la radiobiologie enfin résolue ? *Revue de médecine nucléaire* **40**, 254-257 (2016).
31. M. Maalouf *et al.*, Influence of Linear Energy Transfer on the Nucleo-shuttling of the ATM Protein: A Novel Biological Interpretation Relevant for Particles and Radiation. *International journal of radiation oncology, biology, physics* **103**, 709-718 (2019).





# PROJET INDIRA



## ACTIVITY 04 – PREDICTIVE ASSAYS – Team 2

**PURPOSE:** The goal of this work package was to develop predictive radiosensitivity tests for Team 2 (Objective 1).

**SUMMARY:** Within the INDIRA project, which aimed to better understand the concept of individual radiosensitivity, Team 2's specific objective was to search for new genomic and epigenomic markers of individual radiosensitivity. It developed its research on susceptibility to radiation-induced pathologies along two axes: radiation-induced cancer and damage to healthy tissue. The tools used were those of cell biology and integrative genomics.

For cell biology, existing collections of radiosensitive patients and a collection of healthy donors established by the laboratory were studied.

1) COPERNIC collection: fibroblast lines from patients who developed complications in healthy tissue after radiotherapy and lines from patients who did not develop complications. This collection was established by N. Foray's team at INSERM, in collaboration with numerous radiotherapy departments.

2) Gorlin fibroblast lines, derived from patients with Gorlin syndrome, linked to mutations in the PTCH1 gene. This syndrome is known for its predisposition to radiation-induced cancer.

3) Fibroblast lines obtained at the CEA from healthy donors, for which we characterized intrinsic radiosensitivity after high and low doses.

For integrative genomics, we combined high-throughput DNA sequencing (exome), which allows us to identify DNA sequence variants, and RNA sequencing using RNA-Seq (transcriptome). The latter allows for a functional approach to individual radiosensitivity as well as the discovery of new markers, which are sought within the coding and non-coding transcriptome.

### 1. Markers of radiation-induced cancer risk

Regarding radiation-induced risk, the team has participated in major international journals and developed three studies on specific biological pathways.



## **1.1 Journal publications on radiosensitivity**

Team 2 has published summaries on radiosensitivity, particularly cutaneous radiosensitivity (1-3), including two for international institutions (ICRP).

1. Niwa O, et al. CRP Publication 131: Stem Cell Biology with Respect to Carcinogenesis Aspects of Radiological Protection. December 2015, Annals of the ICRP 44(3-4):7-357. Doi: 10.1177/0146645315595585

**2. Hendry JH, Niwa O, Barcellos-Hoff MH, Globus RK, Harrison JD, Martin MT, Seed TM, Shay JW, Story MD, Suzuki K, Yamashita S. Stem Cell Biology with Respect to Carcinogenesis Aspects of Radiological Protection. ICRP (International Commission on Radiological Protection) Publication 131. Annals of the ICRP, March 2016. Doi: 10.1177/0146645315621849.**

**3. MT Martin, A Vulin, JH Hendry. Human epidermal stem cells: role in skin reactions and carcinogenesis from radiation. Mutation Research, 2016, 770, 349-368. Mutat Res. 2016 Oct-Dec;770(Pt B):349-368. Doi: 10.1016/j.mrrev.2016.08.004**

## **1.2 Study of the Sonic Hedgehog track**

Gorlin syndrome, or NBCCS, is a genetic disease linked to heterozygous mutations in the membrane receptor PATCHED1. This syndrome has been classified as radiosensitive because these patients develop numerous radiation-induced cancers. The team has shown that patients with the highest receptor deficiency exhibit the highest cellular radiosensitivity, both after low and high doses (4). This deficiency is linked to the type of mutation acquired in the PTCH1 gene. Furthermore, in a collaboration with W. Rachidi's team (CEA, Grenoble), it was shown that Gorlin fibroblasts are deficient in the BER (base excision repair) pathway, which is involved in the repair of oxidative DNA damage (5). The expression level of the PATCHED1 receptor, as well as that of BER activity, could therefore constitute prognostic tests for high radiosensitivity in Gorlin patients who must be exposed to ionizing radiation for medical purposes.

4. A Vulin, M Sedkaoui, S Moratille, N Sevenet, P Soularue, O Rigaud, L Guibbal, J Dulong, P Jeggo, JF Deleuze, J Lamartine and MT Martin. Severe PATCHED1 deficiency in cancer-prone Gorlin patient cells results in intrinsic radiosensitivity. Int J Radiat Oncol Biol Phys. 2018, Oct 1;102(2):417-425. Doi: 10.1016/j.ijrobp.2018.05.057.

5. Charazac A, Fayyad N, Beal D, Bourgoïn-Voillard S, Seve M, Sauvaigo S, Lamartine J, Soularue P, Moratille S, Martin MT, Ravanat JL, Douki T and Rachidi W. Impairment of base excision repair in dermal fibroblasts isolated from Nevoid Basal Cell Carcinoma patients. Front Oncol, 2020, Aug 7;10:1551. Doi: 10.3389/fonc.2020.01551.



### **1.3. Study of the NFATC2 Pathway**

The team collaborated with that of J. Lamartine (Université Lyon 1) for this study. Comparison of fibroblasts from radiosensitive patients (Copernic collection) with fibroblasts from healthy donors demonstrated that the NFATC2 gene was particularly deregulated in the radiosensitive context, and that the NFATC2 protein is involved in cellular radiosensitivity and DNA repair (6). A current publication shows that this protein activates the repair of DNA double-strand breaks via a direct interaction with the Ku80 protein (7).

6. Dulong J, Kouakou C, Mesloub Y, Rorteau J, Moratille S, Chevalier F, Vinasco Sandoval T, Martin MT and Lamartine J. NFATC2 modulates radiation sensitivity of dermal fibroblasts from patients with severe side-effects of radiotherapy. *Front Oncol*, 2020 Dec 16;10:589168. Doi.org/10.3389/fonc.2020.589168.

7. In preparation: Barthelemy T, Lamartine J, et al. NFATC2 potentiates DNA double-strand breaks repair by direct interaction with Ku80.

### **1.4. Effects of low doses of radiation**

La collection de cellules de donneurs sains a été utilisée pour étudier l'effet d'une exposition unique à 50 mGy de rayons X, dans un modèle d'organoïde cutané. Nous montrons que cette exposition induit le processus de transition épithélio-mésenchymateux (EMT), notamment par l'activité de la protéine ZEB1, qui crée un environnement favorable à la cancérogenèse (8).

8. Cavallero S, Neves Granito R, Stockholm D, Azzolin P, Martin MT, Fortunel NO. Exposure of Human Skin Organoids to Low Genotoxic Stress Can Promote Epithelial-to-Mesenchymal Transition in Regenerating Keratinocyte Precursor Cells. *Cells*, 2020, Aug 18;9(8):E1912. Doi: 10.3390/cells9081912.

Markers of the risk of radiation-induced fibrosis

To search for new markers of damage in healthy tissue, the transcriptomes of patients who developed severe complications after radiotherapy for breast cancer were established and analyzed. This research is based on the study of cell lines from the Copernic collection, which consists of primary, non-transformed fibroblast lines derived from skin biopsies taken from patients outside the radiation field.

We focused our research on one of the most common complications of radiotherapy, fibrosis, for which clinical data were available. A subpopulation consisting exclusively of patients treated with radiotherapy for breast cancer was defined, including 10 patients who developed severe breast fibrosis and 9 patients who did not develop objective fibrosis after radiotherapy.

Fibrosis is one of the most common late complications of high-dose localized exposure. It corresponds to the progressive invasion of a functional tissue by a pathological extracellular matrix, leading to a loss of function of the target organ. Its development involves the trans-differentiation of local tissue fibroblasts into myofibroblasts, which proliferate and synthesize fibrous components, notably collagens. While mechanisms leading to the development of fibrosis have been characterized for the coding part of the genome, and in particular the involvement of the TGFB1-related gene network, knowledge relating to the non-coding part of the



genome is only emerging. Non-coding RNAs are classified according to their size, ranging from small RNAs (less than 30 nucleotides, including microRNAs), to long non-coding RNAs of more than 500 nucleotides (lncRNAs). Understanding the functions of lncRNAs is currently a challenge for biology and radiobiology (9,10). We developed specific analytical tools to study them in our models (11, 12).

We identified a breast fibrosis susceptibility signature comprising 15 lncRNAs (13). Among them, the lncRNA VIM-AS1 was statistically the best biomarker of fibrosis. As we found this marker in other types of non-radiation-induced fibrosis, it could be a general marker of tissue fibrosis risk. Functional studies showed that VIM-AS1 was involved in a key step in the development of fibrosis: the activation of myofibroblasts, which will deposit the collagen matrix in response to the growth factor TGFB1. The study of the mechanisms points to transcriptional (cis) regulation mediated by vimentin, as well as post-translational (trans) regulation involving miRNAs (Figure 1). In conclusion, our study shows that prognostic tests based on non-coding RNA expression signatures could be included in the battery of tests needed to predict the risk of developing severe complications after anticancer treatment. High production in normal tissues of a non-coding RNA called VIM-AS1 is a risk factor for breast fibrosis. Reducing the production of this RNA before radiotherapy could attenuate the intrinsic radiosensitivity of these patients.

9. MT Martin. Non coding RNAs: a new mechanism to regulate sensitivity to ionizing radiation. EU review posted on Europa-website, November 2017: <http://ec.europa.eu/energy/node/1216>.

10. MT Martin. Long non-coding RNAs: new mechanisms regulating sensitivity to ionizing radiation. European Commission Proceedings, 2019, Epigenetic effects, potential impact on radiation protection, Radiation Protection n°189, November, 32-39. ISSN 1681-6803.

11. Auvré F, Coutier J, Martin MT, Fortunel NO. Quantitative Detection of Low-Abundance Transcripts at Single-Cell Level in Human Epidermal Keratinocytes by Digital Droplet Reverse Transcription-Polymerase Chain Reaction. *Methods Mol Biol.*, 2019;1879:31-41. Doi: 10.1007/7651\_2018\_149.

12. Vinasco-Sandoval T, Lemaître G, Soularue P, Martin MT, and Fortunel NO. Deciphering ‘immaturity-stemness’ in human epidermal stem cells at the levels of protein-coding and non-coding genomes: a prospective computational approach. *Int J Mol Sci*, 2024, 25, 3353. <https://doi.org/10.3390/ijms25063353>.

13. Vinasco-Sandoval T, Moratille S, Crechet F, Mesloub Y, Montanari J, Auvré F, Deleuze JF, Foray N, Fortunel NO, and Martin MT. Long Noncoding VIM-AS1: Biomarker of Breast Fibrosis Susceptibility After Radiation Therapy and Promoter of Transforming Growth Factor- $\beta$ 1-Driven Fibrosis. *Int J Radiat Oncol Biol Phys*, 2024, in press.

**CONCLUSIONS:** The achievements of Team 2 with its integrative genomic approach also support a specific description of individual radiosensitivity with the functional identification of a VIM-AS1 biomarker, identified in the global signature of 20 lncRNAs of radiosensitive individuals. This biomarker is involved in the development of fibrosis, a pathology that constitutes a major radiation-induced complication. The objective of a test based on a genomic approach is therefore achieved.





## PROJET INDIRA



### ACTIVITY 05 – PREDICTIVE ASSAYS – Team 3

**PURPOSE :** The aim of this workpackage was to develop predictive radiosensitivity tests for Team 3 (objective 1).

#### **SYNTHESIS<sup>1</sup> :**

**Our predictive approach is based on a determination of the phosphorylation of H2AX histones, with lymphocytes and hair follicles being used as reporters. In 2014, we established the first correlations between the hair follicle response and the lymphocyte response, which is generally taken as a cellular standard for measuring an individual's irradiation. Indeed, we showed on 10 individuals a direct and linear relationship between the responses of hair follicles and lymphocyte cells. In 2015, we finalized the new test geometry allowing the treatment of more than 10 people per hour in order to prepare for the full-scale test on the cohort selected for this project. Based on the samples taken in 2015, we developed a measurement correction model that takes into account the variability of responses between individuals published in 2017.**

During the period 2016 - 2017, we completed the validation of the test, both from a technical-operational point of view, for implementation in real conditions, and from a biotechnological point of view for the measurement, in particular:

- On cell lines, in particular the COPENIC collection of human fibroblasts (Team 1) which is studied in the framework of this project by the other two groups.
- On a sample of individuals irradiated as part of an interventional radiology, through a blinded clinical trial.
- On samples irradiated at different doses from volunteers.

To validate the biotechnological component of our test, we launched the study on the cell line of the COPENIC collection. The objective is to use the radiosensitivity correction factor developed in the test to classify lines based on radiosensitivity. Preliminary blinded trials on 7 lines were conducted in 2016. The protocol used consists, after the recultivation of the lines, in irradiating an aliquot from each line at one of the doses 0.5, 1, 2, 4 and 8 Gy, then in measuring the phosphorylation of H2AX histones after 1 h. After normalization by the radiosensitivity coefficient of the assay, the variation in dose response becomes similar for all lines. The work carried out in 2017 on the COPENIC lines is currently being analysed. The validation of the test is completed by a clinical trial set up with the Clermont-Ferrand University Hospital on 9 individuals treated in interventional radiology in the context of embolism and aneurysm.

<sup>1</sup> This is the last text that Team 3 left for the 2017 activity report.



During the procedure, patients receive varying doses to different areas of the head, depending on the morphology and duration of the procedure.

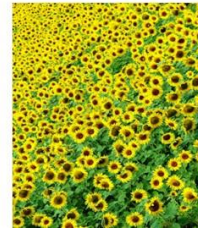
We are currently working to better integrate radiosensitivity variability into a point measurement in order to improve the accuracy of blinded measurement, especially for irradiations between 3 and 5 Gy. In particular, as part of the hair studies and while waiting for the INDIRA cohort samples to be available, we have undertaken a complementary study to the study conducted on the COPERNIC lines, in order to evaluate the possibility of studying radiosensitivity by working on the cells of the hair bulb. Indeed, we wanted to check whether it was possible to work simultaneously on hair and blood samples from the same individual. Tests were first performed on irradiated whole mice where the results showed a good correlation between blood and hair bulb results. Unfortunately, we do not have comparable results on ex vivo irradiation of hair bulbs which are not reproducible enough to carry out an analysis comparable to blood, to be able to carry out a radiosensitivity study of the hair bulbs and the blood of the same individual, it will probably be necessary to develop a method of culture of the bulb after sampling, in order to be able to irradiate the hairs ex vivo and obtain a reproducible result. Nevertheless, before launching this culture, we wanted to verify that the ex vivo irradiation of a hair sample held in the skin made it possible to carry out a radiodosimeter measurement according to the process we developed. To do this, we used a model of monkey skin and monkey blood that we irradiated, before assaying the protein of interest. This experiment confirms that the hair bulb remains a good study model provided that the hair is irradiated directly into the skin. To carry out the experiments on the hair samples of the test cohort, we will now work on a model of hair culture that will keep it alive in optimal conditions during irradiation and protein extraction.

**CONCLUSIONS:** It seems that the choice of hair follicles as tissue poses technological and methodological problems that do not support a sufficiently accurate individual radiosensitivity test since Team 3 stopped in 2018. In addition, the lymphocyte test has not been sufficiently documented and the clinical study referred to in this text has not been documented by Team 3 either. Finally, the use and validation of the radiosensitivity coefficient was not presented or explained by Team 3 either. In conclusion, the objectives that Team 3 had set for itself were not achieved and the task of an intercomparison of the tests of all the teams was not carried out by Team 3: alternative measures were taken to compensate for this lack of deliverables (see governance sheet ACTIVITY 01). L'Equipe 3 announced its cessation of activity in 2018.





# PROJET INDIRA



## ACTIVITY 06 – ASSAYS INTERCOMPARISON

**PURPOSE:** The purpose of this workpackage was to compare radiosensitivity tests. This task was originally assigned to Team 3, but was ultimately carried out by Team 1.

**SUMMARY:** Once Team 3 withdrew from the research/development of radiosensitivity tests, as hair follicles appeared to be a difficult tissue to manipulate, it remained to compare the tests produced by Team 1 (functional tests) based on the cytonuclear transit of the ATM protein and the genomic tests produced by Team 2. However, whereas Team 1 considered CTCAE grades (i.e. grades of severity of post-radiotherapy tissue reactions as a whole), Team 2 focused on better detecting radiation fibrosis, a very specific aspect of post-radiotherapy tissue reactions, with Team 2's test becoming more specific. As radiosensitivity tests were developed throughout the project, we decided to compare the tests proposed in the literature and not just those produced by the INDIRA project, in order to provide a more global view of the state of the art in this field.

Firstly, Guillaume Vogin's paper enabled us to compare our tests derived directly from the ATM transit model with those developed by Neolys Diagnostics, which are based not on immunofluorescence but on ELISA tests. It appears that the latter perform less well, particularly as these tests determine a CTCAE grade group (e.g. (0, 1 or 2) or (3 or 4)) whereas there is a direct mathematical link between the maximum pATM foci rate (pATMmax) and the CTCAE grade (1, 2).

More generally, the predictive power of radiosensitivity with clonogenic survival tests has been compared with that derived from ATM transit. This time, it is the cumbersome experimental protocol and not the statistical robustness that is at issue: survival curves cannot be integrated into a routine process for measuring radiosensitivity (3, 4)

With regard to the  $\gamma$ H2AX immunofluorescence test, in line with what we have already published, the measurement of the rate of foci remaining 24 h after 2 Gy is not specific enough to discriminate cells over a wide range of radiosensitivity (5). All the other functional tests appear to be less robust than the pATMmax test. Paradoxically, the pATMmax test takes the longest to set up, which leads us to conclude (Figure 1) that the longer the test, the more robust it is (4, 6, 7).



## Intercomparisons between predictive assays

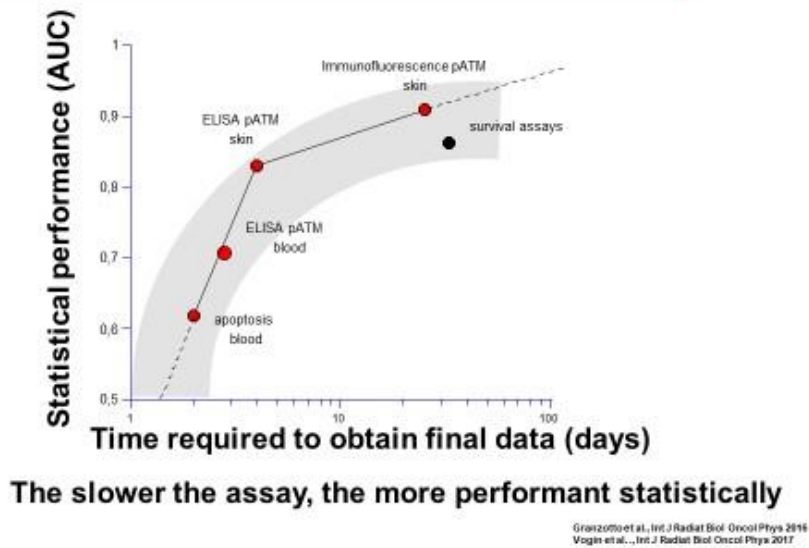


Fig 1 : Area under the curve (AUC) of the current predictive assays . From (1)

Finally, another way of approaching the scientific robustness and consistency of the bases of radiosensitivity predictive tests is to look for multi-scale correlations by analysing the mathematical relationships that may exist between CTCAE grades, clonogenic survival at 2 Gy (SF2) and the various biomarkers from the RIANS model. The result is a mathematical mesh linking the different biomarkers, which now enables us not only to consolidate the mathematical consistency of our model but also to detect outliers (4).

**CONCLUSIONS:** After more than ten years of research, it appears that there is no very rapid, very robust test. On the contrary, a complete test that can detect any range of radiosensitivity of any kind requires a long cell culture (establishment of the biopsy) and a test that is not necessarily super-fast (24-hour protocol at most). The RIANS model offers us a new vision of the individual response to radiation, with multiple areas of validity and well-documented multi-scale mathematical relationships. Conversely, there may be genomic tests that are predictive of very specific reactions (e.g. radiation fibrosis) but which are not necessarily predictive of other types of tissue reaction. The cross-comparison of tests in articles 1, 4 and 6 shows us that the objectives have been achieved by the 2 teams 1 and 2, but that the comparison is becoming increasingly qualitative as the tests proposed today are so different and meet so many different expectations.

## PUBLICATIONS RELATED TO THIS ACTIVITY

1. G. Vogin *et al.*, The Phosphorylated ATM Immunofluorescence Assay: A High-performance Radiosensitivity Assay to Predict Postradiation Therapy Overreactions. *International journal of radiation oncology, biology, physics* **101**, 690-693 (2018).
2. G. Vogin *et al.*, OC-0221: High-performance radiosensitivity assay to predict post radiation overreactions. *Radiotherapy and Oncology* **123**, S110-S111 (2017).

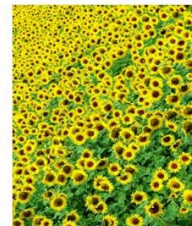


3. N. Foray, M. Bourguignon, N. Hamada, Individual response to ionizing radiation. *Mutation Research Review* **770**, 369-386 (2016).
4. E. Le Reun *et al.*, Quantitative correlations between radiosensitivity biomarkers show that the ATM protein kinase is strongly involved in the radiotoxicities observed after radiotherapy. *International journal of molecular sciences* **23**, (2022).
5. A. Granzotto *et al.*, Influence of Nucleoshuttling of the ATM Protein in the Healthy Tissues Response to Radiation Therapy: Toward a Molecular Classification of Human Radiosensitivity. *International journal of radiation oncology, biology, physics* **94**, 450-460 (2016).
6. L. Sonzogni *et al.*, Prediction of radiotherapy toxicity: 20 years of COPERNIC radiosensitivity diagnosis procedure. *Cancer radiotherapie : journal de la Societe francaise de radiotherapie oncologique*, (2024).
7. D. Averbeck *et al.*, Establishing mechanisms affecting the individual response to ionizing radiation. *International journal of radiation biology* **96**, 297-323 (2020).





# PROJET INDIRA



## ACTIVITY 07 – VALORIZATION

**PURPOSE:** The purpose of this workpackage was to develop the results of the INDIRA project both industrially (deliverable 1: patents in particular) and socially (deliverable 2: conferences for the general public).

**SUMMARY:** As far as Team 1 is concerned, at the end of the INDIRA project, the economic benefits can be summed up as 6 patents registered and licensed, 1 patent registered, a database registered, a Soleau envelope registered and a start-up created: Neolys Diagnostics, which has since been bought by the ALARA group in 2021. The foundation of this start-up and its work to set up patents, licences, CE and COFRAC accreditations is a first in the field and has been very useful to us in moving forward.

The societal benefits are reflected in the large number of conferences and public events at which INDIRA's results have been directly or indirectly cited. For the project coordinator, for example, the number of public conferences at which INDIRA data has been disseminated can be estimated at one per month. Details will be provided in the activity report.

### 1. Industrial and economic valorisation

#### 1.1 Team 1

During the INDIRA project, realising that Team 1 (N. Foray) was regularly receiving skin biopsies to diagnose in terms of radiosensitivity, we founded a start-up called NEOLYS DIAGNOSTICS on 1/4/2014 in Lyon (Gilles Devillers, Julien Gillet-Daubin and Nicolas Foray being co-founders) to better meet the diagnostic demand. This start-up has been a pioneer in the field of individual radiosensitivity diagnostics in all areas (setting up the legal and regulatory framework, accreditations, certifications, etc.). It was behind the filing of patents covering each stage of the radiosensitivity tests developed by Team 1 (Table 1). Unfortunately, the strategy of patenting each stage rather than a single protocol was to no avail and the company was forced to officially cease trading on 7/10/2020.

Neolys Diagnostics was bought out by the ALARA group based in Strasbourg (Entzheim) a few months later. However, no member of Team 1 or the INDIRA teams is active in this company. The development of new radiosensitivity tests, still based on the ATM protein but above all on the ELISA approach (immunological measurement of ATM molecule levels), which was the subject



of a publication with N. Foray as the last author. However, these tests are less effective than the original tests developed by Team 1. The last patent filed by Team 1 (on Alzheimer's disease) was co-owned by the 2nd company Neolys Diagnostics.

**Conflicts of interest:** Some members of the Team, co-inventors of the patents, were 'small' shareholders in the first Neolys Diagnostics company for small sums (<100 Euros) and never received any subsidies. The work of Nicolas Foray, co-founder and small shareholder, and above all scientific advisor to Neolys Diagnostics, was governed by a scientific assistance agreement signed by Inserm Transfert and validated by the Inserm Ethics Commission. N. Foray, as scientific advisor, will have received only the sum of 2000 Euros from Neolys Diagnostics for the duration of the project and the company. No links of interest are to be declared with Neolys Diagnostics 2 or the members of Team 1.

Neolys Diagnostics 1 supplied the sampling kits for the INDIRA volunteers of the Paris Samu. Neolys Diagnostics 2 funded a CIFRE thesis (Clément Devic) on low-dose radiation and the RIANs model.

### 1.2 Team 3

Sylvie Chevillard (CEA), head of Team 3, has been involved in the creation of a start-up called ACUBENS, the aim of which was to offer biological dosimetry kits for mass nuclear or radiological accidents in order to better "sort" exposed individuals. The link between ACUBENS and Team 3's investment in the INDIRA project should not be direct, since INDIRA's aim is not to offer tests for estimating the dose received (biodosimetry) but rather tests for predicting individual radiosensitivity. In other words, biodosimetry assumes that all exposed individuals are radioresistant and receive different doses (a single chart), whereas the INDIRA project introduces the notion of radiosensitive sub-populations receiving different doses. Originally, Team 3 proposed to use blood or hair follicles (or another deliverable) to assess the differences between individuals. Unfortunately, Team 3, in the absence of the availability of the INDIRA cohort, refused the proposals of Teams 1 and 2 to make provisional use of Team 1's COPERNIC collection on a long-term scale (several years). Team 3 preferred to use samples from the Clermont-Ferrand University Hospital, and authorisations were never provided. In 2018, Team 3 announced that it was withdrawing from the INDIRA project, even though it was supposed to provide at least the final intercomparison of the radiosensitivity tests proposed by each Team 1: clearly, the tests developed either on blood or on hair follicles were not reliable or accurate enough to compete with the approaches adopted by Teams 1 and 2, as suggested in Team 3's latest INDIRA report (see also Activity 05).

**Conflicts of interest:** no information on the status of ACUBENS or its scientific collaboration agreement has been provided to clarify the relationship between the company and Team 3. It should be noted that ACUBENS ceased its activities on 10 November 2021. See also the information on Team 3 (activity 05).

**CONCLUSIONS:** Neolys Diagnostics 2 currently offers variants of tests based on ATM transit using ELISA methodology. Conversely, U1296 is still carrying out its expert activity using historical tests. For the moment, no diagnostic test for Alzheimer's disease based on ATM transit has yet been proposed. As regards the work of Team 3, we have therefore had to reorganise the project (see ACTIVITY SHEETS 01 and 05).



**Table 1: patents field during the INDIRA project by Team 1**

DIAGNOSIS OF ALZHEIMER'S DISEASE	EP2024050282	08/01/2024	INSERM, NEOLYS DIAGNOSTICS	FORAY NICOLAS, BERTHEL ELISE, PEREIRA SANDRINE,
INDIVIDUAL METHOD FOR PREDICTING THE GENOTOXIC EFFECTS OF DNA-BREAKING CHEMICAL OR BIOCHEMICAL AGENTS	FR1559962	20/10/2015	CENTRE LEON BERARD, NEOLYS DIAGNOSTICS, INSERM, CNRS, UNIVERSITE CLAUDE BERNARD LYON 1	NICOLAS FORAY, MELANIE FERLAZZO, LAURENE SONZOGNI, LARRY BODGI, SANDRINE PEREIRA
INDIVIDUAL METHOD FOR PREDICTING THE GENOTOXIC EFFECTS OF CHEMICAL OR BIOCHEMICAL AGENTS THAT BREAK DNA	FR2016052083	16/08/2016	INSERM, CENTRE LEON BERARD, CNRS, UNIVERSITE CLAUDE BERNARD LYON 1	FORAY NICOLAS, FERLAZZO MÉLANIE, , SONZOGNI LAURÈNE, BODGI LARRY, PEREIRA
INDIVIDUAL METHOD FOR PREDICTING THE GENOTOXIC EFFECTS OF CHEMICAL OR BIOCHEMICAL AGENTS THAT BREAK DNA	EP16763915	16/08/2016	INSERM, CENTRE LEON BERARD, CNRS, UNIVERSITE CLAUDE BERNARD LYON 1	FORAY NICOLAS, FORAY, Nicolas, FERLAZZO MÉLANIE, FERLAZZO, Mélanie, SONZOGNI LAURÈNE, SONZOGNI, Laurène, BODGI LARRY, BODGI, Larry, PEREIRA SANDRINE, PEREIRA, Sandrine
METHOD FOR PREDICTING AND ASSESSING EXCESS DOSE DUE TO IODINATED CONTRAST PRODUCTS INJECTED DURING RADIODIAGNOSTIC EXAMINATIONS	FR1559963	20/10/2015	INSERM, CENTRE LEON BERARD, CNRS, UNIVERSITE CLAUDE BERNARD LYON 1	NICOLAS FORAY, ADELINE GRANZOTTO, CLEMENT DEVIC, MELANIE FERLAZZO, LARRY BODGI, SANDRINE PEREIRA
METHOD FOR PREDICTING AND ASSESSING EXCESS DOSE DUE TO IODINATED CONTRAST PRODUCTS INJECTED DURING RADIODIAGNOSTIC EXAMINATIONS	FR2016052084	16/08/2016	INSERM, CENTRE LEON BERARD, CNRS, UNIVERSITE CLAUDE BERNARD LYON 1	FORAY NICOLAS, FORAY, Nicolas, GRANZOTTO ADELINE, GRANZOTTO, Adeline, DEVIC CLÉMENT, DEVIC, Clément, FERLAZZO MÉLANIE, FERLAZZO, Mélanie, BODGI LARRY, BODGI, Larry, PERREIRA SANDRINE, PERREIRA, Sandrine
METHOD FOR PREDICTING AND ASSESSING EXCESS DOSE DUE TO IODINATED CONTRAST PRODUCTS INJECTED DURING RADIODIAGNOSTIC EXAMINATIONS	EP16763916	16/08/2016	INSERM, CENTRE LEON BERARD, CNRS, UNIVERSITE CLAUDE BERNARD LYON 1	FORAY NICOLAS, FORAY, Nicolas, GRANZOTTO ADELINE, GRANZOTTO, Adeline, DEVIC CLÉMENT, DEVIC, Clément, FERLAZZO MÉLANIE, FERLAZZO, Mélanie, BODGI LARRY, BODGI, Larry, PEREIRA



				SANDRINE, PEREIRA, Sandrine
PREDICTIVE METHOD FOR CHARACTERISING A PATIENT'S RADIOSENSITIVITY AND TISSUE REACTION TO THERAPEUTIC IONISING RADIATION	FR2015050365	16/02/2015	INSERM, CENTRE LEON BERARD, CNRS, UNIVERSITE CLAUDE BERNARD LYON 1	FORAY NICOLAS, FORAY, NICOLAS, GRANZOTTO ADELINE, GRANZOTTO, ADELINE, DEVIC CLÉMENT, DEVIC, CLÉMENT
PREDICTIVE METHOD FOR CHARACTERISING A PATIENT'S RADIOSENSITIVITY AND TISSUE REACTION TO IONISING RADIATION THERAPY	EP15709253.7	16/02/2015	INSERM, CENTRE LEON BERARD, CNRS, UNIVERSITE CLAUDE BERNARD LYON 1	FORAY, Nicolas, GRANZOTTO, Adeline, DEVIC, Clément
PREDICTIVE METHOD FOR CHARACTERISING A PATIENT'S RADIOSENSITIVITY AND TISSUE REACTION TO IONISING RADIATION THERAPY	FR1451215	17/02/2014	INSERM, CENTRE LEON BERARD, CNRS, UNIVERSITE CLAUDE BERNARD LYON 1	NICOLAS FORAY, ADELINE GRANZOTTO, CLEMENT DEVIC
PREDICTIVE METHOD FOR CHARACTERISING THE SENSITIVITY OF A TUMOUR IN RESPONSE TO A DNA-BREAKING TREATMENT	FR1559961	20/10/2015	INSERM, CENTRE LEON BERARD, CNRS, UNIVERSITE CLAUDE BERNARD LYON 1	NICOLAS FORAY, LARRY BODGI, SANDRINE PEREIRA
PREDICTIVE METHOD FOR CHARACTERISING THE SENSITIVITY OF A TUMOUR IN RESPONSE TO A DNA-BREAKING TREATMENT	FR2016052082	16/08/2016	INSERM, CENTRE LEON BERARD, CNRS, UNIVERSITE CLAUDE BERNARD LYON 1	FORAY NICOLAS, FORAY, Nicolas, BODGI LARRY, BODGI, Larry, PERREIRA SANDRINE, PERREIRA, Sandrine
PREDICTIVE METHOD FOR CHARACTERISING THE SENSITIVITY OF A TUMOUR IN RESPONSE TO A DNA-BREAKING TREATMENT	EP16763914	16/08/2016	INSERM, CENTRE LEON BERARD, CNRS, UNIVERSITE CLAUDE BERNARD LYON 1	FORAY NICOLAS, FORAY, Nicolas, BODGI LARRY, BODGI, Larry, PEREIRA SANDRINE, PEREIRA, Sandrine
PREDICTIVE METHOD FOR DETERMINING TISSUE RADIOSENSITIVITY	FR2015050370	16/02/2015	INSERM, CENTRE LEON BERARD, CNRS, UNIVERSITE CLAUDE BERNARD LYON 1	FORAY NICOLAS, GRANZOTTO, ADELINE, DEVIC, CLÉMENT
PREDICTIVE METHOD FOR DETERMINING TISSUE RADIOSENSITIVITY	EP15709256.0	16/02/2015	INSERM, CENTRE LEON BERARD, CNRS, UNIVERSITE CLAUDE BERNARD LYON 1	FORAY, Nicolas, GRANZOTTO, Adeline, DEVIC, Clément
PREDICTIVE METHOD FOR DETERMINING TISSUE RADIOSENSITIVITY	FR1451216	17/02/2014	INSERM, CENTRE LEON BERARD, CNRS, UNIVERSITE CLAUDE BERNARD LYON 1	NICOLAS FORAY, ADELINE GRANZOTTO, CLEMENT DEVIC
RAPID PREDICTIVE METHOD FOR CHARACTERISING A PATIENT'S RADIOSENSITIVITY TO IRRADIATION WITH IONISING RADIATION	FR1563362	28/12/2015	INSERM, CENTRE LEON BERARD, CNRS, UNIVERSITE CLAUDE BERNARD LYON 1	NICOLAS FORAY, ADELINE GRANZOTTO, CLEMENT DEVIC, MELANIE FERLAZZO, LARRY



				BODGI, SANDRINE PEREIRA
RAPID PREDICTIVE METHOD FOR CHARACTERISING A PATIENT'S RADIOSENSITIVITY TO IRRADIATION WITH IONISING RADIATION	FR2016053322	09/12/2016	INSERM, CENTRE LEON BERARD, CNRS, UNIVERSITE CLAUDE BERNARD LYON 1	NICOLAS FORAY, ADELINE GRANZOTTO, CLEMENT DEVIC, MELANIE FERLAZZO, LARRY BODGI, SANDRINE PEREIRA
RAPID PREDICTIVE METHOD FOR CHARACTERISING A PATIENT'S RADIOSENSITIVITY TO IRRADIATION WITH IONISING RADIATION	EP16825476.1	09/12/2016	INSERM, CENTRE LEON BERARD, CNRS, UNIVERSITE CLAUDE BERNARD LYON 1	NICOLAS FORAY, ADELINE GRANZOTTO, CLEMENT DEVIC, MELANIE FERLAZZO, LARRY BODGI, SANDRINE PEREIRA
DIAGNOSIS OF ALZHEIMER'S DISEASE	EP2024050282	08/01/2024	INSERM, CENTRE LEON BERARD, CNRS, UNIVERSITE CLAUDE BERNARD LYON 1	NICOLAS FORAY, ADELINE GRANZOTTO, CLEMENT DEVIC, MELANIE FERLAZZO, LARRY BODGI, SANDRINE PEREIRA
INDIVIDUAL METHOD FOR PREDICTING THE GENOTOXIC EFFECTS OF DNA-BREAKING CHEMICAL OR BIOCHEMICAL AGENTS	FR1559962	20/10/2015	CEN	NICOLAS FORAY, MELANIE FERLAZZO, LAURENE SONZOGNI, LARRY BODGI, SANDRINE PEREIRA
INDIVIDUAL METHOD FOR PREDICTING THE GENOTOXIC EFFECTS OF DNA-BREAKING CHEMICAL OR BIOCHEMICAL AGENTS	FR2016052083	16/08/2016	INSERM, CENTRE LEON BERARD, CNRS, UNIVERSITE CLAUDE BERNARD LYON 1	NICOLAS FORAY, ADELINE GRANZOTTO, SONZOGNE LAUREE CLEMENT DEVIC, MELANIE FERLAZZO, LARRY BODGI, SANDRINE PEREIRA
INDIVIDUAL METHOD FOR PREDICTING THE GENOTOXIC EFFECTS OF DNA-BREAKING CHEMICAL OR BIOCHEMICAL AGENTS	EP16763915	16/08/2016	INSERM, CENTRE LEON BERARD, CNRS, UNIVERSITE CLAUDE BERNARD LYON 1	FORAY NICOLAS, , FERLAZZO, MELANIE, SONZOGNI LAURÉNE, BODGI LARRY, PEREIRA SANDRINE,





# PROJET INDIRA



## 1<sup>ER</sup> REFUND

### ACTIVITY 08-1 – LOW/HIGH DOSES

**PURPOSE:** The aim of this workpackage was to verify the validity of the RIANS model for low doses of radiation (less than 0.5 Gy) and to elucidate the enigmas of radiobiology represented by hypersensitivity to low doses, the adaptive response and hormesis. More recently, due to the redistribution of the balance of Team 3, we proposed to carry out the same approach for high doses of radiation (greater than 4 Gy) by initiating fundamental research on acute radiation syndrome.

**SUMMARY :** At doses below 0.5 Gy, 3 specific phenomena whose mechanisms are still unknown emerge and constitute real enigmas of radiobiology since at least the 1980s: hypersensitivity to low doses (1), adaptive response (2) and hormesis (3). Thanks to the RIANS model and Clément Devic's thesis, we were able to propose a coherent explanation for these 3 phenomena:

- **Low dose hypersensitivity:** First described by Lambin et al. (4) and Marples and Joiner (5), hyper-radiosensitivity to low dose (HRS) results, for a single  $d_{HRS}$  HRS dose between 1 and 800 mGy (6), in a significant reduction in clonogenic survival and thus results in a biological effect equivalent to a much higher dose. Low dose hypersensitivity is not only limited to a decrease in cell survival but is also associated with an increase in unrepaired DSBs and an increase in the number of micronuclei (301). This phenomenon does not only concern cell death and radiosensitivity pathways (7). The maximum magnitude of HFD was observed at a  $d_{HFDmax}$  dose between  $d_{HFDmax}$  0.1 and 0.8 Gy (the most frequent  $d_{HFDmax}$  is 0.2 Gy) corresponding to a biological effect equivalent to a dose 5 to 10 times higher (6, 8). Furthermore,  $d_{HFDmax}$  can also vary with dose rate (8). In the RIANS model, at low dose exposure, the number of ATM monomers produced by irradiation in the cytoplasm is naturally reduced (because it is proportional to the dose). Thus, the number of ATM monomers that diffuse into the nucleus will also be reduced at low doses. This is particularly true in radiosensitive group II cells because, in addition, X proteins sequester some ATM monomers. Figure 49 indicates that after 10 min post-irradiation, a dose of 0.2 Gy ( $d_{HFDmax}$ ) provides the nucleus with about 2.5 times more ATM monomers in a group I cell than in a group II cell. At such a dose, only about 8 DSBs per cell are produced. In group II cells, few monomers are able to diffuse to the nucleus and it is very likely that of the 8 induced DSBs, the majority are not recognized by suture repair (NHEJ) and will therefore remain either unrepaired (dramatic drop in the cell survival curve) or poorly repaired (increased risk of mutations). For



slightly higher doses, the number of ATM monomers increases and is sufficient to recognize more DSBs: the probability that a DSB remains unrecognized and unrepaired decreases and the survival curve returns to its classic shape (3).

**- Adaptive response (AR) :** the adaptive response is observed if, during a succession of doses  $d_{RA} + \Delta t_{RA} + D_{RA}$ , the biological effect is more beneficial than a single dose  $D_{RA}$ . AR is observed specifically in cells with intermediate radiosensitivity. Within the framework of the ATM transit theory, for radioresistant cells (group I), the ATM flux is more than sufficient for the benefit of  $d_{RA} + \Delta t_{RA}$  before the delivery of  $D_{RA}$  to be significant. Consequently, the AR phenomenon is not measurable for radioresistant cells. For hyperradiosensitive cells (group III), the effect of  $d_{RA} + \Delta t_{RA}$  is already deleterious and therefore adds to that of  $D_{RA}$ : AR is not observed either. In the case of moderately radiosensitive cells (group II) subjected to a  $d_{RA}$  between 0.001 and 0.5 Gy, the diffusion of ATM monomers is approximately 2 times less important than in radioresistant cells. For example, approximately 40,000 and 20,000 ATM monomers pass the nuclear membrane respectively after 0.2 Gy followed by 6 h ( $d_{RA} + \Delta t_{RA}$ ) for radioresistant and moderately radiosensitive cells. However, a dose of 2 Gy ( $D_{RA}$ ) produces in 10 min, for the same type of cells respectively, approximately 30,000 and 16,000 ATM monomers (2). During  $\Delta t_{RA}$ , ATM monomers produced by  $d_{RA}$  can lose their activity by “redimerizing”. However, even if approximately 20% of ATM monomers supplied by  $d_{RA}$  remain active during  $\Delta t_{RA}$  (i.e. approximately 4,000 monomers in our case), this contribution represents approximately 25% (4,000 out of 16,000) of the additional active ATM monomers to respond to  $D_{RA}$ . In this specific case, a  $\Delta t_{AR}$  that is too short would not allow sufficient flux; a  $\Delta t_{AR}$  that is too long would result in inactive monomers. Thus, in group II radiosensitive cells,  $d_{AR} + \Delta t_{AR}$  could therefore produce a stimulation of DSB recognition by an additional supply of ATM monomers. The occurrence and extent of the RA phenomenon would therefore strongly depend on the radiosensitivity of the irradiated cells. The RA phenomenon (i.e. the reduction of the biological effect of a high dose of radiation by a lower dose) is therefore not technically an artifact but it is observable but under specific experimental conditions:

- An exposure scenario of the  $d_{RA} + \Delta t_{RA} + D_{RA}$  type must be applied, with  $d_{RA}$  between 0.001 and 0.5 Gy,  $\Delta t_{RA}$  between 2 and 24 h, and  $D_{RA}$  between 0.1 and 5 Gy.
- This phenomenon can be observed on many cell types, but the cells must be characterized by a certain radiosensitivity or radiosusceptibility (group II): RA is not measurable on radioresistant cells or on hyperradiosensitive cells. It therefore depends heavily on genetic status.
- The benefit of this phenomenon for humans remains very limited, if not nonexistent, especially since the first condition makes this exposure scenario feasible almost exclusively in the laboratory. However, in clinical practice, it should be verified whether a positioning CT scan followed by a dose of radiotherapy can lead to tumor radioprotection.
- Just as with low-dose hypersensitivity (LDH), the ATM transit theory now provides a molecular explanation for this phenomenon. Contrary to historical hypotheses, and although the priming dose is reminiscent of vaccination, this phenomenon has nothing to do with the laws of immunology.
  - After much semantic drift and misinterpretation, the existence of AR, based on the succession of a low dose and a high dose (which is often itself toxic or mutagenic) and which is only observed in radiosensitive or transformed cells, does not constitute proof that low doses are beneficial.



**-Hormesis:** Hormesis describes beneficial irradiation. The phenomenon of hormesis, triggered by a single dose  $d_{\text{horm}}$  in the dose range [20-75 mGy], is preferentially observed in radioresistant cells. Recognition and repair of radiation-induced DSBs is complete for doses less than or equal to 2 Gy in these cells (9). However, they may exhibit low but significant genomic instability with spontaneous single-strand break (SSB) rates due to reactive oxygen species or nuclease activity (10). This spontaneously elevated nuclease activity contributes to aging and genomic instability by increasing DNA damage (10, 11). In the dose range where hormesis is observed, the number of radio-induced CSBs does not normally exceed 75 CSBs per cell, which, moreover, is not statistically sufficient to create an additional DSB (remember that a DSB cannot be the result of 2 DSBs unless they are sufficiently close (less than 50 bp) or if the second CSB is an abnormal consequence of the repair of the first). On the other hand, even if there are few or no induced DSBs, a flow of several thousand ATM monomers diffuses very quickly into the nucleus (3). This contribution of ATM monomers, without influencing the efficiency of recognition of DSBs induced by a dose of  $d_{\text{horm}}$ , could, however, allow cells to repair spontaneous damage (DSBs or BSCs). Thus, this "detoxification" of cells would reduce the potential risks of cancer or aging linked to this spontaneous damage, obviously provided that these are associated with a particular clinical risk. This effect could not occur in radiosensitive cells, particularly those from individuals predisposed to cancer, since, on the contrary,  $d_{\text{horm}}$  would directly or indirectly produce DSBs linked to hyper-recombination in addition to the spontaneous damage which may be more numerous for this type of genomically unstable cells than for radioresistant cells. The contribution of ATM monomers would not be able to compensate for the additional damage induced by  $d_{\text{horm}}$ . Just like HFD and RA, the phenomenon of hormesis would therefore also have a meaning at the molecular level. Within the framework of the ATM transit model, to the extent that the chosen parameters depend on the activity of the ATM kinase in the nucleus, the biological consequences of hormesis can be of great diversity. Indeed, the ATM protein has been shown to be upstream of a phosphorylation cascade of its substrates by obeying a functional and temporal hierarchy: phosphorylation of ATM substrates involved in the recognition of DNA damage, then in the repair of this damage, then in the control of the cell cycle and finally in cell death pathways (12). Interestingly, all steps of the molecular and cellular response to radiation are known to be facilitated by high nuclear ATM kinase activity, which makes our model consistent with the phenomenon of hormesis. The consequences of high ATM activity can also be observed at the cellular level downstream of the steps of DSB recognition and repair. This is particularly the case for clinical features that occur at the tissue level, such as immune and inflammatory reactions (12). However, additional experimental data on ATM are needed to establish a quantitative and qualitative link between the cellular event and tissue responses. Thus, hormesis may contribute to reducing spontaneous cell death, genomic instability, and aging in radioresistant cells. However, the consequences of a hormetic phenomenon may show different magnitudes depending on the molecular, cellular, tissue, or clinical scales considered. For example, the recognition and repair of DSBs and chromosomes are "bounded" notions: when all lesions are recognized or repaired, a dose of hormesis cannot contribute to recognizing or repairing more. Therefore, if the recognition or repair of DSBs and chromosomal lesions are considered as parameters for measuring hormesis, the dose response may present a threshold or even not be measurable at the molecular or cellular level but be observed at a larger scale.

We also undertook to verify the validity of the RIANS model, i.e., in the context of acute radiation syndrome. For doses above 4 Gy, the RIANS model predicts that the number of radiation-induced ATM monomers is so high that the monomers redimerize and therefore cannot diffuse into the nucleus: the cessation of DSB recognition is total and the number of  $\gamma$ H2AX foci must decrease



(because ATM cannot phosphorylate H2AX in the nucleus) while the number of radiation-induced DSBs increases with the dose. The experimental data obtained fully validate this hypothesis, to the point that a very late increase (24-72 h after irradiation) in the number of  $\gamma$ H2AX foci, also predicted by the RIANs model, was predicted. In parallel, radioprotective drugs added under the same conditions allowed us to modulate the response to high doses. These experiments were carried out on skin and intestinal fibroblasts to document the tissue-dependence of the response to high doses. Finally, using ELISA kits and flow cytometry, we were able to measure the quantity and overexpression of 6 pro- or anti-inflammatory cytokines both inside and outside the cell. A mathematical model governing both DNA damage (DSB), its recognition ( $\gamma$ H2AX and pATM foci) and cytokine induction is currently being developed: coupled with a mechanistic model, these two models could revolutionize our vision of acute radiation syndrome by introducing the ATM protein which could then explain:

- The prodrome with the cessation of repair functions
- The lag phase with the return of very late ATM monomers to the nucleus
- The pro- or anti-inflammatory nature of cytokines depending on whether they are phosphorylated and/or interact with ATM
- The tissue-dependence of acute radiation syndrome
- The effectiveness of new-generation radioprotective drugs

A thesis on the subject is expected to begin early next year and a first publication is expected to be submitted in early 2025.

**CONCLUSIONS:** The RIANs model now makes it possible to interpret the biological mechanisms of radiobiological phenomena specific to low doses, each time with a mathematical model that better predicts the response following the modification of certain parameters. Furthermore, the RIANs model has made it possible to initiate research on high doses of radiation: once again, the hypotheses of the RIANs model have been experimentally verified, and we are preparing a specific study of acute radiation syndrome, where the ATM protein appears to play a key regulatory role.

## PUBLICATIONS DIRECTLY RELATED TO THE ACTIVITY

Asterisks mark publications that are not from the INDIRA project.

1. L. Bodgi, N. Foray, The nucleo-shuttling of the ATM protein as a basis for a novel theory of radiation response: resolution of the linear-quadratic model. *International journal of radiation biology* **92**, 117-131 (2016).
2. C. Devic, M. L. Ferlazzo, N. Foray, Influence of Individual Radiosensitivity on the Adaptive Response Phenomenon: Toward a Mechanistic Explanation Based on the Nucleo-Shuttling of ATM Protein. *Dose-response : a publication of International Hormesis Society* **16**, 1-11 (2018).
3. C. Devic, M. L. Ferlazzo, E. Berthel, N. Foray, Influence of Individual Radiosensitivity on the Hormesis Phenomenon: Toward a Mechanistic Explanation Based on the Nucleoshuttling of ATM Protein. *Dose-response : a publication of International Hormesis Society* **18**, 1559325820913784 (2020).



- 4.\* P. Lambin, B. Marples, B. Fertil, E. P. Malaise, M. C. Joiner, Hypersensitivity of a human tumour cell line to very low radiation doses. *International journal of radiation biology* **63**, 639-650 (1993).
- 5.\* B. Marples, M. C. Joiner, The response of Chinese hamster V79 cells to low radiation doses: evidence of enhanced sensitivity of the whole cell population. *Radiation research* **133**, 41-51 (1993).
- 6.\* M. C. Joiner, B. Marples, P. Lambin, S. C. Short, I. Turesson, Low-dose hypersensitivity: current status and possible mechanisms. *International journal of radiation oncology, biology, physics* **49**, 379-389 (2001).
- 7.\* L. Xue *et al.*, ATM-dependent hyper-radiosensitivity in mammalian cells irradiated by heavy ions. *International journal of radiation oncology, biology, physics* **75**, 235-243 (2009).
8. C. Thomas *et al.*, Impact of dose-rate on the low-dose hyper-radiosensitivity and induced radioresistance (HRS/IRR) response. *International journal of radiation biology* **89**, 813-822 (2013).
9. A. Granzotto *et al.*, Influence of Nucleoshuttling of the ATM Protein in the Healthy Tissues Response to Radiation Therapy: Toward a Molecular Classification of Human Radiosensitivity. *International journal of radiation oncology, biology, physics* **94**, 450-460 (2016).
- 10.\* M. Schieber, N. S. Chandel, ROS function in redox signaling and oxidative stress. *Curr Biol* **24**, R453-462 (2014).
- 11.\* M. S. Cooke, M. D. Evans, M. Dizdaroglu, J. Lunec, Oxidative DNA damage: mechanisms, mutation, and disease. *FASEB J* **17**, 1195-1214 (2003).
12. N. Foray, [Radiobiological features of anti-cancer treatments involving synchrotron radiation: outcome and perspectives]. *Cancer radiotherapie : journal de la Societe francaise de radiotherapie oncologique* **14**, 145-154 (2010).





# PROJET INDIRA



## 1<sup>ST</sup> REFUND

### ACTIVITY 08-2 – RADIOSUSCEPTIBILITY/SENSITIVITY/DEGENERESCENCE

**OBJECTIVE:** The aim of this workpackage was to distinguish radiosensitivity, radiosusceptibility and radiodegeneration using specific tests and biomarkers

**SUMMARY:** In a recently published review (1, 2), we showed that cancer syndromes are predominantly associated with the mutation of X proteins that are overexpressed and randomly distributed in the cytoplasm, whereas aging syndromes are associated with X proteins that are rather perinuclear. The study of radiosensitivity related to Alzheimer's disease (AD) allowed us to go further in this analysis. Indeed, in the 1980s, cells from AD patients were considered radiosensitive to ionizing radiation (3). We recently showed that AD fibroblasts are part of radiosensitivity group II with a significant delay in ATM transit. Moreover, fibroblasts from AD patients systematically showed spontaneous perinuclear localization of phosphorylated ATM forms (pATM) (4) (Fig. 1). Our data and a mathematical approach through a completely new model suggest that in response to progressive and cumulative stress, cytoplasmic ATM monomers phosphorylate the APOE protein (pAPOE) close to the nuclear membrane and overexpressed in AD cells (4). ATM monomers aggregate around the nucleus, preventing their own entry into the nucleus and therefore the recognition and repair of DSBs, thus promoting an aging process (Fig. 1) (4). Similar observations (but with a different X protein, dystrophin) have been made on cells from Duchesne muscular dystrophy. A patent has been filed (see activity sheet 07). Even more recently, we have also observed perinuclear ATM coronas on tissues that age either spontaneously (e.g., the lens (5)) or after low-dose-rate irradiation (6).

In addition to the specific localizations of X proteins, it appears that cells from syndromes associated with a predisposition to cancer show early MRE11 foci (within the first minutes after 2 Gy). Conversely, cells from accelerated aging syndromes show late MRE11 foci (24 h post-irradiation). Knowing that MRE11 foci only appear after phosphorylation of the MRE11 nuclease by ATM, our observations suggest that only ATM monomers that can rapidly access the nucleus would be responsible for the formation of MRE11 foci (1, 2). Conversely, for accelerated aging, access to the nucleus would be very limited for ATM monomers.



Finally, even more recently, we have highlighted, thanks to the thesis of Laura El-Nachef, that the excess risk of cancer could be determined by a double test measuring on the one hand mutability and on the other hand the capacity for proliferation (7).

**CONCLUSIONS:** For several months, we have been able to confirm that, using the specific biomarkers detailed above, we can distinguish cells predisposed to cancer from cells predisposed to accelerated aging. The RIANS model therefore offers a comprehensive view of the individual response to radiation by integrating the different clinical consequences of irradiation. The objectives have been achieved.

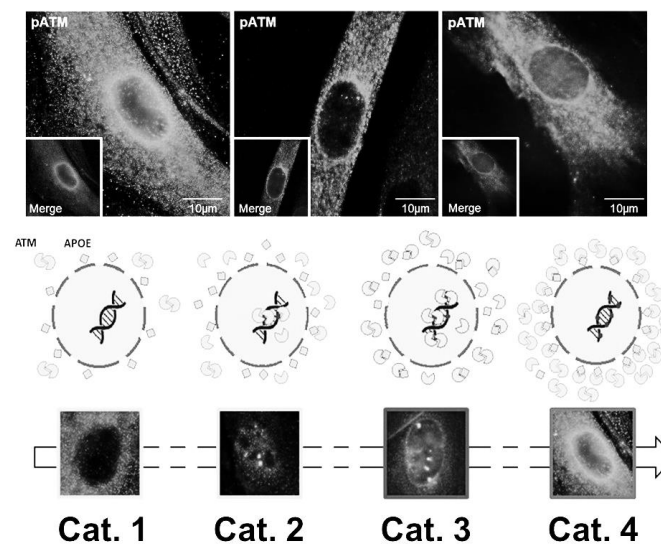


**Fig. 1:** Representative examples of perinuclear ATM coronas observed on fibroblasts from patients with Alzheimer's disease (taken from (4)). The aging process would first begin with the formation of ATM-APOE complexes that would not hinder the arrival of ATM in the nucleus to recognize and trigger the repair of DNA breaks (visible in the form of bright green foci). Then gradually the first ATM-APOE layer would cover the entire nucleus (a thin green corona appears while still observing foci) then finally the ATM dimers accumulate and thicken the corona by preventing any ATM from penetrating into the nucleus (the DNA breaks are there but no longer recognized (no foci)).

## PUBLICATIONS LIEES DIRECTEMENT A CETTE ACTIVITE

1. L. El-Nachef *et al.*, Human Radiosensitivity and Radiosusceptibility: What Are the Differences? *International journal of molecular sciences* **22**, 7158 (2021).
2. L. El Nachef *et al.*, Cancer and Radiosensitivity Syndromes: Is Impaired Nuclear ATM Kinase Activity the Primum Movens? *Cancers* **14**, (2022).
3. J. H. Robbins *et al.*, Parkinson's disease and Alzheimer's disease: hypersensitivity to X rays in cultured cell lines. *J Neurol Neurosurg Psychiatry* **48**, 916-923 (1985).
4. E. Berthel *et al.*, Toward an early diagnosis for Alzheimer's disease based on the perinuclear localization of the ATM protein. *Cells* **12**, 1747 (2023).
5. J. Al-Choboq *et al.*, The Radiobiological Characterization of Human and Porcine Lens Cells Suggests the Importance of the ATM Kinase in Radiation-Induced Cataractogenesis. *Cells* **12**, (2023).
6. J. Restier-Verlet *et al.*, Accelerated aging effects observed in vitro after an exposure to gamma-rays delivered at very low and continuous dose-rate equivalent to 1-5 weeks in International Space Station. *Cells* **in press**, (2024).
7. L. El Nachef *et al.*, Prediction of Cancer Proneness under Influence of X-rays with Four DNA Mutability and/or Three Cellular Proliferation Assays. *Cancers* **16**, (2024).





# PROJET INDIRA



## 1<sup>ST</sup> RE-FUND

### ACTIVITEY08-3 – HUMAN AND SOCIAL SCIENCES STUDY

**OBJECTIVES :** The aim of this workpackage was to develop and carry out an SHS study on healthy donors from the INDIRA cohort.

**SUMMARY:** The INDIRA results show that it is now possible to predict the level of individual sensitivity after exposure to ionizing radiation, for common medical exposures. This work raises questions about the possible reactions of patients after this type of predictive announcement. To investigate this question, the theoretical framework offered by the sociogenetic approach to social representations seems most appropriate. This perspective on social representations makes it possible to highlight, on the one hand, the genesis of collective thought in social discourse and, on the other hand, its practical and useful purpose in behaviors. This work aims to study the representations of ionizing radiation and health prediction and through it, the possible impact of such a prediction. Given the lack of prior work on this subject, this study will begin with exploratory interviews in order to refine the main data collection. Based on the analysis of the interviews, a questionnaire will be constructed to investigate, on the one hand, the social representations of ionizing radiation and, on the other hand, the question of disease prediction. The qualitative data will be subject to a thematic content analysis and descriptive statistics. As for the quantitative data, they will be described statistically before looking for possible correlations between socio-demographic data and the answers to the questions. The analysis of the results should highlight the motivations and obstacles to carrying out this type of predictive tests, but also to understand how ionizing radiation is viewed by the general public.

#### Research Questions and Objectives

By combining these various elements of the literature with the knowledge already identified by the INDIRA project, we formulated the following research questions :

- What are the social representations of ionizing radiation in the general population?
- What are the perceptions of the possible prediction of cancer?

**Main objective:** To study the representations of ionizing radiation and prediction in health.

**Secondary objective:** To study the impact of predicting individual radiosensitivity on health behaviors.



The study of the general public's perception and prediction of cancer involved a deeper exploration of social representations of radiation. The ambivalence surrounding the perception of risks and exposure to ionizing radiation from the general public's perspective prompted us to study this issue from the following perspectives:

- Research on social representations from a sociogenetic perspective. In this way, it is possible to study group thinking around a complex subject in common-sense discourse.
- Research on disease prediction, as other diseases are already the subject of early genetic testing.
- Health norms that implicitly guide our thoughts and behaviors.

Our results showed that representations of radiation are part of a cautious dimension but they are immediately associated with nuclear power plants before thinking about the medical aspects of their uses. Considering the development of a disease remains worrying for everyone because people only feel reassured by the possible actions to delay or treat the disease. The health objective remains a priority and normative. Finally, the notion of increased risks of disease depending on radiation is rather known by respondents who are aware of the risks of radiation in general. As a reminder, 65.53% of participants responded that radiation is dangerous for health and 100% responded that radiation increases the risk of cancer (32.26% from a small exposure and 70.97% when exposure is repeated or intense).

**CONCLUSION:** This study highlights the need for multidisciplinary support for predictive testing. Concerns, even anxieties, associated with the results should be addressed by a psychologist. Support appears necessary whether the test results place patients in a group with normal responses to DNA double-strand break repair or a radiosensitive group. This point is a lesson learned from the work on individuals tested for Huntington's disease. Finally, support regarding possible preventive measures or tests, as well as possible treatments for the diseases, also appears essential and desired by respondents.



# PROJET INDIRA



## 2<sup>nd</sup> REFUND

### ACTIVITY 09 – INTER-TISSUE DIFFERENCES

**PURPOSE:** The aim of this workpackage was to provide an initial reading of the differences in radiosensitivity between human tissues with the biomarkers previously established by work on predictive radiosensitivity tests with avenues for moving from the reference tissue "skin" to other tissues

**SYNTHESIS :** During the INDIRA project and the various other projects that Team 1 has developed, at least 7 different tissues have been studied: skin, bone, heart, lens, retina, prostate, brain, and breast. These 7 tissues, however, represent 5 cell types (fibroblasts, epithelial cells, osteoblasts, astrocytes, and myocytes). It should also be noted that these fibroblasts do not necessarily come from the same donor. The partnership with the Léon Bérard Center (Team 5), however, allowed us to collect pairs of skin fibroblasts and osteoblasts from the same donor and to be able to collect breast fibroblasts. The rest of the lines come from the American company ScienceCell (USA). According to our data obtained from approximately 25 cell lines, 4 major parameters seem to characterize the response to radiation of a given tissue:

- **The abundance of ATM protein** and the mobilization of ATM monomers from the cell: this is particularly the case for astrocytes, known to be ATM-poor: all characterized astrocytes are classified as group II (low ATM flux and delayed transit). A theoretical study is underway to refine the RIANS model on this subject (1).
- **The width/length of the cytoplasm**, which imposes a more or less long transit time for ATM dimers to reach the nucleus: this is also the case for astrocytes compared to lymphocytes, for example, which have a large nucleus and a small cytoplasm. A theoretical study is underway to refine the RIANS model on this subject (1).
- **The cell's content** and its capacity to mobilize calcium (Ca<sup>2+</sup>). Team 1 published a fundamental article on the bystander effect where it is shown that at each irradiation, whatever its nature, the released Ca<sup>2+</sup> ions can contaminate the surrounding cells (whether they are irradiated or not) and contribute to the dose (nearly 30% more dose) (2). In addition, Team 1 has accumulated over the last 3 months data on the quantity of calcium released after a given dose (from 0.1 to 10 Gy), for given times (from 10 min to 4 h) and for given numbers of irradiated cells (from 100,000 to 10,000,000 cells). A



publication is being prepared to compare the radiation-induced calcium fluxes according to the nature of the irradiated cells.

- **The tissue X protein(s):** According to the RIANS model, each tissue is characterized by "tissue" X proteins, proteins abundant more specifically in the tissue in question and carrying SQ and TQ sites of phosphorylation by ATM. Recently, through Joëlle Al-Choboq's thesis on eye pathologies and radiation-induced cataracts, we demonstrated that the FSP2 protein is a lens X protein (3). More recently, premature aging of the ovaries has become a subject of study with a systematic search for the X protein of this particular tissue (Al-Choboq et al., in preparation).
- Another, more general article will take stock of the different mathematical laws observed between skin fibroblasts and all the tissues cited (planned for early 2025).

Another, more general article will review the different mathematical laws observed between skin fibroblasts and all the tissues mentioned (planned for early 2025).

**CONCLUSIONS:** This latest work package opens a new avenue towards refining predictions of radiosensitivity, as well as radiosusceptibility and radiodegeneration for all human tissues. It is now clear that the individual response to radiation is complicated by tissue specificity, which can lead to a risk of toxicity, cancer, or accelerated aging. The transition from tissue to tissue is multifactorial and could represent a major challenge in future radiation protection by better documenting, as the Sievert system attempts to do, the differences in responses and therefore risks. This last topic could represent a very interesting perspective for the INDIRA project.

#### **PUBLICATIONS CONCERNEES DIRECTEMENT PAR CETTE ACTIVITE**

1. L. Bodgi, N. Foray *Effets biologiques des radiations ionisantes. Une théorie basée sur le transit cyto-nucléaire de la protéine ATM. Applications à la radiothérapie* (Editions universitaires européennes, Sarrebruck, Allemagne, 2016).
2. J. Restier-Verlet *et al.*, X-rays-Induced Bystander Effect Consists in the Formation of DNA Breaks in a Calcium-Dependent Manner: Influence of the Experimental Procedure and the Individual Factor. *Biomolecules* **13**, 542 (2023).
3. J. Al-Choboq *et al.*, The Radiobiological Characterization of Human and Porcine Lens Cells Suggests the Importance of the ATM Kinase in Radiation-Induced Cataractogenesis. *Cells* **12**, (2023).









Article

# Quantitative Correlations between Radiosensitivity Biomarkers Show That the ATM Protein Kinase Is Strongly Involved in the Radiotoxicities Observed after Radiotherapy

Eymeric Le Reun <sup>1,†</sup>, Larry Bodgi <sup>1,2,3,†</sup> , Adeline Granzotto <sup>1</sup>, Laurène Sonzogni <sup>1</sup>, Mélanie L. Ferlazzo <sup>1</sup>, Joëlle Al-Choboq <sup>1</sup> , Laura El-Nachef <sup>1</sup>, Juliette Restier-Verlet <sup>1</sup>, Elise Berthel <sup>1</sup> , Clément Devic <sup>1</sup> , Audrey Bouchet <sup>1</sup> , Michel Bourguignon <sup>1,4</sup> and Nicolas Foray <sup>1,\*</sup>

<sup>1</sup> Inserm, U1296 Unit, «Radiation: Defense, Health and Environment», Centre Léon-Bérard, 28, rue Laennec, 69008 Lyon, France

<sup>2</sup> Department of Radiation Oncology, American University of Beirut Medical Center, Riad El-Solh, Beirut 1107-2020, Lebanon

<sup>3</sup> Department of Anatomy, Cell Biology and Physiological Sciences, Faculty of Medicine, American University of Beirut, Bliss Street, 11-0236 Riad El-Solh, Beirut 1107-2020, Lebanon

<sup>4</sup> Department of Biophysics and Nuclear Medicine, Université Paris Saclay Versailles St. Quentin en Yvelines, 78035 Versailles, France

\* Correspondence: nicolas.foray@inserm.fr; Tel.: +33-4-78-78-28-28

† These authors contributed equally to this work.



**Citation:** Le Reun, E.; Bodgi, L.; Granzotto, A.; Sonzogni, L.; Ferlazzo, M.L.; Al-Choboq, J.; El-Nachef, L.; Restier-Verlet, J.; Berthel, E.; Devic, C.; et al. Quantitative Correlations between Radiosensitivity Biomarkers Show That the ATM Protein Kinase Is Strongly Involved in the Radiotoxicities Observed after Radiotherapy. *Int. J. Mol. Sci.* **2022**, *23*, 10434. <https://doi.org/10.3390/ijms231810434>

Academic Editors: Yi-Jang Lee and Yu-Chan Chang

Received: 30 July 2022

Accepted: 7 September 2022

Published: 9 September 2022

**Publisher's Note:** MDPI stays neutral with regard to jurisdictional claims in published maps and institutional affiliations.



**Copyright:** © 2022 by the authors. Licensee MDPI, Basel, Switzerland. This article is an open access article distributed under the terms and conditions of the Creative Commons Attribution (CC BY) license (<https://creativecommons.org/licenses/by/4.0/>).

**Abstract:** Tissue overreactions (OR), whether called adverse effects, radiotoxicity, or radiosensitivity reactions, may occur during or after anti-cancer radiotherapy (RT). They represent a medical, economic, and societal issue and raise the question of individual response to radiation. To predict and prevent them are among the major tasks of radiobiologists. To this aim, radiobiologists have developed a number of predictive assays involving different cellular models and endpoints. To date, while no consensus has been reached to consider one assay as the best predictor of the OR occurrence and severity, radiation oncologists have proposed consensual scales to quantify OR in six different grades of severity, whatever the organ/tissue concerned and their early/late features. This is notably the case with the Common Terminology Criteria for Adverse Events (CTCAE). Few radiobiological studies have used the CTCAE scale as a clinical endpoint to evaluate the statistical robustness of the molecular and cellular predictive assays in the largest range of human radiosensitivity. Here, by using 200 untransformed skin fibroblast cell lines derived from RT-treated cancer patients eliciting OR in the six CTCAE grades range, correlations between CTCAE grades and the major molecular and cellular endpoints proposed to predict OR (namely, cell survival at 2 Gy (SF2), yields of micronuclei, recognized and unrepaired DSBs assessed by immunofluorescence with  $\gamma$ H2AX and pATM markers) were examined. To our knowledge, this was the first time that the major radiosensitivity endpoints were compared together with the same cohort and irradiation conditions. Both SF2 and the maximal number of pATM foci reached after 2 Gy appear to be the best predictors of the OR, whatever the CTCAE grades range. All these major radiosensitivity endpoints are mathematically linked in a single mechanistic model of individual response to radiation in which the ATM kinase plays a major role.

**Keywords:** radiosensitivity; radiotherapy; DNA double-strand breaks; ATM; overreactions; predictive assays

## 1. Introduction

Among cancer patients treated with radiation therapy (RT), about 5 to 20% may elicit tissue overreactions (OR) (also called adverse effects, radiotoxicity, or radiosensitivity reactions) occurring during or after the treatment. Such ORs can limit the application of the scheduled treatment and increase morbidity: ORs represent therefore a significant medical,



economic, and societal issue [1–10]. One of the major tasks of radiobiologists is to better understand, predict, and prevent them [11]. However, the diversity of the predictive assays proposed, the number of different experimental protocols, cohorts, and cellular models, the biases linked to the extrapolation of data from animal models, and the lack of a systematic biomathematical approach that would justify and consolidate each step of the prediction process have not helped radiobiologists to reach a consensus about the predictive assay to be applied in routine [3,11,12].

First, the existence of ORs, which is likely to be specific to each individual, has long been debated: since ORs may be similar to the tissue reactions expected after a dose excess, ORs have been suggested to be caused by dosimetry errors. However, the RT accident in Epinal (France) demonstrated that the same dose excess may produce a large spectrum of OR severities among treated patients, likely reflecting individual responses to RT [13,14]. This last statement must be modulated by the considerable progress in the quantification of the physical dose of ionizing radiation (IR) in the irradiated tissue area. In addition, a number of genetic diseases associated with significant radiosensitivity have highlighted the impact of individual predisposition in the final outcome of RT-treated patients, independently of any dosimetry error [3,15].

In order to establish the requirements for a relevant and robust prediction of ORs, let us survey the major features of the post-RT ORs based on clinical observations:

- *Spectrum of OR severities*: ORs show a large and continuous spectrum of severities, from non-hazardous effects on irradiated healthy tissues to fatal reactions. Hence, any relevant predictive assay should reflect this spectrum with constant statistical robustness. In other terms, the power of OR prediction of the predictive assays should be independent of the OR severity [3].
- *Dose–response*: The higher the dose, the more severe and the earlier the OR. Such observations suggest that predictive assays should also be consistent with the dose–response relationships observed both in vivo and in vitro [5].
- *Early/late OR prediction*: The early or late occurrence of ORs does not condition their severities. In other terms, both early and late ORs may show a large spectrum of severities, from non-hazardous effects on irradiated healthy tissues to fatal reactions. Hence, the power of the OR prediction of the predictive assays should be independent of the early or late nature of ORs [6,16,17].
- *Tissue representativeness*: ORs potentially concern all the irradiated organs/tissues of the body. Hence, the molecular and cellular models chosen for the predictive assay should be representative enough to account for ORs occurring in all the tissues of the human body [3].
- *OR severity scales endpoint*: In practice, OR occurrence and severity are generally estimated with the local experience of each oncologist and each medical staff of each radiotherapy department. To alleviate the subjectivity of such approaches, some grading severity scales have been proposed to characterize post-RT ORs for each irradiated organ/tissue of the body. This is notably the case of the Common Terminology Criteria for Adverse Events (CTCAE) [16,17] and the Radiation Therapy Oncology Group (RTOG) [6] scales, which are the most extensively used. These two scales consist of classifying OR severity into six grades (from grade 0: no event, to grade 5: death). Hence, to establish a statistically robust correlation between the clinical features of ORs and molecular and/or cellular assays, the OR severity scales should be systematically used as clinical endpoints to quantify the individual response of each treated patient to RT [6,16,17].

Several approaches have been chosen by radiobiologists to develop predictive assays [3,11]. Among them, the *genomic* approach based on the determination of DNA sequences whether through single nucleotide polymorphisms (SNPs) or genome-wide association studies (GWAS) cannot reach the above dose–response requirement since DNA sequences, whatever their form, cannot predict the dose–response specific to each tissue and individual since it does not change after irradiation [18,19]. Hence, one SNP cannot be



associated with a unique dose–response of a given healthy tissue for a given RT schedule. Conversely, a genomic approach consisting of a systematic analysis of all the mutations of all the genes potentially involved in radiotoxicity is interesting, particularly if some mutations are found in common with patients with the same nature and occurrence of OR [3]. However, even if the genotype/phenotype relationships are well known for one specific gene, such an approach would not reach the above dose–response requirement because many other mutated genes can interplay to provide a specific dose–response observed in each patient. Lastly, a genomic approach that would consist of quantifying the dose-dependent expression of one given gene involved in the individual response to IR is very promising, but further investigations are still needed to better understand the interplay with the radiation-induced expression of other genes involved in the final outcome [20,21].

Unlike the genomic approach, the *functional* approach privileges the assessment of biological functions essential for a normal individual response to IR, *independently of the knowledge of the DNA sequence* or the genes involved [3]. Such a “blind” approach reaches all the above requirements but does not directly provide a diagnosis of the mutations of the gene(s) that cause(s) ORs. The data accumulated all along the history of radiobiology converge to propose the clonogenic cell survival assay as the gold standard for predicting individual response to IR. The clonogenic cell survival assay is considered as belonging to the functional approach since it is based on the assessment of the whole radiation-induced (RI) cell death, independently of its nature (mitotic death, senescence, or apoptosis) [22–27]. Unfortunately, the clonogenic cell survival assay is too time-consuming to ensure a routine prediction of ORs. The same conclusions were reached with predictive assays based on cytogenetics endpoints, similarly to the micronuclei and the chromosome breaks assays that have been also found correlated to cell survival [3,28,29]. Lastly, since cell survival, micronuclei, and chromosome breaks were found to be correlated with unrepaired DNA double-strand breaks (DSBs), the yield of unrepaired DSBs may be of interest to predicting ORs [30–35]. However, according to the technique applied, there are numerous DSB endpoints proposed in the literature [36–40]. This is notably the case of immunofluorescence against the phosphorylated forms of the variant X of the H2AX histone ( $\gamma$ H2AX) [38,41] and the phosphorylated forms of the ATM protein (pATM) [42] that both form nuclear foci at the DSB sites. Unfortunately, low yields of unrepaired DSBs were not accurate in predicting moderate radiosensitivity [40,43].

ATM kinase, whose mutations cause ataxia telangiectasia, the human syndrome associated with the highest radiosensitivity, is upstream of the major DSB repair and signaling pathways [44–46]. Since 2003, our group has accumulated hundreds of skin fibroblasts from RT-treated patients eliciting a large range of OR severities, the COPERNIC collection [35]. From the COPERNIC collection, we have provided experimental and theoretical clues showing that the radiation-induced (RI) nucleoshuttling of ATM (RIANS) is a statistically robust and reliable predictor of OR [43,47,48]. Lastly, it is noteworthy that the RIANS model is also at the basis of a novel resolution of the linear quadratic (LQ) model, the general formula that aims to link cell survival and radiation dose and whose biological interpretation has remained unsolved since the 1970s [49,50].

Here, with 200 COPERNIC skin fibroblast cell lines deriving from OR patients, inter-correlations between CTCAE grades, cell survival, micronuclei, and yields of recognized and unrepaired DSBs from  $\gamma$ H2AX and pATM data were examined. A general, coherent, and multi-parametric analysis of the prediction of post-RT OR is proposed from quantitative correlations between the above radiosensitivity endpoints.

## 2. Results

### 2.1. Clonogenic Cell Survival vs. CTCAE Grades

Since a dose of 2 Gy X-rays generally represents the current dose applied per standard radiotherapy session, the survival fraction at 2 Gy (SF2) has been used to quantify radiosensitivity [22,24]. Here, the clonogenic cell survival assay was not systematically applied to all



the cell lines of the COPERNIC collection but to a representative subset of 36 COPERNIC cell lines (including 10, 1, 6, 6, 6, and 7 cell lines derived from patients with CTCAE grade 0, 1, 2, 3, and 6 reactions, respectively (Figure 1A)). It must be stressed that, in practice, the clinical criteria of CTCAE grade 1 still remain subjective and some grade 1 ORs may be preferentially and provisionally graded to 0 or 2 CTCAE grade. No significant correlation was observed between the clonogenicity (plating efficiency) and the corresponding CTCAE grades, suggesting that the proliferation capacity is not a predictor of OR. The SF2 data were plotted against the corresponding CTCAE grades. The SF2 data from the patients who were apparently healthy or did not show ORs were not found significantly different ( $p > 0.8$ ), and the corresponding SF2 values were in agreement with the most radioresistant cells in the literature (average SF2 value:  $62.1 \pm 1.4\%$ ; CTCAE grade 0). The SF2 values corresponding to patients who succumbed to RT (here, *ATM*- and *LIG4*-mutated patients) were also found consistent with published data (average SF2 value:  $3.3 \pm 0.5\%$ ; CTCAE grade 5). Hence, to obey the mathematical constraints, these bounded values suggested either a linear or a sigmoidal law between SF2 data and CTCAE grades. By plotting all the SF2 data available, the best data fit chosen among the current mathematical laws was found to be a linear law (Table 1):

$$\text{SF2 (\%)} = 61.55 - 11.72 \times \text{grade}; r^2 = 0.98. \quad (1)$$

**Table 1.** Fitting parameters for the relationships between the radiosensitivity endpoints.

Endpoints Concerned	Fitting Function	Adjusted a1 Value *	Adjusted a2 Value *	Adjusted $r^2$	SSE **	RMS ***
SF2 = f(grade)	$f(x) = a \cdot x + a2$	−11.72 (−12.3, −11.15)	61.55 (59.77, 63.32)	0.9805	329.9	3.162
SF2 = f(MN <sub>24h</sub> )	$f(x) = a \cdot \exp(b \cdot x)$	68.55 (62.39, 74.72)	−0.1142 (−0.1363, −0.09208)	0.8839	1966	7.719
SF2 = f(H2AX <sub>24h</sub> )	$f(x) = a \cdot \exp(b \cdot x)$	62.56 (57.25, 67.87)	−0.2168 (−0.261, −0.1726)	0.8685	2228	8.217
pATMmax = f(grade)	$f(x) = a1 \cdot x + a2$	−6.786 (−7.356, −6.215)	41.72 (39.99, 43.45)	0.7399	3912	4.514
SF2 = f(pATMmax)	$f(x) = a1 \cdot x$	1.422 (1.322, 1.523)	NA	0.8794	1971	7.848

\* with 95% confidence bounds; \*\* SSE: sum squared error; \*\*\* RMSE: root mean square error; NA: non-applicable. See also Materials and Methods.

Whatever the variation of grade 1 data, a sigmoidal law between SF2 and CTCAE grades was not possible. Altogether, our data suggest that decreasing every 11.72% cell survival increment leads to a decrease in one additional CTCAE grade (Figure 1A). It must be stressed here that such a conclusion was reached in the largest OR severity range possible. Altogether, these data consolidate the power of the OR prediction of the clonogenic cell survival assay. Interestingly, by calculating the average SF2 corresponding to each grade data (grade 0:  $62.1 \pm 1.4\%$ ; grade 1:  $51.0\%$ ; grade 2:  $37.2 \pm 3.8\%$ ; grade 3:  $23.0 \pm 1.4\%$ ; grade 4:  $17.8 \pm 0.6\%$ ), some similarities appeared with the SF2 values associated with some well-characterized genetic diseases and the database of our research group [15]. These diseases are mentioned in Figure 1B. Such findings strengthened the fact that ORs and the radiosensitivity of genetic origin reflect the same large and continuous spectrum of responses to IR. Reciprocally, the CTCAE grades showed the relevant values that can be found in the case of the IR exposure of the patients suffering from the indicated genetic diseases associated with radiosensitivity (Figure 1B).

It is noteworthy that no fibroblast cell line of the COPERNIC collection elicited apoptotic death, whether irradiated or not. Since the COPERNIC fibroblasts cover the largest OR severity range possible, the absence of apoptosis suggests that this specific cellular death cannot explain radiotoxicity observed in fibroblasts, which represents the majority of human tissues.



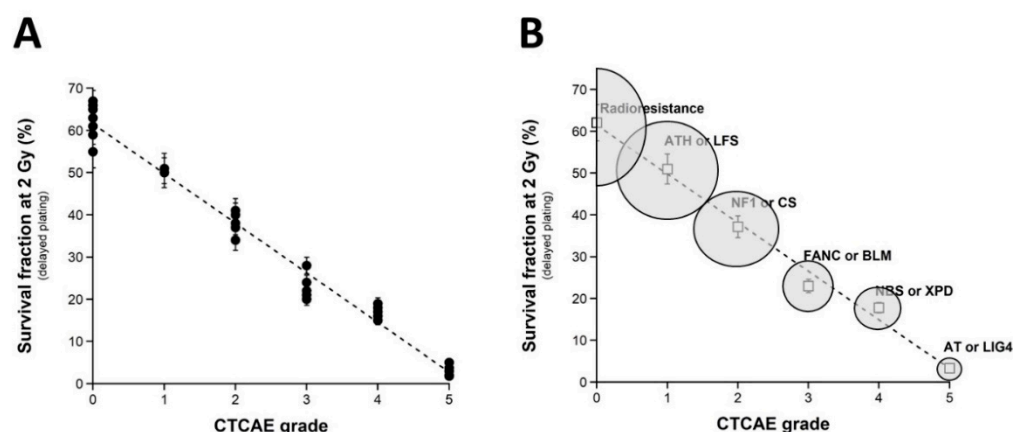


**Figure 1.** Clonogenic cell survival vs. CTCAE grades. **(A)** The SF2 data from 36 COPENIC cell lines were plotted against the corresponding CTCAE grade values (closed circles). Each point corresponds to the mean  $\pm$  standard error of the mean (SEM) of three independent triplicates, at least. The best data fit was obtained with the linear law:  $SF2 (\%) = 61.55 - 11.72 \times \text{grade}$ ;  $r^2 = 0.98$  (dotted line). **(B)** The average SF2 values ( $\pm$ SEM) of the data shown in Fig1A were plotted against the corresponding CTCAE grade (open squares). The dotted line is the reproduction of the data fit shown in (A). An arbitrary 25% relative error was applied to the SF2 and grade values. The resulting 25% confidence circle zones were built in grey. They schematically reproduce the average SF2 values observed from fibroblasts deriving from patients suffering from the indicated syndromes (AT: ataxia telangiectasia, homozygous mutations of *ATM*; LIG4: homozygous mutations of *LIG4*; NBS: Nijmegen's syndrome, homozygous mutations of *NBS1*; XPD, xeroderma pigmentosum D, homozygous mutations of *XPD*; BLM, Bloom's syndrome, homozygous mutations of *BLM*; FANC, Fanconi anemia, homozygous mutations of *FANC*; NF1, neurofibromatosis type 1, heterozygous mutations of neurofibromin; CS, Cockayne's syndrome, homozygous mutations of *CS*; LFS: Li-Fraumeni's syndrome, heterozygous mutations of *p53*; ATH, heterozygous mutations of *ATM*). The syndromes data were obtained from our lab and published elsewhere [3,15].

## 2.2. Number of Micronuclei vs. CTCAE Grades and SF2-Micronuclei Relationships

Micronuclei lead to irreversibly damaged chromosomal fragments causing mitotic death [51]. Micronuclei have been shown to be quantitatively correlated with cellular radiosensitivity when assessed by the clonogenic cell survival assay [28,52–54]. However, to our knowledge, such cytogenetic endpoints have not yet been tested in a large spectrum of CTCAE grades, with the notable exception of our previous report gathering 117 COPENIC cell lines [43]. Here, micronuclei were scored before or 24 h after irradiation in 200 COPENIC cells. With regard to spontaneous micronuclei, no significant correlation was found with the CTCAE grades (Figure 2A). Conversely, when 24 h data were plotted against the CTCAE grades, a tendency appeared suggesting that the higher the number of micronuclei assessed at 24 h post-irradiation, the larger the CTCAE grade. However, the prediction of the CTCAE grades from the residual micronuclei was not reliable, with the notable exception of grades 0 and 5 ORs (Figure 2B). In addition, Table 2 showed that the number of micronuclei assessed 24 h post-irradiation cannot discriminate grade 2 from grade 3 and grade 3 from grade 4 ORs at a high degree of significance. The mathematical law that would link the number of micronuclei assessed at 24 h post-irradiation to CTCAE grades appeared complex. Further analysis will be discussed in the next chapters.

Since a correlation between SF2 and micronuclei has been previously established, we investigated the link between these two endpoints by plotting SF2 data against micronuclei assessed at 24 h post-irradiation. Among the current mathematical laws, an exponential law appeared to provide the best fit to link SF2 and the number of micronuclei assessed 24 h post-irradiation ( $MN_{24h}$ ) (Figure 3A) (Table 1):

$$SF2 (\%) = 62.2 \exp (-0.107 \times MN_{24h}); r^2 = 0.939 \quad (2)$$



Such a mathematical law is relevant whatever the CTCAE grade and appeared also relevant for fitting data from cell lines provided from genetic syndromes associated with radiosensitivity (published data, [3,15,30,43]), supporting again the fact that radiosensitivity from genetic syndromes obeys the same mathematical laws as radiotoxicity observed in cells from RT-treated patients (Figure 3B).

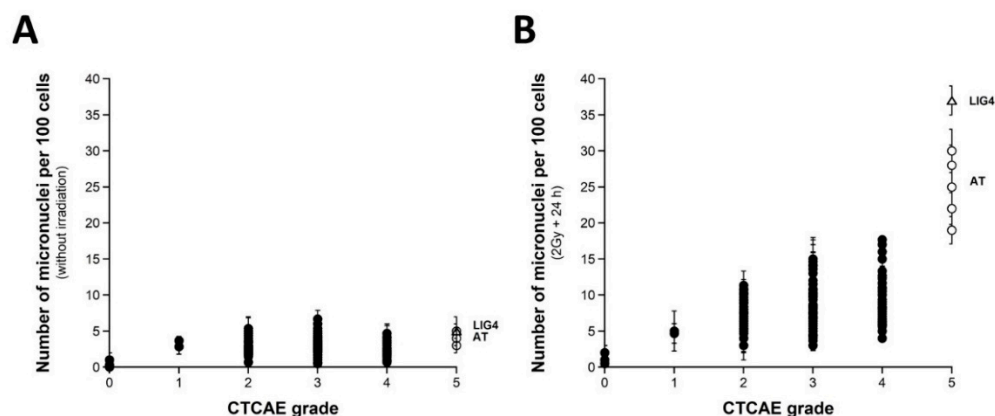


**Figure 2.** Micronuclei vs. CTCAE grades. The number of spontaneous micronuclei per 100 cells (A) or micronuclei assessed 24 h post-irradiation per 100 cells (B) from 200 COPENIC cell lines were plotted against the corresponding CTCAE grade values (closed circles). Each point corresponds to the mean  $\pm$  standard error of the mean (SEM) of three independent triplicates, at least. The points corresponding to the *ATM*- (open circles) and the *LIG4*- (open triangles) mutated cell lines are indicated.

**Table 2.** Discrimination power of the major molecular radiosensitivity endpoints \*.

Compared CTCAE Grades	<i>p</i> Values for MN <sub>24h</sub>	<i>p</i> Values for H2AX <sub>24h</sub>	<i>p</i> Values for pATMmax
2,3 and 4	0.045	0.0115	$8.55 \times 10^{-30}$
2 and 3	0.140	0.018	$4.15 \times 10^{-6}$
3 and 4	0.055	0.017	$6.51 \times 10^{-20}$
2 and 4	0.030	0.81	$2.09 \times 10^{-24}$

\* quantified by one-way ANOVA test. See also Section 4.

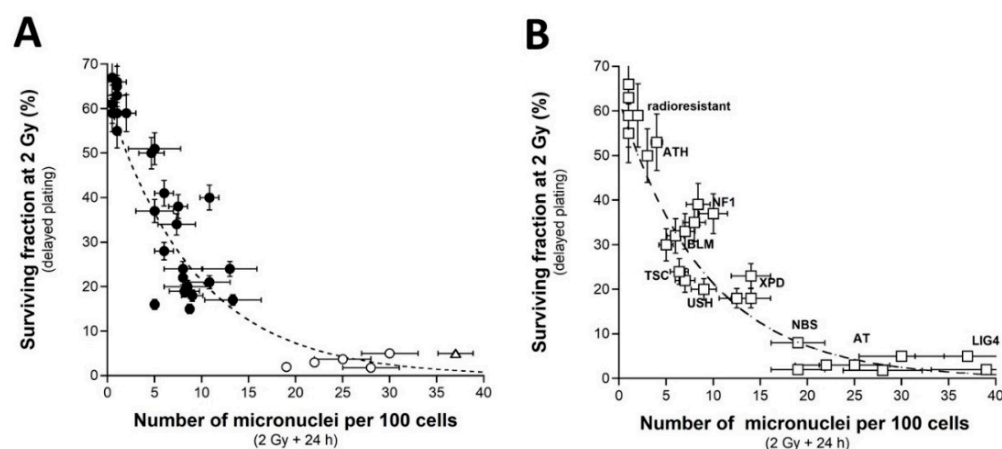


**Figure 3.** SF2 vs. micronuclei. (A) The SF2 data from 36 COPENIC cell lines were plotted against the corresponding number of micronuclei per 100 cells assessed 24 h post-irradiation (closed circles). Each point corresponds to the mean  $\pm$  standard error of the mean (SEM) of three independent triplicates,



at least. The best data fit was obtained with the linear law:  $SF2 (\%) = 62.2 \exp (-0.107 MN_{24h})$ ;  $r^2 = 0.939$  (dotted line). The points corresponding to the *ATM*- (open circles) and the *LIG4*- (open triangles) mutated cell lines are indicated. (B) The SF2 values ( $\pm$ SEM) and the corresponding numbers of micronuclei per 100 cells assessed 24 h post-irradiation ( $\pm$ SEM) from fibroblasts deriving from patients suffering from the indicated syndromes (open squares) (AT: ataxia telangiectasia, homozygous mutations of *ATM*; *LIG4*: homozygous mutations of *LIG4*; NBS: Nijmegen's syndrome, homozygous mutations of *NBS1*; XPD, xeroderma pigmentosum D, homozygous mutations of *XPD*; USH, Usher's syndrome, homozygous mutations of *USH*; TSC, tuberous sclerosis, heterozygous mutation of *TSC*; Bloom's syndrome, homozygous mutations of *BLM*; NF1, neurofibromatosis type 1, heterozygous mutations of neurofibromin; ATH, heterozygous mutations of *ATM*). The dotted line is the reproduction of the data fit shown in (A). The syndromes data were obtained from our lab and published elsewhere [3,15,30,43].

### 2.3. Number of H2AX Foci vs. CTCAE Grades and SF2-Micronuclei- $\gamma$ H2AX Foci Relationships

As evoked above, one of the most current ways of assessing DSBs is the immunofluorescence assay performed with the anti- $\gamma$ H2AX antibody [38,41,55–58]. However, while IR “physically” induces about 40 DSBs per Gy in all the human fibroblasts, whatever their radiosensitivity, the number of  $\gamma$ H2AX foci assessed early (10 min) after irradiation may depend on their radiosensitivity [43]. The nuclear  $\gamma$ H2AX foci have been associated with the DSBs recognized by the ATM-dependent non-homologous end-joining (NHEJ), the most predominant DSB repair and signaling pathways in human quiescent cells [38,41,55–58]. In human radioresistant quiescent fibroblast cell lines, about 40 nuclear  $\gamma$ H2AX foci per Gy per cell have been currently scored early after irradiation. This value was found similar to those deduced from other techniques assessing DSBs, which strongly supports that the anti- $\gamma$ H2AX immunofluorescence permits to detect the great majority of RI DSBs as far as the NHEJ pathway is predominant in the cells tested [3]. However, in radiosensitive cells, the amount of DSBs recognized by NHEJ was shown to be lower than the number of DSBs “physically” induced by IR [42,43], suggesting an impairment in the DSB recognition by NHEJ in these cells [42,43]. We, therefore, examined the number of early and residual  $\gamma$ H2AX foci in the 200 COPERNIC cells. The COPERNIC cells have been exposed to 2 Gy X-rays followed by 10 min, 1, 4 (not shown), and 24 h for repair. No significant correlation was found between spontaneous  $\gamma$ H2AX foci and CTCAE grades, in agreement with previous data [43]. The number of  $\gamma$ H2AX foci assessed 24 h post-irradiation ( $H2AX_{24h}$ ) was plotted against the corresponding CTCAE grade (Figure 4). In agreement with the literature, the radioresistant controls showed the lowest  $H2AX_{24h}$  [41]. Cells from *ATM*-mutated patients did not show  $\gamma$ H2AX foci (since the phosphorylation of H2AX is strongly ATM-dependent) or, if any,  $\gamma$ H2AX foci were found very tiny and dispersed [43,59]. Hence, the number of  $\gamma$ H2AX foci in *ATM*-mutated cells can be considered either as nil (grey square in Figure 4) by defining the  $\gamma$ H2AX foci as similar to that of the other cell lines or as non-nil by taking into account the tiny  $\gamma$ H2AX foci. In the fibroblast cell line (180BR) derived from a *LIG4*-mutated patient who succumbed to RT, the  $\gamma$ H2AX foci data were found to be very specific: while the 180BR cells showed an SF2 value similar to those of the *ATM*-mutated cell lines, they elicited a number of early  $\gamma$ H2AX foci similar to that observed in radioresistant controls (which suggests a normal DSB recognition) but with a number of residual  $\gamma$ H2AX foci higher than 30 (which suggests a gross DSB repair defect). These data were found in agreement with literature that has provided a relevant interpretation of these specific radiobiological features: in fact, in 180BR cells, the recognition step is not affected by the *LIG4* mutations while the DSB repair step is strongly impaired [60–62]. All the other COPERNIC cell lines that correspond to grades 1–4 showed intermediate  $H2AX_{24h}$  [43]. As for micronuclei, there was a tendency of  $H2AX_{24h}$  to increase with the CTCAE grade. However, unlike with micronuclei, statistical analysis showed that  $H2AX_{24h}$  can discriminate between grades 2 and 3, and 3 and 4 but not between grades 2 and 4 (Table 2). Similarly for micronuclei, the mathematical law that would link  $\gamma$ H2AX<sub>24h</sub> with



CTCAE grades appeared complex. Further mathematical analysis will be discussed in the next chapters.

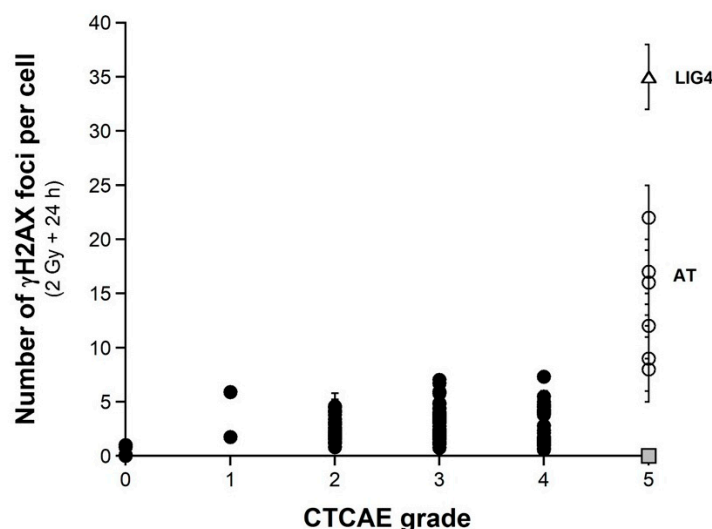


**Figure 4.**  $\gamma$ H2AX foci vs. CTCAE grades. The number of  $\gamma$ H2AX foci assessed 24 h post-irradiation from 200 COPENIC cell lines were plotted against the corresponding CTCAE grade values (closed circles). Each point corresponds to the mean  $\pm$  standard error of the mean (SEM) of three independent triplicates, at least. The points corresponding to the *ATM*- (open circles) and the *LIG4*- (open triangles) mutated cell lines are indicated. The grey square indicates all the *AT* data if considering  $\gamma$ H2AX foci in *ATM*-mutated cells as absent.

Since a correlation between SF2 and unrepaired DSBs has been established already [30], we investigated the link between these two endpoints by plotting SF2 data against  $\gamma$ H2AX<sub>24h</sub>. Among the current mathematical laws, an exponential function appeared to provide the best fit between SF2 and  $\gamma$ H2AX<sub>24h</sub> (Figure 5A) (Table 1):

$$\text{SF2 (\%)} = 62.56 \exp(-0.216 \times \gamma\text{H2AX}_{24h}); r^2 = 0.87 \quad (3)$$

Such mathematical law did not change with the pattern of the  $\gamma$ H2AX foci defined from the *ATM*-mutated cells. These data strongly suggested that the SF2 decreased with  $\gamma$ H2AX<sub>24h</sub>. However, for the cases showing intermediate radiosensitivity, while the corresponding SF2 values ranged from 7 to 60%,  $\gamma$ H2AX<sub>24h</sub> varied only from 0 to 10%. In other terms, the intermediate radiosensitivity is poorly predicted by  $\gamma$ H2AX<sub>24h</sub> but provides higher statistical performance than the micronuclei assay (Table 2). This mathematical law was found to be relevant to fit data from fibroblasts deriving from genetic syndromes (Figure 5B). Again, these findings support that radiotoxicity observed after RT and radiosensitivity observed in cells deriving from genetic syndromes obey similar quantitative links between cellular and molecular endpoints of radiosensitivity.

When plotted against  $\gamma$ H2AX<sub>24h</sub>, MN<sub>24h</sub> obeyed a linear or else a curvilinear function depending on whether the data corresponding to the *LIG4*-mutated cell line has been taken into account. Further mathematical analysis will be discussed in the next chapters. Such correlation shows that the  $\gamma$ H2AX foci and/or else micronuclei are not relevant to predict the cases corresponding to the OR with CTCAE grades ranging from 1 to 4 (Figure 5C).



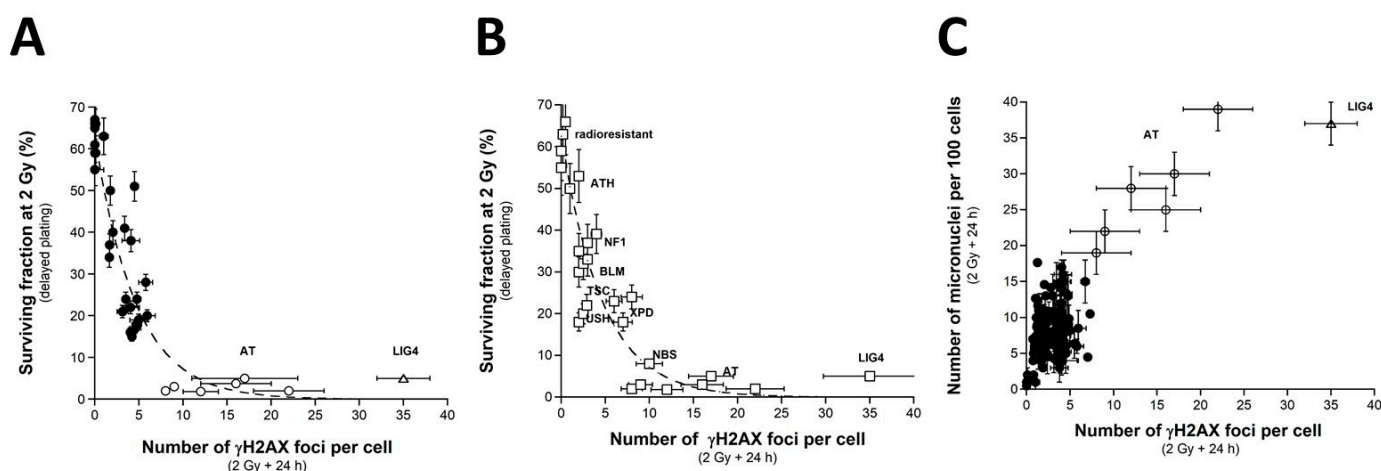


**Figure 5.** SF2 vs.  $\gamma$ H2AX foci and micronuclei vs.  $\gamma$ H2AX foci (A) The SF2 data from 36 COPERNIC cell lines were plotted against the corresponding number of  $\gamma$ H2AX foci per cell assessed 24 h post-irradiation (closed circles). Each point corresponds to the mean  $\pm$  standard error of the mean (SEM) of three independent triplicates, at least. The best data fit was obtained with the linear law:  $SF2 (\%) = 62.56 \exp(-0.216 H2AX_{24h})$ ;  $r^2 = 0.87$  (dotted line). (B) The SF2 values ( $\pm$ SEM) and the  $\gamma$ H2AX foci assessed 24 h post-irradiation ( $\pm$ SEM) from fibroblasts deriving from patients suffering from the indicated syndromes (open squares) (AT: ataxia telangiectasia, homozygous mutations of *ATM*; LIG4: homozygous mutations of *LIG4*; NBS: Nijmegen's syndrome, homozygous mutations of *NBS1*; XPD, xeroderma pigmentosum D, homozygous mutations of *XPD*; USH, Usher's syndrome, homozygous mutations of *USH*; TSC, tuberous sclerosis, heterozygous mutation of *TSC*; Bloom's syndrome, homozygous mutations of *BLM*; NF1, neurofibromatosis type 1, heterozygous mutations of neurofibromin; ATH, heterozygous mutations of *ATM*). The dotted line is the reproduction of the data fit shown in (A). The syndromes data were obtained from our lab and published elsewhere [3,15,30,43]. (C) The number of micronuclei assessed 24 h post-irradiation shown in Figure 2A (from 200 COPERNIC cell lines) was plotted against the corresponding numbers of  $\gamma$ H2AX foci per cell assessed 24 h post-irradiation shown in Figure 4. The points corresponding to the *ATM*- (open circles) and the *LIG4*- (open triangles) mutated cell lines are indicated.

#### 2.4. Number of pATM Foci vs. CTCAE Grades and SF2-Micronuclei- $\gamma$ H2AX Foci vs. pATM Foci Relationships

As described elsewhere, and as Section 2.3 suggests, the number of RI  $\gamma$ H2AX foci scored 10 min after irradiation in the COPERNIC fibroblasts was found to be systematically lower than those of the radioresistant controls [43]. These data do not suggest that fewer DSBs were physically induced but that fewer DSBs were recognized by the ATM phosphorylation of H2AX histone at the DSB sites via NHEJ. The RIANS model is based on the assumption that any delay in the ATM nucleoshuttling is responsible for radiosensitivity and abnormal individual response [42]. IR triggers the monomerization of cytoplasmic pATM dimers. ATM monomers diffuse in the nucleus, and re-associate as dimers at the DSB sites once the DSBs are recognized [42,49]. From our historical data, an exposure to 2 Gy X-rays generally results in the formation of about 40 pATM foci per cell at 10 min post-irradiation in radioresistant fibroblast controls. In the *ATM*-mutated cells, no pATM foci were observed. The number of pATM foci, therefore, varies from about 40 to 0 [43]. Such a hypothesis was verified by plotting the pATM foci against the CTCAE. As already reported in a published paper with 117 COPERNIC cell lines [43], the 200 COPERNIC cells tested here showed a maximal number of pATM foci at 10 min or else at 1 h after 2 Gy. Hence, the maximal number of pATM foci reached at 10 min or 1 h post-irradiation, pATMmax, reflects the maximal ATM kinase activity in the nucleus [43]. When plotted against the corresponding CTCAE grades, the number of pATM foci per cell assessed 10 min (Figure 6A) or 1 h (Figure 6B) post-irradiation decreased by obeying a



linear law whose correlation coefficient varied and appeared low ( $r^2 = 0.70$  and  $r^2 = 0.38$ , respectively). Interestingly, the number of pATM foci assessed at 1 h post-irradiation in radioresistant controls were found systematically lower than the 10 min data values and, than those of the other COPERNIC cells, suggesting that DSB repair was already efficient at this post-irradiation time (Figure 6A,B). Furthermore, the dispersion of pATM data for both conditions appeared too large to discriminate data in the CTCAE grade 2 to 4 range (Figure 6 A,B). Such findings reflect the differences in the kinetics of the nuclear ATM kinase activity that may exist in human cells. Hence, pATM data assessed either at 10 min or else 1 h post-irradiation cannot predict CTCAE grades reliably. By contrast, by plotting pATMmax with the corresponding CTCAE grade data, a linear function of the grade associated with a good discrimination of CTCAE grades appeared (Figure 6C) (Table 1):

$$\text{pATMmax (grade)} = 41.72 - 6.78 \times \text{grade}; r^2 = 0.74 \quad (4)$$

Interestingly, such a mathematical formula suggests that decreasing every 6.78 arly pATM foci per cell increment leads to a decrease in one additional CTCAE grade (Figure 6C). Such conclusions did not significantly depend on whether the *LIG4*-mutated cell data are integrated or not in the calculations.

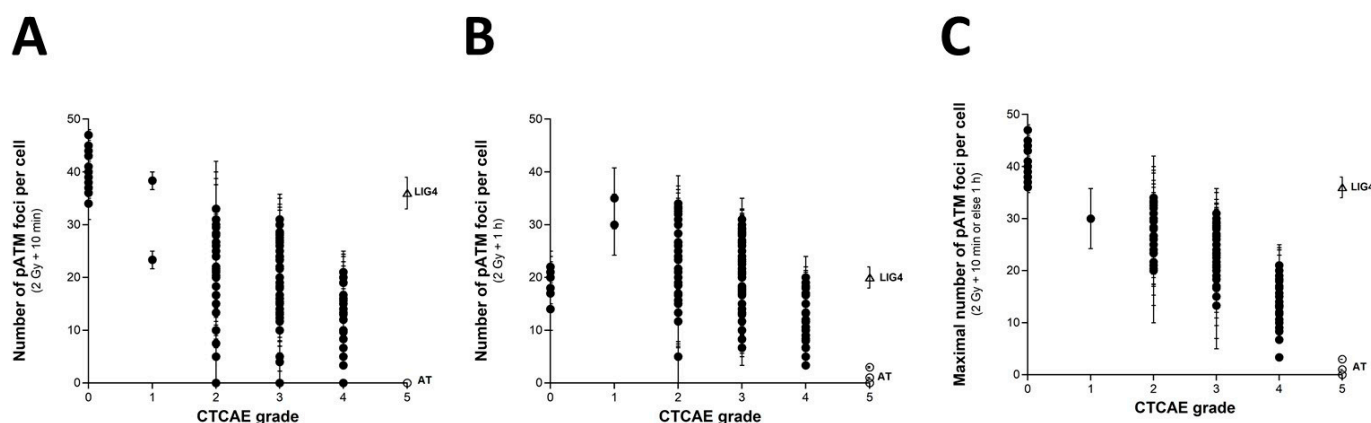


**Figure 6.**  $\gamma$ H2AX foci vs. CTCAE grades. The number of pATM foci per cell assessed 10 min (A) or 1 h (B) post-irradiation from 200 COPERNIC cell lines was plotted against the corresponding CTCAE grade values (closed circles). Each point corresponds to the mean  $\pm$  standard error of the mean (SEM) of 3 independent triplicates, at least. (C) The maximal number of pATM foci per cell among the 10 min and 1h data shown in panels (A,B) was plotted against the corresponding CTCAE grade values (closed circles). The best data fit was obtained with the linear law:  $\text{pATMmax (grade)} = 41.72 - 6.78 \times \text{grade}$  ( $r^2 = 0.74$ ) (dotted line). The points corresponding to the *ATM*- (open circles) and the *LIG4*- (open triangles) mutated cell lines are indicated.

It must be stressed that, among the molecular endpoints tested here, the pATMmax provided the best discrimination of the CTCAE grades (Table 2).

When SF2 values are plotted against the corresponding pATMmax values, a linear correlation appeared between the two endpoints (Figure 7A) (Table 1):

$$\text{SF2 (pATMmax)} = 1.422 \times \text{pATMmax}; r^2 = 0.87 \quad (5)$$

Such a linear correlation was found consistent with the fact that both SF2 and pATMmax elicited a linear correlation with CTCAE grades. The value of the coefficient of proportionality will be discussed in the next chapters.

Lastly, by plotting the pATMmax with  $\text{MN}_{24\text{h}}$  or else  $\text{H2AX}_{24\text{h}}$ , it appeared that the higher the pATMmax, the lower the  $\text{MN}_{24\text{h}}$ , and the lower the  $\text{H2AX}_{24\text{h}}$ , in coherence with the existence of a linear or a curvilinear law between these last two endpoints (see above chapters) (Figure 7B,C). Again, these last findings showed that data can be discriminated



into three distinct categories: the radioresistant cell lines (corresponding to CTCAE grade 0), the hyper-radiosensitive cell lines (corresponding to CTCAE grade 5), and the cell lines showing an intermediate radiosensitivity (corresponding to CTCAE grades 1–4). The case of the unique *LIG4*-mutated cell lines can be considered as a fourth category.

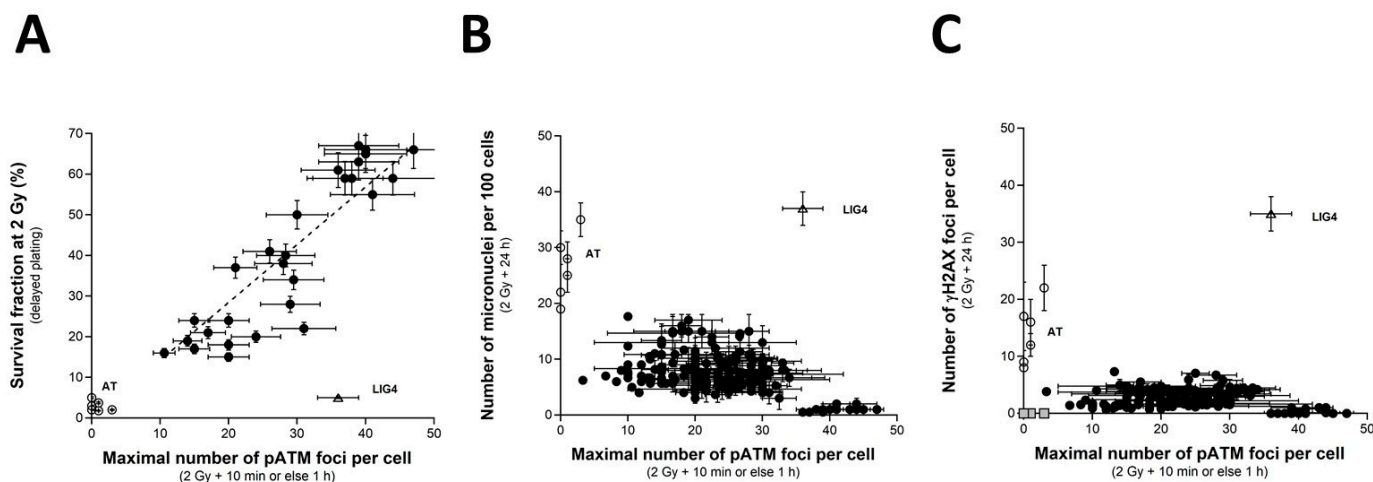


**Figure 7.** SF2 vs. pATMmax, pATmax vs. MN<sub>24h</sub> and pATMmax vs. H2AX<sub>24h</sub> relationships. **(A)** The SF2 data from 36 COPENIC cell lines were plotted against the corresponding number of γH2AX foci per cell assessed 24 h post-irradiation (closed circles). Each point corresponds to the mean  $\pm$  standard error of the mean (SEM) of three independent triplicates, at least. The best data fit was obtained with the linear law:  $SF2(pATMmax) = 1.422 \times pATMmax$ ;  $r^2 = 0.87$  (dotted line). **(B)** The pATMmax from 200 COPENIC cells were plotted against the corresponding number of micronuclei assessed 24 h post-irradiation **(B)** or the corresponding number of micronuclei assessed 24 h post-irradiation **(C)** Each point corresponds to the mean  $\pm$  standard error of the mean (SEM) of three independent triplicates, at least. The grey square indicates all the AT data if considering γH2AX foci in *ATM*-mutated cells as absent. The points corresponding to the *ATM*- (open circles) and the *LIG4*- (open triangles) mutated cell lines are indicated.

## 2.5. A Global Inter-Correlations System with the Major Radiosensitivity Endpoints

Altogether, our findings confirm the existence of multiple correlations between the major radiosensitivity endpoints, namely the CTCAE grades, SF2, MN<sub>24h</sub>, H2AX<sub>24h</sub>, and pATMmax. If we define max(SF2), min(SF2), and  $\Delta SF2$  as the maximal SF2 reflecting the highest radioresistance, the highest radiosensitivity observed in human fibroblasts, and the difference between max(SF2) and min(SF2), respectively:

Formula (1) suggests that:

$$SF2(\text{grade}) = \max(SF2) - \frac{\Delta SF2}{5} \text{grade} \quad (6)$$

Formula (6) suggests a solution of the following differential equation:

$$\frac{dSF2(\text{grade})}{d\text{grade}} = -k_0 \quad (7)$$

in which:

$$k_0 = \frac{\Delta SF2}{5} \quad (8)$$

If we define max(MN<sub>24h</sub>) as the maximal MN<sub>24h</sub> value:

Formula (2) suggests that:

$$SF2(MN_{24h}) = \max(SF2)e^{-k_1 MN_{24h}} \quad (9)$$



in which:

$$k_1 = \ln(\max(\text{SF2})/\min(\text{SF2}))/\max(\text{MN}_{24\text{h}}) \quad (10)$$

Formula (9) is the solution of the following differential equation:

$$\frac{d\text{SF2}(\text{MN}_{24\text{h}})}{d\text{MN}_{24\text{h}}} = -k_1 \text{SF2} \quad (11)$$

If we define  $\max(\text{H2AX}_{24\text{h}})$  as the maximal  $\text{H2AX}_{24\text{h}}$ :  
Formula (3) suggests that:

$$\text{SF2}(\text{H2AX}_{24\text{h}}) = \max(\text{SF2})e^{-k_2 \text{H2AX}_{24\text{h}}} \quad (12)$$

in which:

$$k_2 = \ln(\max(\text{SF2})/\min(\text{SF2}))/\max(\text{H2AX}_{24\text{h}}) \quad (13)$$

Formula (12) is the solution of the following differential equation:

$$\frac{d\text{SF2}(\text{H2AX}_{24\text{h}})}{d\text{H2AX}_{24\text{h}}} = -k_2 \text{SF2} \quad (14)$$

If we define  $\max(\text{pATMmax})$ ,  $\min(\text{pATMmax})$ , and  $\Delta\text{pATMmax}$  as the highest, the lowest values taken among the  $\text{pATMmax}$ , and the difference between  $\max(\text{pATMmax})$  and  $\min(\text{pATMmax})$ , respectively (i.e., corresponding to the radioresistant controls), Formula (3) suggests that:

$$\text{pATMmax}(\text{grade}) = \max(\text{pATMmax}) - \frac{\Delta\text{pATMmax}}{5}\text{grade} \quad (15)$$

Formula (15) suggests the following differential equation:

$$\frac{dp\text{ATMmax}(\text{grade})}{d\text{grade}} = -k_3 \quad (16)$$

in which:

$$k_3 = \frac{\Delta\text{pATMmax}}{5} \quad (17)$$

Formula (5) suggests that:

$$\text{SF2}(\text{pATMmax}) = k_4 \times \text{pATMmax} \quad (18)$$

in which:

$$k_4 = \max(\text{SF2})/\max(\text{pATMmax}) \quad (19)$$

Formula (18) is the solution of the following differential equation:

$$\frac{d\text{SF2}(\text{pATMmax})}{dp\text{ATmax}} = k_4 \quad (20)$$

It is noteworthy that Formulas (6), (9), (12) and (15) provide:

$$\text{MN}_{24\text{h}}(\text{grade}) = \ln\left(\frac{1}{-k_0 \text{grade}}\right)^{1/k_1} \quad (21)$$

$$\text{H2AX}_{24\text{h}}(\text{grade}) = \ln\left(\frac{1}{-k_0 \text{grade}}\right)^{1/k_2} \quad (22)$$

$$\text{MN}_{24\text{h}}(\text{H2AX}_{24\text{h}}) = \frac{k_2}{k_1} \text{H2AX}_{24\text{h}} \quad (23)$$



$$pATM_{max}(MN_{24h}) = \frac{\max(SF2)}{k_4} e^{-k_1 MN_{24h}} \quad (24)$$

$$pATM_{max}(H2AX_{24h}) = \frac{\max(SF2)}{k_4} e^{-k_2 H2AX_{24h}} \quad (25)$$

Interestingly, all of Formula (11) is in agreement with the shape of the data shown in Figures 2B, 4, 5C and 7B,C.

Altogether, these formulas suggest the following global system:

$$\left\{ \begin{array}{l} \frac{dSF2(grade)}{dgrade} = -k_0 \\ \frac{dSF2(MN_{24h})}{dMN_{24h}} = -k_1 SF2 \\ \frac{dSF2(H2AX_{24h})}{dH2AX_{24h}} = -k_2 SF2 \\ \frac{d(pATM_{max})}{dgrade} = -k_3 \\ \frac{dSF2(pATM_{max})}{dpATM_{max}} = k_4 \end{array} \right. \quad (26)$$

### 3. Discussion

#### 3.1. The Prediction of OR, a Clinical, Technological, Economical, and Legal Issue

In RT, the dose delivered to the tumor is often a compromise between two antagonistic goals: to reach the maximal anti-tumor efficiency and to limit the occurrence and the severity of OR in the locoregional tissues [6,7]. Indeed, OR can alter the patient quality of life during the treatment [8] and even up to several years [9,10]. The occurrence of OR during treatment may also threaten the compliance to RT by not exposing the patient to the full prescribed dose. Before the end of RT, ORs can modify the anatomy of the organs surrounding the target (by generating weight loss during a head and neck treatment for example) and thus lead to a modified dosimetry—inasmuch as tumor volume reduction can modify target dosimetry [63]. If new RT techniques, such as intensity-modulated RT (IMRT), stereotactic RT with CyberKnife irradiators, protontherapy, or hadrontherapy, tend to improve the risk–benefit balance with a better dose conformation to the target volume, none of them allow for RT without risk for patients [64,65]. Besides, new techniques are not even always superior to reducing ORs [64,66,67]. Above all, according to recent data, it is also noteworthy that ORs may be underestimated by clinicians [68].

In parallel, it must be stressed that ORs with CTCAE grades 2–5 represent a significant but small subset of post-RT events generally evaluated to about 5 to 20% of patients [3]. Furthermore, the CTCAE grade-distribution of ORs may show a semi-gaussian shape with subsets of CTCAE grades 0, 1, 2, 3, 4, and 5, representing, from previous COPERNIC data and in agreement with the literature [43], about 65, 17, 10, 5, 2.5, and 0.5% of RT-treated patients (with a relative error of about 20% each), respectively. Besides, such estimation strongly depends on whether the CTCAE grade 1 ORs are still considered as tissue reactions without significant clinical consequence or as radiosensitivity reactions. Furthermore, such grade distribution strongly depends on the RT modality and the type of tumor to be treated. The fatal reactions remain very exceptional and are likely due to a genetic predisposition to hyper-radiosensitivity similarly to for *ATM* and *LIG4* mutations [3,15]. Interestingly, the frequency of genetic syndromes as a function of the radiosensitivity level (SF2) reported previously [15] obeys a similar shape to the CTCAE grade distribution of ORs (Figure 8).



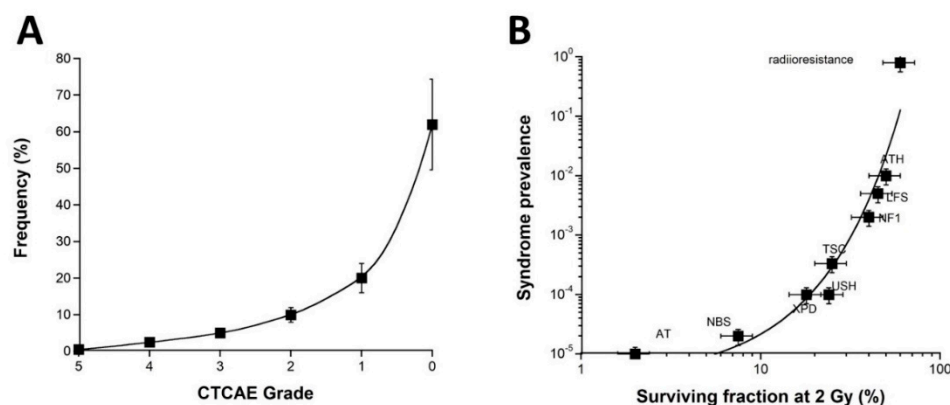


**Figure 8.** (A) Frequency of the OR as a function of the CTCAE grades. These data were established from the COPERNIC collection ([43] and N.F. personal communication). (A) A 20% relative error was applied to all the data. The best data fit was obtained with an exponential law. (B) Prevalence of the indicated genetic syndromes associated with radiosensitivity as a function of SF2 data [43]. These data have been published in a previous report in another form. Error bars were built on the basis of 20% relative error for SF2 and prevalence, respectively. (AT: ataxia telangiectasia, homozygous mutations of *ATM*; NBS: Nijmegen's syndrome, homozygous mutations of *NBS1*; XPD, xeroderma pigmentosum D, homozygous mutations of *XPD*; USH, Usher's syndrome, homozygous mutations of *USH*; TSC, tuberous sclerosis, heterozygous mutation of *TSC*; NF1, neurofibromatosis type 1, heterozygous mutations of neurofibromin; LF2, Li-Fraumeni's syndrome, heterozygous mutations of *p53*; ATH, heterozygous mutations of *ATM*). The best data fit was obtained with an exponential law.

Such a statement strengthens again the fact that the clinical, cellular, and biostatistical features of the radiotoxicity observed in RT are similar to those of the radiosensitivity observed with genetic diseases. Another important consequence of such a statement is that the CTCAE grade distribution may introduce some biases in the analysis of the data from clinical studies. Indeed, since severe ORs remain exceptional, the prospective studies may be based on cohorts of RT-treated patients with a majority of radioresistant patients and a minority of radiosensitive ones. Consequently, in this case, the statistical robustness of any predictive assay may be overestimated for the lowest grades and underestimated for the highest ones. Conversely, the retrospective studies can be based on a specific distribution of the cohorts: hence, the best compromise would be to obtain the same number of cases for each CTCAE grade to ensure an OR prediction that would not be dependent on the severity grade of the OR [3]. Further investigations are needed to optimize the methodology and all these statistical constraints.

### 3.2. The Diverse Predictive Assays and Their Associated Endpoints

There is a large body of evidence that ORs are the clinical consequences of RI cell death [3,6,16,17]. The clonogenic survival assay, first developed in 1956 by Puck and Markus, is the current measurement of RI death in vitro [69,70]. In 1981, a quantitative correlation between tumor radio responsiveness (quantified in vivo by using tumor local control as an endpoint) and cellular radiosensitivity (quantified in vitro by using SF2 as an endpoint) was pointed out for the first time, validating the clonogenic cell survival assay as the most reliable predictive assay of anti-tumor efficiency of the RT [24]. The clonogenic cell survival assay has been also applied to a number of non-tumor cellular models, notably lymphoblasts and fibroblasts [26,27,71]; in 1975, Taylor et al. pointed out, for the first time with the clonogenic cell survival assay, the extreme radiosensitivity associated with ataxia telangiectasia (*ATM* mutations) [45]. After this discovery, a considerable number of studies have reported the radiobiological characterization of various genetic syndromes which permits to propose, to date, a complete view of human radiosensitivity [22,52–54,72–76]. Conversely, with regard to the radiobiological characterization of cells provided from OR patients, there are a few reports about the link between clonogenic cell survival data and



the CTCAE grade. For example, Pouliliou et al. (2015) investigated SF2 in peripheral blood lymphocytes from RT-treated patients. However, the corresponding CTCAE grades of this study were grouped into three categories of grades of early reactions (0, 1, and 2 + 3) [77]. To our knowledge, no report with SF2 has involved the full range of CTCAE grades like our work published in 2016 [43] and this present study. Lastly, it must be stressed that the range of SF2 observed in cells from OR patients is similar to that observed in cells from patients suffering from genetic syndromes, which demonstrates that the two phenomena are similar. Besides, all the young *ATM*- or *LIG4*-mutated patients suffering from hyper-radiosensitivity and treated with RT succumbed by eliciting CTCAE grade 5 ORs [45,60,78–80]. To date, the clonogenic cell survival assay as a predictive assay for OR occurrence and severity has been abandoned because it is based on a long procedure of cell culture: (1) the plating efficiency of each cell line tested must be determined with precision by seeding a series of numbers of non-irradiated cells and scoring the resulting colonies that generally appear in 7 to 14 days; (2) in order to avoid the feeder effects, the concentration of cells giving the highest plating efficiency is then deduced; (3) a series of numbers of irradiated cells are seeded and the resulting colonies and fractions of cell survival are calculated. Hence, the clonogenic cell survival protocol requires some weeks, which means its routine clinical application is very complex [70].

The clonogenic cell survival accounts for the whole RI cell death and is not specific to a particular cell death pathway (Figure 9). The major RI cell deaths are mitotic death, senescence, and apoptosis [3]. Mitotic death is predominant in cells that can proliferate, whether that be fibroblasts or lymphocytes. Micronuclei are one of the current endpoints reflecting mitotic death and they have been observed when NHEJ or any other DSB repair pathways (like homologous recombination) were impaired, suggesting that micronuclei do not occur only when NHEJ is faulty [3,51] (Figure 9). Furthermore, the occurrence of a micronucleus requires not only unrepaired DNA breaks but, overall, a bypass of G2/M arrest. However, radiosensitivity may be independent of the G2/M arrest status [15]. For example, the ratio between unrepaired breaks and micronuclei may drastically differ between cells from aging syndromes (generally arrested in G0/G1) and cells from cancer syndromes (generally impaired in G2/M arrest) [15]. Together with clonogenic assays, cytogenetic assays, similarly to the micronuclei assay, were initially based on the staining techniques like Giemsa and require metaphases and therefore a significant period of time to reach new cell cycle phases [28]. Hence, the most current protocol for scoring micronuclei is based on the cytokinesis block with cytochalasin B that accelerates the passage in the G2/M phase. However, this step may introduce bias by mixing the capacity of cells to pass G2/M (and therefore by artificially increasing the micronuclei production rate) with the dose-dependent ratio between micronuclei and unrepaired chromosome breaks [28,81–83]. To overcome such bias, the micronuclei assay protocol applied in the present study did not involve any artificial block cells in G2/M but followed the same protocol as that applied in  $\gamma$ H2AX and pATM immunofluorescence to better facilitate data inter-comparisons (see materials and methods). A high number of unrepaired chromosome breaks (and therefore micronuclei) has been shown to characterize many radiosensitive genetic syndromes [34,83–85]. Conversely, the great majority of studies failed to confirm the applicability of the micronuclei assay to predict OR for RT-treated patients [83]. Furthermore, to our knowledge, no report has investigated the relationships between yields of micronuclei and a large range of CTCAE grades. This short review is consistent with the fact that the micronuclei assay is unable to discriminate the CTCAE grades 1 to 4 ORs reliably. The fact that Cornforth and Bedford demonstrated that one unrepaired chromosome break corresponds to one lethal event for non-transformed human fibroblasts does not contradict the general tendency observed in the present study (*the higher the number of micronuclei, the higher the radiosensitivity, the more severe the OR*) but illustrates well that the ratio between unrepaired DSB and micronuclei may differ among the human cell lines according to their radiosensitivity status and their capacity to bypass the G2/M arrest [15,34].



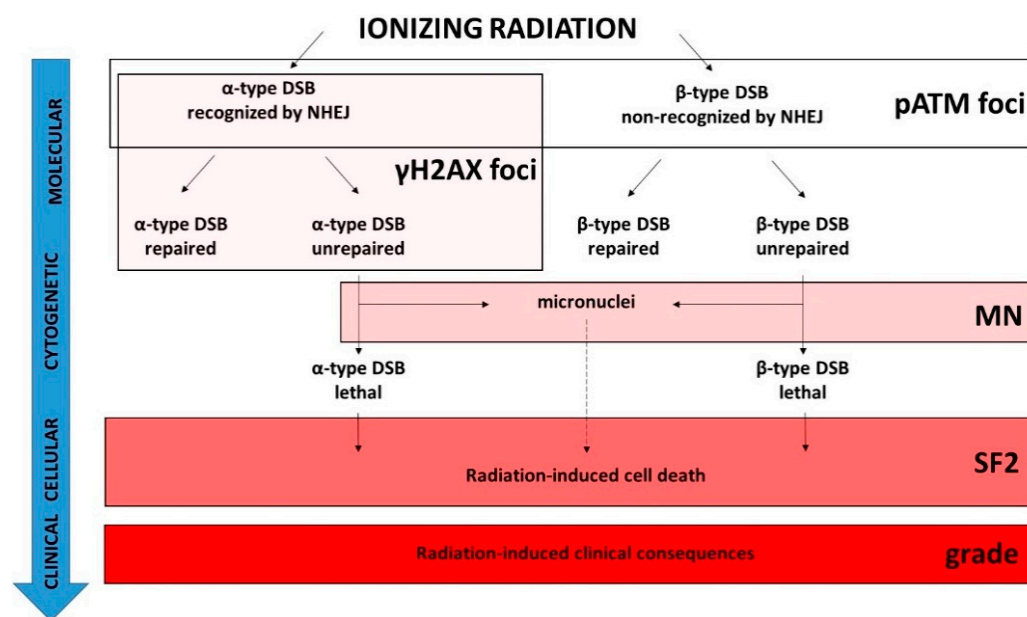


**Figure 9.** Schematic view of the molecular, cytogenetic, cellular, and clinical consequences of exposure to IR and the validity domain of the major radiosensitivity endpoints. IR induces two types of DSB. The  $\alpha$ -type DSBs are recognized by the NHEJ DSB repair pathway while the  $\beta$ -type DSBs are not [49]. For each type of DSB, there are some subsets of unrepaired DSB [49]. Among them, some may be unrepairable and contribute to the lethal effect. Some unrepaired DSBs may also provide micronuclei according to the radiosensitivity status and the capacity of irradiated cells to bypass the G2/M arrest [15]. The pATM foci biomarker detects the DSBs recognized by NHEJ, and the DSBs non-recognized by NHEJ or recognized by another DSB repair pathway can be deduced from the induction rate of DSBs “physically” induced by IR. The  $\gamma$ H2AX foci biomarker detects the  $\alpha$ -type DSBs only. Both  $\alpha$ - and  $\beta$ -type unrepaired DSBs may provide some micronuclei, but the ratio between unrepaired DSBs and micronuclei is not necessarily equal to 1. Some subsets of micronuclei can contribute to the lethal effect. SF2 reflects all the RI cell deaths and therefore reflects the whole cellular response to IR independently of the DSB repair pathways involved. The dashed line indicates that the link is different from a one-to-one correlation.

In coherence with the causal links between SF2, micronuclei, and unrepaired DSBs, there is a plethora of studies aiming to characterize radiosensitivity with DSB repair assays [3,15,36,37]. In the 1990s, radiobiologists focused on the yield of unrepaired DSBs as a potential radiosensitivity predictor by using notably pulsed-field gel electrophoresis (PFGE), comet, and immunofluorescence techniques [12,36]. The major advantage of DSB repair assays based on the assessment of RI DNA fragmentation like PFGE, elution, or sucrose sedimentation is that they provide data independent of any specific DSB repair pathway. Conversely, their major inconvenience is that they require very high doses (often non-biologically relevant) to allow the DNA breaks to be detectable, which raises the question of the dose-dependence of the DSB repair rate when assessed by these techniques [3]. By contrast, the  $\gamma$ H2AX immunofluorescence assay requires the same dose range as those applied in RT, clonogenic cell survival, and micronuclei assays. However, does each nuclear  $\gamma$ H2AX foci correspond to one DSB, whatever the cell lines, their radiosensitivity status, and the irradiation conditions? As evoked in Section 2.3, the formation of  $\gamma$ H2AX foci is ATM-dependent and represents a major early step of NHEJ. The number of  $\gamma$ H2AX foci assessed per Gy early after irradiation is similar to the number of DSBs induced per Gy by using PFGE [38,41,55–58]. However, such an observation has been performed with the radioresistant quiescent human cells and with the *LIG4*-mutated cell lines that show normal ATM kinase activity [42,43]. Conversely, in radiosensitive cells that show impaired ATM kinase activity, the number of early  $\gamma$ H2AX foci was shown to be lower than the number of



DSBs “physically” induced by IR, suggesting an impairment in DSB recognition by NHEJ in these cells [42,43]. Hence, the  $\gamma$ H2AX foci represent a limited subset of all the RI DSBs: the DSBs recognized by NHEJ only. Consequently, the residual (or persistent)  $\gamma$ H2AX foci observed 24 h post-irradiation do not necessarily represent all the DSBs that contribute to the RI lethal effect (Figure 9). The RIANS model has integrated two types of RI and lethal DSBs [49]: (1) the  $\alpha$ -type DSBs, recognized by the ATM monomers in the nucleus (therefore by NHEJ) early after irradiation (presence of  $\gamma$ H2AX foci). Some of them may remain unreparable and contribute to the RI lethal effect (persistent  $\gamma$ H2AX foci). Their number was demonstrated to be proportional to the dose [49]; (2) the  $\beta$ -type DSB, not recognized by the ATM monomers in the nucleus (therefore not managed by NHEJ) because of a delay or an absence of the RIANS. Some of them may remain unreparable and contribute to the RI lethal effect. However, these DSBs are not visible by using  $\gamma$ H2AX immunofluorescence. Their number was demonstrated to be proportional to the square of the dose [49]. As a result, the number of all these lethal DSBs is the same as the linear-quadratic expression found in the LQ model [49] (Figure 9). Besides, such a definition of  $\alpha$ - and  $\beta$ -type DSBs is also consistent with the radiobiological features of the unique *LIG4*-mutated 180BR cell line.

How does one explain the pATM data and their prediction power? As evoked in Sections 2.3 and 2.4, the fact that less early  $\gamma$ H2AX foci were observed in the radiosensitive COPERNIC cells does not suggest that fewer DSBs are induced “physically” in these cells but, rather than fewer DSBs are recognized by the ATM-dependent phosphorylation of H2AX, consistently with lower nuclear ATM kinase activity, caused by a delay in the RIANS [43]. In a previous report, with 117 COPERNIC cell lines, the correlation between pATMmax, and the CTCAE grade was found to be significant (concordance coefficient:  $p = 0.86$ ) [43]. By adding here 83 additional COPERNIC fibroblasts, the statistical robustness of the correlation between pATMmax and the CTCAE grade was confirmed (Figure 6). To our knowledge, there is no equivalent of such correlation in the literature with the complete range of CTCAE grades. Logically, by considering a binary approach, i.e., by gathering OR of grades 0, 1, and 2 in one category and grades 3, 4, and 5 in another category, the superiority of pATMmax and SF2 in the prediction of ORs was also found to be enhanced, in agreement with previous reports [43,47,48] (Table 3). Since our group particularly focuses on the RIANS model, there is no equivalent of SF2-pATMmax, MN<sub>24h</sub>-pATMmax, and  $\gamma$ H2AX<sub>24h</sub>-pATMmax correlation in the literature either. Our findings strongly suggest that, with SF2, pATMmax appears to be the most powerful predictor of the CTCAE grade ORs.

**Table 3.** Discrimination power of the major molecular radiosensitivity endpoints in a binary approach \*.

<i>p</i> Values for SF2	<i>p</i> Values for MN <sub>24h</sub>	<i>p</i> Values for H2AX <sub>24h</sub>	<i>p</i> Values for pATMmax
$1.90 \times 10^{-12}$	$1.52 \times 10^{-6}$	$1.51 \times 10^{-4}$	$9.91 \times 10^{-20}$

\* Patients were divided into two groups, radioresistant (CTCAE scores of 0, 1, and 2) and radiosensitive (CTCAE scores of 3, 4, and 5). A One-Way ANOVA test was performed to assess the discrimination power of each molecular endpoint.

The conclusion that both SF2 and pATMmax appear to be the best predictors of ORs has been reached but not simply because a linear function has been found between these endpoints and the CTCAE grades. Some correlation coefficients may be higher with other mathematical laws and other endpoints. The high prediction power of the pATMmax endpoint is based on the fact that the pATM foci account for all the DSBs managed by NHEJ and that the number of the DSBs managed by other DSB repair pathways, if any, can be easily estimated from the well-documented DSB induction rate of about 40 DSBs per Gy per human untransformed fibroblast [42]. Hence, by integrating all the RI DSBs that may potentially contribute to the lethal effect, independently of any DSB repair pathway involved or impaired, both SF2 and pATMmax provide a more exact view of the radiobiological response of human cells. The other endpoints (micronuclei and  $\gamma$ H2AX foci) reflect only a limited subset of the RI DSBs (Figure 9). In addition to this explanation, it



must be also stressed that both SF2 and pATMmax vary in ranges ([3–62%] and [0–42 pATM foci], respectively) larger than those of the other endpoints tested. Hence, the different levels of cellular and molecular response to IR can be better discriminated with SF2 and pATMmax [3,42].

### 3.3. The Detection of Radiosensitivity, a Unique Multiparametric System?

The mathematical approach applied in this study consisted in:

- considering that some causal or partially causal link documented by the literature exists between each of the endpoints tested.
- the nature of such links can be reflected by a specific mathematical link between each of the endpoints tested.
- the data-fitting analysis was conducted with some current mathematical laws (linear, curvilinear, exponential, and power functions). Hence, some other (but more complex) mathematical laws can be tested in further investigations.
- we have considered that the best data fit was the solution of a differential equation linking two endpoints.
- the k-coefficient, the type, and the order of each differential equation found were hypothesized to reflect the complexity of the link between the two endpoints considered.

The differential equations described in the last sections of the Results chapter may suggest Michaelis–Menten equations. However, the CTCAE grades, the cell survival (SF2), the number of micronuclei, and the number of  $\gamma$ H2AX and pATM foci do not represent the same scale (cell, chromosome, DNA, and proteins, respectively) and these endpoints cannot be considered as interplaying substrates: consequently, the theory of enzymatic kinetics is not applicable here.

Conversely, the biological features and specificities of each endpoint tested (summarized in Figure 9) and their mathematical constraints may lead to the following interpretations that illustrate the direct (linear) and indirect or incomplete (non-linear) links between the endpoints tested (Figure 10):

- the k0 coefficient represents the direct link between the RI cellular death (SF2) and the clinical OR (grade). It illustrates that any clonogenic cell death corresponds to an RI tissue event. The mathematical constraints are simple: the k0 coefficient only depends on the maximal range of the scale (i.e., six grades and therefore five inter-grade intervals for CTCAE) and the range of SF2 (i.e.,  $\Delta$ SF2) (see Formula (8). Quantitatively, decreasing every 11.72% cell survival increment leads to a decrease in one CTCAE grade.
- the k3 coefficient represents the direct link between the maximal nuclear RI ATM kinase activity (pATMmax) and the clinical OR (grade). It illustrates the fact that the pATM foci lacking (due to the non-recognition of DSBs by NHEJ or by another DSB repair pathway) directly represent a subset proportional to the number of lethal DSBs responsible for an RI tissue event. As for k0, the k3 coefficient only depends on the maximal range of the scale (i.e., six grades and therefore five inter-grade intervals for CTCAE) and the range of pATMmax (i.e.,  $\Delta$ pATMmax) (see Formula (17). Quantitatively, decreasing every 6.78 pATM foci per cell increment leads to a decrease of one CTCAE grade.
- the k4 coefficient supports that the maximal nuclear ATM kinase activity (pATMmax) directly conditions cell survival: the higher the pATMmax, the higher the SF2. As specified above, pATMmax reflects the maximal nuclear RI ATM kinase activity. By combining Formulas (6) and (15), the k4 coefficient appears to directly depend on k0, k3, max(SF2), and max(pATMmax). Quantitatively, decreasing every 6.78 early pATM foci per cell increment leads to a decrease of 11.72% cell survival.
- the k2 coefficient represents the number of DSBs that contribute to the RI lethal event among the unrepaired DSBs reflected by persistent  $\gamma$ H2AX foci (i.e., recognized by NHEJ) (Figure 9). Since  $k_2 = 0.21$ , our findings suggest that about one event per five unrepaired DSBs recognized by NHEJ may be lethal. Such interpretation leads to the



notion of the tolerance of DSBs: some unrepaired DSBs may be not lethal, which is in agreement with previous reports and the current observation that some cells can elicit a significant number of spontaneous DSBs without impacting on their capacity of repair [30,43]. It is noteworthy that Formula (22), deduced from the other formulas, fits well when the  $H2AX_{24h}$  data are plotted against the CTCAE grades (Figure 4).

- the  $k_1$  coefficient represents the number of micronuclei per 100 cells that contribute to the RI lethal event among all the micronuclei detected. Since  $k_1 = 0.107$ , our findings suggest that about 1 per about 10 micronuclei observed per 100 cells is lethal. As for  $H2AX_{24h}$ , such interpretation also leads to the notion that some micronuclei may not contribute to the RI lethal event, maybe by enhancing the transformation (misrepair) of the cells [30,43]. It is noteworthy that Formula (21), deduced from the other formulas, fits well when the  $MN_{24h}$  data are plotted against the CTCAE grades (Figure 3). Interestingly, the link between  $MN_{24h}$  and  $H2AX_{24h}$ , illustrated by Formula (23), suggests that there is a constant subset of unrepaired DSBs reflected by  $\gamma H2AX$  foci that leads to the formation of micronuclei. According to Formula (23), this rate suggests that all the unrepaired DSBs recognized by NHEJ do not lead to the formation of micronuclei.

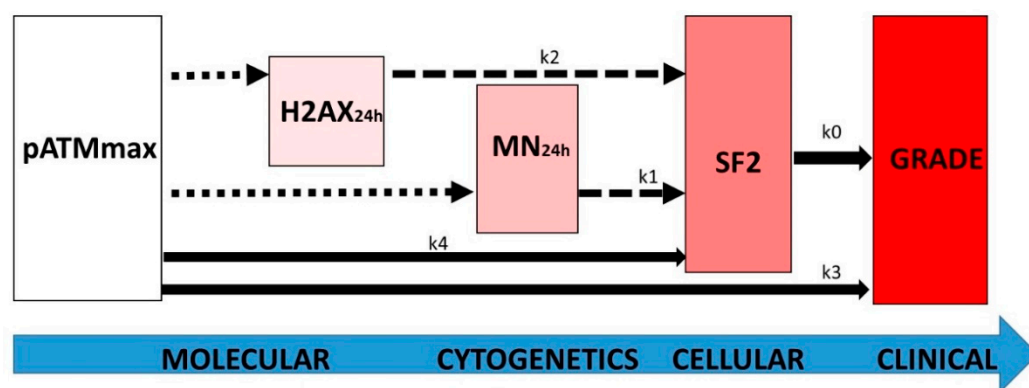


**Figure 10.** Schematic view of the link between the major radiosensitivity endpoints with the  $k$  coefficients of the differential equations described at the end of the Results chapter. The dotted, dashed, and full-line arrows represent complex, exponential, and linear laws, respectively.

Interestingly, the resulting equations system linking the major radiosensitivity endpoints described by Formula (26) may be also relevant for all mammalian cells, especially for rodent models. Indeed, the  $k$  coefficients linking the SF2,  $MN_{24h}$ ,  $H2AX_{24h}$ , and pATM-max endpoints were shown to depend on their maximal and minimal values. It must be stressed that the most radioresistant and the most radiosensitive rodent cellular models show similar bounded values as those observed in humans. For example, SF2 is generally limited to 1 to 80% in mammals. This is also the case for the yields of residual micronuclei and unrepaired DSB yields [40].

## 4. Materials and Methods

### 4.1. Fibroblast Cell Lines

All of the experiments were performed with untransformed skin fibroblast cells in the plateau phase of growth under standard culture conditions described elsewhere [43,54]. Skin biopsies sampling was performed in unirradiated areas (generally under the forearm) after local anesthesia, similarly to standardized dermatologic punch. All the anonymous patients were informed and gave signed consent according to the ethics recommendations. Clinical data on tumor characteristics and therapy regimens were extracted from the medical records. The OR severity was graded by two independent clinicians according to the Common Terminology Criteria for Adverse Events (CTCAE) version 4.03. Only OR patients with consensual clinical grading were included in this study. Both early and



late reactions were considered. Cancer patients suffered from breast, prostate, nose ear throat, lymphoma, nervous system (central and peripheral), lung, anal canal, pediatrics, cervix, sarcoma, skin, testis, bone, rectum, and esophagus cancer. In order to avoid bias, no tumor type subset represented more than 40% of the collection. There was no correlation between the CTCAE grade and age, sex, regimen, or total cumulated dose of the treatment. All the sampling procedures were done in the frame of the experimental protocol of the “COPERNIC” collection, approved by the national ethical committee in agreement with the current national regulations about the clinical studies. The resulting fibroblast cell lines were declared under the numbers DC2008-585, DC2011-1437, and DC2021-3957 to the Ministry of Research. This study involved 200 COPERNIC fibroblast cell lines, including:

- A total of 117 COPERNIC cell lines already described in a published report. This subset is composed of 12 radioresistant, 4 ATM-mutated, and 1 LIG4-mutated gifted cell lines and the 100 first registered cell lines of the COPERNIC collection derived from RT-treated patients who showed grades 1–4 CTCAE ORs. The Radiobiological Database of this subset is protected under the reference IDDN.FR.001.510017.000.D.P.2014.000.10300
- A total of 82 additional COPERNIC cell lines. This subset is composed of 2 additional radioresistant, 2 ATM-mutated cell lines, and 78 cell lines of the COPERNIC collection derived from RT-treated patients who showed grades 1–4 CTCAE ORs that were chosen randomly in a subset of 150 available ones. The protection procedure of the radiobiological database of this subset is in progress.

#### 4.2. X-rays Irradiation

Irradiations were performed with a 6 MeV X-ray medical irradiator (SL 15 Philips) (dose-rate:  $6 \text{ Gy} \cdot \text{min}^{-1}$ ) at the anti-cancer Centre Léon-Bérard (Lyon, France) [43,86]. In all the experiments, a dose of 2 Gy was chosen because it simulates a current dose per session in a standard radiotherapy. The dosimetry was certified by radiophysicists of the Centre Léon-Bérard.

#### 4.3. Clonogenic Cell Survival

The intrinsic cellular radiosensitivity was quantified from clonogenic cell survival data obtained from standard delayed plating procedures that were described elsewhere [24]. Cells in the plateau phase of growth were irradiated at the indicated doses, incubated for 24 h at 37 °C, harvested, counted using hemocytometer, and then diluted to a pre-defined number of cells to be seeded in Petri dishes. After 15 days at 37 °C in a CO<sub>2</sub> incubator, the cells were and stained in crystal violet. Only the colonies with more than 50 cells were scored. The survival data were fitted to the linear-quadratic (LQ) model that describes the cell survival  $S$  as a function of dose  $D$ , as follows:  $S = e^{-(\alpha D + \beta D^2)}$ , in which  $\alpha$  and  $\beta$  are adjustable parameters to be determined. The intrinsic radiosensitivity was quantified by calculating the surviving fraction at 2 Gy (SF2) [49].

#### 4.4. Immunofluorescence

The immunofluorescence protocol and nuclear protein foci scoring was described elsewhere [43,54]. Anti- $\gamma\text{H2AX}^{\text{ser139}}$  antibody (#05-636; Merck Millipore, Burlington, VT, USA) was used at 1:800. The monoclonal anti-mouse anti- $\text{pATM}^{\text{ser1981}}$  (#05-740) from Merck Millipore was used at 1:100. Incubations with anti-mouse fluorescein (FITC) and rhodamine (TRITC) secondary antibodies were performed at 1:100 at 37 °C for 20 min. By following the same procedure, micronuclei were scored on the same slides by using 4',6'-Diamidino-2-Phényl-indole (DAPI)-counter staining. Foci and micronuclei were scored by eye with an Olympus BX51 fluorescence microscope. For each of the three independent experiments, 100 nuclei were analyzed. The patented procedures of foci scoring have been detailed elsewhere [26]. It is noteworthy that post-irradiation times indicated in the text represent an equal period of time of the incubation of cells at 37 °C without any genotoxic stress (i.e., under standard culture conditions). Such a period is currently considered to be a time for repair [43,54].



#### 4.5. Statistical Analysis

Statistical analysis was performed by using Kaleidagraph v4 (Synergy Software, Reading, PA, USA), Graphpad Prism (San Diego, CA, USA) and MATLAB R2020B (MathWorks, Natick, MA, USA). Since each experiment is the result of three independent replicates, the mean is given with the standard error of the mean (SEM) of the three independent experiments. The discrimination power of each molecular endpoints was performed with the one-way ANOVA test.

The mathematical analysis of correlations between the different endpoints was based on the following procedure: (1) The data fitting analysis was attempted with the current mathematical laws (linear, curvilinear, exponential, and power functions). The adjustable parameters and the quality of fit were calculated systematically. If the data fitting is not acceptable, the link between the two endpoints is considered as “complex” and is thereafter deduced from the other links established (crossed resolution). (2) The differential equation whose solution is provided by the best data fit is established. (3) The k-coefficient and all the bounded values were deduced numerically.

#### 5. Conclusions

By analyzing radiobiological data from 200 skin fibroblast cell lines from RT-treated patients showing a large spectrum of OR severity grades obtained with the major assays predicting radiosensitivity, it appears that SF2 and the maximal number of early pATM foci are the best predictors of all the CTCAE grades while the number of residual micronuclei and  $\gamma$ H2AX foci do not predict well the intermediate grades. These findings are consistent with the fact that the clonogenic cell survival assay account for all the dead cells, independently of the cell death pathway. Similarly, the pATM immunofluorescence permits the quantification of DSBs unrecognized by the predominant NHEJ pathway, which directly impact on the RI cell death. Conversely, the residual micronuclei and the  $\gamma$ H2AX foci correspond to a limited subset of lethal DSB. Gathered all in a differential equations system, these major radiosensitivity endpoints are mathematically linked in a single mechanistic model of individual response to radiation in which the ATM kinase plays a major role. Further investigations are needed to better exploit this system in the prediction of the deleterious effects of any exposure of mammalian cells to IR and, more generally, to any DSB-inducer agent.

**Author Contributions:** The authors of this manuscript have contributed in the following manners: Conceptualization, E.L.R., L.B., N.F. and M.B.; data acquisition and methodology, A.G., L.S., M.L.F., J.A.-C., L.E.-N., J.R.-V., C.D., E.B. and A.B.; data analysis, E.L.R., L.B. and N.F.; writing and original draft preparation, J.A.-C., E.B. and N.F.; writing, reviewing and editing, all the authors; project administration, and funding acquisition, N.F., A.B. and M.B. All authors have read and agreed to the published version of the manuscript.

**Funding:** This work was supported by the Commissariat General à l'Investissement (Programmes Investissement d'avenir—INDIRA project), the Institut National du Cancer (InCa)—PROUST project, the National Space Agency (CNES)—ICARE project, the French-Lebanon partenariat Hubert Curien—CEDRE 47880PE project, Région Auvergne Rhône-Alpes—ERATOSTHENE R21107CC project.

**Institutional Review Board Statement:** As already mentioned in Materials and Methods, this study has been performed with human fibroblast cell lines that belong to the COPERNIC collection of the lab that has been approved by the regional Ethical Committee. Cell lines were declared under the numbers DC2008-585, DC2011-1437, and DC2021-3957 to the Ministry of Research.

**Informed Consent Statement:** All of the anonymous donors of the COPERNIC collection evoked above were informed and signed consent according to the ethics and regulatory recommendations, notably for their consent to participate and for publication of anonymous data.

**Data Availability Statement:** All the data can be provided on reasonable request.



**Conflicts of Interest:** N.F. reports the following related patents: FR3040178A1, FR3040179A1, WO-2017098190A1, EP3685163A. The authors declare no conflict of interest. The funders had no role in the design of the study; in the collection, analyses, or interpretation of data; in the writing of the manuscript, or in the decision to publish the results.

## References

1. Turesson, I.; Nyman, J.; Holmberg, E.; Oden, A. Prognostic factors for acute and late skin reactions in radiotherapy patients. *Int. J. Radiat. Oncol. Biol. Phys.* **1996**, *36*, 1065–1075. [\[CrossRef\]](#)
2. ICRP Publication 105. Radiation protection in medicine. *Ann. ICRP* **2007**, *37*, 1–63. [\[CrossRef\]](#)
3. Foray, N.; Bourguignon, M.; Hamada, N. Individual response to ionizing radiation. *Mutat. Res. Rev.* **2016**, *770*, 369–386. [\[CrossRef\]](#)
4. Dorr, W. Skin and other reactions to radiotherapy—Clinical presentation and radiobiology of skin reactions. *Front. Radiat. Ther. Oncol.* **2006**, *39*, 96–101. [\[PubMed\]](#)
5. Stewart, F.A.; Akleyev, A.V.; Hauer-Jensen, M.; Hendry, J.H.; Kleiman, N.J.; Macvittie, T.J.; Aleman, B.M.; Edgar, A.B.; Mabuchi, K.; Muirhead, C.R.; et al. ICRP publication 118: ICRP statement on tissue reactions and early and late effects of radiation in normal tissues and organs—Threshold doses for tissue reactions in a radiation protection context. *Ann. ICRP* **2012**, *41*, 1–322. [\[CrossRef\]](#)
6. Cox, J.D.; Stetz, J.; Pajak, T.F. Toxicity criteria of the Radiation Therapy Oncology Group (RTOG) and the European Organization for Research and Treatment of Cancer (EORTC). *Int. J. Radiat. Oncol. Biol. Phys.* **1995**, *31*, 1341–1346. [\[CrossRef\]](#)
7. Stone, H.B.; Coleman, C.N.; Anscher, M.S.; McBride, W.H. Effects of radiation on normal tissue: Consequences and mechanisms. *Lancet Oncol.* **2003**, *4*, 529–536. [\[CrossRef\]](#)
8. Fuzissaki, M.A.; Paiva, C.E.; Oliveira, M.A.; Lajolo Canto, P.P.; Paiva Maia, Y.C. The Impact of Radiodermatitis on Breast Cancer Patients' Quality of Life during Radiotherapy: A Prospective Cohort Study. *J. Pain Symptom Manag.* **2019**, *58*, 92–99.e1. [\[CrossRef\]](#)
9. Alicikus, Z.A.; Yamada, Y.; Zhang, Z.; Pei, X.; Hunt, M.; Kollmeier, M.; Cox, B.; Zelefsky, M.J. Ten-year outcomes of high-dose, intensity-modulated radiotherapy for localized prostate cancer. *Cancer* **2011**, *117*, 1429–1437. [\[CrossRef\]](#)
10. Zhao, J.; Yorke, E.D.; Li, L.; Kavanagh, B.D.; Li, X.A.; Das, S.; Miften, M.; Rimner, A.; Campbell, J.; Xue, J.; et al. Simple Factors Associated with Radiation-Induced Lung Toxicity after Stereotactic Body Radiation Therapy of the Thorax: A Pooled Analysis of 88 Studies. *Int. J. Radiat. Oncol. Biol. Phys.* **2016**, *95*, 1357–1366. [\[CrossRef\]](#)
11. Averbeck, D.; Candeias, S.; Chandna, S.; Foray, N.; Friedl, A.A.; Haghdoust, S.; Jeggo, P.A.; Lumniczky, K.; Paris, F.; Quintens, R.; et al. Establishing mechanisms affecting the individual response to ionizing radiation. *Int. J. Radiat. Biol.* **2020**, *96*, 297–323. [\[CrossRef\]](#) [\[PubMed\]](#)
12. Ferlazzo, M.L.; Bourguignon, M.; Foray, N. Functional Assays for Individual Radiosensitivity: A Critical Review. *Semin. Radiat. Oncol.* **2017**, *27*, 310–315. [\[CrossRef\]](#) [\[PubMed\]](#)
13. Ash, D. Lessons from Epinal. *Clin. Oncol.* **2007**, *19*, 614–615. [\[CrossRef\]](#) [\[PubMed\]](#)
14. Peiffert, D.; Simon, J.M.; Eschwege, F. Epinal radiotherapy accident: Passed, present, future. *Cancer Radiother. J. Soc. Fr. Radiother. Oncol.* **2007**, *11*, 309–312.
15. El-Nachef, L.; Al-Choboq, J.; Restier-Verlet, J.; Granzotto, A.; Berthel, E.; Sonzogni, L.; Ferlazzo, M.L.; Bouchet, A.; Leblond, P.; Combemale, P.; et al. Human Radiosensitivity and Radiosusceptibility: What Are the Differences? *Int. J. Mol. Sci.* **2021**, *22*, 7158. [\[CrossRef\]](#)
16. National Institutes of Health; National Cancer Institute. *Common Terminology Criteria for Adverse Events (CTCAE) Version 4.0*. May 28, 2009 (v4.03: June 14, 2010); National Institutes of Health: Bethesda, MD, USA, 2010.
17. Trotti, A.; Colevas, A.D.; Setser, A.; Rusch, V.; Jaques, D.; Budach, V.; Langer, C.; Murphy, B.; Cumberlin, R.; Coleman, C.N.; et al. CTCAE v3.0: Development of a comprehensive grading system for the adverse effects of cancer treatment. *Semin. Radiat. Oncol.* **2003**, *13*, 176–181. [\[CrossRef\]](#)
18. Barnett, G.C.; Coles, C.E.; Elliott, R.M.; Baynes, C.; Luccarini, C.; Conroy, D.; Wilkinson, J.S.; Tyrer, J.; Misra, V.; Platte, R.; et al. Independent validation of genes and polymorphisms reported to be associated with radiation toxicity: A prospective analysis study. *Lancet Oncol.* **2012**, *13*, 65–77. [\[CrossRef\]](#)
19. Barnett, G.C.; Thompson, D.; Fachal, L.; Kerns, S.; Talbot, C.; Elliott, R.M.; Dorling, L.; Coles, C.E.; Dearnaley, D.P.; Rosenstein, B.S.; et al. A genome wide association study (GWAS) providing evidence of an association between common genetic variants and late radiotherapy toxicity. *Radiother. Oncol. J. Eur. Soc. Ther. Radiol. Oncol.* **2014**, *111*, 178–185. [\[CrossRef\]](#)
20. Badie, C.; Dziwura, S.; Raffy, C.; Tsigani, T.; Alsbeih, G.; Moody, J.; Finnon, P.; Levine, E.; Scott, D.; Bouffler, S. Aberrant CDKN1A transcriptional response associates with abnormal sensitivity to radiation treatment. *Br. J. Cancer* **2008**, *98*, 1845–1851. [\[CrossRef\]](#)
21. Badie, C.; Kabacik, S.; Balagurunathan, Y.; Bernard, N.; Brengues, M.; Faggioni, G.; Greither, R.; Lista, F.; Peinnequin, A.; Poyot, T.; et al. Laboratory intercomparison of gene expression assays. *Radiat. Res.* **2013**, *180*, 138–148. [\[CrossRef\]](#)
22. Deschavanne, P.J.; Fertil, B. A review of human cell radiosensitivity in vitro. *Int. J. Radiat. Oncol. Biol. Phys.* **1996**, *34*, 251–266. [\[CrossRef\]](#)
23. Fertil, B.; Dertinger, H.; Courdi, A.; Malaise, E.P. Mean inactivation dose: A useful concept for intercomparison of human cell survival curves. *Radiat. Res.* **1984**, *99*, 73–84. [\[CrossRef\]](#) [\[PubMed\]](#)
24. Fertil, B.; Malaise, E.P. Inherent cellular radiosensitivity as a basic concept for human tumor radiotherapy. *Int. J. Radiat. Oncol. Biol. Phys.* **1981**, *7*, 621–629. [\[CrossRef\]](#)



25. Fertil, B.; Deschavanne, P.J. Relationships between colony forming efficiency and parameters of intrinsic radiosensitivity. *Int. J. Radiat. Biol.* **1999**, *75*, 1275–1282. [[PubMed](#)]
26. Little, J.B.; Nichols, W.W.; Troilo, P.; Nagasawa, H.; Strong, L.C. Radiation sensitivity of cell strains from families with genetic disorders predisposing to radiation-induced cancer. *Cancer Res.* **1989**, *49*, 4705–4714.
27. Arlett, C.F.; Harcourt, S.A. Survey of radiosensitivity in a variety of human cell strains. *Cancer Res.* **1980**, *40*, 926–932.
28. Fenech, M. The in vitro micronucleus technique. *Mutat. Res.* **2000**, *455*, 81–95. [[CrossRef](#)]
29. Darroudi, F.; Fomina, J.; Meijers, M.; Natajara, A.T. Kinetics of the formation of chromosome aberrations in X-irradiated human lymphocytes, using PCC and FISH. *Mutat. Res.* **1998**, *404*, 55–65. [[CrossRef](#)]
30. Joubert, A.; Zimmerman, K.M.; Bencokova, Z.; Gastaldo, J.; Rénier, W.; Chavaudra, N.; Favaudon, V.; Arlett, C.; Foray, N. DNA double-strand break repair defects in syndromes associated with acute radiation response: At least two different assays to predict intrinsic radiosensitivity? *Int. J. Radiat. Biol.* **2008**, *84*, 107–125. [[CrossRef](#)]
31. Dikomey, E.; Borgmann, K.; Brammer, I.; Kasten-Pisula, U. Molecular mechanisms of individual radiosensitivity studied in normal diploid human fibroblasts. *Toxicology* **2003**, *193*, 125–135. [[CrossRef](#)]
32. Nunez, M.I.; Villalobos, M.; Olea, N.; Valenzuela, M.T.; Pedraza, V.; McMillan, T.J.; Ruiz de Almodovar, J.M. Radiation-induced DNA double-strand break rejoining in human tumour cells. *Br. J. Cancer* **1995**, *71*, 311–316. [[CrossRef](#)] [[PubMed](#)]
33. Ruiz de Almodovar, J.M.; Nunez, M.I.; McMillan, T.J.; Olea, N.; Mort, C.; Villalobos, M.; Pedraza, V.; Steel, G.G. Initial radiation-induced DNA damage in human tumour cell lines: A correlation with intrinsic cellular radiosensitivity. *Br. J. Cancer* **1994**, *69*, 457–462. [[CrossRef](#)]
34. Cornforth, M.N.; Bedford, J.S. A quantitative comparison of potentially lethal damage repair and the rejoining of interphase chromosome breaks in low passage normal human fibroblasts. *Radiat. Res.* **1987**, *111*, 385–405. [[CrossRef](#)] [[PubMed](#)]
35. Granzotto, A.; Bencokova, Z.; Vogin, G.; Devic, C.; Joubert, A.; Balosso, J.; Foray, N. DNA double-strand breaks repair and signaling of human gliomas and normal brain cells in response to radiation: Potential impact of the ATM- and BRCA1-dependent pathways. In *Brain Tumors—Current and Emerging Therapeutic Strategies*; Abujamra, A.L., Ed.; Intechweb: Rijeka, Croatia, 2011.
36. Iliakis, G. The role of DNA double strand breaks in ionizing radiation-induced killing of eukaryotic cells. *BioEssays News Rev. Mol. Cell. Dev. Biol.* **1991**, *13*, 641–648.
37. Jeggo, P.A.; Lobrich, M. DNA double-strand breaks: Their cellular and clinical impact? *Oncogene* **2007**, *26*, 7717–7719. [[CrossRef](#)]
38. Kinner, A.; Wu, W.; Staudt, C.; Iliakis, G. Gamma-H2AX in recognition and signaling of DNA double-strand breaks in the context of chromatin. *Nucleic Acids Res.* **2008**, *36*, 5678–5694. [[CrossRef](#)]
39. Ganguly, T.; Iliakis, G. A cell-free assay using cytoplasmic cell extracts to study rejoining of radiation-induced DNA double-strand breaks in human cell nuclei. *Int. J. Radiat. Biol.* **1995**, *68*, 447–457. [[CrossRef](#)]
40. Berthel, E.; Ferlazzo, M.L.; Devic, C.; Bourguignon, M.; Foray, N. What does the History of Research on the Repair of DNA Double-Strand Breaks Tell Us?—A Comprehensive Review of Human Radiosensitivity. *Int. J. Mol. Sci.* **2019**, *20*, 5339. [[CrossRef](#)]
41. Rothkamm, K.; Lobrich, M. Evidence for a lack of DNA double-strand break repair in human cells exposed to very low x-ray doses. *Proc. Natl. Acad. Sci. USA* **2003**, *100*, 5057–5062. [[CrossRef](#)]
42. Berthel, E.; Foray, N.; Ferlazzo, M.L. The Nucleoshuttling of the ATM Protein: A Unified Model to Describe the Individual Response to High- and Low-Dose of Radiation? *Cancers* **2019**, *11*, 905. [[CrossRef](#)]
43. Granzotto, A.; Benadjaoud, M.A.; Vogin, G.; Devic, C.; Ferlazzo, M.L.; Bodgi, L.; Pereira, S.; Sonzogni, L.; Forcheron, F.; Viau, M.; et al. Influence of Nucleoshuttling of the ATM Protein in the Healthy Tissues Response to Radiation Therapy: Toward a Molecular Classification of Human Radiosensitivity. *Int. J. Radiat. Oncol. Biol. Phys.* **2016**, *94*, 450–460. [[CrossRef](#)]
44. Lobrich, M.; Jeggo, P.A. The two edges of the ATM sword: Co-operation between repair and checkpoint functions. *Radiother. Oncol. J. Eur. Soc. Ther. Radiol. Oncol.* **2005**, *76*, 112–118. [[CrossRef](#)]
45. Taylor, A.M.; Harnden, D.G.; Arlett, C.F.; Harcourt, S.A.; Lehmann, A.R.; Stevens, S.; Bridges, B.A. Ataxia telangiectasia: A human mutation with abnormal radiation sensitivity. *Nature* **1975**, *258*, 427–429. [[CrossRef](#)]
46. Foray, N.; Marot, D.; Gabriel, A.; Randrianarison, V.; Carr, A.M.; Perricaudet, M.; Ashworth, A.; Jeggo, P. A subset of ATM- and ATR-dependent phosphorylation events requires the BRCA1 protein. *EMBO J.* **2003**, *22*, 2860–2871. [[CrossRef](#)]
47. Vogin, G.; Bastogne, T.; Bodgi, L.; Gillet-Daubin, J.; Canet, A.; Pereira, S.; Foray, N. The Phosphorylated ATM Immunofluorescence Assay: A High-performance Radiosensitivity Assay to Predict Postradiation Therapy Overreactions. *Int. J. Radiat. Oncol. Biol. Phys.* **2018**, *101*, 690–693. [[CrossRef](#)]
48. Pereira, S.; Bodgi, L.; Duclos, M.; Canet, A.; Ferlazzo, M.L.; Devic, C.; Granzotto, A.; Deneuve, S.; Vogin, G.; Foray, N. Fast and binary assay for predicting radiosensitivity based on the nucleoshuttling of ATM protein: Development, validation and performances. *Int. J. Radiat. Oncol. Biol. Phys.* **2018**, *100*, 353–360. [[CrossRef](#)]
49. Bodgi, L.; Foray, N. The nucleo-shuttling of the ATM protein as a basis for a novel theory of radiation response: Resolution of the linear-quadratic model. *Int. J. Radiat. Biol.* **2016**, *92*, 117–131. [[CrossRef](#)]
50. Bodgi, L.; Canet, A.; Pujo-Menjouet, L.; Lesne, A.; Victor, J.M.; Foray, N. Mathematical models of radiation action on living cells: From the target theory to the modern approaches. A historical and critical review. *J. Theor. Biol.* **2016**, *394*, 93–101. [[CrossRef](#)]
51. Grote, S.J.; Joshi, G.P.; Revell, S.H.; Shaw, C.A. Observations of radiation-induced chromosome fragment loss in live mammalian cells in culture, and its effect on colony-forming ability. *Int. J. Radiat. Biol. Relat. Stud. Phys. Chem. Med.* **1981**, *39*, 395–408. [[CrossRef](#)]



52. Al-Choboq, J.; Ferlazzo, M.L.; Sonzogni, L.; Granzotto, A.; El-Nachef, L.; Maalouf, M.; Berthel, E.; Foray, N. Usher Syndrome Belongs to the Genetic Diseases Associated with Radiosensitivity: Influence of the ATM Protein Kinase. *Int. J. Mol. Sci.* **2022**, *23*, 1570. [\[CrossRef\]](#)
53. Combemale, P.; Sonzogni, L.; Devic, C.; Bencokova, Z.; Ferlazzo, M.L.; Granzotto, A.; Burlet, S.F.; Pinson, S.; Amini-Adle, M.; Al-Choboq, J.; et al. Individual Response to Radiation of Individuals with Neurofibromatosis Type I: Role of the ATM Protein and Influence of Statins and Bisphosphonates. *Mol. Neurobiol.* **2022**, *59*, 556–573. [\[CrossRef\]](#)
54. Ferlazzo, M.; Berthel, E.; Granzotto, A.; Devic, C.; Sonzogni, L.; Bachelet, J.T.; Pereira, S.; Bourguignon, M.; Sarasin, A.; Mezzina, M.; et al. Some mutations in the xeroderma pigmentosum D gene may lead to moderate but significant radiosensitivity associated with a delayed radiation-induced ATM nuclear localization. *Int. J. Radiat. Biol.* **2019**, *96*, 394–410. [\[CrossRef\]](#)
55. Rogakou, E.P.; Pilch, D.R.; Orr, A.H.; Ivanova, V.S.; Bonner, W.M. DNA double-stranded breaks induce histone H2AX phosphorylation on serine 139. *J. Biol. Chem.* **1998**, *273*, 5858–5868. [\[CrossRef\]](#)
56. Sedelnikova, O.A.; Rogakou, E.P.; Panyutin, I.G.; Bonner, W.M. Quantitative detection of (125)IdU-induced DNA double-strand breaks with gamma-H2AX antibody. *Radiat. Res.* **2002**, *158*, 486–492. [\[CrossRef\]](#)
57. Burma, S.; Chen, B.P.; Murphy, M.; Kurimasa, A.; Chen, D.J. ATM phosphorylates histone H2AX in response to DNA double-strand breaks. *J. Biol. Chem.* **2001**, *276*, 42462–42467. [\[CrossRef\]](#)
58. Rothkamm, K.; Kruger, I.; Thompson, L.H.; Lobrich, M. Pathways of DNA double-strand break repair during the mammalian cell cycle. *Mol. Cell. Biol.* **2003**, *23*, 5706–5715. [\[CrossRef\]](#)
59. Kuhne, M.; Riballo, E.; Rief, N.; Rothkamm, K.; Jeggo, P.A.; Lobrich, M. A double-strand break repair defect in ATM-deficient cells contributes to radiosensitivity. *Cancer Res.* **2004**, *64*, 500–508. [\[CrossRef\]](#)
60. Badie, C.; Goodhardt, M.; Waugh, A.; Doyen, N.; Foray, N.; Calsou, P.; Singleton, B.; Gell, D.; Salles, B.; Jeggo, P.; et al. A DNA double-strand break defective fibroblast cell line (180BR) derived from a radiosensitive patient represents a new mutant phenotype. *Cancer Res.* **1997**, *57*, 4600–4607.
61. Badie, C.; Iliakis, G.; Foray, N.; Alsbeih, G.; Cedervall, B.; Chavaudra, N.; Pantelias, G.; Arlett, C.; Malaise, E.P. Induction and rejoining of DNA double-strand breaks and interphase chromosome breaks after exposure to X rays in one normal and two hypersensitive human fibroblast cell lines. *Radiat. Res.* **1995**, *144*, 26–35. [\[CrossRef\]](#)
62. Badie, C.; Iliakis, G.; Foray, N.; Alsbeih, G.; Pantelias, G.E.; Okayasu, R.; Cheong, N.; Russell, N.S.; Begg, A.C.; Arlett, C.F.; et al. Defective repair of DNA double-strand breaks and chromosome damage in fibroblasts from a radiosensitive leukemia patient. *Cancer Res.* **1995**, *55*, 1232–1234.
63. Yang, S.N.; Liao, C.Y.; Chen, S.W.; Liang, J.A.; Tsai, M.H.; Hua, C.H.; Lin, F.J. Clinical implications of the tumor volume reduction rate in head-and-neck cancer during definitive intensity-modulated radiotherapy for organ preservation. *Int. J. Radiat. Oncol. Biol. Phys.* **2011**, *79*, 1096–1103. [\[CrossRef\]](#)
64. Pozniak-Balicka, R.; Chomiak, B.; Woskowiak, P.; Nowicki, N.; Bojarski, J.; Salagierski, M. Does the radiation approach affect acute toxicity in prostate cancer patients? A comparison of four radiation techniques. *Cent. Eur. J. Urol.* **2020**, *73*, 295–299.
65. Amaldi, U. Future trends in cancer therapy with particle accelerators. *Z. Med. Phys.* **2004**, *14*, 7–16. [\[CrossRef\]](#) [\[PubMed\]](#)
66. Le Reun, E.; Casutt, A.; Durham, A.; Bouchaab, H.; Romano, E.; Lovis, A.; Krueger, T.; Von Garnier, C.; Ozshahin, E.M.; Kinj, R. Lung stereotactic radiation therapy: Intercomparison of irradiation devices in terms of outcome and predictive factors. *Cancer Radiother. J. Soc. Fr. Radiother. Oncol.* **2022**, in press. [\[CrossRef\]](#) [\[PubMed\]](#)
67. Thomas, A.; Keller, A.; Menoux, I.; Brahimi, Y.; Vigneron, C.; Le Fevre, C.; Chambrelant, I.; Pietta, G.A.; Guihard, S.; Clavier, J.B.; et al. Prognostic factors of acute radiodermatitis in breast cancer after adjuvant radiotherapy treated with RT3D or IMRT. *Cancer Radiother. J. Soc. Fr. Radiother. Oncol.* **2022**, *26*, 684–691.
68. Lapen, K.; King, C.; Braunstein, L.Z.; Khan, A.J.; Kamrava, M.R.; Gillespie, E.F.; Cook, K.A. A Comparison of Patient- and Clinician-Reported Acute Toxicity during Radiotherapy for Primary Breast Cancer. *Int. J. Radiat. Oncol. Biol. Phys.* **2022**, *114*, 301–309. [\[CrossRef\]](#)
69. Puck, T.T.; Marcus, P.I. Action of x-rays on mammalian cells. *J. Exp. Med.* **1956**, *103*, 653–666. [\[CrossRef\]](#)
70. Elkind, M.M.; Whitmore, G.F. *The Radiobiology of Cultured Mammalian Cells*; Gordon and Breach: New York, NY, USA, 1967.
71. Arlett, C.F.; Green, M.H.; Priestley, A.; Harcourt, S.A.; Mayne, L.V. Comparative human cellular radiosensitivity: I. The effect of SV40 transformation and immortalisation on the gamma-irradiation survival of skin derived fibroblasts from normal individuals and from ataxia-telangiectasia patients and heterozygotes. *Int. J. Radiat. Biol.* **1988**, *54*, 911–928. [\[CrossRef\]](#)
72. Ferlazzo, M.L.; Bach-Tobdj, M.K.E.; Djerad, A.; Sonzogni, L.; Burlet, S.F.; Devic, C.; Granzotto, A.; Bodgi, L.; Djefal-Kerrar, A.; Foray, N. Radiobiological characterization of tuberous sclerosis: A delay in the nucleo-shuttling of ATM may be responsible for radiosensitivity. *Mol. Neurobiol.* **2017**, *55*, 4973–4983. [\[CrossRef\]](#)
73. Ferlazzo, M.L.; Sonzogni, L.; Granzotto, A.; Bodgi, L.; Lartin, O.; Devic, C.; Vogin, G.; Pereira, S.; Foray, N. Mutations of the Huntington's Disease Protein Impact on the ATM-Dependent Signaling and Repair Pathways of the Radiation-Induced DNA Double-Strand Breaks: Corrective Effect of Statins and Bisphosphonates. *Mol. Neurobiol.* **2014**, *49*, 1200–1211. [\[CrossRef\]](#)
74. Moulay Lakhdar, I.; Ferlazzo, M.L.; Al Choboq, J.; Berthel, E.; Sonzogni, L.; Devic, C.; Granzotto, A.; Thariat, J.; Foray, N. Fibroblasts from Retinoblastoma Patients Show Radiosensitivity Linked to Abnormal Localization of the ATM Protein. *Curr. Eye Res.* **2020**, *46*, 546–557. [\[CrossRef\]](#) [\[PubMed\]](#)



75. Bachelet, J.T.; Granzotto, A.; Ferlazzo, M.L.; Sonzogni, L.; Berthel, E.; Devic, C.; Foray, N. First Radiobiological Characterization of Skin and Bone Cells from a Patient Suffering from the PI3KCA-Related Overgrowth Spectrum (PROS) Syndrome. *Arch. Med. Clin. Case Rep.* **2020**, *4*, 1052–1066. [[CrossRef](#)]
76. Bachelet, J.T.; Granzotto, A.; Ferlazzo, M.; Sonzogni, L.; Berthel, E.; Devic, C.; Foray, N. First radiobiological characterization of the McCune-Albright syndrome: Influence of the ATM protein and effect of statins + bisphosphonates treatment. *Int. J. Radiat. Biol.* **2021**, *97*, 317–328. [[CrossRef](#)] [[PubMed](#)]
77. Pouliliou, S.E.; Lialiaris, T.S.; Dimitriou, T.; Giatromanolaki, A.; Papazoglou, D.; Pappa, A.; Pistevou, K.; Kalamida, D.; Koukourakis, M.I. Survival Fraction at 2 Gy and gammaH2AX Expression Kinetics in Peripheral Blood Lymphocytes from Cancer Patients: Relationship with Acute Radiation-Induced Toxicities. *Int. J. Radiat. Oncol. Biol. Phys.* **2015**, *92*, 667–674. [[CrossRef](#)]
78. Attard-Montalto, S.P.; Saha, V.; Kingston, J.; Plowman, N.; Taylor, M.; Arlett, C.; Bridges, B.; Eden, O. Increased radiosensitivity in a child with T-cell non-Hodgkin's lymphoma. *Med. Pediatr. Oncol.* **1996**, *27*, 564–570. [[CrossRef](#)]
79. Plowman, P.N.; Bridges, B.A.; Arlett, C.F.; Hinney, A.; Kingston, J.E. An instance of clinical radiation morbidity and cellular radiosensitivity, not associated with ataxia-telangiectasia. *Br. J. Radiol.* **1990**, *63*, 624–628. [[CrossRef](#)]
80. Pietrucha, B.M.; Heropolitanska-Pliszka, E.; Wakulinska, A.; Skopczynska, H.; Gatti, R.A.; Bernatowska, E. Ataxia-telangiectasia with hyper-IgM and Wilms tumor: Fatal reaction to irradiation. *J. Pediatr. Hematol. Oncol.* **2010**, *32*, e28–e30. [[CrossRef](#)]
81. Scott, D.; Barber, J.B.; Levine, E.L.; Burrill, W.; Roberts, S.A. Radiation-induced micronucleus induction in lymphocytes identifies a high frequency of radiosensitive cases among breast cancer patients: A test for predisposition? *Br. J. Cancer* **1998**, *77*, 614–620. [[CrossRef](#)]
82. Rothfuss, A.; Schutz, P.; Bochum, S.; Volm, T.; Eberhardt, E.; Kreienberg, R.; Vogel, W.; Speit, G. Induced micronucleus frequencies in peripheral lymphocytes as a screening test for carriers of a BRCA1 mutation in breast cancer families. *Cancer Res.* **2000**, *60*, 390–394.
83. Sommer, S.; Buraczewska, I.; Kruszewski, M. Micronucleus Assay: The State of Art, and Future Directions. *Int. J. Mol. Sci.* **2020**, *21*, 1534. [[CrossRef](#)]
84. Duker, N.J. Chromosome breakage syndromes and cancer. *Am. J. Med. Genet.* **2002**, *115*, 125–129. [[CrossRef](#)] [[PubMed](#)]
85. Bedford, J.S.; Cornforth, M.N. Relationship between the recovery from sublethal X-ray damage and the rejoining of chromosome breaks in normal human fibroblasts. *Radiat. Res.* **1987**, *111*, 406–423. [[CrossRef](#)] [[PubMed](#)]
86. Foray, N.; Priestley, A.; Alsbeih, G.; Badie, C.; Capulas, E.P.; Arlett, C.F.; Malaise, E.P. Hypersensitivity of ataxia telangiectasia fibroblasts to ionizing radiation is associated with a repair deficiency of DNA double-strand breaks. *Int. J. Radiat. Biol.* **1997**, *72*, 271–283. [[PubMed](#)]






# UP Defense



## Article

# Molecular Influence of the ATM Protein in the Treatment of Human Cells with Different Radioprotective Drugs: Comparisons between Antioxidative and Pro-Episkevic Strategies

Juliette Restier-Verlet <sup>1,†</sup>, Michel Drouet <sup>1,2,†</sup>, Pauline Pras <sup>1,†</sup>, Mélanie L. Ferlazzo <sup>1</sup>, Adeline Granzotto <sup>1</sup>, Laurene Sonzogni <sup>1</sup>, Joëlle Al-Choboq <sup>1</sup> , Laura El Nacheff <sup>1</sup> , Sabine François <sup>1,2</sup>, Michel Bourguignon <sup>1,3</sup> and Nicolas Foray <sup>1,\*</sup> 

<sup>1</sup> INSERM U1296 Unit “Radiation: Defense, Health, Environment”, Centre Léon-Bérard, 69008 Lyon, France

<sup>2</sup> Division Défense NRBC, Institut de Recherche Biomédicale des Armées, 91220 Brétigny-sur-Orge, France

<sup>3</sup> Department of Biophysics and Nuclear Medicine, Université Paris Saclay Versailles St Quentin en Yvelines, 78035 Versailles, France

\* Correspondence: nicolas.foray@inserm.fr; Tel.: +33-4-78-78-28-28

† These authors contributed equally to this work.

**Abstract:** The radiation protection strategy with chemical agents has long been based on an antioxidative approach consisting in reducing the number of radical oxygen and nitrogen species responsible for the formation of the radiation-induced (RI) DNA damage, notably the DNA double-strand breaks (DSB), whose subset participates in the RI lethal effect as unreparable damage. Conversely, a DSB repair-stimulating strategy that may be called the “pro-episkevic” approach (from the ancient Greek *episkeve*, meaning repair) can be proposed. The pro-episkevic approach directly derives from a mechanistic model based on the RI nucleoshuttling of the ATM protein (RIANS) and contributes to increase the number of DSB managed by NHEJ, the most predominant DSB repair and signaling pathway in mammals. Here, three radioresistant and three radiosensitive human fibroblast cell lines were pretreated with antioxidative agents (N-acetylcysteine or amifostine) or to two pro-episkevic agents (zoledronate or pravastatin or both (ZOPRA)) before X-ray irradiation. The fate of the RI DSB was analyzed by using  $\gamma$ H2AX and pATM immunofluorescence. While amifostine pretreatment appeared to be the most efficient antioxidative process, ZOPRA shows the most powerful radiation protection, suggesting that the pro-episkevic strategy may be an alternative to the antioxidative one. Additional investigations are needed to develop some new drugs that may elicit both antioxidative and pro-episkevic properties and to quantify the radiation protection action of both types of drugs applied concomitantly.

**Keywords:** radioprotectors; N-acetylcysteine; amifostine; statin; bisphosphonates; ATM



**Citation:** Restier-Verlet, J.; Drouet, M.; Pras, P.; Ferlazzo, M.L.; Granzotto, A.; Sonzogni, L.; Al-Choboq, J.; El Nacheff, L.; François, S.; Bourguignon, M.; et al. Molecular Influence of the ATM Protein in the Treatment of Human Cells with Different Radioprotective Drugs: Comparisons between Antioxidative and Pro-Episkevic Strategies. *Biomolecules* **2023**, *13*, 524. <https://doi.org/10.3390/biom13030524>

Academic Editors: Michael Van Dyke and Vladimir N. Uversky

Received: 12 September 2022

Revised: 3 March 2023

Accepted: 9 March 2023

Published: 13 March 2023



**Copyright:** © 2023 by the authors. Licensee MDPI, Basel, Switzerland. This article is an open access article distributed under the terms and conditions of the Creative Commons Attribution (CC BY) license (<https://creativecommons.org/licenses/by/4.0/>).

## 1. Introduction

Exposure to ionizing radiation (IR) causes a large spectrum of DNA damage and cellular deaths and affects individuals by increasing risks of radiation-induced (RI) tissue/organ injuries (radiosensitivity), cancers (radiosusceptibility) and/or aging (radiodegeneration) [1]. Since the first studies initiated in 1942 by the scientists of the Manhattan Project at Walter Reed General Hospital (Washington, DC, USA) and by Antoine Lacasagne at Institut Curie (Paris, France), radiobiologists have endeavored to develop chemical countermeasures aiming to protect DNA, cells, tissues and individuals from the clinical consequences of exposure to IR [2–7]. In the field of radiation protection, specific terms are currently used to describe the different radioprotective agents, whether they are administered before (prophylactic drugs), during or after (mitigation drugs) irradiation [2]. The



radioprotective agents should be efficient in different scenarios, such as after accidental, military, occupational and clinical exposures to IR (Figure 1):

- High-intensity warfare has recently emerged as a reality in Europe: Old cold war challenges are currently largely under review, among which the place of radioprotector countermeasures should usefully be revisited. Military operations under radiological/nuclear threat (even limited to tactical level) could result in numerous cases of acute radiation syndrome. Targeting fallout may be more realistic and could offer opportunities for innovative radioprotectors use. As an example, nuclear power plant security during military operations has been a concern for some years in NATO strategy, and recent operations in Ukraine (Tchernobyl area and Zaporizhia power plant) clearly illustrate some of these various scenarios. In such context, maintaining the freedom of action of forces may result in deliberate or accidental limited irradiation of soldiers up to 750 mGy [8].
- Space radiation represents the most hazardous factor of space exploration [9]. For the astronauts in their spacecraft, exposure to space radiation can be summarized as a continuous low dose rate of X- and gamma-rays (the “bath of radiation”) and a flux of low-energy particles emitted from the metallic shielding [9]. Hence, specific radiation protection countermeasures are needed to protect astronauts.
- Radioprotective agents are useful in the medical context, notably in anticancer radiotherapy (RT) to specifically protect healthy tissues surrounding the tumor [2,3,10,11]. There has been a plethora of RT trials involving radioprotectors, generally sulfhydryl compounds and other antioxidants. Analogs of cysteine, notably cysteamine, and glutathione were applied to irradiated animals and then cancer patients; the development of new thiol-containing agents was a major axis of research in this field [12–16]. More than 4000 candidate compounds were tested in the Walter Reed Army Research Center (USA) [7]. Among them, WR2721 (ethyol and amifostine) appeared to be the most efficient radioprotective drug in RT. Amifostine was notably shown to reduce IR-induced esophagitis, mucositis, lung inflammation and cisplatin-related nephrotoxicity. Despite some side effects, the application of amifostine during RT generally permits to achieve high rates of complete response [17–23]. Since 1999, the use of amifostine in RT is permitted by the US Federal Drug Agency agreement to reduce xerostomia in patients undergoing postoperative RT for head and neck cancer [21].

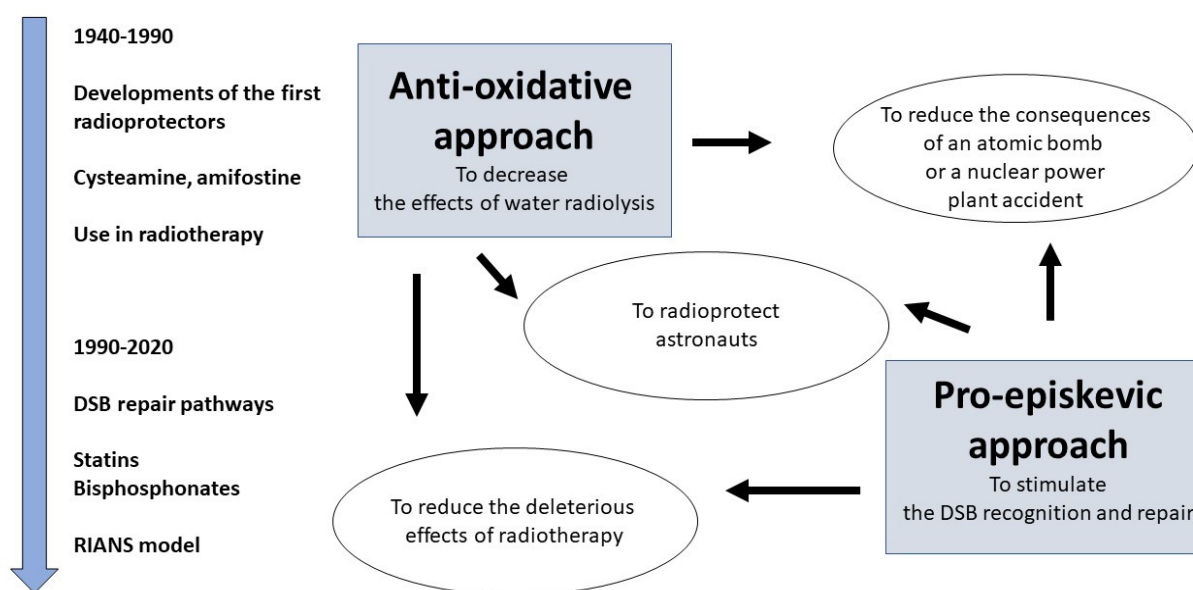


Figure 1. Schematic view of the two different approaches of radioprotection, their major principles and their historical milestones.



In addition to amifostine, a number of antioxidants such as glutathione, vitamin E, selenium or N-acetylcysteine (NAC) have been used concomitantly with chemo- and radiotherapy [2,3,24]. Among the antioxidants, NAC is one of the most extensively used and provides the advantage of a low cost and the absence of toxicity. The major action of NAC is the increase in glutathione levels, which facilitates the prevention against the pathologies linked to free radicals and reactive species [25]. Mainly supported by experiments on exposed rats, first RT trials with NAC have revealed a significant heart and lung protection [26,27]. However, whatever the antioxidants tested, the experimental protocols are so various that a very small minority of trials involved the same drug, which does not permit to conclude a real benefit of any antioxidative drug during anticancer RT, and reciprocally, it does not facilitate reliable intercomparisons between the different antioxidants [2,3] (Figure 1).

To date, the great majority of the studies about radioprotectors follow the same *antioxidative* approach, based on the reduction in the ROS levels that produce RI DNA damage. Consistently, this approach results in decreasing the number of DNA breaks, notably that of DNA double-strand breaks (DSB), the key damage of the cell killing [28,29]. An alternative approach would consist rather in *stimulating DSB repair* than *reducing the number of the RI DSB*. Such a strategy has been named the *pro-episkevic* approach (from the ancient Greek επισκευε (episkeve), meaning “repair”). This term was first mentioned in the PhD thesis dissertation of M.L.F presented in 2017 at the University of Lyon, France [30]. The pro-episkevic approach has been mainly documented in the frame of the RI nucleoshuttling of the ATM protein (RIANS) model [31–34]. The ATM protein is a major actor in the individual response to IR and DNA-breaking agents. The RIANS model is based on the following molecular steps of the stress response of quiescent cells: (1) RI oxidative stress results in both induction of DSB in nucleus and monomerization of the cytoplasmic ATM dimers; (2) the resulting ATM monomers diffuse from cytoplasm to nucleus; (3) the ATM monomers phosphorylate H2AX histones, which produces nuclear  $\gamma$ H2AX foci at the DSB sites (easily visible and quantifiable by immunofluorescence) and contribute to the recognition of DSB by the nonhomologous end-joining (NHEJ) pathway, predominant in human quiescent cells [35–37]; (4) a complete DSB repair produces the trans-autophosphorylation of ATM proteins (pATM) that forms ATM dimers in nucleus, reflected by pATM foci at the DSB sites, again easily visible and quantifiable by immunofluorescence [34,36,38,39]. A delayed RIANS may be caused by an overexpression of some ATM phosphorylation substrate proteins (called X-proteins) in cytoplasm. The cytoplasmic X-proteins sequester the ATM monomers. As a consequence, either the *unrecognized* DSB remain unrepaired and participate in cell death, or else, they are *misrepaired* by error-prone recombination-like pathways and participate in cell transformation and cancer [34,36,38,39]. A combination of statins and bisphosphonates was shown to accelerate the RIANS by increasing the permeability of the nuclear membranes to the ATM monomers and to provide various levels of radioprotection according the genetic syndromes tested [31–34,40,41] (Figure 1).

Recently, from 200 human fibroblast cell lines showing a large spectrum of radiosensitivity, we provided clues that some quantitative correlations exist between the cellular radiosensitivity of quiescent human cells and  $\gamma$ H2AX and pATM biomarkers [42]. Other biomarkers such as DNA-PK foci, Ku expression, or cell-free plasmid end-joining assays were not chosen because of potential technical artifacts, low dose dependence and difficulties to extrapolate data to in vivo experiments, respectively [1,42,43]. Hence, here, by using the number of  $\gamma$ H2AX and pATM foci as endpoints, the antioxidative approach (with NAC and amifostine, the most documented antioxidative drugs) and the pro-episkevic approach (with statins and bisphosphonates, the most documented pro-episkevic drugs) were compared with three radioresistant and three radiosensitive human quiescent fibroblasts, pretreated with drug concentrations already tested in the literature and exposed to IR. Our major goal is to better understand the molecular features of the radioprotection process by quantifying the reduction of the molecular effect induced by a reference IR dose (here, 2 Gy X-rays, mimicking a standard RT session) after a 24 h drug pretreatment.



## 2. Materials and Methods

### 2.1. Cell Lines

All the skin fibroblasts tested were untransformed to avoid any bias linked to genomic stability in the plateau phase of growth (95–99% in G0/G1) to overcome any cell cycle and homologous recombination effects. Skin fibroblasts were routinely cultured at 37 °C in 5% CO<sub>2</sub> humid conditions as monolayers with Dulbecco's modified Eagle's minimum medium (DMEM) (Gibco-Invitrogen-France, Cergy-Pontoise, France), supplemented with 20% fetal calf serum, penicillin and streptomycin. The origin and the radiobiological features of the RIANs-normal radioresistant AG1521, 1BR3 and 149BR controls are published elsewhere [39,44,45]. The radiosensitive RIANs-delayed 09CLB, 11CLB and 15CLB fibroblasts were provided from skin biopsy from donors who show adverse tissue reaction after anticancer RT. These cell lines belong to the "COPERNIC" collection managed by our lab and approved by the regional Ethical Committee. The COPERNIC cell lines were declared under the numbers DC2008-585, DC2011-1437 and DC2021-3957 to the Ministry of Research. The radiobiological database was protected under the reference as IDD.N.FR.001.510017.000.D.P.2014.000.10300 [39]. The surviving 2 Gy (SF2) of the cell lines used in this study is assessed and published elsewhere [42]. Briefly, while the SF2 of the radioresistant AG1521, 1BR3 and 149BR controls ranged between 60 and 65%, the SF2 of 09CLB, 11CLB and 15CLB fibroblast cell lines were found to be  $35 \pm 5$ ,  $42 \pm 8$  and  $37 \pm 4\%$ , respectively. It is noteworthy that 09CLB, 11CLB and 15CLB donors suffered from severity grades 4, 3 and 4 tissue post RT reaction [39,42].

### 2.2. Radioprotective Drugs

With regard to the antioxidative drugs, N-acetyl-L-cysteine (NAC) and amifostine (2-(3-Aminopropyl)aminoethyl phosphorothioate, WR2721, Ethyol) were purchased from Sigma-Aldrich (Saint-Quentin-Fallavier, France; #9165 and #A5922, respectively). Cells were incubated with these two last drugs separately for 24 h at 37 °C at 10–300 mM NAC or at 24–96 mM for amifostine. The choice of these drug concentrations was motivated by preliminary experiments based on the assessment of  $\gamma$ H2AX foci when drug was applied alone to radioresistant fibroblasts. All the conditions leading to the production of more than 2  $\gamma$ H2AX foci per cell were excluded. With regard to the pro-episkevic drugs, cells were incubated with either 1  $\mu$ M pravastatin (#P4498, Sigma-Aldrich) for 24 h at 37 °C alone or 1  $\mu$ M zoledronate (#SML0223, Sigma-Aldrich) for 12 h at 37 °C alone (to permit intercomparisons) or together (ZOPRA treatment) [46]. The choice of these drug concentrations was notably motivated by our previous data published in [46].

### 2.3. X-ray Irradiations

Irradiations were performed with a 6 MeV X-ray medical irradiator (SL 15 Philips) (dose rate: 6 Gy.min<sup>-1</sup>) at the anticancer Center Léon-Bérard (Lyon, France) [39,45]. In all the experiments, a dose of 2 Gy was applied. It is noteworthy that 2 Gy X-rays represent a reference dose equivalent to a session of a standard anticancer RT.

### 2.4. Immunofluorescence

The immunofluorescence protocol was described elsewhere [47,48]. Briefly, cells were fixed in paraformaldehyde for 10 min at room temperature and were permeabilized in 0.5% Triton X-100 solution for 5 min at 4 °C. Primary and secondary antibody incubations were performed for 40 and 20 min at 37 °C, respectively. Anti- $\gamma$ H2AX<sup>ser139</sup> antibody (#05636; Upstate Biotechnology-Euromedex, Mundolsheim, France) was used at 1:800. The monoclonal anti-mouse anti-pATM<sup>ser1981</sup> (#ab2888) from Abcam (Cambridge, UK) was used at 1:100. Incubations with anti-mouse fluorescein (FITC) and rhodamine (TRITC) secondary antibodies were performed at 1:100 at 37 °C for 20 min. Slides were mounted in 4',6'-Diamidino-2-Phenyl-indole (DAPI)-stained Vectashield (Abcys, Paris, France), and foci were examined with Olympus fluorescence microscope. The foci scoring procedure applied here received the certification agreement of CE mark and ISO-13485 quality management



system norms. Our foci scoring procedure also developed some features that are protected in the frame of the Soleau Envelop and patents (FR3017625 A1, FR3045071 A1, EP3108252 A1) [48]. More than 50 nuclei were analyzed per experiment and at least 3 independent replicates were performed for each condition [39]. It is noteworthy that  $\gamma$ H2AX foci reveal only the presence of DSB recognized by the NHEJ pathway: vis-à-vis the DSB induced “physically” by IR, the proportion of DSB recognized by NHEJ is maximal in radioresistant cells, while the number of  $\gamma$ H2AX foci may be lower than the total number of DSB induced in radiosensitive cells, notably in those eliciting a delayed RANS [38,39,42].

### 2.5. Statistical Analysis

Statistical significance between data points was verified with the one-way ANOVA test. Statistical analysis was performed by using Kaleidagraph v4 (Synergy Software, Reading, PA, USA).

## 3. Results

### 3.1. Radioprotective Effect of the Antioxidative N-Acetylcysteine (NAC)

Before irradiation, while NAC did not significantly impact the number of spontaneous  $\gamma$ H2AX foci in radioresistant controls below 150 mM, the NAC pretreatment decreased the number of  $\gamma$ H2AX foci in all the radiosensitive fibroblasts tested ( $p < 0.001$ ,  $p < 0.01$  and  $p < 0.05$  for the 09CLB, 11CLB and 15 CLB fibroblasts, respectively) (Figure 2A). Interestingly, the effect of NAC on radiosensitive cells fitted well with a sigmoidal curve (all the correlation coefficients'  $r$  were found higher than 0.8) that converged to an average minimal value of  $0.3 \pm 0.1$   $\gamma$ H2AX foci per cell ( $0.1 \pm 0.1$   $\gamma$ H2AX foci per cell for the radioresistant controls,  $p < 0.05$ ). These findings suggest that millimolar concentrations of NAC may decrease the number of spontaneous DSB (Figure 2A).

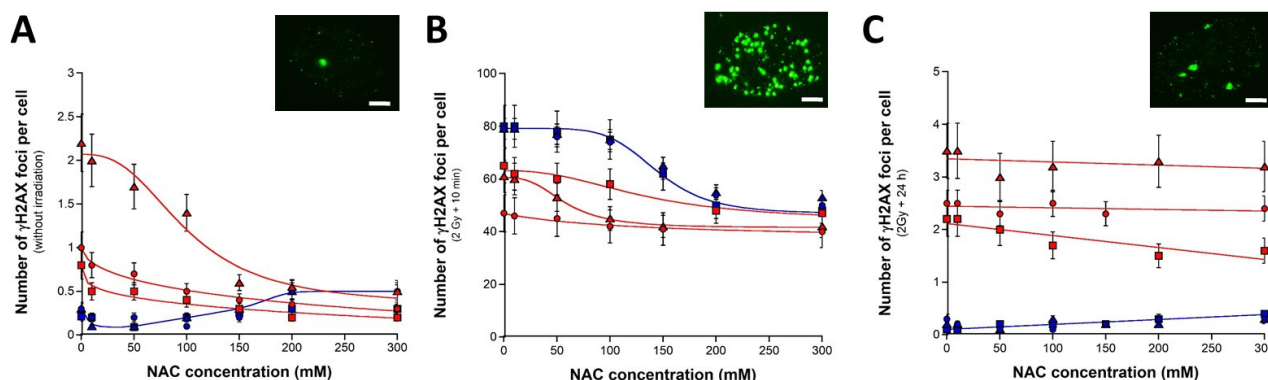


**Figure 2.** Radioprotective effect of a pretreatment with NAC. Number of  $\gamma$ H2AX foci per cell in the human untransformed radioresistant AG1521 (blue squares), 1BR3 (blue triangles) and 149BR (blue circles) fibroblasts in the radiosensitive 09CLB (red triangles), 11CLB (red squares) and 15CLB (red circles) fibroblasts after pretreatment with NAC (A), followed by 2 Gy X-rays and 10 min (B) or 24 h (C) incubation. Each point represents the mean  $\pm$  standard error (SEM) of at least three replicates. Sigmoidal or linear functions were used for data fitting. Inserts show representative examples of 300 mM pretreated 09CLB nuclei with  $\gamma$ H2AX foci assessed at the indicated conditions. White bar represents 5  $\mu$ m.

When the number of  $\gamma$ H2AX foci was assessed 10 min post irradiation, the untreated radioresistant controls showed an average of  $79.5 \pm 1.5$   $\gamma$ H2AX foci per cell, in agreement with the literature data and with a DSB induction rate of  $37 \pm 4$   $\gamma$ H2AX foci per Gy per cell ( $p > 0.8$ ) [45] (Figure 2B). After NAC pretreatment, the number of  $\gamma$ H2AX foci assessed 10 min post irradiation was shown to decrease significantly by obeying a sigmoidal function of the NAC concentration in all the radioresistant controls. In these cases, all the correlation coefficients'  $r$  were found higher than 0.9, and the lowest average value corresponded to



$50.3 \pm 1.5$   $\gamma$ H2AX foci. The radiosensitive fibroblasts showed a significantly lower number of  $\gamma$ H2AX foci without NAC pretreatment than radioresistant controls ( $p < 0.01$ ), according to previous data [39]. The NAC pretreatment led to decrease the number of  $\gamma$ H2AX foci assessed 10 min post irradiation, suggesting that millimolar concentration of NAC may significantly decrease the number of DSB induced by IR and recognized by NHEJ. However, the lowest average number of  $\gamma$ H2AX foci reached with radiosensitive cells was not found significantly different from that reached by radioresistant controls ( $p > 0.1$ ) (Figure 2B).

Finally, the number of  $\gamma$ H2AX foci assessed 24 h post irradiation was examined. As previously reported, the numbers of  $\gamma$ H2AX foci assessed 24 h post irradiation were found not significantly different from zero in the untreated radioresistant controls ( $p > 0.5$ ) (Figure 2C). The NAC pretreatment did not significantly change these values ( $p > 0.3$ ). Interestingly, this last conclusion was also reached with the 09CLB and 15CLB radiosensitive fibroblasts ( $p > 0.3$ ), even if the  $\gamma$ H2AX foci values were significantly higher than those found with the radioresistant controls ( $p < 0.01$ ). In the radiosensitive 11CLB fibroblasts, the NAC pretreatment was found to decrease significantly the number of  $\gamma$ H2AX foci assessed 24 h post irradiation ( $p < 0.01$ ) (Figure 2C). Altogether, these data suggest that the NAC pretreatment may produce a significant radioprotective effect on spontaneous DSB, as well as on a subset of recognized DSB (Figure 2).

### 3.2. Radioprotective Effect of the Antioxidative Amifostine (Ethyol)

Fibroblasts were pretreated to 24–96 mM amifostine for 24 h and irradiated thereafter. Despite a systematic decrease with concentration, the amifostine pretreatment did not significantly impact the number of spontaneous  $\gamma$ H2AX foci in the radioresistant controls ( $p > 0.2$ ) (Figure 3A). Conversely, in the radiosensitive fibroblasts, the amifostine pretreatment resulted in a significant decrease in the number of spontaneous  $\gamma$ H2AX foci that obeyed a decreasing exponential function of the amifostine concentration for the 09CLB cells ( $r = 0.9$ ) and a sigmoidal function for the two other radiosensitive cell lines tested ( $r = 0.8$ ) for both. These findings suggest that millimolar concentrations of amifostine may decrease the number of spontaneous DSB recognized by NHEJ in radiosensitive cells (Figure 3A).

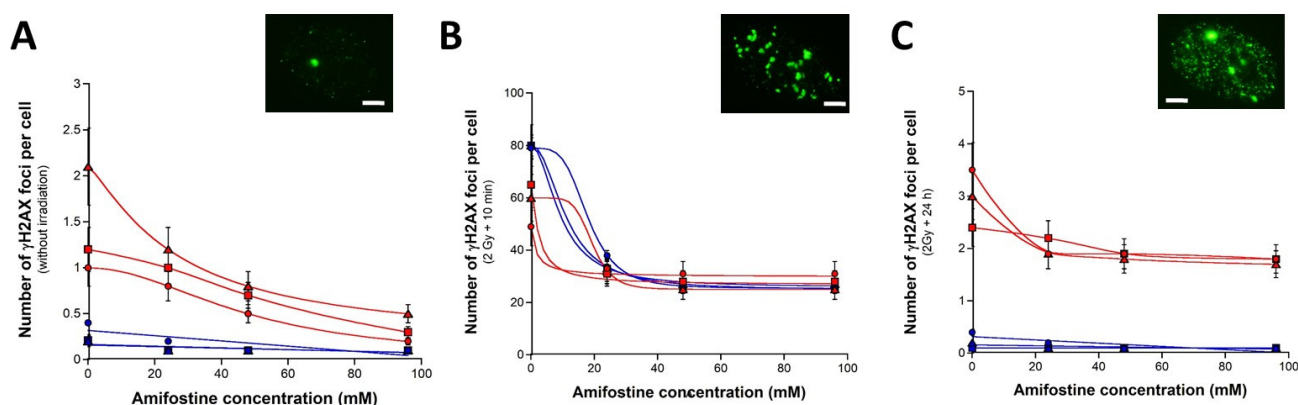


**Figure 3.** Radioprotective effect of a pretreatment with amifostine. Number of  $\gamma$ H2AX foci per cell in the human untransformed radioresistant AG1521 (blue squares), 1BR3 (blue triangles) and 149BR (blue circles) fibroblasts and in the radiosensitive 09CLB (red triangles), 11CLB (red squares) and 15CLB (red circles) fibroblasts after pretreatment with amifostine (A), followed by 2 Gy X-rays and 10 min (B) or 24 h (C) incubation. Each point represents the mean  $\pm$  standard error (SEM) of at least three replicates. Exponential, sigmoidal or linear functions were used for data fitting. Inserts show representative examples of 96 mM pretreated 09CLB nuclei with  $\gamma$ H2AX foci assessed at the indicated conditions. White bar represents 5  $\mu$ m.

The number of  $\gamma$ H2AX foci assessed 10 min post irradiation was shown to decrease significantly by obeying a sigmoidal function of the amifostine concentration in all the



fibroblasts tested (all the correlation coefficients'  $r$  were found higher than 0.8) (Figure 3B). The lowest  $\gamma$ H2AX foci reached 96 mM amifostine and corresponded to an average of  $26 \pm 0.5$  and  $28 \pm 2$   $\gamma$ H2AX foci per cell for the radioresistant and radiosensitive cells, respectively ( $p > 0.4$ ). Interestingly, this value was found significantly lower than that obtained with the NAC pretreatment ( $p < 0.001$ ). These findings support that amifostine results in significantly decreasing the number of DSB induced by IR and recognized by NHEJ (Figure 3B).

Lastly, the amifostine pretreatment did not significantly change the number of  $\gamma$ H2AX foci assessed 24 h post irradiation in the radioresistant controls ( $p > 0.5$ ) (Figure 3C). Conversely, the amifostine pretreatment led to a significant decrease in the number of  $\gamma$ H2AX foci in the 09CLB and 15CLB radiosensitive cell lines ( $p < 0.04$ ) from 26 mM and in the 11CLB cell lines ( $p < 0.05$ ) at 96 mM amifostine (Figure 3C). In these conditions, the action of amifostine was found more efficient for the three radiosensitive cell lines tested than with NAC ( $p < 0.03$ ). Altogether, these data suggest that amifostine pretreatment provides a radioprotective effect on spontaneous DSB, a reduction in the number of DSB recognized by NHEJ in a larger extent than with NAC pretreatment and a significant reduction in the remaining unrepaired DSB (Figure 3).

### 3.3. Radioprotective Effect of the Pro-Episkevic Drugs Zoledronate and Pravastatin

The findings described above showed that the pretreatment with NAC or amifostine antioxidative agents consisted in decreasing the number of  $\gamma$ H2AX foci, likely because they contribute to reduce the ROS and therefore the number of DSB induced by IR in general. Such reduction is likely to be performed chemically, i.e., independently of any DSB repair and signaling pathway recognizing the DSB induced by IR. Conversely, pro-episkevic drugs such as zoledronate and pravastatin accelerate the RIANS and therefore increase the number of DSB recognized by NHEJ [34]. Hence, as far as the  $\gamma$ H2AX foci reflect the DSB managed by NHEJ, we can expect an increase in the number of DSB recognized by NHEJ (i.e., early  $\gamma$ H2AX foci), while the number of DSB "physically" induced by IR should remain constant.

The fibroblasts were pretreated to zoledronate and pravastatin separately, as well as with the combination of both drugs (ZOPRA). In the radioresistant controls pretreated with zoledronate and pravastatin separately or concomitantly, the number of  $\gamma$ H2AX foci assessed before irradiation was found to be significantly lower than that observed in the non-pre-treated cells ( $p < 0.03$ ) (Figure 4A). The same value was reached whether cells were pretreated with zoledronate or pravastatin, taken separately or with ZOPRA ( $p > 0.8$ ). The extent of such a decrease is the same as that found with the pretreatment with amifostine ( $p > 0.1$ ). In radiosensitive cells, the picture changed, since more DSB recognized by NHEJ are expected:  $0.5 \pm 0.1$   $\gamma$ H2AX foci vs.  $0.3 \pm 0.1$   $\gamma$ H2AX foci per cell were found on average with the pro-episkevic drugs and the antioxidative drugs, respectively ( $p < 0.01$ ). Altogether, these data suggest that zoledronate, pravastatin and ZOPRA may significantly reduce the number of spontaneous DSB but not to the same extent as antioxidative agents such as NAC or amifostine (Figure 4A).

In the radioresistant controls, the pretreatment of cells with zoledronate and pravastatin, separately and ZOPRA, has no significant effect on the number of  $\gamma$ H2AX foci assessed 10 min post irradiation ( $p > 0.8$ ), in agreement with the hypothesis that all the RI DSB are recognized by NHEJ in radioresistant cells (Figure 4B). Conversely, in the radiosensitive fibroblasts, the number of  $\gamma$ H2AX foci assessed 10 min post irradiation increased with the pro-episkevic drugs pretreatment (by comparison with the untreated conditions), but this tendency was not significant ( $p < 0.08$ ). The ZOPRA combination provided the largest increase by reaching the values of the radioresistant controls for the 09CLB and 11CLB cell lines. Such a tendency was drastically different from the reduction in the number of  $\gamma$ H2AX foci assessed 10 min post irradiation observed with antioxidative agents, ( $p > 0.5$  with NAC and  $p > 0.8$  with amifostine). These findings suggested that the pro-episkevic drugs increase the number of DSB recognized by NHEJ among the DSB physically induced



by IR, while the antioxidative drugs decrease the number of all the DSB physically induced by IR (Figure 4B).

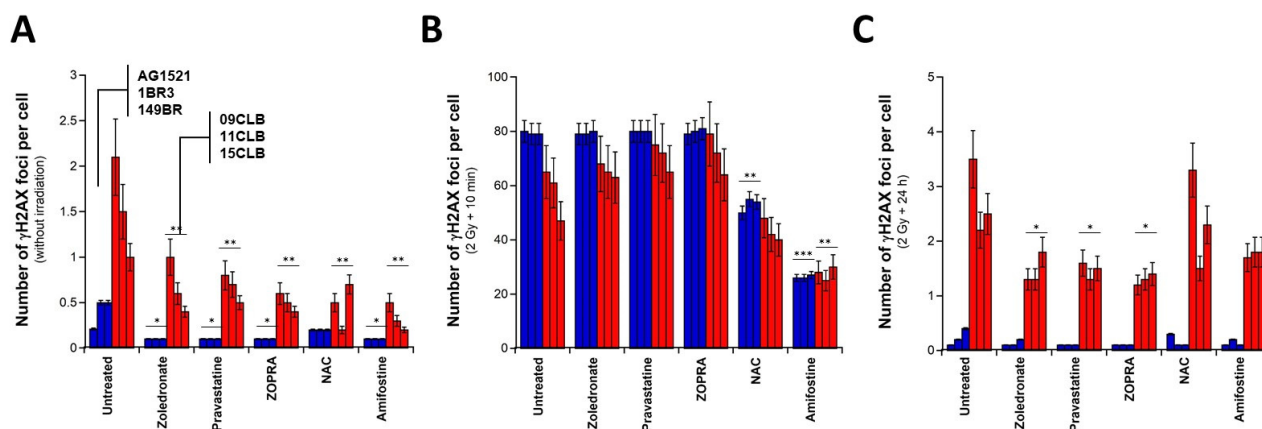


**Figure 4.** Radioprotective effect of a pretreatment with zoledronate, pravastatine and ZOPRA. Number of  $\gamma$ H2AX foci per cell assessed in the indicated pretreatment and after the indicated pretreatment (A), followed by 2 Gy X-rays and 10 min (B) or 24 h (C) incubation. Each bar represents the mean  $\pm$  standard error (SEM) of at least three replicates. The NAC and amifostine data are those already shown in Figures 3 and 4 with pretreatment of 300 mM NAC and 96 mM amifostine. one, two and three asterisks indicate  $p < 0.05$ ,  $p < 0.01$  and  $p < 0.001$ , respectively, by comparison with untreated controls.

By comparing it with data from untreated cells, the number of  $\gamma$ H2AX foci assessed 24 h post irradiation in radioresistant controls did not change when pretreated with the pro-episkevic drugs, whether the drugs were applied separately or concomitantly ( $p > 0.8$ ). By contrast, in radiosensitive cells, the number of  $\gamma$ H2AX foci assessed 24 h post irradiation decreased significantly with pro-episkevic drugs ( $p < 0.03$  with NAC and  $p < 0.04$  with amifostine) and reached its lowest values with ZOPRA pretreatment (Figure 4C).

To better illustrate such differences, the percentage of  $\gamma$ H2AX foci remaining at 24 h post irradiation was calculated by dividing the number of  $\gamma$ H2AX foci assessed 24 h post irradiation by the number of  $\gamma$ H2AX foci assessed 10 min post irradiation. The resulting percentage was found to be the lowest with the ZOPRA pretreatment and the highest with the antioxidative drugs. Considering such percentage resulted in increasing the differences between ZOPRA on one hand and NAC and amifostine on the other hand ( $p < 0.001$ ). These findings suggested that, even if NAC and amifostine may reduce the DSB physically induced by IR, they do not reduce the severity of the DSB remaining (Figure 5). Let us recall again that  $\gamma$ H2AX foci represent the DSB recognized by the ATM-dependent NHEJ pathway [34], that the pro-episkevic drugs act on the NHEJ pathway specifically and that the antioxidative agents act on all the DSB, whatever the pathway involved.

### 3.4. Influence of the ATM Protein in the Antioxidative and Pro-Episkevic Approaches

In the frame of the RIANS model, the cytoplasmic ATM monomers diffuse to the nucleus and contribute to the recognition of DSB via NHEJ by phosphorylating H2AX molecules at the DSB sites [34]. Once the recognition and DSB repair steps are completed, the ATM monomers reassociate via a trans-autophosphorylation responsible of the formation of pATM foci [38,39]. We therefore examined the different action of the antioxidative NAC and amifostine and the pro-episkevic ZOPRA pretreatments by using pATM immunofluorescence. No spontaneous pATM focus was observed, whatever the conditions (data not shown). By contrast, the number of pATM foci assessed 10 min post irradiation reached similar conclusions as that with  $\gamma$ H2AX foci, with the lowest values obtained with the pretreatment with the antioxidative drugs and the highest values with the pretreatment with ZOPRA (Figure 6A). The 24 h data reached similar conclusions as those reached with



$\gamma$ H2AX data, with a nearly complete absence of pATM foci in ZOPRA pretreated cells ( $p < 0.001$  by comparison with untreated conditions) and lower reduction with NAC and amifostine pretreatment ( $p < 0.04$  by comparison with untreated conditions) (Figure 6B).

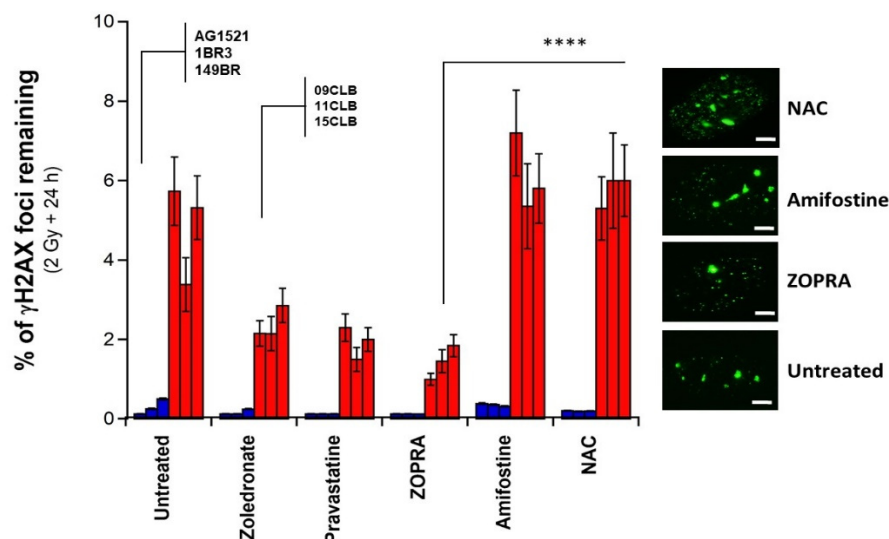


**Figure 5.** Relative radioprotective effect of a pretreatment with zoledronate, pravastatine, ZOPRA, NAC and amifostine. The data shown in Figure 3C are expressed as percentage of  $\gamma$ H2AX foci remaining, calculated by dividing the number of  $\gamma$ H2AX foci assessed 24 h post irradiation (Figure 4C) by the number of  $\gamma$ H2AX foci assessed 10 min post irradiation (Figure 4B). Inserts show representative examples of untreated and ZOPRA, 300 mM amifostine and 96 mM NAC pretreated 09CLB nuclei with  $\gamma$ H2AX foci assessed at the indicated conditions. White bar represents 5  $\mu$ m. Four asterisks indicate  $p < 0.0001$ , respectively, between ZOPRA data and NAC and amifostine data.

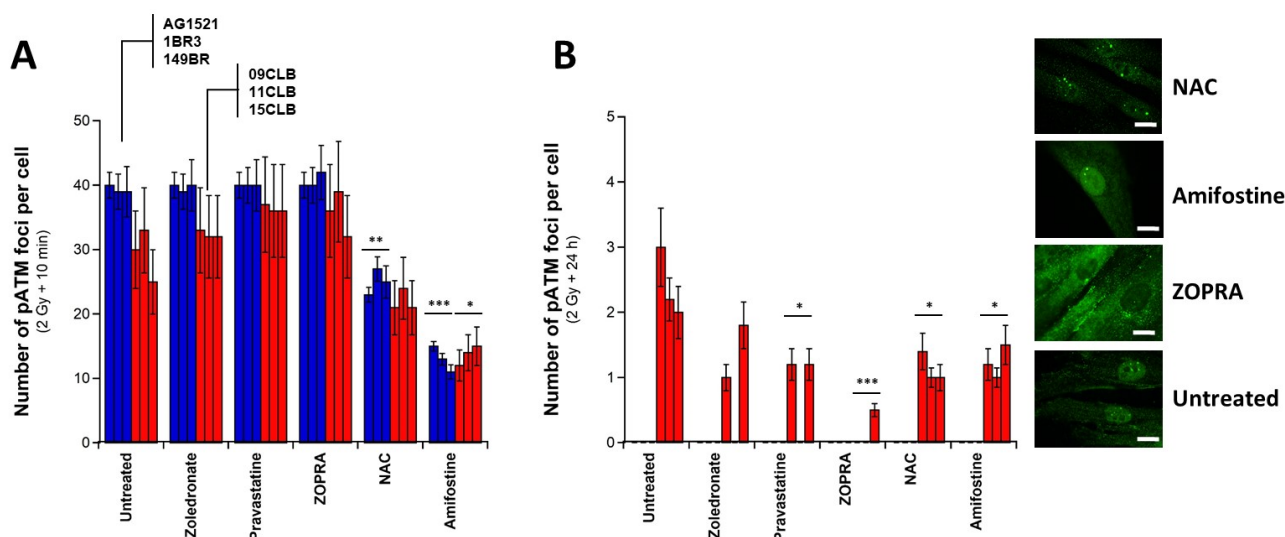


**Figure 6.** Radioprotective effect of a pretreatment with zoledronate, pravastatine and ZOPRA assessed with pATM foci. Number of pATM foci per cell assessed in the indicated pretreatment and after the indicated pretreatment, followed by 2 Gy X-rays and 10 min (A) or 24 h (B) incubation. Each point represents the mean  $\pm$  standard error (SEM) of at least three replicates. Inserts show representative examples of untreated and ZOPRA, 300 mM amifostine and 96 mM NAC pretreated 09CLB nuclei with pATM foci assessed at 24 h post irradiation at the indicated conditions. White bar represents 10  $\mu$ m. one, two and three asterisks indicate  $p < 0.05$ ,  $p < 0.01$  and  $p < 0.001$ , respectively, by comparison with the untreated controls.



### 3.5. Review of the Radioprotective Action of the Pro-Episkevic ZOPRA Combinations

Since 2008, our research group has endeavored to document the major radiobiological features of genetic syndromes associated with radiosensitivity [43]. For the first time, by focusing on the pATM data only, we gathered the data involving ZOPRA pretreatment in 10 diseases, namely Usher's syndrome (USH) [41], PROS syndrome (PROS) [49], McCune-Albright syndrome (MAC) [33], retinoblastoma (RB) [50], Tuberous Sclerosis Complex syndrome (TSC) [32], Huntington Disease (HD) [40], Xeroderma Pigmentosum D (XPD) [48], Neurofibromatosis 1 (NF1) [31], LIG4 syndrome (LIG4) [51] and ataxia telangiectasia (AT) [52]. When the numbers of pATM foci assessed at 10 min post irradiation with and without ZOPRA pretreatment were plotted together, a sigmoidal function appeared, indicating that there is no significant ZOPRA protective effect for cells eliciting fewer than 10 pATM foci per cell, such as the two ATM-mutated hyper-radiosensitive cell lines (Figure 7). Furthermore, for fibroblasts showing more than 10 but fewer than 25 pATM foci at 10 min post irradiation, the ZOPRA protective effect was found proportional to the number of pATM foci (Figure 7). From 30 pATM up to the maximal 40 pATM foci values, the ZOPRA protective effect reached a plateau ( $p > 0.8$ ) (Figure 7). The sigmoidal function indicated that the maximal ZOPRA effect can add 15 additional recognized DSB to a number of 20 DSB already managed by NHEJ, which corresponds to a relative increase of 75%. Altogether, these findings suggest that ZOPRA cannot correct, on one hand, the hyper-radiosensitive cells with no or nearly absent nuclear ATM kinase activity, and on the other hand, the hyper-radiosensitive LIG4-mutated cells and radioresistant controls that all show a normal ATM kinase activity. Such data therefore support that the ZOPRA pretreatment is particularly adapted to correct moderate but significant radiosensitivity. Additional investigations are needed to identify more efficient pro-episkevic drugs and to ask whatever the combination of antioxidative and pro-episkevic agents may lead to an enhanced protection against IR.

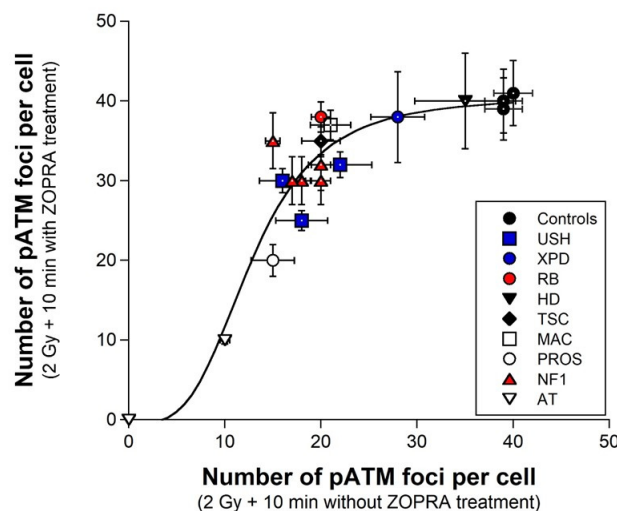


**Figure 7. Radioprotective effect of ZOPRA in fibroblasts from 10 genetic syndromes with pATM foci.** The number of pATM foci assessed at 10 min post irradiation (X-rays) with and without ZOPRA pretreatment were plotted together. Fibroblasts were derived from the indicated syndromes: Usher's syndrome (USH), PROS syndrome (PROS), McCune-Albright syndrome (MAC), retinoblastoma (RB), Tuberous Sclerosis Complex syndrome (TSC), Huntington Disease (HD), Xeroderma Pigmentosum D (XPD), Neurofibromatosis 1 (NF1), LIG4 syndrome (LIG4) and ataxia telangiectasia (AT). Note the AT data are obtained from historical data of the N.F. lab; all these data were published elsewhere [31–33,40,41,48–50]. Each point represents the mean  $\pm$  standard error (SEM) of at least three replicates. Data were fitted to the following sigmoidal function:  $y = 40.53 + (40.10)/(1 + (x/12.797)^{3.51})$ ;  $r = 0.944$ .



## 4. Discussion

### 4.1. Documented Evidence That NAC and Amifostine May Act as Radioprotectors

An exposure to IR triggers the formation of a large spectrum of reactive oxygen and nitrogen species [53]. The natural antioxidative agents produced in cells are mostly related to glutathione (GSH) [54]. However, at high IR dose, the levels of endogenous RI-induced GSH molecules may be not sufficient to provide a significant radioprotective effect: exogenous thiols are required. A plethora of antioxidative thiol compounds have been developed to serve as countermeasures of IR-induced toxicity. Among them, NAC and amifostine appear as the most efficient radioprotectors [2]. NAC has been recommended as mucolytic and against acetaminophen overdose [55,56]. The great majority of radiobiological studies with NAC have been conducted with rats [2,3,24]. However, its radioprotective effect has also been documented in RT trials, notably in non-small-cell lung cancers [27]. For example, the pretreatment with NAC was shown to improve anastomoses and wound healing, to decrease post-irradiation toxicity and show anti-inflammatory effects in the liver, gastrointestinal tract, cochlea, bones and skin [55,56]. NAC has the double advantage of being cheap and to present few side effects. Historically, NAC is one of the simplest molecules proposed in the group of cysteine-containing agents. However, in the present study, the radioprotective effect of NAC was found to be lower than amifostine, the most extensively used radioprotector [2]. The actions of these two drugs have often been compared [24,57,58]. NAC may have two concomitant actions: (1) A reduction effect through which the free SH-groups of NAC break the disulfur R-S-S-R' bridges of different proteins. As indicated above, such hydrolysis is exploited in gastric mucus to provide mucolytic properties [59]. (2) A cysteine production effect through which the deacetylation of NAC produces cysteine required for GSH production [60]. Conversely, amifostine is transformed to an active thiol when dephosphorylated by alkaline phosphatases, which is very abundant in the cellular membranes, to provide an SH group. Its two amine functions and SH permit a high power of chelation of ions, including  $\text{Ca}^{2+}$  ions, particularly produced after exposure to IR [61]. These various action modes of NAC and amifostine may explain some discrepancies in their radioprotective effect, likely due to tissue specificities and differences in experimental protocols. For example, by using clonogenic cell surviving fraction and yields of  $\gamma\text{H2AX}$  foci as endpoints, Kataoka et al. (2007) systematically showed that amifostine was a better radioprotector than NAC in a human endothelial cell line [58]. Conversely, NAC was reported to be a better cytoprotective drug than amifostine in methotrexate-treated hepatic rat tissues [62]. Seker et al. did not find differences between the two drugs in RT-induced uterine tissue injuries in rats [63]. Despite such discrepancies, amifostine remains the only radioprotective agent approved in RT by FDA [2]. In this study, the pretreatment with 96 mM amifostine was found to be more efficient to protect cells against IR injuries than the most efficient concentration of NAC. It is also important to mention that amifostine (WR2721) is the thiophosphate prodrug of an active thiol form (WR1065) that is usually applied in culture medium at lower concentrations and that shows a radioprotective effect earlier than amifostine [2,64]. However, we deliberately chose to apply the drug recommended by the FDA as a 24 h pretreatment, as with the other drugs tested here, to facilitate intercomparisons.

Finally, with regard to the concentrations used, while it must be stressed that the drug concentrations used in ZOPRA treatment correspond to the posology applied in standard antiosteoporosis and anticholesterolemiant treatments [46], the question of translation to clinical use is more complex with regard to antioxidative drugs, even if the concentrations applied here have been extensively used in the literature and even if they currently present few side effects [2].



#### 4.2. Documented Evidence That Statins and Bisphosphonates May Act as Radioprotectors

Pravastatin is currently used as countermeasure of hypercholesterolemia and has showed anti-inflammatory properties associated with the inhibition of Rho and Rho-associated kinases involved in a number of RI tissue injuries [65]. Pravastatin is known as an inhibitor of 3-hydroxy-3-methyl-glutaryl-coenzyme A reductase (HMG-coA). However, although such property may explain its anticholesterolemic action, the molecular mechanisms at the origin of its radioprotective effect remain unknown, inasmuch as some adverse side effects have been reported when statins are applied for a long period [66]. Some authors have suggested that statins may accelerate the DSB repair and can also increase the expression of some DNA repair proteins [67,68]. However, statins may induce ROS and some toxicities [69], so that they may be associated with antioxidative drugs. While its protective action in prostate cancer patients becomes more and more documented, no mechanistic model of the action of statins is still consensual [68].

In parallel, bisphosphonates in general, and zoledronate in particular, are currently used in treatment of osteoporosis and of cancer linked to hypercalcemia [70]. Bisphosphonates were shown to reduce skeletal events, notably pain, in the treatment against bone metastasis [71]. Bisphosphonates have the property to bind to exposed calcium areas and to cause apoptosis in osteoclasts [72]. Hence, like statins, while the molecular action of bisphosphonates is well-documented as a hypercalcemia countermeasure, no mechanistic model still explains its action in radioprotection.

A combined action of statins and aminobisphosphonates leads to the inhibition of both farnesylation and geranylgeranylation of progerin and prelamin A proteins, which are notably found cumulated in the nuclear membrane of progeroid cells [46]. Interestingly, these two drugs lead to increase the permeability of membranes, particularly those of mitochondria. With regard to statins, it is well known that cholesterol influences the organization of the membranes' structure by inducing conformational ordering of the lipid chains: an anticholesterolemic action may therefore impact the lipid layers' permeability [73]. With regard to bisphosphonates, their impact on  $\text{Ca}^{2+}$  ions strongly suggests an important role in the regulation of the pores of the nuclear membranes [74]. Hence, to better document the radioprotective actions of each pro-episkevic drug alone and to compare them with the action of each antioxidative drug tested, it was useful to evaluate both applications of these drugs (i.e., alone or in association). Altogether, the literature and our data suggest that there is a body of evidence that a combination of statins and bisphosphonates would act on the protein trafficking between cytoplasm and nucleus. However, what is the link between such nucleoshuttling and radioprotection?

#### 4.3. Toward a Unified Model for Chemical Radioprotection?

As evoked in the Introduction, the RIANS model is based on the occurrence of some important molecular steps [34]:

- DSB and ATM monomers induction: Immediately after irradiation, cytoplasmic ATM dimers dissociate in ATM monomers in a linearly dose-dependent manner; in parallel, in the nucleus, the RI DNA damage, and notably, the RI DSB, are induced in a dose-dependent manner as well [38]. During this step, the antioxidative approach leads to reduce the ROS in both cytoplasm and nucleus. Hence, the antioxidative approach would result in the decrease in the number of both RI-induced ATM monomers and DSB. This action should equally affect the DSB recognized by NHEJ and those recognized by any other pathways or even DSB that are not recognized at all. As a result, the number of early  $\gamma\text{H2AX}$  foci decreases [31–33,40,41,48–50]. In the case of normal-RIANS quiescent cells, all the DSB are recognized by NHEJ: the number of  $\gamma\text{H2AX}$  foci corresponds to the DSB physically induced by IR. Hence, the radioprotective effect of any antioxidative drug can be easily quantified on radioresistant controls. Conversely, in the case of delayed-RIANS quiescent cells, the difference between the number of DSB physically induced (about 40 per Gy) and the number of DSB recognized by NHEJ reflected by the  $\gamma\text{H2AX}$  foci corresponds to the number of



the DSB non-recognized by NHEJ or recognized by other pathways than NHEJ. At this step, the pro-episkevic drugs may not significantly impact the process.

- ATM monomers diffusion and DSB recognition: The RI ATM monomers diffuse in the nucleus. The pro-episkevic approach may result in accelerating and facilitating the diffusion of ATM monomers in the nucleus. Consequently, the number of pATM monomers that diffuse in the nucleus increases [31–33,40,41,48–50]. In the normal-RIANS quiescent cells, the number of ATM monomers available is sufficient to recognize all the DSB physically induced: no effect is observed. Conversely, in the delayed-RIANS quiescent cells, a larger number of ATM monomers contributes to recognize some additional DSB that are not recognized at all or that are recognized by other pathways than NHEJ. Hence, the number of  $\gamma$ H2AX foci increases [31–33,40,41,48–50].
- DSB repair: In the case of the normal-RIANS quiescent cells, the pro-episkevic approach has no significant effect, while the antioxidative approach that leads to decrease the number of DSB does not reduce the proportion of unrepairable DSB. In the case of delayed-RIANS quiescent cells, the pro-episkevic approach contributes to increase the subset of DSB repaired by NHEJ, which decreases the RI lethal effect, while the antioxidative approach is not efficient enough to make the unrepaired DSB disappear.

The linear–quadratic (LQ) model is an empirical formula that links the cell survival to the IR dose. Since the 1970s, such a formula has been extensively used by radiobiologists and radiation oncologists to describe the individual response to IR [75]. The LQ model describes the clonogenic cell survival  $S$  as a function of dose  $D$  as follows:

$$S = e^{-(\alpha D + \beta D^2)} \quad (1)$$

in which  $\alpha$  and  $\beta$  are adjustable parameters to be determined [75].

In 2016, the RIANS model provided a coherent interpretation of the two LQ parameters,  $\alpha$  and  $\beta$ , by defining two types of RI and lethal DSB [38]: (1) The  $\alpha$ -type DSB that are recognized by the ATM monomers in nucleus and therefore by NHEJ early after irradiation. Their number was demonstrated to be proportional to the dose [38]. (2) The  $\beta$ -type DSB that are not recognized by the ATM monomers in the nucleus (therefore not managed by NHEJ) because of a delay or an absence of the RIANS. Their number was demonstrated to be proportional to the square of the dose. It is noteworthy that the total number of DSB induced by IR (whatever their type,  $\alpha$  or  $\beta$ ) remains proportional to the dose [38]. A certain proportion of  $\alpha$ - and  $\beta$ -type DSB may remain unrepairable and participate in the RI lethal effect. However, only the  $\alpha$ -type DSB are detectable by  $\gamma$ H2AX and pATM immunofluorescence. Hence, from the hypotheses developed above, the antioxidative approach results in the reduction in the number of DSB induced, whatever their type,  $\alpha$  or  $\beta$ , while the pro-episkevic approach tends to transform the  $\beta$ -type DSB into  $\alpha$ -type DSB (Figure 8). In other terms, the antioxidative approach may not change the mutation rate induced by IR, while the pro-episkevic approach may decrease it. Additional investigations are needed to verify such hypotheses.



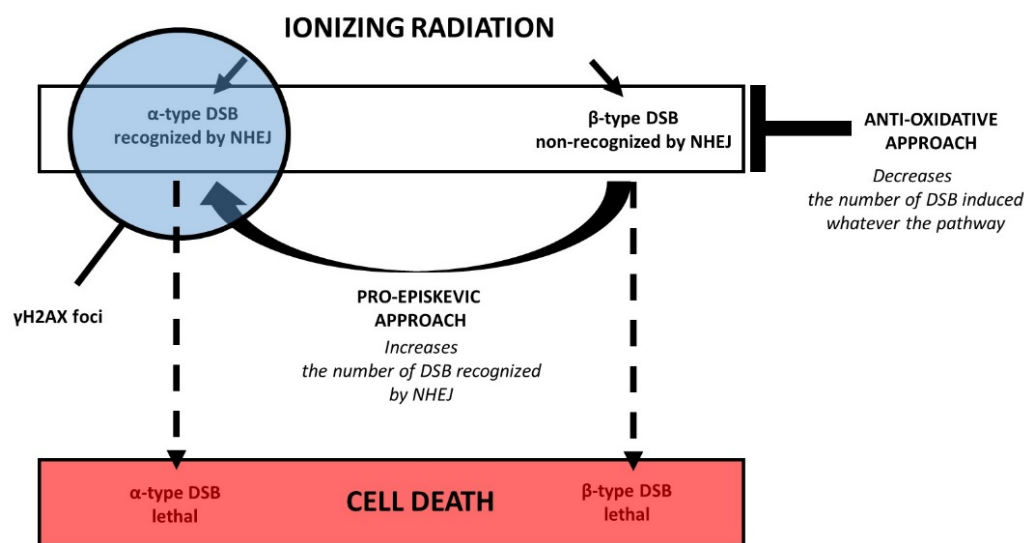


**Figure 8.** Schematic view of the molecular and cellular consequences of an exposure to IR inducing two types of DSB. The  $\alpha$ -type DSB are recognized by the NHEJ DSB repair pathway, while the  $\beta$ -type DSB are not [38]. For each type of DSB, there are some subsets of unrepaired DSB [38]. Among them, some may be unrepairable and participate in the lethal effect. The  $\gamma$ H2AX foci reveal the  $\alpha$ -type DSB only. The antioxidative approach consists in reducing the number of DSB involved by IR, independently of the DSB repair pathways involved in their recognition. The pro-episkevic approach consists in increasing the number of DSB recognized by NHEJ by accelerating and facilitating the RIANs and therefore by stimulating the efficiency of NHEJ.

## 5. Conclusions

In this study, we aimed to investigate and compare the molecular features of two different approaches of radioprotection. These investigations were performed, as a first step, with quiescent human fibroblasts and in standard conditions of a current RT session. Altogether, our findings suggest the following:

- The radiation protection strategy has long been based on an *antioxidative approach* consisting in reducing the oxidation process of the RI water radiolysis through an efficient reduction in ROS:
  - o The number of DSB induced by IR decreases significantly;
  - o Our findings confirm the efficiency of amifostine as one of the most efficient antioxidative drugs.
- The *pro-episkevic approach*, directly deriving from the RIANs model, aims at stimulating repair and contributes to increase the number of DSB managed by NHEJ—the most predominant DSB repair and signaling pathway in mammals:
  - o The combination of pravastatin and zoledronate (ZOPRA) shows a significant pro-episkevic property that appears to be more efficient than amifostine;
  - o In the case of genetic syndromes associated with the loss of function of some genes essential for DSB repair, the effect of ZOPRA appears to be limited.

Additional investigations are needed to develop some new drugs that may elicit both antioxidative and pro-episkevic properties and to quantify the radiation protection action of both types of drugs applied together, whether on quiescent or proliferating cells. The question of the innocuity of long-term treatments should also be examined.

**Author Contributions:** Conceptualization, J.R.-V., P.P., M.L.F. and N.F.; data acquisition and methodology, P.P., M.L.F., A.G., L.S., J.A.-C. and L.E.N.; validation and data analysis, M.D., M.B. and N.F.; writing—original draft preparation, N.F.; writing, reviewing and editing, M.D., S.F., M.B. and N.F.; project administration and funding acquisition, N.F. All authors have read and agreed to the published version of the manuscript.



**Funding:** This work was supported by the Commissariat General à l'Investissement (Programmes Investissement d'Avenir (INDIRA Project)) and the Centre National d'Etudes Spatiales (ICARE Project).

**Institutional Review Board Statement:** As already mentioned in Materials and Methods, this study was performed with human fibroblast cell lines that belong to the COPERNIC collection of the lab that was approved by the regional Ethical Committee. Cell lines were declared under the numbers DC2008-585, DC2011-1437 and DC2021-3957 to the Ministry of Research.

**Informed Consent Statement:** All the anonymous donors of the COPERNIC collection evoked above were informed and signed consent according to the ethics and regulatory recommendations, notably for their consent to participate and for publication of anonymous data.

**Data Availability Statement:** All the data can be provided on reasonable request.

**Conflicts of Interest:** The authors declare no conflict of interest. The opinions or assertions contained herein are the private views of the authors and are not necessarily those of the French Ministry of Defense.

## References

- Foray, N.; Bourguignon, M.; Hamada, N. Individual response to ionizing radiation. *Mutat. Res. Rev.* **2016**, *770*, 369–386. [\[CrossRef\]](#) [\[PubMed\]](#)
- Weiss, J.F.; Landauer, M.R. History and development of radiation-protective agents. *Int. J. Radiat. Biol.* **2009**, *85*, 539–573. [\[CrossRef\]](#) [\[PubMed\]](#)
- Citrin, D.; Cotrim, A.P.; Hyodo, F.; Baum, B.J.; Krishna, M.C.; Mitchell, J.B. Radioprotectors and mitigators of radiation-induced normal tissue injury. *Oncologist* **2010**, *15*, 360–371. [\[CrossRef\]](#) [\[PubMed\]](#)
- Mönig, H.; Messerschmidt, O.; Streffer, C. Chemical radioprotection in mammals and in man. In *Radiation Exposure and Occupational Risks*; Scherer, E., Streffer, C., Trott, K.R., Eds.; Springer: Berlin, Germany, 1990; pp. 97–143.
- Lacassagne, A. Chute de la sensibilité aux rayons X chez la souris nouveau-née en état d'asphyxie. *C. R. L'académie Des. Sci.* **1942**, *616*, 231–232.
- Akerfeldt, S. Preparation and determination of sodium hydrogen S-(2-aminoethyl)-phosphorothioate. *Acta Chem. Scand.* **1959**, *13*, 1479–1480. [\[CrossRef\]](#)
- Sweeney, T.R. *A Survey of Compounds from the Antiradiation Drug Development Program of the US Army Medical Research and Development Command*; Walter Reed Army Institute of Research: Washington, DC, USA, 1979.
- Walker, R.I. Requirements of radioprotectors for military and emergency needs. *Pharmacol. Ther.* **1988**, *39*, 13–20. [\[CrossRef\]](#)
- Restier-Verlet, J.; El-Nachef, L.; Ferlazzo, M.L.; Al-Choboq, J.; Granzotto, A.; Bouchet, A.; Foray, N. Radiation on Earth or in Space: What Does It Change? *Int. J. Mol. Sci.* **2021**, *22*, 3739. [\[CrossRef\]](#)
- Nair, C.K.; Parida, D.K.; Nomura, T. Radioprotectors in radiotherapy. *J. Radiat. Res.* **2001**, *42*, 21–37. [\[CrossRef\]](#)
- Weiss, J.F. Pharmacologic approaches to protection against radiation-induced lethality and other damage. *Environ. Health Perspect.* **1997**, *105* (Suppl. 6), 1473–1478. [\[CrossRef\]](#)
- Vachon, A.; Roman, V.; Lecomte, C.; Folcher, G.; Fatome, M.; Braquet, P.; Berleur, F. A radioprotector: Cysteamine, inhibits oxygen transport in lipidic membranes. *Int. J. Radiat. Biol. Relat. Stud. Phys. Chem. Med.* **1987**, *52*, 847–852. [\[CrossRef\]](#)
- Deschavanne, P.J.; Midander, J.; Debieu, D.; Malaise, E.P.; Revesz, L. Radioprotective effect of cysteamine in glutathione synthetase-deficient cells. *Int. J. Radiat. Biol. Relat. Stud. Phys. Chem. Med.* **1986**, *49*, 85–101. [\[CrossRef\]](#) [\[PubMed\]](#)
- Lespinasse, F.; Oiry, J.; Fatome, M.; Ardouin, P.; Imbach, J.; Malaise, E.P.; Guichard, M. Radioprotection of EMT6 tumor by a new class of radioprotectors based on a pseudo-peptide cysteamine combination. *Int. J. Radiat. Oncol. Biol. Phys.* **1985**, *11*, 1035–1038. [\[CrossRef\]](#) [\[PubMed\]](#)
- Bansal, A.; Simon, M.C. Glutathione metabolism in cancer progression and treatment resistance. *J. Cell Biol.* **2018**, *217*, 2291–2298. [\[CrossRef\]](#) [\[PubMed\]](#)
- Jadhav, G.K.; Bhanumathi, P.; Devi, P.U.; Seetharamaiah, T.; Vidyasagar, M.S.; Rao, K.K.; Hospet, C.S.; Solomon, J.G. Possible role of glutathione in predicting radiotherapy response of cervix cancer. *Int. J. Radiat. Oncol. Biol. Phys.* **1998**, *41*, 3–5. [\[CrossRef\]](#)
- Utley, J.F.; Phillips, T.L.; Kane, L.J. Protection of normal tissues by WR2721 during fractionated irradiation. *Int. J. Radiat. Oncol. Biol. Phys.* **1976**, *1*, 699–703. [\[CrossRef\]](#)
- Wadler, S.; Haynes, H.; Beitler, J.J.; Goldberg, G.; Holland, J.F.; Hochster, H.; Bruckner, H.; Mandeli, J.; Smith, H.; Runowicz, C. Management of hypocalcemic effects of WR2721 administered on a daily times five schedule with cisplatin and radiation therapy. The New York Gynecologic Oncology Group. *J. Clin. Oncol. Off. J. Am. Soc. Clin. Oncol.* **1993**, *11*, 1517–1522. [\[CrossRef\]](#)
- Treskes, M.; Boven, E.; van de Loosdrecht, A.A.; Wijffels, J.F.; Cloos, J.; Peters, G.J.; Pinedo, H.M.; van der Vijgh, W.J. Effects of the modulating agent WR2721 on myelotoxicity and antitumour activity in carboplatin-treated mice. *Eur. J. Cancer* **1994**, *30*, 183–187. [\[CrossRef\]](#) [\[PubMed\]](#)
- Wynn, R.B.; Mehta, V. Reduction of treatment breaks and radiation-induced esophagitis and pneumonitis using amifostine in unresectable non-small cell lung cancer patients receiving definitive concurrent chemotherapy and radiation therapy: A prospective community-based clinical trial. *Semin. Oncol.* **2005**, *32*, S99–S104. [\[CrossRef\]](#)



21. King, M.; Joseph, S.; Albert, A.; Thomas, T.V.; Nittala, M.R.; Woods, W.C.; Vijayakumar, S.; Packianathan, S. Use of Amifostine for Cytoprotection during Radiation Therapy: A Review. *Oncology* **2020**, *98*, 61–80. [\[CrossRef\]](#)
22. Seed, T.M.; Inal, C.E.; Singh, V.K. Radioprotection of hematopoietic progenitors by low dose amifostine prophylaxis. *Int. J. Radiat. Biol.* **2014**, *90*, 594–604. [\[CrossRef\]](#)
23. Singh, V.K.; Seed, T.M. The efficacy and safety of amifostine for the acute radiation syndrome. *Expert Opin. Drug Saf.* **2019**, *18*, 1077–1090. [\[CrossRef\]](#) [\[PubMed\]](#)
24. Demirel, C.; Kilciksiz, S.; Ay, O.I.; Gurgul, S.; Ay, M.E.; Erdal, N. Effect of N-acetylcysteine on radiation-induced genotoxicity and cytotoxicity in rat bone marrow. *J. Radiat. Res.* **2009**, *50*, 43–50. [\[CrossRef\]](#) [\[PubMed\]](#)
25. Samuni, Y.; Goldstein, S.; Dean, O.M.; Berk, M. The chemistry and biological activities of N-acetylcysteine. *Biochim. Biophys. Acta* **2013**, *1830*, 4117–4129. [\[CrossRef\]](#)
26. Barlaz Us, S.; Vezir, O.; Yildirim, M.; Bayrak, G.; Yalin, S.; Balli, E.; Yalin, A.E.; Comelekoglu, U. Protective effect of N-acetyl cysteine against radiotherapy-induced cardiac damage. *Int. J. Radiat. Biol.* **2020**, *96*, 661–670. [\[CrossRef\]](#)
27. Maasilta, P.; Holsti, L.R.; Blomqvist, P.; Kivisaari, L.; Mattson, K. N-acetylcysteine in combination with radiotherapy in the treatment of non-small cell lung cancer: A feasibility study. *Radiother. Oncol. J. Eur. Soc. Ther. Radiol. Oncol.* **1992**, *25*, 192–195. [\[CrossRef\]](#) [\[PubMed\]](#)
28. Kryston, T.B.; Georgiev, A.B.; Pissis, P.; Georgakilas, A.G. Role of oxidative stress and DNA damage in human carcinogenesis. *Mutat. Res.* **2011**, *711*, 193–201. [\[CrossRef\]](#) [\[PubMed\]](#)
29. Kurashige, T.; Shimamura, M.; Nagayama, Y. N-Acetyl-L-cysteine protects thyroid cells against DNA damage induced by external and internal irradiation. *Radiat. Environ. Biophys.* **2017**, *56*, 405–412. [\[CrossRef\]](#) [\[PubMed\]](#)
30. Ferlazzo, M. Impact of the Nucleoshuttling of the ATM Protein in Response to Ionizing Radiation: Notions of Pro- and Anti-Epishevic Features. PhD Thesis, University of Lyon, Lyon, France, 2017.
31. Combemale, P.; Sonzogni, L.; Devic, C.; Bencokova, Z.; Ferlazzo, M.L.; Granzotto, A.; Burlet, S.F.; Pinson, S.; Amini-Adle, M.; Al-Choboq, J.; et al. Individual Response to Radiation of Individuals with Neurofibromatosis Type I: Role of the ATM Protein and Influence of Statins and Bisphosphonates. *Mol. Neurobiol.* **2022**, *59*, 556–573. [\[CrossRef\]](#) [\[PubMed\]](#)
32. Ferlazzo, M.L.; Bach-Tobdji, M.K.E.; Djerad, A.; Sonzogni, L.; Burlet, S.F.; Devic, C.; Granzotto, A.; Bodgi, L.; Djefal-Kerrar, A.; Foray, N. Radiobiological characterization of tuberous sclerosis: A delay in the nucleo-shuttling of ATM may be responsible for radiosensitivity. *Mol. Neurobiol.* **2017**, *55*, 4973–4983. [\[CrossRef\]](#)
33. Bachelet, J.T.; Granzotto, A.; Ferlazzo, M.; Sonzogni, L.; Berthel, E.; Devic, C.; Foray, N. First radiobiological characterization of the McCune-Albright syndrome: Influence of the ATM protein and effect of statins + bisphosphonates treatment. *Int. J. Radiat. Biol.* **2021**, *97*, 317–328. [\[CrossRef\]](#)
34. Berthel, E.; Foray, N.; Ferlazzo, M.L. The Nucleoshuttling of the ATM Protein: A Unified Model to Describe the Individual Response to High- and Low-Dose of Radiation? *Cancers* **2019**, *11*, 905. [\[CrossRef\]](#)
35. Georgoulis, A.; Vorgias, C.E.; Chrousos, G.P.; Rogakou, E.P. Genome Instability and gammaH2AX. *Int. J. Mol. Sci.* **2017**, *18*, 1979. [\[CrossRef\]](#)
36. Berthel, E.; Ferlazzo, M.C.D.; Bourguignon, M.; Foray, N. What does the History of Research on the Repair of DNA Double-Strand Breaks Tell Us?—A Comprehensive Review of Human Radiosensitivity. *Int. J. Mol. Sci.* **2019**, *20*, 5339. [\[CrossRef\]](#) [\[PubMed\]](#)
37. Rothkamm, K.; Lobrich, M. Evidence for a lack of DNA double-strand break repair in human cells exposed to very low x-ray doses. *Proc. Natl. Acad. Sci. USA* **2003**, *100*, 5057–5062. [\[CrossRef\]](#) [\[PubMed\]](#)
38. Bodgi, L.; Foray, N. The nucleo-shuttling of the ATM protein as a basis for a novel theory of radiation response: Resolution of the linear-quadratic model. *Int. J. Radiat. Biol.* **2016**, *92*, 117–131. [\[CrossRef\]](#)
39. Granzotto, A.; Benadjaoud, M.A.; Vogin, G.; Devic, C.; Ferlazzo, M.L.; Bodgi, L.; Pereira, S.; Sonzogni, L.; Forcheron, F.; Viau, M.; et al. Influence of Nucleoshuttling of the ATM Protein in the Healthy Tissues Response to Radiation Therapy: Toward a Molecular Classification of Human Radiosensitivity. *Int. J. Radiat. Oncol. Biol. Phys.* **2016**, *94*, 450–460. [\[CrossRef\]](#) [\[PubMed\]](#)
40. Ferlazzo, M.L.; Sonzogni, L.; Granzotto, A.; Bodgi, L.; Lartin, O.; Devic, C.; Vogin, G.; Pereira, S.; Foray, N. Mutations of the Huntington's Disease Protein Impact on the ATM-Dependent Signaling and Repair Pathways of the Radiation-Induced DNA Double-Strand Breaks: Corrective Effect of Statins and Bisphosphonates. *Mol. Neurobiol.* **2014**, *49*, 1200–1211. [\[CrossRef\]](#) [\[PubMed\]](#)
41. Al-Choboq, J.; Ferlazzo, M.L.; Sonzogni, L.; Granzotto, A.; El-Nachef, L.; Maalouf, M.; Berthel, E.; Foray, N. Usher Syndrome Belongs to the Genetic Diseases Associated with Radiosensitivity: Influence of the ATM Protein Kinase. *Int. J. Mol. Sci.* **2022**, *23*, 1570. [\[CrossRef\]](#)
42. Le Reun, E.; Bodgi, L.; Granzotto, A.; Sonzogni, L.; Ferlazzo, M.L.; Al-Choboq, J.; El-Nachef, L.; Restier-Verlet, J.; Berthel, E.; Devic, C.; et al. Quantitative correlations between radiosensitivity biomarkers show that the ATM protein kinase is strongly involved in the radiotoxicities observed after radiotherapy. *Int. J. Mol. Sci.* **2022**, *23*, 10434. [\[CrossRef\]](#)
43. Joubert, A.; Zimmerman, K.M.; Bencokova, Z.; Gastaldo, J.; Rénier, W.; Chavaudra, N.; Favaudon, V.; Arlett, C.; Foray, N. DNA double-strand break repair defects in syndromes associated with acute radiation response: At least two different assays to predict intrinsic radiosensitivity? *Int. J. Radiat. Biol.* **2008**, *84*, 107–125. [\[CrossRef\]](#)
44. Foray, N.; Fertil, B.; Alsbeih, M.G.; Badie, C.; Chavaudra, N.; Iliakis, G.; Malaise, E.P. Dose-rate effect on radiation-induced DNA double-strand breaks in the human fibroblast HF19 cell line. *Int. J. Radiat. Biol.* **1996**, *69*, 241–249. [\[CrossRef\]](#) [\[PubMed\]](#)



45. Foray, N.; Priestley, A.; Alsbeih, G.; Badie, C.; Capulas, E.P.; Arlett, C.F.; Malaise, E.P. Hypersensitivity of ataxia telangiectasia fibroblasts to ionizing radiation is associated with a repair deficiency of DNA double-strand breaks. *Int. J. Radiat. Biol.* **1997**, *72*, 271–283. [[PubMed](#)]
46. Varela, I.; Pereira, S.; Ugalde, A.P.; Navarro, C.L.; Suarez, M.F.; Cau, P.; Cadinanos, J.; Osorio, F.G.; Foray, N.; Cobo, J.; et al. Combined treatment with statins and aminobisphosphonates extends longevity in a mouse model of human premature aging. *Nat. Med.* **2008**, *14*, 767–772. [[CrossRef](#)] [[PubMed](#)]
47. Foray, N.; Marot, D.; Gabriel, A.; Randrianarison, V.; Carr, A.M.; Perricaudet, M.; Ashworth, A.; Jeggo, P. A subset of ATM- and ATR-dependent phosphorylation events requires the BRCA1 protein. *EMBO J.* **2003**, *22*, 2860–2871. [[CrossRef](#)]
48. Ferlazzo, M.; Berthel, E.; Granzotto, A.; Devic, C.; Sonzogni, L.; Bachelet, J.T.; Pereira, S.; Bourguignon, M.; Sarasin, A.; Mezzina, M.; et al. Some mutations in the xeroderma pigmentosum D gene may lead to moderate but significant radiosensitivity associated with a delayed radiation-induced ATM nuclear localization. *Int. J. Radiat. Biol.* **2019**, *96*, 394–410. [[CrossRef](#)]
49. Bachelet, J.T.A.G.; Ferlazzo, M.; Sonzogni, L.; Berthel, E.C.D.; Foray, N. First Radiobiological Characterization of Skin and Bone Cells from A Patient Suffering from the PI3KCA-Related Overgrowth Spectrum (PROS) Syndrome. *Arch. Med. Clin. Case Rep.* **2020**, *4*, 1052–1066. [[CrossRef](#)]
50. Moulay Lakhdar, I.; Ferlazzo, M.L.; Al Choboq, J.; Berthel, E.; Sonzogni, L.; Devic, C.; Granzotto, A.; Thariat, J.; Foray, N. Fibroblasts from Retinoblastoma Patients Show Radiosensitivity Linked to Abnormal Localization of the ATM Protein. *Curr. Eye Res.* **2020**, *46*, 546–557. [[CrossRef](#)]
51. Badie, C.; Goodhardt, M.; Waugh, A.; Doyen, N.; Foray, N.; Calsou, P.; Singleton, B.; Gell, D.; Salles, B.; Jeggo, P.; et al. A DNA double-strand break defective fibroblast cell line (180BR) derived from a radiosensitive patient represents a new mutant phenotype. *Cancer Res.* **1997**, *57*, 4600–4607.
52. McKinnon, P.J. Ataxia-telangiectasia: An inherited disorder of ionizing-radiation sensitivity in man. Progress in the elucidation of the underlying biochemical defect. *Hum. Genet.* **1987**, *75*, 197–208. [[CrossRef](#)]
53. Srinivas, U.S.; Tan, B.W.Q.; Vellayappan, B.A.; Jeyasekharan, A.D. ROS and the DNA damage response in cancer. *Redox Biol.* **2019**, *25*, 101084. [[CrossRef](#)]
54. Forman, H.J.; Zhang, H.; Rinna, A. Glutathione: Overview of its protective roles, measurement, and biosynthesis. *Mol. Asp. Med.* **2009**, *30*, 1–12. [[CrossRef](#)] [[PubMed](#)]
55. Raghu, G.; Berk, M.; Campochiaro, P.A.; Jaeschke, H.; Marenzi, G.; Richeldi, L.; Wen, F.Q.; Nicoletti, F.; Calverley, P.M.A. The Multifaceted Therapeutic Role of N-Acetylcysteine (NAC) in Disorders Characterized by Oxidative Stress. *Curr. Neuropharmacol.* **2021**, *19*, 1202–1224. [[CrossRef](#)]
56. Tenorio, M.; Graciliano, N.G.; Moura, F.A.; Oliveira, A.C.M.; Goulart, M.O.F. N-Acetylcysteine (NAC): Impacts on Human Health. *Antioxidants* **2021**, *10*, 967. [[CrossRef](#)] [[PubMed](#)]
57. Verhey, L.J.; Sedlacek, R. Determination of the radioprotective effects of topical applications of MEA, WR-2721, and N-acetylcysteine on murine skin. *Radiat. Res.* **1983**, *93*, 175–183. [[CrossRef](#)]
58. Kataoka, Y.; Murley, J.S.; Baker, K.L.; Grdina, D.J. Relationship between phosphorylated histone H2AX formation and cell survival in human microvascular endothelial cells (HMEC) as a function of ionizing radiation exposure in the presence or absence of thiol-containing drugs. *Radiat. Res.* **2007**, *168*, 106–114. [[CrossRef](#)] [[PubMed](#)]
59. Pedre, B.; Barayeu, U.; Ezerina, D.; Dick, T.P. The mechanism of action of N-acetylcysteine (NAC): The emerging role of H<sub>2</sub>S and sulfane sulfur species. *Pharmacol. Ther.* **2021**, *228*, 107916. [[CrossRef](#)]
60. Whillier, S.; Raftos, J.E.; Chapman, B.; Kuchel, P.W. Role of N-acetylcysteine and cystine in glutathione synthesis in human erythrocytes. *Redox Rep.* **2009**, *14*, 115–124. [[CrossRef](#)]
61. Glover, D.; Riley, L.; Carmichael, K.; Spar, B.; Glick, J.; Kligerman, M.M.; Agus, Z.S.; Slatopolsky, E.; Attie, M.; Goldfarb, S. Hypocalcemia and inhibition of parathyroid hormone secretion after administration of WR-2721 (a radioprotective and chemoprotective agent). *N. Engl. J. Med.* **1983**, *309*, 1137–1141. [[CrossRef](#)]
62. Akbulut, S.; Elbe, H.; Eris, C.; Dogan, Z.; Toprak, G.; Otan, E.; Erdemli, E.; Turkoz, Y. Cytoprotective effects of amifostine, ascorbic acid and N-acetylcysteine against methotrexate-induced hepatotoxicity in rats. *World J. Gastroenterol.* **2014**, *20*, 10158–10165. [[CrossRef](#)]
63. Onalan, G.; Gulumser, C.; Mulyayim, B.; Dagdeviren, A.; Zeyneloglu, H. Effects of amifostine on endometriosis, comparison with N-acetyl cysteine, and leuprolide as a new treatment alternative: A randomized controlled trial. *Arch. Gynecol. Obstet.* **2014**, *289*, 193–200. [[CrossRef](#)]
64. Murray, D.; Prager, A.; Milas, L. Radioprotection of cultured mammalian cells by the aminothiols WR-1065 and WR-255591: Correlation between protection against DNA double-strand breaks and cell killing after gamma radiation. *Radiat. Res.* **1989**, *120*, 154–163. [[CrossRef](#)] [[PubMed](#)]
65. Haydont, V.; Bourcier, C.; Pocard, M.; Lusinchi, A.; Aigueperse, J.; Mathe, D.; Bourhis, J.; Vozenin-Brotans, M.C. Pravastatin Inhibits the Rho/CCN2/extracellular matrix cascade in human fibrosis explants and improves radiation-induced intestinal fibrosis in rats. *Clin. Cancer Res. Off. J. Am. Assoc. Cancer Res.* **2007**, *13*, 5331–5340. [[CrossRef](#)] [[PubMed](#)]
66. Balasubramanian, R.; Maideen, N.M.P. HMG-CoA Reductase Inhibitors (Statins) and their Drug Interactions Involving CYP Enzymes, P-glycoprotein and OATP Transporters-An Overview. *Curr. Drug Metab.* **2021**, *22*, 328–341. [[CrossRef](#)] [[PubMed](#)]



67. Ziegler, V.; Henninger, C.; Simiantonakis, I.; Buchholzer, M.; Ahmadian, M.R.; Budach, W.; Fritz, G. Rho inhibition by lovastatin affects apoptosis and DSB repair of primary human lung cells in vitro and lung tissue in vivo following fractionated irradiation. *Cell Death Dis.* **2017**, *8*, e2978. [[CrossRef](#)] [[PubMed](#)]
68. Efimova, E.V.; Ricco, N.; Labay, E.; Mauceri, H.J.; Flor, A.C.; Ramamurthy, A.; Sutton, H.G.; Weichselbaum, R.R.; Kron, S.J. HMG-CoA Reductase Inhibition Delays DNA Repair and Promotes Senescence After Tumor Irradiation. *Mol. Cancer Ther.* **2018**, *17*, 407–418. [[CrossRef](#)]
69. Sehitoglu, I.; Tumkaya, L.; Bedir, R.; Kalkan, Y.; Cure, M.C.; Yucel, A.F.; Zorba, O.U.; Yuce, S.; Cure, E. Zoledronic acid aggravates kidney damage during ischemia reperfusion injury in rat. *J. Environ. Pathol. Toxicol. Oncol.* **2015**, *34*, 53–61. [[CrossRef](#)]
70. Mirrakhimov, A.E. Hypercalcemia of Malignancy: An Update on Pathogenesis and Management. *N. Am. J. Med. Sci.* **2015**, *7*, 483–493. [[CrossRef](#)]
71. Wei, Z.; Pan, B.; Jia, D.; Yu, Y. Long-term safety and efficacy of bisphosphonate therapy in advanced lung cancer with bone metastasis. *Future Oncol.* **2022**, *18*, 2257–2267. [[CrossRef](#)]
72. Srivichit, B.; Thonusin, C.; Chattipakorn, N.; Chattipakorn, S.C. Impacts of bisphosphonates on the bone and its surrounding tissues: Mechanistic insights into medication-related osteonecrosis of the jaw. *Arch. Toxicol.* **2022**, *96*, 1227–1255. [[CrossRef](#)]
73. Zaborowska, M.; Broniatowski, M.; Wydro, P.; Matyszevska, D.; Bilewicz, R. Structural modifications of lipid membranes exposed to statins—Langmuir monolayer and PM-IRRAS study. *J. Mol. Lipids* **2020**, *313*, 113570. [[CrossRef](#)]
74. Bootman, M.D.; Fearnley, C.; Smyrnias, I.; MacDonald, F.; Roderick, H.L. An update on nuclear calcium signalling. *J. Cell Sci.* **2009**, *122*, 2337–2350. [[CrossRef](#)] [[PubMed](#)]
75. Bodgi, L.; Canet, A.; Pujo-Menjouet, L.; Lesne, A.; Victor, J.M.; Foray, N. Mathematical models of radiation action on living cells: From the target theory to the modern approaches. A historical and critical review. *J. Theor. Biol.* **2016**, *394*, 93–101. [[CrossRef](#)] [[PubMed](#)]

**Disclaimer/Publisher's Note:** The statements, opinions and data contained in all publications are solely those of the individual author(s) and contributor(s) and not of MDPI and/or the editor(s). MDPI and/or the editor(s) disclaim responsibility for any injury to people or property resulting from any ideas, methods, instructions or products referred to in the content.



# 6<sup>th</sup> RADIOBIOLOGY SYMPOSIUM

International Military Radiation & Innovation Symposium

## IMRIS



10<sup>th</sup>  
Anniversary

November 17, 2022

The Department of Radiations Bioeffects of the French Armed Forces Biomedical Research Institute has the pleasure of welcoming you the **17<sup>th</sup> of November 2022** for the 6<sup>th</sup> Radiobiology Symposium:

### International Military Radiation and Innovation Symposium (IMRIS)

To celebrate its 10<sup>th</sup> Anniversary, it will be held at the French National Armed Forces Club (Cercle National des Armées, CNA) in Paris, France

*Cercle National des Armées  
8 Place Saint Augustin  
75008 PARIS*

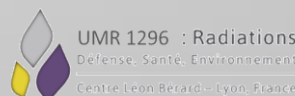
Metro stations: Saint Lazare (M 3 12 13 14) ; Saint Augustin (M 9)

Free registration

Limited places available, registration required by email

Contact for registration, abstract submission and questions:

[radiobiology.workshop@gmail.com](mailto:radiobiology.workshop@gmail.com)





# 7<sup>th</sup> RADIOBIOLOGY SYMPOSIUM

International **M**military **R**adiation & **I**nnovation **S**ymposium

In PARIS,  
October 8-9 2024



## PRE-PLANNING

### Tuesday the 8th of October

8h45-9h30 : Welcome of the attendees -  
Coffee

9h30-9h40: Opening Speech

#### Session 1

**Ionizing radiations: Dosimetry and  
exposure biomarkers**

12h30-13h30 : Lunch- Poster session

#### Session 2

**Radiological physiopathology and  
contamination**

#### Session 3 (Part 1)

**Radiobiology and medical  
countermeasures**

### Wednesday the 9th of October

8h45- 9h00 : Welcome of the attendees

#### Session 3 (Part 2)

**Radiobiology and medical  
countermeasures**

#### Session 4 (Part 1)

**Environmental pollutants**

12h30-13h30 : Lunch- Poster session

#### Session 4 (Part 2)

**Environmental pollutants**

#### Session 5

**Electromagnetic radiations**

17h10-17h30 : Poster award –  
Closing speech








**UP Health**



## Article

# Influence of the Hypersensitivity to Low Dose Phenomenon on the Tumor Response to Hypofractionated Stereotactic Body Radiation Therapy

Eymeric Le Reun <sup>1,2,†</sup>, Adeline Granzotto <sup>1,†</sup>, Adeline Pêtre <sup>1,3,†</sup>, Larry Bodgi <sup>4</sup> , Guillaume Beldjoudi <sup>3</sup> , Thomas Lacornerie <sup>5</sup>, Véronique Vallet <sup>2</sup>, Audrey Bouchet <sup>1</sup> , Joëlle Al-Choboq <sup>1</sup> , Michel Bourguignon <sup>1,6</sup>, Juliette Thariat <sup>7</sup>, Jean Bourhis <sup>2</sup>, Eric Lartigau <sup>5</sup> and Nicolas Foray <sup>1,\*</sup> 

<sup>1</sup> U1296 Unit, “Radiation: Defense, Health and Environment”, Centre Léon-Bérard, Inserm, 28 Rue Laennec, 69008 Lyon, France; eymeric.le-reun@inserm.fr (E.L.R.); adeline.granzotto@inserm.fr (A.G.); adeline.petre@lyon.unicancer.fr (A.P.); audrey.bouchet@inserm.fr (A.B.); joelle.al-choboq@inserm.fr (J.A.-C.); michel.bourguignon@inserm.fr (M.B.)

<sup>2</sup> Service de Radio-Oncologie, Centre Hospitalier Universitaire Vaudois (CHUV), 46 Rue du Bugnon, 1011 Lausanne, Switzerland; veronique.vallet@chuv.ch (V.V.); jean.bourhis@chuv.ch (J.B.)

<sup>3</sup> Département de Radiothérapie, Centre Léon-Bérard, 28 Rue Laennec, 69008 Lyon, France; guillaume.beldjoudi@lyon.unicancer.fr

<sup>4</sup> Department of Radiation Oncology, American University of Beirut Medical Center, Riad El-Solh, Beirut 1107-2020, Lebanon; lb38@aub.edu.lb

<sup>5</sup> Département de Radiothérapie, Centre Oscar-Lambret, 3 Rue Frédéric Combemale, 59000 Lille, France; t-lacornerie@o-lambret.fr (T.L.); e-lartigau@o-lambret.fr (E.L.)

<sup>6</sup> Département de Biophysique et Médecine Nucléaire, Université Paris Saclay, Versailles St. Quentin en Yvelines, 78035 Versailles, France

<sup>7</sup> Département de Radiothérapie, Centre François-Baclesse, 3 Avenue du Général Harris, 14076 Caen, France; j.thariat@baclesse.unicancer.fr

\* Correspondence: nicolas.foray@inserm.fr; Tel.: +33-478782828

† These authors contributed equally to this work.



**Citation:** Le Reun, E.; Granzotto, A.; Pêtre, A.; Bodgi, L.; Beldjoudi, G.; Lacornerie, T.; Vallet, V.; Bouchet, A.; Al-Choboq, J.; Bourguignon, M.; et al. Influence of the Hypersensitivity to Low Dose Phenomenon on the Tumor Response to Hypofractionated Stereotactic Body Radiation Therapy. *Cancers* **2023**, *15*, 3979. <https://doi.org/10.3390/cancers15153979>

Academic Editor: Franz Rödel

Received: 4 July 2023

Revised: 30 July 2023

Accepted: 3 August 2023

Published: 5 August 2023



**Copyright:** © 2023 by the authors. Licensee MDPI, Basel, Switzerland. This article is an open access article distributed under the terms and conditions of the Creative Commons Attribution (CC BY) license (<https://creativecommons.org/licenses/by/4.0/>).

**Simple Summary:** We demonstrated the possible occurrence of the hypersensitivity to low dose (HRS) phenomenon in SBRT modality in both tumor and healthy cells. In HRS-positive cells, the response to SBRT was found exacerbated. Notably, a subset of highly damaged cells can appear and increase the efficiency of the treatment. Hence, each SBRT session can be viewed as hyperfractionated dose delivery by means of hundreds of low dose minibeam. To determine the HRS status of tumors and healthy tissues appears to be useful to increase SBRT efficiency and decrease the risk of adverse reactions.

**Abstract:** Stereotactic body radiation therapy (SBRT) has made the hypofractionation of high doses delivered in a few sessions more acceptable. While the benefits of hypofractionated SBRT have been attributed to additional vascular, immune effects, or specific cell deaths, a radiobiological and mechanistic model is still needed. By considering each session of SBRT, the dose is divided into hundreds of minibeam delivering some fractions of Gy. In such a dose range, the hypersensitivity to low dose (HRS) phenomenon can occur. HRS produces a biological effect equivalent to that produced by a dose 5-to-10 times higher. To examine whether HRS could contribute to enhancing radiation effects under SBRT conditions, we exposed tumor cells of different HRS statuses to SBRT. Four human HRS-positive and two HRS-negative tumor cell lines were exposed to different dose delivery modes: a single dose of 0.2 Gy, 2 Gy, 10 × 0.2 Gy, and a single dose of 2 Gy using a non-coplanar isocentric minibeam irradiation mode were delivered. Anti- $\gamma$ H2AX immunofluorescence, assessing DNA double-strand breaks (DSB), was applied. In the HRS-positive cells, the DSB produced by 10 × 0.2 Gy and 2 Gy, delivered by tens of minibeam, appeared to be more severe, and they provided more highly damaged cells than in the HRS-negative cells, suggesting that more severe DSB are induced in the “SBRT modes” conditions when HRS occurs in tumor. Each SBRT session can be viewed as hyperfractionated dose delivery by means of hundreds of low dose minibeam. Under current SBRT conditions (i.e., low dose per minibeam and not using ultra-high dose-rate), the response of



HRS-positive tumors to SBRT may be enhanced significantly. Interestingly, similar conclusions were reached with HRS-positive and HRS-negative untransformed fibroblast cell lines, suggesting that the HRS phenomenon may also impact the risk of post-RT tissue overreactions.

**Keywords:** low-dose; radiation therapy; SBRT; LDRT; radiosensitivity; cancer; HRS phenomenon

## 1. Introduction

Over the last decades, numerous technological advances in radiotherapy (RT)—notably, via stereotactic approaches—have permitted better tumor targeting and a drastic reduction in the volume of irradiated healthy tissues. This is, notably, the case of the stereotactic body radiation therapy (SBRT). Considering the great diversity of SBRT protocols, with various doses per fraction, number of fractions, dose gradient, etc., it appears more rigorous to describe SBRT from its physical features, i.e., as a RT modality delivering many non-coplanar minibeam converging to the tumor with sub-millimetric accuracy, as defined by the International Commission on Radiation Units and Measurements (ICRU) [1–6]. Particularly, hypofractionated SBRT has been shown to improve anti-tumor efficiency and decrease the volume of irradiated healthy tissues for numerous tumor indications, including spine metastasis [7–9], prostate cancer [10], liver metastasis [11], as well as lung carcinoma and metastasis [7,12,13].

In stereotactic approaches, a precise tumor target is reached in each session by hundreds of minibeam delivering subfractions of Gy [14]. For example, during one SBRT session, the targeted tumor may be exposed to a hyperfractionation of low doses of the order of cGy. Furthermore, some minibeam may overlap in the same regions of the targeted tumor; hence, in a given tumor region, a session of SBRT results in some repeated low doses that are separated by some seconds to some minutes (Figure 1).

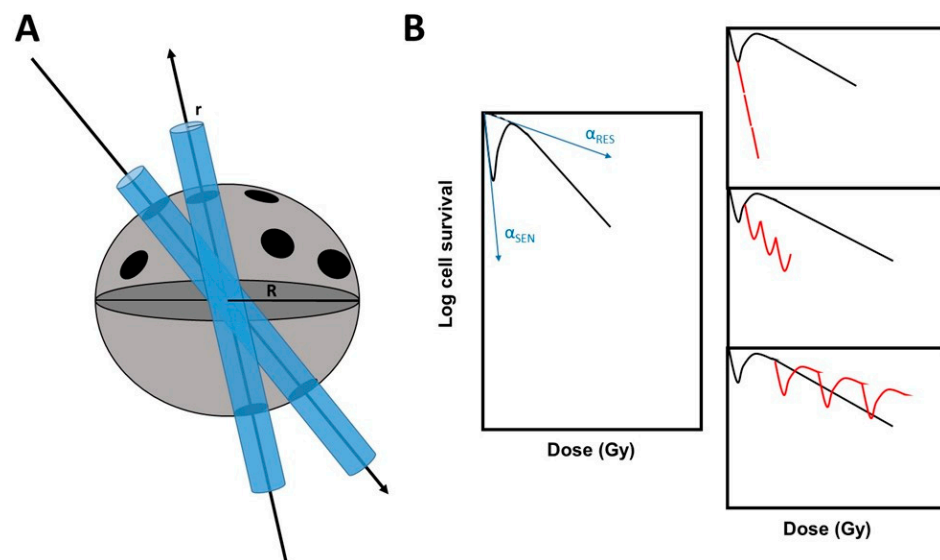


**Figure 1.** SBRT and the hypersensitivity to low doses phenomenon (HRS). (A) A schematic view of SBRT centripetal minibeam crossing a spherical tumor. (B) On the left, there is a representative example of a survival curve showing HRS phenomenon. The HRS parameters defined in Material and Methods are indicated. On the right, the survival effect of repeated low doses in an HRS-positive cell at different doses is shown. Red lines indicate the expected fractionation effect.

Interestingly, at the ranges of doses and dose-rates involved during an SBRT session, the hypersensitivity to low dose (HRS) phenomenon can occur and result in enhancing the effect of the low dose to an effect that is equivalent to a dose 5 to 10 times greater [15–17].



Any HRS-positive tumor treated by SBRT could, therefore, elicit a considerable dose enhancement effect caused by HRS. (Figure 1). At high dose-rate (some Gy/min), the maximal HRS effect generally ranges from 0.1 to 0.8 Gy. However, the dose at which the maximal HRS effect occurs has been shown to decrease with dose-rate reaching a maximal HRS effect in the mGy to cGy range [18]. By using unrepaired DSB as an endpoint, such dose enhancement may be quantified after one single SBRT session.

The present study aims to investigate the potential influence of the HRS phenomenon in the response of tumor and normal cells exposed to SBRT, as defined above. In order to verify such a hypothesis, four HRS-negative and two HRS-positive human tumor cell lines were exposed to a single dose of 0.2 Gy, 2 Gy,  $10 \times 0.2$  Gy, and a single dose of 2 Gy using a non-coplanar isocentric minibeam irradiation mode at Centre Léon-Bérard (CLB), Lyon, France and at Centre Hospitalier Universitaire Vaudois (CHUV), Lausanne, Switzerland. There were also one HRS-negative and one HRS-positive human untransformed fibroblast cell lines used to evaluate the influence of the HRS status on the response of healthy tissues to SBRT. The immunofluorescence against the phosphorylated forms of the variant X of the H2A histone ( $\gamma$ H2AX), a current biomarker of DSB recognized by the non-homologous end-joining (NHEJ), the most predominant DSB repair pathway in mammals [19,20], was applied to each condition to investigate the DSB repair and signaling response.

## 2. Materials and Methods

### 2.1. Cell Lines

There were four HRS-positive and two HRS-negative commercial human tumor cell lines used in this study. Their major biological and radiobiological features were detailed in Table 1. All the experiments with tumor cell lines were performed in the log phase of growth with similar relative distributions in the cell cycle phases (70–80% in G0/G1; 10–15% in S and 10–20% in G2/M) [21]. In addition, to evaluate the influence of the HRS status on the response of healthy tissues to SBRT, one HRS-negative (AG1521) and one HRS-positive (13HNG) human untransformed fibroblast cell line were irradiated in the same conditions as those used for tumor, to the notable exception that they were irradiated in plateau phase of growth [22]. While the AG1521 fibroblast cell line is provided from a commercial cell repository (Table 1), the 13HNG cell line belongs to the COPERNIC collection (N.F.'s lab), which has been abundantly documented and composed of radioresistant and radiosensitive fibroblast cell lines derived from RT-treated patients. The COPERNIC radiobiological database is protected under the reference IDDN.FR.001.510017.000.D.P.2014.000.10300. All sampling protocols of the COPERNIC collection were approved by the national ethical committee in agreement with the current national regulations. The resulting cells were declared under the numbers DC2008-585, DC2011-1437, and DC2020-3957 to the Ministry of Research. All the cells used in this study were routinely cultured with Dulbecco's modified Eagle's minimum medium (DMEM) (Gibco-Invitrogen-France, Cergy-Pontoise, France), which was supplemented with 20% fetal calf serum, penicillin, and streptomycin.

**Table 1.** Biological features of the tumor and fibroblast cell lines used in this study.

Cell Line	Origin	HRS Status
HT29	Grade II colon adenocarcinoma isolated from a primary tumor from a white Caucasian female patient	#HTB-38, ATCC <sup>a</sup> +
A549	lung carcinoma from a white Caucasian male patient	#CCL-185, ATCC <sup>a</sup> +
U373 MG	glioblastoma astrocytoma from a malignant tumor	#08061901, ECACC <sup>b</sup> –
U87 MG	from malignant glioma from a male patient	#HTB-14, ATCC <sup>a</sup> +



Table 1. Cont.

Cell Line	Origin		HRS Status
LN229	from the right frontal parieto-occipital cortex of a white female patient with glioblastoma.	#CRL-2611, ATCC <sup>a</sup>	+
SNU475	from an hepatocellular carcinoma	#CRL-2236 ATCC <sup>a</sup>	—
AG1521	Skin (foreskin) fibroblast from a foreskin of a 3 day child	#AG01521, Coriell Institute Repository <sup>c</sup>	—
13HNG	Skin fibroblast from a cancer patient showing adverse tissue after radiotherapy	COPERNIC Collection	+

<sup>a</sup> American Type Culture Collection (ATCC), (Manassas, VA, USA); <sup>b</sup> European Collection of Authenticated Cell Cultures (ECACC), Health Security Agency, (Salisbury, UK); <sup>c</sup> Coriell Institute Repository (Camden, NJ, USA). + and — mean HRS-positive and -negative status, respectively.

## 2.2. Irradiation

Irradiations simulating a hyperfractionated RT were performed with a 6 MV X-rays medical irradiator (SL 15 Philips) (dose-rate: 4 Gy.min<sup>−1</sup>) at Centre Léon-Bérard (Lyon, France) [23]. In all the experiments, a dose of 2 Gy was chosen as reference since it simulates a current dose per RT session. Cells in Petri dishes were exposed in a static irradiation described elsewhere [23]. Dosimetry was certified by radiophysicists of the Centre Léon-Bérard. SBRT Irradiations were performed with a CyberKnife<sup>TM</sup> treatment unit (Accuray Inc, Sunnyvale, CA, USA) at Centre Léon Bérard (Lyon, France) or at CHUV (Lausanne, Switzerland) [24]. First, cells in Petri dishes were exposed with static irradiation: dishes were positioned on the floor on 10 cm of water equivalent plates, for backscattering purposes, and under 5 cm of water equivalent plates. A fixed collimator of 60 mm was used. In these conditions, dose-rate to the cells was estimated to about 1.5 Gy.min<sup>−1</sup>. Cells were irradiated by considering three schemes: 2 Gy delivered in one time (“2 Gy”), 0.2 Gy delivered in one time (“0.2 Gy”), and 2 Gy delivered in 10 subfractions of 0.2 Gy, with a 2 min time interruption between each fraction, leading to a planned delivery time of about 20 min (“10 × 0.2 Gy”). A second setup was considered with a CyberKnife<sup>TM</sup> treatment unit: Petri dishes were positioned inside a homemade phantom containing fiducials that could be seen by the CyberKnife<sup>TM</sup> system, and a CT scan was performed. Multiplan<sup>TM</sup> (Accuray Inc., Sunnyvale, CA, USA) treatment planning system was used to create a clinical plan, and the fixed 20 mm, 35 mm, and 50 mm collimators were chosen. A homogeneous dose of 2 Gy was planned for the target volume, containing the Petri dishes plus isotropic extension margins, of 5 mm to account for setup uncertainties. The treatment consisted of 82 minibeam, including 8, 71, and 3 minibeam provided by fixed 20, 35, and 50 mm collimators, respectively. The planned delivery time was about 20 min. It will be further referred to, in this paper, as the (“2 Gy Cyber”) condition.

## 2.3. Cell Survival

Standard clonogenic assays were used for the assessment of intrinsic radiosensitivity, as previously described [25,26]. For HRS-negative cells, the linear-quadratic (LQ) model describes the cell survival *S* as a function of dose *D*, as follows:

$$S(D) = \exp(-\alpha D - \beta D^2) \quad (1)$$

in which  $\alpha$  and  $\beta$  are adjustable parameters to be determined.



For HRS-positive cells, the induced repair model describes the cell survival  $S$  as a function of dose  $D$ , similar to the LQ model, but by integrating the HRS phenomenon with the following modifications on the  $\alpha$  parameter, by defining the HRS variant LQ model as follows:

$$S(D) = \exp(-\alpha_{\text{res}} (1 + g \exp(-D/D_c))D - \beta D^2) \quad (2)$$

in which  $D_c$  is an adjustable parameter and  $g$  is the amount by which  $\alpha$ , at the very low doses ( $\alpha_{\text{sen}}$ ), is larger than  $\alpha$  at high doses ( $\alpha_{\text{res}}$ ). Hence,  $\alpha_{\text{sen}} = \alpha_{\text{res}} (1 + g)$  for the hyperradiosensitive cells [27] (Figure 1). The HRS/IRR ratio can also be used to quantify the extent of the HRS phenomenon. It is defined as the ratio of high and low doses, providing the lowest survival values at low doses and corresponding to the maximal HRS effect.

#### 2.4. Immunofluorescence

The immunofluorescence protocol and foci scoring were described elsewhere [23]. Briefly, cells were fixed in 4% (*w/v*) paraformaldehyde solution for 10 min at room temperature, and they were permeabilized in 0.5% Triton X-100 solution for 5 min at 4 °C. Primary and secondary antibody incubations were performed for 40 and 20 min at 37 °C, respectively. Anti- $\gamma$ H2AX<sup>ser139</sup> antibody (#05-636; Merck Millipore, Burlington, VT, USA) was used at a 1:800 ratio. Anti-mouse fluorescein (FITC) secondary antibody was used at a 1:100 ratio. Slides were mounted and counterstained in 4',6'-Diamidino-2-Phenyl-indole (DAPI)-stained Vectashield (Abcys, Paris, France), and nuclei were examined with a BX51 Olympus fluorescence microscope. For each of the three independent replicates, 100 nuclei were analyzed. The foci scoring procedure applied here has received the certification agreement of CE mark and ISO-13485 quality management system norms. Our foci scoring procedure also developed some features that are protected in the frame of the patents (FR3017625 A1 and FR3045071 A1).

#### 2.5. Statistical Analysis

Statistical analysis was performed by using Kaleidagraph v4 (Synergy Software, Reading, PA, USA), Graphpad Prism (San Diego, CA, USA), and MATLAB R2020B (Math-Work, Natick, MA, USA). Each experiment is the result of three independent replicates, so the mean is given with the standard error of the mean (SEM).

### 3. Results

#### 3.1. HRS Status of the 6 Tumor Cell Lines Used in This Study

Using a standard orthovoltage irradiator, delivering X-rays at high dose-rate, clonogenic cell survival assays were applied to the HT29, A549, U373, U87, LN229, and SNU475 cell lines. With regard to cell survival, while the U373 and SNU475 cells were found to be HRS-negative by obeying the classical LQ model data fitting, the HT29, A549, U87, and LN229 cells showed a specific hyperradiosensitivity in the range of 0.1 to 0.5 Gy, and they obeyed the HRS variant LQ model (Figure 2; Table 2). It is noteworthy that the surviving fractions, at 2 Gy (SF2) of the HRS-positive LN229 and the HRS-negative U373 cells, were not significantly different ( $61 \pm 3\%$  and  $58 \pm 6\%$ , respectively;  $p > 0.8$ ), while the SF2 values of the LN229 (HRS-positive) and the A549 (HRS-positive) were significantly different ( $61 \pm 3\%$  and  $80 \pm 4\%$ , respectively;  $p < 0.001$ ). These findings suggest that the extent of HRS phenomenon may be observed independently of the SF2 value. A similar conclusion can be reached with the cell cycle since all the cell lines have been irradiated in similar distributions of cell cycle phases. Our results were found to be in agreement with literature data [28–30] (Figure 2).



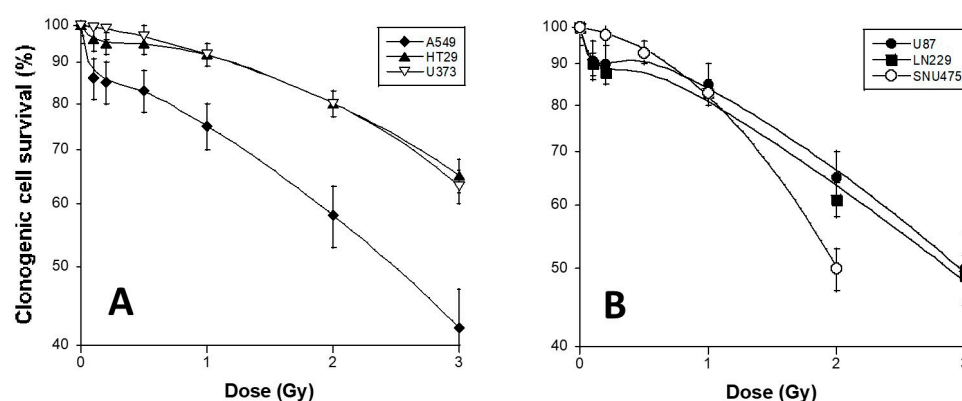


**Figure 2.** Clonogenic cell survival of the 6 tumor cell lines used in this study. Cell survival data were plotted as a function of X-ray dose delivered at high dose rate (4 Gy/min) by a standard orthovoltage irradiator. Each point represents the mean of triplicate experiments  $\pm$  SEM. Survival data were fitted to the LQ model and HRS LQ variant model. The HRS-positive cell lines are represented by closed symbols, while the HRS-negative cell lines are represented by open symbols. The (A) panel represents the A549, HT29, and U373 data and the (B) panel represents the U87, LN229, and SNU475 data.

**Table 2.** Numerical values of the adjustable parameters defining the variant LQ model for the tumor cell lines used here \*.

Cell Lines	HRS Status	$\alpha_{\text{res}}$ (Gy $^{-1}$ )	g	Dc (Gy)	HRS/IRR Ratio	$\beta$ (Gy $^{-2}$ )	SF2 (%)
U373	—	0.05	0	NA	1	0.029	58 $\pm$ 6
SNU475	—	0.05	0	NA	1	0.14	50 $\pm$ 4
A549	+	0.273	8.11	0.17	4.5	0.0003	80 $\pm$ 4
HT29	+	0.001	12.63	0.15	6	0.003	80 $\pm$ 6
U87	+	0.14	12.05	0.13	3.75	0.03	65 $\pm$ 6
LN229	+	0.19	7.03	0.15	7.5	0.016	61 $\pm$ 3

\* Survival data shown in Figure 2 were fitted to  $S(D) = \exp(-\alpha_{\text{res}} (1 + g \exp(-D/D_c))D - \beta D^2)$  (Formula (2)). It is noteworthy that all the data fit provided correlation coefficients larger than 0.98; + and — mean HRS-positive and -negative status, respectively; NA: non applicable.

### 3.2. $\gamma$ H2AX Foci Kinetics of the 6 Tumor Cell Lines Used in This Study

The formation of nuclear  $\gamma$ H2AX foci reveals the DSB, which is recognized by the non-homologous end-joining pathway (NHEJ), the most predominant DSB repair and signaling in mammals [20]. The early (10 min)  $\gamma$ H2AX foci document the recognition step of the DSB managed by NHEJ, while the residual (24 h)  $\gamma$ H2AX foci reflect the DSB repair step [20]. After 2 Gy, the anti- $\gamma$ H2AX immunofluorescence revealed a maximal number of  $\gamma$ H2AX foci reached at 10 min post-irradiation and corresponding to  $80 \pm 5$  and  $78 \pm 4$   $\gamma$ H2AX foci in the U373 and the HT29 cells ( $p > 0.2$ ), respectively. Conversely, in the A549 cells, this number was found to be significantly lower ( $65 \pm 4$   $\gamma$ H2AX foci;  $p < 0.005$ ), suggesting an impaired DSB recognition, which was in agreement with literature [20] (Figure 3). At 24 h after 2 Gy, the amounts of residual  $\gamma$ H2AX foci in the three cell lines tested were found to be similar ( $p > 0.2$ ), suggesting that, at 2 Gy, (1) the DSB recognized by H2AX phosphorylation are repaired similarly, and (2) the differences between cell survival (SF2) values are likely due to DSB that are not recognized by NHEJ and not revealed by  $\gamma$ H2AX foci [17] (Figure 3). After a single dose of 0.2 Gy, the number of  $\gamma$ H2AX foci were about 10 times lower for all the cells. However, the HRS-positive cells elicited a lower number of  $\gamma$ H2AX foci, assessed 10 min post-irradiation, than the HRS-negative cells ( $p < 0.05$ ), suggesting a DSB recognition impairment at 0.2 Gy. Furthermore, the HRS-positive cells elicited a higher number of  $\gamma$ H2AX foci 24 h post-irradiation than the HRS-negative cells ( $p > 0.001$ ), suggesting a slower DSB repair (Figure 3). Altogether, these findings suggest that, at 0.2 Gy, unlike the HRS-negative U373 cells, the HRS-positive HT29 and A549 cells showed a lack of DSB recognition by NHEJ pathway and a larger amount of unrepaired



DSB, which documents the HRS phenomenon (Figure 3). Similar conclusions were reached with the HRS-positive U87 and LN229 cells and the HRS-negative SNU475 cells.

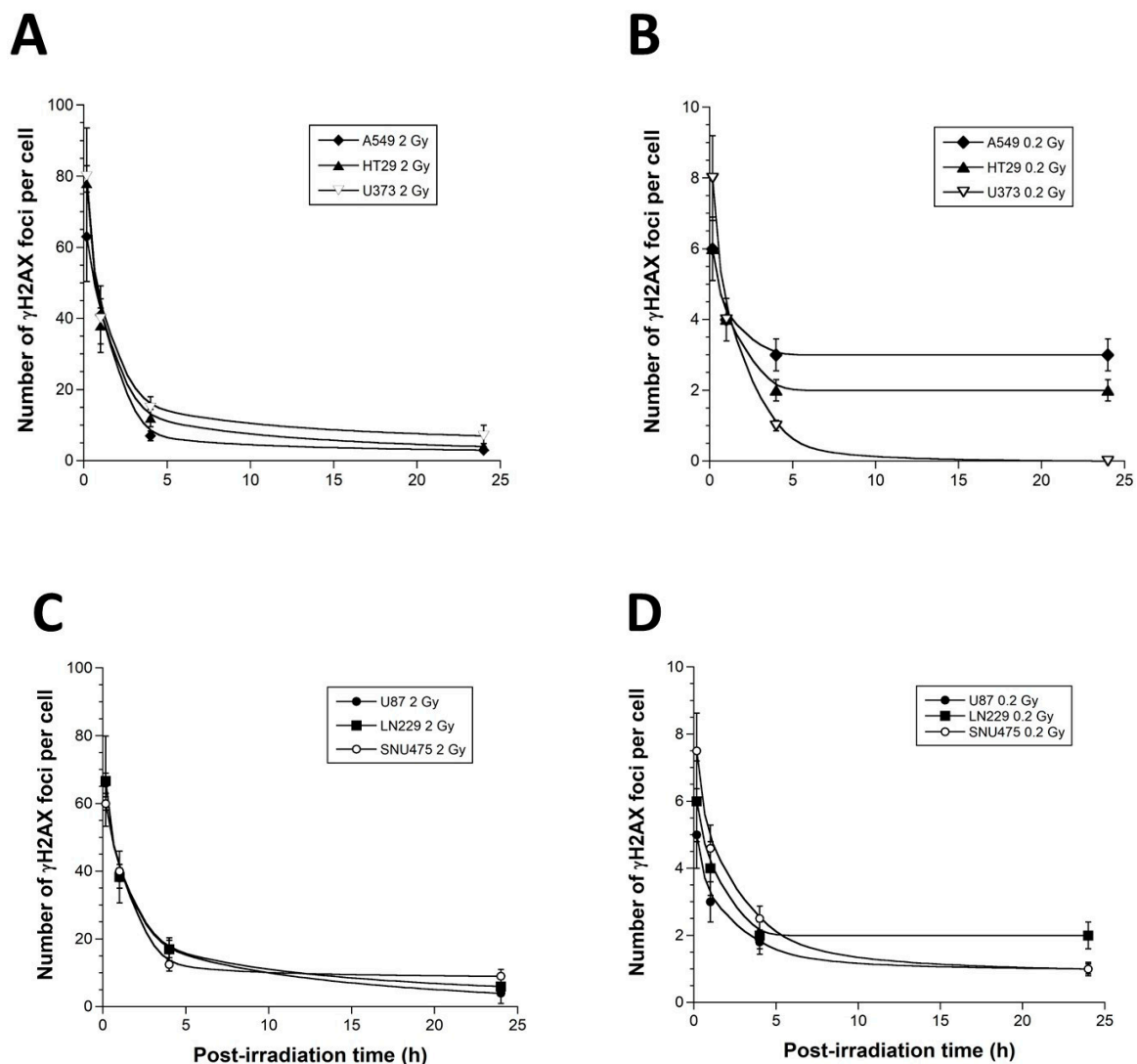


**Figure 3.** Radiation-induced  $\gamma$ H2AX foci kinetics of the 6 tumor cell lines used in this study. The  $\gamma$ H2AX foci data were expressed as a number of  $\gamma$ H2AX foci per cell, as a function of post-irradiation time, after a dose of 2 Gy (A,C) and 0.2 Gy (B,D) X-ray delivered at high dose rate (4 Gy/min) by a standard orthovoltage irradiator. Each point represents the mean of triplicate experiments  $\pm$  SEM.

Among the most current questions with regard the relevance of the HRS phenomenon is how a low dose, such as 0.2 Gy, can provide a similar lethal effect to higher doses such as 2 Gy. In fact, the link between unrecognized/unrepaired DSB and cell survival is now very clearly documented [20]. Literature data converge to the conclusion that one to two unrepaired DSB is a lethal event for human fibroblasts [31], and the same link is true about two to three unrepaired DSB for human tumors since tumors may tolerate more unrepaired DSB than healthy tissues [14,20,32]. Furthermore, we have already shown that HRS phenomenon results in the lack of recognition and repair of DSB by the NHEJ pathway [19,20]. Hence, in order to consolidate the relevance of our data with regard to these two features, we have plotted the number of residual  $\gamma$ H2AX foci with the corresponding cell survival data at 2 Gy (SF2) and 0.2 Gy (SF0.2) (Figure 4).



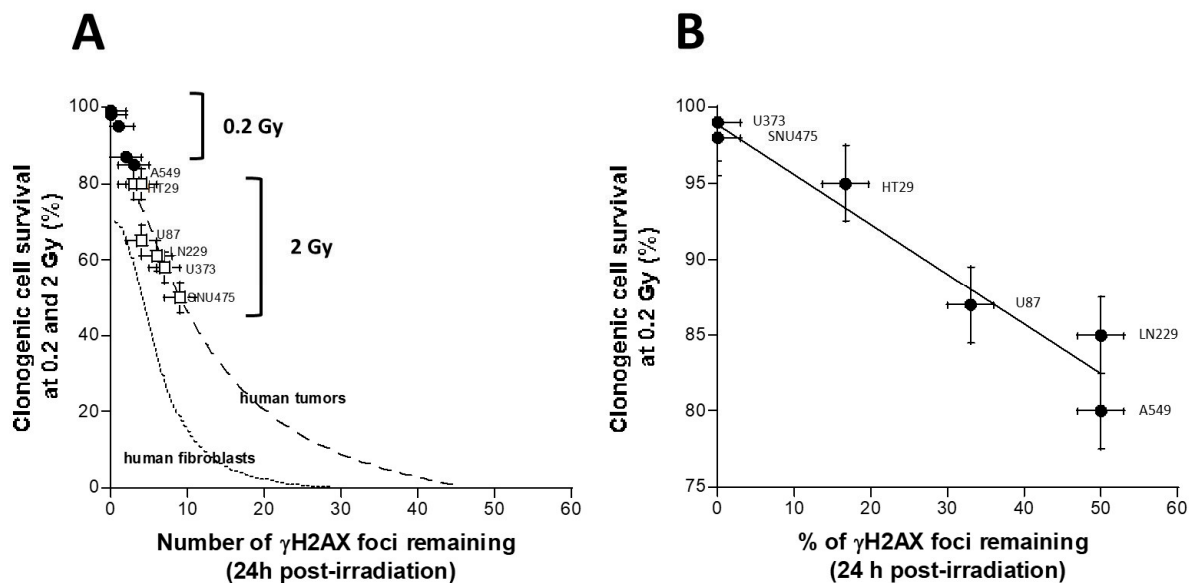


**Figure 4.** Relationships between the cell survival and the  $\gamma$ H2AX data. **A.** The survival data assessed at 0.2 (SF0.2) and 2 Gy (SF2), shown in Figure 2, were plotted against the corresponding  $\gamma$ H2AX data assessed at 24 h post-irradiation, shown in Figure 3, and obtained from the indicated human tumor cell lines. Each point represents the mean of triplicate experiments  $\pm$  SEM. The dashed and the dotted lines represent the links between the SF2 and the number of residual  $\gamma$ H2AX foci obtained from 40 human tumor cell lines described in [32], as well as 200 human fibroblast cell lines described in [20]. **(B)** The survival data assessed at 0.2 (SF0.2), shown in panel (A), were plotted against the corresponding percentage of  $\gamma$ H2AX data assessed at 24 h post-irradiation (24 h data divided by 10 min data, shown in Figure 3, and obtained from the indicated human tumor cell lines). Each point represents the mean of triplicate experiments  $\pm$  SEM. The line represents the formula  $y = 98.8 - 0.32x$  ( $r = 0.97$ ).

The relationship between the SF2 data, shown in Figure 2, and the corresponding  $\gamma$ H2AX foci assessed at 24 h post-irradiation, shown in Figure 3, was found to be in agreement with the link between SF2 and the number of unrepaired DSB reflected by the  $\gamma$ H2AX foci described in [32] (Figure 4A). It is also noteworthy that data obtained with a dose of 0.2 Gy obeyed the same relationship (Figure 4A), supporting, again, that a very small number of unrepaired DSB can lead to cellular death. Lastly, the clonogenic cell survival at 0.2 Gy appeared to be inversely proportional to the percentage of DSB recognized and repaired by the NHEJ (Figure 4B). The formula deduced from the data fits suggested that cell survival decreased by 1% each time the percentage of DSB recognized and repaired by NHEJ decreased by one-third (Figure 4B).

### 3.3. Molecular Response to SBRT of the 6 Tumor Cell Lines Used in This Study

In order to further examine the potential impact of the HRS status in the response to SBRT, we applied 2 and 0.2 Gy delivered at one time, 2 Gy delivered in 10 subfractions of 0.2 Gy, and 2 Gy delivered in CyberKnife conditions, with minibeam to the 6 tumor cell lines. The first series was performed with a CyberKnife irradiator of CLB (Lyon, France) with the HT29, A549, and U373 cells. The second parallel series was performed in the same conditions with a CyberKnife irradiator of the CHUV (Lausanne, France).

The  $\gamma$ H2AX foci kinetics after the “2 Gy” condition were not found to be significantly different from those obtained with an orthovoltage X-ray irradiator ( $p > 0.2$ ) (Figure 4). After the “0.2 Gy” condition, in the two HRS-positive cells, the number of  $\gamma$ H2AX foci was found to be lower at 10 min and higher at 24 h post-irradiation than in the HRS-negative cells ( $p < 0.01$ ) (Figure 5). Interestingly, the “10  $\times$  0.2 Gy” condition resulted in a number of early  $\gamma$ H2AX foci, assessed 10 min post-irradiation, similar to that assessed in the “2 Gy” condition ( $p > 0.4$ ) (Figure 5). At 24 h post-irradiation, the “10  $\times$  0.2 Gy” condition resulted



in increasing the amount of residual  $\gamma$ H2AX foci reflecting unrepaired DSB in the two HRS-positive cells by comparison with the “2 Gy” condition ( $p < 0.02$ ). Conversely, the “ $10 \times 0.2$  Gy” condition did not significantly change the number of residual  $\gamma$ H2AX foci in the HRS-negative cells ( $p > 0.2$ ). These findings suggest that the severity of DSB only increases in HRS-positive cells (Figure 5). The “2 Gy Cyber” condition was found to amplify the differences already noticed with the “0.2 Gy” condition ( $p < 0.02$ ) again. The “2 Gy Cyber” and “ $10 \times 0.2$  Gy” conditions showed the most severe DSB and the largest differences between the HRS-negative and positive cells, (Figure 5). Similar conclusions were reached with the U87, LN229, and SNU475 cell lines.

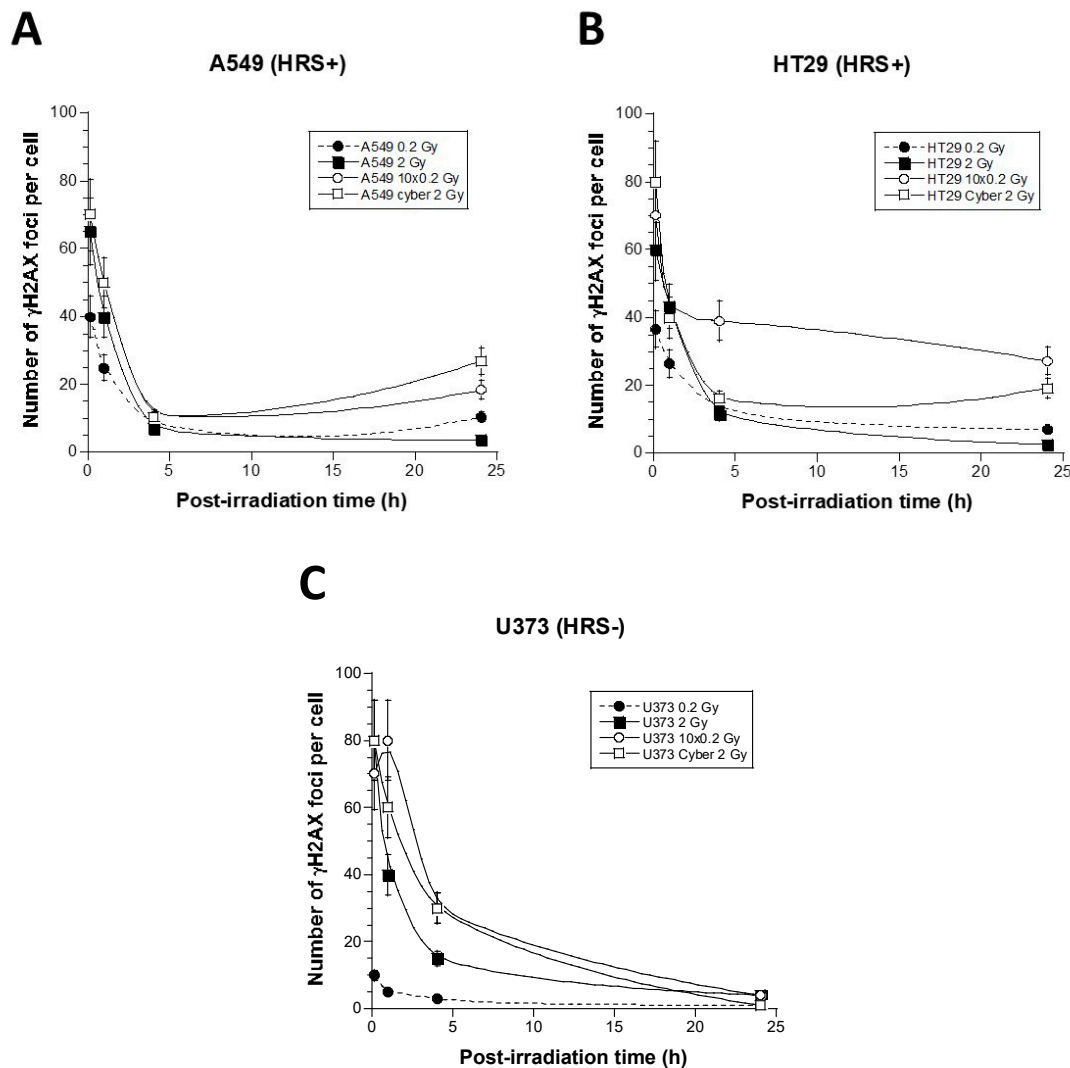


**Figure 5.** Radiation-induced  $\gamma$ H2AX foci kinetics of the A549 (HRS-positive) (A), HT29 (HRS-positive) (B), and U373 (HRS-negative) (C) tumor cell lines irradiated with different SBRT delivery mode. For each cell line, the  $\gamma$ H2AX foci data were expressed as a number of  $\gamma$ H2AX foci per cell and a function of post-irradiation time (top) after a single dose of 2 Gy (2 Gy), 0.2 Gy (0.2 Gy), a series of 10 times 0.2 Gy ( $10 \times 0.2$  Gy), and a dose of 2 Gy delivered by CyberKnife (2 Gy Cyber). Each point represents the mean of triplicate experiments  $\pm$  SEM.

During our experiments, we observed some cells showing a number of  $\gamma$ H2AX foci higher than 100, i.e., they were difficult to score with precision. Such highly damaged cells (HDC) appeared to be a specific feature of the HRS-positive cells that was mainly observed in “ $10 \times 0.2$  Gy” and in “2 Gy Cyber” conditions (Figure 6). In order to account for HDC, we have re-expressed the previous data by considering four categories of cells:



no  $\gamma$ H2AX foci, no more than 15  $\gamma$ H2AX foci, more than 15  $\gamma$ H2AX foci, and HDC. The 24 h data did not show any HDC after a single dose of 2 Gy (Figures 6 and 7). The HDC were observed in HRS-positive cells in the “0.2 Gy” conditions, and such features increased in “10  $\times$  0.2 Gy” and “2 Gy Cyber” conditions in the HRS-positive cells only, suggesting a specific biological dose-enhancement. Conversely, with regards to the HRS-negative cells, a non-significant amount of HDC was observed. No cell with more than 15 foci was observed in HRS-negative cells. (Figures 6 and 7). These findings suggest that a considerable amount of additional DSB may be specifically induced in the HRS-positive cells when the dose is delivered in the hyper-fractionated SBRT conditions.

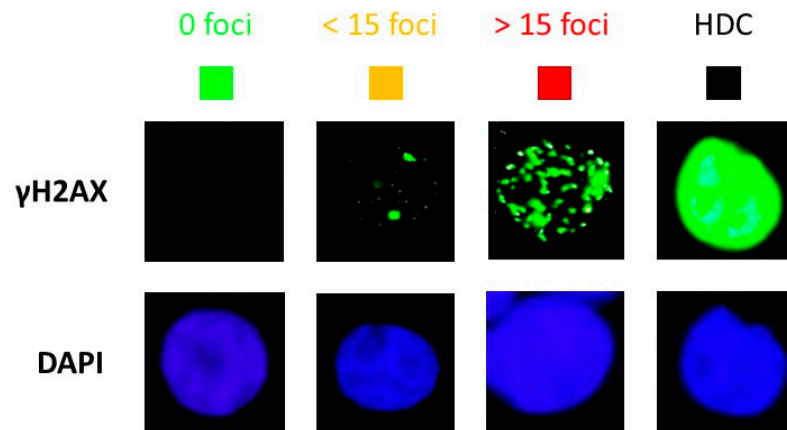


**Figure 6.** Representative images of the four categories of cells observed 24 h post-irradiation: cells showing no  $\gamma$ H2AX foci, no more than 15  $\gamma$ H2AX foci, more than 15  $\gamma$ H2AX foci, and HDC. The  $\gamma$ H2AX staining is in green, and the corresponding DAPI counterstaining is in blue.

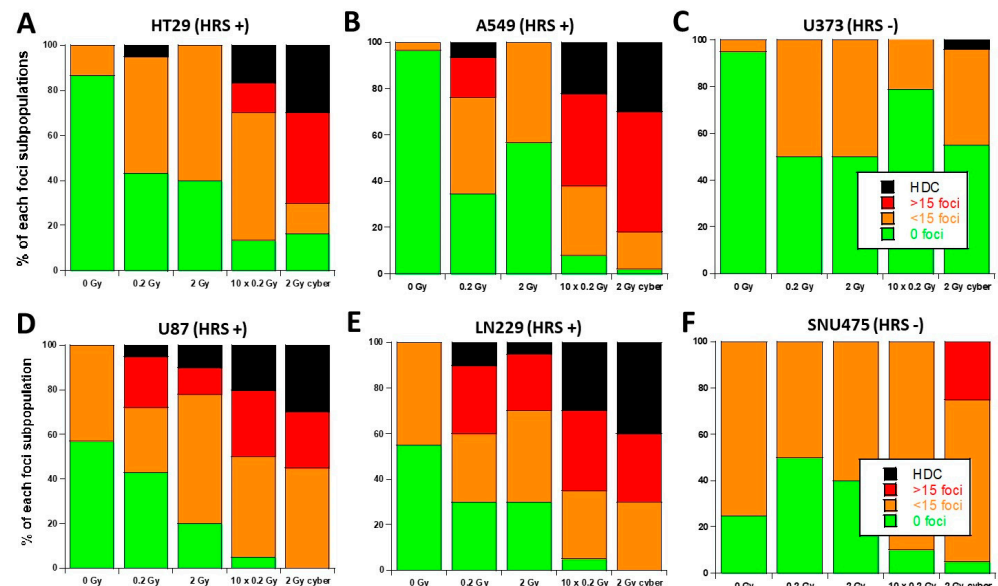


**Figure 7.** Stacked bar chart of 24 h  $\gamma$ H2AX foci data from the 6 tumor cell lines used this study. The 24 h data obtained from the 6 indicated tumor cell lines were re-expressed by considering four categories of cells defined in Figure 6. Each point represents the mean of triplicate experiments  $\pm$  SEM.

### 3.4. Molecular Response to SBRT of the 13HNG and AG1521 Skin Fibroblast Cell Lines

The HRS phenomenon is not limited to the tumor cell lines; it has also been observed in healthy tissues such as skin fibroblasts [33–37]. Hence, if the SBRT irradiation would concern the healthy tissues around the tumor, some over-reaction would also be expected. Hence, in order to examine the influence of the HRS status in the response of



skin fibroblasts to SBRT, we applied the same irradiation conditions as described above to two untransformed skin fibroblast cell lines: AG1521 (HRS-positive) and 13HNG (HRS-negative) (Figure 8). The HDC were only observed in HRS-positive cells in the “0.2 Gy” and “2 Gy” conditions, and such features increased in “10 × 0.2 Gy” and “2 Gy Cyber” conditions. Such data confirm again that the positive HRS status may lead to a specific biological dose-enhancement in SBRT irradiation conditions (Figure 8).

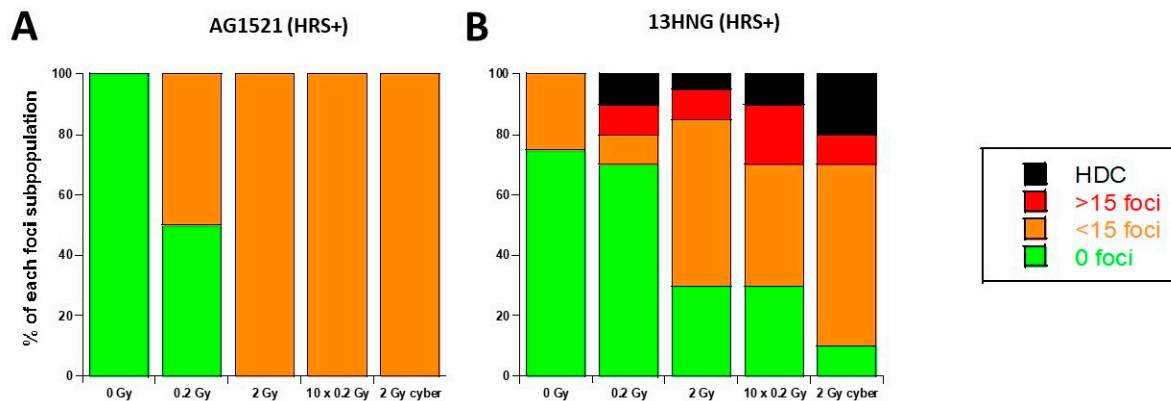


**Figure 8.** Stacked bar chart of 24 h  $\gamma$ H2AX foci data. The 24 h data obtained from the 2 indicated healthy tissue cell lines were re-expressed by considering four categories of cells defined in Figure 6. Each point represents the mean of triplicate experiments  $\pm$  SEM.

### 3.5. Quantified Relationship between the HRS/IRR Ratio and the Percentage of HDC

The HDC appeared to be a biomarker specific to a repeated HRS phenomenon. In order to examine whether a quantified link exists between the percentage of HDC and the HRS/IRR ratio, these two parameters, obtained from the four HRS-positive tumor cells, were plotted together (Figure 9). Interestingly, the higher the HRS/IRR ratio, the larger the percentage of HDC. Furthermore, the percentage of HDC increased with the number of SBRT sessions by obeying a linear function close to a one-to-one correlation. Hence, each infinitesimal extent of HRS corresponds to about a 1% increase in HDC. The HRS/IRR ratio is a bounded value, so the percentage of HDC is expected to be a curvilinear function of the number of SBRT sessions. However, further investigations will be needed to document the occurrence of the HRS phenomenon in the SBRT sessions and to verify such a hypothesis.

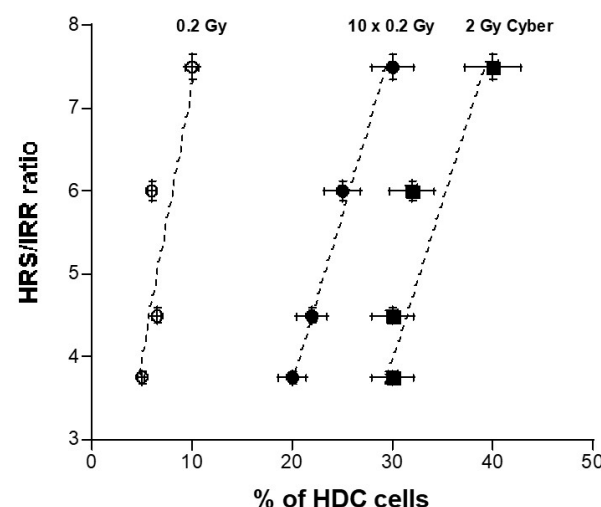


**Figure 9.** HRS/IRR ratio as a function of percentage of HDC. The HRS/IRR ratios mentioned for the four HRS-positive tumor cells in Table 2 were plotted against the corresponding percentage of HDC in the 0.2 Gy, 10 × 0.2 Gy, and 2 Gy Cyber conditions shown in Figure 6. Dotted lines correspond to a linear function used for data fitting.



## 4. Discussion

### 4.1. From Hypofractionated to Stereotactic RT Modalities

The occurrence of the HRS phenomenon in RT depends on the dose, the dose-rate, and the HRS status of the irradiated cells. To date, some hypofractionated and/or stereotactic RT modalities may include conditions in which the HRS phenomenon may occur and may be repeated. In this study, we have applied particular hypofractionated SBRT conditions (those of CyberKnife<sup>TM</sup> RT). Theoretically, as far as the HRS phenomenon can occur and be repeated, our conclusions may be relevant for any stereotactic delivery of the dose. Furthermore, our results showed that the HRS phenomenon is independent of the tumor cell type (glioblastoma, lung adenocarcinoma...), and therefore, many SBRT or stereotactic radiosurgery (SRS) protocols can be concerned by such conditions. Further investigations are therefore needed to document the occurrence of HRS in other RT modalities.

Historically, hypofractionated RT has long been associated with severe complications, while hyperfractionated RT, with several sessions of about 2 Gy, was known to reduce them [38–40]. In the 1930s, the “German School” with Holzknecht and Wintz preferentially applied hypofractionated RT, while the “French school”, represented by the medical staff of the Curie Institute in Paris with Regaud, Coutard, and Del Regato, promoted hyperfractionated RT [38–40]. First developed in the 1950s, the stereotactic approach has significantly improved the tumor targeting, which has revived the old debate about hypo or else hyperfractionated RT [41]. Particularly, while hypofractionation may concern other RT modalities, it remains intimately linked to SBRT, and the efficiency of such specific modality has been often attributed, at least partially, to hypofractionation [42,43]. Some authors have suggested that long periods between two RT sessions may facilitate immune reactions, tumor reoxygenation, or repopulation, but these last features have not been correlated to radiosensitivity in a unified model yet [14,44,45]. Furthermore, immune reactions and tumor repopulation require a significant cell killing effect. With regards to DNA damage, if the 24 h repair time is protracted, no significant number of additional DNA damage is created or repaired, and therefore, no additional cell killing effect is produced [14]. In other terms, by considering unrepaired DNA breaks, protracting the time between RT sessions over 24 h should not protect significantly more healthy tissues or kill more tumor cells and, consequently, should not favor the occurrence of immune reactions and tumor repopulation [14]. In a hypofractionated RT modality (whether SBRT or not), hypofractionation of the total dose is likely to produce additive, but not supra-additive, effects. Conversely, by not considering the hypofractionation of high doses delivered during all the treatment but the hyperfractionation of low doses during each session, a significant dose-enhancement may be observed if the HRS phenomenon occurs, i.e., if some doses and dose-rates obey HRS conditions [18]. In addition, by producing an excess of cell lethality, HRS may also impact on vascular damage and immune response. Hence, our model is compatible with other hypotheses evoked above.

### 4.2. HRS Phenomenon and Stereotactic RT

The HRS phenomenon results in a significant reduction in clonogenic cell survival, increase in chromosome breaks, micronuclei, and unrepaired DSB, but also an increase in mutation frequency after a single low-dose ranging between 1 and 800 mGy [18,46]. At a dose-rate higher than 1 Gy/min, HRS generally occurs between 1 and 800 mGy. At 0.1 Gy/min, HRS is expected at few cGy [18]. In 2016, we have provided a relevant biological interpretation of the HRS phenomenon in the frame of the radiation-induced ATM nucleoshuttling (RIANS) model [17]. Briefly, in the RIANS model, IR induce DNA damage (similarly to DSB), but they also induce monomerization of the cytoplasmic ATM dimers in a dose-dependent manner. The resulting ATM monomers diffuse to the nucleus to participate in the DSB recognition by NHEJ [47]. The delay of the RIANS was shown to be correlated with the cell survival and severity grade of post-RT tissue reactions [20,23]. The RIANS is very fast (some minutes after 2 Gy) in radioresistant cells (SF2 > 60%) called group I cells. It is not functional in hyperradiosensitive cells (SF2 < 10%) called group III



cells. In cells showing significant but intermediate radiosensitivity ( $10\% < \text{SF}_2 < 60\%$ ), called group II cells, the RIANS is delayed by the cytoplasmic over-expression of some proteins called X-proteins [17,47]. At low doses, the number of ATM monomers that diffuse in the nucleus and the number of DSB induced by IR decrease together but not at the same rate. Indeed, the number of DSB induced by IR decreases by obeying an induction rate of about 40 DSB induced per Gy per cell, regardless of the group of radiosensitivity. In group II cells, because ATM monomers are sequestered by X-proteins in the cytoplasm, the number of ATM monomers decreases faster than in group I cells. Consequently, the ratio of ATM monomers that diffuse in the nucleus per DSB is much lower in group II than group I cells [17,47]. In a specific mGy dose range, the flux of ATM monomers may not be sufficient for recognizing the few DSB induced. In the case of non-recognition of some DSB, the survival rate, the number of unrepaired DSB, micronuclei, or mutations may be affected significantly. Hence, the HRS-positive cells necessarily belong to the group II, i.e., they are characterized by a moderate radiosensitivity and a delayed RIANS. It must be stressed that such a hypothesis is relevant for both healthy tissues and tumors [17,47].

#### 4.3. Evidence That Each SBRT Session Results in a Repetition of Low Doses

Through the graphical demonstration of Figure 1, there is evidence that each SBRT session results in a repetition of low doses. Hence, let us consider the cell survival of the irradiated tumor  $S(d)$ , at a dose  $d$ , delivered by one single minibeam: the resulting cell survival  $S_{\text{SBRT}}$  after one SBRT session of  $\rho$  repeated doses delivered by  $\rho$  minibeam is:

$$S_{\text{SBRT}} = [S(d)]^\rho \quad (3)$$

By using the HT29, A549, and U373 tumor data described above and applying the Equation (3), let us consider that each minibeam delivered 10 cGy on average: the HRS-negative cells show a cell survival  $S(d)$  of about 0.9999, while the HRS-positive cells show a cell survival  $S(d)$  ranging from 0.98 to 0.93. Hence, by taking a numerical example with  $\rho = 10$  minibeam overlapping in the same region of the tumor, the resulting cell survival  $S_{\text{SBRT}}$ , after one SBRT session for HRS-negative and positive tumors, is  $0.9999^{10} = 0.999$  and  $0.98^{10} = 0.817$  to  $0.91^{10} = 0.39$ , respectively. Hence, in the HRS-positive cells exposed to one SBRT session, the final survival rate may reach a survival from 1.2 to 2.5 times lower than the HRS-negative cells. Altogether, such experimental and calculated data are consistent with a significant dose enhancement due to the specific occurrence of an HRS phenomenon repeated several times during each SBRT session.

#### 4.4. The HRS Phenomenon in Stereotactic RT Modalities: Towards New Predictive Assays?

If the HRS-positive cells show an enhanced killing effect, our findings raise two important questions: (1) What would be the effect on healthy tissues if they are also HRS-positive? (2) How can we predict whether a tumor/healthy tissue is HRS-positive or negative? For the first question, it appears obvious that healthy tissues can also be HRS-positive and that the HRS phenomenon is not a specific feature of tumors, as demonstrated by the Slonina's group [33–37]. However, it is important to note that the HRS statuses of tumor and healthy tissues, as with their radiosensitivity at high doses, are independent. If healthy tissues are HRS-positive, or even if both healthy tissues and tumors are HRS-positive, the benefit of a hyperfractionation of low-doses may be reduced. However, it must be stressed again that, in the particular case of SBRT, the tumor targeting is particularly precise, and therefore, healthy tissues may be spared more than with any other RT modality. The benefit of SBRT may be not negligible in this case.

With regards to the second question, the frequency of a positive HRS status in tumors is still unknown. However, a predictive assay, based on the irradiation of 2 and 0.2 Gy at high dose rate by taking DSB biomarkers as endpoints, may be informative enough to verify the HRS status of a given tumor, even if the feasibility of such a specific assay may be strongly linked to the accessibility of the tumor to perform biopsies. Fortunately, in radiation oncology, a tumor sample is, in the vast majority of cases, a prerequisite before



irradiation, whether in the form of a surgical specimen or a biopsy. With regard to healthy tissues, it is always possible to perform cutaneous biopsies or blood lymphocyte assays to verify the HRS status.

#### 4.5. Towards a Biology-Guided Radiation Therapy (BGRT)?

In the long term, determining the HRS status of both tumors and healthy tissues, may improve RT efficiency and increase its safety. Indeed, healthy tissues exhibiting an HRS-negative radiosensitivity surrounding an HRS-positive tumor would be a good candidate for a treatment technique favoring discontinuous microbeams, such as CyberKnife™, rather than volumetric modulated arc therapy (VMAT) or 3D RT modalities that involve a few beams. In this case, a de-escalation of the dose could even be considered in order to reduce the risk of radiotoxicity while safely maintaining anti-tumor efficiency. It must be stressed that such a biomolecular selection of the patients would be entirely compatible with all current SBRT techniques, allowing for increased treatment precision [48,49].

### 5. Conclusions

As mentioned in the above paragraph, the practical requirements for the occurrence of the HRS phenomenon depends on some specific ranges of dose and dose-rate. For example, some 3D-conformational RT protocols (i.e., several non-coplanar arcs) may also include such conditions and concern HRS-positive cells. Hence, our approach should be considered as a first step of investigations about the impact of the HRS phenomenon on certain modalities of RT. For the first time to our knowledge, it is suggested, here, that the benefit of the SBRT modalities may not be due to the hypofractionation of the dose through the whole treatment but, rather, to the hyperfractionation of the low dose delivered by each minibeam during each session, as well as the occurrence of the HRS phenomenon, in cells exhibiting HRS positive status. Further experiments are needed to document these findings in other SBRT modalities and, even, to better evaluate the risk of exposing HRS-positive healthy tissues and the benefit of treating HRS-positive tumors.

**Author Contributions:** Conceptualization, E.L.R., A.G., A.P. and N.F.; data acquisition and methodology, E.L.R., A.G., A.P., L.B., G.B., T.L., V.V., A.B. and J.A.-C.; validation and data analysis, E.L.R., A.G., A.P., L.B., G.B., T.L., V.V., A.B., J.A.-C., M.B., J.T., J.B., E.L. and N.F.; writing and original draft preparation, and review and editing: all the authors; project administration, and funding acquisition, N.F. All authors have read and agreed to the published version of the manuscript.

**Funding:** This research was funded by Commissariat General à l'Investissement (Programmes Investissement d'avenir—INDIRA project, NF), National Space Agency (CNES) (ATHENA and BERNADOTTE projects, NF), and by Région Auvergne Rhône-Alpes (PAI ERATOSTHENE project) and Campus France CEDRE project (47880PE).

**Institutional Review Board Statement:** To the notable exception of the 13HNG cell line belonging to the COPERNIC collection (see Table 1), all the fibroblast and tumor cell lines used in this study were purchased from commercial repositories (see Materials and Methods). The COPERNIC collection has been approved by the regional Ethical Committee. The COPERNIC Cell lines were declared under the numbers DC2008-585, DC2011-1437 and DC2021-3957 to the Ministry of Research. Database was protected under the reference IDDN.FR.001.510017.000.D.P.2014.000.10300.

**Informed Consent Statement:** The commercial repositories that have provided the fibroblast cell lines used in this study applied all the ethics and regulations related to the human samplings. All the anonymous COPERNIC patients were informed and signed consent according to the ethics recommendation, notably for their consent to participate and for publication of anonymous data (informed and written consent, anonymization and acceptance for publication).

**Data Availability Statement:** The data presented here are either present in a deposited database (see Section 2) or will be made available on reasonable request.

**Conflicts of Interest:** The authors declare no conflict of interest.



## References

- Bondiau, P.Y.; Benezery, K.; Beckendorf, V.; Peiffert, D.; Gerard, J.P.; Mirabel, X.; Noel, A.; Marchesi, V.; Lacornerie, T.; Dubus, F.; et al. CyberKnife robotic stereotactic radiotherapy: Technical aspects and medical indications. *Cancer Radiother. J. Soc. Fr. Radiother. Oncol.* **2007**, *11*, 338–344. [\[CrossRef\]](#)
- Kilby, W.; Dooley, J.R.; Kuduvalli, G.; Sayeh, S.; Maure, C.R. The CyberKnife® Robotic Radiosurgery System in 2010. *Technol. Cancer Res. Treat.* **2010**, *9*, 433–452. [\[CrossRef\]](#) [\[PubMed\]](#)
- De Jong, E.E.C.; Guckenberger, M.; Andratschke, N.; Dieckmann, K.; Hoogeman, M.S.; Milder, M.; Moller, D.S.; Nyeng, T.B.; Tanadini-Lang, S.; Lartigau, E.; et al. Variation in current prescription practice of stereotactic body radiotherapy for peripherally located early stage non-small cell lung cancer: Recommendations for prescribing and recording according to the ACROP guideline and ICRU report 91. *Radiother. Oncol. J. Eur. Soc. Ther. Radiol. Oncol.* **2020**, *142*, 217–223. [\[CrossRef\]](#) [\[PubMed\]](#)
- Wilke, L.; Andratschke, N.; Blanck, O.; Brunner, T.B.; Combs, S.E.; Grosu, A.L.; Moustakis, C.; Schmitt, D.; Baus, W.W.; Guckenberger, M. ICRU report 91 on prescribing, recording, and reporting of stereotactic treatments with small photon beams: Statement from the DEGRO/DGMP working group stereotactic radiotherapy and radiosurgery. *Strahlenther. Onkol. Organ Dtsch. Rontgenes.* **2019**, *195*, 193–198. [\[CrossRef\]](#) [\[PubMed\]](#)
- Biston, M.C.; Dupuis, P.; Gassa, F.; Gregoire, V. Do all the linear accelerators comply with the ICRU 91's constraints for stereotactic body radiation therapy treatments? *Cancer Radiother. J. Soc. Fr. Radiother. Oncol.* **2019**, *23*, 625–629. [\[CrossRef\]](#)
- ICRU. ICRU Report 91, Prescribing, Recording, and Reporting of Stereotactic Treatments with Small Photon Beams; International Commission on Radiation Units and Measurements: Bethesda, MD, USA, 2017.
- Calcerrada Diaz-Santos, N.; Blasco Amaro, J.A.; Cardiel, G.A.; Andradas Aragones, E. The safety and efficacy of robotic image-guided radiosurgery system treatment for intra- and extracranial lesions: A systematic review of the literature. *Radiother. Oncol. J. Eur. Soc. Ther. Radiol. Oncol.* **2008**, *89*, 245–253. [\[CrossRef\]](#)
- Gibbs, I.C.; Kamnerdsupaphon, P.; Ryu, M.R.; Dodd, R.; Kiernan, M.; Chang, S.D.; Adler, J.R., Jr. Image-guided robotic radiosurgery for spinal metastases. *Radiother. Oncol. J. Eur. Soc. Ther. Radiol. Oncol.* **2007**, *82*, 185–190. [\[CrossRef\]](#)
- Ehret, F.; Senger, C.; Kufeld, M.; Furweger, C.; Kord, M.; Haidenberger, A.; Windisch, P.; Ruess, D.; Kaul, D.; Ruge, M.; et al. Image-Guided Robotic Radiosurgery for the Management of Intramedullary Spinal Cord Metastases-A Multicenter Experience. *Cancers* **2021**, *13*, 297. [\[CrossRef\]](#)
- Jereczek-Fossa, B.A.; Beltramo, G.; Fariselli, L.; Fodor, C.; Santoro, L.; Vavassori, A.; Zerini, D.; Gherardi, F.; Ascione, C.; Bossi-Zanetti, I.; et al. Robotic image-guided stereotactic radiotherapy, for isolated recurrent primary, lymph node or metastatic prostate cancer. *Int. J. Radiat. Oncol. Biol. Phys.* **2012**, *82*, 889–897. [\[CrossRef\]](#)
- Ihnat, P.; Skacelikova, E.; Tesar, M.; Penka, I. Stereotactic body radiotherapy using the CyberKnife((R)) system in the treatment of patients with liver metastases: State of the art. *OncoTargets Ther.* **2018**, *11*, 4685–4691. [\[CrossRef\]](#)
- Khadije, M.; Salleron, J.; Marchesi, V.; Oldrini, G.; Peiffert, D.; Beckendorf, V. Cyberknife((R)) stereotactic radiation therapy for stage I lung cancer and pulmonary metastases: Evaluation of local control at 24 months. *J. Thorac. Dis.* **2018**, *10*, 4976–4984. [\[CrossRef\]](#) [\[PubMed\]](#)
- Diamant, A.; Heng, V.J.; Chatterjee, A.; Faria, S.; Bahig, H.; Fillion, E.; Doucet, R.; Khosrow-Khavar, F.; Naqa, I.E.; Seuntjens, J. Comparing local control and distant metastasis in NSCLC patients between CyberKnife and conventional SBRT. *Radiother. Oncol. J. Eur. Soc. Ther. Radiol. Oncol.* **2020**, *144*, 201–208. [\[CrossRef\]](#)
- Foray, N.; Bourguignon, M.; Hamada, N. Individual response to ionizing radiation. *Mutat. Res. Rev.* **2016**, *770*, 369–386. [\[CrossRef\]](#) [\[PubMed\]](#)
- Joiner, M.C.; Marples, B.; Lambin, P.; Short, S.C.; Turesson, I. Low-dose hypersensitivity: Current status and possible mechanisms. *Int. J. Radiat. Oncol. Biol. Phys.* **2001**, *49*, 379–389. [\[CrossRef\]](#)
- Marples, B.; Collis, S.J. Low-dose hyper-radiosensitivity: Past, present, and future. *Int. J. Radiat. Oncol. Biol. Phys.* **2008**, *70*, 1310–1318. [\[CrossRef\]](#)
- Bodgi, L.; Foray, N. The nucleo-shuttling of the ATM protein as a basis for a novel theory of radiation response: Resolution of the linear-quadratic model. *Int. J. Radiat. Biol.* **2016**, *92*, 117–131. [\[CrossRef\]](#) [\[PubMed\]](#)
- Thomas, C.; Martin, J.; Devic, C.; Diserbo, M.; Thariat, J.; Foray, N. Impact of dose-rate on the low-dose hyper-radiosensitivity and induced radioresistance (HRS/IRR) response. *Int. J. Radiat. Biol.* **2013**, *89*, 813–822. [\[CrossRef\]](#) [\[PubMed\]](#)
- Rothkamm, K.; Lobrich, M. Evidence for a lack of DNA double-strand break repair in human cells exposed to very low X-ray doses. *Proc. Natl. Acad. Sci. USA* **2003**, *100*, 5057–5062. [\[CrossRef\]](#)
- Le Reun, E.; Bodgi, L.; Granzotto, A.; Sonzogni, L.; Ferlazzo, M.L.; Al-Choboq, J.; El-Nachef, L.; Restier-Verlet, J.; Berthel, E.; Devic, C.; et al. Quantitative correlations between radiosensitivity biomarkers show that the ATM protein kinase is strongly involved in the radiotoxicities observed after radiotherapy. *Int. J. Mol. Sci.* **2022**, *23*, 10434. [\[CrossRef\]](#)
- Granzotto, A.; Bencokova, Z.; Vogin, G.; Devic, C.; Joubert, A.; Balosso, J.; Foray, N. DNA double-strand breaks repair and signaling of human gliomas and normal brain cells in response to radiation: Potential impact of the ATM- and BRCA1-dependent pathways. In *Brain Tumors/Book 3*; Abujamra, A.L., Ed.; Intechweb: Rijeka, Croatia, 2011.
- Foray, N.; Priestley, A.; Alsbeih, G.; Badie, C.; Capulas, E.P.; Arlett, C.F.; Malaise, E.P. Hypersensitivity of ataxia telangiectasia fibroblasts to ionizing radiation is associated with a repair deficiency of DNA double-strand breaks. *Int. J. Radiat. Biol.* **1997**, *72*, 271–283.



23. Granzotto, A.; Benadjaoud, M.A.; Vogin, G.; Devic, C.; Ferlazzo, M.L.; Bodgi, L.; Pereira, S.; Sonzogni, L.; Forcheron, F.; Viau, M.; et al. Influence of Nucleoshuttling of the ATM Protein in the Healthy Tissues Response to Radiation Therapy: Toward a Molecular Classification of Human Radiosensitivity. *Int. J. Radiat. Oncol. Biol. Phys.* **2016**, *94*, 450–460. [\[CrossRef\]](#)
24. Mengue, L.; Bertaut, A.; Ngo Mbus, L.; Dore, M.; Ayadi, M.; Clement-Colmou, K.; Claude, L.; Carrie, C.; Laude, C.; Tanguy, R.; et al. Brain metastases treated with hypofractionated stereotactic radiotherapy: 8 years experience after Cyberknife installation. *Radiat. Oncol.* **2020**, *15*, 82. [\[CrossRef\]](#)
25. Ferlazzo, M.; Berthel, E.; Granzotto, A.; Devic, C.; Sonzogni, L.; Bachelet, J.T.; Pereira, S.; Bourguignon, M.; Sarasin, A.; Mezzina, M.; et al. Some mutations in the xeroderma pigmentosum D gene may lead to moderate but significant radiosensitivity associated with a delayed radiation-induced ATM nuclear localization. *Int. J. Radiat. Biol.* **2019**, *96*, 394–410. [\[CrossRef\]](#) [\[PubMed\]](#)
26. Al-Choboq, J.; Ferlazzo, M.L.; Sonzogni, L.; Granzotto, A.; El-Nachef, L.; Maalouf, M.; Berthel, E.; Foray, N. Usher Syndrome Belongs to the Genetic Diseases Associated with Radiosensitivity: Influence of the ATM Protein Kinase. *Int. J. Mol. Sci.* **2022**, *23*, 1570. [\[CrossRef\]](#) [\[PubMed\]](#)
27. Marples, B.; Lambin, P.; Skov, K.A.; Joiner, M.C. Low dose hyper-radiosensitivity and increased radioresistance in mammalian cells. *Int. J. Radiat. Biol.* **1997**, *71*, 721–735. [\[CrossRef\]](#) [\[PubMed\]](#)
28. Wang, Q.; Chen, Y.; Chang, H.; Hu, T.; Wang, J.; Xie, Y.; Cheng, J. The Role and Mechanism of ATM-Mediated Autophagy in the Transition from Hyper-Radiosensitivity to Induced Radioresistance in Lung Cancer Under Low-Dose Radiation. *Front. Cell Dev. Biol.* **2021**, *9*, 650819. [\[CrossRef\]](#)
29. Schoenherr, D.; Krueger, S.A.; Martin, L.; Marignol, L.; Wilson, G.D.; Marples, B. Determining if low dose hyper-radiosensitivity (HRS) can be exploited to provide a therapeutic advantage: A cell line study in four glioblastoma multiforme (GBM) cell lines. *Int. J. Radiat. Biol.* **2013**, *89*, 1009–1016. [\[CrossRef\]](#) [\[PubMed\]](#)
30. Ryan, L.A.; Seymour, C.B.; Joiner, M.C.; Mothersill, C.E. Radiation-induced adaptive response is not seen in cell lines showing a bystander effect but is seen in lines showing HRS/IRR response. *Int. J. Radiat. Biol.* **2009**, *85*, 87–95. [\[CrossRef\]](#)
31. Cornforth, M.N.; Bedford, J.S. A quantitative comparison of potentially lethal damage repair and the rejoining of interphase chromosome breaks in low passage normal human fibroblasts. *Radiat. Res.* **1987**, *111*, 385–405. [\[CrossRef\]](#)
32. Chavaudra, N.; Bourhis, J.; Foray, N. Quantified relationship between cellular radiosensitivity, DNA repair defects and chromatin relaxation: A study of 19 human tumour cell lines from different origin. *Radiother. Oncol. J. Eur. Soc. Ther. Radiol. Oncol.* **2004**, *73*, 373–382.
33. Slonina, D.; Biesaga, B.; Urbanski, K.; Kojs, Z. Low-dose radiation response of primary keratinocytes and fibroblasts from patients with cervix cancer. *Radiat. Res.* **2007**, *167*, 251–259. [\[CrossRef\]](#) [\[PubMed\]](#)
34. Slonina, D.; Biesaga, B.; Urbanski, K.; Kojs, Z. The response of primary keratinocytes and fibroblasts from cancer patients to multiple low-dose irradiations. *Radiat. Res.* **2007**, *168*, 631–636. [\[CrossRef\]](#) [\[PubMed\]](#)
35. Slonina, D.; Biesaga, B.; Urbanski, K.; Kojs, Z. Comparison of chromosomal radiosensitivity of normal cells with and without HRS-like response and normal tissue reactions in patients with cervix cancer. *Int. J. Radiat. Biol.* **2008**, *84*, 421–428. [\[CrossRef\]](#) [\[PubMed\]](#)
36. Slonina, D.; Biesaga, B.; Urbanski, K.; Kojs, Z.; Waligorski, M. Evidence of low-dose hyper-radiosensitivity in normal cells of cervix cancer patients? *Radiat. Prot. Dosim.* **2006**, *122*, 282–284. [\[CrossRef\]](#) [\[PubMed\]](#)
37. Slonina, D.; Kowalczyk, A.; Janecka-Widla, A.; Kabat, D.; Szatkowski, W.; Biesaga, B. Low-Dose Hypersensitive Response for Residual pATM and gammaH2AX Foci in Normal Fibroblasts of Cancer Patients. *Int. J. Radiat. Oncol. Biol. Phys.* **2018**, *100*, 756–766. [\[CrossRef\]](#)
38. Del Regato, J.A. Fractionation: A panoramic view. *Int. J. Radiat. Oncol. Biol. Phys.* **1990**, *19*, 1329–1331. [\[CrossRef\]](#)
39. Ellis, F. Fractionation in radiotherapy. In *Modern Trends in Radiotherapy*; Wood, D.A., Ed.; Butterworth: London, UK, 1967; Volume 1, p. 34.
40. Willers, H.; Beck-Bornholdt, H.P. Origins of radiotherapy and radiobiology: Separation of the influence of dose per fraction and overall treatment time on normal tissue damage by Reisner and Miescher in the 1930s. *Radiother. Oncol. J. Eur. Soc. Ther. Radiol. Oncol.* **1996**, *38*, 171–173. [\[CrossRef\]](#)
41. Lasak, J.M.; Gorecki, J.P. The history of stereotactic radiosurgery and radiotherapy. *Otolaryngol. Clin. N. Am.* **2009**, *42*, 593–599. [\[CrossRef\]](#)
42. Klement, R.J.; Sonke, J.J.; Allgauer, M.; Andratschke, N.; Appold, S.; Belderbos, J.; Belka, C.; Dieckmann, K.; Eich, H.T.; Flentje, M.; et al. Estimation of the alpha/beta ratio of non-small cell lung cancer treated with stereotactic body radiotherapy. *Radiother. Oncol. J. Eur. Soc. Ther. Radiol. Oncol.* **2020**, *142*, 210–216. [\[CrossRef\]](#)
43. Stuschke, M.; Pottgen, C. Altered fractionation schemes in radiotherapy. *Front. Radiat. Ther. Oncol.* **2010**, *42*, 150–156. [\[CrossRef\]](#)
44. Nahum, A.E. The radiobiology of hypofractionation. *Clin. Oncol. R. Coll. Radiol.* **2015**, *27*, 260–269. [\[CrossRef\]](#)
45. Brand, D.H.; Kirby, A.M.; Yarnold, J.R.; Somaiah, N. How Low Can You Go? The Radiobiology of Hypofractionation. *Clin. Oncol. R. Coll. Radiol.* **2022**, *34*, 280–287. [\[CrossRef\]](#)
46. Thomas, C.; Charrier, J.; Massart, C.; Cherel, M.; Fertil, B.; Barbet, J.; Foray, N. Low-dose hyper-radiosensitivity of progressive and regressive cells isolated from a rat colon tumour: Impact of DNA repair. *Int. J. Radiat. Biol.* **2008**, *84*, 533–548. [\[PubMed\]](#)
47. Berthel, E.; Foray, N.; Ferlazzo, M.L. The Nucleoshuttling of the ATM Protein: A Unified Model to Describe the Individual Response to High- and Low-Dose of Radiation? *Cancers* **2019**, *11*, 905. [\[CrossRef\]](#) [\[PubMed\]](#)



48. Tsang, M.W. Stereotactic body radiotherapy: Current strategies and future development. *J. Thorac. Dis.* **2016**, *8*, S517–S527. [[CrossRef](#)] [[PubMed](#)]
49. Ferro, M.; Crocetto, F.; Lucarelli, G.; Lievore, E.; Barone, B. Radiotherapy to the Primary Tumor: The First Step of a Tailored Therapy in Metastatic Prostate Cancer. *Diagnostics* **2022**, *12*, 1981. [[CrossRef](#)]

**Disclaimer/Publisher’s Note:** The statements, opinions and data contained in all publications are solely those of the individual author(s) and contributor(s) and not of MDPI and/or the editor(s). MDPI and/or the editor(s) disclaim responsibility for any injury to people or property resulting from any ideas, methods, instructions or products referred to in the content.



# **UP Environment and Space**





## Original research

# Long-term exposure to air pollution at residential and workplace addresses and breast cancer risk: A case-control study nested in the French E3N-Général cohort from 1990 to 2011

Margaux Duboeuf<sup>a,b</sup>, Amina Amadou<sup>a,b</sup>, Thomas Coudon<sup>a,b</sup>, Lény Grassot<sup>a,b</sup>, Marie Ramel-Delobel<sup>a,b,d</sup>, Elodie Faure<sup>c</sup>, Pietro Salizzoni<sup>d,e</sup>, John Gulliver<sup>f</sup>, Gianluca Severi<sup>c,g</sup>, Francesca Romana Mancini<sup>c</sup>, Béatrice Fervers<sup>a,b</sup>, Delphine Praud<sup>a,b,\*</sup>

<sup>a</sup> Department of Prevention Cancer Environment, Centre Léon Bérard, Lyon, France

<sup>b</sup> Inserm, U1296 Unit, "Radiation: Defense, Health and Environment", Lyon, France

<sup>c</sup> Paris-Saclay University, UVSQ, Inserm U1018 unit, Gustave Roussy, Centre de Recherche en Épidémiologie et Santé des Populations (CESP), Villejuif, France

<sup>d</sup> Laboratoire de Mécanique des Fluides et d'Acoustique, University of Lyon, CNRS UMR 5509, Ecole Centrale de Lyon, INSA Lyon, Université Claude Bernard Lyon 1, Ecully, France

<sup>e</sup> Department of Environmental, Land, and Infrastructure Engineering, Politecnico di Torino, Turin, Italy

<sup>f</sup> Centre for Environmental Health and Sustainability, School of Geography, Geology and the Environment, University of Leicester, United Kingdom

<sup>g</sup> Département de Statistiques, Computer Science and Applications "G. Parenti", University of Florence, Italy



## ARTICLE INFO

## Keywords:

Air pollution

Breast cancer

Case-control study

Land use regression

Nitrogen dioxide

Particulate matters

Workplace history

Residential history

## ABSTRACT

**Background:** An increasing evidence links air pollution to breast cancer (BC) risk. Yet, pollutant exposure estimates at the workplace location in pollution exposure assessment have not been considered.

**Objectives:** This study investigates the association between particulate matters (PM<sub>2.5</sub>, PM<sub>10</sub>) and nitrogen dioxide (NO<sub>2</sub>) atmospheric concentrations (1990–2011), at the women's residential and workplace locations, and BC risk.

**Methods:** This case-control study of 2419 BC cases and 2984 controls, was nested in the French prospective E3N cohort. The annual mean PM<sub>2.5</sub>, PM<sub>10</sub> and NO<sub>2</sub> concentrations were estimated using a Land Use Regression model (50 m x 50 m resolution) and assigned to the women's geocoded residential and workplace locations, from cohort recruitment to their index date (date of case diagnosis). Odds ratios (OR) and 95 % confidence intervals (CI) were estimated using multivariate logistic regression models.

**Results:** An increased BC risk was observed for a 10 µg/m<sup>3</sup> increase of the 1990–2011 average PM<sub>2.5</sub> concentration estimates (OR=1.28; CI 1.00, 1.63). An increased risk was suggested for a 10 µg/m<sup>3</sup> increase for PM<sub>10</sub> (OR=1.09; CI 0.92, 1.30) and NO<sub>2</sub> (OR=1.05; CI 0.97, 1.13). No effect modification by menopausal status, nor difference by hormone receptor status were observed.

**Discussion:** This study is the first to estimate BC risk and long-term air pollutant exposure from both, residential and workplace location histories. Results suggest that residential PM<sub>2.5</sub>, PM<sub>10</sub> and NO<sub>2</sub> concentrations are strongly correlated with workplace ones, indicating that residential data may serve as proxy for overall exposure. Future studies should consider exposure during commuting.

## 1. Introduction

Breast cancer is the most common female cancer worldwide, with nearly 2.3 million cases in 2020, and the leading cause of cancer deaths among women (approximately 685,000 deaths in 2020) [1]. Advanced

age, genetic predisposition, hormonal and reproductive factors, and lifestyle are the main risk factors identified to date [2]. However, these remain insufficient to explain all cases of breast cancer. There is an increasing body of evidence and compelling data suggesting an association between some environmental exposures, including outdoor air

\* Correspondence to: Département Prévention Cancer Environnement, Centre Léon Bérard, Inserm U1296 Radiations: Défense, Santé, Environnement, 28 rue Laënnec, 69373 CEDEX 08 Lyon, France.

E-mail address: [delphine.praud@lyon.unicancer.fr](mailto:delphine.praud@lyon.unicancer.fr) (D. Praud).

<https://doi.org/10.1016/j.ejca.2024.114293>

Available online 22 August 2024

0959-8049/© 2024 The Authors. Published by Elsevier Ltd. This is an open access article under the CC BY license (<http://creativecommons.org/licenses/by/4.0/>).



pollution and breast cancer risk [3,4]. Outdoor air pollution is a major public health concern, classified carcinogenic to humans in 2013, by the International Agency for Research on Cancer (IARC) [5]. Air pollution is an ubiquitous complex mixture of solid and liquid particles and gases. Particulate matter (PM) and nitrogen dioxide (NO<sub>2</sub>) are the main components of air pollution in particular in urban areas. PM originating from the residential sector, road traffic, industry and agriculture are classified according to their size, mainly particles with aerodynamic diameters of 10 µm or smaller (PM<sub>10</sub>), and particles of 2.5 µm in diameter or smaller (PM<sub>2.5</sub>). The smaller the particles, the deeper they are able to penetrate into the respiratory system. NO<sub>2</sub> are principally emitted from road traffic and fuel combustion (e.g. heating, power generation). Inhalation is the main exposure route to these pollutants.

A causal link between air pollution and lung cancer and biological mechanisms involved, has been established [6]. However, the link with other cancer sites, including breast cancer, remains more controversial. Several studies supported a statistically significant increased breast cancer risk associated with higher NO<sub>2</sub> atmospheric concentration [7], as well as higher PM<sub>2.5</sub> or PM<sub>10</sub> concentrations [8], while others reported no evidence of an association. The latest meta-analysis on the effect of NO<sub>2</sub>, highlighted a small but significant increase in breast cancer risk with increasing NO<sub>2</sub> concentration (13 studies; RR=1.015; 95 % Confidence Interval (CI) 1.003, 1.028, for a 10 µg/m<sup>3</sup> increase in NO<sub>2</sub>) [7]. Conversely, the most recent meta-analysis on the effect of PM did not show a statistically-significant association neither for PM<sub>2.5</sub> (8 studies; RR=1.006; CI 0.941, 1.076, for a 10 µg/m<sup>3</sup> increase in PM<sub>2.5</sub>), nor PM<sub>10</sub> (7 studies; RR=1.047; CI 0.984, 1.113, for a 10 µg/m<sup>3</sup> increase in PM<sub>10</sub>) [8].

Reliable assessment of PM and NO<sub>2</sub> atmospheric concentrations, emitted from various sources unevenly distributed over the territory with large spatio-temporal concentration variability, is critical to epidemiological studies. The challenge to accurately estimate air pollution exposure is amplified in studies investigating cancer risk, as the latency requires the reconstruction of exposures over long periods [9]. Most published studies to date, in particular those investigating breast cancer risk, relied on exposure estimates at a single point in time (e.g. at inclusion) [10–15] and/or did not consider the subjects' residential history [10–13,16–18]. The uncertainties arising from these estimates may be source of measurement errors, potentially resulting in biased estimates of the exposure effect [19,20]. Moreover, it has been suggested that outdoor air pollution exposure is insufficiently captured when limiting assessment to the residential location. Considering air pollution levels at the workplace location, may better account for variations in daily activity patterns and further enhance the reliability of exposure estimates [21]. However, to our knowledge, workplace location has not been considered in previous studies investigating the link between air pollution and risk of breast cancer.

To overcome these limitations, the present study examines the association of breast cancer risk with long-term PM<sub>2.5</sub>, PM<sub>10</sub> and NO<sub>2</sub> concentrations, estimated at a fine spatial scale at the residential and workplace locations combined. Since breast cancer is a heterogeneous disease, we also investigate this relationship by menopausal status and hormonal subtypes.

## 2. Material and Methods

### 2.1. E3N study

E3N-Génération (Etude Epidémiologique auprès de femmes de l'Education Nationale) is a prospective, national cohort study investigating factors associated with cancer and other chronic diseases in women. To participate in the E3N study, women had to be between 40 and 65 years old, live in metropolitan France, and be insured by a national health insurance plan covering mostly teachers (Mutuelle Générale de l'Education Nationale, MGEN) at the time of inclusion in the cohort between June 1990 and November 1991. They were included

after returning a self-questionnaire and signing an informed consent, in accordance with the French National Commission for Data Protection and Privacy (CNIL). At inclusion, 98,995 women completed the questionnaire, providing information on sociodemographic characteristics, anthropometric measurements, reproductive history, lifestyle, medical history and familial history of cancer [22]. In addition, the participants' birthplace was obtained from the first questionnaire and assigned an urban/rural status based on data from the closest national census. Follow-up questionnaires were sent every 2 to 3 years, with a total of 13 follow-up questionnaires to date. Alcohol-intake was collected from the dietary questionnaire sent in 1993. Breast cancer cases were identified mainly by self-reporting through follow-up questionnaires but for a few from insurance data or the National Service on Causes of Deaths. Overall, nearly 90 % of cases were histologically confirmed.

### 2.2. Study design

The present study used data from the XENAIR case-control study nested in the E3N-Génération cohort [23]. Histologically confirmed incident cases of invasive breast cancer diagnosed between 1990 (inclusion in the E3N-Génération cohort) and 2011 (the 10th questionnaire) were included in the nested case-control study. Breast cancer cases without pathology report confirmation were included because of the very low proportion of self-reported false positives (<5 %). For cases with multiple tumours detected at the same time, the most advanced tumour was considered. Cases must not have a prior diagnosis of any other cancers to be included.

For each breast cancer case, one control was randomly selected by incidence density sampling. At the index date of the case, the controls needed to be in follow-up and without any history of cancer diagnosis. Two groups of cases based on the availability of biological samples (blood or saliva) were used, to ensure the best choice of controls selection and to allow ancillary objectives based on biological samples. For the first group (with a blood sample), controls were matched to cases on the department of residence, age (± 1 year), date (± 3 months), and menopausal status at blood collection. Controls for the second group (without a blood sample) were matched on the same criteria, but at baseline, and additionally matched on availability of a saliva sample.

Women who had missing data on matching variables, as well as their pairs, were excluded (N = 6).

### 2.3. Collection of history of residential and workplace locations

In addition to the information collected in the inclusion and follow-up questionnaires, the addresses of residential and workplace locations (start and end dates for each residence and job) were collected through a specific questionnaire sent out to the participants of the XENAIR case-control study in March 2017. Reminders were sent in June and November 2017. The present study focuses on residential and workplace addresses between 1990 and 2011, corresponding to the follow-up period covered by the XENAIR study [23].

### 2.4. Estimation of long-term PM<sub>2.5</sub>, PM<sub>10</sub> and NO<sub>2</sub> concentrations

In this study, we used modelled pollutant concentration estimates at the residence and workplace locations as a proxy for individual exposure to ambient PM<sub>2.5</sub>, PM<sub>10</sub> and NO<sub>2</sub> concentrations. PM<sub>2.5</sub>, PM<sub>10</sub> and NO<sub>2</sub> concentration levels were estimated at the residential and workplace addresses using a LUR model with 50 m x 50 m spatial resolution and coverage from 1990 to 2011. The LUR model has been described previously [24]. Briefly, LUR is a statistical method using geographical data such as topography (land use, road network, buildings height, etc.), and emission sources (road traffic volume, industrial density, etc.) to predict the concentrations at a given site. The parameters used in each LUR model differ according to the pollutant. In the present study, the LUR models for PM<sub>2.5</sub>, PM<sub>10</sub> and NO<sub>2</sub>, included estimates from a chemical



transport model, length of roads and major roads, density of agriculture and forestry or urban land, residential and commercial density. This model has been validated for the years 2010 and 2011 by comparing its estimates with experimental data collected at monitoring sites, through a hold-out validation, and a back-extrapolation to reconstruct exposure until 1990.

Subjects' residential and workplace addresses were geocoded using a Geographic Information System software ArcMap 10.0 (ArcGIS Locator version 10.0, Environmental System Research Institute – ESRI, Redlands, CA, USA) and the reference street network database (BD Adresse from the French National Geographic Institute (X and Y coordinates) [23]. Addresses were geocoded automatically and 28 % of residential addresses and 65 % of occupational addresses were manually relocated by a trained GIS-technician to improve their accuracy – the high rate for occupational addresses is linked to the fact that people regularly provide the name of the workplace (such as school, university predominantly) rather than the street address. Overall a total of 75 % of residential and 70 % of occupational addresses were geocoded to the exact address, 14 % of residential and 15 % of occupational addresses were located to the street segment and 11 % of residential and 16 % of occupational addresses were geocoded with an accuracy level lower than street segment, i.e., town hall, postal code or city. Annual means of the PM<sub>2.5</sub>, PM<sub>10</sub> and NO<sub>2</sub> concentration estimates were further calculated for each woman, for each calendar year (from 1990 to the index date (date of diagnosis for cases and sampling date for controls)), separately for residential and workplace addresses. The average of the annual mean concentrations (from 1990 to index date) was then calculated for each pollutant, separately for residential and workplace locations. We assumed that E3N women working in the national education system, spent on average nine hours daily at the workplace (including two hours of lunchbreak onsite), five days a week, for at least 36 weeks (i.e. school time) per year, resulting in 18.5 % of the time spent at the workplace. Given that working hours varies according to positions, we rounded up this proportion to 20 %. We further weighted the average pollutant concentrations by the proportion of time spent at home (80 %) and at the workplace (20 %). From the women's retirement, only their residential addresses were taken into account. The combined residential-workplace concentrations for each pollutant refers hereafter to the average of the annual means of the pollutant concentration estimates, weighted according to the time spent at the residence and workplace locations.

## 2.5. Handling of missing data

Under the assumption of missing data at random, multiple imputation was performed for the following variables: education level (3.7 % of missing data), body mass index (BMI) (1.6 % of missing data), alcohol intake (20.7 % of missing data), smoking status (0.5 % of missing data), age at menarche (1.9 % of missing data), parity and age at first full-term pregnancy (AFP) (1.4 % of missing data), and family history of breast cancer (0.8 % of missing data) [25]. We carried out 10 imputations, each with 10 iterations with a multivariate imputation via a chained equations approach (MICE) [25]. Predictors were all variables considered in the different adjustment models. Models specified for multiple imputation were: logistic regression models for binary variables, polynomial logistic regression models for categorical variables with more than two categories and predictive matching models for quantitative variables. The analyses were then performed in parallel for the 10 imputed datasets, and then pooled into imputed data sets and then pooled using Rubin's laws.

Simple imputation was used for menopausal status at inclusion. If age at menopause was missing and a woman's age at inclusion was less than 51 years (median age at menopause of women in the E3N-Généralistes cohort), women were considered premenopausal at inclusion, otherwise, women were considered postmenopausal at inclusion [26].

All women with missing data on oral contraceptive use at index date,

had reported 'never use' at baseline. We assumed for these women continued 'never use' during follow-up, since age at cohort inclusion was 40 to 65 years. No imputation was performed for menopausal hormone therapy (MHT) as this variable is highly dependent on age and menopausal status, but a missing data category was created.

## 2.6. Statistical methods

Baseline socio-demographic characteristics and main risk factors for breast cancer have been described by case-control status. The combined residential-workplace pollutant concentration (main exposure) was estimated on a continuous scale. The linearity of the logit of the effect of the quantitative variables on breast cancer risk was investigated using fractional polynomials of degree 2.

Associations of PM<sub>2.5</sub>, PM<sub>10</sub> and NO<sub>2</sub> with breast cancer risk were modelled using unconditional logistic regression models to estimate odds ratios (OR) for a 10-µg/m<sup>3</sup> increase in combined residential-workplace pollutant concentrations and their 95 % confidence intervals (CI). Unconditional logistic regression models were performed in order to prevent the exclusion of incomplete case-control pairs since not all cases and controls within the same pair from the XENAIR study answered to the specific questionnaire on residential and workplace.

Adjustment variables were selected from a literature review and a directed acyclic graph (DAG), and two models emerged from the DAG (Supplementary material, Fig. S1). The first model was adjusted for matching variables (department of residence, age, date, and menopausal status at baseline or at blood collection), education level, urban/rural status of birthplace and follow-up duration (Model 1). The second model was adjusted for matching variables, urban/rural status of birthplace, follow-up duration, and instead of education level was adjusted for physical activity, BMI, alcohol-intake, smoking- status, oral contraceptive use, MHT, mammography, parity, AFP, and breastfeeding (Model 2). We also considered an additional model adding other adjustment variables widely found in the literature: age at menarche, menopausal status at index date, previous history of personal benign breast disease, previous family history of breast cancer (Model 3). All adjustment variables were taken at baseline with the exception of oral contraceptive and MHT variables, collected from the last questionnaire before the index date, and alcohol intake from the dietary questionnaire (Q3, in 1993).

Additional subgroup analyses were conducted according to breast cancer hormone receptor status (oestrogen receptors (ER), progesterone receptors (PR)). These analyses were carried out using an unconditional logistic regression model comparing cases of each hormonal subtype with all controls, adjusted for the variables of the first model (Model 1).

Effect modification analyses by menopausal status during follow-up (considering menopausal status at inclusion and menopausal status at index date), physical activity, BMI, smoking status and urban/rural status of birthplace, were performed. Menopausal status during follow-up was considered in three categories: premenopausal (women who reported premenopausal on the last returned questionnaire), postmenopausal (women who reported postmenopausal on the last returned questionnaire) and women premenopausal at inclusion who transitioned to postmenopausal status before the index date. Test for interaction for each potential effect modifier was computed by the likelihood ratio test.

## 2.7. Additional and sensitivity analyses

Subjects that could not be included in the analyses because of incomplete workplace history have been described by case-control status.

Additional analyses were performed to investigate the association between air pollution and breast cancer risk depending on the grade, stage and histological subtype of the tumor.

A first sensitivity analysis was carried out considering that women spent 30% of the daily time at the workplace (vs. 20% in our main



analysis) [21]. In a second sensitivity analysis, subjects with short follow-up (<2years) were excluded. In addition, to facilitate comparisons with previous studies, we focused analyses on concentration data evaluated at the residential address only. Finally, we performed an analysis considering only active women at baseline.

All statistical tests were two-sided and p values < 0.05 were considered statistically-significant. All analyses were performed using R Studio software version 4.2.0.

3. Results

3.1. Characteristics of the study population

The selection flowchart of the participants in this case-control study is described in Fig. S2. Briefly, within the E3N cohort, 11,421 women were included in the nested XENAIR case-control study, and received the questionnaire collecting history of residence and workplace locations. Overall, 7824 women returned this questionnaire and were eligible for the present study. Of the 7806 women who completed at least one information in the questionnaire, 5403 had a complete residential and workplace history.

Characteristics of the 2419 breast cancer cases and the 2984 controls are presented in Table 1. The distribution by age was similar in the two groups. Cases were diagnosed, on average at 59.5 ( ± 7.4) years. Cases and controls had a mean follow-up of 12.0 ( ± 5.6) years. Education-level, urban/rural status at birthplace, lifestyle factors, age at menarche, menopausal status and use of oral contraceptives were similar between cases and controls. However, compared to controls, cases had less frequently a child (86.6% vs. 88.8%) and breastfed (54.8% vs. 56.7%). Conversely, cases were more likely to be MHT users (57.0% vs. 55.2%), to have a mammography before inclusion (76.6% vs. 72.0%), and to have a family history of breast cancer in first-degree relatives (17.5% vs. 11.6%) or history of personal benign breast disease (30.1% vs. 23.9%).

The distribution of the combined residential-workplace pollutant concentrations was similar in cases and controls (26.2 ( ± 5.9) µg/m<sup>3</sup> among cases vs. 26.2 ( ± 5.8) µg/m<sup>3</sup> among controls for PM<sub>2.5</sub>; 35.4 ( ± 8.0) µg/m<sup>3</sup> among cases vs. 35.3 ( ± 7.7) µg/m<sup>3</sup> among controls for PM<sub>10</sub>; 30.7 ( ± 15.1) µg/m<sup>3</sup> among cases vs 30.1 ( ± 14.6) µg/m<sup>3</sup> among controls for NO<sub>2</sub>) (Table 1, Figure 1). All women were exposed above the thresholds recommended by World Health Organization (WHO) in 2005 and 2021 [27].

Characteristics of the 1089 subjects (457 cases and 632 controls) who had a complete residential history but an incomplete workplace history are described in Table S1. These subjects were on average older compared to women with a complete residential and workplace history at inclusion (51.3 ( ± 6.5) vs. 47.4 ( ± 5.1) years for cases and 51.8 ( ± 6.4) vs. 47.4 ( ± 5.1) years for controls) and at diagnosis (62.9 ( ± 8.3) vs. 59.4 ( ± 7.4) years respectively) and were more likely to have a secondary education level (16.0% vs. 8.6% respectively). They were comparable in terms of lifestyle factors, except that they were more physically active. Age at menarche was also similar between the two groups. Subjects with an incomplete workplace history had used less frequently an oral contraceptive and were less likely to be nulliparous. However, they were more likely to have used MHT and to have breastfed. The proportion of women who had had menopause was higher at inclusion and at the index date. They were less likely to have a personal or family history of cancer or other breast diseases. Women with incomplete workplace history had similar average annual mean pollutant concentration estimates at the residential address, except for NO<sub>2</sub> whose concentrations were slightly lower compared to women with complete workplace history (28.6 ( ± 14.9) µg/m<sup>3</sup> vs 30.7 ( ± 15.1) µg/m<sup>3</sup> for cases and 28.1 ( ± 13.9) µg/m<sup>3</sup> vs 30.1 ( ± 14.6) µg/m<sup>3</sup> for controls, respectively).

Table 1  
Characteristics of the 2419 cases and 2984 controls, France, 1990–2011.

Characteristics	Cases (n = 2419)	Controls (n = 2984)
	n (%) or mean ± sd	n (%) or mean ± sd
Age at baseline (years)	47.4 ± 5.1	47.4 ± 5.1
Age at diagnosis (years)	59.5 ± 7.4	
Follow-up duration (years)	12.0 ± 5.7	12.0 ± 5.5
LUR PM <sub>2.5</sub> concentration <sup>a</sup> (µg/m <sup>3</sup> )	26.2 ± 5.9	26.2 ± 5.8
LUR PM <sub>10</sub> concentration <sup>a</sup> (µg/m <sup>3</sup> )	35.4 ± 8.0	35.3 ± 7.7
LUR NO <sub>2</sub> concentration <sup>a</sup> (µg/m <sup>3</sup> )	30.7 ± 15.1	30.1 ± 14.6
Level of education		
Secondary	208 (8.6)	246 (8.2)
1- to 2-year university degree	1138 (47.0)	1530 (51.3)
≥ 3 year university degree	978 (40.4)	1105 (37.0)
Missing	95 (3.9)	103 (3.5)
Status of the birthplace		
Rural	730 (30.2)	921 (30.9)
Urban	1689 (69.8)	2063 (69.1)
Body mass index (kg/m <sup>2</sup> )	22.3 ± 2.8	22.2 ± 2.9
Missing	37 (1.5)	50 (1.7)
Physical activity (METs-h/week)	38.2 ± 24.4	39.7 ± 25.4
Alcohol drinking <sup>b</sup> (g/day)	12.6 (14.5)	11.5 (13.7)
Missing	521 (21.5)	595 (19.9)
Smoking status		
Never or former smoker	1257 (52.0)	1582 (53.0)
Current smoker	1149 (47.4)	1388 (46.5)
Missing	13 (0.5)	14 (0.5)
Age at menarche (years)	12.7 ± 1.4	12.8 ± 1.4
Missing	46 (1.9)	59 (2.0)
Previous use of oral contraceptives <sup>c</sup>		
Yes	1600 (66.1)	2000 (67.0)
No	819 (33.9)	984 (33.0)
Parity and age at first full-term pregnancy (years)		
Nulliparous	324 (13.4)	334 (11.2)
1 or 2 children and AFP < 30	1239 (51.2)	1551 (52.0)
1 or 2 children and AFP ≥ 30	290 (12.0)	267 (8.9)
≥ 3	527 (21.8)	794 (26.6)
Missing	39 (1.6)	38 (1.3)
Breastfeeding	2.6 ± 4.0	2.8 ± 4.3
Menopausal status at inclusion		
Premenopausal	1771 (73.2)	2206 (73.9)
Postmenopausal	646 (26.7)	769 (25.8)
Missing	2 (0.1)	9 (0.3)
Menopausal status at index date		
Premenopausal	453 (18.7)	495 (16.6)
Postmenopausal	1966 (81.3)	2489 (83.4)
Use of menopausal replacement therapy <sup>d</sup>		
Yes	1378 (57.0)	1647 (55.2)
No	1020 (42.2)	1304 (43.7)
Missing	21 (0.9)	33 (1.1)
Mammography during the previous follow-up period		
Yes	1853 (76.6)	2149 (72.0)
No	566 (23.4)	835 (28.0)
Previous family history of breast cancer		
First-degree relative <sup>e</sup>	424 (17.5)	347 (11.6)
Second degree relatives	362 (15.0)	379 (12.7)
No familial history	1616 (66.8)	2230 (74.7)
Missing	17 (0.7)	28 (0.9)
Previous history of personal benign breast disease		
Yes	728 (30.1)	713 (23.9)
No	1691 (69.9)	2271 (76.1)

SD, standard deviation; MET, metabolic Equivalent of Task; AFP, age at first full-term pregnancy; PM<sub>2.5</sub>, particulate matter with a diameter < 2.5 µg/m<sup>3</sup>; PM<sub>10</sub>, particulate matter with a diameter < 10 µg/m<sup>3</sup>; NO<sub>2</sub>, nitrogen dioxide

<sup>a</sup> PM<sub>2.5</sub>, PM<sub>10</sub> and NO<sub>2</sub> concentrations correspond to the average of the annual means (1990-index date) at the subject's residential and workplace location combined

<sup>b</sup> Alcohol consumption collected through the food questionnaire (Q3)

<sup>c</sup> Use of oral contraceptive collected between Q1 and index date

<sup>d</sup> Use of menopausal replacement therapy collected between Q2 and index date

<sup>e</sup> Breast cancer among parents, siblings or children



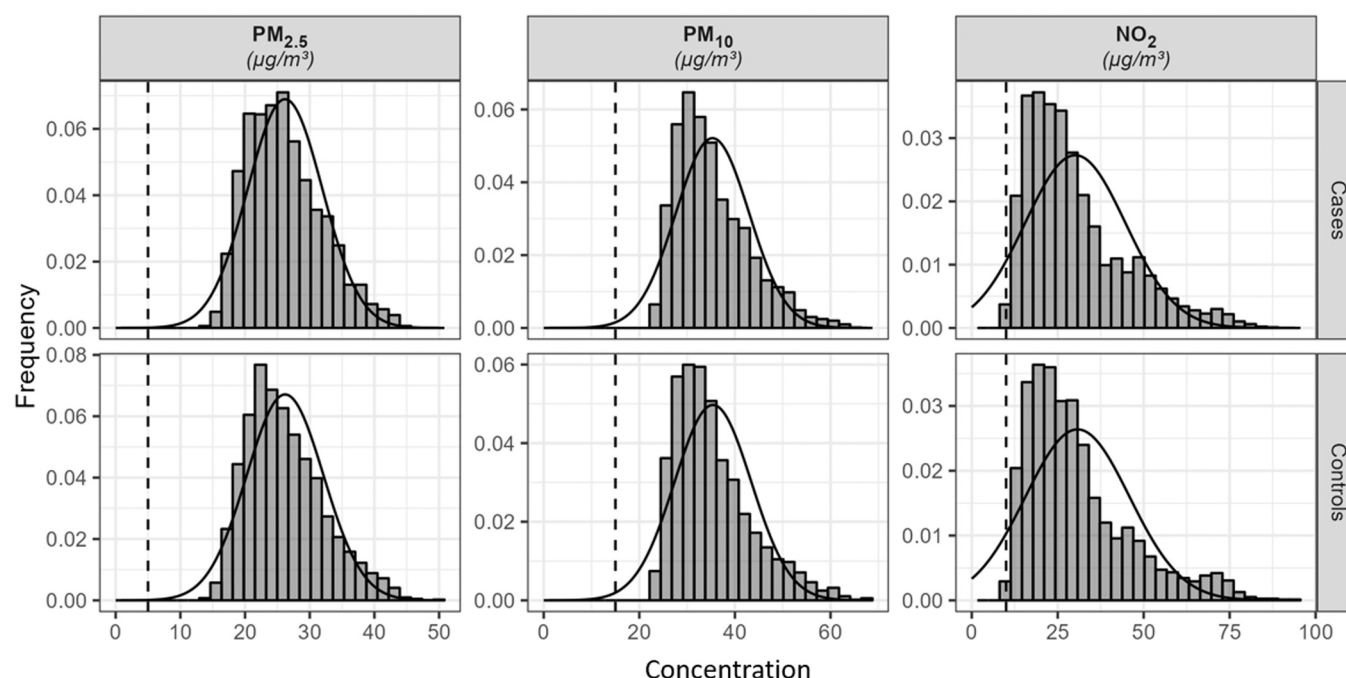


**Fig. 1.** Distribution of the average annual mean exposure to PM<sub>2.5</sub>, PM<sub>10</sub> and NO<sub>2</sub>, at residential and workplace combined during follow-up by case/control status, France, 1990–2011. The solid curve represents the distribution of the mean annual concentration levels for PM<sub>2.5</sub>, PM<sub>10</sub> and NO<sub>2</sub>, if it followed a normal distribution. The vertical dashed line corresponds to the 2021 WHO reference guidelines for PM<sub>2.5</sub>, PM<sub>10</sub> and NO<sub>2</sub>.

### 3.2. Evolution of PM<sub>2.5</sub>, PM<sub>10</sub> and NO<sub>2</sub> concentrations

In 1990, the median PM<sub>2.5</sub>, PM<sub>10</sub> and NO<sub>2</sub> concentrations, were respectively 29.2 µg/m<sup>3</sup> (interquartile range, IQR=9.4 µg/m<sup>3</sup>), 38.0 µg/m<sup>3</sup> (IQR=10.6 µg/m<sup>3</sup>) and 26.6 µg/m<sup>3</sup> (IQR=19.4 µg/m<sup>3</sup>) for residential addresses and respectively 29.7 µg/m<sup>3</sup> (IQR=9.5 µg/m<sup>3</sup>), 38.0 µg/m<sup>3</sup> (IQR=11.0 µg/m<sup>3</sup>) and 28.1 µg/m<sup>3</sup> (IQR=20.2 µg/m<sup>3</sup>) for workplace addresses (Figure 2). PM<sub>2.5</sub> and PM<sub>10</sub> concentrations decreased

largely until 2000, gradually between 2000 and 2011, except in 2003 when particulate concentrations peaked, mainly due to specific weather conditions (a very long European heatwave) resulting in poor dispersion of the pollutants. The decrease in NO<sub>2</sub> concentrations was progressive over the whole follow-up period. In 2011, the median PM<sub>2.5</sub>, PM<sub>10</sub> and NO<sub>2</sub> concentrations were respectively 16.2 µg/m<sup>3</sup> (IQR=4.3 µg/m<sup>3</sup>), 22.2 µg/m<sup>3</sup> (IQR=5.9 µg/m<sup>3</sup>) and 19.3 µg/m<sup>3</sup> (IQR=12.4 µg/m<sup>3</sup>) for residential locations and 16.4 µg/m<sup>3</sup> (IQR=4.4 µg/m<sup>3</sup>), 22.4 µg/m<sup>3</sup>

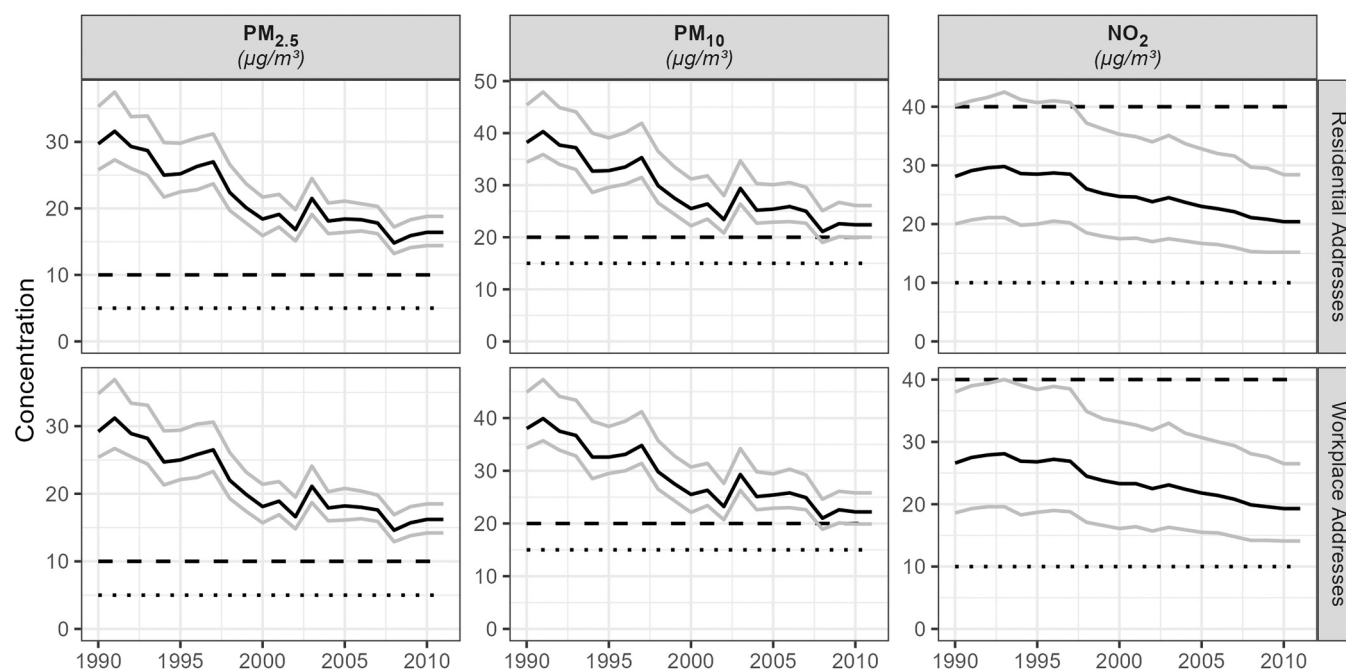


**Fig. 2.** Evolution of the annual mean hourly atmospheric concentrations (median, 1<sup>st</sup> and 3<sup>rd</sup> quartiles) for PM<sub>2.5</sub>, PM<sub>10</sub> and NO<sub>2</sub>, at the residential addresses and workplace addresses of the study subjects, France, 1990–2011. Horizontal dashed lines correspond to 2005 and 2021 WHO reference guidelines for PM<sub>2.5</sub>, PM<sub>10</sub> and NO<sub>2</sub>.



(IQR=6.1 µg/m<sup>3</sup>) and 20.4 µg/m<sup>3</sup> (IQR=13.2 µg/m<sup>3</sup>) for workplace locations. In 2011, these concentrations remained well above the current WHO thresholds, especially for PM<sub>2.5</sub>. Correlation between the average of the annual mean exposure to PM<sub>2.5</sub>, PM<sub>10</sub> and NO<sub>2</sub> at residential and workplace combined were high, 0.91 for PM<sub>2.5</sub> and PM<sub>10</sub>, 0.82 for PM<sub>2.5</sub> and NO<sub>2</sub> and 0.83 for PM<sub>10</sub> and NO<sub>2</sub> (Supplementary material, Table S2).

3.3. Association between PM2.5, PM10 and NO2 concentrations and breast cancer risk

There was a positive association between combined residential-workplace concentration estimates for PM<sub>2.5</sub> and risk of breast cancer, with ORs of 1.28 (CI 1.00, 1.63) and 1.28 (CI 1.00, 1.64) per each 10-µg/m<sup>3</sup> increment, for first and second model, respectively (Table 2). For the third adjustment model, the association with PM<sub>2.5</sub> was not statistically-significant but suggested a trend towards increased risk of breast cancer with OR of 1.24 (CI 0.97, 1.58). For PM<sub>10</sub> and NO<sub>2</sub> concentrations, a statistically non-significant positive association with breast cancer risk was observed in the three models (as an example: OR=1.09; CI 0.92, 1.30 for PM<sub>10</sub> and OR=1.05; CI 0.97, 1.13 for NO<sub>2</sub> in Model 1) (Table 2). Given that risk estimates in the main analyses were similar for the three adjustment models, all additional and sensitivity analyses were performed using the first model, containing fewer variables and thus less uncertainties arising from multiple imputations.

When considering pollutant concentration estimates at the residential address only, ORs were similar to those obtained by weighted residential-workplace pollutant concentrations (OR=1.29; CI 1.02, 1.62 for PM<sub>2.5</sub>; OR=1.10; CI 0.93, 1.31 for PM<sub>10</sub> and OR=1.05; CI 0.98, 1.13 for NO<sub>2</sub>) (Table 3).

By hormone receptor status, an increase of breast cancer risk, albeit

Table 2

Odds ratios (ORs), 95% confidence intervals (95% CIs) and associated *p* values, of breast cancer among 2419 cases and 2984 controls, for the association with the average of the annual mean exposure to PM<sub>2.5</sub> PM<sub>10</sub> and NO<sub>2</sub>, at residential and workplace addresses combined, in all women, France, 1990–2011.

	OR (95% CI)	<i>P</i> value
PM <sub>2.5</sub> (for an increase of 10 µg/m <sup>3</sup> )		
Model 1 <sup>f</sup>	1.28 (1.00, 1.63)	0.047
Model 2 <sup>g</sup>	1.28 (1.00, 1.64)	0.046
Model 3 <sup>h</sup>	1.24 (0.97, 1.58)	0.086
PM <sub>10</sub> (for an increase of 10 µg/m <sup>3</sup> )		
Model 1 <sup>f</sup>	1.09 (0.92, 1.30)	0.318
Model 2 <sup>g</sup>	1.10 (0.92, 1.31)	0.291
Model 3 <sup>h</sup>	1.07 (0.90, 1.28)	0.455
NO <sub>2</sub> (for an increase of 10 µg/m <sup>3</sup> )		
Model 1 <sup>f</sup>	1.05 (0.97, 1.13)	0.222
Model 2 <sup>g</sup>	1.05 (0.97, 1.13)	0.210
Model 3 <sup>h</sup>	1.05 (0.97, 1.13)	0.242

OR, Odds ratio; 95% CI, 95% confidence intervals; PM<sub>2.5</sub>, particulate matters with a diameter < 2.5 µg/m<sup>3</sup>; PM<sub>10</sub>, particulate matters with a diameter < 10 µg/m<sup>3</sup>; NO<sub>2</sub>, nitrogen dioxide

<sup>f</sup> Adjusted for matching variables (age at inclusion or at blood collection, date of return of inclusion questionnaire or at blood collection, menopausal status at inclusion or at blood collection, department of residence at inclusion or at blood collection, availability of a salivary sample), level of education, urban/rural status of birthplace and follow-up duration.

<sup>g</sup> Adjusted for matching variables (age at inclusion or at blood collection, date of return of inclusion questionnaire or at blood collection, menopausal status at inclusion or at blood collection, department of residence at inclusion or at blood collection, availability of a salivary sample), and physical activity, body mass index, alcohol intake, smoking status, oral contraceptive use, menopausal hormone therapy use, mammography, parity, age at first full-term pregnancy, breastfeeding and follow-up duration.

<sup>h</sup> Adjusted for model 1 variables, and age at menarche, previous family of breast cancer, personal history of benign breast cancer, menopausal status at index date and follow-up duration.

Table 3

Odds ratios (ORs) and 95% confidence intervals (95% CIs) for the association between breast cancer and average of the annual means concentrations at residential location, France, 1990–2011.

	Cases/controls	OR <sup>i</sup> (95% CI)
PM <sub>2.5</sub> (for an increment of 10 µg/m <sup>3</sup> )	2419/2984	1.29 (1.02, 1.62)
PM <sub>10</sub> (for an increment of 10 µg/m <sup>3</sup> )	2419/2984	1.10 (0.93, 1.31)
NO <sub>2</sub> (for an increment of 10 µg/m <sup>3</sup> )	2419/2984	1.05 (0.98, 1.13)

OR, Odds ratio; 95% CI, 95% confidence intervals; PM<sub>2.5</sub>, particulate matters with a diameter < 2.5 µg/m<sup>3</sup>; PM<sub>10</sub>, particulate matters with a diameter < 10 µg/m<sup>3</sup>; NO<sub>2</sub>, nitrogen dioxide

<sup>i</sup> Adjusted for matching variables (age at inclusion or at blood collection, date of return of inclusion questionnaire or at blood collection, department of residence at inclusion or at blood collection, availability of a salivary sample), level of education, urban/rural status of birthplace, and follow-up duration (Model 1)

not statistically significant, was observed for ER-positive (ER+) breast cancer (OR=1.31; CI 0.99, 1.73 for PM<sub>2.5</sub> and OR=1.05; CI 0.96, 1.14 for NO<sub>2</sub>) and for ER-positive and PR-positive (ER+PR+) breast cancer (OR=1.32; CI 0.97, 1.79 for PM<sub>2.5</sub> and OR=1.04; CI 0.95, 1.14 for NO<sub>2</sub>) (Table 4). Results were similar for ER-negative (ER-) breast cancer and for ER-negative PR-negative (ER-PR-) breast cancer, although with wider 95% CI probably due to the limited number of cases included in this analysis (Table 4).

There were no statistically significant interactions with menopausal status for any of the pollutants (all *p* values for interaction>0.05). Nevertheless, considering the relevance of menopausal status in the

Table 4

Odds ratios (ORs) and 95% confidence intervals (95% CIs) for the association between breast cancer and average of the annual mean exposure to PM<sub>2.5</sub> PM<sub>10</sub> and NO<sub>2</sub>, at residential and workplace combined, by hormone receptor status, France, 1990–2011.

	Cases/controls	OR <sup>j</sup> (95% CI)
PM <sub>2.5</sub> (for an increment of 10 µg/m <sup>3</sup> )		
ER-	347/2984	1.29 (0.77, 2.16)
ER+	1662/2984	1.31 (0.99, 1.73)
PR-	681/2984	1.28 (0.87, 1.89)
PR+	1328/2984	1.30 (0.96, 1.76)
ER-/PR-	282/2984	1.36 (0.76, 2.41)
ER-/PR+	65/2984	0.97 (0.33, 2.83)
ER+ /PR-	399/2984	1.26 (0.78, 2.03)
ER+ /PR+	1254/2984	1.32 (0.97, 1.79)
Missing	403/2984	1.12 (0.72, 1.74)
PM <sub>10</sub> (for an increment of 10 µg/m <sup>3</sup> )		
ER-	347/2984	1.06 (0.73, 1.53)
ER+	1662/2984	1.06 (0.87, 1.30)
PR-	681/2984	1.00 (0.75, 1.32)
PR+	1328/2984	1.09 (0.88, 1.35)
ER-/PR-	282/2984	1.06 (0.70, 1.61)
ER-/PR+	65/2984	0.97 (0.44, 2.11)
ER+ /PR-	399/2984	0.97 (0.69, 1.38)
ER+ /PR+	1254/2984	1.09 (0.88, 1.37)
Missing	403/2984	1.14 (0.84, 1.56)
NO <sub>2</sub> (for an increment of 10 µg/m <sup>3</sup> )		
ER-	347/2984	1.06 (0.91, 1.24)
ER+	16462/2984	1.05 (0.96, 1.14)
PR-	681/2984	1.08 (0.96 –1.21)
PR+	1328/2984	1.03 (0.94, 1.13)
ER-/PR-	282/2984	1.08 (0.91, 1.29)
ER-/PR+	65/2984	0.96 (0.67, 1.36)
ER+ /PR-	399/2984	1.07 (0.92, 1.24)
ER+ /PR+	1254/2984	1.04 (0.95, 1.14)
Missing	410/2984	1.04 (0.90, 1.20)

OR, Odds ratio; 95% CI, 95% confidence intervals; PM<sub>2.5</sub>, particulate matters with a diameter < 2.5 µg/m<sup>3</sup>; PM<sub>10</sub>, particulate matters with a diameter < 10 µg/m<sup>3</sup>; NO<sub>2</sub>, nitrogen dioxide

<sup>j</sup> Adjusted for matching variables (age at inclusion or at blood collection, date of return of inclusion questionnaire or at blood collection, department of residence at inclusion or at blood collection, availability of a salivary sample), level of education, urban/rural status of birthplace and follow-up duration (Model 1)



aetiology of breast cancer, we performed stratified analyses on menopausal status during follow-up. The results suggested a similar increase risk associated with PM<sub>2.5</sub> and NO<sub>2</sub> in premenopausal women, in women who transitioned to postmenopausal status before the index date and in postmenopausal women (Table 5).

There was no evidence of effect modification by education level, total physical activity, BMI, smoking status and breastfeeding (p for interaction>0.05) (Table S3).

3.4. Additional and sensitivity analyses

The association between air pollution and breast cancer risk was not substantially different depending on the grade, stage and histological subtype (Supplementary material, Table S4). Similar results were also obtained when increasing the time spent at the workplace location (30%, vs. 20% in the main analyses) (OR= 1.27; CI 0.99, 1.62 for PM<sub>2.5</sub>; OR= 1.09; CI 0.91, 1.29 for PM<sub>10</sub> and OR= 1.05; CI 0.97, 1.13 for NO<sub>2</sub>) (Supplementary material, Table S5). Moreover, after excluding women followed for less than two years (n = 248), the ORs associated with a 10-µg/m<sup>3</sup> increase of combined residential-workplace concentration were consistent with ORs for the overall population (OR=1.30; CI 1.01, 1.67 for PM<sub>2.5</sub>; OR=1.08; CI 0.90, 1.30 for PM<sub>10</sub> and OR=1.05; CI 0.97, 1.13 for NO<sub>2</sub>) (Supplementary material, Table S6).

When excluding women who were already retired at baseline (606 cases and 722 controls), the OR was slightly higher than for the overall study population for PM<sub>2.5</sub>, (OR=1.61; CI 0.96, 2.71) and similar for PM<sub>10</sub> and NO<sub>2</sub> (OR=1.02; CI 0.71, 1.45 for PM<sub>10</sub> and OR=0.99; CI 0.85, 1.16 for NO<sub>2</sub>) (Supplementary material Table S7).

4. Discussion

To the best of our knowledge, this case-control study is the first study

**Table 5**  
Odds ratios (ORs) and 95% confidence intervals (95% CIs) for the association between breast cancer and average of the annual mean exposure to PM<sub>2.5</sub> PM<sub>10</sub> and NO<sub>2</sub>, at residential and workplace combined, by menopausal status during follow-up, France, 1990–2011.

	Cases/ controls	OR <sup>k</sup> (95% CI)	p- value <sup>l</sup>
PM <sub>2.5</sub> (for an increment of 10 µg/m <sup>3</sup> )			0.99
Premenopausal	453/495	1.26 (0.94, 1.70)	
Premenopausal at inclusion & postmenopausal before index date	1312/1700	1.28 (0.98, 1.67)	
Postmenopausal	633/756	1.27 (0.95, 1.70)	
PM <sub>10</sub> (for an increment of 10 µg/m <sup>3</sup> )			0.90
Premenopausal	453/495	1.09 (0.87, 1.36)	
Premenopausal at inclusion & postmenopausal before index date	1312/1700	1.07 (0.89, 1.30)	
Postmenopausal	633/756	1.13 (0.91, 1.39)	
NO <sub>2</sub> (for an increment of 10 µg/m <sup>3</sup> )			0.86
Premenopausal	453/495	1.07 (0.96, 1.19)	
Premenopausal at inclusion & postmenopausal before index date	1312/1700	1.05 (0.97, 1.14)	
Postmenopausal	633/756	1.04 (0.94, 1.15)	

OR, Odds ratio; 95% CI, 95% confidence intervals; PM<sub>2.5</sub>, particulate matters with a diameter < 2.5 µg/m<sup>3</sup>; PM<sub>10</sub>, particulate matters with a diameter < 10 µg/m<sup>3</sup>; NO<sub>2</sub>, nitrogen dioxide

<sup>k</sup> Adjusted for matching variables (age at inclusion or at blood collection, date of return of inclusion questionnaire or at blood collection, department of residence at inclusion or at blood collection, availability of a salivary sample), level of education, urban/rural status of birthplace and follow-up duration (Model 1)

<sup>l</sup> P-values derived from a likelihood ratio test

to investigate combined residential-workplace air pollution exposure over 22 years, and its association with breast cancer risk. Our results suggest a positive association between cumulative long-term exposure to air pollution including PM<sub>2.5</sub>, PM<sub>10</sub> and NO<sub>2</sub> exposure. Results were consistent across the three adjustment models and robust to sensitivity analyses. Findings were comparable when using only residence concentration estimates suggesting that residential data could serve as a proxy for overall exposure in the population of the present study.

These findings are in line with several previous studies that have found an increase in breast cancer risk among subjects exposed to higher levels of PM<sub>2.5</sub> and similar to our study [8], two studies investigated PM<sub>2.5</sub> exposure level estimates over a period of over 20 years [12,28]. A recent meta-analysis summarized these results and reported a pooled RR of 1.006 (CI 0.941–1.076) [8]. However, none of these studies considered workplace concentrations in addition to residential concentrations. Of note, the mean of PM<sub>2.5</sub> exposure levels over all studies included in this meta-analysis of 10.9 µg/m<sup>3</sup>, was quite lower than in the present study.

Our results on PM<sub>10</sub> exposure are in line with the last published meta-analysis showing a border line positive association with breast cancer risk [8]. Among the seven studies published to date, only one reported a statistically significant increased breast cancer risk (OR=1.19; CI 1.09, 1.31), for a 10 µg/m<sup>3</sup> increment of PM<sub>10</sub> [8].

Current evidence for an association with breast cancer risk appears to be stronger for NO<sub>2</sub> [7]. Our findings of a positive association, was consistent with the results of a previous study on NO<sub>2</sub> exposure in a larger sample of the E3N cohort population, associated with a significant increase of breast cancer risk (OR=1.09; CI: 1.01, 1.31) for an inter-quartile range increase in NO<sub>2</sub> levels (estimated with a LUR model = 17.8 µg/m<sup>3</sup>) [24], as well as the results of two recent meta-analyses reporting an association for NO<sub>2</sub> with breast cancer risk (RR=1.015; CI 1.003, 1.028 and RR= 1.023; CI 1.005, 1.041) [7,8].

Our study did not suggest a differential effect according to menopausal status, unlike several previous studies [12,14,17,29–31]. However, the question of whether air pollution affects breast cancer risk differently according to menopausal status is still open and needs to be investigated further.

The results do not support that the relationship between pollutant concentrations and breast cancer risk varies by hormone receptor status. However we observed a trend towards an increased risk of ER+ and ER+PR+ breast cancers consistent with several other studies [4,28,32].

The differences might be due to the higher exposure levels observed in our study population compared to those in previous studies [7,8]. However, difference in exposure assessment methodology may also explain the heterogeneity of results between studies in terms of spatial resolution (from <100 m to 10 kilometres), geographical coverage (regional to national coverage) and temporal resolution[7,8]. Previous studies have investigated whether combined residential-workplace concentration of NO<sub>2</sub> better reflects overall personal concentration, suggesting that workplace locations are strong determinants of NO<sub>2</sub> concentration[33,34]. Nethery et al. in their review on air pollution exposure technologies in 2008 concluded that combining workplace location pollutant concentrations with residential location concentrations improves estimates of personal exposure by taking into account variation in time-activity patterns that result in exposure differences for individuals living in the same community, in fact correlation between NO estimates with land use regression and measurements changed from r = 0.49 to r = 0.55 [33]. Two studies assessed the impact of NO<sub>2</sub> and PM concentrations at the school or workplace on health effects (such as birth outcomes, overweight and obesity), over shorter periods, with divergent findings [35,36]. The study by de Bont et al. investigating the associations between ambient air pollution exposure at both home and school location, and obesity in children, reported higher risks for childhood overweight and obesity, especially for a higher exposure at school location [35]. Conversely, in the study by Dibben et al., studying maternal ambient air pollution exposure related to birth outcomes, the



inclusion of workplace location exposure showed negligible differences in the effect size compared to considering residential exposure only [36].

No previous studies considered combined residential-workplace concentration over long periods, and none of the studies published to date on the effects of air pollution on breast cancer risk considered concentrations at the workplace addresses. In this study, the small differences observed in breast cancer risk estimates, whether or not the workplace concentration was considered and the strong correlation between concentration at the residential and workplace locations ( $r = 0.95$  for  $PM_{2.5}$ ;  $r = 0.93$  for  $PM_{10}$ ;  $r = 0.90$  for  $NO_2$ ) may suggest that concentrations at the residential address may be a good proxy of the overall exposure [33]. Yet, we did not consider daily variations in pollutant concentrations. Daytime concentrations at the workplace, especially for  $NO_2$  could be higher than concentrations averaged over 24 h. Moreover, the lack of difference in risk estimates could also be explained by the high proportion of retired women (*i.e.* 38% were already retired at baseline).

Although the biological mechanisms by which air pollution may cause breast cancer remains unclear, several key biological mechanisms have been proposed. Air pollution has been reported to increase breast density [37], which is an important risk factor for breast cancer [38]. In addition, several pollutants, including  $NO_2$ , are suspected of having endocrine-disrupting properties [39]. Hormone exposure is one of the key drivers in the development of breast cancer [40]. Also, air pollution, including PM is reported to induce inflammation and oxidation stress, associated with both breast cancer development and progression [41]. Air pollutants can also cause epigenetic modifications, such as DNA methylation, involved in tumorigenesis [42]. Furthermore,  $PM_{2.5}$ ,  $PM_{10}$  and  $NO_2$  are traffic-related air pollutants (TRAP), representing a complex mixture of several pollutants such as polycyclic aromatic hydrocarbons (PAHs) suspected of being carcinogenic due to their potential cytotoxic, mutagenic, epigenetic, inflammatory and endocrine-disrupting effects [39,43]. Finally, exposure to air pollution can alter immune function, resulting in suppression of immune responses and modulation of immune cell activity [44].

This study presents several strengths. First, it is based on a relatively large sample size (5403 subjects), from a large prospective cohort with a high participation rate during follow-up questionnaires, ranging from 77% to 92% [22]. The participation rate in the present study for the specific questionnaire, gathering information of residential and workplace history, is relatively high (65%) given the advanced average age of the participants at the time of data collection (74 years) and that some have since died. Thanks to the large amount of data collected within the E3N-Générations cohort, we could adjust for most of the potential confounding factors known to date. Moreover, the long-term follow-up of up to 22 years allowed for consider the effect of chronic exposure to  $PM_{2.5}$ ,  $PM_{10}$  and  $NO_2$ , in contrast to most other studies that measure exposure over shorter periods [7,8]. A major strength of our study was the availability of the residential and workplace history to obtain the finest possible air pollutant concentration estimates. Furthermore, most women from the E3N-Générations cohort were teachers or worked in affiliated occupations, thus it can be assumed that exposures related to the occupational tasks were homogeneously low among study participants.

This present study has also several limitations. Despite the two decades of follow-up, concentration information for the three pollutants before 1990 was lacking. This is due to scarcity of historical air pollutant concentration data precluding assessment of air pollution concentration before 1990, leading to left truncation lifetime exposure data on potentially relevant critical windows exposure for breast cancer (in utero, early years of life, puberty, *etc.*) [39,45,46]. Nonetheless, we adjusted for urban/rural status at the birthplace as a surrogate of air pollution concentration before inclusion into the cohort. Moreover, we took into account menopausal status in our analysis. We looked at this association specifically in women who had undergone menopause

during follow-up (pre-menopausal at inclusion and post-menopausal before index date) which is a significant period in a woman's life, marked by hormonal changes that may influence her susceptibility to various health conditions, including breast cancer due to structural and functional changes in breast tissue [45]. Failure to consider exposure during windows of susceptibility have led to non-differential bias in the OR estimates, resulting in inaccurate estimation of the true impact of air pollution on breast cancer risk [46]. Finally, given that the majority of our population lived and worked in urban areas (where most of the emission sources of the pollutants taken into account in this study are located), the exposure contrast was perhaps insufficient to identify a differential risk between residential and combined residential and workplace exposure.

## 5. Conclusion

In conclusion, this study found a positive association between the average of the annual means of  $PM_{2.5}$  atmospheric concentrations at residential and workplace locations combined and the risk of overall breast cancer. An increased risk of breast cancer was also suggested for  $PM_{10}$  and  $NO_2$ . Yet, these results need to be confirmed by future studies in other population.

Future epidemiological studies should also explore the impact of exposure while commuting and of diurnal variations in pollutants' concentrations on the risk of breast cancer.

## Funding

This work was financially supported by The French National Research Program for Environmental and Occupational Health of Anses (2019/1/242), Fondation de France (n°00099899) and the canceropole of Lyon Auvergne Rhône-Alpes (Grant OncoStarter). The part of the project allowing to collect residential and workplace addresses was financially supported by the French National Institute for Cancer (INCa) (SHSESP17-070). The research was carried out using data from the French National Institute of Health and Medical Research (Inserm) E3N-generation cohort, which was established and maintained with the support of the Mutuelle Générale de l'Éducation Nationale (MGEN), the Gustave Roussy Institute and the Ligue Contre le Cancer. E3N-Generations cohort is also supported by the French National Research Agency (ANR) under the Investment for the future Program (PIA) (ANR-10-COHO-0006); and by the French Ministry of Higher Education, Research and Innovation (#2103 586016). Marie Ramel-Delobel was supported with a PhD fellowship from the French League against cancer. Amina Amadou was supported by the Regional Committee of the French League against Cancer of the Savoie Region. The funding body had no role in the conception, design, planning, or writing of the study.

## CRedit authorship contribution statement

**Pietro Salizzoni:** Writing – review & editing. **John Gulliver:** Writing – review & editing. **Gianluca Severi:** Writing – review & editing. **Francesca Romana Mancini:** Writing – review & editing. **Thomas Coudon:** Writing – review & editing, Funding acquisition, Data curation. **Lény Grassot:** Writing – review & editing, Software, Data curation. **Marie Ramel-Delobel:** Writing – review & editing, Software, Methodology, Data curation. **Elodie Faure:** Writing – review & editing, Data curation. **Delphine Praud:** Writing – review & editing, Validation, Supervision, Project administration, Methodology, Funding acquisition, Conceptualization. **Margaux Duboeuf:** Writing – original draft, Software, Methodology, Formal analysis. **Amina Amadou:** Writing – review & editing. **Béatrice Fervers:** Writing – review & editing, Funding acquisition.



## Declaration of Competing Interest

The authors declare that they have no known competing financial interests or personal relationships that could have appeared to influence the work reported in this paper.

## Acknowledgments

We gratefully acknowledge the E3N-generation cohort participants for providing data and the practitioners for providing pathology reports. We also thank Charlotte Carretero, Matthieu Dubuis and Kathleen Godet for addresses geocoding, Elodie Belladame for the datamanagement of residential and workplace addresses, Céline Kernaléguen, Maxime Valdenaire, Laureen Dartois, Roselyn Gomes-Rima, and Amandine Gelot for the data management and the assistance for the cohort data collection.

## Data sharing

Access to the data can be requested from the corresponding author upon reasonable request and after acceptance by the E3N-generation cohort coordinator and its scientific board.

## Appendix A. Supporting information

Supplementary data associated with this article can be found in the online version at [doi:10.1016/j.ejca.2024.114293](https://doi.org/10.1016/j.ejca.2024.114293).

## References

- [1] Sung H, Ferlay J, Siegel RL, Laversanne M, Soerjomataram I, Jemal A, et al. Global Cancer Statistics 2020: GLOBOCAN Estimates of Incidence and Mortality Worldwide for 36 Cancers in 185 Countries. *CA Cancer J Clin* 2021;71:209–49. <https://doi.org/10.3322/caac.21660>.
- [2] Akram M, Iqbal M, Daniyal M, Khan AU. Awareness and current knowledge of breast cancer. *Biol Res* 2017;50:33. <https://doi.org/10.1186/s40659-017-0140-9>.
- [3] Gamboa-Loira B, López-Carrillo L, Mar-Sánchez Y, Stern D, Cebrían ME. Epidemiologic evidence of exposure to polycyclic aromatic hydrocarbons and breast cancer: A systematic review and meta-analysis. *Chemosphere* 2022;290:133237. <https://doi.org/10.1016/j.chemosphere.2021.133237>.
- [4] White AJ, Bradshaw PT, Hamra GB. Air pollution and Breast Cancer: A Review. *Curr Epidemiol Rep* 2018;5:92–100. <https://doi.org/10.1007/s40471-018-0143-2>.
- [5] Loomis D, Grosse Y, Lauby-Secretan B, Ghissassi FE, Bouvard V, Benbrahim-Tallaa L, et al. The carcinogenicity of outdoor air pollution. *Lancet Oncol* 2013;14:1262–3. [https://doi.org/10.1016/S1470-2045\(13\)70487-X](https://doi.org/10.1016/S1470-2045(13)70487-X).
- [6] Hamra GB, Laden F, Cohen AJ, Raaschou-Nielsen O, Brauer M, Loomis D. Lung Cancer and Exposure to Nitrogen Dioxide and Traffic: A Systematic Review and Meta-Analysis. *Environ Health Perspect* 2015;123:1107–12. <https://doi.org/10.1289/ehp.1408882>.
- [7] Praud D, Deygas F, Amadou A, Bouilly M, Turati F, Bravi F, et al. Traffic-Related Air Pollution and Breast Cancer Risk: A Systematic Review and Meta-Analysis of Observational Studies. *Cancers* 2023;15:927. <https://doi.org/10.3390/cancers15030927>.
- [8] Gabet S, Lemarchand C, Guénel P, Slama R. Breast Cancer Risk in Association with Atmospheric Pollution Exposure: A Meta-Analysis of Effect Estimates Followed by a Health Impact Assessment. *Environ Health Perspect* 2021;129:057012. <https://doi.org/10.1289/EHP8419>.
- [9] Coudon T, Nguyen CV, Volta P, Grassot L, Couvidat F, Souhac L, et al. Retrospective Modeling of NO<sub>2</sub> and PM<sub>10</sub> Concentrations over the Lyon Metropolitan Area (France), 1990–2010—Performance Evaluation, Exposure Assessment and Correlation between Pollutants. *Atmosphere* 2021;12:239. <https://doi.org/10.3390/atmos12020239>.
- [10] Andersen ZJ, Stafoggia M, Weinmayr G, Pedersen M, Galassi C, Jørgensen JT, et al. Long-Term Exposure to Ambient Air Pollution and Incidence of Postmenopausal Breast Cancer in 15 European Cohorts within the ESCAPE Project. *Environ Health Perspect* 2017;125:107005. <https://doi.org/10.1289/EHP1742>.
- [11] Datzmann T, Markevych I, Trautmann F, Heinrich J, Schmitt J, Tesch F. Outdoor air pollution, green space, and cancer incidence in Saxony: a semi-individual cohort study. *BMC Public Health* 2018;18:715. <https://doi.org/10.1186/s12889-018-5615-2>.
- [12] White AJ, Keller JP, Zhao S, Carroll R, Kaufman JD, Sandler DP. Air Pollution, Clustering of Particulate Matter Components, and Breast Cancer in the Sister Study: A U.S.-Wide Cohort. *Environ Health Perspect* 2019;127:107002. <https://doi.org/10.1289/EHP5131>.
- [13] White AJ, Gregoire AM, Niehoff NM, Bertrand KA, Palmer JR, Coogan PF, et al. Air pollution and breast cancer risk in the Black Women's Health Study. *Environ Res* 2021;194:110651. <https://doi.org/10.1016/j.envres.2020.110651>.
- [14] Goldberg MS, Villeneuve PJ, Crouse D, To T, Weichenthal SA, Wall C, et al. Associations between incident breast cancer and ambient concentrations of nitrogen dioxide from a national land use regression model in the Canadian National Breast Screening Study. *Environ Int* 2019;133:105182. <https://doi.org/10.1016/j.envint.2019.105182>.
- [15] Goldberg MS, Labreche F, Weichenthal S, Lavigne E, Valois M-F, Hatzopoulou M, et al. The association between the incidence of postmenopausal breast cancer and concentrations at street-level of nitrogen dioxide and ultrafine particles. *Environ Res* 2017;158:7–15. <https://doi.org/10.1016/j.envres.2017.05.038>.
- [16] Crouse DL, Goldberg MS, Ross NA, Chen H, Labreche F. Postmenopausal Breast Cancer Is Associated with Exposure to Traffic-Related Air Pollution in Montreal, Canada: A Case-Control Study. *Environ Health Perspect* 2010;118:1578–83. <https://doi.org/10.1289/ehp.1002221>.
- [17] Villeneuve PJ, Goldberg MS, Crouse DL, To T, Weichenthal SA, Wall C, et al. Residential exposure to fine particulate matter air pollution and incident breast cancer in a cohort of Canadian women. *Environ Epidemiol* 2018;2:e021. <https://doi.org/10.1097/EE9.0000000000000021>.
- [18] To T, Zhu J, Villeneuve PJ, Simatovic J, Feldman L, Gao C, et al. Chronic disease prevalence in women and air pollution — A 30-year longitudinal cohort study. *Environ Int* 2015;80:26–32. <https://doi.org/10.1016/j.envint.2015.03.017>.
- [19] Basagaña X, Aguilera I, Rivera M, Agis D, Foraster M, Marrugat J, et al. Measurement Error in Epidemiologic Studies of Air Pollution Based on Land-Use Regression Models. *Am J Epidemiol* 2013;178:1342–6. <https://doi.org/10.1093/aje/kwt127>.
- [20] Wei Y, Qiu X, Yazdi MD, Shtein A, Shi L, Yang J, et al. The Impact of Exposure Measurement Error on the Estimated Concentration-Response Relationship between Long-Term Exposure to PM<sub>2.5</sub> and Mortality. *Environ Health Perspect* 2022;130:077006. <https://doi.org/10.1289/EHP10389>.
- [21] Reis S, Liška T, Vieno M, Carnell EJ, Beck R, Clemens T, et al. The influence of residential and workday population mobility on exposure to air pollution in the UK. *Environ Int* 2018;121:803–13. <https://doi.org/10.1016/j.envint.2018.10.005>.
- [22] Clavel-Chapelon F. Cohort Profile: The French E3N Cohort Study. *Int J Epidemiol* 2015;44:801–9. <https://doi.org/10.1093/ije/dyu184>.
- [23] Amadou A, Coudon T, Praud D, Salizzoni P, Leffondre K, Lévesque E, et al. Chronic Low-Dose Exposure to Xenoestrogen Ambient Air Pollutants and Breast Cancer Risk: XENAIR Protocol for a Case-Control Study Nested Within the French E3N Cohort. *JMIR Res Protoc* 2020;9:e15167. <https://doi.org/10.2196/15167>.
- [24] Amadou A, Praud D, Coudon T, Deygas F, Grassot L, Dubuis M, et al. Long-term exposure to nitrogen dioxide air pollution and breast cancer risk: A nested case-control within the French E3N cohort study. *Env Pollut* 2022;317:120719. <https://doi.org/10.1016/j.envpol.2022.120719>.
- [25] Buuren S van, Groothuis-Oudshoorn K. Mice: multivariate imputation by chained equations in R. *J Stat Softw* 2011;45:1–67. <https://doi.org/10.18637/jss.v045.i03>.
- [26] Garcia-Acosta S, Clavel-Chapelon F. Dealing with missing, abnormal and incoherent data in E3N cohort study. *Rev Dépidémiologie St Publique* 1999;47:515–23.
- [27] World Health Organization. Air quality guidelines 2021. <https://apps.who.int/iris/bitstream/handle/10665/345329/9789240034228-eng.pdf?sequence=1&isAllowed=y> (accessed April 10, 2023).
- [28] White AJ, Fisher JA, Sweeney MR, Freedman ND, Kaufman JD, Silverman DT, et al. Ambient fine particulate matter and breast cancer incidence in a large prospective US cohort. *djad170 J Natl Cancer Inst* 2023. <https://doi.org/10.1093/jnci/djad170>.
- [29] Andersen ZJ, Ravnskjaer L, Andersen KK, Loft S, Brandt J, Becker T, et al. Long-term Exposure to Fine Particulate Matter and Breast Cancer Incidence in the Danish Nurse Cohort Study. *Cancer Epidemiol Biomark Prev* 2017;26:428–30. <https://doi.org/10.1158/1055-9965.EPI-16-0578>.
- [30] Hart JE, Bertrand KA, DuPre N, James P, Vieira VM, Tamimi RM, et al. Long-Term Particulate Matter Exposures During Adulthood and Risk of Breast Cancer Incidence in the Nurses' Health Study II Prospective Cohort. *Cancer Epidemiol Biomark Prev* 2016;25:1274–6. <https://doi.org/10.1158/1055-9965.EPI-16-0246>.
- [31] Hystad P, Villeneuve PJ, Goldberg MS, Crouse DL, Johnson K. Exposure to traffic-related air pollution and the risk of developing breast cancer among women in eight Canadian provinces: A case-control study. *Environ Int* 2015;74:240–8. <https://doi.org/10.1016/j.envint.2014.09.004>.
- [32] Lemarchand C, Gabet S, Cénée S, Tvardik N, Slama R, Guénel P. Breast cancer risk in relation to ambient concentrations of nitrogen dioxide and particulate matter: results of a population-based case-control study corrected for potential selection bias (the CECILE study). *Environ Int* 2021;155:106604. <https://doi.org/10.1016/j.envint.2021.106604>.
- [33] Nethery E, Leckie SE, Teschke K, Brauer M. From measures to models: an evaluation of air pollution exposure assessment for epidemiological studies of pregnant women. *Occup Environ Med* 2008;65:579–86. <https://doi.org/10.1136/oem.2007.035337>.
- [34] Rotko T, Kousa A, Alm S, Jantunen M. Exposures to nitrogen dioxide in EXPOLIS-Helsinki: microenvironment, behavioral and sociodemographic factors. *J Expo Sci Environ Epidemiol* 2001;11:216–23. <https://doi.org/10.1038/sj.jea.7500162>.
- [35] de Bont J, Casas M, Barrera-Gómez J, Cirach M, Rivas I, Valvi D, et al. Ambient air pollution and overweight and obesity in school-aged children in Barcelona, Spain. *Environ Int* 2019;125:58–64. <https://doi.org/10.1016/j.envint.2019.01.048>.
- [36] Dibben C, Clemens T. Place of work and residential exposure to ambient air pollution and birth outcomes in Scotland, using geographically fine pollution climate mapping estimates. *Environ Res* 2015;140:535–41. <https://doi.org/10.1016/j.envres.2015.05.010>.
- [37] Yaghjian L, Arao R, Brokamp C, O'Meara ES, Sprague BL, Ghita G, et al. Association between air pollution and mammographic breast density in the Breast



- Cancer Surveillance Consortium. Breast Cancer Res BCR 2017;19:36. <https://doi.org/10.1186/s13058-017-0828-3>.
- [38] McCormack VA, Dos Santos Silva I. Breast Density and Parenchymal Patterns as Markers of Breast Cancer Risk: A Meta-analysis. *Cancer Epidemiol Biomark Prev* 2006;15:1159–69. <https://doi.org/10.1158/1055-9965.EPI-06-0034>.
- [39] Rodgers KM, Udesky JO, Rudel RA, Brody JG. Environmental chemicals and breast cancer: An updated review of epidemiological literature informed by biological mechanisms. *Environ Res* 2018;160:152–82. <https://doi.org/10.1016/j.envres.2017.08.045>.
- [40] Darbre PD. Endocrine disrupting chemicals and breast cancer cells. *Adv Pharm* 2021;92:485–520. <https://doi.org/10.1016/bs.apha.2021.04.006>.
- [41] Turner MC, Andersen ZJ, Baccarelli A, Diver WR, Gapstur SM, Pope CA, et al. Outdoor air pollution and cancer: An overview of the current evidence and public health recommendations. *CA Cancer J Clin* 2020;70:460–79. <https://doi.org/10.3322/caac.21632>.
- [42] Mukherjee S, Dasgupta S, Mishra PK, Chaudhury K. Air pollution-induced epigenetic changes: disease development and a possible link with hypersensitivity pneumonitis. *Environ Sci Pollut Res* 2021;28:55981–6002. <https://doi.org/10.1007/s11356-021-16056-x>.
- [43] White AJ, Bradshaw PT, Herring AH, Teitelbaum SL, Beyea J, Stellman SD, et al. Exposure to multiple sources of polycyclic aromatic hydrocarbons and breast cancer incidence. *Environ Int* 2016;89–90:185–92. <https://doi.org/10.1016/j.envint.2016.02.009>.
- [44] Glencross DA, Ho T-R, Camiña N, Hawrylowicz CM, Pfeffer PE. Air pollution and its effects on the immune system. *Free Radic Biol Med* 2020;151:56–68. <https://doi.org/10.1016/j.freeradbiomed.2020.01.179>.
- [45] Terry MB, Michels KB, Brody JG, Byrne C, Chen S, Jerry DJ, et al. Environmental exposures during windows of susceptibility for breast cancer: a framework for prevention research. *Breast Cancer Res* 2019;21:96. <https://doi.org/10.1186/s13058-019-1168-2>.
- [46] Zhai Y, Amadou A, Mercier C, Praud D, Faure E, Iwaz J, et al. The impact of left truncation of exposure in environmental case-control studies: evidence from breast cancer risk associated with airborne dioxin. *Eur J Epidemiol* 2022;37:79–93. <https://doi.org/10.1007/s10654-021-00776-y>.





Full length article

# Multi-pollutant exposure profiles associated with breast cancer risk: A Bayesian profile regression analysis in the French E3N cohort

Camille Giampiccolo<sup>a,b,c</sup>, Amina Amadou<sup>a,b,\*</sup>, Thomas Coudon<sup>a,b</sup>, Delphine Praud<sup>a,b</sup>,  
Lény Grassot<sup>a,b</sup>, Elodie Faure<sup>d</sup>, Florian Couvidat<sup>e</sup>, Gianluca Severi<sup>d,f</sup>,  
Francesca Romana Mancini<sup>d</sup>, Béatrice Fervers<sup>a,b,1</sup>, Pascal Roy<sup>c,g,h,1</sup>

<sup>a</sup> Department of Prevention Cancer Environnement, Centre Léon Bérard, Lyon, France

<sup>b</sup> Inserm U1296 Radiations : Défense, Santé, Environnement, Lyon, France

<sup>c</sup> Laboratoire de Biométrie Et Biologie Evolutive, CNRS UMR 5558, Villeurbanne, France

<sup>d</sup> Université Paris-Saclay, UVSQ, Inserm, Gustave Roussy, Villejuif, France

<sup>e</sup> National Institute for Industrial Environment and Risks (INERIS), Verneuil-en-Halatte, France

<sup>f</sup> Department of Statistics, Computer Science and Applications (DISIA), University of Florence, Florence, Italy

<sup>g</sup> Université Claude Bernard Lyon 1, Lyon, France

<sup>h</sup> Service de Biostatistique-Bioinformatique, Pole Sante Publique, Hospices Civils de Lyon, Lyon, France



## ARTICLE INFO

Handling Editor: Adrian Covaci

### Keywords:

Breast cancer

Air pollutants

Mixture

Correlated exposures

Bayesian profile regression

Cluster

## ABSTRACT

**Background:** Human exposure to air pollution involves complex mixtures of multiple correlated air pollutants. To date, very few studies have assessed the combined effects of exposure to multiple air pollutants on breast cancer (BC) risk.

**Objectives:** We aimed to assess the association between combined exposures to multiple air pollutants and breast cancer risk.

**Methods:** The study was based on a case-control study nested within the French E3N cohort (5222 incident BC cases/5222 matched controls). For each woman, the average of the mean annual exposure to eight pollutants (benzo(a)pyrene, cadmium, dioxins, polychlorinated biphenyls (PCB153), nitrogen dioxide (NO<sub>2</sub>), ozone, particulate matter and fine particles (PMs)) was estimated from cohort inclusion in 1990 to the index date. We used the Bayesian Profile Regression (BPR) model, which groups individuals according to their exposure and risk levels, and assigns a risk to each cluster identified. The model was adjusted on a combination of matching variables and confounders to better consider the design of the nested case-control study. Odds ratios (OR) and their 95 % credible intervals (CrI) were estimated.

**Results:** Among the 21 clusters identified, the cluster characterised by low exposures to all pollutants, except ozone, was taken as reference. A consistent increase in BC risk compared to the reference cluster was observed for 3 clusters: cluster 9 (OR=1.61; CrI=1.13,2.26), cluster 16 (OR=1.59; CrI=1.10,2.30) and cluster 15 (OR=1.38; CrI=1.00,1.88) characterised by high levels of NO<sub>2</sub>, PMs and PCB153. The other clusters showed no consistent association with BC.

**Discussion:** This is the first study assessing the effect of exposure to a mixture of eight air pollutants on BC risk, using the BPR approach. Overall, results showed evidence of a positive joint effect of exposure to high levels to most pollutants, particularly high for NO<sub>2</sub>, PMs and PCB153, on the risk of BC.

**Abbreviations:** AFP, Age at first full-term pregnancy; BaP, Benzo[a]pyrene; BC, Breast cancer; BMI, Body Mass Index; BPR, Bayesian Profile Regression; CI, Confidence Interval; CrI, Credible Interval; CNIL, National Commission for Data Protection and Privacy; DPM, Dirichlet Process Mixture; E3N, Etude Epidémiologique auprès de femmes de la Mutuelle Générale de l'Éducation Nationale; IARC, International Agency for Research on Cancer; IGN, National Geographic Institute; MCMC, Markov Chain Monte Carlo; MET, Metabolic equivalent task; NO<sub>2</sub>, Nitrogen dioxide; ORs, Odds ratios; O<sub>3</sub>, Ozone; PAM, Partitioning Around Medoids; PCBs, Polychlorinated biphenyls; PCB153, group III of the Wolff's classification of polychlorinated biphenyls; PMs, Particles (including PM<sub>10</sub> and PM<sub>2.5</sub>); PM<sub>10</sub>, Particles (diameter < 10 µm); PM<sub>2.5</sub>, Fine particles (diameter < 2.5 µm); SD, Standard deviation.

\* Corresponding author at: Département Prévention Cancer Environnement, Centre Léon Bérard, Inserm U1296 Radiations : Défense, Santé, Environnement, 28 rue Laënnec 69373, Lyon, France.

E-mail address: [amina.amadou@lyon.unicancer.fr](mailto:amina.amadou@lyon.unicancer.fr) (A. Amadou).

<sup>1</sup> These authors contributed equally to this work and share last authorship.

<https://doi.org/10.1016/j.envint.2024.108943>

Received 25 April 2024; Received in revised form 2 August 2024; Accepted 6 August 2024

Available online 8 August 2024

0160-4120/© 2024 The Authors. Published by Elsevier Ltd. This is an open access article under the CC BY license (<http://creativecommons.org/licenses/by/4.0/>).



## 1. Introduction

Exposure to air pollutants is a major public health concern because of its many adverse effects on human health, including cancer (Turner et al., 2020). Air pollution is a complex mixture of highly correlated pollutants from multiple sources (Billionnet et al., 2012). The International Agency for Research on Cancer (IARC) has classified outdoor air pollution as a whole, and particulate matter (PM) as carcinogenic to humans with sufficient evidence for lung cancer and a positive association for bladder cancer (Loomis et al., 2013). Other chemical contaminants present in the air have been classified as carcinogenic to humans, such as benzo(a)pyrene (BaP), cadmium, dioxins, and polychlorinated biphenyls (PCBs). Exposure to chemical air contaminants, in particular those with endocrine disrupting effects are strongly suspected to play a role in breast cancer (BC) development (Darbre, 2021; Wan et al., 2022; Yilmaz et al., 2020), the most common cancer in women worldwide (2.3 million new cases estimated in 2020) (Sung et al., 2021).

The body of evidence reporting positive associations between exposure to air pollutants and risk of BC is steadily increasing, both for pollutants with endocrine disrupting effects as well as for nitrogen dioxide (NO<sub>2</sub>) and PMs (Gabet et al., 2021; Niehoff et al., 2022; Praud et al., 2023; White et al., 2021, 2018). An increased BC risk has been shown for BaP exposure (Amadou et al., 2021; Large and Wei, 2017), while inconsistent findings have been reported from epidemiological studies for dioxins (Danjou et al., 2019; Fiolet et al., 2022; VoPham et al., 2020; Xu et al., 2016), cadmium (Amadou et al., 2020b; Filippini et al., 2020; Florez-Garcia et al., 2023), as well as PCBs (Deygas et al., 2021; Fiolet et al., 2022). Several studies have shown an increased BC risk related to NO<sub>2</sub> exposure, largely emitted from road traffic (Amadou et al., 2023; Gabet et al., 2021; Praud et al., 2023; Wei et al., 2021). Concerning PM<sub>10</sub> and PM<sub>2.5</sub>, although positive associations were reported in some studies, the findings remained globally inconsistent across studies (Wei et al., 2021; Zhang et al., 2019). With regard to ozone (O<sub>3</sub>), a “secondary” pollutant, the available studies showed no association between BC risk and high exposure to O<sub>3</sub> (Bai et al., 2020; White et al., 2021), but an inverse association has been observed in relation to breast density, a well-established risk factor for BC (Yaghjian et al., 2017).

While the population is exposed simultaneously to multiple air pollutants, previous studies have mainly investigated the adverse effects of exposure to air pollutants considering one pollutant at a time. Traditional epidemiological methods, such as multiple logistic regression, are not adapted to investigate joint health effects of simultaneous exposure to multiple highly correlated pollutants leading to variance inflation of the estimates (Agier et al., 2016; Farrar and Glauber, 1967; Hoerl and Kennard, 1970; MacLehose et al., 2007). Consequently, parameter estimates of the model may not be significantly different from zero in multivariate analyses adjusted on correlated variables, even when an effective relationship between exposure and health exists. There is thus a great interest in assessing the impact of exposure to correlated pollutant mixtures on BC risk, using more appropriate methods (Bellavia, 2023).

An increasing number of statistical methods for considering exposure to pollutant mixtures have been described in the literature to investigate these complex relationships. Among these methods, Bayesian profile regression (BPR) analysis, is a pertinent approach, for identifying at-risk groups of individuals who share similar exposure profiles of correlated pollutants, and assigning a risk to each of these groups (Molitor et al., 2010).

The main objective of this study was to estimate the joint effect of exposure to eight air pollutants (BaP, cadmium, dioxins, PCB153, NO<sub>2</sub>, O<sub>3</sub>, PM<sub>10</sub> and PM<sub>2.5</sub>) on the risk of BC in a matched case-control study nested within the French E3N cohort using BPR analysis (Liverani et al., 2015; Molitor et al., 2010).

## 2. Material and methods

### 2.1. The cohort study population

The E3N-Generation prospective study is an ongoing French familial cohort study established as an extension of the E3N cohort of women (Etude Epidémiologique auprès des femmes de la Mutuelle Générale de l'Éducation Nationale) including the E3N women's children, their fathers and, in the future, their grandchildren. The present study focuses only on the E3N part of the cohort that was created in 1990 with the recruitment of 98,995 women that at that time were the E3N cohort of women (Etude Epidémiologique auprès des femmes de la Mutuelle Générale de l'Éducation Nationale) including the E3N women's children, their fathers and, in the future, their grandchildren. The present study focus only on the E3N part of the cohort that was created in 1990 with the recruitment of 98,995 women that at that time were aged 40–65 years, were living in France and were affiliated to the national health insurance covering workers from the French National Education System (Mutuelle Général de l'Éducation Nationale, MGEN) (Clavel-Chapelon and E3N Study Group, 2015). The E3N cohort is still followed-up after more than 30 years with self-administered questionnaires including data on socio-demographic characteristics, lifestyle, reproductive factors, anthropometry, past medical history, and familial history of cancer. The addresses of the cohort participants included in the study were collected at baseline (1990), and at each of the twelve follow-up questionnaires. BC occurrence was self-reported in follow-up questionnaires and a few additional cases were retrieved from health insurance data or from mortality data including causes of death obtained from the National Services on Causes of Deaths (CépiDC- Inserm). Self-reported cases were validated through retrieval of medical records from treating physicians and pathological confirmation was obtained for 93 % of cases. Since the false-positive rate of self-reports was low in the cohort population (<5%), we also included the cases that were not pathologically confirmed. For one fourth of the cohort blood samples were collected between 1995 and 1998 and are stored in liquid nitrogen as aliquots of buffy coat, plasma, serum and erythrocytes. The study was approved by the French National Commission for Data Protection and Privacy (CNIL), and informed consent was obtained from each participant.

### 2.2. The nested case-control study

This study is based on data from a case-control study nested in the E3N cohort described in previous articles (Amadou et al., 2020a). In brief, the study included participants without any cancer at baseline, who had reported their home address at baseline, and lived in metropolitan France during the follow-up period from 1990 to 2011 (Deygas et al., 2021). Of the 6,298 invasive BC cases diagnosed during follow-up, we excluded women with phyllodes tumours which are biologically and clinically different (N=19) (Zhang and Kleer, 2016), those with missing data on matching variables (N=3) and those with more than one missing address (N=1,054 cases) (Amadou et al., 2021; Deygas et al., 2021). For each case, one control free of cancer was randomly selected by incidence density sampling, among cohort participants at risk of BC at the time of case diagnosis (Amadou et al., 2020a). This incidence density sampling is an efficient method of choice for obtaining unbiased results, in which controls are selected without replacement from all persons at risk at the time of case occurrence, excluding the index case itself (Richardson, 2004). Two matchings were done according to the availability of a biological sample (blood or saliva) (Amadou et al., 2020a). This variable was one of the matching variables, as the case-control study was originally designed to also address additional objectives (impact of exposure on DNA methylation and interactions with genetic polymorphisms). The protocol of the matched nested case control study has been published in JMIR protocol (Amadou et al., 2020a). Briefly, cases having blood samples collected before diagnosis were matched to controls with a



blood sample collected before the index date of the matched case, and matched on the department of residence, age ( $\pm 1$  year), date ( $\pm 3$  months), and menopausal status, all at the time of blood collection. Cases without a blood sample were matched to controls on the same criteria, at inclusion, and additionally matched on availability of a saliva sample. The final study population included 5,222 women diagnosed with an invasive BC and 5,222 matched controls. The flow chart is presented in [Supplementary Figure S1](#).

### 2.3. Assessment of long-term exposure to eight atmospheric pollutants

The approach used to estimate the subjects' atmospheric exposure based on the pollutant concentrations at the women's consecutive residential addresses has been applied in our previous studies and described elsewhere ([Amadou et al., 2023, 2021](#)). Briefly, mean annual atmospheric BaP ( $\text{ng}/\text{m}^3$ ), cadmium ( $\text{pg}/\text{m}^3$ ), dioxins ( $\text{fg-TEQ}/\text{m}^3$ ), PCB153 ( $\text{pg}/\text{m}^3$ ),  $\text{NO}_2$  ( $\mu\text{g}/\text{m}^3$ ),  $\text{O}_3$  ( $\text{pp}/\text{m}^3$ ),  $\text{PM}_{10}$  ( $\mu\text{g}/\text{m}^3$ ) and  $\text{PM}_{2.5}$  ( $\mu\text{g}/\text{m}^3$ ) concentrations were estimated at the women's geocoded consecutive residence addresses, from 1990 to their index date using a chemistry-transport model (CHIMERE) with a spatial resolution of  $0.125 \times 0.0625$  (approximately  $7 \times 7$  km) ([Couvidat et al., 2018](#)). This deterministic model simulates pollutant concentrations on large scales using emission inventories and meteorological data as input data ([Couvidat et al., 2018](#); [Guerreiro et al., 2016](#); [Menut et al., 2013](#)). The CHIMERE model has been validated by comparisons with pollutant measurements ([Clément et al., 2017](#); [Couvidat et al., 2018](#)) and has been used to estimate for example BaP exposure and other air pollutants in Europe ([Guerreiro et al., 2016](#)). French departments are administrative divisions of territories ("NUTS-3" in the classification of territorial divisions of the European Union) ([Eurostat, 2024](#)) with surfaces sufficiently large to exhibit heterogeneous exposure profiles with the CHIMERE model ( $7 \times 7$  km spatial resolution). Surface areas range from 105 to 10,000  $\text{km}^2$  (with 25th, 50th, and 75th percentiles of 5147  $\text{km}^2$ , 5954  $\text{km}^2$ , and 6775  $\text{km}^2$  respectively); with population size varying from 76,604 to 2,608,346 persons ([Amadou et al., 2023](#); [INSEE, 2024](#)).

The consecutive residential addresses of the participants were geocoded with the ArcGIS Software (ArcGIS Locator version 10.0, Environmental System Research Institute – ESRI, Redlands, CA, USA), and its reference street network database, BD Adresse® from the National Geographic Institute (IGN) ([Faure et al., 2017](#)).

Weighted annual estimates of pollutant concentrations were assigned to the subsequent geocoded residential addresses of subjects for each year during the 1990–2011 follow-up period. For each woman, mean concentration levels of pollutant exposure at the residential address were calculated, from their entry into the cohort to their index date. Entry into the E3N (1990) cohort is thus the starting point for the exposure assessment in the present nested case-control study. Exposure assessment is performed until the index date (corresponding to the date of BC diagnosis for cases and date of selection for controls). The average of the mean annual concentrations for each pollutant prior to BC diagnosis and used as an estimate of the actual pollutant exposure in the present study ([Amadou et al., 2023, 2021](#); [Deygas et al., 2021](#)).

### 2.4. Statistical analyses

#### 2.4.1. Descriptive analysis

Exposure estimates for each pollutant, socio-demographic characteristics, and other covariates of the participants were described using mean and standard deviation (SD) for continuous variables, and frequency and percentage for categorical variables. The Pearson correlation coefficients were computed to assess the correlations between exposure to different pollutants ([Gallo et al., 2018](#)).

#### 2.4.2. Bayesian profile regression (BPR)

BPR was used to assess the association between the combined exposure to the eight pollutants and the risk of BC by estimating the odds

ratio (OR) between groups of individuals sharing a similar exposure profile. BPR assigns individuals to clusters according to an assignment model. When grouping individuals into clusters, the assignment model considers both the information on joint exposures, provided by an exposure sub-model, and the expected cluster effect on BC estimated from risk provided by a disease sub-model ([Liverani et al., 2015](#); [Molitor et al., 2010](#)).

Details of the BPR model are described in [supplementary material](#). Briefly, the assignment sub-model is based on a Dirichlet Process Mixture (DPM) model, a non-parametric model used for probabilistic clustering of mixture profiles ([Molitor et al., 2010](#)). This sub-model estimates the optimal number of clusters and calculates the probability that an individual belongs to each cluster. The exposure sub-model determines the exposure profile of each cluster ([Belloni et al., 2020](#)). The eight exposure variables, represent the average of the mean annual exposure levels of BaP, cadmium, dioxins, PCB153,  $\text{NO}_2$ ,  $\text{O}_3$ ,  $\text{PM}_{10}$  and  $\text{PM}_{2.5}$  respectively during the follow-up period of the woman, and were continuous.

The disease sub-model links clusters of profiles to the outcome, by estimating the risk of BC within each cluster. An unconditional logistic regression model adjusted for confounders was therefore fitted. The binary indicator  $Y_i$  specified the woman's  $i$  status (1 for cases and 0 for controls). This model included specific parameters for each cluster and a vector of parameters shared by all clusters. The assignment model is written by specifying the respective contributions of the exposure and disease sub-models.

The number of clusters and the construction of the mixing weights  $\psi_c$  were defined by a "stick-breaking" process, with the maximum number of clusters  $C_{\max}$  specified ([Molitor et al., 2010](#)). From the elements of the likelihood, the posterior probabilities of a given individual belonging to each cluster was calculated using Bayes theorem. According to this, an individual was assigned to the cluster with the highest probability. This was repeated for each individual.

The parameters of the BPR model were estimated by a Bayesian approach using a Markov chain Monte Carlo (MCMC) algorithm, with 30,000 iterations after a burn-in sample of 10,000 iterations. Every iteration of the MCMC algorithm assigned each individual to a cluster therefore partitioning the study population. As the MCMC algorithm finds it harder to split clusters than to merge them, and given the large population of the present study (including 10,444 participants), the initial number of clusters was set to a large number, namely 2,500. During the MCMC simulation, the number of clusters could vary and the label associated with each cluster changed during the iterations, thus postprocessing of the MCMC output was carried out to obtain an optimal partition. First, a score matrix of  $(n \times n)$  ( $n$  being the total number of individuals) size, was generated at each iteration, to determine whether two individuals belonged to the same cluster or not. Second, a probability matrix of  $(n \times n)$  size was created, to indicate the probability that 2 individuals belonged to the same cluster, by averaging each matrix score. Lastly, based on this probability matrix, an optimal partition was obtained by maximising the average silhouette width across various partitions obtained by partitioning Around Medoids (PAM) ([Molitor et al., 2010](#)).

Posterior distribution of cluster parameters was obtained from MCMC output. For each iteration of the MCMC sampler, the risk associated with a given cluster  $k$  is the average of the risk obtained, for all individuals included in the cluster  $k$ . Repeating this for all iterations provides a distribution for the risk for the optimal partition, applied for all cluster parameters ([Molitor et al., 2010](#)).

The MCMC algorithm was run five times with different initial positions randomly assigned and the marginal posterior distributions of the  $\alpha$  parameter of DPM were compared between the five runs to assess convergence. The final partition selected was the one maximising the average silhouette clustering score among the optimal partitions obtained by post-processing ([Lengyel and Botta-Dukát, 2019](#); [Liverani et al., 2015](#)).



Confounders were identified using a directed acyclic graph (Supplementary figure S2). Two minimal sufficient adjustment sets of variables have been proposed. The first includes physical activity (<25.3, 25.3–35.5, 35.6–51.8, and  $\geq 51.8$  METs-h/week), alcohol intake (0, 1–6.7, > 6.7 g/day), body mass index (BMI) (<25, 25–<30, and  $\geq 30$  kg/m<sup>2</sup>), breastfeeding (ever, never), oral contraceptive use (ever, never), menopausal hormone treatment (ever, never), status of birthplace (rural, urban), status of inclusion (rural, urban), smoking status (never, current, and former), parity and age at first full-term pregnancy (AFP) (0, 1–2 children & AFP<30 years, 1–2 children & AFP $\geq$ 30 years, and 3 children), and mammography screening (yes, no). The second includes the level of education, considered as a proxy of socio-economic status. The model with more adjustment variables was selected for the analysis. Confounding variables with less than 5 % missing data were imputed using the median for continuous variables and the mode for categorical variables, based on control population data. Covariates with more than 5 % missing values, specifically alcohol consumption and birthplace, were treated as a separate category (Amadou et al., 2020a).

Analyses were run in R (version 4.0.2; R Core Team 2020). The R PRemium package (Liverani et al., 2015) designed to fit the BPR model includes an unconditional logistic regression disease sub-model but not the conditional regression model more suitable for the matched case-control design of the present study. In consequence, we fitted the unconditional logistic regression model, adjusted on the combination of matching variables (including department of residence, age ( $\pm 1$  year), date ( $\pm 3$  months), menopausal status at blood collection (menopausal or not) and availability of a saliva sample (yes, no), in addition to confounders as proposed by Pearce (Pearce, 2016). To fit mixtures and potentially link covariates with responses, we identified covariates that actively influence the mixture components and those that exhibit characteristics common to all components through variable selection available in PRemium package. Odds ratios (ORs) of BC risk associated with combined exposure to the 8 pollutants in each cluster, and their 95 % credible intervals (CrIs) were estimated (Coker et al., 2020). The average exposure profiles of each cluster also assessed and presented with boxplot and heat map. The geocoded residential locations of all women were graphically displayed by cluster.

Sensitivity analyses were further conducted by defining exposure profiles solely based on the exposure variables, without considering the risk provided by the disease sub-model in the profile regression, using an option of the BPR model in the R PRemium package that excludes the outcome variable from the profile regression model. To assess the model's convergence, we followed the same approach as in the main analyses. Associations between these exposure profiles and BC risk were analysed using unconditional logistic regression models and adjusted on the matching variables and previously defined confounders.

### 3. Results

#### 3.1. Characteristics of the study population

General characteristics of the study population are presented in Supplementary Table S1. Overall, women were included on average at age 49.6 (6.3) years, 54.5% were ever smokers, 62.1 % were born in urban areas, 37 % were in the highest tertile level of alcohol intake (>6.7 g/day), 83 % had normal BMI (<25 kg/m<sup>2</sup>). Fig. 1 shows the Pearson correlation matrix between the average of the annual mean concentrations (1990–2011) for each of the eight pollutants. Overall, moderate to strong positive correlations were observed between the majority of the pollutants. The strongest correlations were observed between PM<sub>2.5</sub> and PM<sub>10</sub> (0.99), between PCB153 and PM (0.93 and 0.94, for PM<sub>10</sub> and PM<sub>2.5</sub>, respectively), between NO<sub>2</sub> and PM (0.87 and 0.86 for PM<sub>10</sub> and PM<sub>2.5</sub>, respectively) and between PCB153 and NO<sub>2</sub> (0.81). In contrast, O<sub>3</sub> was negatively correlated with all other pollutants, with a strong negative correlation for NO<sub>2</sub> (−0.92), PM<sub>10</sub> (−0.90), PM<sub>2.5</sub> (−0.89), and PCB153 (−0.83).

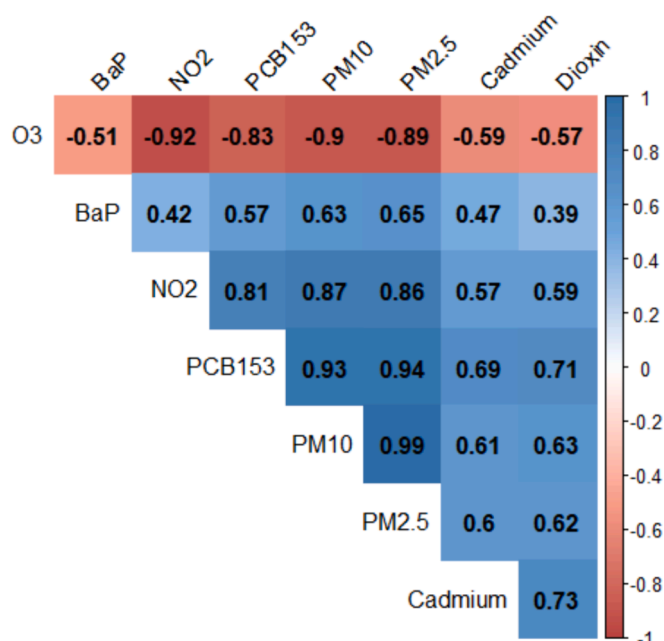


Fig. 1. Pearson's correlation matrix between the average of the annual mean concentrations (1990–2011) for each of the eight pollutants (BaP, dioxins, cadmium, PCB153, NO<sub>2</sub>, O<sub>3</sub>, PM<sub>10</sub>, PM<sub>2.5</sub>) in the case-control study nested within the E3N-generation cohort, France, 1990–2011.

#### 3.2. Association between exposure profiles and BC risk

The marginal posterior distributions of the  $\alpha$  parameter (Markov chains), shown in Supplementary Figure S3, overlapped among the five runs of the MCMC algorithm and showed the model convergence. Supplementary Table S2 presents the number of clusters for each partition, ranging from 18 to 26 clusters, and the associated average silhouette score. Partition 2, with 21 clusters, maximising the silhouette average score (0.866), was selected as the final partition. Visual comparison of the five post-processed partitions with the highest silhouette average scores (0.79–0.87), showed similar exposure profiles, supporting the convergence of the model (data not shown).

During the iterations of the MCMC algorithm, the selection probability for each pollutant remained consistently above 0.8 (Supplementary Figure S4).

For a visual overview of cluster exposure profiles, Fig. 2 shows the normalised posterior means of each of the eight pollutants, for the 21 clusters ordered by decreasing levels of O<sub>3</sub> exposure. The Supplementary Figure S5 shows a heat map of the posterior clustering. Average concentration estimates of the pollutants for the 21 resulting clusters are shown in Table 1. The number of subjects in each cluster ranged from 52 (cluster 3) to 1,223 (cluster 11). Table 2 shows the ORs and corresponding 95 % credible intervals for each cluster.

Cluster 1 (1141 women), characterised by low exposure to all pollutants except O<sub>3</sub> was selected as the reference cluster (Fig. 2). Graphical displays of women residential locations by cluster, shows that women in the reference cluster were scattered over a wide area of France (Fig. 3).

The three clusters with the highest ORs were characterised by quite similar pollutant patterns with varying levels of exposures (Table 1, Table 2, Fig. 2 and Supplementary Figure S6): cluster 9 (265 participants; OR=1.61; CrI=1.13,2.26), cluster 16 (210 participants; OR=1.59; CrI=1.10,2.30) and cluster 15 (357 participants; OR=1.38; CrI=1.00,1.88). Cluster 9 corresponded to women with very high NO<sub>2</sub> exposure levels and high exposure to PCB153, PM<sub>10</sub> and PM<sub>2.5</sub>. However, exposure to BaP, cadmium and dioxins were lower than the other pollutants and exposure to O<sub>3</sub> was extremely low. Cluster 16 represented women with very high exposure levels for NO<sub>2</sub>, PCB153, PM<sub>10</sub> and



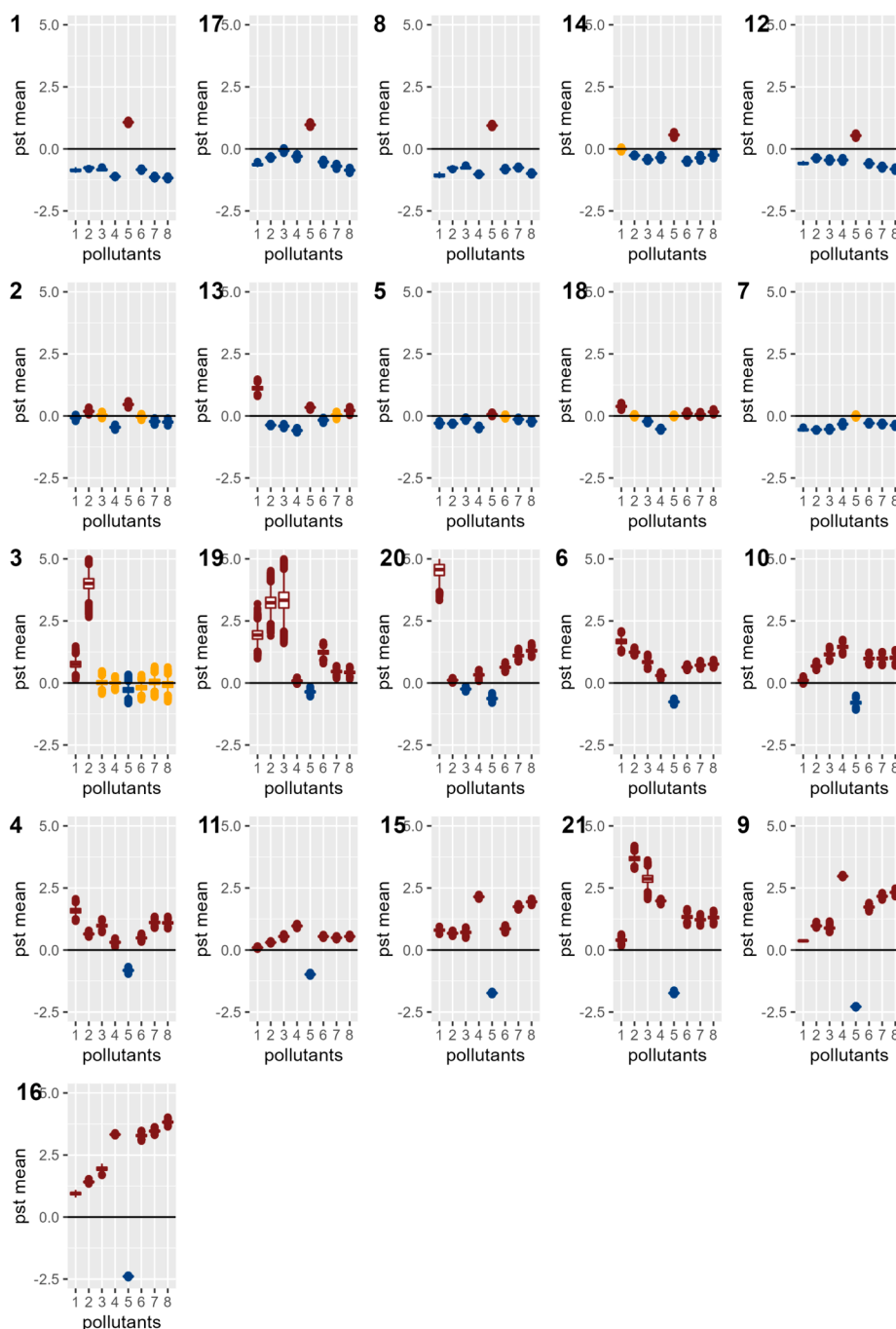


**Fig. 2.** Characterization of the exposure profiles associated to each cluster using BPR, in the case-control study nested within the E3N-generation cohort, France, 1990–2011. Clusters were numbered from 1 to 21 and ordered by decreasing levels of  $O_3$  exposure. For each cluster, the boxplot of the normalised means distribution of each pollutant were represented from left to right in the following order: BaP (1), cadmium (2), dioxin (3),  $NO_2$  (4),  $O_3$  (5), PCB153 (6),  $PM_{10}$  (7),  $PM_{2.5}$  (8). These distributions came from MCMC algorithm of BPR model. The two different colours, blue and red, correspond to a 95 % credible interval, respectively under or upper 0 which represents low or high exposure level respectively. Orange colour shows no evidence of high or low values of exposures. Pst mean: normalised posterior mean of the exposures within cluster. (For interpretation of the references to colour in this figure legend, the reader is referred to the web version of this article.)

$PM_{2.5}$ , lower exposure to BaP, cadmium and dioxins and low exposure to  $O_3$ . Cluster 15 was characterised by high exposure levels for  $NO_2$  and PMs, lower exposures to BaP, cadmium, dioxins and PCB153, and low exposure to  $O_3$  (Table 1, Table 2 and Fig. 2). Women in these three clusters were mainly located in urban metropolitan areas of Paris and Lyon (Fig. 3). Two other clusters with less elevated ORs and CrI limits showed close profiles with lower exposure levels: cluster 11 (1,223 participants; OR=1.21; CrI=0.95,1.55) and cluster 10 (285 participants; OR=1.22; CrI=0.91,1.64).

Seven other clusters essentially characterised by higher exposure levels for cadmium, dioxins and/or BaP, were not associated with BC risk (Table 1, Fig. 2). Of these, six clusters had ORs greater than 1: cluster 3 (52 participants; OR=1.08; CrI=0.64,1.83), cluster 4 (249 participants; OR=1.08; CrI=0.75,1.53), cluster 6 (361 participants; OR=1.11; CrI=0.81,1.52), cluster 19 (148 participants; OR=1.26; CrI=0.87,1.80), cluster 20 (158 participants; OR=1.22; CrI=0.66,2.28) and cluster 21 (54 participants; OR=1.26; CrI=0.72,2.20). One cluster, cluster 13 was associated with an OR below 1 (321 participants; OR=0.74;



**Table 1**

Characterization of the exposure profiles associated to each cluster when fitting a BPR model, in the case-control study nested within the E3N-generation cohort, France, 1990–2011.

Cluster Label	Bap*	Cadmium*	Dioxin*	PCB153*	NO2*	O3*	PM2.5*	PM10*
1	0.09 (0.09,0.10)	71.88 (67.98,73.11)	2.83 (2.51,3.45)	6.40 (6.31,6.49)	2.83 (2.70,2.96)	32.44 (32.26,32.61)	12.00 (11.84,12.16)	14.47 (14.32,14.62)
2	0.18 (0.18,0.19)	178.05 (172.33,185.09)	10.23 (9.74,10.73)	9.65 (9.43,9.86)	8.91 (8.50,9.34)	28.68 (28.33,29.02)	17.48 (17.12,17.85)	20.13 (19.78,20.48)
3	0.28 (0.25,0.31)	608.34 (548.34,660.23)	10.09 (8.57,11.60)	9.06 (8.27,9.84)	13.21 (12.15,14.16)	24.10 (22.82,25.54)	18.58 (16.99,20.09)	21.78 (20.31,23.19)
4	0.37 (0.35,0.39)	230.08 (224.20,236.25)	18.27 (17.25,19.21)	11.80 (11.52,12.07)	16.00 (15.34,16.65)	20.79 (20.42,21.17)	25.42 (24.86,25.98)	28.35 (27.80,28.91)
5	0.16 (0.15,0.16)	122.72 (120.35,124.87)	8.87 (8.61,9.12)	9.71 (9.56,9.85)	8.85 (8.57,9.14)	26.22 (26.02,26.42)	17.64 (17.44,17.85)	20.65 (20.46,20.84)
6	0.38 (0.36,0.40)	296.52 (289.68,305.75)	17.11 (16.11,18.10)	12.40 (12.20,12.61)	15.90 (15.39,16.42)	21.15 (20.87,21.44)	23.43 (23.07,23.80)	25.91 (25.54,26.29)
7	0.13 (0.12,0.14)	95.12 (92.25,96.61)	5.38 (5.12,5.79)	8.63 (8.52,8.73)	10.07 (9.72,10.42)	25.81 (25.64,25.99)	16.70 (16.54,16.86)	19.54 (19.38,19.69)
8	0.07 (0.06,0.08)	70.76 (66.83,72.14)	3.46 (3.15, 4.02)	6.46 (6.36,6.56)	3.67 (3.53,3.82)	31.62 (31.43,31.81)	13.06 (12.93,13.20)	16.84 (16.72,16.96)
9	0.23 (0.23,0.24)	266.46 (262.44,272.62)	17.45 (16.74,18.06)	16.89 (16.62,17.17)	40.58 (40.40,40.78)	11.79 (11.70,11.88)	32.70 (32.33,33.08)	34.86 (34.52,35.20)
10	0.20 (0.20,0.21)	233.93 (225.73,242.40)	19.72 (18.65,20.72)	13.85 (13.41,14.28)	26.55 (25.40,27.71)	20.95 (20.21,21.67)	24.96 (24.15,25.79)	27.61 (26.87,28.36)
11	0.20 (0.20,0.21)	191.42 (189.15,193.90)	14.57 (14.13,14.92)	12.04 (11.93,12.16)	22.08 (21.73,22.42)	19.81 (19.65,19.97)	22.17 (21.97,22.36)	24.56 (24.37,24.74)
12	0.13 (0.12,0.13)	115.25 (112.75,117.47)	6.10 (5.83,6.47)	7.39 (7.29,7.49)	8.99 (8.67,9.31)	29.14 (28.90,29.37)	14.11 (13.93,14.29)	16.99 (16.82,17.16)
13	0.32 (0.30,0.34)	115.97 (113.32,118.51)	6.48 (6.15,6.84)	9.12 (8.94,9.31)	7.71 (7.36,8.09)	27.94 (27.70,28.15)	20.23 (19.85,20.61)	21.73 (21.37,22.09)
14	0.19 (0.19,0.19)	127.83 (125.60,129.94)	6.30 (6.04,6.64)	7.78 (7.65,7.91)	9.86 (9.50,10.23)	29.30 (29.00,29.61)	17.46 (17.13,17.79)	19.29 (18.97,19.61)
15	0.28 (0.27,0.29)	233.15 (228.11,238.57)	15.98 (15.21,16.72)	13.30 (13.04,13.57)	32.93 (32.61,33.25)	15.18 (15.04,15.31)	30.44 (30.11,30.78)	32.26 (31.96,32.55)
16	0.30 (0.29,0.31)	316.04 (312.01,323.39)	26.53 (25.08,27.38)	23.23 (22.88,23.59)	43.85 (43.66,44.03)	11.12 (11.02,11.23)	41.59 (41.12,42.05)	42.87 (42.45,43.29)
17	0.12 (0.12,0.13)	118.94 (116.12,121.50)	9.41 (9.09,9.72)	7.67 (7.50,7.84)	10.34 (9.97,10.72)	31.82 (31.57,32.07)	13.85 (13.60,14.11)	17.20 (16.93,17.47)
18	0.24 (0.23,0.24)	157.88 (154.35,161.46)	8.08 (7.80,8.36)	10.23 (10.06,10.39)	8.20 (7.95,8.46)	25.84 (25.68,26.00)	19.91 (19.64,20.17)	21.89 (21.64,22.14)
19	0.41 (0.37,0.46)	520.90 (462.90,580.59)	38.17 (31.75,44.88)	14.87 (14.18,15.56)	13.91 (13.39,14.43)	23.64 (23.16,24.11)	21.47 (20.88,22.06)	24.35 (23.77,24.94)
20	0.72 (0.65,0.78)	170.05 (165.58,174.05)	7.89 (7.50,8.27)	12.40 (12.09,12.71)	16.14 (15.28,16.91)	21.97 (21.53,22.48)	26.65 (26.00,27.29)	28.31 (27.67,28.93)
21	0.24 (0.23,0.25)	571.19 (551.52,594.23)	34.24 (31.47,36.84)	15.26 (14.75, 15.7)	31.40 (31.07,31.72)	15.16 (15.04,15.29)	26.71 (26.06,27.33)	29.03 (28.47,29.58)
Overall	0.19	157.32	9.96	9.82	13.12	25.84	18.94	21.51

BaP was expressed in ng/m<sup>3</sup>, PCB153 in pg/m<sup>3</sup>, cadmium in pg/m<sup>3</sup>, dioxin in fg-TEQ/m<sup>3</sup>, PM10 in µm<sup>3</sup>, PM2.5 in µg/m<sup>3</sup>, NO2 in µg/m<sup>3</sup>, O3 in pp/m<sup>3</sup>.

\* : estimated mean (95 %CrI).

CrI=0.49,1.17) (Table 2).

Four further clusters associated with exposures relatively close to the overall average for each pollutant were found (Table 1, Fig. 2): cluster 5 (656 participants; OR=1.13; CrI=0.85,1.48), cluster 18 (562 participants; OR=1.15; CrI=0.87,1.54), cluster 7 (792 participants; OR=1.23; CrI=0.97,1.56) and cluster 2 (529 participants; OR=1.20; CrI=0.97,1.49) (Table 2).

The remaining four clusters exhibited high O<sub>3</sub> levels and low exposures to other pollutants (Table 1, Fig. 2): cluster 17 (662 participants; OR=1.24; CrI=0.93,1.66), cluster 8 (767 participants; OR=1.10; CrI=0.84,1.45), cluster 14 (842 participants; OR=1.03; CrI=0.79,1.33) and cluster 12 (810 participants; OR=0.96; CrI=0.77,1.18) (Table 2).

### 3.3. Sensitivity analyses

The results of the sensitivity analyses of pollutant exposure profiles, without considering the risk, are shown in Supplementary Figures S7 and S8, and, Supplementary Tables S3, S4 and S5. The marginal posterior distributions of the parameter (Markov chains) overlapped among the five runs of the MCMC algorithm and showed the model convergence (Supplementary Figure S7). Partition 3, with 18 clusters, maximising the silhouette average score (0.863), was selected as the final partition

(Supplementary Table S3). Cluster S1 (1,085 women), characterised by low exposure to all pollutants except O<sub>3</sub> was selected as the reference cluster (Supplementary Figure S8). The three clusters with the highest ORs of BC risk were cluster S7 (88 participants; OR=1.99; CI=1.15,3.46), cluster S9 (290 participants; OR=1.96; CI=1.29,2.98) and cluster S12 (1,433 participants; OR=1.36; CI=1.03,1.80) (Supplementary Table S4). Cluster S7 and S9 were characterised by quite similar pollutant patterns with women exposed to very high levels of NO<sub>2</sub>, PCB153, PM<sub>10</sub> and PM<sub>2.5</sub> (Supplementary Figure S8). Clusters S7 and S9 displayed similar pollutant profiles than clusters 9, 15 and 16 in the main analyses, but with slightly higher ORs. In contrast, cluster S12 corresponded to women considerably exposed to NO<sub>2</sub> and moderately or slightly exposed to all other pollutants (Supplementary Figure S8). Characteristics of women in cluster S12 did not substantially differ from the overall population (Supplementary Figure S5).

## 4. Discussion

To the best of our knowledge, this is the first study assessing the association between the combined exposure to eight highly correlated air pollutants and BC risk using the BPR model.

Overall, the present study demonstrated a positive association



**Table 2**

Association between BC risk and clusters, using BPRmodel, in the case-control study nested within the E3N-generation cohort, France, 1990–2011.

Clusters Label	Cases/controls	OR (95 % CrI)
1	559/582	Reference
2	282/247	1.20(0.97,1.49)
3	26/26	1.08(0.64,1.83)
4	123/126	1.08 (0.75,1.53)
5	329/327	1.13 (0.85,1.48)
6	174/187	1.11 (0.81,1.52)
7	410/382	1.23 (0.97,1.56)
8	377/390	1.10 (0.84,1.45)
9	151/114	1.61 (1.13,2.26)
10	138/147	1.22 (0.91,1.64)
11	595/628	1.21 (0.95,1.55)
12	384/426	0.96 (0.77,1.18)
13	152/169	0.74 (0.49,1.17)
14	410/432	1.03 (0.79,1.33)
15	186/171	1.38 (1.00,1.88)
16	121/89	1.59 (1.10,2.30)
17	337/325	1.24 (0.93,1.66)
18	287/275	1.15 (0.87,1.54)
19	78/70	1.26 (0.87,1.80)
20	80/78	1.22 (0.66,2.28)
21	23/31	1.26 (0.72,2.20)

BPR model were adjusted for physical activity, alcohol intake, body mass index, breast-feeding, oral contraceptive use, menopausal hormone treatment, status of birthplace, status of inclusion smoking status, parity and age at first full-term pregnancy, mammography screening, department of residence, menopausal status and availability of a saliva sample.

OR: Odds Ratio; CrI: credible interval.

between BC risk and exposure to combinations of the eight pollutants, with significant evidence only for three clusters, characterised mainly by high levels of NO<sub>2</sub>, PM<sub>10</sub>, PM<sub>2.5</sub>, and PCB153. Women in these three clusters (9, 15 and 16) were mainly located in high-density urban environments of Paris and Lyon. Two other clusters (10 and 11) with close exposure profiles but lower exposure levels, likewise predominantly located in high-density urban areas, were associated with increased ORs of lower magnitude. Moreover, several clusters (3, 4, 6, 19, 20, and 21) driven by high exposure levels to cadmium, dioxins, and / or BaP, were associated with positive ORs, although not consistent. Women in these clusters were mainly located in eastern France, near the border with Germany and Belgium (cluster 4, 6 and 20), and potentially subject to cross-border pollution, or located in highly industrialised areas known to be associated with industrial emissions (clusters 3, 19 and 21) (Jeanjean et al., 2021).

Most studies have investigated the effects of single air pollutants on BC risk, with classical and well-known methods such as multiple linear or logistic regression (Niehoff et al., 2022; White et al., 2021, 2018). The results observed for the three clusters associated with highest risk are consistent with results obtained from single pollutant analyses. Increased risks of BC have been constantly found in previous studies for NO<sub>2</sub> (Gabet et al., 2021; Praud et al., 2023), including a previous study in the same nested case-control study with OR=1.15 (95 % CI= 1.06,1.26) (Amadou et al., 2023). Likewise, there was a statistically significant positive association between cumulative atmospheric exposure to PCB153 and BC risk (OR=1.19; 95 % CI= 1.08,1.31) (Deygas et al., 2021). Yet, divergent results were reported between PM (PM<sub>2.5</sub> and PM<sub>10</sub>) and BC risk (Gabet et al., 2021; Wei et al., 2021; Zhang et al., 2019). However, the ORs for clusters of combined exposures (cluster 9 (OR=1.61; CrI=1.13,2.26), cluster 16 (OR=1.59; CrI=1.10,2.30) and cluster 15 (OR=1.38; CrI=1.00,1.88)) were superior to the ORs observed in the single pollutant studies.

Our study has revealed that exposure profiles with high exposure to cadmium, dioxin, and BaP, showed no consistent increase of BC risk. Similar to these findings, single epidemiological analyses available on the association between cadmium and dioxins and risk of BC showed divergent results (Amadou et al., 2020b; Danjou et al., 2019; Filippini

et al., 2020; Fiolet et al., 2022; Florez-Garcia et al., 2023; VoPham et al., 2020; Xu et al., 2016). A recent meta-analysis showed that exposure to higher levels of cadmium (dietary, airborne, and biomarker measures) was associated with an increased risk of BC (Florez-Garcia et al., 2023), while our previous study found no evidence of an association between single airborne exposure to cadmium and overall risk of BC (Amadou et al., 2020b). Regarding dioxins, a study by Danjou et al. showed no increased risk of BC in relation to higher dioxin exposure levels (Danjou et al., 2019). In contrast, evidence of increased risk of BC associated with exposure to BaP was reported in the present nested-case control study by Amadou et al. (OR=1.15; 95 %CI= 1.04,1.27) (Amadou et al., 2021).

Of note, one prospective cohort study has investigated the combined effect of multiple metallic air pollutants exposures (including cadmium) on the risk of BC, using the weighted quantile sum regression (WQS) method. This study showed a statistically significant association between the WQS index (combined exposure to ten air toxic metals) and postmenopausal BC (OR=1.06; 95 %CI= 1.00–1.13) (White et al., 2019). Regarding air pollutant exposure profile approaches, our findings are notably consistent with the study by Niehoff et al., in which classification and regression tree method has been used to identify patterns and combinations of 29 air toxics related to BC. This exploratory analysis identified combinations of age, methylene chloride, BMI and four other toxic substances (propylene dichloride, ethylene dibromide, ethylene dichloride, styrene) associated with overall BC risk, highlighting the complex association between these pollutants and BC risk (Niehoff et al., 2019). However, no study has employed the BPR model to estimate the joint effect of long-term exposure to several air pollutants on the risk of BC in the context of correlated exposures.

The BPR model was selected for the present study, as it considers the risk of BC in addition to the level of exposure, as well as its interest to jointly analyse positively correlated exposures, and also negatively correlated ones (O<sub>3</sub>). In this study, the MCMC algorithm converged to 21 clusters ( $\pm 3$  clusters depending on the initial positions of the Markov chains), a number slightly higher than those obtained in most previous studies, which often had between five and 15 clusters (Coker et al., 2020, 2023; Hoover et al., 2023; Mattei et al., 2016; Rouanet et al., 2021). For example, a study assessing the association between metal mixtures and Preterm birth among pregnant Indigenous women from the Navajo Birth Cohort Study, based on 417 individuals, has estimated six clusters (Hoover et al., 2023). Another study investigating the effect of occupational exposures to organic solvents on lung cancer risk, based on 5,012 individuals, identified 13 exposure profiles (Mattei et al., 2016). Of note, the observed difference in the number of clusters can be explained by the size of our study population, including 10,444 women, exceeding that of most published studies with between 551 and 5,012 subjects (Coker et al., 2023; Hoover et al., 2023; Mattei et al., 2016). It has been shown that the MCMC algorithm of a DPM tends to converge towards a higher number of clusters with increasing population size (Chaumeny et al., 2022). It should be highlighted that the MCMC algorithm with the PreMiuM R package has a superior performance to merge rather than to split clusters (Liverani et al., 2015). It is then important that the number of clusters selected at the initiation of the MCMC algorithm is substantially higher than the true number of clusters, possibly in the dataset. If the number of clusters at MCMC initiation is too low, the final number of clusters may be overestimated by a DPM as the algorithm might be unable to converge to the optimal number of clusters (Hastie et al., 2015). In response to this, the initial number of clusters at initialization of the MCMC algorithm in the present study was fixed at 2,500. We observed a similar number of final clusters produced by the five runs of the MCMC chain with convergence of the model as shown by the marginal posterior distributions of the  $\alpha$  parameters.

The sensitivity analyses, ignoring the risk provided by the disease sub-model in the clustering process, yielded similar average exposure profiles than the full BPR model, with slightly higher ORs for the two clusters (S7 and S9) characterised by high levels of NO<sub>2</sub>, PM<sub>10</sub>, PM<sub>2.5</sub>, and PCB153, than clusters 9, 15 and 16 in the main analysis. However,



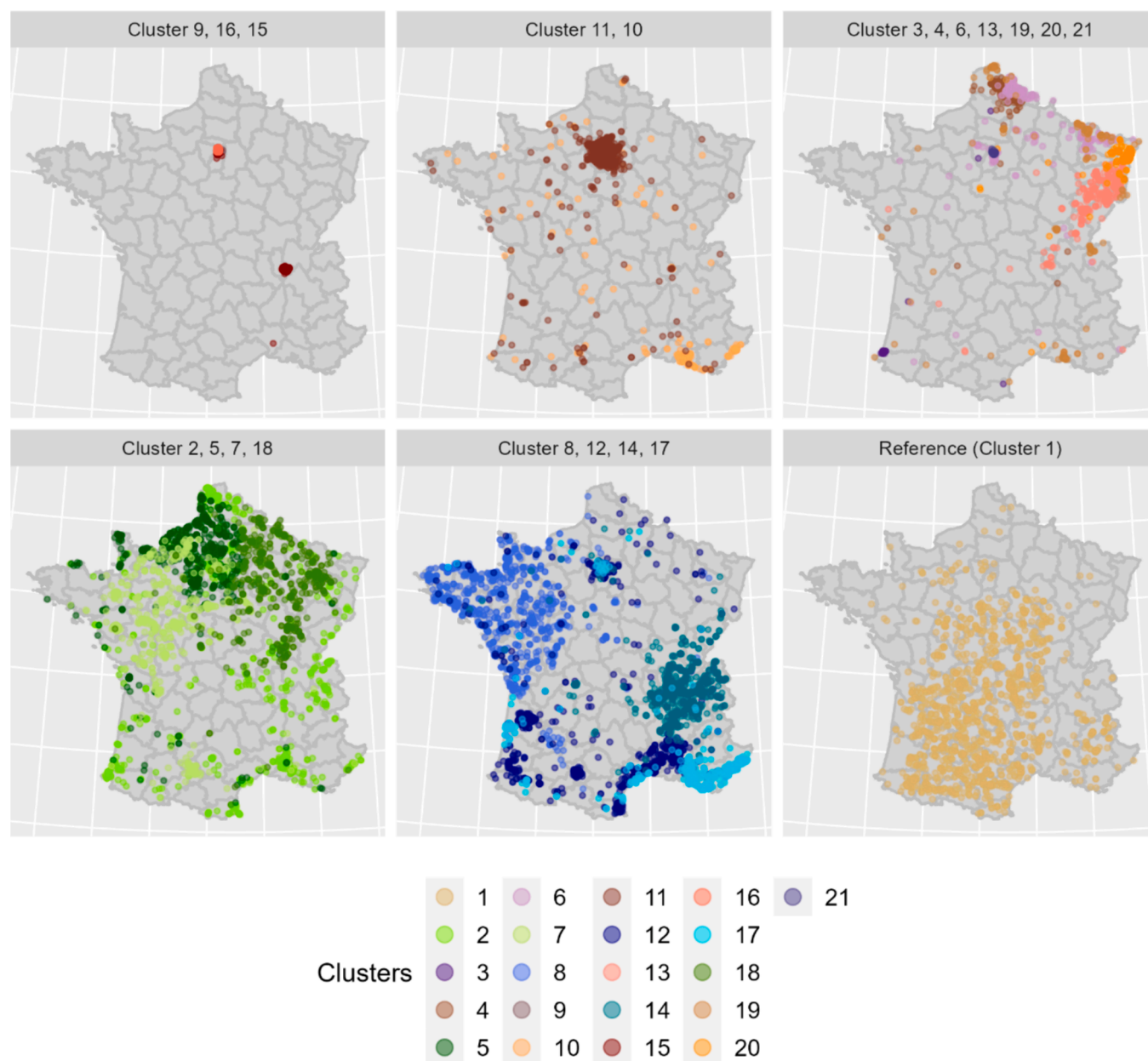


**Fig. 3.** Geographic location of women in France, based on their addresses. Women's residential address coloured by cluster at all addresses. "Cluster 9, 16, 15": associated with women at highest risk; "Cluster 10, 11": characterised by high exposure to NO<sub>2</sub>, PCB153, PM<sub>2.5</sub> or PM<sub>10</sub>; "Cluster 3, 4, 6, 13, 19, 10, 21": characterised by higher exposure levels for cadmium, dioxins and/or BaP; Cluster 2, 5, 7, 18: characterised by exposures relatively close to the overall average for each pollutant; "Cluster 8, 12, 14, 17": characterised by high O<sub>3</sub> levels and low exposures to other pollutants.

as a difference we observed a profile significantly associated with BC risk (cluster 12) consisting of women with low exposure to most pollutants. This profile was not observed with the full BPR model. Grouping individuals together based on their similarity in terms of both, the exposure profile and probability of outcome, the full BPR model may achieve clustering of more homogenous groups of individuals.

One of the strengths of the present study is the use of the BPR method to estimate the risk of BC in the presence of multiple correlated air pollutants, with concentration levels of the eight pollutants estimated over a long period (up to 22 years). With the use of BPR, the limitations of unstable estimates encountered in traditional methods such as multiple regression in presence of multiple correlated predictors are circumvented. This method could be applied to other multiple exposures and diseases risks. Another strength of this study is the design of the nested case-control study within the large prospective French E3N-

generation cohort providing the availability of information on a wide range of potential confounders. The low percentages of missing data reflect the high quality of the data.

Despite these strengths, it is important to note some limitations. The non-implementation of the likelihood of a conditional logistic regression model in the R premium package, as a disease sub-model, required thorough consideration of applying the BPR model to the matched case-control study. Further adjusting the models for matching variables, allowed us to get correct estimates comparable to that obtained with a conditioned model. Another limitation is that the main pollutants responsible for the association with BC have not been identified. This method is unable to provide any evidence of interactions throughout the mixture. Moreover, BPR tends to estimate a greater number of clusters when dealing with a larger population (Chaumeny et al., 2022), of note several clusters have comparable ORs and exposure profiles, suggesting



that there is redundancy in the partitioning of the study population.

## 5. Conclusion

Overall, this study supports evidence of a positive association between a mixture of air pollutant exposures and risk of BC, with greater risk observed for clusters with high concentrations levels of NO<sub>2</sub>, PMs and PCB153. BPR was an appropriate model for the present research, considering women's levels of risk and air pollutant exposure profiles. Overall, this is the first time that BPR was applied to estimate the joint effects of exposure to eight air pollutants on the risk of BC. This study suggests the importance of considering combinations of air pollutants when estimating BC risk, in order to identify specific subgroups at high risk, to inform public health policies and development of preventive strategies.

## 6. Research ethics and patient consent ethical approval

Our research is based on the existing French national cohort E3N. Informed consent was obtained from all participants and the study was approved by the French National Commission for Data Protection and Privacy (CNIL). The datasets generated and/or analysed during the current study are not publicly available for ethical reasons and in accordance with the specific consent signed by the participants. Data are available from the E3N-Generations team through the corresponding author on reasonable request.

## Funding

This work was supported by ADEME (21ESD0020), the Regional Committee of the French League against Cancer of the Savoie Region (18-383-C). CG is supported by a doctoral fellowship of the Regional Committee of the French League Against Cancer of Rhône. The research was carried out using data from the Inserm (French National Institute for Health and Medical Research) E3N-Generation cohort, which was established and maintained with the support of the Mutuelle Générale de l'Éducation Nationale (MGEN), Gustave Roussy, and the French League against Cancer (LNCC). The E3N-Generation cohort is also supported by the French National Research Agency (ANR) under the Investment for the future Program (PIA; ANR-10-COHO-0006) and by the French Ministry of Higher Education, Research and Innovation (subsidy for public service charges No. 2102 918823, 2103236497, and 2103586016).

## CRediT authorship contribution statement

**Camille Giampiccolo:** Writing – review & editing, Writing – original draft, Methodology, Formal analysis, Conceptualization. **Amina Amadou:** Supervision, Resources, Project administration, Conceptualization. **Thomas Coudon:** Writing – review & editing, Supervision, Resources, Conceptualization. **Delphine Praud:** Writing – review & editing, Data curation, Conceptualization. **Lény Grassot:** Writing – review & editing, Resources, Data curation. **Elodie Faure:** Writing – review & editing, Resources, Data curation. **Florian Couvidat:** Writing – review & editing, Resources, Data curation. **Gianluca Severi:** Writing – review & editing, Resources, Data curation, Conceptualization. **Francesca Romana Mancini:** Writing – review & editing, Resources, Data curation. **Béatrice Fervers:** Writing – review & editing, Supervision, Resources, Project administration, Conceptualization. **Pascal Roy:** Writing – review & editing, Validation, Supervision, Methodology, Conceptualization.

## Declaration of competing interest

The authors declare that they have no known competing financial interests or personal relationships that could have appeared to influence

the work reported in this paper.

## Data availability

Data will be made available on request.

## Acknowledgments

We sincerely thank John Molitor, Silvia Liverani, Muriel Rabilloud and Sophie Ancelet for their advice on the application of the BPR model. The authors are grateful to the study participants for their continued participation and to medical practitioners for providing pathology reports.

## Appendix A. Supplementary material

Supplementary data to this article can be found online at <https://doi.org/10.1016/j.envint.2024.108943>.

## References

- Agier, L., Portengen, L., Chadeau-Hyam, M., Basagaña, X., Giorgis-Allemand, L., Siroux, V., Robinson, O., Vlaanderen, J., González, J.R., Nieuwenhuijsen, M.J., Vineis, P., Vrijheid, M., Slama, R., Vermeulen, R., 2016. A systematic comparison of linear regression-based statistical methods to assess exposome-health associations. *Environ. Health Perspect.* 124, 1848–1856. <https://doi.org/10.1289/EHP172>.
- Amadou, A., Coudon, T., Praud, D., Salizzoni, P., Leffondre, K., Lévêque, E., Boutron-Ruault, M.-C., Danjou, A.M.N., Morelli, X., Le Cornet, C., Perrier, L., Couvidat, F., Bessagnet, B., Caudeville, J., Faure, E., Mancini, F.R., Gulliver, J., Severi, G., Fervers, B., 2020a. Chronic low-dose exposure to xenoestrogen ambient air pollutants and breast cancer risk: XENAIR protocol for a case-control study nested within the French E3N Cohort. *JMIR Res. Protoc.* 9, e15167 <https://doi.org/10.2196/15167>.
- Amadou, A., Praud, D., Coudon, T., Danjou, A.M.N., Faure, E., Leffondré, K., Le Romancer, M., Severi, G., Salizzoni, P., Mancini, F.R., Fervers, B., 2020b. Chronic long-term exposure to cadmium air pollution and breast cancer risk in the French E3N cohort. *Int. J. Cancer* 146, 341–351. <https://doi.org/10.1002/ijc.32257>.
- Amadou, A., Praud, D., Coudon, T., Deygas, F., Grassot, L., Faure, E., Couvidat, F., Caudeville, J., Bessagnet, B., Salizzoni, P., Gulliver, J., Leffondré, K., Severi, G., Mancini, F.R., Fervers, B., 2021. Risk of breast cancer associated with long-term exposure to benzo[a]pyrene (BaP) air pollution: Evidence from the French E3N cohort study. *Environ. Int.* 149, 106399 <https://doi.org/10.1016/j.envint.2021.106399>.
- Amadou, A., Praud, D., Coudon, T., Deygas, F., Grassot, L., Dubuis, M., Faure, E., Couvidat, F., Caudeville, J., Bessagnet, B., Salizzoni, P., Leffondré, K., Gulliver, J., Severi, G., Mancini, F.R., Fervers, B., 2023. Long-term exposure to nitrogen dioxide air pollution and breast cancer risk: A nested case-control within the French E3N cohort study. *Environ. Pollut.* 317, 120719 <https://doi.org/10.1016/j.envpol.2022.120719>.
- Bai, L., Shin, S., Burnett, R.T., Kwong, J.C., Hystad, P., van Donkelaar, A., Goldberg, M. S., Lavigne, E., Weichenthal, S., Martin, R.V., Copes, R., Kopp, A., Chen, H., 2020. Exposure to ambient air pollution and the incidence of lung cancer and breast cancer in the Ontario Population Health and Environment Cohort. *Int. J. Cancer* 146, 2450–2459. <https://doi.org/10.1002/ijc.32575>.
- Bellavia, A., 2023. 1.1 Environmental mixtures | Statistical Methods for Environmental Mixtures.
- Belloni, M., Laurent, O., Guihenneuc, C., Ancelet, S., 2020. Bayesian Profile Regression to Deal With Multiple Highly Correlated Exposures and a Censored Survival Outcome. First Application in Ionizing Radiation Epidemiology. *Frontiers in Public Health* 8.
- Billionnet, C., Sherrill, D., Annesi-Maesano, I., GERIE study, 2012. Estimating the health effects of exposure to multi-pollutant mixture. *Ann Epidemiol* 22, 126–141. Doi: 10.1016/j.annepidem.2011.11.004.
- Chaumeny, Davison, J. van der M.M., Anthony C., Paul D. W. Kirk, 2022. Bayesian nonparametric mixture inconsistency for the number of components: How worried should we be in practice?.
- Clavel-Chapelon, F., E3N Study Group, 2015. Cohort Profile: The French E3N Cohort Study. *Int J Epidemiol* 44, 801–809. Doi: 10.1093/ije/dyu184.
- Clément, F., Xu, X., Donini, C.F., Clément, A., Omarjee, S., Delay, E., Treilleux, I., Fervers, B., Le Romancer, M., Cohen, P.A., Maguer-Satta, V., 2017. Long-term exposure to bisphenol A or benzo(a)pyrene alters the fate of human mammary epithelial stem cells in response to BMP2 and BMP4, by pre-activating BMP signaling. *Cell Death Differ.* 24, 155–166. <https://doi.org/10.1038/cdd.2016.107>.
- Coker, E., Katamba, A., Kizito, S., Eskenazi, B., Davis, J.L., 2020. Household air pollution profiles associated with persistent childhood cough in urban Uganda. *Environ. Int.* 136, 105471 <https://doi.org/10.1016/j.envint.2020.105471>.
- Coker, E.S., Molitor, J., Liverani, S., Martin, J., Maranzano, P., Pontarollo, N., Vergalli, S., 2023. Bayesian profile regression to study the ecologic associations of correlated environmental exposures with excess mortality risk during the first year of the Covid-19 epidemic in Lombardy, Italy. *Environ. Res.* 216, 114484 <https://doi.org/10.1016/j.envres.2022.114484>.



- Couvidat, F., Bessagnet, B., Garcia-Vivanco, M., Real, E., Menut, L., Colette, A., 2018. Development of an inorganic and organic aerosol model (CHIMERE 2017 $\beta$  v1.0): Seasonal and spatial evaluation over Europe. *Geosci. Model Dev.* 11, 165–194. <https://doi.org/10.5194/gmd-11-165-2018>.
- Danjou, A.M.N., Coudon, T., Praud, D., L  v  que, E., Faure, E., Salizzoni, P., Le Romancer, M., Severi, G., Mancini, F.R., L  fondr  , K., Dossus, L., Fervers, B., 2019. Long-term airborne dioxin exposure and breast cancer risk in a case-control study nested within the French E3N prospective cohort. *Environ. Int.* 124, 236–248. <https://doi.org/10.1016/j.envint.2019.01.001>.
- Darbre, P.D., 2021. Endocrine disrupting chemicals and breast cancer cells. *Adv. Pharmacol.* 92, 485–520. <https://doi.org/10.1016/bs.apha.2021.04.006>.
- Deygas, F., Amadou, A., Coudon, T., Grassot, L., Couvidat, F., Bessagnet, B., Faure, E., Salizzoni, P., Gulliver, J., Caudeville, J., Severi, G., Mancini, F.R., L  fondr  , K., Fervers, B., Praud, D., 2021. Long-term atmospheric exposure to PCB153 and breast cancer risk in a case-control study nested in the French E3N cohort from 1990 to 2011. *Environ. Res.* 195, 110743. <https://doi.org/10.1016/j.envres.2021.110743>.
- Eurostat, 2024. Contexte - NUTS - Nomenclature des unit  s territoriales statistiques - Eurostat [WWW Document]. URL [https://ec.europa.eu/cas/login?loginRequestId=ECAS\\_LR-16888280-M3H0v1bFbSx4npCwalt3EYeABmoVSGOmK3oP8LD1n0HWZkzHVziwLbVvXhmGj8nw0v6y5SoBztCSwzQAK5xMzG-yntOf97TTHqmOIW4k0Hqea-KhMAUIv0cJlr2StB9kuYZ40zkrCXZcQPenDWbu74zvAZSLJXD7UqXdk3U8FrueHdYnv4zJXfmlDsREUeazq2sO](https://ec.europa.eu/cas/login?loginRequestId=ECAS_LR-16888280-M3H0v1bFbSx4npCwalt3EYeABmoVSGOmK3oP8LD1n0HWZkzHVziwLbVvXhmGj8nw0v6y5SoBztCSwzQAK5xMzG-yntOf97TTHqmOIW4k0Hqea-KhMAUIv0cJlr2StB9kuYZ40zkrCXZcQPenDWbu74zvAZSLJXD7UqXdk3U8FrueHdYnv4zJXfmlDsREUeazq2sO) (accessed 8.2.24).
- Farrar, D.E., Glauber, R.R., 1967. Multicollinearity in regression analysis: The problem revisited. *Rev. Econ. Stat.* 49, 92–107. <https://doi.org/10.2307/1937887>.
- Faure, E., Danjou, A.M.N., Clavel-Chapelon, F., Boutron-Ruault, M.-C., Dossus, L., Fervers, B., 2017. Accuracy of two geocoding methods for geographic information system-based exposure assessment in epidemiological studies. *Environ. Health* 16, 15. <https://doi.org/10.1186/s12940-017-0217-5>.
- Filippini, T., Torres, D., Lopes, C., Carvalho, C., Moreira, P., Naska, A., Kasdagli, M.-I., Malavolti, M., Orsini, N., Vinceti, M., 2020. Cadmium exposure and risk of breast cancer: A dose-response meta-analysis of cohort studies. *Environ. Int.* 142, 105879. <https://doi.org/10.1016/j.envint.2020.105879>.
- Fiolet, T., Casagrande, C., Nicolas, G., Horvath, Z., Frenoy, P., Weiderpass, E., Katzke, V., Kaaks, R., Rodriguez-Barranco, M., Panico, S., Sacerdote, C., Manjer, J., Sonestedt, E., Grioni, S., Agudo, A., Rylander, C., Haugdahl N  st, T., Skeie, G., T  nnel  nd, A., Raaschou-Nielsen, O., Ardanaz, E., Amiano, P., Dolores Chirlaque L  pez, M., Schulze, M.B., Wennberg, M., Harlid, S., Cairat, M., Kvaskoff, M., Huybrechts, I., Romana Mancini, F., 2022. Dietary intakes of dioxins and polychlorobiphenyls (PCBs) and breast cancer risk in 9 European countries. *Environ Int* 163, 107213. <https://doi.org/10.1016/j.envint.2022.107213>.
- Florez-Garcia, V.A., Guevara-Romero, E.C., Hawkins, M.M., Bautista, L.E., Jenson, T.E., Yu, J., Kalkbrenner, A.E., 2023. Cadmium exposure and risk of breast cancer: A meta-analysis. *Environ. Res.* 219, 115109. <https://doi.org/10.1016/j.envres.2022.115109>.
- Gabet, S., Lemarchand, C., Gu  nel, P., Slama, R., 2021. Breast cancer risk in association with atmospheric pollution exposure: A meta-analysis of effect estimates followed by a health impact assessment. *Environ. Health Perspect.* 129, 57012. <https://doi.org/10.1289/EHP8419>.
- Gallo, A., Agnese, V., Coronello, C., Raffa, G.M., Bellavia, D., Conaldi, P.G., Pilato, M., Pasta, S., 2018. On the prospect of serum exosomal miRNA profiling and protein biomarkers for the diagnosis of ascending aortic dilatation in patients with bicuspid and tricuspid aortic valve. *Int. J. Cardiol.* 273, 230–236. <https://doi.org/10.1016/j.ijcard.2018.10.005>.
- Guerreiro, C.B.B., Hor  lek, J., de Leeuw, F., Couvidat, F., 2016. Benzo(a)pyrene in Europe: Ambient air concentrations, population exposure and health effects. *Environ. Pollut.* 214, 657–667. <https://doi.org/10.1016/j.envpoll.2016.04.081>.
- Hastie, D.I., Liverani, S., Richardson, S., 2015. Sampling from Dirichlet process mixture models with unknown concentration parameter: Mixing issues in large data implementations. *Stat. Comput.* 25, 1023–1037. <https://doi.org/10.1007/s11222-014-9471-3>.
- Hoerl, A.E., Kennard, R.W., 1970. Ridge regression: Biased estimation for nonorthogonal problems. *Technometrics* 12, 55–67. <https://doi.org/10.1080/00401706.1970.10488634>.
- Hoover, J.H., Coker, E.S., Erdei, E., Luo, L., Begay, D., MacKenzie, D., NBCS Study Team, Lewis, J., 2023. Preterm Birth and Metal Mixture Exposure among Pregnant Women from the Navajo Birth Cohort Study. *Environmental Health Perspectives* 131, 127014. <https://doi.org/10.1289/EHP10361>.
- INSEE, 2024. Base du comparateur de territoires [WWW Document]. URL <https://www.insee.fr/fr/statistiques/2521169> (accessed 8.2.24).
- Jeanjean, M., Goix, S., Periot, M., Douib, K., Dron, J., Etienne, M.-P., Marchand, P., Austruy, A., Revenko, G., Chamaret, P., 2021. Environmental and dietary exposures near a major industrial harbour (Fos-sur-Mer, France) identified as a significant pathway for PCBs and PCDD/Fs accumulation in residents' blood serum. *Expo. Health* 13, 447–464. <https://doi.org/10.1007/s12403-021-00395-8>.
- Large, C., Wei, Y., 2017. Geographic variations in female breast cancer incidence in relation to ambient air emissions of polycyclic aromatic hydrocarbons. *Environ. Sci. Pollut. Res. Int.* 24, 17874–17880. <https://doi.org/10.1007/s11356-017-9395-5>.
- Lengyel, A., Botta-Duk  t, Z., 2019. Silhouette width using generalized mean—A flexible method for assessing clustering efficiency. *Ecol. Evol.* 9, 13231–13243. <https://doi.org/10.1002/ece3.5774>.
- Liverani, S., Hastie, D.I., Azizi, L., Papathomas, M., Richardson, S., 2015. PRemiuM: An R package for profile regression mixture models using Dirichlet processes. *J. Stat. Softw.* 64, 1–30. <https://doi.org/10.18637/jss.v064.i07>.
- Loomis, D., Grosse, Y., Lauby-Secretan, B., El Ghissassi, F., Bouvard, V., Benbrahim-Tallaa, L., Guha, N., Baan, R., Mattock, H., Straif, K., International Agency for Research on Cancer Monograph Working Group IARC, 2013. The carcinogenicity of outdoor air pollution. *Lancet Oncol* 14, 1262–1263. [https://doi.org/10.1016/s1470-2045\(13\)70487-x](https://doi.org/10.1016/s1470-2045(13)70487-x).
- MacLehose, R.F., Dunson, D.B., Herring, A.H., Hoppin, J.A., 2007. Bayesian methods for highly correlated exposure data. *Epidemiology* 18, 199–207. <https://doi.org/10.1097/01.ede.00000256320.30737.c0>.
- Mattei, F., Liverani, S., Guida, F., Matrat, M., Cen  e, S., Azizi, L., Menvielle, G., Sanchez, M., P  lorget, C., Lap  tre-Ledoux, B., Luce, D., Richardson, S., St  cker, I., 2016. Multidimensional analysis of the effect of occupational exposure to organic solvents on lung cancer risk: the ICARE study. *Occup. Environ. Med.* 73, 368–377. <https://doi.org/10.1136/oemed-2015-103177>.
- Menut, L., Bessagnet, B., Khvorostyanov, D., Beekmann, M., Blond, N., Colette, A., Coll, I., Curci, G., Foret, G., Hodzic, A., Mailler, S., Meleux, F., Monge, J.-L., Pison, I., Siour, G., Turquet, S., Valari, M., Vautard, R., Vivanco, M.G., 2013. CHIMERE 2013: A model for regional atmospheric composition modelling. *Geosci. Model Dev.* 6, 981–1028. <https://doi.org/10.5194/gmd-6-981-2013>.
- Molitor, J., Papathomas, M., Jerrett, M., Richardson, S., 2010. Bayesian profile regression with an application to the National survey of children's health. *Biostatistics* 11, 484–498. <https://doi.org/10.1093/biostatistics/kxq013>.
- Niehoff, N.M., Gammon, M.D., Keil, A.P., Nichols, H.B., Engel, L.S., Sandler, D.P., White, A.J., 2019. Airborne mammary carcinogens and breast cancer risk in the Sister Study. *Environ. Int.* 130, 104897. <https://doi.org/10.1016/j.envint.2019.06.007>.
- Niehoff, N.M., Terry, M.B., Bookwalter, D.B., Kaufman, J.D., O'Brien, K.M., Sandler, D.P., White, A.J., 2022. Air pollution and breast cancer: An examination of modification by underlying familial breast cancer risk. *Cancer Epidemiol. Biomark. Prev.* 31, 422–429. <https://doi.org/10.1158/1055-9965.EPI-21-1140>.
- Pearce, N., 2016. Analysis of matched case-control studies. *BMJ* 352, i969. <https://doi.org/10.1136/bmj.i969>.
- Praud, D., Deygas, F., Amadou, A., Bouilly, M., Turati, F., Bravi, F., Xu, T., Grassot, L., Coudon, T., Fervers, B., 2023. Traffic-related air pollution and breast cancer risk: A systematic review and meta-analysis of observational studies. *Cancers (Basel)* 15, 927. <https://doi.org/10.3390/cancers15030927>.
- Richardson, D., 2004. An incidence density sampling program for nested case-control analyses. *Occup. Environ. Med.* 61, e59. <https://doi.org/10.1136/oem.2004.014472>.
- Rouanet, A., Johnson, R., Strauss, M.E., Richardson, S., Tom, B.D., White, S.R., Kirk, P.D. W., 2021. Bayesian profile regression for clustering analysis involving a longitudinal response and explanatory variables. *arXiv:2111.04518 [stat]*.
- Sung, H., Ferlay, J., Siegel, R.L., Laversanne, M., Soerjomataram, I., Jemal, A., Bray, F., 2021. Global cancer statistics 2020: GLOBOCAN estimates of incidence and mortality worldwide for 36 cancers in 185 countries. *CA Cancer J. Clin.* 71, 209–249. <https://doi.org/10.3322/caac.21660>.
- Turner, M.C., Andersen, Z.J., Baccarelli, A., Diver, W.R., Gapstur, S.M., Pope, C.A., Prada, D., Samet, J., Thurston, G., Cohen, A., 2020. Outdoor air pollution and cancer: An overview of the current evidence and public health recommendations. *CA Cancer J. Clin.* <https://doi.org/10.3322/caac.21632>.
- Vopham, T., Bertrand, K.A., Jones, R.R., Deziel, N.C., DuPr  , N.C., James, P., Liu, Y., Vieira, V.M., Tamimi, R.M., Hart, J.E., Ward, H., Laden, F., 2020. Dioxin exposure and breast cancer risk in a prospective cohort study. *Environ. Res.* 186, 109516. <https://doi.org/10.1016/j.envres.2020.109516>.
- Wan, M.L.Y., Co, V.A., El-Nezami, H., 2022. Endocrine disrupting chemicals and breast cancer: A systematic review of epidemiological studies. *Crit. Rev. Food Sci. Nutr.* 62, 6549–6576. <https://doi.org/10.1080/10408398.2021.193382>.
- Wei, W., Wu, B.-J., Wu, Y., Tong, Z.-T., Zhong, F., Hu, C.-Y., 2021. Association between long-term ambient air pollution exposure and the risk of breast cancer: a systematic review and meta-analysis. *Environ. Sci. Pollut. Res.* 28, 63278–63296. <https://doi.org/10.1007/s11356-021-14903-5>.
- White, A.J., Bradshaw, P.T., Hamra, G.B., 2018. Air pollution and breast cancer: A review. *Curr. Epidemiol. Rep.* 5, 92–100. <https://doi.org/10.1007/s40471-018-0143-2>.
- White, A.J., O'Brien, K.M., Niehoff, N.M., Carroll, R., Sandler, D.P., 2019. Metallic air pollutants and breast cancer risk in a nationwide cohort study. *Epidemiology* 30, 20–28. <https://doi.org/10.1097/EDE.0000000000000917>.
- White, A.J., Gregoire, A.M., Niehoff, N.M., Bertrand, K.A., Palmer, J.R., Coogan, P.F., Bethea, T.N., 2021. Air pollution and breast cancer risk in the Black Women's Health Study. *Environ. Res.* 194, 110651. <https://doi.org/10.1016/j.envres.2020.110651>.
- Xu, J., Ye, Y., Huang, F., Chen, H., Wu, H., Huang, J., Hu, J., Xia, D., Wu, Y., 2016. Association between dioxin and cancer incidence and mortality: A meta-analysis. *Sci. Rep.* 6, 38012. <https://doi.org/10.1038/srep38012>.
- Yaghjian, L., Arao, R., Brokamp, C., O'Meara, E.S., Sprague, B.L., Ghita, G., Ryan, P., 2017. Association between air pollution and mammographic breast density in the Breast Cancer Surveillance Consortium. *Breast Cancer Res.* 19, 36. <https://doi.org/10.1186/s13058-017-0828-3>.
- Yilmaz, B., Terekci, H., Sandal, S., Kelestimur, F., 2020. Endocrine disrupting chemicals: Exposure, effects on human health, mechanism of action, models for testing and strategies for prevention. *Rev. Endocr. Metab. Disord.* 21, 127–147. <https://doi.org/10.1007/s11554-019-09521-z>.
- Zhang, Y., Kleer, C.G., 2016. Phyllodes tumor of the breast: histopathologic features, differential diagnosis, and molecular/genetic updates. *Arch. Pathol. Lab. Med.* 140, 665–671. <https://doi.org/10.5858/arpa.2016-0042-RA>.
- Zhang, Z., Yan, W., Chen, Q., Zhou, N., Xu, Y., 2019. The relationship between exposure to particulate matter and breast cancer incidence and mortality: A meta-analysis. *Medicine (Baltimore)* 98, e18349. <https://doi.org/10.1097/MD.00000000000018349>.





Review

# Radiation on Earth or in Space: What Does It Change?

Juliette Restier-Verlet <sup>†</sup>, Laura El-Nachef <sup>†</sup>, Mélanie L. Ferlazzo <sup>†</sup>, Joëlle Al-Choboq, Adeline Granzotto, Audrey Bouchet and Nicolas Foray <sup>\*</sup>

Inserm, U1296 Unit, «Radiation: Defense, Health and Environment», Centre Léon-Bérard, 28, Rue Laennec, 69008 Lyon, France; juliette.restier-verlet@inserm.fr (J.R.-V.); laure.el-nachef@inserm.fr (L.E.-N.); melanie.ferlazzo@inserm.fr (M.L.F.); joelle.al-choboq@inserm.fr (J.A.-C.); adeline.granzotto@inserm.fr (A.G.); audrey.bouchet@inserm.fr (A.B.)

<sup>\*</sup> Correspondence: Nicolas.foray@inserm.fr; Tel.: +33-4-78-78-28-28

<sup>†</sup> These three authors have contributed equally.

**Abstract:** After having been an instrument of the Cold War, space exploration has become a major technological, scientific and societal challenge for a number of countries. With new projects to return to the Moon and go to Mars, radiobiologists have been called upon to better assess the risks linked to exposure to radiation emitted from space (IRS), one of the major hazards for astronauts. To this aim, a major task is to identify the specificities of the different sources of IRS that concern astronauts. By considering the probabilities of the impact of IRS against spacecraft shielding, three conclusions can be drawn: (1) The impacts of heavy ions are rare and their contribution to radiation dose may be low during low Earth orbit; (2) secondary particles, including neutrons emitted at low energy from the spacecraft shielding, may be common in deep space and may preferentially target surface tissues such as the eyes and skin; (3) a “bath of radiation” composed of residual rays and fast neutrons inside the spacecraft may present a concern for deep tissues such as bones and the cardiovascular system. Hence, skin melanoma, cataracts, loss of bone mass, and aging of the cardiovascular system are possible, dependent on the dose, dose-rate, and individual factors. This suggests that both radiosusceptibility and radiodegeneration may be concerns related to space exploration. In addition, in the particular case of extreme solar events, radiosensitivity reactions—such as those observed in acute radiation syndrome—may occur and affect blood composition, gastrointestinal and neurologic systems. This review summarizes the specificities of space radiobiology and opens the debate as regards refinements of current radiation protection concepts that will be useful for the better estimation of risks.

**Keywords:** space radiobiology; radiosusceptibility; radiosensitivity; radiodegeneration



**Citation:** Restier-Verlet, J.; El-Nachef, L.; Ferlazzo, M.L.; Al-Choboq, J.; Granzotto, A.; Bouchet, A.; Foray, N. Radiation on Earth or in Space: What Does It Change?. *Int. J. Mol. Sci.* **2021**, *22*, 3739. <https://doi.org/10.3390/ijms22073739>

Academic Editor:  
Dimitris Emfietzoglou

Received: 24 February 2021

Accepted: 29 March 2021

Published: 3 April 2021

**Publisher's Note:** MDPI stays neutral with regard to jurisdictional claims in published maps and institutional affiliations.



**Copyright:** © 2021 by the authors. Licensee MDPI, Basel, Switzerland. This article is an open access article distributed under the terms and conditions of the Creative Commons Attribution (CC BY) license (<https://creativecommons.org/licenses/by/4.0/>).

## 1. Introduction

To date, exposure to ionizing radiation (IR) is one of the major concerns for space exploration [1–4]. IR remove electrons from atoms, which triggers the production of reactive oxygen species (ROS) and DNA damage, leading to significant injuries at the molecular, cellular, tissue and/or clinical levels in a dose-dependent manner [5]. While radiobiology is a pluridisciplinary study of the biological effects of IR, space radiobiology is a particular subdomain, in which investigations are made difficult by the very specific physical features of IR emitted from space (IRS). While the sources of IRS are well known, the contribution of each type of IRS to the dose delivered to astronauts needs to be better documented. Furthermore, since space missions generally correspond to exposure to low-dose radiation, space radiobiology should also integrate the uncertainties related to rare physical events, the specificity of some radiobiological phenomena occurring at low-doses, and their contribution to radiation-induced risks [6]. In addition, a complete review of the specific human organs/tissues at risk of low-dose radiation is required, while the specificities of the clinical risks related to cellular death (radiosensitivity), cellular



transformation (radiosusceptibility) and cellular aging (radiodegeneration) should be identified and documented. In addition, it is noteworthy that the perception of these clinical consequences by society is different [5,7] (also see below). Lastly, the current international radiation protection recommendations do not integrate individual factors in the radiation response or various specific features of low-energy particles that may be important in the context of space radiobiology [5]. Hence, data controversies, differences in the estimations of the risks and confusion in the terms used have progressively appeared, together with societal interest in the field which has been enhanced by topics such as the International Space Station (ISS) end-of-life and the initiation of projects to travel to the Moon and to Mars. Therefore, better documenting these different issues and clarifying the messages represent the major objectives of this review.

## 2. The Three Sources of Ionizing Radiation Emitted from Space

### 2.1. Historical Features

As part of his work related to low electrical currents, and just before the discovery of radium thanks to Marie Curie, his wife, Pierre Curie developed very sensitive electrometers at the beginning of the 20th century [8]. In 1910, by setting up a Curie electroscope at the top of the Eiffel tower, Wulf, a Jesuit priest, demonstrated that 50% of the electricity in the air was lost by comparison with that assessed at the Earth's surface [9]. In 1912, by using balloons, Hess demonstrated that the ionization density of the atmosphere decreases up to 1000 m, but increases above 1800 m, suggesting the existence of radiation emitted from space, *the cosmic rays*—even though this term was first proposed by Millikan. Later, with more specific tools, it was shown that cosmic rays are composed of high energy particles. The Nobel Prize in Physics was awarded in 1936 to Hess for his work related to space radiation. In the same year, Solomon published a theory about the interaction between matter and cosmic rays [10]. Between 1930 and 1940, a body of research related to the nucleosynthesis of the universe led to the production of evidence that heavy elements are abundant in the cosmos, namely, *galactic cosmic radiation* (GCR) [6,9,11,12] (Figure 1).

The 1950s correspond to a technological revolution in the field of cosmology: experiments with balloons were replaced by physics and chemistry assessments in artificial satellites. Notably, the data generated by the first Explorer and Pioneer satellites permitted Van Allen and Franck to point out the existence of the Earth's radiation belt; that is, a high intensity band of corpuscular radiation temporarily trapped in the Earth's magnetic field, the *Van Allen radiation belt*. They revealed, thereafter, that this belt is composed of protons and electrons that are mainly generated as secondary particles from neutrons emitted from cosmic charged particles [13,14]. In the same period, considerable advances were made in regard to solar radiation. Notably, protons were also considered to be the most abundant particles emitted from the Sun [15,16].

In the 1960s, thanks to the acceleration of spatial technology progress emulated by the Cold War, the specific composition and energy-distribution of the inner and outer Van Allen radiation belt and solar flares were almost completely defined. Astrophysicists and geophysicists pointed out a specific area where the inner Van Allen radiation belt is the closest to the Earth surface, (above Brazil and South Atlantic Ocean): The *South Atlantic Anomaly* (SAA). This area is characterized by an impressive flux of protons and electrons (100–1000 protons/cm<sup>2</sup>/s at 500 km). Numerous hypotheses were formulated about the injuries that such particle flux may cause on electronics, materials, and overall, on human health at each passage above the SAA. From this period, on-board radiation dosimetry was systematically set up for each space mission [16–18].

### 2.2. From the Cosmos to the Shielding: The Three Sources of IRS and Their Physical Features

To date, IRS is generally divided into three major sources: the cosmos, the Sun and the Van Allen radiation belt. Their physical features are fairly well known [16,17] (Figure 1):

- *The cosmos: Galactic cosmic radiation* (GCR) is composed of 85% protons, 14% helium ions, and about 1% heavier elements, such as iron. In GCR, the corresponding fluxes



are about four particles/cm<sup>2</sup>/s for protons, 0.4 for helium ions and 10<sup>−4</sup> to 10<sup>−2</sup> for heavier ions. Their energy can be very high (more than 10<sup>11</sup> MeV). The probability of impact of the heaviest ions to astronauts can be considered as negligible in low Earth orbit (LEO) but not in deep space [19]. For quantifying the risks during LEO, GCR can be reasonably reduced as a flux of protons and helium ions [6].

- *The Sun:* Solar flares generally consist of 92% protons, 6% helium ions and about 2% heavier elements at various MeV values. The solar wind is an intense (about 10<sup>8</sup> protons/cm<sup>2</sup>/s) flux of protons at various keV values. Solar flares, storms and winds are infrequent events (generally obeying a cycle of 11 years for solar flares) [20]. Even if space missions are scheduled to avoid such events, some missions, such as Apollo-XIV, Skylab-4, and Mir-15, have been exposed to some significant solar events, at least partially: The crews received 11.4 mGy in 9 days, 77 mGy in 90 days, and 92.9 mGy in 185 days. All these values were obtained from on-board dosimeters that included the GCR contribution [6] (Figure 2). However, no significant injury was reported to astronauts or electronics, probably because the duration of the mission was short and/or the excess of dose remained limited. Predicting solar events should, therefore, be an essential part of ensuring the radiological protection of astronauts. By excluding exceptional solar events, one can reasonably consider the Sun as a simple source of protons emitted at high flux but at a relatively low energy.
- *The Van Allen radiation belt* is made of two layers: An “outer” belt composed of electrons, the energy of which ranges from 40 keV to 7 MeV (in electron radiotherapy, the energy of electrons is 6–25 MeV), and an “inner” belt, mostly composed of protons, the energy of which ranges from 100 keV and 400 MeV (in proton therapy, the energy of protons is 60–280 MeV). As described above, the particularity of the Van Allen belt is the excess of radiation observed in the SAA. At each passage above the SAA, electronic devices and astronauts receive a peak of dose that may represent a dose six-fold higher than the average one experienced outside the SAA [18]. Lastly, it is noteworthy that inside the Van Allen belt, the flux and the nature of the particles that impact the spacecraft are greatly conditioned by the flight parameters (notably, day/night and orbit inclination [21,22]. Hence, significant differences may appear when comparing data from the Apollo missions—that spent some time outside the Van Allen belt—and the ISS that remains in LEO, protected inside the magnetosphere [23]. The assessed and calculated doses are discussed below.

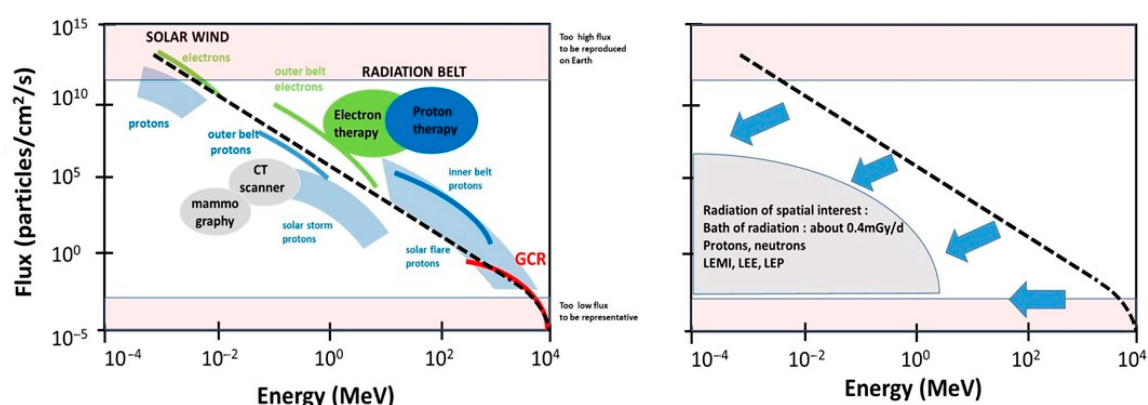


**Figure 1.** Schematic representation of the 3 major sources of space radiation as a function of energy and flux: Galactic cosmic radiation (GCR), solar radiation component and Van Allen radiation belt. Left panel. The dotted line represents the general relationship between flux and energy. The confidence zones represent the physical features of rays and particles used in proton therapy, electron therapy, computerized tomography (CT) scan and mammography. Right panel. Through their interaction with the shielding, space radiation is degraded in nature, flux and energy to give protons, neutrons, low-energy-metal ions (LEMI), low-energy-electrons (LEE), low-energy-protons (LEP) and a “bath” of residual radiation at about 0.4 mGy/d [6]. Blue arrows represent the effect of the spacecraft shielding to the IRS.



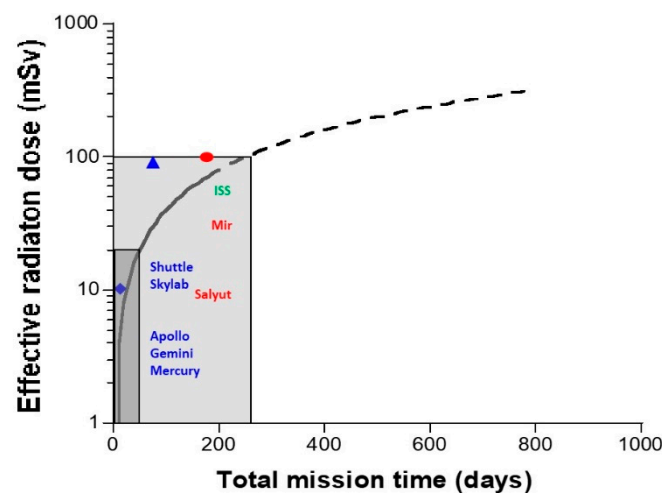


**Figure 2.** Schematic representation of effective dose per day of space mission. *Left panel.* The black solid line and its dotted line extension represents the average over the whole duration of the mission from all of the space mission's on-board dosimetry data until 1990s [6]. Blue losange, blue triangle and red circle represent the Apollo XIV, Skylab4 and Mir 15 missions' on-board dosimetry data, respectively. Dark and light grey zones represent the annual and the 5-year limits of occupational exposure to ionizing radiation (IR) (20 mSv/y and 100 mSv/y, respectively).

By integrating all these data and excluding exceptional solar events, an empirical formula can be deduced between the flux,  $F_{outside}$ —assessed outside the spacecraft and expressed in particles/cm<sup>2</sup>/s—at the energy,  $E$ , expressed in MeV. This formula fits the proton component particularly well:

$$F_{outside}(E) = \left( \frac{10}{\sqrt{E}} \right)^5 \quad (1)$$

### 2.3. Inside the Shielding: Occurrence of a Variety of Electronic and Nuclear Reactions

Since the 1960s, the shielding composition designed to protect astronauts and electronic equipment has been the subject of a number of reports [2,17,24–30]. While very dense elements such as lead or depleted uranium would theoretically offer the best protection against radiation, the aluminum-containing shieldings have been considered as the best compromise between the highest density and the best protection. However, to date, there are a plethora of projects focused on different new shieldings combining multilayers of dense elements that stop charged particles and materials of low atomic numbers, such as hydrogen, that absorb neutrons [2,17,24–29].

However, whatever the final shielding, the energy and flux ranges of IRS are impossible to reproduce on Earth. Consequently, the radiation dose received by astronauts inside their spacecraft must be calculated from the physical interactions between the IRS and the shielding components, simulated by a Monte Carlo approach and transport equations. This task is particularly difficult since the choice of the simulation code, the values of the cut-off energies and the uncertainties of cross-sections related to reactions involving high-energy particles, represent sources of discrepancies between research groups [31].

The shielding serves as a *filter* and is a *transformer*: In other words, the collision between the IRS and the shielding provides primary and secondary rays and particles that obey the following trends.

- *A general decrease in the flux:* The flux of the secondary particles provided from the spacecraft shielding must be lower than that of the incident particles. A decreased flux leads to a lower absorbed dose: By omitting exceptional solar events, the dose delivered to astronauts is generally in the order of mGy per day. The decrease in the



flux by the shielding can be roughly represented by a vertical shift in the data plotted in Figure 1.

- *A general degradation of the energy combined with changes in the nature of radiation:* The energy of the secondary particles provided from the spacecraft shielding must be lower than the incident particles and their nature can be changed. The decrease in energy can be roughly represented by a horizontal shift in the data plotted in Figure 1. High-energy particles interact with matter to produce atomic displacements and/or electronic ionizations and excitations. If the kinetic energy of the incident particle transferred to the nucleus of the atoms of the shielding is sufficient, the moving atom may serve as a projectile to produce secondary displacements or ionize or excite other atoms adjacent to its path [32]. For example, while electrons emitted from space may be stopped by shielding, they can produce a non-negligible effect through the bremsstrahlung phenomenon, which results in an intense ray build-up behind the shielding [21,22]. With regard to protons emitted from space, numerous excitations and ionizations are expected inside the shielding, together with the emission of low-energy metal ions (LEMI) [32,33]. In addition, secondary neutrons provided from the aluminum-containing shielding have also been detected in low earth orbiting spacecraft [34,35]. However, although their energy spectrum is difficult to measure, the long duration exposure facility (LDEF) mission has provided data suggesting that neutrons of more than 1 MeV are the most abundant and responsible for most of the total equivalent neutron dose [36]. At this stage, it is important to address whether neutrons may be responsible for some of the activation reactions in the spacecraft. In general, the mechanical properties of metals and ceramics that are present in the spacecraft do not significantly suffer from a flux that is lower than  $10^{17}/\text{cm}^2$  for protons  $> 1$  MeV,  $10^{17}/\text{cm}^2$  for neutrons  $> 1$  keV and  $10^{18}/\text{cm}^2$  for electrons  $> 1$  MeV [32]. The neutron activation and the neutron photo-emission or spallation of oxygen inside the spacecraft may result in  $^{19}\text{O}$  and  $^{15}\text{O}$ , respectively. However, the lifetimes of these oxygen isotopes are too short to obtain reliable measurements. Conversely,  $^7\text{Be}$ ,  $^{22}\text{Na}$  and  $^{24}\text{Na}$ , are the major activable gamma-ray-emitting radioisotopes present in the body, with half-lives that are long enough to be measurable. Additionally, in 1969, Brodzinski et al. proposed to quantify the radiation dose to Apollo astronauts from the assessment of such activated nuclides. Relevant dosimetry data were obtained, suggesting that measurable activation events occur in the spacecraft [37]. Unfortunately, to our knowledge, no data have been published in regard to this technique being applied in the ISS, maybe because the physical conditions of neutron activation are not so favorable at LEO. Further investigations are, however, needed to document the impact of this particular process on the dose.

#### 2.4. From the Shielding to Astronauts: The Contribution of Each IRF to the Radiation Dose

From the two trends explained above, three major types of radiation must be considered: *Low-energy particles* (mostly protons, electrons and metal ions directly produced by the shielding), neutrons, and a “*bath of radiation*” resulting from a mixture of all the secondary rays that result from Bremsstrahlung and activation emitted in the spacecraft. To illustrate these specific types of rays and particles emitted inside the spacecraft, presented below are two representative examples:

- At the end of the 1960s, it was reported that helmets used during the Apollo missions were impacted by specific low-energy metal ions (LEMI). As described above, the probability of the impact of such GCR metal ions is approximately a few particles per  $\text{km}^2$  per century. Thus, the LEMIs detected in the helmets did not come from the cosmos, but were generated from the walls of the spacecraft made of iron, zinc, aluminum, nickel, and copper. These particles resulted from the interaction between the incident protons from space with the metal shielding. LEMIs were found to emit at a few keV to several MeV [33]. In addition to these LEMIs, some low-energy protons (LEP) and low-energy electrons (LEE) can be emitted from the shielding and may



have a significant impact on electronics [38]. It is noteworthy that LEMI, LEP and LEE deliver nearly all their energy at the surface of matter (with an average track path of several mm to nm) [39,40]. Hence, these particles preferentially target the external parts of the human body, such as the skin and eyes (Figure 1). It is noteworthy that this low-energy particle component may be reduced in the ISS in comparison with deep space missions.

- The other rays and particles directly or indirectly produced by these secondary particles represent a constant “bath of radiation”, notably made of the build-up of X-rays and gamma-rays. An overview of the dosimetry of all space missions, from that of Gagarin in 1962 to the most recent with the Space Shuttle, has shown that the dose received by astronauts is strongly time-dependent [6] (Figure 2). Whether the mission concerns LEO, the surface of the Moon or a trip from Earth to the Moon (Apollo missions only), the data review indicates a constant dose rate of about 0.4 mGy/d (Table 1). Such a “bath of radiation” is mainly made of X-rays and gamma-rays and should concern the human body as a whole, even at depth [6].

Despite the relative simplicity of the above description, the contribution of GCR and that of neutrons to the dose has been a subject of controversy. For example, in 2001, Benton and Benton (2001) reported that “roughly half the dose on the ISS is expected to come from trapped protons and half from GCR” [41], while Cucinotta et al. (2008) supported that “80% or more of organ dose equivalents on the ISS are from GCR and only a small contribution from trapped protons” [42]. As described above, such differences are likely due to different simulation methodologies and reveal the difficulties of measuring and predicting a very complex spectrum of rays and particles emitted from space and targeting the spacecraft. These differences could also be due to the meaning of the term “GCR” that may evoke connotations of heavy ions only and not necessarily protons, helium ions and heavier ions.

Similarly, the contribution of neutrons to the dose is still not well established, notably because of the difficulties to introduce high-energy neutrons features into measurements and calculations. While the contribution of neutrons with an energy lower than 1 MeV to the dose has been found to be less than 5%, calculations show that 1–10 MeV neutrons should contribute to half of the total dose in the space shuttle [34,43]. More recently, the measured neutron spectrum (12–436 MeV) in the ISS was found to produce a dose rate of  $3.8 \pm 1.2 \mu\text{Gy/d}$ . Extrapolation of the spectrum at 0.1–1000 MeV led to a total neutron-induced dose rate of  $6 \pm 2 \mu\text{Gy/day}$  [44].

In addition to these uncertainties regarding high-energy neutrons, the estimation of the dose is made difficult by the dependence of GCR fluxes with the solar cycle (*solar modulation*): The GCR flux is maximal when solar activity is minimal. Differences between solar minimum and solar maximum are a factor of approximately five and also explain the range of uncertainties [19,29]. Similar explanations are relevant for explaining the night/day differences on the Moon and Mars surface [45].

## 2.5. From the Assessment of the Absorbed Dose to the Calculation of the Effective Dose

The same absorbed dose does not lead to the same biological effects, rather it is dependent on the type of radiation and/or the irradiated tissue. For this reason, the *equivalent dose* is a useful way to calculate the radiation-induced risk when exposed to IR involving different types of radiation. Similarly, the effective dose permits one to quantify the radiation-induced risks when different parts of the body, sensitive or not, are exposed to IR. As part of the international radiation protection recommendations of the International Commission of Radiological Protection (ICRP), calculation of the equivalent dose  $H_T$  and effective dose  $E$  are based on the dimensionless weighting factors  $W_R$  and  $W_T$ , related to the nature of the radiation type and the tissue, respectively [46]. The equivalent dose  $H$  is



defined as the probability of a stochastic event (namely radiation-induced cancer) for an absorbed dose  $D$  in the tissue  $T$  irradiated with the radiation type  $R$ :

$$H_T = \sum_R W_R \cdot D_{T,R} \quad (2)$$

The effective dose  $E$  is defined as the probability of radiation-induced cancer for a mass-averaged absorbed dose  $\bar{D}$  in tissue  $T$ , irradiated with radiation type  $R$ :

$$E_T = \sum_T W_T \cdot H_T = \sum_T W_T \cdot \sum_R W_R \bar{D}_{T,R} \quad (3)$$

The relevance of the dose equivalent and the effective dose depend on the relevance of the weighting factors  $W_R$  and  $W_T$ . The specificity of space radiobiology is that the  $W_R$  of some very high- or very low-energy particles may not be consensual. The relevance of weighting factors  $W$  will be discussed in the following paragraphs. Notwithstanding the question of relevance, a non-exhaustive list of reports on estimated doses of spatial interest shows a relatively good agreement between the absorbed doses and the effective doses proposed for the ISS, Moon and Mars [47–52] (Table 1). Again, the range of values are explained by solar modulation.

**Table 1.** Non-exhaustive list of reports about estimated doses of spatial interest.

Missions	References	Absorbed Dose/Day (mGy/d)	Effective Dose/Day (mSv/d)
Missions before ISS	[41]	Salyut: 0.1–0.3 Apollo: 0.22–1.27	
Missions from Gagarin to Space Shuttle	[6]	0.2–1.26 Average: 0.4	
ISS	[23]		0.153–0.231
ISS during Solar event	[23]		0.535
ISS	[35]		0.15
ISS during Solar event	[20]	10.48	
	[19]		0.37–0.97
Moon surface	[47]		0.3–1
	[48]		0.31
	[19]		0.17–0.325
Mars surface	[49]		0.002–0.9
	[52]		0.15
	[51]		0.33

## 2.6. Comparison with the Natural Radiation Backgrounds on Earth, the Moon and Mars

As far as any shielding is used during the exposure, the low-energy particle component does not exist on Earth. In contrast, the natural radiation background can be considered as a “bath of radiation” composed of three major components:

- *The telluric radiation component:* The three major radioactive decay chains of natural radiation, such as uranium ( $^{235}\text{U}$  or  $^{238}\text{U}$ ) and thorium ( $^{232}\text{Th}$ ), are present on Earth and continuously provide several unstable and stable radionuclides. The major part of the telluric radiation component comes from radon, a naturally radioactive gas resulting from the decay of uranium and radium naturally present in the soil. The average effective dose inhaled in air produced by radon is about 1.3 mSv/y, while terrestrial radiation from the ground represents about 0.5 mSv/y.
- *The organic radiation component:* An effective dose-rate of about 0.3 mSv/y comes from organic products that contain naturally radioactive substances such as potassium ( $^{40}\text{K}$ ) and carbon ( $^{14}\text{C}$ ).
- *The cosmic radiation component:* At sea level, an effective dose-rate of 0.3 mSv/y comes from cosmic radiation.



The average worldwide effective dose-rate provided by the natural radiation background is about 2.4 mSv/y. However, this value can vary greatly in various regions of the world. In Japan, it is about 0.5 mSv/y (the lowest value), while in certain regions of Brazil, India, and Iran, the amount of radiation is about 140 times higher and can reach 70 mSv/y (e.g., Ramsar, Iran). Some effective dose-rate values of 260 mSv/y have been also reported in a district of Ramsar [50]. It is noteworthy that the cancer incidence ratio between Ramsar and Japan is likely to be much lower than 140-fold, notwithstanding the confounding factors linked to the environment, suggesting that no evident risk threshold can be pointed out between 0.5 and 70 mSv/y. In contrast, some reports have suggested a lower incidence of cancer and radiation-induced diseases in Ramsar (hormesis phenomenon). However, the number of inhabitants in Ramsar is small. Consequently, further investigations are needed with larger cohorts of individuals [50].

The continuous “bath” of space radiation of about 0.4 mGy/d described above, corresponds to an effective dose rate ranging from 0.1 to 0.3 mSv/d without solar flares and about 0.5 mSv/d with solar flares (Table 1). Considering the average values given in Table 1, one year in the ISS corresponds to an effective dose ranging from 110 to 180 mSv/y. These values are much higher than the average worldwide background. The surfaces of the Moon and Mars appear to be more radioactive: According to the time of day, the natural radiation backgrounds assessed on the Moon and Mars are 110–380 and 130–260 mSv/y, respectively [47–51] (Tables 1 and 2). This is mainly due to the absence of significant magnetic protection and to a higher telluric component. These values should, therefore, be taken into account in the evaluation of the radiation-induced risks for astronauts (Figure 2) (Table 1). To date, the exploration of Mars is thought to require about 900 days or more with more than one year being spent in deep space, where shielding will not be able to protect astronauts significantly from GCR. The latest estimation of the effective dose for such a mission stated a value of approximately 1200 mSv, corresponding, therefore, to an average of 1.3 mSv/d (i.e., 475 mSv/y, corresponding to 200 times higher than the average worldwide natural radiation background) (Tables 1 and 2).

**Table 2.** Current average effective dose and dose-rates of interest for different exposures to IR.

	On Earth		In Space
	700–12,000	Acute radiation syndrome (irradiation accident)	ARS during solar events?
Effective dose (mSv)	2000	Tumor dose per fraction in radiotherapy	
	200	Dose per fraction in total body irradiation	
	100	Threshold dose for solid cancer	500 days in ISS
	20	Threshold dose for leukemia	
	0.3–0.5	Coronarography	50 days in ISS
	0.01	2 mammography views	1 day in ISS
		1 day for a nuclear worker	
Effective dose-rate (mSv/y)	0.5	Radiation background in Japan	
	2.4	Worldwide radiation background	
	70	Radiation background in Ramsar	
	110–180		In LEO (ISS)
	130–260		At the surface of Mars
	110–300		At the surface of the Moon
	500–700		In deep space

Such estimation raises the question of the acceptability of such excess of risk vis-à-vis society and current regulations on Earth. As part of the international radiation protection rules, the annual occupational exposure limit is 20 mSv/y (and no more than 100 mSv in 5 years). This suggests that the limit may be exceeded by space missions of more than 50 days or alternatively, astronauts may partake in a space mission of 250 days but should not take part in any other mission for the next 4 years. The exploration of Mars is far beyond this in terms of the involved risk. Therefore, a prominent question is how to manage such risks?



### 3. The Potential Radiation-Induced Risks for the Astronauts: What Do We Expect?

As part of the international radiation protection rules, radiation-induced risks are generally based on the notion of deterministic/stochastic events and the calculation of the dose equivalent and effective dose [46]. However, as detailed in the next chapter, such approach is not necessarily consensual, notably, to identify all the clinical consequences of an exposure to IR. Therefore, let us consider that IR can produce three distinct types of clinical effects: Radiosensitivity, radiosusceptibility and radiodegeneration [5].

#### 3.1. Radiosensitivity in Space

**Radiosensitivity** has been defined as the proneness to adverse tissue effects (burns, dermatitis, proctites), generally attributable to cell death [5]. Radiosensitivity reactions are likely to occur at high doses, often above 0.7 Gy. Radiosensitivity reactions are generally observed during/after radiotherapy treatment due to effects on a specific organ targeted by irradiation, such as dermatitis or proctites or the entire body (notably in case of total body irradiation). The radiopathology of acute radiation syndrome (ARS) is fairly well described: It can occur at 0.7 Gy or more and is generally divided into three sub-syndromes: Bone marrow (0.7–6 Gy), gastrointestinal (6–8 Gy) and neurovascular (8–12 Gy) (Table 2) [53]. So far, no case of ARS has been observed among the astronauts. Except for intense solar events, no radiosensitivity reactions are expected during space missions. The reference to ARS in relation to solar events may explain why blood forming organs, gastrointestinal and central neurologic systems are cited in the risks related to the exploration of Mars [54,55].

With regard to genetic predisposition, a number of syndromes are associated with individual radiosensitivity and have been well characterized to date. However, the clinical features of these syndromes are so precocious and severe that it is unlikely that over-selected astronauts will be affected by such genetic diseases [5]. In conclusion, if radiosensitivity reactions may be theoretically possible during exceptional solar events, none have been observed, likely because all the past space missions have corresponded to too low-doses and no significant solar events. A mission to Mars may raise this question.

#### 3.2. Radiosusceptibility in Space

Radiosusceptibility has been defined as the proneness to radiation-induced cancers, generally attributable to cell transformation [5]. Radiosusceptibility reactions are generally encountered either in areas irradiated by radiotherapy (secondary cancers), or after accidental or occupational exposure. The epidemiological data of the Hiroshima bomb survivors represent the only source of consensual data to describe the risk of radiation-induced cancer as a function of dose: The risk of radiation-induced leukemia and solid cancers increases significantly from a threshold dose of 100 and 200 mSv, respectively [56] (Table 2). However, these data are only valid for exposures delivered in a few minutes (flash exposures), which is possible in case of solar events, but does not answer the question of protracted exposures during long space missions. There are no consensual data of radiation-induced cancer as a function of the dose-rate. However, it is considered that as the length of time that the dose is delivered for increases, the less hazardous the radiation response is expected to be [5]. Thus, the threshold dose of radiation-induced cancers for low-dose-rated exposures is expected to be much greater than 100–200 mSv/y, but its actual value needs to be documented. Furthermore, to date, the number of astronauts who have performed long missions of more than 250 days is too low to deduce any reliable numerical value [6]. Despite this lack of data, there are a number of emerging mathematical models that propose cancer risk predictions with different scenarios of space missions [57,58]. To determine the risk of cancer as a function of dose-rate is an important challenge for space radiobiology but also for radiobiology in general. Indeed, the potential cancer risks linked to mammography (about 2 mGy per s) and to CT scan exams (some tens mGy per min) raise the question of the dose-rate effect on cancer occurrence [59,60] (Table 2).

What type of radiation-induced cancer do we expect from exposure to space radiation? Since LEMI, LEP and LEE preferentially target the surface of body, they might increase



the occurrence of radiation-induced cancer in the skin and eyes, notably, skin and eye melanoma (Table 3):

- Recently, an increase in mortality from skin melanoma has been reported among astronauts. This increase was shown to be consistent with skin melanoma observed among aircraft pilots. Ultraviolet radiation and lifestyle were suggested as potential causes. However, it must be stressed that neutrons, LEMI, LEP and LEE may also present a cause of concern for aircraft pilots, similarly to astronauts. Conversely, ultraviolet radiation cannot be suggested as a cause in the case of astronauts [61,62]. Further investigations are, therefore, needed to document the potential physical causes of skin melanoma in both aircraft and spacecraft crews. It is noteworthy that the physical parameters of the flights (notably LEO or non-LEO) significantly affects the occurrence of such tumors [63].
- With regard to radiation-induced eye tumors, although rare, choroid melanoma is the most frequent primarily adult tumor in the eye [64]. However, to our knowledge, no IR-induced choroid melanoma has been observed so far. No choroid melanoma has been reported in astronauts. Retinoblastoma, another common tumor of the ocular system can be evoked. However, the retina may be too deep in the eye to be reached by energy deposition from LEMI, LEP and LEE (the average distance between the iris and retina is about 2 cm). Again, the flight parameters and the relatively low duration of previous space missions may limit the occurrence of such specific events.

**Table 3.** Major radiation-induced risks for astronauts after long-term space mission in absence of severe solar events.

Radiation-Induced Consequences	Type of Space Radiation	Type of Tissues	Clinical Consequences	Countermeasures
<b>Radiosusceptibility</b> The 100–200 mGy thresholds for cancer risks derived from Hiroshima survivors are the only consensual series of data.	Low energy ions/particles including neutrons	<i>“surface tissues”</i> : Eye Skin	Eye melanoma Skin melanoma	Glasses? Water-filled worksuits?
	“Bath of radiation” including fast neutrons	<i>“deep tissues”</i> : Cardiovascular System Bones General	No cancer observed yet Osteosarcoma Leukemia	Radioprotective drugs
<b>Radiodegeneration</b> There are no well-defined dose thresholds (>0.1 Gy?) nor biomarkers that are specific to aging yet.	Low energy ions/particles including neutrons	<i>“surface tissues”</i> : Eye Skin	Cataracts Aging	Glasses? Water-filled worksuits?
	“Bath of radiation” including fast neutrons	<i>“deep tissues”</i> : Cardiovascular System Bones General	Heart attacks Loss of bone mass To be investigated	Radioprotective drugs

Unlike LEMI, LEP and LEE, the “bath of radiation” composed of more energetic rays and particles targets deeper tissues. In this specific case, leukemia represents the most probable radiation-induced cancer. However, Hiroshima bomb survivors’ data suggest that the occurrence of this form of cancer requires much more than a cumulative exposure of 100 mSv, and therefore, much more than 1 year in space. Hence, no radiation-induced leukemia has been reported yet in the astronauts’ corps, probably because previous space missions were not long enough. For the exploration of Mars, such risk has to be considered.

With regard to the potential genetic predisposition that may be a cause for concern among astronauts, a number of genetic syndromes are associated with individual cancer proneness that also increase the risk of radiation-induced cancer. Unlike the syndromes associated with radiosensitivity, the syndromes associated with cancer proneness and radiosusceptibility are generally caused by heterozygous gene mutations and their related clinical features may not be detectable without DNA sequencing before cancer occurrence. This is notably the case of the heterozygous mutations of ATM, BRCA1, BRCA2, p53, and Rb genes that confer a high risk of breast cancer and retinoblastoma, respectively [5]. Additionally, it is noteworthy that carriers of heterozygous mutations of ATM may represent



1% of the whole population [5]. However, there is no known gene that has been identified as being associated with radiation-induced skin or eye melanoma or specific to radiation-induced leukemia. Hence, while some actual risk of radiation-induced melanoma emerges, further investigations about specific biomarkers of radiosusceptibility are needed (Table 3).

### 3.3. Radiodegeneration in Space

Radiodegeneration has been defined as the proneness to radiation-induced accelerated aging of specific tissues, generally attributable to tolerance of a certain amount of DNA damage [5]. The most frequent radiodegeneration reactions include radiation-induced cataracts. To date, this appears as the most probable consequence of exposure to cosmic radiation [65]. Forty-eight cases of severe lens opacification (16.2%) were observed among the 295 NASA astronauts who participated in the LSAH (Longitudinal Study of Astronaut Health) study, but 86% of the astronauts who stayed in space suffered from a pathology of the eye. An increased risk of cataracts was generally observed after exposure to doses above 8 mGy, which corresponds to approximately 20 mission days [66,67]. Interestingly, on Earth, radiation-induced cataracts have long been considered as a relatively rare condition, requiring an estimated dose threshold of about 2 Gy to the eyes. However, recent data suggest that this dose threshold could be much lower than 2 Gy. A general discussion about the relevance of the ICRP recommendations related to the response of the ocular system to IR can be found in the next chapter [6].

In addition to the acceleration of aging of lens that leads to cataracts, the potential radiation-induced aging of the skin is another pressing concern. Surprisingly, while the skin represents a much greater surface area for the impact of LEMI, LEP and LEE than lens, to date, no quantitative assessment of space radiation-induced aging of the skin has been conducted. Such an absence of any data may be explained not only by the current wearing of worksuits during space missions (only the forearms may be eventually exposed inside the spacecraft), but also by the lack of specific biomarkers for aging [5]. The location of skin melanoma or any change of texture should be therefore registered carefully. The question of radiodegeneration has been recently raised by space experiments on twins [68–72]. During a one-year ISS mission, one male twin was on board while his monozygotic twin served as a genetically matched ground control. His telomeres were found to be longer during spaceflight but shortened rapidly upon return to Earth. An increase in the number of chromosomal inversions was also found to persist after spaceflight [69]. However, while telomere biomarkers have been found to be associated with aging, further investigations are needed to demonstrate whether chromosomal inversions are correlated with radiosusceptibility or radiodegeneration [5].

With regard to the potential aging consequences of the “bath of radiation”, two specific tissues should attract our attention: Bone and the cardiovascular system (Table 3):

- The loss of bone mass in astronauts, especially in weight-bearing bones, is a current observation performed after each space mission, that may have consequences for the immune system. The loss of bone mass was hypothesized to be similar to osteoporosis [73–76]. Although the inherent mechanisms of this loss of bone mass have been based on animal models data, it appears that a reduced osteoblast function leads to decreased bone formation, while bone resorption is unaltered or increased. The loss of bone mass has long been attributed to microgravity [73]. However, while the molecular and cellular pathways by which microgravity may act in the form of biochemical signals are still unknown, some emerging data suggest that radiation (and logically, the “bath of radiation”) may also affect bones [77]. Interestingly, by radiobiologically characterizing various genetic syndromes associated with facial dysmorphism, osteoblasts were shown to be more radiosensitive than the skin of the same donor, which may suggest that IR contribution to the loss of bone mass in astronauts has been underestimated [78]. Further studies are, therefore, needed to document the radiodegeneration of bone in response to IRS. In the following chapters, we discuss the advantages of anti-osteoporosis drugs as countermeasures.



- Epidemiology data of women patients with breast cancer have shown that more than 50% of women are at risk of a heart attack for 10 years post-radiotherapy [79–82]. Such examples, suggest that the cardiovascular system may be mechanically affected by radiation and sensitive to low-dose. To date, there is no evidence of any cardiovascular disease in astronauts caused by exposure to IRS [62,83]. Again, the microgravity contribution should be separated from the radiation contribution [84]. However, even though the cohorts investigated have been too small, the potential radiodegeneration of heart tissue needs to be further investigated.

#### 4. Radiation Protection Factors and Radiobiological Effects Specific to Low-Dose Radiation to Be Considered

##### 4.1. Radiation Protection Factors to Be Investigated to Refine the Estimation of Risks

While the calculations of the risks are based on the dose equivalent and effective dose defined by the formulas (2) and (3), it is noteworthy that the weighting factor  $W_R$  has been defined as equal to 1 for electrons, X-rays and gamma-rays, and equal to 2 for protons regardless of their energy levels [46]. However, there is now evidence that the considerable energy deposited locally by LEMI, LEP or LEE at the surface of the matter has more significant biological and clinical consequences than the same particles being emitted at a higher energy [85,86]. Hence, the definition of the  $W_R$  for electrons and protons should be refined and become a function of energy.

In addition to the problem of the energy-dependence of  $W_R$ , it must be stressed that, a given  $W_T$  corresponds to a mis-defined clinical consequence. For example, when the  $W_T$  of the eyes, breast and skin is considered, it is more likely to illustrate the risk of cataracts, radiation-induced breast cancer and the occurrence of radiodermatitis, respectively [87]. Hence, to date, it is necessary to evaluate the risks of radiosensitivity, radiosusceptibility and radiodegeneration, separately, since the management, cure and prevention of radiation-induced cataracts, breast cancer and dermatitis are not the same.

Lastly, even if the individual proneness to radiosensitivity, radiosusceptibility and radiodegeneration is limited by the over-selection of astronauts, it is practically possible that an individual who appears to be apparently healthy up to the age of 40 could be a carrier of a cancer-prone gene mutation. Let us return to the fact that ATM heterozygotes represent about 1% of the whole population. Hence, it is important to consider the excess of risks due to the genetic status of an astronaut, that may be more than 10 according to the gene mutations [5]. Consequently, a new weighting factor quantifying the individual factors involved may be useful.

Taken together, our examples suggest that space radiobiology raises important questions related to the ICRP recommendations and the definition of some major notions of radiation protection.

##### 4.2. Radiobiological Effects Specific to Low-Dose Radiation to Be Investigated to Refine the Estimation of Risks

In addition to the refinements proposed above, it is necessary to discuss some specific radiobiological phenomena that render the dose–response curve non-linearly dose-dependence and the quantification of the risks more complex.

The hypersensitivity to low-dose (HRS) phenomenon was described for the first time by Lambin et al. (1993) [88] and Marples and Joiner (1993) [89]. In vitro, this phenomenon results in a significant reduction in clonogenic cell survival, an increase in chromosome breaks, micronuclei, unrepaired DNA double-strand breaks (DSB) and/or gene mutations after a single low-dose generally belonging to the 100–800 mGy dose range. However, this range may vary with the dose-rate and the HRS may be maximal at lower doses [90]. At a dose-rate higher than Gy/min, the maximal HRS effect is generally obtained at 200 mGy in human cells and corresponds to a biological effect equivalent to a dose that is five to ten times higher (i.e., to 1 to 2 Gy) [90,91]. It is noteworthy that this phenomenon has been observed in normal human tissues and, notably, skin cells [92] and a mechanistic model has been recently proposed [93,94]. While no current radiation protection regulation integrates



this yet, the HRS phenomenon may theoretically increase the risks related to small solar events (between 100 and 800 mGy). Further investigations as regards the occurrence of this phenomenon are needed.

The *hormesis phenomenon* was described for the first time in the radiation research field by Luckey [95]. It is described as a J-shaped dose- or dose-rate dependent phenomenon, associated with a specific threshold, under which, stress is considered to be “positive” and above which it is detrimental [96,97]. Hormesis appeared to be more frequently observed in human untransformed radioresistant cells exposed at the doses belonging to the 20–75 mGy range and corresponds to a negative cancer risk in the Hiroshima survivors data [94]. Again, the occurrence of the hormesis phenomenon depends on the dose-rate but this field needs to be better documented for human cells.

The *bystander effect* is defined as any biological effect expressed in cells that are not directly targeted by irradiation but that are situated within the close vicinity of irradiated cells [98,99]. *Stricto sensu*, the bystander effect is not a radiobiological phenomenon specific to low-dose radiation, but bystander cells generally show levels of DNA and chromosome damage, mutations and cell death very similar to those encountered at low-dose radiation. If a bystander effect occurs after the impact of low-energy particles, the energy deposition that initially targets a small number of cells may indirectly concern a larger surface as if surrounding cells have been exposed to low-dose radiation. Hence, the bystander effect produced by IRS should be documented to refine our estimation of the risks.

## 5. Countermeasures

From the above analyses, we distinguished that low-energy ions/particles that produce a massive energy deposition at the surface of the skin and eyes, and the “bath of radiation” that may impact deeper tissues and neutrons may concern both. The contribution to the total dose of these three types of events can vary with the flight parameters (e.g., LEO vs. deep space). To reduce the specific risks related to low-energy particles, a simple form of protection may be sufficient: Indeed, special glasses and worksuits may protect both the skin and eyes significantly. Despite the fact that the majority of studies concern either extravehicular mobility [100,101] or orthostatic intolerance [102], a water-filled garment to protect astronauts has been developed recently in the ISS [103] (Table 3).

With regard to protection against the “bath of radiation” that may affect deep tissues, considerable efforts have been aimed at developing chemical radioprotectors to reduce the results of radiolysis and the amount of radiation-induced DNA damage. At present, the only effective radioprotective agent to protect healthy tissues during radiotherapy is ethylol (amifostine). Amifostine treatment results in a significant decrease in the amount of DNA damage due to its powerful anti-oxidative effect [104–106]. However, this drug induces disabling hypotension and would, therefore, be unusable for the protection of astronauts.

In fact, the great majority of chemical radioprotectors consist of reducing the amount of DNA damage *induced* but not necessarily the amount of DNA damage *to be repaired*. More recently, our lab has proposed a general mechanistic model of radiation action based on the radiation-induced nucleo-shuttling of the ATM protein (RIANS) [107]. After irradiation, the ATM dimers become monomers and diffuse into the nucleus to recognize DNA double-strand breaks and trigger their repair through the phosphorylation of the histone variant H2AX ( $\gamma$ H2AX). Any delay in the RIANS causes radiosensitivity, radiosusceptibility and/or radiodegeneration [5]. Interestingly, we have provided clues that a combination of statins (anti-cholesterol-lowering drugs) and bisphosphonates (anti-osteoporosis) was shown to facilitate the entry of the ATM kinase into the nucleus to trigger DNA damage repair [5,78]. Such a treatment (notably combining pravastatin and zoledronate (ZOPRA)) was found to be more effective than current anti-oxidative drugs such as ethylol or N-acetylcysteine (N. Foray, personal communication; paper in preparation). Hence, it may be interesting to test the long-term action of ZOPRA during long-flight missions.



## 6. Conclusions and Perspectives

A careful analysis of the flux/energy-spectrum of space radiation and the study of the secondary particles emitted from the shielding has refined the definition of the potential clinical consequences of occupational exposure to IRS for astronauts. We have identified the risks related to high localized energy deposition due to low energy particles/ions that concern the *surface tissues* (such as the skin and eyes), while the low-dose-rated “bath of radiation”—including fast neutrons—concerns the *deep tissues* (such as the bones and cardiovascular system). By omitting the consequences of severe solar events, both radiosusceptibility and radiodegeneration reactions are expected: Radiation-induced melanomas and cataracts for surface tissues and loss of bone mass and accelerated aging of the cardiovascular system for deep tissues. Specific countermeasures may be considered for each situation: Glasses and special suits for surface tissue risks and chemical radioprotective drugs for the deeper tissue risks. Therefore, the countermeasures represent a major axis of space radiation research. Lastly, a debate about the impact of the specific radiobiological phenomena occurring at low-dose radiation, including the bystander effect and a refinement of the radiation protection rules, should be organized rapidly in collaboration with all the key players in space radiobiology.

**Author Contributions:** The authors of this manuscript have contributed in the following manners: Conceptualization, N.F.; writing—review and editing, J.R.-V., L.E.-N., M.L.F. J.A.-C., A.G., A.B. and N.F. All authors approve the submitted version of this manuscript and agree to be personally accountable for their individual contributions and for ensuring that questions related to the accuracy or integrity of the work are appropriately investigated, resolved, and documented in the literature. All authors have read and agreed to the published version of the manuscript.

**Funding:** This research received the support of the Commissariat Général à l’Investissement (INDIRA Project); Centre National d’Etudes Spatiales (ATHENA and BERNADOTTE Projects).

**Conflicts of Interest:** The authors declare no conflict of interest.

## References

1. Cucinotta, F.A.; Schimmerling, W.; Wilson, J.W.; Peterson, L.E.; Badhmar, G.D.; Saganti, P.B.; Dicello, J.F. *Space Radiation Cancer Risk Projections for Exploration Missions: Uncertainty Reduction and Mitigation*; NASA: Hanover, MD, USA, 2002; JSC-29295.
2. Cucinotta, F.A.; Kim, M.H.; Ren, L. *Managing Luna and Mars Mission Radiation Risks. Part I: Cancer Risks, Uncertainties and Shielding Effectiveness*; NASA: Hanover, MD, USA, 2005; TP-2005-213164.
3. Durante, M. New challenges in high-energy particle radiobiology. *Br. J. Radiol.* **2014**, *87*, 20130626. [\[CrossRef\]](#)
4. Durante, M.; Cucinotta, F.A. Heavy ion carcinogenesis and human space exploration. *Nat. Rev. Cancer* **2008**, *8*, 465–472. [\[CrossRef\]](#) [\[PubMed\]](#)
5. Foray, N.; Bourguignon, M.; Hamada, N. Individual response to ionizing radiation. *Mutat. Res. Rev.* **2016**, *770*, 369–386. [\[CrossRef\]](#) [\[PubMed\]](#)
6. Maalouf, M.; Durante, M.; Foray, N. Biological effects of space radiation on human cells: History, advances and outcomes. *J. Radiat. Res.* **2011**, *52*, 126–146. [\[CrossRef\]](#)
7. Ferlazzo, M.L.; Foray, N. Space radiobiology needs realistic hypotheses and relevant methodology. *Proc. Natl. Acad. Sci. USA* **2017**, *114*, E6733. [\[CrossRef\]](#) [\[PubMed\]](#)
8. Curie, P. *Oeuvres de Pierre Curie*; Editions des Archives Contemporaines: Paris, France, 1984.
9. Todd, P.; Tobias, C.A.; Silver, I.L. Current topics in space radiation biology. In *Space Radiation Biology and Related Topics*; Tobias, C., Todd, P., Eds.; Academic Press: New York, NY, USA; London, UK, 1974; pp. 1–18.
10. Solomon, J. *Théorie du Passage des Rayons Cosmiques à Travers la Matière*; Hermann: Paris, France, 1936.
11. Millikan, R.A. *Electrons (+ and -), Protons, Photons, Neutrons, Mesotrons and Cosmic Rays*; University of Chicago Press: Chicago, IL, USA, 1947.
12. Hess, V.F.; Eugster, J.A.G. *Cosmic Radiation and Its Biological Effects*; Fordham University Press: New York, NY, USA, 1949.
13. Van Allen, J.A.; Franck, L.A. Radiation around the earth to a radial distance of 107,400 km. *Nature* **1959**, *183*, 430. [\[CrossRef\]](#)
14. Van Allen, J.A.; Franck, L.A. Radiation measurements to 658,300 km with Pioneer IV. *Nature* **1959**, *184*, 219. [\[CrossRef\]](#)
15. Neugebauer, M.; Snyder, C.W. Interplanetary solar wind measurements by Mariner II. In *Space Research*; Muller, P., Ed.; North-Holland Publications: Amsterdam, The Netherlands, 1964; Volume 4, pp. 89–113.
16. Hellweg, C.E.; Matthiä, D.; Berger, T.; Baumstark-Khan, C. *Radiation in Space: Relevance and Risk for Human Missions*; Springer: Cham, Switzerland, 2020.



17. Wilson, J.W. Environmental geophysics and SPS shielding. In Proceedings of the Workshop on the Radiation Environment of the Satellite Power System, Berkeley, CA, USA, 15 September 1978; Report LBL-8581. California Univ.: Berkeley, CA, USA, 1978.
18. Bottollier-Depois, J.F.; Siegrist, M.; Petrov, V.M.; Shurshakov, V.V.; Bengin, V.; Koslova, S.B. TEPC measurements obtained on the Mir space station. *Radiat. Meas.* **2002**, *35*, 485–488. [\[CrossRef\]](#)
19. Hellweg, C.E.; Baumstark-Khan, C. Getting ready for the manned mission to Mars: The astronauts' risk from space radiation. *Naturwissenschaften* **2007**, *94*, 517–526. [\[CrossRef\]](#)
20. Dachev, T.P.; Tomov, B.T.; Matviichuk, Y.N.; Dimitrov, P.G.; Bankov, N.G. High dose rates obtained outside ISS in June 2015 during SEP event. *Life Sci. Space Res.* **2016**, *9*, 84–92. [\[CrossRef\]](#)
21. NASA. *Human Health and Performance Risks for Space Exploration Missions*. NASA-SP-2009-3405; NASA: Houston, TX, USA, 2009.
22. NASA. *Second Symposium on Protection against Radiations in Space-SP71*; NASA: Galtinburg, TE, USA, 1964.
23. Reitz, G.; Beaujean, R.; Benton, E.; Burmeister, S.; Dachev, T.; Deme, S.; Luszik-Bhadra, M.; Olko, P. Space radiation measurements on-board ISS—the DOSMAP experiment. *Radiat. Prot. Dosim.* **2005**, *116*, 374–379. [\[CrossRef\]](#) [\[PubMed\]](#)
24. Haffner, J.W. (Ed.) *Radiation and Shielding in Space*; Academic Press: New York, NY, USA, 1967.
25. Jorgensen, A.M.; Patamia, S.E.; Gassend, B. Passive radiation shielding considerations for the proposed space elevator. *Acta Astronaut.* **2007**, *60*, 198–209. [\[CrossRef\]](#)
26. Parker, E.N. Shielding space travelers. *Sci. Am.* **2006**, *294*, 40–47. [\[CrossRef\]](#) [\[PubMed\]](#)
27. Pugliese, M.; Bengin, V.; Casolino, M.; Roca, V.; Zanini, A.; Durante, M. Tests of shielding effectiveness of Kevlar and Nextel onboard the International Space Station and the Foton-M3 capsule. *Radiat. Environ. Biophys.* **2010**, *49*, 359–363. [\[CrossRef\]](#)
28. Spillantini, P.; Casolino, M.; Durante, M.; Mueller-Mellin, R.; Reitz, G.; Rossi, L.; Shurshakov, V.; Sorbi, M. Shielding from cosmic radiation for interplanetary missions: Active and passive methods. *Radiat. Meas.* **2007**, *42*, 14–23. [\[CrossRef\]](#)
29. Wilson, J.W.; Cucinotta, F.A.; Shinn, J.L.; Simonsen, L.C.; Dubey, R.R.; Jordan, W.R.; Jones, T.D.; Chang, C.K.; Kim, M.Y. Shielding from solar particle event exposures in deep space. *Radiat. Meas.* **1999**, *30*, 361–382. [\[CrossRef\]](#)
30. Sihver, L.; Sato, T.; Puchalska, M.; Reitz, G. Simulations of the MATROSHKA experiment at the international space station using PHITS. *Radiat. Environ. Biophys.* **2010**, *49*, 351–357. [\[CrossRef\]](#)
31. Villagrasa, C.; Bordage, M.C.; Bueno, M.; Bug, M.; Chiriotti, S.; Gargioni, E.; Heide, B.; Nettelbeck, H.; Parisi, A.; Rabus, H. Assessing the Contribution of Cross-Sections to the Uncertainty of Monte Carlo Calculations in Micro- and Nanodosimetry. *Radiat. Prot. Dosim.* **2019**, *183*, 11–16. [\[CrossRef\]](#) [\[PubMed\]](#)
32. NASA. *Nuclear and Space Radiation Effects on Materials*; NASA: Springfield, Virginia, 1970.
33. Fleischer, R.L.; Hart, H.R., Jr.; Giard, W.R. Particle track identification: Application of a new technique to apollo helmets. *Science* **1970**, *170*, 1189–1191. [\[CrossRef\]](#)
34. Badhwar, G.D.; Keith, J.E.; Cleghorn, T.F. Neutron measurements onboard the space shuttle. *Radiat. Meas.* **2001**, *33*, 235–241. [\[CrossRef\]](#)
35. Smith, M.B.; Khulapko, S.; Andrews, H.R.; Arkhangelsky, V.; Ing, H.; Koslowksy, M.R.; Lewis, B.J.; Machrafi, R.; Nikolaev, I.; Shurshakov, V. Bubble-detector measurements of neutron radiation in the international space station: ISS-34 to ISS-37. *Radiat. Prot. Dosim.* **2016**, *168*, 154–166. [\[CrossRef\]](#)
36. Benton, E.R.; Benton, E.V.; Frank, A.L. Neutron dosimetry in low-earth orbit using passive detectors. *Radiat. Meas.* **2001**, *33*, 255–263. [\[CrossRef\]](#)
37. Brodzinski, R.L.; Wognan, N.A.; Perkins, R.W. Cosmic-rat-induced radioactivity in astronauts as a measure of radiation dose. *Space Life Sci.* **1969**, *2*, 69.
38. Rodbell, K.P. Low-energy protons-Where and why “rare events” matter. *IEEE Trans. Nucl. Sci.* **2020**, *67*, 1204–1215. [\[CrossRef\]](#)
39. Francis, Z.; Villagrasa, C.; Clairand, I. Simulation of DNA damage clustering after proton irradiation using an adapted DBSCAN algorithm. *Comput. Methods Programs Biomed.* **2011**, *101*, 265–270. [\[CrossRef\]](#)
40. Uehara, S.; Toburen, L.H.; Nikjoo, H. Development of a Monte Carlo track structure code for low-energy protons in water. *Int. J. Radiat. Biol.* **2001**, *77*, 139–154. [\[CrossRef\]](#)
41. Benton, E.R.; Benton, E.V. Space radiation dosimetry in low-Earth orbit and beyond. *Nucl. Instrum. Methods Phys. Res. B* **2001**, *184*, 255–294. [\[CrossRef\]](#)
42. Cucinotta, F.A.; Kim, M.H.; Willingham, V.; George, K.A. Physical and biological organ dosimetry analysis for international space station astronauts. *Radiat. Res.* **2008**, *170*, 127–138. [\[CrossRef\]](#)
43. Stricklin, D.; VanHorne-Sealy, J.; Rios, C.I.; Carnell, L.S.; Taliaferro, L.P. Neutron Radiobiology and Dosimetry. *Radiat. Res.* **2021**. [\[CrossRef\]](#)
44. Kohler, J.; Ehresmann, B.; Zeitlin, C.; Wimmer-Schweingruber, R.F.; Hassler, D.M.; Reitz, G.; Brinza, D.E.; Appel, J.; Bottcher, S.; Bohm, E.; et al. Measurements of the neutron spectrum in transit to Mars on the Mars Science Laboratory. *Life Sci. Space Res.* **2015**, *5*, 6–12. [\[CrossRef\]](#)
45. Hassler, D.M.; Zeitlin, C.; Wimmer-Schweingruber, R.F.; Ehresmann, B.; Rafkin, S.; Eigenbrode, J.L.; Brinza, D.E.; Weigle, G.; Bottcher, S.; Bohm, E.; et al. Mars' surface radiation environment measured with the Mars Science Laboratory's Curiosity rover. *Science* **2014**, *343*, 1244797. [\[CrossRef\]](#)
46. ICRP. Recommendations of the International Commission on Radiological Protection. ICRP publication 103. *Ann. ICRP* **2007**, *37*, 1–332.
47. Reitz, G.; Berger, T.; Mattiae, D. Radiation exposure to the Moon environment. *Planet. Space Sci.* **2012**, *74*, 78–83. [\[CrossRef\]](#)



48. Zhang, S.; Wimmer-Schweingruber, R.F.; Yu, J.; Wang, C.; Fu, Q.; Zou, Y.; Sun, Y.; Wang, C.; Hou, D.; Bottcher, S.I.; et al. First measurements of the radiation dose on the lunar surface. *Sci. Adv.* **2020**, *6*, eaaz1334. [\[CrossRef\]](#)
49. Straume, T.; Blattinig, S.; Zeitlin, C. Radiation Hazards and the Colonization of Mars. In *The Human Mission to Mars: Colonizing the Red Planet*; Levine, J.S., Schild, E.R.E., Eds.; Cosmology Science Publishers: Cambridge, MA, USA, 2010; pp. 803–850.
50. Abbasi, S.; Mortazavi, S.A.R.; Mortazavi, S.M.J. Martian Residents: Mass Media and Ramsar High Background Radiation Areas. *J. Biomed. Phys. Eng.* **2019**, *9*, 483–486. [\[CrossRef\]](#) [\[PubMed\]](#)
51. Zeitlin, C.; Hassler, D.M.; Cucinotta, F.A.; Ehresmann, B.; Wimmer-Schweingruber, R.F.; Brinza, D.E.; Kang, S.; Weigle, G.; Bottcher, S.; Bohm, E.; et al. Measurements of energetic particle radiation in transit to Mars on the Mars Science Laboratory. *Science* **2013**, *340*, 1080–1084. [\[CrossRef\]](#)
52. Dartnell, L.R. Ionizing radiation and life. *Astrobiology* **2011**, *11*, 551–582. [\[CrossRef\]](#) [\[PubMed\]](#)
53. Dainiak, N.; Gent, R.N.; Carr, Z.; Schneider, R.; Bader, J.; Buglova, E.; Chao, N.; Coleman, C.N.; Ganser, A.; Gorin, C.; et al. Literature review and global consensus on management of acute radiation syndrome affecting nonhematopoietic organ systems. *Disaster Med. Public Health Prep.* **2011**, *5*, 183–201. [\[CrossRef\]](#) [\[PubMed\]](#)
54. Chancellor, J.C.; Scott, G.B.; Sutton, J.P. Space Radiation: The Number One Risk to Astronaut Health beyond Low Earth Orbit. *Life* **2014**, *4*, 491–510. [\[CrossRef\]](#)
55. Cucinotta, F.A.; Alp, M.; Sulzman, F.M.; Wang, M. Space radiation risks to the central nervous system. *Life Sci. Space Res.* **2014**, *2*, 54–69. [\[CrossRef\]](#)
56. Preston, D.L.; Shimizu, Y.; Pierce, D.A.; Suyama, A.; Mabuchi, K. Studies of Mortality of Atomic Bomb Survivors; Report 13: Solid Cancer and Noncancer Disease Mortality: 1950–1997. *Radiat. Res.* **2003**, *160*, 381–407. [\[CrossRef\]](#) [\[PubMed\]](#)
57. Cucinotta, F.A. A new approach to reduce uncertainties in space radiation cancer risk predictions. *PLoS ONE* **2015**, *10*, e0120717. [\[CrossRef\]](#) [\[PubMed\]](#)
58. Cucinotta, F.; Schimmerling, W.; Wilson, J.W.; Peterson, L.E.; Badhwar, G.D.; Saganti, P.B.; Dicello, J.F. Space radiation cancer risks and uncertainties for Mars missions. *Radiat. Res.* **2001**, *156*, 682–688. [\[CrossRef\]](#)
59. Tang, F.R.; Loganovsky, K. Low dose or low dose rate ionizing radiation-induced health effect in the human. *J. Environ. Radioact.* **2018**, *192*, 32–47. [\[CrossRef\]](#) [\[PubMed\]](#)
60. Tang, F.R.; Loke, W.K.; Khoo, B.C. Low-dose or low-dose-rate ionizing radiation-induced bioeffects in animal models. *J. Radiat. Res.* **2017**, *58*, 165–182. [\[CrossRef\]](#)
61. Di Trollo, R.; Di Lorenzo, G.; Fumo, B.; Ascierto, P.A. Cosmic radiation and cancer: Is there a link? *Future Oncol.* **2015**, *11*, 1123–1135. [\[CrossRef\]](#) [\[PubMed\]](#)
62. Reynolds, R.; Little, M.P.; Day, S.M.; Charvat, J.; Blattinig, S.; Huff, J.L.; Patel, Z.S. Cancer Incidence and Mortality in the U.S. Astronaut Corps, 1959–2017. *Res. Sq.* **2020**, in press.
63. Meier, M.M.; Matthia, D. Assessment of the skin dose for aircrew. *J. Radiol. Prot.* **2017**, *37*, 321–328. [\[CrossRef\]](#)
64. Kaliki, S.; Shields, C.L. Uveal melanoma: Relatively rare and deadly cancer. *Eye* **2017**, *31*, 241–257. [\[CrossRef\]](#)
65. Aleci, C. From international ophthalmology to space ophthalmology: The threats to vision on the way to Moon and Mars colonization. *Int. Ophthalmol.* **2020**, *40*, 775–786. [\[CrossRef\]](#)
66. Cucinotta, F.A.; Manuel, F.K.; Jones, J.; Iszard, G.; Murrey, J.; Djojonegro, B.; Wear, M. Space radiation and cataracts in astronauts. *Radiat. Res.* **2001**, *156*, 460–466. [\[CrossRef\]](#)
67. Blakely, E.A.; Chang, P.Y. A review of ground-based heavy ion radiobiology relevant to space radiation risk assessment: Cataracts and CNS effects. *Adv. Space Res.* **2007**, *40*, 1307–1319. [\[CrossRef\]](#)
68. Witze, A. Astronaut twins study spots subtle genetic changes caused by space travel. *Nature* **2019**. [\[CrossRef\]](#)
69. Luxton, J.J.; Bailey, S.M. Twins, Telomeres, and Aging-in Space! *Plast. Reconstr. Surg.* **2021**, *147*, 7S–14S. [\[CrossRef\]](#) [\[PubMed\]](#)
70. Garrett-Bakelman, F.E.; Darshi, M.; Green, S.J.; Gur, R.C.; Lin, L.; Macias, B.R.; McKenna, M.J.; Meydan, C.; Mishra, T.; Nasrini, J.; et al. The NASA Twins Study: A multidimensional analysis of a year-long human spaceflight. *Science* **2019**, *364*. [\[CrossRef\]](#)
71. Dai, Z.; Lei, X.; Yang, C.; Zhao, L.; Lu, L.; Li, Y. Systematic biomedical research of the NASA Twins Study facilitates the hazard risk assessment of long-term spaceflight missions. *Protein Cell* **2019**, *10*, 628–630. [\[CrossRef\]](#) [\[PubMed\]](#)
72. Schmidt, M.A.; Meydan, C.; Schmidt, C.M.; Afshinnekoo, E.; Mason, C.E. The NASA Twins Study: The Effect of One Year in Space on Long-Chain Fatty Acid Desaturases and Elongases. *Lifestyle Genom.* **2020**, *13*, 107–121. [\[CrossRef\]](#) [\[PubMed\]](#)
73. Vico, L.; Hargens, A. Skeletal changes during and after spaceflight. *Nat. Rev. Rheumatol.* **2018**, *14*, 229–245. [\[CrossRef\]](#) [\[PubMed\]](#)
74. Axpe, E.; Chan, D.; Abegaz, M.F.; Schreurs, A.S.; Alwood, J.S.; Globus, R.K.; Appel, E.A. A human mission to Mars: Predicting the bone mineral density loss of astronauts. *PLoS ONE* **2020**, *15*, e0226434. [\[CrossRef\]](#) [\[PubMed\]](#)
75. Garcia, H.D.; Hays, S.M.; Tsuji, J.S. Modeling of blood lead levels in astronauts exposed to lead from microgravity-accelerated bone loss. *Aviat. Space Environ. Med.* **2013**, *84*, 1229–1234. [\[CrossRef\]](#)
76. Iwamoto, J.; Takeda, T.; Sato, Y. Interventions to prevent bone loss in astronauts during space flight. *Keio J. Med.* **2005**, *54*, 55–59. [\[CrossRef\]](#)
77. Farley, A.; Gnyubkin, V.; Vanden-Bossche, A.; Laroche, N.; Neefs, M.; Baatout, S.; Baselet, B.; Vico, L.; Mastrandrea, C. Unloading-Induced Cortical Bone Loss is Exacerbated by Low-Dose Irradiation During a Simulated Deep Space Exploration Mission. *Calcif. Tissue Int.* **2020**, *107*, 170–179. [\[CrossRef\]](#)



78. Bachelet, J.T.; Granzotto, A.; Ferlazzo, M.L.; Sonzogni, L.; Berthel, E.; Devic, C.; Foray, N. First Radiobiological Characterization of Skin and Bone Cells from A Patient Suffering from the PI3KCA-Related Overgrowth Spectrum (PROS) Syndrome. *Arch. Med. Clin. Case Rep.* **2020**, *4*, 1052–1066. [\[CrossRef\]](#)
79. Seddon, B.; Cook, A.; Gothard, L.; Salmon, E.; Latus, K.; Underwood, S.R.; Yarnold, J. Detection of defects in myocardial perfusion imaging in patients with early breast cancer treated with radiotherapy. *Radiother. Oncol. J. Eur. Soc. Ther. Radiol. Oncol.* **2002**, *64*, 53–63. [\[CrossRef\]](#)
80. Tang, S.; Otton, J.; Holloway, L.; Delaney, G.P.; Liney, G.; George, A.; Jameson, M.; Tran, D.; Baturalai, V.; Thomas, L.; et al. Quantification of cardiac subvolume dosimetry using a 17 segment model of the left ventricle in breast cancer patients receiving tangential beam radiotherapy. *Radiother. Oncol. J. Eur. Soc. Ther. Radiol. Oncol.* **2019**, *132*, 257–265. [\[CrossRef\]](#) [\[PubMed\]](#)
81. Taylor, C.; McGale, P.; Bronnum, D.; Correa, C.; Cutter, D.; Duane, F.K.; Gigante, B.; Jensen, M.B.; Lorenzen, E.; Rahimi, K.; et al. Cardiac Structure Injury After Radiotherapy for Breast Cancer: Cross-Sectional Study With Individual Patient Data. *J. Clin. Oncol. Off. J. Am. Soc. Clin. Oncol.* **2018**, *36*, 2288–2296. [\[CrossRef\]](#)
82. Darby, S.C.; Ewertz, M.; Hall, P. Ischemic heart disease after breast cancer radiotherapy. *N. Engl. J. Med.* **2013**, *368*, 2527. [\[CrossRef\]](#) [\[PubMed\]](#)
83. Reynolds, R.J.; Day, S.M. Mortality due to cardiovascular disease among Apollo Lunar astronauts. *Aerosp. Med. Hum. Perform.* **2017**, *88*, 492–496. [\[CrossRef\]](#) [\[PubMed\]](#)
84. Hughson, R.L.; Helm, A.; Durante, M. Heart in space: Effect of the extraterrestrial environment on the cardiovascular system. *Nat. Rev. Cardiol.* **2018**, *15*, 167–180. [\[CrossRef\]](#)
85. Nikjoo, H.; Lindborg, L. RBE of low energy electrons and photons. *Phys. Med. Biol.* **2010**, *55*, R65–R109. [\[CrossRef\]](#) [\[PubMed\]](#)
86. Bianco, D.; Villagrasa, C.; Dos Santos, M. Multi-Scale Analysis of Simulated Proton and Alpha Irradiation. *Radiat. Prot. Dosim.* **2014**. [\[CrossRef\]](#)
87. Britel, M.; Bourguignon, M.; Foray, N. Radiosensitivity: A term with various meanings at the origin of numerous confusions. A semantic analysis. *Int. J. Radiat. Biol.* **2018**, *94*, 503–512. [\[CrossRef\]](#) [\[PubMed\]](#)
88. Lambin, P.; Marples, B.; Fertil, B.; Malaise, E.P.; Joiner, M.C. Hypersensitivity of a human tumour cell line to very low radiation doses. *Int. J. Radiat. Biol.* **1993**, *63*, 639–650. [\[CrossRef\]](#)
89. Marples, B.; Joiner, M.C. The response of Chinese hamster V79 cells to low radiation doses: Evidence of enhanced sensitivity of the whole cell population. *Radiat. Res.* **1993**, *133*, 41–51. [\[CrossRef\]](#) [\[PubMed\]](#)
90. Thomas, C.; Martin, J.; Devic, C.; Diserbo, M.; Thariat, J.; Foray, N. Impact of dose-rate on the low-dose hyper-radiosensitivity and induced radioresistance (HRS/IRR) response. *Int. J. Radiat. Biol.* **2013**, *89*, 813–822. [\[CrossRef\]](#) [\[PubMed\]](#)
91. Joiner, M.C.; Marples, B.; Lambin, P.; Short, S.C.; Turesson, I. Low-dose hypersensitivity: Current status and possible mechanisms. *Int. J. Radiat. Oncol. Biol. Phys.* **2001**, *49*, 379–389. [\[CrossRef\]](#)
92. Slonina, D.; Kowalczyk, A.; Janecka-Widla, A.; Kabat, D.; Szatkowski, W.; Biesaga, B. Low-Dose Hypersensitive Response for Residual pATM and gammaH2AX Foci in Normal Fibroblasts of Cancer Patients. *Int. J. Radiat. Oncol. Biol. Phys.* **2018**, *100*, 756–766. [\[CrossRef\]](#) [\[PubMed\]](#)
93. Bodgi, L.; Foray, N. The nucleo-shuttling of the ATM protein as a basis for a novel theory of radiation response: Resolution of the linear-quadratic model. *Int. J. Radiat. Biol.* **2016**, *92*, 117–131. [\[CrossRef\]](#)
94. Devic, C.; Ferlazzo, M.L.; Berthel, E.; Foray, N. Influence of Individual Radiosensitivity on the Hormesis Phenomenon: Toward a Mechanistic Explanation Based on the Nucleoshuttling of ATM Protein. *Dose-Response A Publ. Int. Hormesis Soc.* **2020**, *18*, 1559325820913784. [\[CrossRef\]](#)
95. Luckey, T.D. *Hormesis with Ionizing Radiation*; CRC Press: New York, NY, USA, 1980.
96. Calabrese, E.J. Hormesis is central to toxicology, pharmacology and risk assessment. *Hum. Exp. Toxicol.* **2008**, *29*, 249–261. [\[CrossRef\]](#)
97. Calabrese, E.J. Hormesis: A fundamental concept in biology. *Microb. Cell* **2014**, *1*, 145–149. [\[CrossRef\]](#)
98. Mothersill, C.; Seymour, C.B. Radiation-induced bystander effects—implications for cancer. *Nat. Rev. Cancer* **2004**, *4*, 158–164.
99. Mothersill, C.; Seymour, C. Radiation-induced bystander effects, carcinogenesis and models. *Oncogene* **2003**, *22*, 7028–7033. [\[CrossRef\]](#) [\[PubMed\]](#)
100. Strauss, S.; Krog, R.L.; Feiveson, A.H. Extravehicular mobility unit training and astronaut injuries. *Aviat. Space Environ. Med.* **2005**, *76*, 469–474.
101. Beggs, J.C. Design and development of the Apollo extravehicular mobility unit. *Ann. N. Y. Acad. Sci.* **1965**, *134*, 441–451. [\[CrossRef\]](#) [\[PubMed\]](#)
102. Convertino, V.A.; Cooke, W.H.; Lukie, K.G. Inspiratory resistance as a potential treatment for orthostatic intolerance and hemorrhagic shock. *Aviat. Space Environ. Med.* **2005**, *76*, 319–325. [\[PubMed\]](#)
103. Baiocco, G.; Giraudo, M.; Bocchini, L.; Barbieri, S.; Locantore, I.; Brussolo, E.; Giacosa, D.; Meucci, L.; Steffenino, S.; Ballario, A.; et al. A water-filled garment to protect astronauts during interplanetary missions tested on board the ISS. *Life Sci. Space Res.* **2018**, *18*, 1–11. [\[CrossRef\]](#)
104. Phillips, T.L. Rationale for initial clinical trials and future development of radioprotectors. *Cancer Clin. Trials* **1980**, *3*, 165–173.
105. Weiss, J.F.; Landauer, M.R. History and development of radiation-protective agents. *Int. J. Radiat. Biol.* **2009**, *85*, 539–573. [\[CrossRef\]](#)



- 
106. Langell, J.; Jennings, R.; Clarck, J.; Ward Jr, J.B. Pharmacological agents for the prevention and treatment of toxic radiation exposure in spaceflight. *Aviat. Space Environ. Med.* **2008**, *79*, 651–660. [[CrossRef](#)]
  107. Berthel, E.; Foray, N.; Ferlazzo, M.L. The Nucleoshuttling of the ATM Protein: A Unified Model to Describe the Individual Response to High- and Low-Dose of Radiation? *Cancers* **2019**, *11*, 905. [[CrossRef](#)] [[PubMed](#)]



## Exposure of human tissues to stratosphere radiation behind different shieldings: data from a campaign of three balloon flights

Human tissues exposed to stratospheric radiation

Juliette Restier-Verlet,<sup>1†</sup> Adeline Granzotto,<sup>1†</sup> Mélanie L. Ferlazzo,<sup>1†</sup> François Kormann,<sup>2</sup> Aurélie Joubert,<sup>3</sup> Clément Devic,<sup>1</sup> Eymeric Le Reun,<sup>1</sup> François Trompier,<sup>3</sup> Michel Bourguignon,<sup>1,4</sup> Nicolas Foray<sup>1\*</sup>

<sup>1</sup>U1296 Inserm Unit “Radiation: Defense, Health, Environment”, 28 Rue Laennec, 69008 Lyon, France ;

<sup>2</sup>ATTA02, 4 rue du Welschbruch, 67200 Strasbourg, France ;

<sup>3</sup>IRSN, Institut de Radioprotection and de Sécurité Nucléaire, 31 Avenue de la Division Leclerc, 92260 Fontenay-aux-Roses, France ;

<sup>4</sup>Département de Biophysique et Médecine Nucléaire, Université Paris Saclay, Versailles St. Quentin en Yvelines, 78035 Versailles, France

<sup>†</sup>The authors have contributed equally to this work;

\*For correspondence : Nicolas.foray@inserm.fr

### Abstract

While some physico-chemical features of the stratosphere are similar to those existing at the equatorial surface of Mars, few balloon campaigns have dealt with the biological effect of stratospheric radiation on human cells. Here, we present data from a campaign of 3 stratospheric balloon flights in which human cutaneous fibroblasts, epithelial lens, osteoblasts and heart myocytes and fibroblasts were exposed frozen to stratosphere in multi-alveolar containers containing boxes made of different shielding materials. Active and passive dosimetry was ensured all along the flight. Once returned in the laboratory, cells were thawed and a 30 min-24 h repair time was applied to them. Recognition and repair of the DNA double-strand breaks (DSB) were investigated. Despite a relatively low dose, flights revealed that stratosphere radiation produce severe DSB: their severity increases with repair time according to the nature of the exposed tissues until the formation of unrepairable highly damaged cells (HDC) cell. Lens and bones cells appeared to be the most radiosensitive.

### Teaser

Stratospheric radiation induce DNA breaks in human tissues even behind shielding



## INTRODUCTION

The era of gas-filled balloons began in France with the Montgolfier brothers who flew safely a balloon made of paper and inflated with oxygen to Versailles in front of the king on September 19, 1783. In the big basket that served as gondola, there was a duck, a rooster and a sheep (1). Surprisingly, history rather remembers as the first milestone the flight of the physicist Jacques Charles's balloon at the Tuileries Gardens in Paris on December 1, 1783, probably because his balloon was made from waterproof taffeta covered with elastic rubber, inflated with hydrogen (lighter than oxygen) and was equipped with a gondola, valve, net, and ballast, still used today (1, 2). It is also this flight which was commemorated by the Olympic cauldron during the Games of Paris 2024. Then followed a considerable number of experiments based on balloons which reached increasingly higher altitudes. In particular, the pioneering insights of Hess in 1912 and Piccard in the 1930s laid the foundation for modern research into ionizing radiation from space, marking essential milestones in the quest to explore and understand the cosmic environment (2). To date, some important discoveries can be credited to scientific ballooning, like the observation of an ozone hole at the South Pole (3) or the accumulation of knowledge of physical features about the stratosphere (2).

Earth's stratosphere spans from 17 to 50 km above sea level (ASL). Stratosphere contains sulfuric acid-water aerosol droplets (4) and oxygen transformed into ozone molecules by intense UV radiation. Interestingly, the physico-chemical features of the stratosphere at about 32-35 km ASL are very similar to those existing at the equatorial surface of Mars. Such a particularity has encouraged astrobiologists to organize some stratospheric balloons campaigns to investigate the survival of some microorganisms in Mars conditions (2). With regard to ionizing radiation reigning in stratosphere, some balloon flights have shown that the composition of physical particles varies with altitude and inclination. The average dose in high stratosphere (36.6 km ASL) is about 64  $\mu\text{Gy/day}$  (i.e. 2.6  $\mu\text{Gy/h}$ ) and the average linear energy transfer increases with altitude (5). High-energy particles interact and produce neutrons: from 15 km ASL, the contributions of neutrons and protons to the total dose represent about 55% and 15%, respectively, the rest being due to gamma- and X-rays (6). However, it must be stressed that the final spectrum of particles and rays that impact actually on living organisms is the result of secondary fragmentations products with the shielding materials (7, 8). Monte-Carlo simulations are required to determine their actual nature and their specific features, although the databases at such altitudes remains limited (9). Lastly, the stratospheric balloons flights with cells and more especially human cells are rare: two reports should nevertheless be cited: Wiese et al.,



1988 and Galleri et al; 2003 who exposed human tumor and blood cells to the stratosphere by maintaining cells in 37°C, respectively (10, 11). Another approach consists in exposing frozen cells to the stratosphere radiation to avoid any repair process during the flight, in thawing them thereafter in laboratory for applying given post-exposure times in order to study DNA damage repair kinetics. To this aim, the gondola should content devices for maintaining temperature below °C for all the duration of the flight.

In a previous review, we have shown that skin, eye, bones and heart may be considered as tissues at risk for space exploration (7, 12). Interestingly, to our knowledge, such human tissues have not been exposed to stratosphere radiation yet. Hence, in order to quantify the radiobiological effects of human cutaneous fibroblasts, epithelial lens, osteoblasts and heart myocytes after an exposure to stratospheric radiation, we designed multi-alveolar containers set in gondola containing frozen cells in boxes made of different shielding materials to prevent neutrons or charged particles to impact cells. In parallel, one container containing dosimeters ensured the active and passive dosimetry all along the flight notably by quantifying the neutron contribution to the dose. The Bernadotte campaign made of three stratospheric balloons flights was organized between 2019 and 2022: the first flight was performed in 2019, from the Timmins base (Canada) and served as preliminary experiment and feasibility test. The two other flights were performed from Kiruna base (Sweden) in 2021 and from Timmins in 2022 (Fig. 1 and 2). The biological effects of stratospheric radiation were evaluated on exposed cells by using immunofluorescence against the phosphorylation of the H2AX variant histone, an early marker of the recognition and repair of the DNA double-strand breaks (DSB), the key-damage of the radiation response (13).



# BERNADOTTE stratospheric balloons campaign

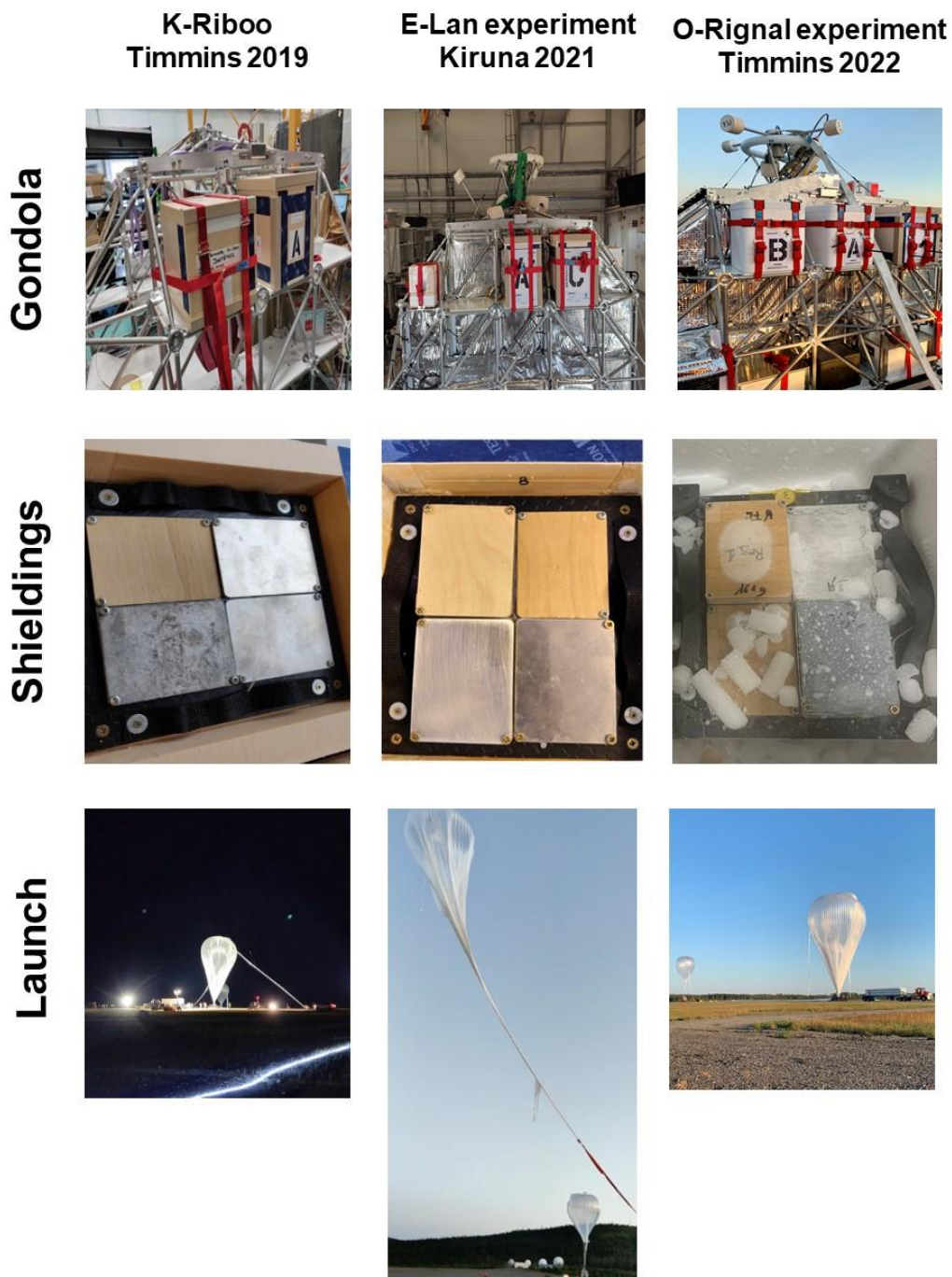


**Fig. 1 : Representative pictures of each flight of the BERNADOTTE campaign**



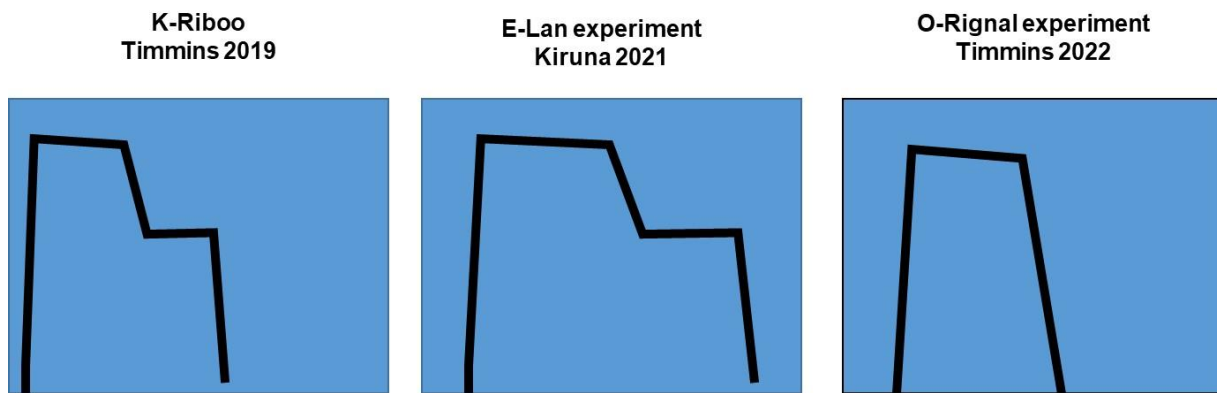


**Fig. 2 : Flight profile and dosimetry features of each flight**

## RESULTS

### *First flight – K-riboo experiment - Timmins (Canada) 2019*

Considering the practical complexity to design and organize stratospheric balloons flights containing human frozen cells, transported abroad from our lab to the launching base abroad, and reciprocally, transported from the launching base to the lab after the flight, we considered the first flight launched in 2019 from the Timmins (Canada) base as a feasibility test. For this flight, only one radioresistant cutaneous fibroblast cell line chosen among the most documented ones of our collection has been exposed to an 8 h-flight (3 h at 32 km and 4 h30 at 19 km) whose profile was shown in Fig. 2. Unfortunately, all the dosimeters could not be triggered during the flight and only the dosimetry data concerning low/high LET radiation was available for this flight (Fig. 2; Table 1). Inside the multi-alveolar gondola, four shielding types were designed: wood (serving as negative control shielding), Pb, Paraffin+Pb, and Al. The number of  $\gamma$ H2AX foci per cell (reflecting the number of DNA double-strand breaks (DSB)) was assessed in all the conditions. Particularly, in non-exposed controls (whether cells maintained at 37°C in Lyon lab or in Timmins base) was found to be  $0.8 \pm 0.5$ , in agreement with published data about non-exposed cells (14, 15). Cells were exposed frozen during all the flight and maintained frozen up to the Lyon lab for analysis. After thawing cells in the lab, 24 h incubation at 37°C was applied to investigate the reparability of the DSB induced by radiation in each condition of shielding (Fig. 3).



**Table 1:** Summary of the absorbed doses in tissue of the low and the high LET component measured per flight with dosimeters EPDN2 type with specific calibration for galactic cosmic radiation

	Absorbed dose in tissue (μGy)	
	Low LET*	High LET**
<b>Flight 1</b> <b>K-Riboo experiment</b> <b>2019</b>	88	35
<b>Flight 2</b> <b>E-Lan experiment</b> <b>2021</b>	138	48
<b>Flight 3</b> <b>O-Rignal experiment</b> <b>2022</b>	53	21

\*relative uncertainties are estimated at 20% (k=2); \*\*relative uncertainties are estimated at 40% (k=2)

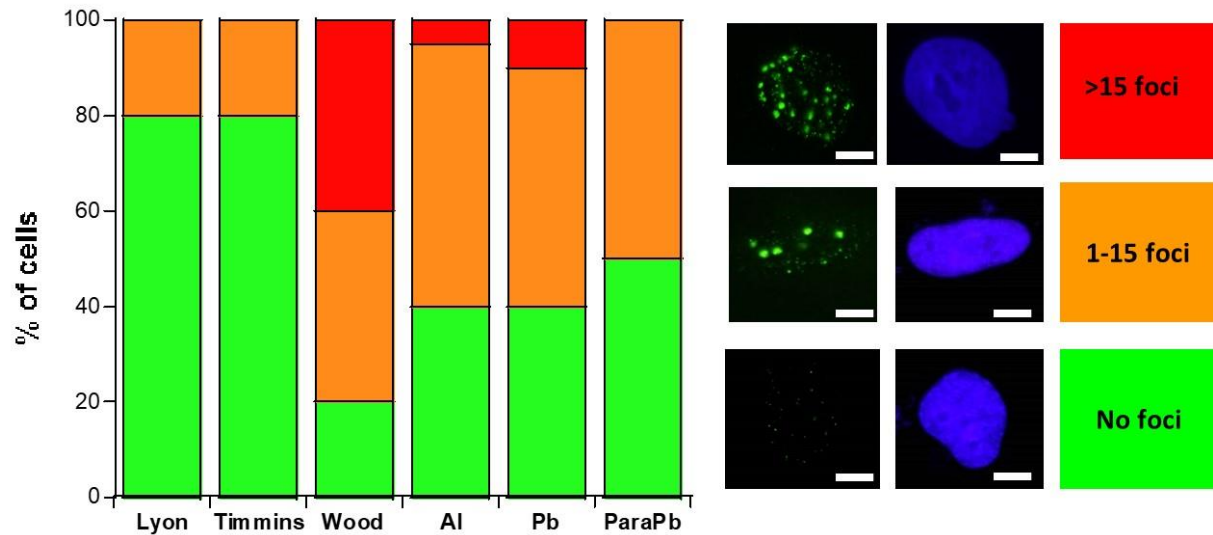


**Fig. 3: Percentage of cells showing the different foci categories for the flight 1.** Frozen radioresistant skin fibroblasts were exposed to stratosphere radiation during flight 1 – K-Riboo experiment and a 24 h post-irradiation period at 37°C was applied once cells were returned in Lyon lab. Anti-γH2AX immunofluorescence was applied to cells and nuclear γH2AX foci was scored in 100 nuclei, at least. Data are represented as the indicated categories (nuclei showing no foci, 1-15 foci or >15 foci). Representative images of each category are shown with DAPI counterstaining. White bar represents 5 μm.



With wood shielding, the number of  $\gamma$ H2AX foci remaining per cell was found to be  $6.9 \pm 2.0$  at 24 h post-irradiation. Interestingly, in our hands, radioresistant fibroblasts reached such amount of remaining  $\gamma$ H2AX foci only after an exposure of low-energy-protons (16) or neutrons (17). In addition, among cell exposed, we observed a subset of damaged cells showing more than 15  $\gamma$ H2AX foci per cell ( $>15$  foci cells). By considering an average dose of  $2.6 \mu\text{Gy/h}$  in the stratosphere (i.e.  $21.33 \mu\text{Gy}$  for this flight) (5) and the very documented DSB induction rate of 40 DSB per Gy per human radioresistant diploid fibroblast cell (13), an average number of about 7 residual DSB assessed 24 h post-irradiation and the existence of a subset of cells showing more than 15  $\gamma$ H2AX foci per cell strongly suggest that stratosphere radiation produce a significant subset of slowly repairable DSB. These findings encouraged us to define categories of  $\gamma$ H2AX foci as shown in Fig. 3, in order to provide both quantitative and qualitative data analysis. Both Pb and ParaPb shieldings were supposed to fully protect cells from stratospheric radiation, notably by arresting specifically neutrons with the paraffin component on one side and ionizing radiation with the Pb component on the other side. However, it must be stressed that electrons impacting Pb may produce bremsstrahlung photons. By comparing data obtained with Pb and ParaPb shieldings, we observed that ParaPb shielding has made disappeared all the  $>15$  foci cells among 40% assessed with wood shielding while it remained 10% of  $>15$  foci cells with Pb shielding. Such findings suggest that neutron component arrested by paraffin was responsible for the formation of at least 30% of  $>15$  foci cells. As evoke above, Pb shielding can produce bremsstrahlung, in a larger extent than Al shielding that showed 5% of  $>15$  foci cells. Altogether, these findings suggested that the formation of  $>15$  foci cells in radioresistant cells was likely due to neutrons (about 30/40 i.e. 75%) but also to the arrest of incident ionizing radiation and to the bremsstrahlung photons (representing each 5/40 i.e. 12.5%). However, it is noteworthy that such hypotheses were made from the number of  $\gamma$ H2AX foci assessed 24 h post-irradiation. Hence, one cannot eliminate the possibility that the DSB repair process produces itself some additional DSB during the 24 h allowed. Hence, for the next flights, it appeared necessary to acquire more repair time data to verify such hypotheses.

## Flight 2 – E-Lan experiment - Kiruna (Sweden) 2021

For the second flight launched from Kiruna base (Sweden) in 2021, 6 human cells deriving from skin, heart, bones and lens were exposed to 16-h 2-stage flight whose profile was shown in Fig. 2. The average dose was XXX and the contribution of neutrons or gamma-rays were found to be



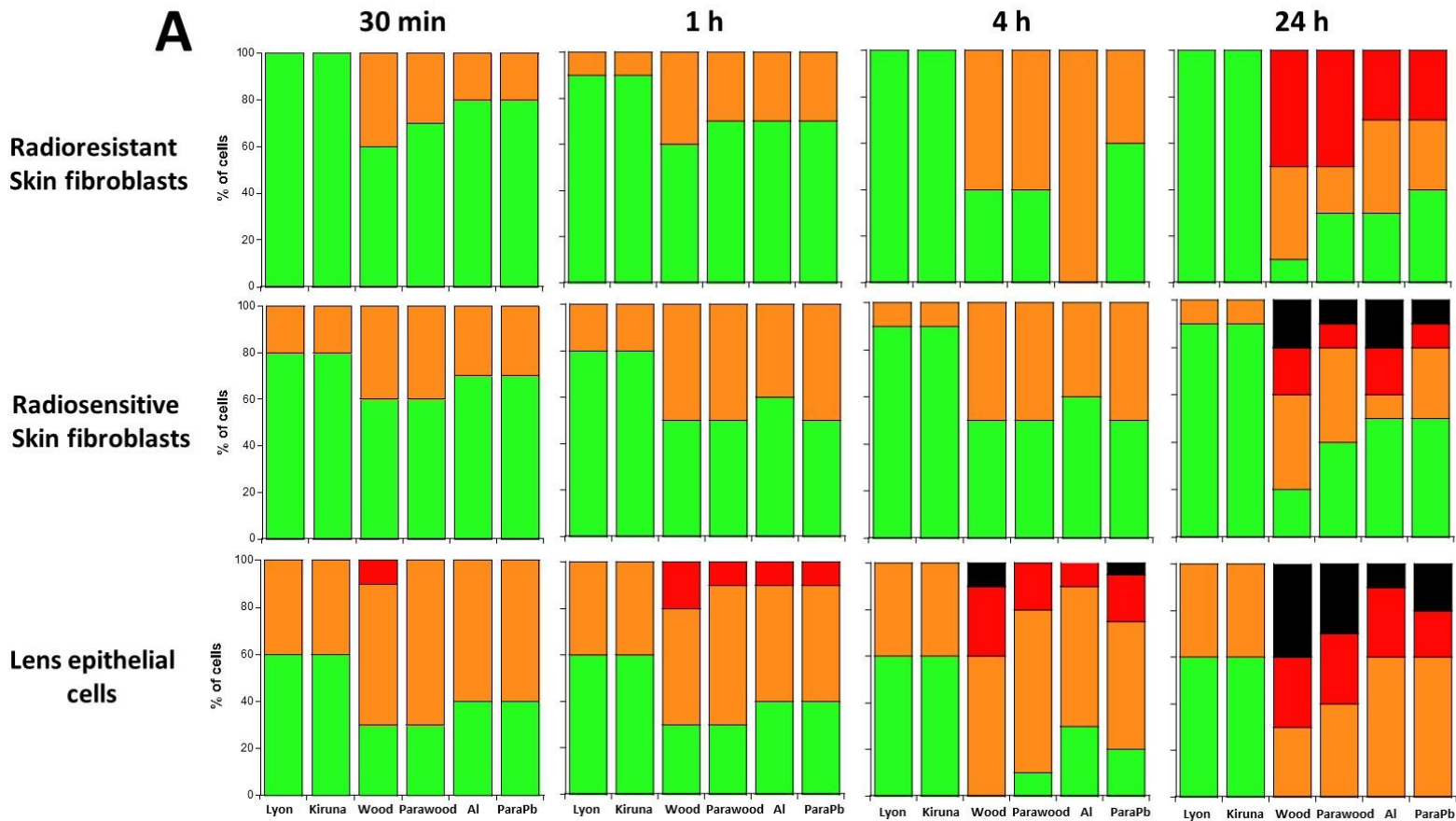
X and Y (Fig. 2). Inside the multi-alveolar containers set in the gondola, four shielding types have been designed: wood, paraffin+wood (Parawood), Al and Paraffin+Pb (ParaPb). One of the major novelties of this flight was that 4 post-irradiation times (30 min, 1h, 4 h and 24 h) were applied to cells in order to investigate the DSB repair kinetics in each situation: hundreds different conditions were therefore examined. For clarity, we presented here the major ones.

The number of  $\gamma$ H2AX foci per assessed in non-exposed radioresistant skin control fibroblasts (whether maintained at 37°C in Lyon lab or in Kiruna base) was found to be  $0.5 \pm 0.5$ , in agreement with published data about non-exposed human cells (14, 15) (Fig. 4). By contrast, without shielding (wood), the number of  $\gamma$ H2AX foci per cell was found to be  $3.7 \pm 0.7$ . at 30 min post-irradiation i.e. significantly higher than unexposed controls ( $p < 0.05$ ) (14, 15).

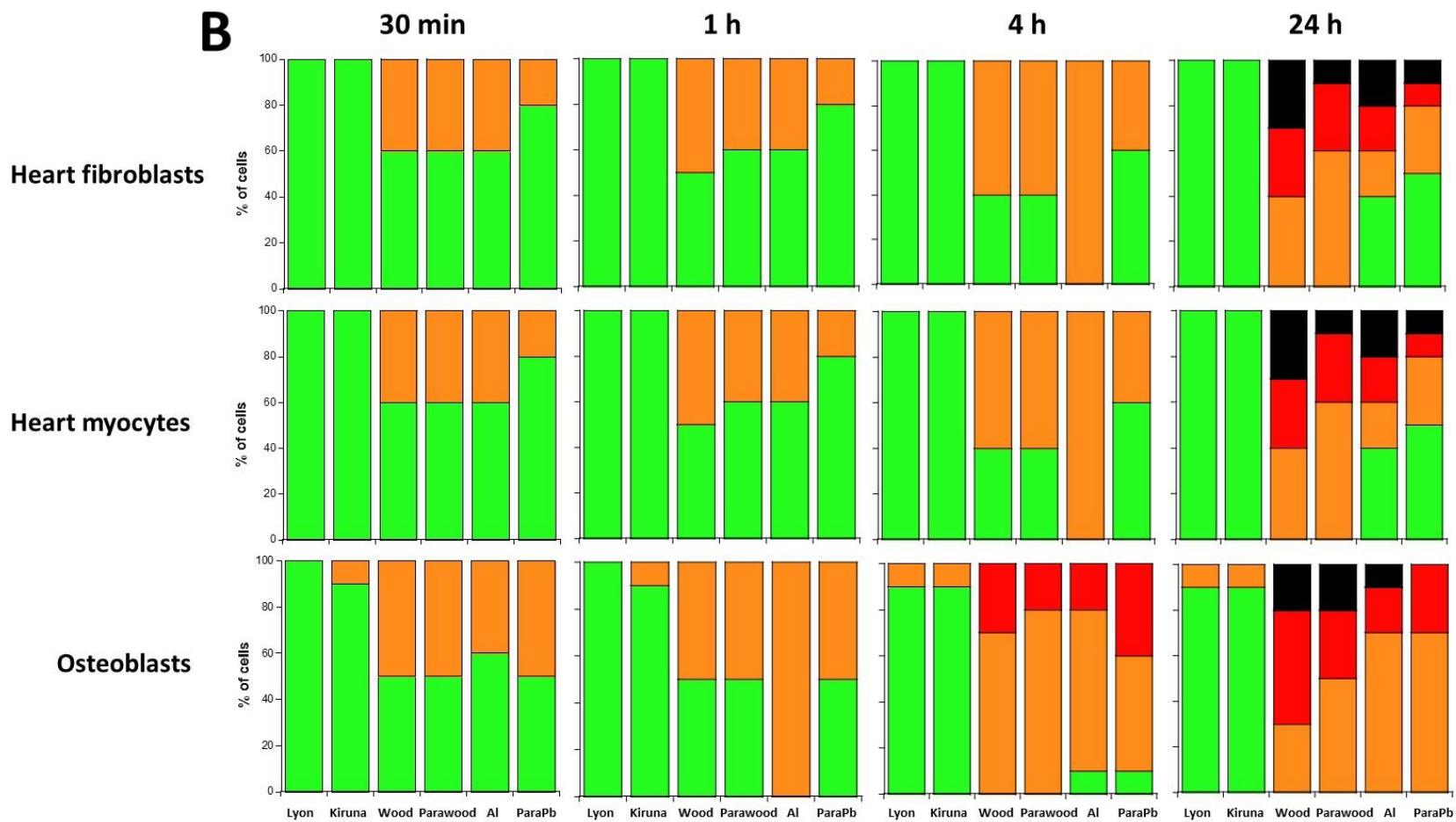
The average number of  $\gamma$ H2AX foci per cell progressively increased with post-irradiation time, suggesting that stratosphere radiation induce DNA damage whose severity (i.e. average number of foci per cell) increased with repair time. For example, with wood shielding, after 24 for repair, the number of  $\gamma$ H2AX foci was found to be  $8.7 \pm 1$ . When the ParaPb shielding was applied, the average number of  $\gamma$ H2AX foci was significantly reduced at 30 min post-irradiation ( $0.6 \pm 0.2$ ) but reached  $5.1 \pm 1$  at 24 h post-irradiation. Same conclusions were reached with Al shielding (Fig.4).

For all the other cell lines tested, the numbers of spontaneous  $\gamma$ H2AX foci were found similar to those assessed in radioresistant skin control fibroblasts ( $p > 0.8$ ). The average numbers of radiation-induced  $\gamma$ H2AX foci also increased with post-irradiation time. However, unlike with radioresistant skin control fibroblasts, the other cell lines tested elicited a subset of cells showing nuclei with very intense and homogenous  $\gamma$ H2AX signal in which foci were not distinguishable: another category of nuclei was therefore defined, namely the highly damaged cells (HDC) category. For all the conditions, the HDC appeared at 4 h post-irradiation for lens cells and at 24 h for all the other cell lines. Interestingly, the number of HDC was found systematically larger with wood shielding than with Parawood, suggesting again that reducing the neutron component may significantly influence the formation of HDC (Fig. 4). Furthermore, for the skin and heart cells, the Al and ParaPb shielding provide significant subsets of cells with no foci, suggesting an efficient protection. This was not the case with lens and bones cells in which cells systematically showed  $\gamma$ H2AX foci even if the subset of HDC was reduced (Fig. 4).











C

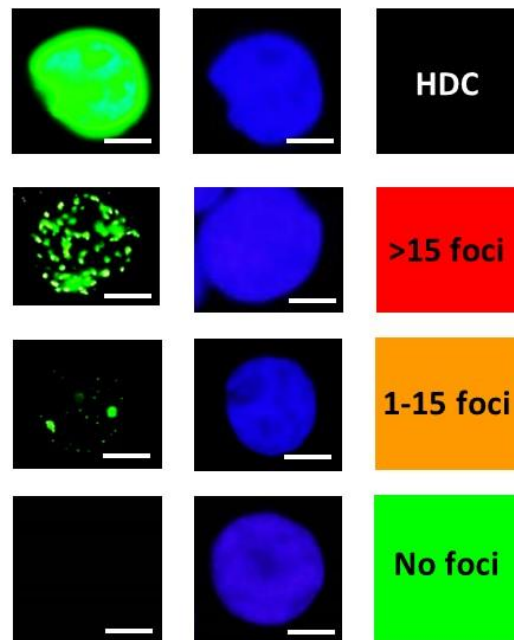


**Fig. 4: Percentage of cells showing the different foci categories for the flight 2.** Frozen radioresistant cells were exposed to stratosphere radiation during flight 2 – E-Lan experiment and a 30 min to 24 h post-irradiation period at 37°C was applied once cells were returned in Lyon lab. A. Skin and lens cells. B. Heart and bone cells. Anti- $\gamma$ H2AX immunofluorescence was applied to cells and nuclear  $\gamma$ H2AX foci was scored in 100 nuclei, at least. Data are represented as the indicated categories (nuclei showing no foci, 1-15 foci, >15 foci and HDC). C. Legend and representative images of each category are shown with DAPI counterstaining. White bar represents 5  $\mu$ m.

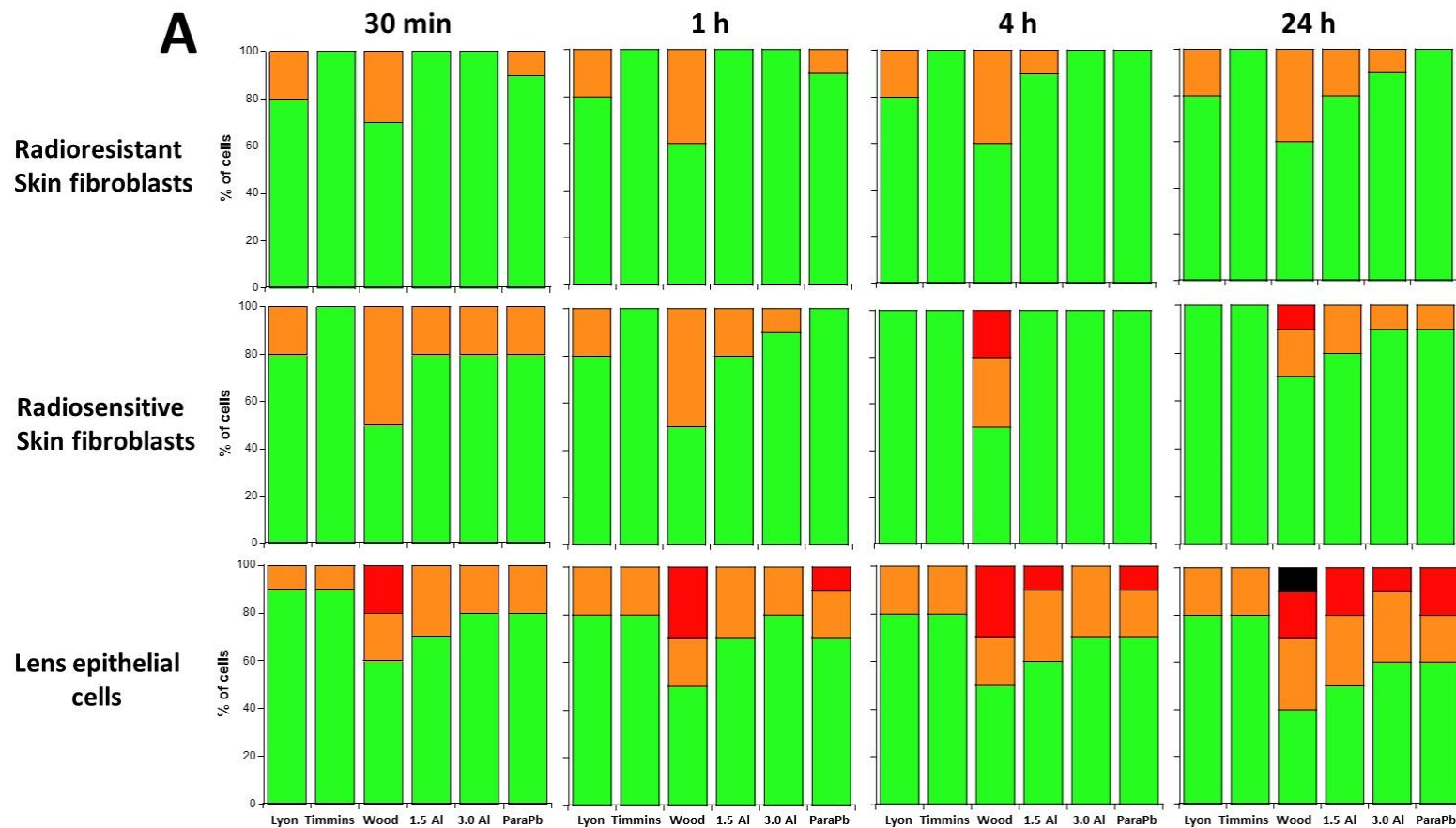


Altogether, the findings of this second flight suggested that: 1) stratosphere radiation produce severe DSB despite a relatively low dose and that their severity increases during the DSB repair process according to the nature of exposed tissue up to the formation of unrepairable HDC; 2) the paraffin that is supposed to decrease the neutron contribution to the dose decreases about 10% of HDC. No shielding tested fully protects the cells from the formation of HDC.

### Flight 3 – O-Rignal experiment – Timmins (Canada) 2022

For the third flight launched from Timmins base (Canada) in 2022, the same human cell lines as those used for the second flight were exposed to 8-h 1-stage flight whose profile was shown in Figure 2. The average dose was XXX and the contribution of neutrons or gamma-rays were found to be X and Y. Inside the multi-alveolar containers set in the gondola, four shielding types have been designed: wood, 1.5 mm Al, 3 mm Al and Parapb. Four post-irradiation times (30 min, 1h, 4h, 24h) were applied to cells in order to investigate the DSB repair kinetics in each situation: hundreds different conditions were therefore examined. The number of  $\gamma$ H2AX foci per assessed in non-exposed radioresistant skin control fibroblasts (whether maintained at 37°C in Lyon lab or in Timmins base) was found to be  $0.3 \pm 0.5$ , in agreement with published data about non-exposed human cells (14, 15). By contrast, without shielding (wood), the number of  $\gamma$ H2AX foci per cell was  $0.6 \pm 0.3$  at 30 min post-irradiation i.e. not significantly different from unexposed controls data ( $p > 0.3$ ) (Fig. 5). Interestingly, the average numbers of  $\gamma$ H2AX foci per cell did not significantly increase with repair time, probably because the cell line was radioresistant and/or that the dose was very low. For example, with wood shielding, after 24 for repair, the number of  $\gamma$ H2AX foci was found to be  $2 \pm 1$ . When the ParaPb shielding was applied, the average number of  $\gamma$ H2AX foci was significantly reduced at 30 min post-irradiation ( $0.3 \pm 0.1$ ) and was found nil at 24 h post-irradiation. Similar conclusions were reached with Al shielding. For all the other cell lines tested, the average numbers of radiation-induced  $\gamma$ H2AX foci did not increase necessarily with post-irradiation time (Fig. 5). All the other cell lines elicited a subset of HDC but this one never exceeded 10% and was only observable at 24 h post-irradiation with wood shielding (Fig.5).







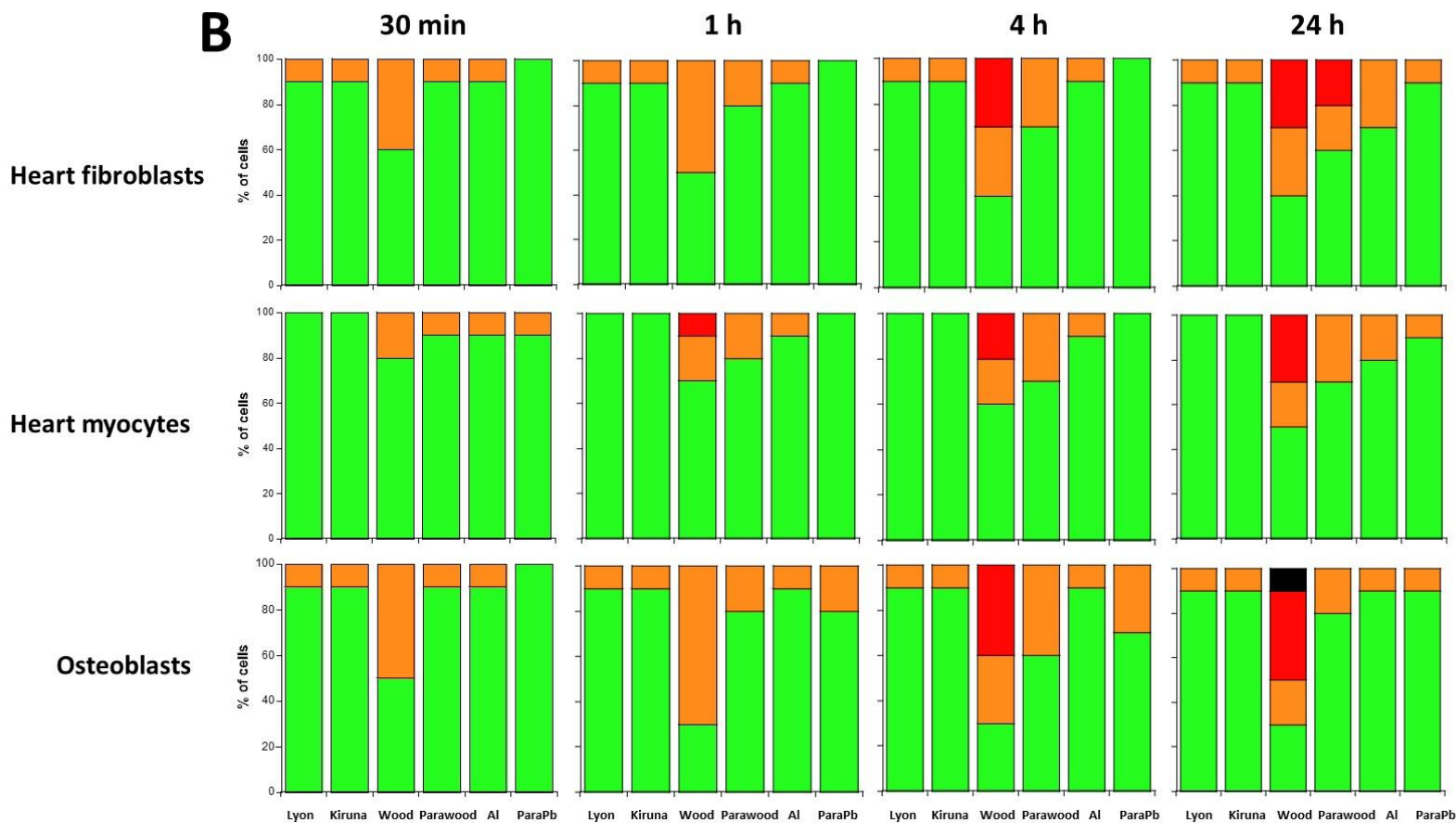


**Fig. 5: Percentage of cells showing the different foci categories for the flight 3.** Frozen radioresistant cells were exposed to stratosphere radiation during flight 3— O-Rignale experiment and a 30 min to 24 h post-irradiation period at 37°C was applied once cells were returned in Lyon lab. A. Skin and lens cells. B. Heart and bone cells. Anti- $\gamma$ H2AX immunofluorescence was applied to cells and nuclear  $\gamma$ H2AX foci was scored in 100 nuclei, at least. Data are represented as the indicated categories (nuclei showing no foci, 1-15 foci, >15 foci and HDC) with the same legend as Fig. 4C.



### DISCUSSION

This report summarizes our findings obtained from the BERNADOTTE campaign of 3 stratospheric balloons flights launched from Kiruna and Timmins bases. The major aim of the study was to determine the number of DSB induced by the stratosphere radiation and remaining after a time for repair in human tissues considered at risk for space exploration, namely skin, bones, lens and heart, kept frozen inside vials set behind different shielding types. Despite that the exposures were performed at low doses and dose-rates, we observed the formation of highly damaged cells (HDC) i.e. cells containing hundreds DSB, which is much higher than the number of DSB expected with the very documented DSB induction rate of 40 DSB/Gy per cell. Such findings suggest that stratosphere radiation induce severe DSB whose repair process is accompanied for 24 h, by the induction of additional DNA stand breaks. Lastly, it must be stressed that the best shieldings (Al and ParaPb) do not fully protect cells. Neutrons and bremsstrahlung appear to be responsible of the majority of the impacts behind the shielding.

HDC, a common feature of human tissues exposed to stratosphere?

In this study, we have considered DSB as the key-DNA damage, responsible for cell lethality, as abundantly documented elsewhere (13). The three major clinical consequences of an exposure to ionizing radiation are toxicity or radiosensitivity reactions, generally due to unrepaired DSB and cell lethality in response to high doses; radiation-induced cancer or radiosusceptibility, generally due to misrepaired DSB and cell transformation in response to repeated low doses; radiation-induced accelerated aging or radiodegeneration, generally due to cumulated DNA strand breaks in response to low dose rate of ionizing radiation (13). In space, the radiation dose received by astronauts is generally low (i.e. lower than 0.5 Gy) and therefore no reaction of radiosensitivity have not been observed yet (7, 12). The formation of HDC have been already reported in different conditions of irradiation involving either cancer risks (18) or accelerating aging (12). For example, through the phenomenon of hyper-sensitivity to low doses (HRS) (19), we showed that in a certain range of doses and dose-rate, the DSB repair systems can panic and provide, through an



exacerbation of nucleases, may a large amount of additional single- and double-strand breaks, rendering the radiation-induced DSB more difficult to be repaired (18, 20, 21). Such phenomenon has been notably observed after an irradiation with an hypofractionated stereotactic body radiation therapy device delivering hundreds micrometric minibeam providing each some fractions of mGy in some seconds. However, in this case, the HRS phenomenon was observed in tumor cells showing HDC (18). More recently, we have provided evidence that, in response to a low dose-rated irradiation equivalent to that reigning in the International Space Station, the ATM protein can accumulate around the nuclear membrane of bones and lens cells by forming perinuclear crown, easily quantifiable by immunofluorescence (12). The ATM crown block the entry to ATM monomers and DNA strand breaks accumulate in the nucleus. When the number of unrecognized DNA breaks reaches a threshold, chromatin decondensation increases the size of nucleus, which permits to some ATM monomers to enter in the nucleus, and to recognize DSB by the phosphorylation of H2AX: HDC appear (12, 22). In both cases precited, the occurrence of HDC is conditioned by chronic or continuous impacts of rays or particle holding subfractions of mGy. Considering that the neutron contribution to the dose is major in our case, the occurrence of HDC should be also linked to the presence of neutrons. Interestingly, we have already observed HDC after the exposure of fibroblasts to 16 MeV-neutrons followed by 24 h for repair. However, further investigations in biology (notably with ATM-immunofluorescence) and in physics (with Monte-Carlo simulations) are needed to better understand the processes caused by stratosphere radiation.

Neutrons vs gamma: the idealistic shielding does not exist

In all the conditions tested, the Al and ParaPb shieldings did not fully protect the cells from the formation of HDC. Interestingly, the flight 1 data suggest that a x mm-paraffin layer is sufficient to reduce the number of HDC by 10%. Unfortunately, we did not investigate further the effect of paraffin or any other materials that may serve as a specific protection against neutrons. However, it appears that HDC formation is not fully due to neutron: protons and bremsstrahlung photons may be also responsible for HDC formation. Hence, even if ParaPb appears to be the most efficient shielding, stratospheric radiation may be sufficiently intense to produce bremsstrahlung photons responsible for the formation or HDC. Conversely, while the occurrence of the bremsstrahlung effect is lower with the Al shielding than with the Pb shielding, the Al shielding offers a lower protection against some



highly ionizing component. Altogether, these statements suggest that there is no idealistic shielding against stratospheric radiation among the shielding types tested.

## MATERIALS AND METHODS

### Cell lines

The cellular characteristics of the cells used in this study are detailed in Table 2. Hs27, a radioresistant cell lines, originating from apparently healthy individual, served as a control. To the exception of the heart myocytes, heart fibroblasts and lens epithelial cell lines purchased from ScienCell research laboratories (Carlsbad, CA, USA) and the skin fibroblast GM03399 cell lines deriving from an *ATM*<sup>+/-</sup>-mutated donor purchased from Coriell Institute (Camden, NJ, USA), all the other cell lines belong to the COPENIC collection of the lab. The COPENIC cell lines were obtained with all sampling protocols approved by the national ethical committee. The resulting cells were declared to the Ministry of Research under the numbers DC2008-585, DC2011-1437, and DC2021-3957. The radiobiological data of the COPENIC collection are protected under reference IDDN.FR.001.510017.000.D.P.2014.000.10300 (Table 2).

**Table 2 :** Major features of the cell lines used in this study

Cell line	Tissue origin	Provider
Hs27	Radioresistant foreskin fibroblast	COPENIC
GM03399	ATM <sup>+/-</sup> skin fibroblast	Coriell Institute
HCF	Heart fibroblast	ScienCell
HCM	Heart myocytes	ScienCell
B3	Lens epithelial cells	ScienCell
EROS080	Osteoblast	COPENIC

All experiments involved human cell lines cultured as monolayers in standard cell culture conditions reported elsewhere (12). In the laboratory, the cell lines were trypsinized, counted and frozen into samples containing 10<sup>6</sup> cells each, before being stored at -80 and transported to the flight sites. The cold chain was maintained at negative temperature until thawing on return to the laboratory. Samples were frozen in 1% of steril glycerol, the DMSO conventionally used being a reducing agent likely to minimize radiation-induced damage.



For each cell line, two batches of samples were frozen, each containing 8 samples loaded on the gondola and two controls, the first remaining in the laboratory and the second serving as a control during transport to the flight site in Sweden or Canada but not flying on the gondola.

#### *Multialveolar box in gondola*

To expose the cells to the stratosphere, we use a device manufactured by the Atta02 prototype manufacturer company (Strasbourg, France). This device comprises 3 polystyrene boxes, two dedicated to the experimental plates containing the cell samples and a third containing the dosimetry devices. Each box contains a set of eutectic plaques to keep the temperature below  $-10^{\circ}\text{C}$  for frozen cells and above  $8^{\circ}\text{C}$  for dosimetry.

The 2 boxes used for the biology section include 2 sets of shields, and positioned above the cold eutectic plaques. the frozen cell samples are located in lead alveoli, closed by the shields, so that the radiation measured is only cosmic, and can only come from above, i.e. through the shields. The dosimetric box is of the same model, and the dosimetry devices are placed on top of the hot eutectic pack and either protected or not by different shields, similar to the conditions of the cold boxes. Furthermore, these modules are placed at the top of the CNES Carmecita gondola.

#### *Dosimetry*

During the stratospheric flight, active and passive dosimetry were used. First, in the hot box, 2 Liulin and 2 EPDN2 were placed without protective shielding, in order to measure the total dose in the stratosphere. Then, RPL, FLI, CR39 and-or GD351 were placed behind similar shields to those protecting the samples. A dosimetric measurement was also performed during the samples transport between the lab and the flight location to avoid any additional radiative exposition (data not shown). The dosimetric analysis of the various devices was carried out in collaboration with IRSN (Institute for Radiation Protection and Nuclear Safety).

#### *Flights features*

Timmins (Canada) CSA balloon base :  $48^{\circ}34'05.2''\text{N } 81^{\circ}22'03.1''\text{W}$

Kiruna (Sweden) SSC Esrange base :  $67^{\circ}53'34.4''\text{N } 21^{\circ}03'41.9''\text{E}$

- Altitudes et paliers éventuels

Timmins 2019 : ??

Kiruna 2021 : plateau 32.7 km 6h50 puis plateau 19 km 6h16



# *Immunofluorescence*

The Labteck CC2 device (xxx) was used to thaw the cell samples. DNA double-strand breaks were assessed by immunofluorescence at 30 min, 1 h, 4 h and 24 h after thawing. For the early time points, we used the fixation and lysis protocol described by M Falk et al [4], which consists in long fixation and permeabilisation with a low concentration of fixative and detergent. For the 4h and 24h time points, we used the immunofluorescence protocol described in our previous publications

The nuclear foci scoring were performed as described elsewhere [5,6]. The foci scoring procedure was performed manually and has received certification under CE mark and ISO-13485 quality management system norms [2]. Furthermore, the foci scoring procedure was applied in the frame of the Soleau Envelop and patents (FR3017625 A1, FR3045071 A1, EP3108252 A1). More than 50 nuclei were analyzed per experiment per post-irradiation time, with three independent replicates performed. The Gaussian distributions of the number of foci were controlled routinely for each condition. Inter-reader foci scoring revealed no significant difference, whether performed manually or by computerized ImageJ v1.5 or Olympus foci scoring software (v2.0) [6].

# *Statistical analysis*

Data were obtained from the indicated number of independent experiments and expressed as the mean  $\pm$  standard error of the mean (SEM). Statistical analyses were performed using PRISM software version 9.5.1 (GraphPad Software, San Diego, CA, USA) or Kaleidagraph version 4.5.4 (Synergy Software, Reading, PA, USA).



## Acknowledgments

Acknowledgments follow the references and notes section but are not numbered. They should include the following information in the order listed below. Each section must be a **separate paragraph** and the heading in bold. Please use the subhead and boldface layout as shown below.).

If applicable, begin the section with text that acknowledges non-author contributions. (Note this section does not have a general heading).

**Funding:** Include all funding sources, including grant numbers, complete funding agency names, and recipient's initials. Each funding source should be listed in a separate paragraph such as:

National Institutes of Health grant U12AV123456 (PV, CHO)

National Institutes of Health grant R01AB123456 (PV, GS)

William K. Bowes Jr Foundation (PV)

German Research Foundation grant AB 1234/1-1

Office of Biological and Environmental Research of the U.S. Department of Energy

Atmospheric System Research Program Interagency Agreement grant DE-SC0000001

National Institute of Health Research UK

**Author contributions:** Each author's contribution(s) to the paper should be listed (we suggest following the CRediT model with each CRediT role given its own line. No punctuation in the initials.

Examples:

Conceptualization: SBB, DLA, MPW

Methodology: HP, FTGS, CW, JRK

Investigation: SBB, DLA, MPW

Visualization: SFB

Supervision: SJE, JLS, EH

Writing—original draft: SBB, DLA

Writing—review & editing: SBB, DLA, PRB, EH

**Competing interests:** Include any financial interests of the authors that could be perceived as being a conflict of interest (including but not limited to financial holdings, professional affiliations, advisory positions, and board memberships). Also include any awarded or filed patents pertaining to the results presented in the paper. If the entire group of authors has no competing interests, the authors should declare this (e.g., "Authors declare that they have no competing interests.") In cases where some authors have competing interests and others do not, note the competing interests and then use the following, "All other authors declare they have no competing interests."

**Data and materials availability:** All data, code, and materials used in the analyses must be available in some form to any researcher for purposes of reproducing or extending the analyses. Include a note explaining any restrictions on materials, such as materials transfer agreements (MTAs). Include accession numbers to any data relevant to the paper and deposited in a public database; include a brief description of the dataset or model with the number. The DMA statement should include the following: "All data are available in the main text or the supplementary materials."



## Supplementary Materials

Please use the *Science Advances* [template](#) to format your Supplementary Materials.

## References

1. F. Simons, *The Early History of Ballooning - The Age of the Aeronaut*. (Read Books, 2014).
2. D. J. Smith, M. B. Sowa, Ballooning for Biologists: Mission Essentials for Flying Life Science Experiments to Near Space on NASA Large Scientific Balloons. *Gravit Space Res* **5**, 52-73 (2017).
3. S. Solomon, Stratospheric ozone depletion: A review of concepts and history. *Reviews of Geophysics* **37**, 275-316 (1999).
4. D. J. Jacob, *Introduction to Atmospheric Chemistry*. (Princeton University Press, Princeton, 1999).
5. C. J. Mertens *et al.*, Cosmic radiation dose measurements from the RaD-X flight campaign. *Space Weather* **14**, 874-898 (2016).
6. W. Schimmerling, Overview of NASA's space radiation research program. *Gravitational and Space Research* **16**, 5-10 (2007).
7. J. Restier-Verlet *et al.*, Radiation on Earth or in Space: What Does It Change? *International journal of molecular sciences* **22**, 3739 (2021).
8. J. Restier-Verlet, N. Foray, Should we extrapolate data from animal models exposed to radiation conditions that poorly reflect cosmic radiation? E-letter about Krukowski et al. (2021). *Nature Advances*, (2021).
9. NCRP, "Information Needed to Make Recommendations for Space Missions Beyond Low-Earth Orbit. Report #153, ," (US National Council for Radiation Protection and Measurements,, Bethesda, MD, 2006).
10. C. Wiese, B. Bechler, G. Lorenzi, A. Cogoli, in *Terrestrial Space Radiation and Its Biological Effects*, P. D. McCormack, C. E. Swenberg, H. Buckner, Eds. (Springer, New York City, 1988), pp. 337-343.
11. G. Galleri *et al.*, in *European Rocket and Balloon Programmes and Related Research*, B. Warmbein, Ed. (ESA, Sankt Gallen, 2003), pp. 571-573.
12. J. Restier-Verlet *et al.*, Accelerated aging effects observed in vitro after an exposure to gamma-rays delivered at very low and continuous dose-rate equivalent to 1-5 weeks in International Space Station. *Cells in press*, (2024).
13. N. Foray, M. Bourguignon, N. Hamada, Individual response to ionizing radiation. *Mutation Research Review* **770**, 369-386 (2016).
14. A. Granzotto *et al.*, Influence of Nucleoshuttling of the ATM Protein in the Healthy Tissues Response to Radiation Therapy: Toward a Molecular Classification of Human Radiosensitivity. *International journal of radiation oncology, biology, physics* **94**, 450-460 (2016).
15. E. Le Reun *et al.*, Quantitative correlations between radiosensitivity biomarkers show that the ATM protein kinase is strongly involved in the radiotoxicities observed after radiotherapy. *International journal of molecular sciences* **23**, (2022).



- 533 16. M. Maalouf *et al.*, Influence of Linear Energy Transfer on the Nucleo-shuttling of the  
534 ATM Protein: A Novel Biological Interpretation Relevant for Particles and Radiation.  
535 *International journal of radiation oncology, biology, physics* **103**, 709-718 (2019).
- 536 17. A. Joubert, N. Foray, in *9ème Colloque International de Radiobiologie Fondamentale et*  
537 *Appliquée*, SIRLAF, Ed. (SIRLAF, Annecy, France, 2009).
- 538 18. E. Le Reun *et al.*, Influence of the Hypersensitivity to Low Dose Phenomenon on the  
539 Tumor Response to Hypofractionated Stereotactic Body Radiation Therapy. *Cancers* **15**,  
540 (2023).
- 541 19. M. C. Joiner, B. Marples, P. Lambin, S. C. Short, I. Turesson, Low-dose hypersensitivity:  
542 current status and possible mechanisms. *International journal of radiation oncology,*  
543 *biology, physics* **49**, 379-389 (2001).
- 544 20. C. Thomas *et al.*, Impact of dose-rate on the low-dose hyper-radiosensitivity and induced  
545 radioresistance (HRS/IRR) response. *International journal of radiation biology* **89**, 813-  
546 822 (2013).
- 547 21. L. Bodgi, N. Foray, The nucleo-shuttling of the ATM protein as a basis for a novel theory  
548 of radiation response: resolution of the linear-quadratic model. *International journal of*  
549 *radiation biology* **92**, 117-131 (2016).
- 550 22. E. Berthel *et al.*, Toward an early diagnosis for Alzheimer's disease based on the  
551 perinuclear localization of the ATM protein. *Cells* **12**, 1747 (2023).
- 552



# **UP Human Social Sciences (PôPS)**





# Measuring reconceptualization and reprioritization during France's first COVID-19-related lockdown in women with and without a history of cancer: an adaptation of the SeiQoL-DW and PGI

Charlotte Bauquier<sup>1</sup> · Stéphanie Ginguéné<sup>1</sup> · Tanguy Leroy<sup>1</sup> · Marjolaine Doumergue<sup>2</sup> · Natacha Lebrun<sup>1</sup> · Claire Della Vecchia<sup>1</sup> · Renaud Mabire-Yon<sup>1</sup> · Sarah Leveaux<sup>1</sup> · Luis Sagaon-Teyssier<sup>3</sup> · Marie Préau<sup>1</sup>

Accepted: 30 January 2024

© The Author(s), under exclusive licence to Springer Nature Switzerland AG 2024

## Abstract

**Purpose** This study aimed to provide a better understanding of the patient-perceived effects of France's first COVID-19-related lockdown on the quality of life (QoL) of women affected by cancer, and to test an ad hoc measurement scale for evaluating quasi-individualized QoL. QoL was measured for both during (i.e., current) and before (i.e., retrospectively) the lockdown. Respondents were women registered on the research platform Seintinelles.

**Methods** A tool for measuring quasi-individualized QoL was adapted from the SeiQoL-DW and PGI. It was distributed as part of a larger online self-questionnaire to a sample of 1303 women with a history of cancer (i.e., former or current) and with no such history.

**Results** Current and retrospective QoL scores were not significantly different between the two respondent groups. An analysis of reconceptualization and reprioritization revealed a cancer-specific effect: women with a history of cancer reconceptualized more, while women with no such history reprioritized more.

**Conclusion** Our novel ad hoc quasi-qualitative tool made it possible to assess the QoL of women with a history of cancer, a particularly vulnerable population in the context of the COVID-19 pandemic. Furthermore, it highlighted a difference in reconceptualization and reprioritization between this population and women with no such history.

**Keywords** Quality of life · Reconceptualization · Reprioritization · Lockdown · Cancer

## Introduction

On March 17, 2020, France's first COVID-19-related lockdown was introduced to limit the spread of the SARS-Cov-2 virus. Measures included the closure of schools and universities, changes to working methods, and the reorganization of hospital and care services. This unprecedented event, which lasted until May 10, 2020, radically changed people's

daily lives. Individuals had to implement adjustment strategies in order to ensure they could manage their familial, professional, and emotional lives as best as possible, and to maintain an acceptable quality of life (QoL) for themselves.

The period was characterized by high levels of uncertainty about the disease, its consequences, measures to manage it, and how long the lockdown would last. The pandemic and lockdown were especially difficult for persons who perceived themselves as more vulnerable to the risk of infection and found it difficult to adequately implement social distancing measures [1]. Women with cancer were one such population [2–4], as the intensely emotional situations they already experienced because of their cancer (e.g., diagnosis announcement, treatment initiation, post-surgical pain, and disease progression) were compounded by the uncertainties listed above, and by specific changes made to cancer care recommendations which were put in place three days before the lockdown started. These changes led to questions being asked by stakeholders—including cancer

Charlotte Bauquier  
charlotte.bauquier@univ-lyon2.fr

<sup>1</sup> Inserm U1296, Radiations: Santé, Défense, Environnement, University Lumière Lyon 2, Lyon, France

<sup>2</sup> Groupe de Recherche en Psychologie Sociale UR 4163, University Lumière Lyon 2, Lyon, France

<sup>3</sup> INSERM, IRD, SESSTIM, Sciences Economiques & Sociales de La Santé & Traitement de L'Information Médicale, ISSPAM, Aix Marseille University, 13005 Marseille, France



patients themselves—about their impact on the quality of care provided, on survival, and on the risk of nosocomial infections [2, 3].

Given the context described above, it seemed particularly relevant to measure the self-reported QoL of women with cancer during the first COVID-19-related lockdown and to compare it with their retrospective evaluation of their QoL before the lockdown started in order to better understand the *patient-perceived* effect of an unpredictable collective health event (in this case, the lockdown) on QoL according to one's personal experience of cancer (i.e., with or without a history of the disease). As part of this exploration, it also seemed relevant to compare patients' self-reported QoL during the lockdown with that of women not personally exposed to cancer.

Several measures exist to assess the QoL of people both in their daily lives and when they are faced with unusual circumstances [5, 6]. Various generic standardized tools (e.g., WHOQOL, EQ-5D, SF-12)—usually in the form of questionnaires—have been developed to be able to compare the QoL of different population groups based on common QoL dimensions. The main limitation of these tools is that because they predefine the dimensions, inter-individual differences in what determines QoL cannot be captured. To overcome this, other tools have been designed which better integrate patients' individual perspectives (e.g., PGI, SeiQoL) [5, 7, 8]. All of these tools (i.e., individual-based or not) measure patient-reported outcome measures (PROMs); more specifically, they measure evaluative (i.e., as opposed to descriptive) PROMs [9]. When constructing a tool to measure PROMs, it is essential to make a cognitive evaluation (i.e., assess what goes through a person's mind he/she responds to questionnaire items) in order to improve the tool's metrological properties (i.e., reliability, validity, and sensitivity) and the quality of interpretation of the results collected [9, 10].

Evaluative PROMs are particularly sensitive to changes in the meaning of the concept of QoL and the items used to measure QoL over time. These changes are known as response shift, a term coined by Sprangers & Schwartz [11, 12]. These two authors defined three aspects of response shift: a) a change in a person's internal standards of measurement (recalibration), b) a change in a person's values (reprioritization), and c) a redefinition by a person of the target construct (reconceptualization). In a recent development of this theory, Vanier et al. [11]—based on previous work by Oort et al. [13]—define response shift in mathematical terms, as a special case of violation of the principle of conditional independence. In their model, recalibration, reprioritization, and reconceptualization inform the 'how' of response shift, but do not in themselves constitute response shift. The authors propose a revised response-shift model, indicating various pathways that a

change in PROMs can take depending on the relationships between the different components—including PROMs—of the model. These components are defined as antecedents (dispositional characteristics and environment in which the individual evolves), catalysts (life experience, necessity to change), mechanisms (individual processes adopted to adjust the catalyst), the target construct (measured concept, e.g., QoL), and measures (self-reported evaluation, e.g., PROMs). Vanier et al. emphasize that a change in self-reported measures by individuals does not necessarily reflect response shift [13].

For the present study, we used Vanier et al.'s theory to measure reprioritization and reconceptualization. The decision to measure these elements was based on the hypothesis that the event in question (i.e., COVID-19 pandemic and first lockdown) likely affected individuals and groups differently (i.e., women with cancer and those without) depending on their prior experience (i.e., antecedents) and adaptations to experience (i.e., mechanisms) they had already implemented.

Moreover, we chose to use an individualized approach to evaluate QoL to avoid predefined dimensions of QoL (see above) in the context of the COVID-19 lockdown. To do this, we developed an ad hoc quasi-individualized tool.

The aim of the study was therefore to provide a better understanding of the patient-perceived effects of France's first COVID-19 lockdown on the QoL of people affected by cancer, and to test a new measurement scale for evaluating quasi-individualized QoL. It had two complementary objectives. The first was to assess quasi-individualized QoL during an unpredictable collective health event (i.e., the lockdown) according to one's personal experience of cancer (i.e., with or without a history of the disease). The second was to assess the reprioritization and reconceptualization aspects of response shift.

## Materials and method

The data used in the present study came from a larger cross-sectional French study entitled 'Social Representations, Adaptations, Risks: Cancer and COVID-19' (RAR2C) [14]. The online self-administered questionnaire used in RAR2C was made available to potential participants on the French collaborative cancer research project platform Seintinelles from April 25 to May 7, 2020. In August 2023, Seintinelles had 38,411 subscribers, 28% of whom currently or previously had cancer; 6% were men (seintinelles.com). These percentages reflected those for 2018 (no data were available for 2020) [15].

RAR2C was conducted in accordance with French research regulations and was approved by the National



Institute for Medical Research's (INSERM) ethical committee (n°20–682) on April 14, 2020.

## Study questionnaire

In order to measure QoL, an ad hoc quasi-individualized tool that combined elements of the Patient Generated Index (PGI) and the Schedule for the Evaluation of Individual Quality of Life-Direct weighting (SEIQoL-DW) was nested inside the larger RAR2C study questionnaire. These are the two most widely used tools to measure individual QoL [5]. Both take the form of an interview guide in which respondents spontaneously name the life domains that are most important to them, rate their satisfaction with each of these domains, and indicate their relative importance to each other. The PGI asks respondents to focus on QoL changes that have occurred due to their disease, while the SeiQoL-DW looks at QoL in general at the time of data collection [5]. While both are semi-structured interview guides, the SeiQoL-DW questions are designed for the general population (i.e., not necessarily persons who are ill), while the PGI structure focuses specifically on persons who are ill. The PGI is more easily adaptable to a questionnaire format because of the standardized list of life domains pre-established.

Our ad hoc quasi-individualized tool had to be adapted to both study populations (i.e., women with and those without a history of cancer). It also had to be easy to complete online by respondents with heterogeneous characteristics. Accordingly, the modifications we made to the PGI and SEIQoL-DW to create the tool aimed to limit the cognitive cost of administering the questionnaire and missing data [16]. More specifically, based on both the standardized list of life domains proposed by the PGI when respondents struggle to spontaneously name five domains of interest to them [17], and on the results of studies conducted using the SeiQoL-DW [18], we first established a list of 15 life domains<sup>1</sup> adapted to the general population and to persons with a history of cancer. From these, participants had to select the five domains which they felt were most important to them *at the time of the study* (i.e., during the lockdown). Following this, participants indicated their level of satisfaction with each of these five domains using Likert-type scales (ranging from 1—*very dissatisfied* to 7—*very satisfied*). They then had to weight (i.e., assign a level of importance to) each of the chosen domains, not by distributing a limited number of

tokens as in the PGI, but by indicating their importance on another Likert-type scale (ranging from 1—*no importance* to 7—*great importance*). If they wished, participants could give equal weight to all five life domains.

After this, the participants answered similar questions about their QoL *before* the lockdown. Specifically, using the same structure as that described above, respondents were asked to choose the five life domains they would have considered to be the most important for them before the lockdown if had they been interviewed *at that time*, and to assess their satisfaction and the importance they would have attributed to them. This retrospective measurement was the only way to evaluate QoL before the lockdown given the context in which the study was conducted.

Besides QoL data, the RAR2C questionnaire also collected the following socio-demographic data: civil status (in a relationship or not); having one or more dependent children (or not); professionally active (or not) during France's first COVID-19-related lockdown; age (continuous variable), number of people self-isolating in the household (continuous variable), perceived economic situation (continuous variable). Furthermore, the following data on physical health were also collected: whether or not the respondent was personally diagnosed with at least one cancer, and for those with more than one cancer, the initial cancer site; whether or not the respondent had been hospitalized because of COVID-19 infection; whether or not a loved one had been hospitalized because of COVID-19 infection.

## Analyses

The present study exclusively focused on female participants in RAR2C ( $N=1303$ ). This decision was based on the fact that men only accounted for 6% ( $N=58$ ) or the RAR2C study sample, and therefore relevant sex-based comparisons would not have been possible.

Descriptive statistical analyses were performed on the socio-demographic data. Two quasi-individualized QoL scores were calculated: one for during the lockdown ('current QoL score' hereafter), and one before the lockdown ('retrospective QoL score' hereafter). These scores corresponded to the average of the satisfaction scores given for each of the five chosen life domains weighted by importance (see above). The QoL scores were then normalized on a QoL scale ranging from 0 (no QoL) to 100 (perfect QoL). Moreover, the difference between these two scores was calculated (i.e., the current score minus the retrospective score). A negative or positive net score reflected a decrease or increase in perceived QoL, respectively.

To study response shift, we also constructed a reconceptualization score and a reprioritization score.

<sup>1</sup> Relationship with children, family; Health and well-being of loved ones; Relationships with friends; Personal well-being and morale; Personal physical health; Hobbies, passions, entertainment; Autonomy, freedom, independence; Sentimental and/or sexual life; Social and cultural life; Professional life; Redesigning living environment; Domestic activities; Animal health and welfare; Involvement in associations / charities; Spiritual and/or religious life.



The former corresponded to the number of important life domains which the participant chose to measure QoL during the lockdown, but which were not selected by the participant when answering the QoL section for before the lockdown (i.e., retrospective measurement). Accordingly, this score varied from 0, reflecting no reconceptualization (i.e., the important domains selected were identical for both measurements), to 5, which reflected total reconceptualization (i.e., all five domains selected were different between the two measurements).

The reprioritization score corresponded to the sum of the distances<sup>2</sup> between the weighting (i.e., level of importance) of each of the study's 15 life domains, during the lockdown and before it. As only 5 life domains were selected by each participant for each measurement (see above), we had to infer the weighting of the 10 life domains not chosen for each measurement. In other words, we had to infer a 'non-chosen domains score.' We assumed the participant gave less importance to all of these 10 life domains than to the domain she selected with the lowest level of importance. Arbitrarily, this difference in importance systematically resulted in one point less in the non-chosen domains score. The distance was calculated according to each life domain. Thus, in the case of total reconceptualization, the 5 life domains chosen by respondents during lockdown were all different from those chosen retrospectively; consequently, 10 life domains had to be included in the calculation of the reprioritization score. Under these conditions (i.e., total reconceptualization and one less point per domain), it was necessary to include all the life domains in the calculation of the reprioritization score to harmonize it across all respondents, irrespective of their 'current' and 'retrospective' life domain choices.

As the ad hoc tool QoL we constructed *obliged* respondents to choose 5 life domains from the list of 15 life domains, we chose not to *automatically* give the 10 life domains which were not chosen a level of importance equal to zero.<sup>3</sup> Of course, if one of the chosen life domains

had the value 1, then these 10 life domains had the value 0. Accordingly, the reprioritization score ranged from 0 (no reprioritization) to 70 (maximum reprioritization).

To be able to compare all five scores (i.e., normalized current and retrospective QoL scores, QoL change score, reconceptualization score, and reprioritization score) between participants with a personal history (i.e., past or present) of cancer ('with cancer' group hereafter) and those with no such history ('without cancer' group), a specific methodological approach was required. More exactly, in this type of observational study, it is impossible to randomly assign participants to one of the two groups; the consequence of this is an imbalance between both groups in terms of socio-demographic characteristics. In our present study, this could have led to erroneous conclusions about the scores we found. Accordingly, to limit confounding variables and to ensure comparability between both groups, we weighted all 5 scores. More specifically, we used the inverse propensity score weighting (IPSW) technique [19, 20], which uses a case-control approach whereby the 'with cancer' and 'without cancer' groups were considered as 'treated' and 'control' groups, respectively.

IPSW makes it possible to construct weights using a propensity score that summarizes participants' socio-demographic characteristics into a single variable. We estimated the propensity score by implementing a probit logistic regression on the dependent variable 'with cancer' = 1 vs. 'without cancer' = 0, as recommended for random-effects models [21]. This propensity score reflected the probability that a participant in the 'without cancer' group would have been part of the 'with cancer' group based on the following characteristics: in a relationship or not (1 or 0, respectively), having one or more dependent children or not (1 or 0), professionally active during the first lockdown (1 or 0), age (continuous variable), perceived economic situation (continuous variable; from the worst situation = 1, to the best possible situation = 10), and the number of people self-isolating in the household (continuous variable). Accordingly, two participants—one from the 'with cancer' group, and the other from the 'without cancer' group—with a similar propensity score would resemble each other in terms of these characteristics. We then constructed weights for each participant as follows for both groups:

'with cancer':  $w = 1/p$  and 'without cancer':  $w = 1/1 - p$ .

These were used to weight the comparisons of means (ANOVA) of all five scores.

Furthermore, for each of the two groups we compared the global QoL change, reprioritization and reconceptualization

<sup>2</sup> The 'distance' is the difference between the weight (i.e., level of importance) assigned by the participant to life domain X during the first lockdown and the level assigned to the same life domain X for before the lockdown (i.e., retrospectively). We chose to use the term distance because we were not interested in the direction (i.e., positive or negative) of change, but simply whether or not there was a change between both measurements. For example, irrespective of whether life domain X was weighted with the value 7 in the 'current' QoL measurement, but only 5 for the 'retrospective' QoL measurement, or vice versa (i.e., net difference of +2 or -2, respectively), the number 2 would be used for the distance in both cases.

<sup>3</sup> As a result of this decision, the scale for calculating distance was changed. The initial Likert scale ranged from 1 to 7. When the minimum weighting given by a respondent to a life domain was 1, the life domains not chosen were given a weighting of 0. Accordingly, the new scale for calculating distance went from 0 to 7. Accordingly, when calculating the reprioritization score, the distance for the life domains—irrespective of their number—never chosen by a respondent

Footnote 3 (continued)

ent (i.e., neither for the 'current' nor 'retrospective' QoL measurements) was zero.



**Table 1** Sociodemographic data ( $N=1303$ )

Sociodemographic characteristics	'Without cancer' group ( $N=936$ ) M (SD) or $N$ (%)	'With cancer' group ( $N=367$ ) M (SD) or $N$ (%)	Comparison tests
Age ( $N=1302$ )	40.4 (13.3)	50.6 (11.7)	$t(1301)=17.954, p<.001$
In a relationship ( $N=1296$ )			
Yes	702 (75.5%)	255 (69.7%)	$\chi^2(1)=4.593, p<.05$
No	228 (24.5%)	111 (30.3%)	
Dependent children			
Yes	534 (57.1%)	287 (78.2%)	$\chi^2(1)=50.598, p<.001$
No	402 (42.9%)	80 (21.8%)	
Number of people self-isolating in household	2.93 (1.52)	2.48 (1.25)	$t(1301)=5.026, p<.001$
Professionally active during lockdown			
No	463 (49.5%)	239 (65.1%)	$\chi^2(2)=29.819, p<.001$
Yes, teleworking*	418 (44.7%)	120 (32.7%)	
Yes, outside the lockdown household*	85 (9.1%)	15 (4.1%)	
Initial cancer site ( $N=367$ )			
Breast		304 (82.8%)	
Other		63 (17.2%)	
At least one loved one hospitalized for COVID-19			
Yes	37 (4.0%)	10 (2.7%)	$\chi^2(1)=1.144$
No	899 (96.0%)	357 (97.3%)	
Perceived economic situation score	6.51 (1.70)	6.49 (1.61)	$t(1301)=0.208$

\*The total of these two lines slightly exceeds 601 because 37 participants (2.8%) conducted both types of activity during the lockdown

scores which had the value 0 to verify statistically that a non-null score (i.e.,  $\neq 0$ ) could be considered as not being due to chance but to a change in response (Appendix 1.).

## Results

### Participants

Among the 1303 female participants in RAR2C whose data were included in the present analysis, a minority (28.2%) had a history of cancer (i.e., past or present). Of these, 82.8% had breast cancer. None of the study sample had been hospitalized for COVID-19 infection, and only 3.6% ( $N=47$ ) had a loved one hospitalized because of the disease (Table 1).

### Quality of life

The current, retrospective, and QoL change scores were not significantly different between women with and without cancer. For both groups, the current QoL score was lower than the retrospective one (median 13 points) (Table 2). Of the five life domains chosen by the participants to describe their current QoL, four (median) were not selected for their retrospective QoL. This high level of reconceptualization

was significantly greater in the 'with cancer' group. Conversely, reprioritization was significantly lower in this group (Table 2).

## Discussion

Our analysis of the QoL data collected in the RAR2C study did not highlight any significant difference between women with and without cancer, irrespective of time (i.e., during the lockdown versus retrospectively). This result echoes findings in the literature where the QoL of people diagnosed with cancer was not necessarily poorer than that of the general population [22]. This has also been observed in fields other than oncology. These somewhat counter-intuitive findings are partly responsible for the increased interest exploring questions surrounding response shift and PROMs [11].

In contrast, with regard to reconceptualization and reprioritization, our analysis highlighted an effect of cancer status: people with a history of cancer reconceptualized more than those with no cancer history. Instead, the latter group reprioritized more. There are several possible explanations for this difference. Bargon et al. [23] put forward the idea that the COVID-19 health crisis accelerated reconceptualization in people with cancer because it promoted a new perspective of the disease. We can therefore hypothesize that



**Table 2** QoL scores before and after inverse propensity score weighting

	‘Without cancer’ group( <i>N</i> =929)		Min;Max	‘With cancer’ group ( <i>N</i> = 366)		Min;Max	F	<i>p</i>
	Mean(SD)	Median[IQR]		Mean(SD)	Median[IQR]			
<b>QoL during lockdown (i.e., current)</b> (0 to 100)								
Before weighting	58.18 (21.76)	61 [31]	0;100	54.72 (25.10)	55 [39]	0;100	6.102	.014
After weighting	56.72 (26.56)	60 [32]	0;100	56.55 (42.20)	57 [37]	0;100	.019	.890
<b>QoL before lockdown (i.e., retrospective)</b> (0 to 100)								
Before weighting	73.01 (16.59)	75 [21]	0;100	73.61 (19.52)	78 [24]	0;100	.314	.575
After weighting	73.87 (20.23)	76 [22]	0;100	72.35 (33.83)	77 [25]	0;100	2.328	.127
<b>Change in QoL</b> (− 100 to 100)								
Before weighting	− 14.63 (24.31)	− 11 [29.5]	− 97;57	− 18.40 (27.55)	− 16 [36.25]	− 97;100	5.861	.016
After weighting	− 16.80 (29.50)	− 13 [32]	− 97;57	− 15.60 (47.93)	− 13 [34]	− 97;100	.704	.401
<b>Reconceptualization</b> (0 to 5)								
Before weighting	3.53 (1.03)	4 [1]	0;5	3.66 (.945)	4 [1]	0;5	5.083	.025
After weighting	3.44 (1.21)	4 [1]	0;5	3.71 (1.72)	4 [1]	0;5	9.488	.002
<b>Reprioritization</b> (0 to 70)								
Before weighting	8.42 (5.61)	8 [7]	0;41	6.98 (4.75)	6 [5]	0;30	18.836	.000
After weighting	8.27 (6.68)	7 [7]	0;41	7.08 (8.31)	7 [6]	0;30	16.995	.000

adapting to the related lockdown also fostered reconceptualization in this population. A second possible explanation is that the process of reconceptualization may have already occurred in people with cancer who experienced a biological rupture after their cancer diagnosis was announced [24]. The upheaval caused by the announcement of a potentially fatal disease can affect individuals' personal and social identities; these people must then implement various strategies to protect their QoL.

The data collected showed a slight deterioration in self-reported QoL (i.e., a low QoL change score) score during France's first lockdown, reflecting international results [25, 26]. The timing of the data collection in the RAR2C study (approximately six weeks after the start of the lockdown on 17 March) may partly explain the deterioration perceived in QoL. More specifically, the data collection period was particularly marked by uncertainty (a lack of knowledge about the virus, how long the lockdown would be kept in place, and about the management of the pandemic post-lockdown) [1].

The lockdown may not have acted as a catalyst event for the entire sample. Ahmed et al. [27] showed that being diagnosed with a chronic disease was, in itself, not enough to cause a change in response (e.g., a patient diagnosed with a chronic disease who does not see his/her health deteriorate will not implement adaptive mechanisms). Accordingly, someone who did not perceive their QoL to be strongly impacted by lockdowns did not need to implement mechanisms to ensure an acceptable QoL. Another explanation is that strategies implemented by the participants to maintain an acceptable QoL during the lockdown may not have been very effective. More advanced analyses integrating coping,

social comparison, and social support into the model [11], which take into account antecedents (positive disease status) and the response shift (reconceptualization or reprioritization), would provide a better understanding of the processes involved.

From a methodological point of view, since the onset of the pandemic and the lockdown measures could not be anticipated, it was impossible to use a prospective study to assess their effects. RAR2C was not designed as a longitudinal study, insofar as the objective of the QoL component was to collect data, while persons were still in lockdown. For the present study, we chose to make a comparison between a 'during the lockdown' measurement and a self-reported retrospective 'before the lockdown' measurement in order to understand the *patient-perceived* effect of an unpredictable collective health event on QoL according to one's personal experience of cancer (i.e., with or without a history of the disease). Not having had QoL measures taken directly before the lockdown prevented us from being able to precisely measure the response shift. Accordingly, our measurements of reconceptualization and reprioritization need to be interpreted with caution. Although the participants were asked for a retrospective evaluation, this study is not anchored in the "then-test" approach [28]. Accordingly, it was not possible to take into account possible respondent recalibration, i.e., the first aspect of response shift (see above). Moreover, as the retrospective QoL measurement involved attempting to remember one's QoL prior to the lockdown, differences in response scores could only be the result of conscious changes in QoL that individuals attributed to the lockdown.



The implicit theory of change is an alternative hypothesis to response-shift theory [11]. In the former, retrospective measurement is less valid than prospective measurement (absent from our study, given there was no pre-lockdown measurement), as it is considered biased. In terms of the present study, according to the former theory, individuals would not remember their past QoL, they would only extrapolate it from their current QoL. On the contrary, in response-shift theory, retrospective measurement is considered more valid because it is based on the same assessment standards as the current measurement with which it will be compared [29].

Various solutions have been proposed to strengthen the choice of favoring response-shift theory over the implicit theory of change [13]. These include proposing a past event that is as salient as possible for individuals, in order to avoid a change of response that could be attributed to mood fluctuations [29] or to recall bias [13]. In our ad hoc QoL questionnaire, the wording of the instructions could have used a more specific time reference (e.g., *immediately* before the start of the lockdown). It must be remembered that the questionnaire was developed relatively hastily given the urgent circumstances of the COVID-19 health crisis in 2020. Despite the limitations associated with our retrospective measurement, it helped us add new knowledge to the literature on the measurement of the evolution of QoL during a health crisis.

Several methods can be used to assess reprioritization and reconceptualization: semi-structured interviews, individualized methods, and even statistical tools under certain conditions (e.g., Structural Equation Modeling) [13]. Questionnaires measuring individualized QoL have the advantage of allowing individuals to define what they consider to be QoL. Furthermore, many more participants can be questioned than with interviews or individualized methods. For the present study, we adapted the PGI and the SeiQoL-DW to create an ad hoc online self-administered questionnaire to measure quasi-individualized QoL (creating an imposed list of 15 predefined life domains). This strategy has the advantage of facilitating standardization, in the sense that this ad hoc tool could be used in the future for the general population in various contexts. Furthermore, it could be used for health comparisons between different groups (e.g., people with a history of cancer, those suffering from chronic diseases, care providers, etc.).

Nevertheless, the imposed list of life domains in the questionnaire constrained respondents' responses to a certain extent. It limited them in terms of how much they could respond spontaneously using their own words, and in how to make sense of their experience.

For this reason, our approach should be considered more quasi-individualized than fully individualized.

Consequently, our reconceptualization scores may have been subject to interpretation bias in our attempt to explain the observed deterioration in individual QoL using the response-shift model [9, 11].

When completing a QoL questionnaire (i.e., in general), if an individual is very worried about certain life domains, he/she will mention them as being important in his/her current life and will provide low satisfaction scores for them. We remind the reader that respondents in our study were obliged to choose 5 life domains—no more and no less—from a fixed list of 15. It is therefore possible that not all the life domains matching the respondents' definition of QoL were covered in their responses. Consequently, the life domains that concerned individuals during the lockdown (and which they listed) may not have been cited for the retrospective measurement. This could be explained by the fact that respondents were aware that these domains did not worry them as much before the lockdown started, and they therefore chose to mention other domains that were more important to them at the time of questionnaire completion. Accordingly, changes in the life domains chosen may have been more an indicator of a heavy emotional burden associated with some life domains at the time of questionnaire completion (i.e., current QoL score) than proof of reconceptualization.

## Conclusion

This study aimed to provide a better understanding of the patient-perceived effects of France's first COVID-19 lockdown on the QoL of people affected by cancer, and to test an ad hoc measurement scale for evaluating quasi-individualized QoL. It had two complementary objectives. The first was to assess quasi-individualized QoL during an unpredictable collective health event—specifically France's first COVID-19-related lockdown—according to one's personal experience of cancer (i.e., with or without a history of the disease). The second was to assess the reprioritization and reconceptualization aspects of response shift.

Our ad hoc tool could be tested in other populations (e.g., men, care providers, persons with pathologies other than cancer, etc.) to measure its acceptability, reliability, and sensitivity to change.

**Supplementary Information** The online version contains supplementary material available at <https://doi.org/10.1007/s11136-024-03626-y>.

**Acknowledgements** The authors would like to thank all the people who contributed to the population-based cross-sectional study RAR2C, which investigated the impact of the COVID-19 crisis and the related first lockdown in France: C. Carpentier (PhD student), J. Devif (PhD student), B. Douffet (PhD student), D. Ferraz (PhD), M. Girodet (PhD), N. Kalampalikis (PhD, PU), A. Le Bonniec (PhD), X. Mabire (PhD), T. Marmorat (PhD student), P. Mercier (PhD student), C. Morin-Messabel (PhD, PU), A.S. Petit (PhD student), M. Perray (PhD student), C.



Puppo (PhD student), S. Rouat (PhD, MCF), A. Siméone (PhD, MCF), and Emilie Vayre (PhD, PU).

**Author contributions** All authors contributed to the study conception and design. CB, SG, TL, and MD conducted the analyses. CB, SG, TL, MD, and MP wrote the first draft of the manuscript. MP supervised this work. All authors commented on the previous versions of the manuscript and read and approved the final manuscript.

**Funding** This work has supported by IDEX Lyon.

**Data availability** The data that support the findings of this study are available from the corresponding author, CB, upon reasonable request.

## Declarations

**Competing interest** The authors have no relevant financial or non-financial interests to disclose.

**Ethical approval** RAR2C was conducted in accordance with French regulations and was approved by the Ethics Evaluation Committee of the National Institute for Medical Research (INSERM) n°20-682 on April 14, 2020.

**Consent to participate** Informed consent was obtained from all individual participants included in the study.

## References

- Fouques, D., Castro, D., Mouret, M., Julien-Sweerts, S., & Romo, L. (2021). Perceptions of the post first-lockdown era in the current covid-19 pandemic: Quantitative and qualitative survey of the French population. *Frontiers in Psychology, 12*, 668961.
- Gultekin, M., Ak, S., Ayhan, A., Strojna, A., Pletnev, A., Fagotti, A., et al. (2021). Perspectives, fears and expectations of patients with gynaecological cancers during the COVID-19 pandemic: A pan-European study of the European Network of Gynaecological Cancer Advocacy Groups (ENGAGE). *Cancer Medicine, 10*, 208–219.
- Institut National du Cancer. (2020). Préconisations pour l'adaptation de l'offre de soins des établissements accueillant les patients atteints de cancer dans le contexte de l'épidémie de COVID-19.
- You, B., Ravaud, A., Canivet, A., Ganem, G., Giraud, P., Guimbaud, R., et al. (2020). The official French guidelines to protect patients with cancer against SARS-CoV-2 infection. *The Lancet Oncology, 21*, 619–621.
- Wettergren, L., Kettis-Lindblad, Å., Sprangers, M., & Ring, L. (2009). The use, feasibility and psychometric properties of an individualised quality-of-life instrument: A systematic review of the SEIQoL-DW. *Quality of Life Research, 18*, 737–746.
- Wettergren, L., Hedlund Lindberg, M., Kettis, Å., Glimelius, B., & Ring, L. (2014). Comparison of two instruments for measurement of quality of life in clinical practice—A qualitative study. *BMC Medical Research Methodology, 14*, 115.
- Ruta, D. A., Garratt, A. M., Leng, M., Russell, I. T., & Macdonald, L. M. (1994). A new approach to the measurement of quality of life: The patient-generated index. *Medical Care, 32*, 1109–1126.
- McGee, H. M., O'Boyle, C. A., Hickey, A., O'Malley, K., & Joyce, C. R. B. (1991). Assessing the quality of life of the individual: The SEIQoL with a healthy and a gastroenterology unit population. *Psychological Medicine, 21*, 749–759.
- Rapkin, B. D., & Schwartz, C. E. (2019). Advancing quality-of-life research by deepening our understanding of response shift: A unifying theory of appraisal. *Quality of Life Research, 28*, 2623–2630.
- Schwartz, C. E., & Rapkin, B. D. (2004). Reconsidering the psychometrics of quality of life assessment in light of response shift and appraisal. *Health and Quality of Life Outcomes, 2*, 16.
- Vanier, A., Oort, F. J., McClimans, L., Ow, N., Gulek, B. G., Böhnke, J. R., et al. (2021). Response shift in patient-reported outcomes: Definition, theory, and a revised model. *Quality of Life Research, 30*, 3309–3322.
- Sprangers, M. A. G., & Schwartz, C. E. (1999). Integrating response shift into health-related quality of life research: A theoretical model. *Social Science & Medicine, 48*, 1507–1515.
- Sprangers, M. A. G., Sawatzky, R., Vanier, A., Böhnke, J. R., Sajobi, T., Mayo, N. E., et al. (2023). Implications of the syntheses on definition, theory, and methods conducted by the response shift—In Sync Working Group. *Quality of Life Research, 32*, 2165–2178.
- Della Vecchia, C., Girodet, M., Ginguéné, S., Carpentier, C., Leroy, T., Siméone, A., et al. (2022). At the heart of the COVID-19 crisis: Perceived concerns of changes in long-term cancer care in French women with cancer. *European J Cancer Care, 31*, e13599.
- Pannard, M., Bauquier, C., Bassoleil, L., Sablone, L., Jacob, G., Rey, F., et al. (2020). Ces citoyen(nes) qui se portent volontaires pour participer aux recherches dans le champ du cancer—résultats du Baromètre Seintinelles 2018. *Bulletin du Cancer, 107*, 333–343.
- Dijkers, M. P. (2003). Individualization in quality of life measurement: Instruments and approaches. *Archives of Physical Medicine and Rehabilitation, 84*, S3–14.
- Botella, M., Zenasni, F., Pocard, M., Gledill, J., & Rodary, C. (2007). Adaptation française du Patient Generated Index: Qualités métrologiques et limites pratiques: French adaptation of the patient generated index: Metric characteristics and practical limitations. *Psycho Oncologie, 1*, 131–140.
- Stone, P. C., Murphy, R. F., Matar, H. E., & Almerie, M. Q. (2008). Measuring the individual quality of life of patients with prostate cancer. *Prostate Cancer and Prostatic Diseases, 11*, 390–396.
- Rosenbaum, P. R., & Rubin, D. B. (1983). The central role of the Propensity score in observational studies for causal effects. *Biometrika, 70*, 41–55.
- Guo, S., & Fraser, M. W. (2015). *Propensity score analysis: Statistical methods and applications* (2nd ed.). Sage Publications, Inc.
- Hahn, E. D., & Soyer, R. (2005). Probit and logit models: differences in the multivariate realm. *The Journal of the Royal Statistical Society, Series B*, 1–12.
- De Haes, J. C. J. M., & Van Knippenberg, F. C. E. (1985). The quality of life of cancer patients: A review of the literature. *Social Science & Medicine, 20*, 809–817.
- Bargon, C., Batenburg, M., van Stam, L., van der Molen, D. M., van Dam, I., van der Leij, F., et al. (2020). The impact of the COVID-19 pandemic on quality of life, physical and psychosocial wellbeing in breast cancer patients—A prospective, multicenter cohort study. *European Journal of Cancer, 138*, S17.
- Bury, M. (1982). Chronic illness as biographical disruption. *Sociology of Health and Illness, 4*, 167–182.
- Epifanio, M. S., Andrei, F., Mancini, G., Agostini, F., Piombo, M. A., Spicuzza, V., et al. (2021). The impact of COVID-19 pandemic and lockdown measures on quality of life among Italian general population. *Journal of Clinical Medicine, 10*, 289.



26. Poder, T., Dufresne, E., He, J., Talba, L., & Da Silva, R. B. (2021). Qualité de vie reliée à la santé et confinement: analyse des effets et des facteurs de risque. *International Journal of Health Preference Research*, 1, 2–26.
27. Ahmed, S., Sawatzky, R., Levesque, J.-F., Ehrmann-Feldman, D., & Schwartz, C. E. (2014). Minimal evidence of response shift in the absence of a catalyst. *Quality of Life Research*, 23, 2421–2430.
28. Ahmed, S., Mayo, N. E., Wood-Dauphinee, S., Hanley, J. A., & Cohen, S. R. (2005). The structural equation modeling technique did not show a response shift, contrary to the results of the then test and the individualized approaches. *Journal of Clinical Epidemiology*, 58, 1125–1133.
29. Norman, G. (2003). Hi! How are you? Response shift, implicit theories and differing epistemologies. *Quality of Life Research*, 12, 239–249.

**Publisher's Note** Springer Nature remains neutral with regard to jurisdictional claims in published maps and institutional affiliations.

Springer Nature or its licensor (e.g. a society or other partner) holds exclusive rights to this article under a publishing agreement with the author(s) or other rightsholder(s); author self-archiving of the accepted manuscript version of this article is solely governed by the terms of such publishing agreement and applicable law.





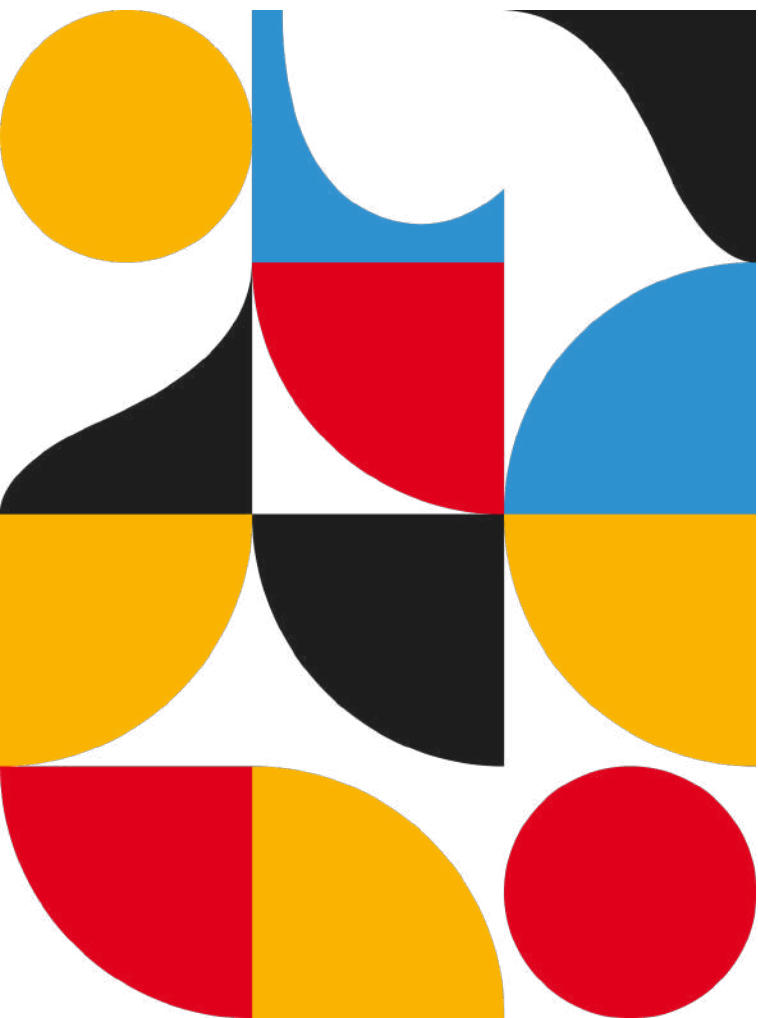
Dulce Ferraz  
Fiocruz Brasília, Fundação Oswaldo Cruz, Brazil  
Institut de Psychologie, Université Lumière Lyon 2, France  
UMR1296

## HIV Prevention

# Community-based research (CBR) for advancing PrEP access among key populations







**I have no conflict of interest to declare**





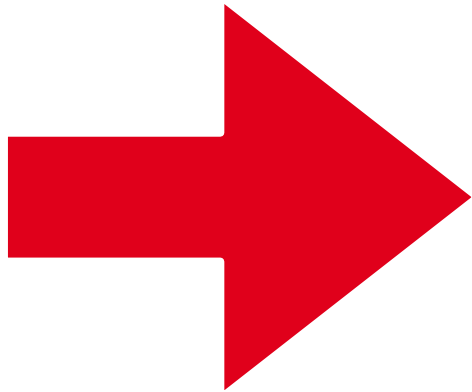
# PrEP access



# PrEP access is slowly progressing globally

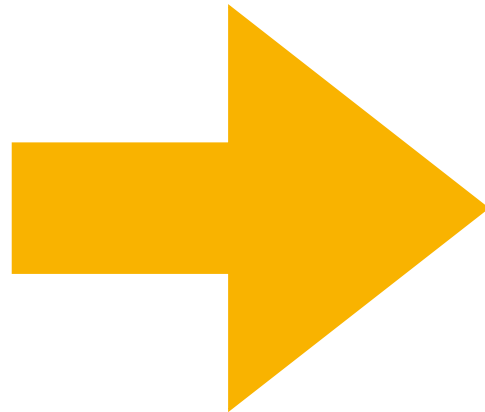


2017



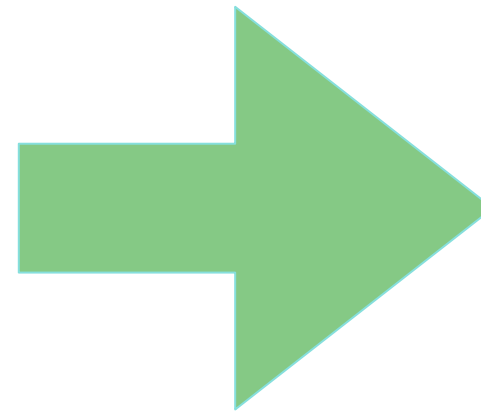
200.000

2023



3.5 million

2025



10 million

2030







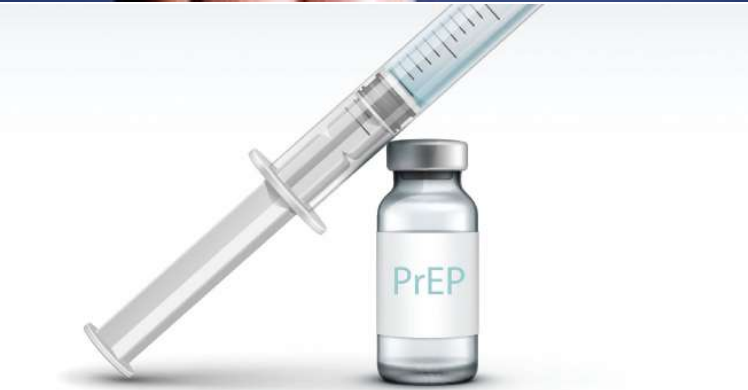
# PrEP has not yet reached scale for impact



Biggest gaps among people from key populations in low- and middle-income countries (Unaids, 2023)

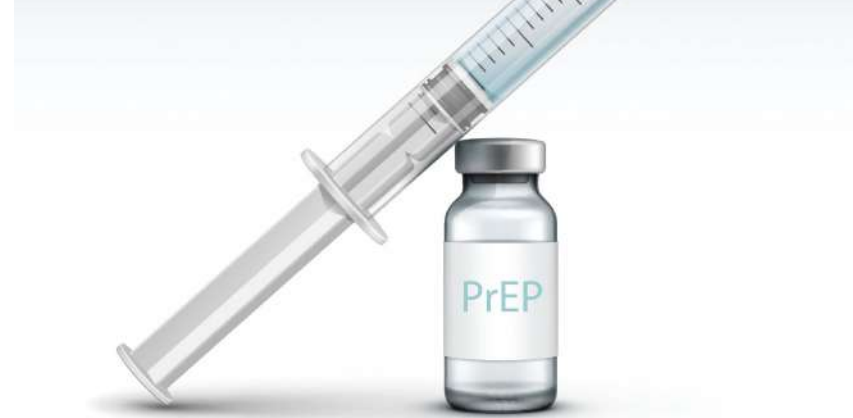
Increasing number of options

Low uptake among KY, despite good levels of awareness and acceptability (Guifang et al, 2023)





# Affordability



# Funding

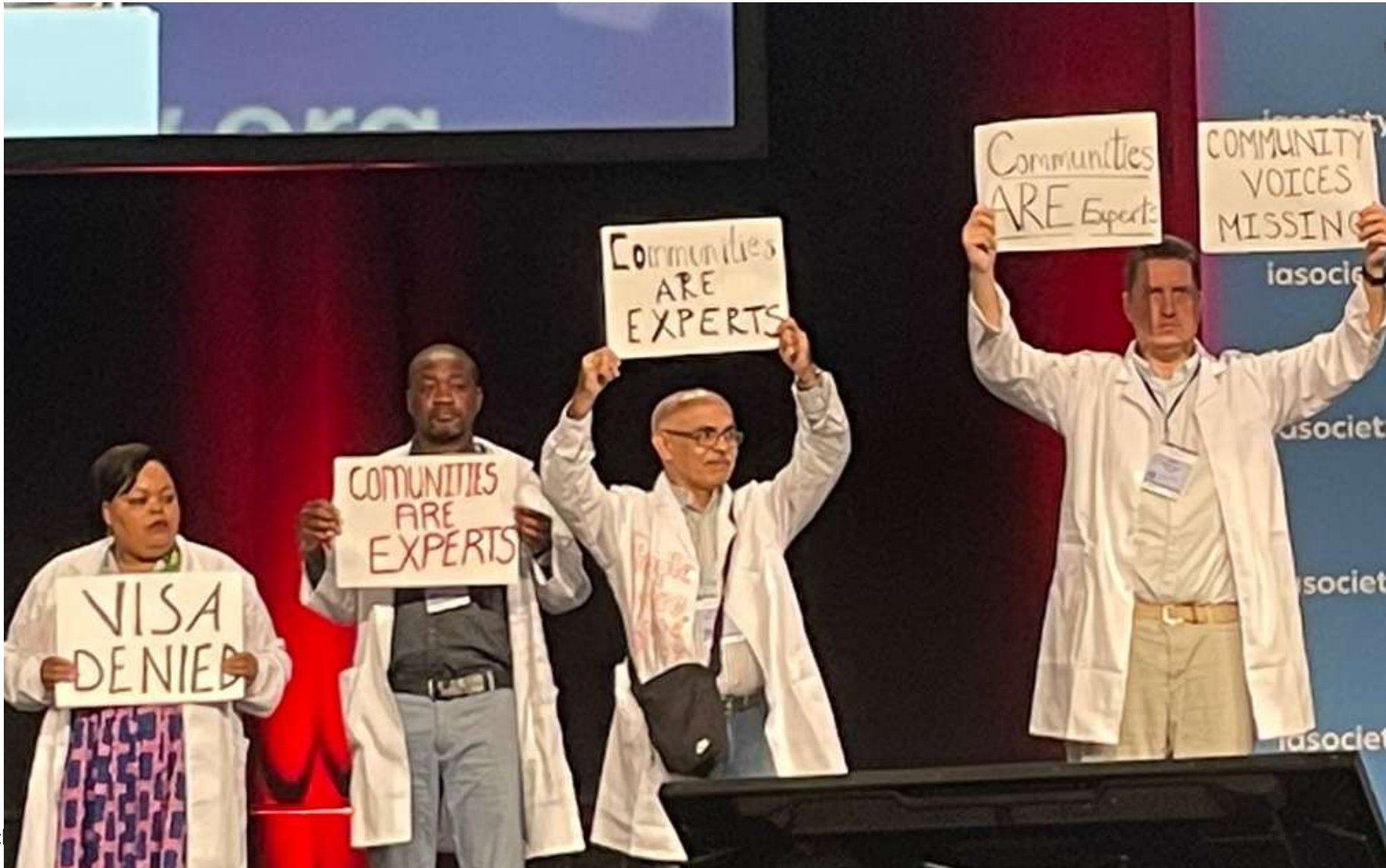


# Political setbacks





# Community-based research





# Community-based research

**Various expertises**

**Experiential knowledge ↔  
technical knowledge**

**Power balance**

**Power balance**

**Communities as agents**

**Bottom-up approach**

**Participation at all stages of  
research**

**Scientific rigor**



# Communities, participation and research



**1940's**

**Kurt Lewin, action research in social psychology, research for social transformation**

**1960/70's**

**1960's, 1970's, SSH searching for methods that would allow science to contribute to social justice: Paulo Freire, Silvia Lane, Orlando Fals-Borda, etc**

**80's - on**

**HIV and the emphasis on participation and research guided by the communities needs  
Community-based research (CBR)**





**FOR HIV-NEGATIVE GUYS**

**Communities of people living with and affected by with HIV have created responses that science would later recognize and demonstrate to be the most effective responses do HIV**





# Communities struggles for social justice led to **human rights-based HIV responses, still the best approaches to HIV**

(Gruskin et al 2010; Becker et al, 2019)



Prevention and treatment are political,  
rather than just technical issues

Solidarity is the response

Participation as a core principle and  
human right





# **Communities and PrEP for Key Populations: what is being done (and published)?**



## Ongoing systematic review on the potentials and barriers of community-based approaches to PrEP delivery\*

**Research question:** What is known about the effectiveness, implementation, and outcomes of delivering HIV pre-exposure prophylaxis (PrEP) through community-based approaches?

**Focus:** different forms of organization of services, their potential and barriers, and the results on PrEP delivery

\*Cristiane Spadacio, Lorrúan Alves, Dulce Ferraz, Marcia Couto, Alexandre Grangeiro



# Ongoing systematic review: methods

("preexposure prophylaxis" OR "pre-exposure prophylaxis" OR PrEP) AND ("HIV" OR "HIV infection") AND ("Community-Based Participatory Research" OR "Community Participation" OR "community-engaged implementation" OR "social participation" OR "peer group" OR "Peer influence" OR "community")

Pubmed, Scopus, WoS, Scielo, Lilacs

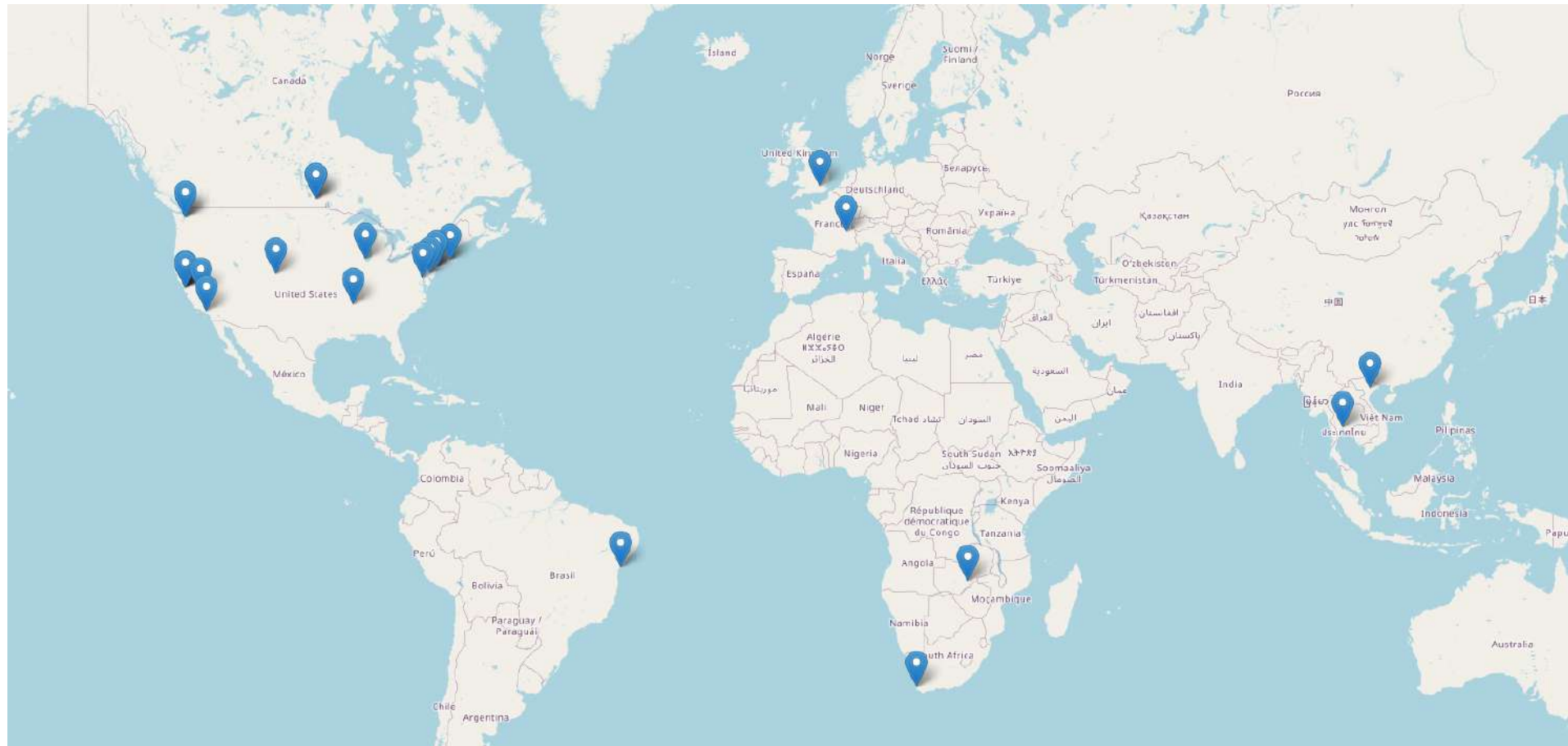
- References: 5.642
  - Duplicates: 3.187
    - Title/abstract read: 2.455
      - Total references for data extraction and analysis: 42
        - **28 included after full-text read**



# Ongoing systematic review: preliminary results



Countries where the 28 studies were conducted





# Ongoing systematic review: preliminary insights



24

Trans women, men who have sex with men, young people, sex workers, LGBT community, cisgender women, fishers, serodiscordant couples



## Demonstration studies

Real-life data contributing to incorporate PrEP on national HIV prevention programs

India, Brazil, Kenya, Uganda, Senegal, South Africa



Often building on community-based health services that **previously existed** and incorporated PrEP

Thailand, India, Kenya and Uganda



# Ongoing systematic review: preliminary insights



More community-based  
**interventions** than research

Different ways of framing and  
naming CBR and participation?  
Insufficient of systematization of  
methods?

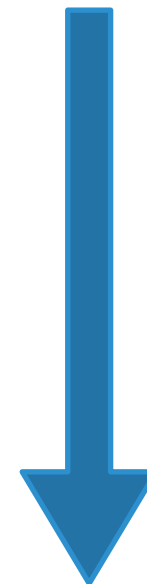


## **Community participation**

Outreach, recruitment, peer-navigation

Community consultation and advisory  
groups providing input on study design  
and implementation PrEP dispensation

Services design, HIV testing, PrEP  
dispensation, communication of test  
results





# Ongoing systematic review: preliminary insights



**Positive results** observed when PrEP is delivered in/by the community, along with evidences of KP preferences for community-based services in some settings, **reinforce the potential benefits of community-led services**

Creating safe spaces and trust

Effectiveness in engaging, recruiting and supporting KP in PrEP

Better adherence and retention than clinical trials



# How can we improve even further community participation on PrEP research with key populations?



Are communities playing key roles in PrEP research?

What are the valued community expertises?

➡ Participation in designing PrEP delivery models ⬅

## LET COMMUNITIES LEAD

 World AIDS Day 2023





**People-centered care**

**Differentiated service delivery**

**Integrated, comprehensive, empowering, stigma-free**

Clinical, hospital settings

Clinically trained providers

Follow-up visits

Community  
settings

Status  
neutral

Home-  
based

School-  
based

Pharmacy-  
based

Mobile  
clinics

PrEP  
machines



**"I dare you to find a  
challenge communities  
cannot solve"**



**CBR supports with:**

Theoretical and methodological tools

Co-developing DSD: efficient organization of care, using resources that were already available, adapting to health systems specificities and limitations

Systematizing and publishing evidences



# Using CBR to let communities lead the design of PrEP services



**Further investing on community-led  
PrEP services design**

**Demedicalize our conceptions of PrEP  
services**

**Developing and systematizing  
community-based conceptions**





## Planning with communities: Designing non-discriminatory, rights-based, youth-friendly PrEP services for adolescents (36)

### Brazil

A study in São Paulo, Brazil, has documented how programmes aimed at improving providers' knowledge of HIV prevention and their ability to provide tailored care can reduce stigma-related barriers. A sub-study, nested within the PrEP 1519 study, interviewed adolescents to learn their perspectives on pre-exposure prophylaxis (PrEP) services. The study concluded that providing youth-friendly differentiated services based on upholding adolescents' human rights is crucial to ensuring their engagement and adherence in HIV prevention and care.

The study explored with participants the importance of various aspects of human rights in service delivery and how these aspects mattered to them. Using an approach grounded in the standards and principles central to a rights-based approach to health service delivery, the study found that all participants valued inclusion and equal treatment, including using clients' chosen pronouns, protecting privacy and confidentiality and seeing themselves represented in the clinic by health care workers who were also part of their community. In addition, the following actions were significant to a person-centred approach:

- ◆ providing a safe space for adolescents to feel accepted
- ◆ relaying information in a youth-friendly way
- ◆ using clear language
- ◆ supporting young people's capacity to make autonomous, well-informed decisions for their own health.

This example shows how embedding a study within a large trial can provide insights on community priorities for addressing stigma, discrimination and human rights. These insights can inform the planning and delivery of quality health services.

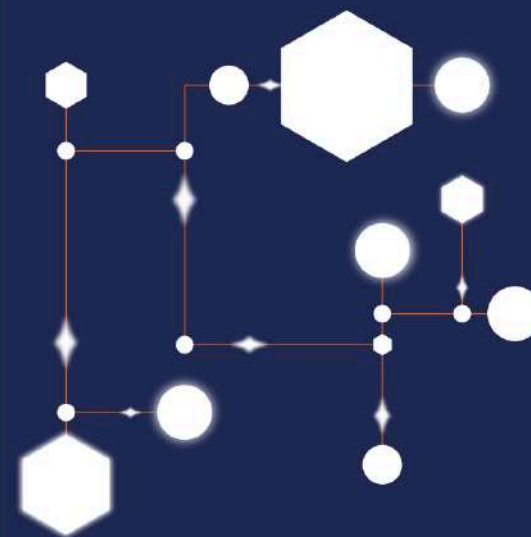
Involving communities in planning and holding facilities to account is an important quality improvement approach and can bring stigma reduction to the fore in HIV prevention services.



© Luiz Felipe Alves de Sousa

## Ensuring quality health care by reducing HIV-related stigma and discrimination

Technical brief





# Funding

## **The gap is widening**

Declines in both international and domestic funding (UNAIDS, 2024)

The end of scale-up of the global AIDS response? (Parker, 2024)

## **Additional public health priorities**

Climate change and its immediate, mid- and long-term impact due to displacement and migration (Ferraz & Barreira, 2024)

## **Reduced number of donors**

66% of all the funds provided by private philanthropic sources: Gilead and BMGF (Parker, 2024)

Bilateral funding from US government: 58% of all international assistance for HIV (UNAIDS, 2023)

## **Rules of research funding often limits communities remuneration**

Failure to recognize the need of experiential expertise in the production of scientific knowledge





# **Beyond delivery models: structural and political barriers to PrEP access**





# Communities struggles for social justice led to **human rights-based HIV responses, still the best approaches to HIV**

(Gruskin et al 2010; Becker et al, 2019)



Prevention and treatment are political,  
rather than just technical issues

Solidarity is the response

Participation as a core principle and  
human right



## Cabotegravir long-acting PrEP out of reach for upper middle-income nations

Keith Alcorn | 8 February 2023 | Estimated reading time 5 minutes



PrEP activists at the AIDS 2022 conference in Montreal. Photo©Jordi Ruiz Cirera/IAS

Most effective PrEP registered for use

ViiV Healthcare: voluntary license allowing 90 countries to buy generic versions of CAB-LA excludes upper UMIC outside Africa

### Excluded countries

122,000 new infections per year (8% of global HIV incidence)

7.7 million people in the excluded countries would need to take cabotegravir to prevent these 122,000 infections

**\$11 billion a year**

(Pepperell et al, 2022)

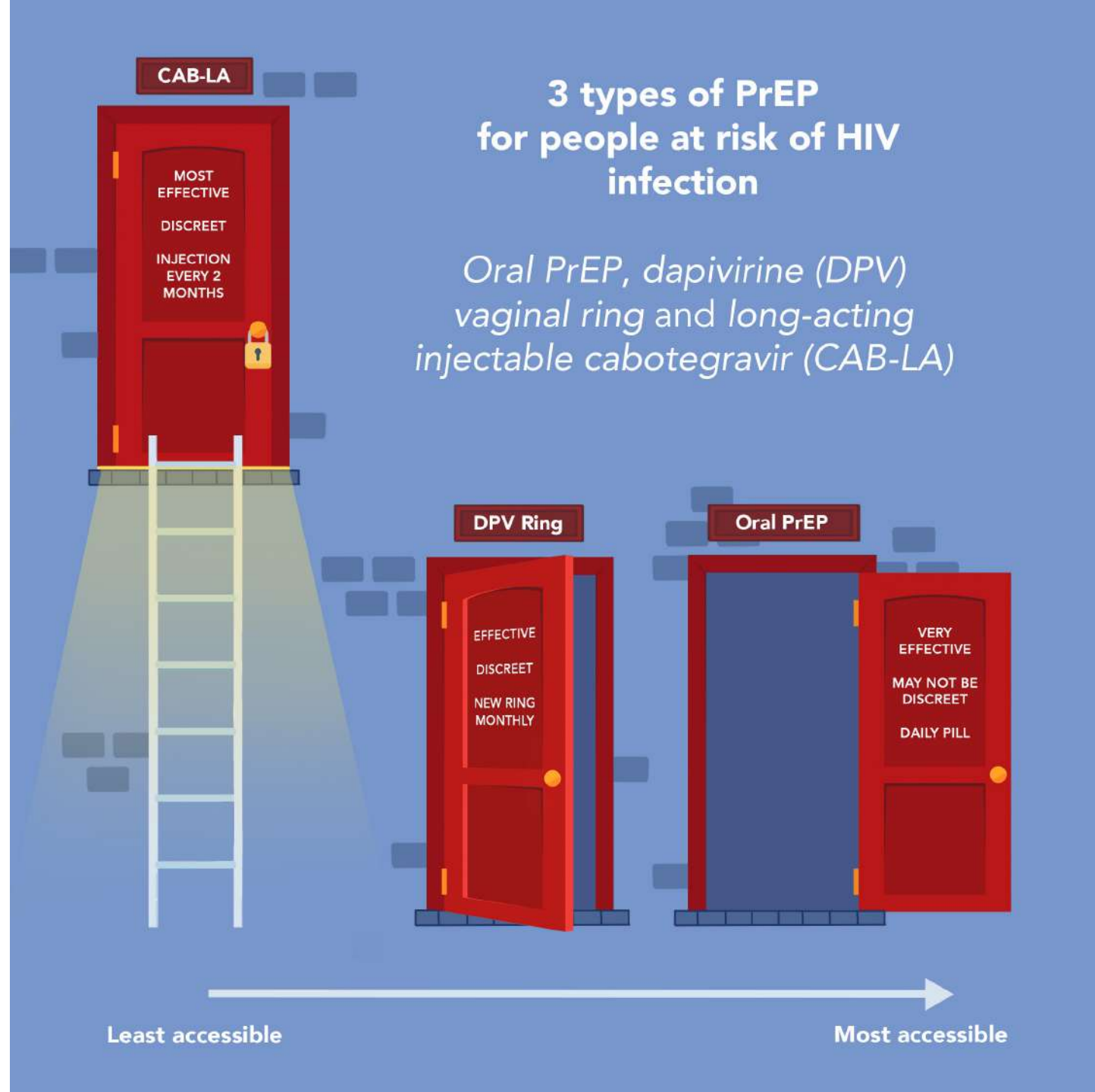


**Affordability is an ongoing challenge and priority**

**Investing in new CBR?**

**Will current demonstration studies on CAB-LA in LIMC effectively inform public policy?**

MSF CAB-LA access campaign





## Lenacapavir injections

"If this PrEP option is made available rapidly and affordably to potential users, it could herald a breakthrough for HIV prevention"

(UNAIDS, 2024)

**Global governance and global solidarity**



**AFRICAN WOMEN**  
**Prevention Community**  
**Accountability Board**

**Acknowledge and celebrate the crucial role of African women and communities in this study**

Call on Gilead to:

Demonstrate its commitment by immediately ensuring access through open-label extension studies

Outline a transparent roadmap for regulatory approvals, manufacturing scale-up, and distribution

**Act quickly in translating these trial results into real-world access**





# Stigma and human-rights abuses



# Global political scenario

Not quite a positive one for (our) communities,  
nor science

Political backlash marked by **anti-democratic**  
movements: anti-rights, anti-gender, anti-  
science



U.S., 2022



Canada, 2023



# Brazil as an example



A case study?

2010's: Advancement of the conservative agenda

Direct attacks on the AIDS response

Government capitulation: negotiating with those attacking our rights + letting go of the political debate on which the technological advances depend on

2018: democratically (?) handing the power to those leading the anti-rights, anti-science agendas



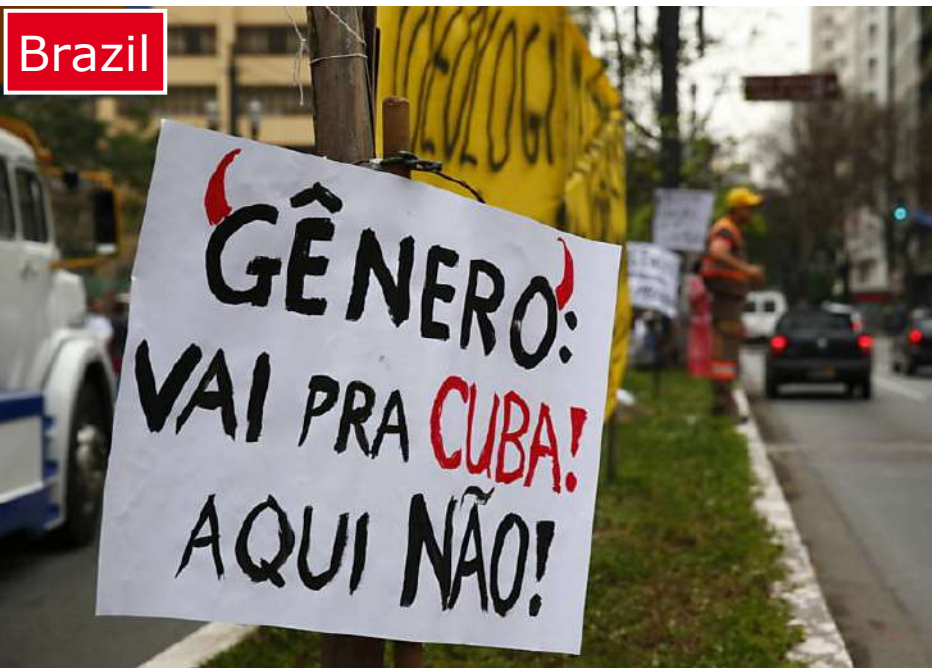


# What happened in Brazil should keep us watchful globally

Anti-gender movements: connected, well funded and spreading (since their defeat in Cairo and Beijing)

Correa, 2018; Murray, 2022

Growth of far-right, democratically elected governments





# Backsliding on SSHR: huge global push on hard-won rights



## Conservative Member States Balk at References to 'Gender' in WHA Resolutions

World Health Assembly 77 28/05/2024 • Kerry Cullinan

## Reverse the Backsliding on Sexual and Reproductive Health and Rights: A Wake-up Call from Independent Scientists and Advisors

Inside View 24/05/2024 • Independent scientists and members of UN advisory groups for SRH



SCIENCEINSIDER HEALTH

# 'A bloodbath': HIV field is reeling after billions in U.S. funding are axed

USAID's promises to support lifesaving efforts are broken, putting millions in peril

28 FEB 2025 • 3:55 PM ET • BY JON COHEN



SHARE:



more useful. Ho



# Global anti-trans crusade

“Strange bed fellows” (Platero, 2023): anti-trans feminists, TERF, conservative parties and their supporters, (some) scientists

Laws prohibiting gender-affirmative care, care that is positively associated with PrEP awareness and uptake (Dang et al, 2022)

Children and young people





# Science without experts?

Review about the provision of care to trans and non-binary youth and children in England and Wales, **commissioned by the NHS in 2020 in response to the increase in children and young people seeking referral to gender identity services**

Headed up by pediatrician with **no prior experience** in trans health + no competitive process

**Expertise = bias?**

**Community participation?**

Concludes that the evidence for trans-affirmative care for these groups is **insufficient**

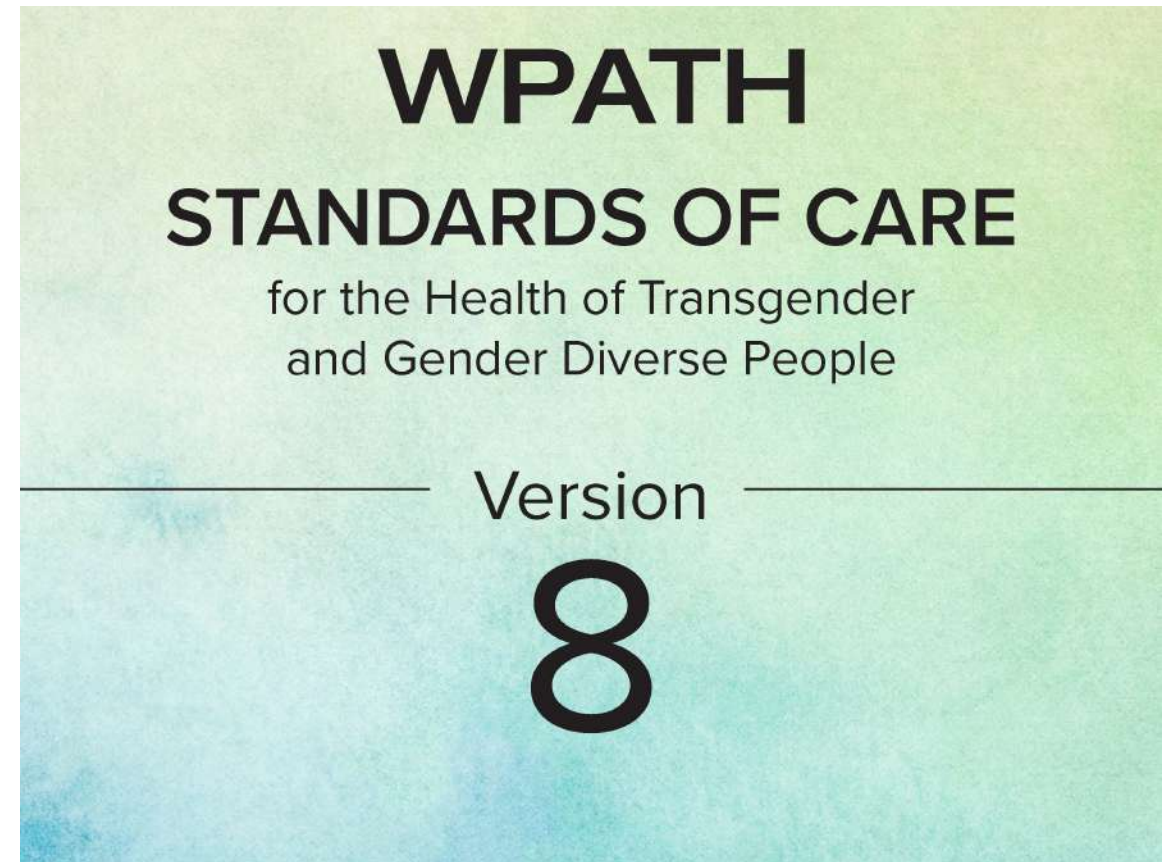




# Scientific, community-based guidelines exist

**"Based on far more systematic reviews that the Cass Review (...) considers that the evidence is such to recommend that providing medical treatment including puberty-blocking medication and hormone therapy is helpful and often life-saving for young TGD people, while withholding such treatment may lead to increased gender dysphoria and adversely affect psychological functioning".**

Access to gender-affirmative care is positively **associated with PrEP awareness and uptake** (Danger al, 2023)







# Methodological flaws and cisnormative scientific bias

## An Evidence-Based Critique of “The Cass Review” on Gender-affirming Care for Adolescent Gender Dysphoria

Meredithe McNamara, MD MSc, Assistant Professor of Pediatrics, Yale School of Medicine

Kellan Baker, PhD, MPH, MA, Executive Director, Whitman-Walker Institute

Kara Connelly, MD, MCR, Associate Professor of Pediatrics, Division of Endocrinology and Metabolism, Oregon Health & Science University

Aron Janssen, MD, Associate Professor of Psychiatry and Behavioral Sciences, Northwestern University



Research Article

## The Cass Review: Cis-supremacy in the UK’s approach to healthcare for trans children

Cal Horton 

Published online: 14 Mar 2024

 Cite this article  <https://doi.org/10.1080/26895269.2024.2328249>



## WPATH AND USPATH COMMENT ON THE CASS REVIEW

May 17, 2024

The recently published Cass Review is the result of a four-year investigation initiated by the United Kingdom’s National Health Service England (NHSE) into the scientific basis of treating gender dysphoria in youth and the experiences of those involved in transgender care in the UK. It makes 12 recommendations for a reorganization of transgender care for youth in England and Wales. The review took place after concerns arose around the increase in referrals, the cost of gender-affirming medical care, and the functioning of the NHS Tavistock Gender Identity Development Service (GIDS), the only national care service with a long history of clinical experience and knowledge, which had operated since 1989 and was closed in March 2024. To date there are no new services in operation, and there will be none in the foreseeable future, despite what NHS England or Hillary Cass may claim. WPATH and USPATH are extremely concerned that this has left young transgender and gender diverse people and families with little opportunity to obtain transgender care. This is a



# Weaponized by anti-trans movements

OPINION

## Bombshell trans report shows ideologues railroad kids into irreversible treatments with no evidence

Key findings of the Cass report: stop giving drugs to children and rushing them into treatment

## Cass Review: A victory for women, children and common sense

The Cass report and the unforgivable puberty blockers scandal

# Services shut down

## Children to stop getting puberty blockers at gender identity clinics, says NHS England

Confirmation comes after public consultation and decision to close Gender Identity Development Service in London







# To conclude



# **Put people first and communities at the centre in PrEP research**

**CBR can continue to help further improving PrEP access among KP**

**Enabling communities to lead service design**

**Adequate funding is needed**



# **Put people first and communities at the centre in PrEP research**

**Solutions may be beyond our medicalized conceptions of healthcare**

**Global action to ensure PrEP access and to protect human rights**

**Solidarity continues to be the key**



# Acknowledgements

## Consulted researchers and community leaders:

- \*Alexandre Grangeiro (USP)
- \*Bruno Spire (Inserm)
- \*Eliana Miura Zucchi (UniSantos)
- \*Erika Castellanos (GATE)
- \*Inês Dourado (UFBA)
- \*Laio Magno (UDEB)
- \*Laura Ferguson (USC)
- \*Marie Préau (Lyon 2)





# Research teams

**Combina Study**



**PI: Alexandre Grangeiro, Marcia Couto**

Lorruan Alves dos Santos, Eliana Miura Zucchi, Dulce Ferraz, Andrea Fache Leal, Denise Lotufo, Érico Arruda, Juliane Santos, Maria Mercedes Escuder, Ramiro Unsain, Renata Moraes, Rosemeire Munhoz, Alan Silveira, Bruno Kauss, Dennis Leite, Jonatan Pereira da Silva, Luiz Fabio Alves de Deus, Maria Eugênia Paiva do Amaral, Thiago Reis

Funding: MoH, CNPq

**PrEP1519 Study**



**PI: Inês Dourado, Alexandre Grangeiro, Dirceu Greco**

Fabiane Soares, Priscilla Caires, Joilson Paim, Lorenza Dezanet, Marluce Carvalho, Beo Leite, Lucas M. Marques, Guilherme B. Campos, Diana Zeballos, Suilan Pedreira, Orlando Ferreira, Nathalia Suzarth, Suelen Seixas, Ícaro Ramos, Thiago Farias, Adenil Neto, Luís Fernando Guimarães, Nathale Lopes, Ívina Lopes, Lua Rodrigues, Andresa Galvão

Dirceu B. Greco, Unaí Tupinambás, Mateus Westin, Walter Ude, Marília Greco, Ana Paula Silva, Érica Dumont, Júlio Andrade, Matheus Alves, Franciele Profeta

Alexandre Grangeiro, Paula Massa, Marcia Couto, Eliana Miura Zucchi, Dulce Ferraz, Lina L. Lucas, Eduardo Oliveira, Luiz Felipe A. De Sousa, Dana Fitipaldi, Dyemison Da Silva, Caroline Dressler de Souza, Eliane Aparecida Sala, Rafael Gonçalves Kosi, Douglas dos Santos, Carolina Cardona, Simone Rocha Figueiredo, Aline Gil Alves Guilloux, Ghabriel Teixeira de Oliveira, Nala Ayaba Santos, Samir dos Santos Junior, Alice Rodrigues Furlaneto, Samylla Costa de Moura, Ramiro Unsain, Luiz Fabio Alves de Deus, Paola Alves de Souza

Funding: Unitaid



# Research teams

## ANRS-COBra

**PI: Inês Dourado and Marie Préau**



22 – 26 July · Munich, Germany and virtual

Funding: ANRS|MIE

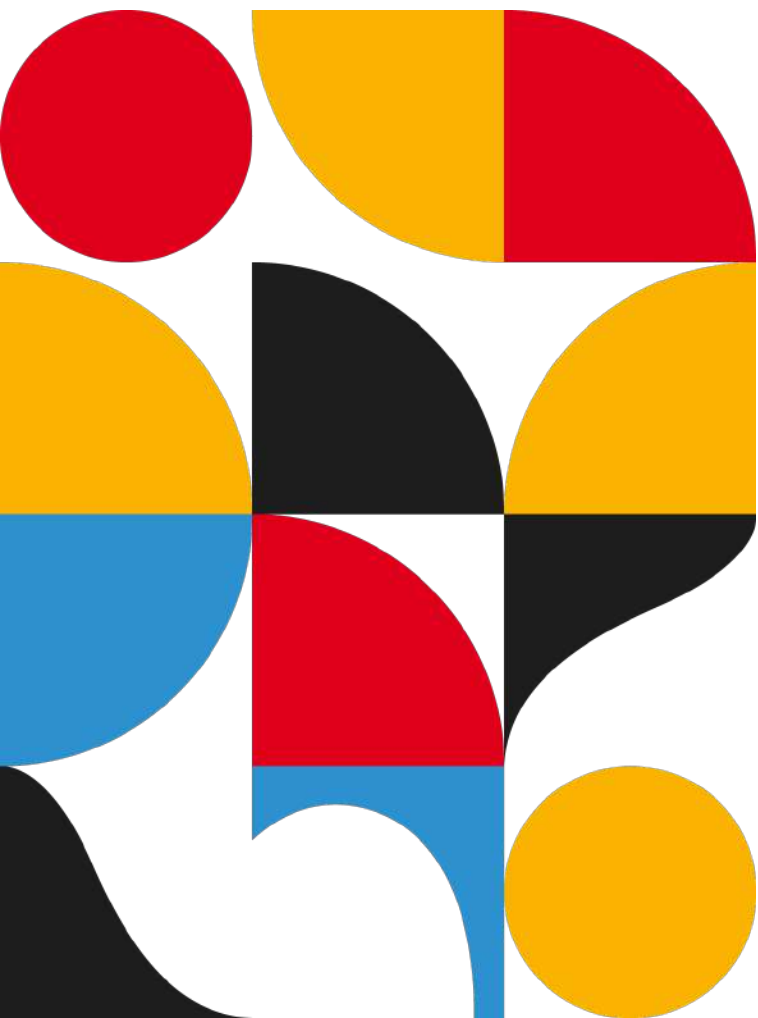
## ANRS-PISTAS

**PI: Dulce Ferraz and Marie Préau**



Funding: ANRS|MIE





# Thank you!

[dulce.ferraz@fiocruz.br](mailto:dulce.ferraz@fiocruz.br)

[d.ferraz@univ-lyon2.fr](mailto:d.ferraz@univ-lyon2.fr)

22 – 26 July · Munich, Germany and virtual

[aids2024.org](https://aids2024.org)



# References



Ayala G, Sprague L, van der Merwe LL, Thomas RM, Chang J, Arreola S, Davis SLM, Taslim A, Mienies K, Nilo A, Mworeko L, Hikuam F, de Leon Moreno CG, Izazola-Licea JA. Peer- and community-led responses to HIV: A scoping review. *PLoS One*. 2021 Dec 1;16(12):e0260555. doi: 10.1371/journal.pone.0260555. PMID: 34852001; PMCID: PMC8635382.

Gruskin, S., Bogecho, D. & Ferguson, L. 'Rights-based approaches' to health policies and programs: Articulations, ambiguities, and assessment. *J Public Health Pol* **31**, 129–145 (2010). <https://doi.org/10.1057/jphp.2010.7>

Oliveri C, Eang R, Ségéral O, Mora M, Puth L, Prom S, Mosnier E, Ouk V, Spire B, Saphonn V, Fiorentino M. High PrEP acceptability and need for tailored implementation in Cambodian key populations: results from a qualitative assessment. *AIDS Care*. 2024 Feb 6;1-8. doi: 10.1080/09540121.2024.2308029. Epub ahead of print. PMID: 38319897.

Macdonald V, Verster A, Baggaley R. A call for differentiated approaches to delivering HIV services to key populations. *J Int AIDS Soc*. 2017 Jul 21;20(Suppl 4):21658. doi: 10.7448/IAS.20.5.21658. PMID: 28770592; PMCID: PMC5577716.

UNAIDS. The path to end aids. Geneva, 2023.

Corrêa, S.. (2018). A "política do gênero": um comentário genealógico. *Cadernos Pagu*, (53), e185301. <https://doi.org/10.1590/18094449201800530001>

Reza-Paul S, Lazarus L, Jana S *et al*. Community Inclusion in PrEP Demonstration Projects: Lessons for Scaling Up [version 2; peer review: 1 approved, 2 approved with reservations]. *Gates Open Res* 2019, **3**:1504 (<https://doi.org/10.12688/gatesopenres.13042.2>)

Reza-Paul, S., Lazarus, L., Maiya, R., Haldar, P., Rewari, B. B., Venugopal, M. S., Hafeez Ur Rahman, S., Venukumar, K. T., Ramaiah, M., Pasha, A., Sharma, M., Steen, R., & Lorway, R. (2020). The Ashodaya PrEP project: Lessons and implications for scaling up PrEP from a community-led demonstration project among female sex workers in Mysore, India. *Global public health*, 15(6), 889–904. <https://doi.org/10.1080/17441692.2020.1724316>

Charest, M., Sharma, M., Chris, A., Schnubb, A., Knox, D. C., Wilton, J., Shahin, R., Chan, A., Mishra, S., Grace, D., Bayoumi, A. M., Maxwell, J., Bogoch, I. I., & Tan, D. H. S. (2021). Decentralizing PrEP delivery: Implementation and dissemination strategies to increase PrEP uptake among MSM in Toronto, Canada. *PloS one*, 16(3), e0248626. <https://doi.org/10.1371/journal.pone.0248626>

Phanuphak N, Sungsing T, Jantarapakde J, Pengnonyang S, Trachunthong D, Mingkwanrungruang P, Sirisakyot W, Phiayura P, Seekaew P, Panpet P, Meekrua P, Praweprai N, Suwan F, Sangtong S, Brutrat P, Wongsri T, Na Nakorn PR, Mills S, Avery M, Vannakit R, Phanuphak P. Princess PrEP program: the first key population-led model to deliver pre-exposure prophylaxis to key populations by key populations in Thailand. *Sex Health*. 2018 Nov;15(6):542-555. doi: 10.1071/SH18065. PMID: 30249317.

Puppo C, Mabire X, Cotte L, Castro DR, Spire B, Cua E, Pialoux G, Monti MS, Pasquet A, Raffi F, Molina JM, Préau M; ANRS-Ipergay Study Group. Community-Based Care in the ANRS-IPERGAY Trial: The Challenges of Combination Prevention. *AIDS Educ Prev*. 2019 Jun;31(3):259-272. doi: 10.1521/aeap.2019.31.3.259. PMID: 31145006.

1. Oliveira RL e S e, Silva LAV da, Duarte FM, Brasil SA, Castellanos MEP, Magno L, et al.. Building bridges to care: the experience of peer navigation in enabling linkage to PrEP for adolescent men who have sex with men and transgender women. *Cad Saúde Pública* [Internet]. 2023;39:e00176821. Available from: <https://doi.org/10.1590/0102-311XEN176821>

Jin G, Shi H, Du J, Guo H, Yuan G, Yang H, Zhu Z, Zhang J, Zhang K, Zhang X, Lu X, Xu W, Wang S, Hao J, Sun Y, Su P, Zhang Z. Pre-Exposure Prophylaxis Care Continuum for HIV Risk Populations: An Umbrella Review of Systematic Reviews and Meta-Analyses. *AIDS Patient Care STDS*. 2023 Dec;37(12):583-615. doi: 10.1089/apc.2023.0158. Epub 2023 Nov 21. PMID: 38011347.

Mann-Jackson, L., Alonzo, J., Garcia, M., Trent, S., Bell, J., Horridge, D. N., & Rhodes, S. D. (2021). Using community-based participatory research to address STI/HIV disparities and social determinants of health among young GBMSM and transgender women of colour in North Carolina, USA. *Health & social care in the community*, 29(5), e192–e203. <https://doi.org/10.1111/hsc.13268>



# References



**AIDS 2024**

Ross, L. E., Pilling, M., Voronka, J., Pitt, K. A., McLean, E., King, C., ... Guta, A. (2023). 'I will play this tokenistic game, I just want something useful for my community': experiences of and resistance to harms of peer research. *Critical Public Health*, 33(5), 735–746. <https://doi.org/10.1080/09581596.2023.2268822>

Préau M. Traité de recherche communautaire en psychologie.

Mora M, Ferraz D, Perray M, Mabire X. Quand la recherche communautaire vulnérabilise. In: Préau M. Traité de recherche communautaire en psychologie.

Parker, R. (2024). Epidemics of signification and global health policy: From the end of AIDS to the end of scale-up of the global AIDS response. *Global Public Health*, 19(1). <https://doi.org/10.1080/17441692.2024.2327523>

Jin, Haiyan Shi, Jun Du, Haiyun Guo, Guojing Yuan, Huayu Yang, Zhihui Zhu, Jianghui Zhang, Kexin Zhang, Xueqing Zhang, Xiaoyan Lu, Wenzhuo Xu, Sainan Wang, Jiahu Hao, Ying Sun, Puyu Su, and Zhihua Zhang [Pre-Exposure Prophylaxis Care Continuum for HIV Risk Populations: An Umbrella Review of Systematic Reviews and Meta-Analyses](#). *AIDS Patient Care and STDs* 2023 37:12, 583-615

Haberer JE, Mujugira A, Mayer KH. The future of HIV pre-exposure prophylaxis adherence: reducing barriers and increasing opportunities. *Lancet HIV*. 2023 Jun;10(6):e404-e411. doi: 10.1016/S2352-3018(23)00079-6. Epub 2023 May 10. PMID: 37178710.

Rousseau, E., Julies, R.F., Madubela, N. *et al.* Novel Platforms for Biomedical HIV Prevention Delivery to Key Populations — Community Mobile Clinics, Peer-Supported, Pharmacy-Led PrEP Delivery, and the Use of Telemedicine. *Curr HIV/AIDS Rep* 18, 500–507 (2021). <https://doi.org/10.1007/s11904-021-00578-7>

Perez-Urbano I, Dilraj A, Pitsi A, Hlongwane N, Abdelatif N, Dietrich J, Ahmed K. Strategies to Close the PrEP Uptake Gap Among Transgender People and Men Who Have Sex with Men in Tshwane, South Africa: Perspectives from the Community. *AIDS Behav*. 2024 Jun;28(6):1999-2014. doi: 10.1007/s10461-024-04300-7. Epub 2024 Mar 1. PMID: 38427124; PMCID: PMC11161427.

Myers JE, Braunstein SL, Xia Q, Scanlin K, Edelstein Z, Harriman G, Tsoi B, Andaluz A, Yu E, Daskalakis D. Redefining Prevention and Care: A Status-Neutral Approach to HIV. *Open Forum Infect Dis*. 2018 May 2;5(6):ofy097. doi: 10.1093/ofid/ofy097. PMID: 29977957; PMCID: PMC6016418.

Vanhamel J, Rotsaert A, Reyniers T, Nöstlinger C, Laga M, Van Landeghem E, Vuylsteke B. The current landscape of pre-exposure prophylaxis service delivery models for HIV prevention: a scoping review. *BMC Health Serv Res*. 2020 Jul 31;20(1):704. doi: 10.1186/s12913-020-05568-w. PMID: 32736626; PMCID: PMC7395423.

Toby Pepperrell, Samuel Cross, Andrew Hill, Cabotegravir—Global Access to Long-Acting Pre-exposure Prophylaxis for HIV, *Open Forum Infectious Diseases*, Volume 10, Issue 1, January 2023, ofac673, <https://doi.org/10.1093/ofid/ofac673>

Platero, L. R., (2023) "Strange Bedfellows: Anti-trans Feminists, VOX Supporters and Biologist Academics", *DiGeSt - Journal of Diversity and Gender Studies* 10(2), 124-130. doi: <https://doi.org/10.21825/digest.89997>

Dang, M., Scheim, A. I., Teti, M., Quinn, K. G., Zarwell, M., Petroll, A. E., Horvath, K. J., & John, S. A. (2022). Barriers and Facilitators to HIV Pre-Exposure Prophylaxis Uptake, Adherence, and Persistence Among Transgender Populations in the United States: A Systematic Review. *AIDS Patient Care and STDs*, 36(6), 236–248. <https://doi.org/10.1089/apc.2021.0236>

Anam, F. R., Nkosi, S., Sebayang, M., Jokonya, M., Dunaway, K., & El Alaoui, T. (2023). Let us lead: community leadership in the AIDS response is its fundamental pillar for success. *Journal of the International AIDS Society*, 26(12), e26196. <https://doi.org/10.1002/jia2.26196>



# Master Psychologie Clinique, Psychopathologie, Psychologie de la santé

**Resp. Mention**  
Marie Préau  
Rémy Potier

**Resp. M1 et M2**  
Myriam Pannard

## Présentation de la formation

Le Master Psychologie Clinique, Psychopathologie et Psychologie de la Santé (PCPPS) s'inscrit dans le champ de la psychologie de la santé / psychologie clinique de la santé, tel que défini notamment par la *Division 38 : Society for Health Psychology* de l'American Psychological Association. La psychologie de la santé a ainsi pour objectif « *d'améliorer la vie des individus et la société en promouvant la santé, en prévenant la maladie et en améliorant les soins de santé à travers la recherche, la pratique, l'éducation, la formation et le plaidoyer* » (APA, 2023).

Le Master PCPPS vise à former des psychologues capables d'accompagner les populations concernées par l'ensemble des aspects propres à la prévention et à la prise en charge des problématiques relatives à la santé (e.g. santé sexuelle et fertilité, inégalités d'accès et de recours aux soins, etc.), et plus particulièrement aux pathologies chroniques somatiques (e.g. cancers, douleurs chroniques, pathologies infectieuses).

Les étudiant·es seront formé·es à construire, déployer et évaluer des interventions – notamment d'accompagnement clinique (e.g. thérapies brèves), mais aussi de promotion et éducation à la santé – auprès de l'ensemble des acteurs·rices et usager·ères du système de santé : les personnes directement concernées (i.e. patient·es, personnes présentant un risque élevé de développer une pathologie donnée), leurs proches et /ou aidant·es, mais aussi les soignant·es impliqué·es dans la prise en charge. En Master 2, les étudiant·es bénéficieront par exemple d'enseignements leur permettant d'obtenir un certificat d'éducation thérapeutique



constituant une réelle plus-value dans un contexte où les personnes atteintes de pathologie chroniques sont encouragées à être de plus en plus autonomes dans la gestion de leur maladie.

La formation dispensée repose sur de solides connaissances théoriques et pratiques relatives à la psychologie de la santé. Ce master propose ainsi une approche innovante en incitant au croisement des regards en psychologie (perspective trans-sous-disciplinaire : psychologie clinique, psychologie sociale, psychologie positive, etc.), en invitant les étudiant·es à construire un regard critique sur la manière de faire science en psychologie de la santé et en leur proposant des espaces d'échanges bienveillants afin de s'initier à la controverse scientifique. Les étudiant·es recevront une formation à et par la recherche en psychologie de la santé afin d'être capables de penser et mener l'ensemble de leurs missions en respectant les principes fondamentaux d'une démarche scientifique et éthique en psychologie.

**Effectifs:** 30 étudiant·es par année

## Des compétences centrées autour de quatre axes majeurs

L'accompagnement  
thérapeutique

La construction, la  
mise en œuvre et  
l'évaluation  
d'interventions en  
promotion de la santé

La recherche en  
psychologie de la  
santé

La supervision et la  
formation

## Description de la formation en Master 1

Au fil des deux années de Master PCPPS, les étudiant·es devront acquérir (1) des compétences théoriques, (2) des compétences méthodologiques liées à la production et à la valorisation de connaissances scientifiques, (3) des compétences praticiennes et d'accompagnement psychologique, et (4) des compétences réflexives et communicationnelles. La formation dispensée en Master 1 PCPPS – structurée autour de trois UE à chaque semestre - vise à construire les bases indispensables à l'acquisition de ces compétences.

Au premier semestre, la première UE sera dédiée à la formation théorique (e.g. psychopathologie, psychologie de la santé) permettant aux étudiant·es d'appréhender de multiples aspects de leur champ d'exercice - notamment grâce à la participation à



des séminaires thématiques inter-niveaux (e.g. addictions, genre et santé, pratiques alimentaires, douleur) facilitant de premiers échanges avec la promotion de Master 2. La seconde UE est consacrée à l'intervention thérapeutique (e.g. pratique de l'étude de cas et de l'accompagnement individuel). La troisième UE est destinée à former les étudiants à la recherche et à l'intervention en psychologie de la santé, notamment grâce à des enseignements méthodologiques et à l'initiation de leur mémoire de recherche.

Le second semestre a pour objectif de favoriser un approfondissement des connaissances théoriques (UE1), mais aussi de permettre une mise en pratique des compétences acquises grâce à la finalisation du mémoire de recherche débuté au premier semestre (UE2) et à la réalisation d'un stage d'une durée de 200 heures minimum (UE3). Le mémoire de recherche et le rapport de stage feront l'objet d'une soutenance en présence de deux membres de l'équipe pédagogique.

Tout au long de l'année, les étudiant-es seront amené-es à développer une réflexion éthique et déontologique concernant leur posture en tant que futur-es psychologues. Ils et elles bénéficieront également de cours d'anglais appliqués à la santé afin de leur permettre (1) de continuer à se former tout au long de leur carrière en s'appuyant notamment sur la littérature scientifique largement publiée en langue anglaise, (2) d'exercer des missions en psychologie de la santé dans un contexte international.

### **Attendus**

Suite à la publication de la Loi n°2016-1828 du 23 décembre 2016, l'admission en Master 1ère année est subordonnée au succès de l'examen d'un dossier de candidature suivi, le cas échéant, d'un entretien et/ou d'épreuves écrites.

L'accès à la première année du Master Psychologie Clinique, Psychopathologie et Psychologie de la Santé est ouvert exclusivement aux titulaires d'une licence de Psychologie après admission.

Dans leur dossier de candidature, les postulant-es à l'entrée en M1 PCCPS doivent (1) présenter d'excellentes compétences académiques illustrées notamment par les résultats antérieurs mais aussi par la rédaction d'un projet de mémoire de recherche, (2) démontrer l'adéquation de leur projet professionnel avec le contenu et les objectifs du master. Disposer d'une ou plusieurs expériences internationales et / ou en lien avec la santé est apprécié mais non obligatoire.

## **Insertion professionnelle**



Les étudiant·es issu·es du Master peuvent exercer en tant que psychologue spécialisé·e en psychologie (clinique) de la santé et / ou en tant qu'ingénieur·e d'études, chef·fe de projet ou encore chargé·e de mission en lien avec la santé. Les lieux d'exercice sont variés et incluent notamment :

- Le système de soins : les institutions et associations de prise en charge du secteur médico-social (e.g. services hospitaliers tels que l'oncologie, les soins palliatifs, la cardiologie, l'addictologie, etc. ; associations et entreprises d'aide à la personne telles que les EPHAD, les Centres Communaux d'Action Social, etc.)
- Les structures œuvrant à la santé publique : organismes de recherche, médecine du travail, cabinets d'études, etc.
- La formation / le conseil : organismes de formation, les IFSI, etc.
- La vie communautaire et sociale : dispositifs communaux, départements et régionaux, agences publiques et semi-publiques d'études et développement sanitaire et social, etc.
- La recherche : universités, services hospitaliers, institutions de santé (INSERM, CNRS, INCa, etc.).

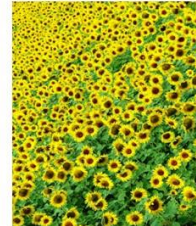
## Contacts

Interlocuteur·rice	Mail
<b>Responsabilité de la mention PCPPS</b>	
Marie Préau Rémy Potier	Marie.preau@univ-lyon2.fr Rémy.potier@univ-lyon2.fr
<b>Responsabilité du M1 et du M2 PCPPS</b>	
Myriam Pannard	M. pannard@univ-lyon2.fr
<b>Scolarité</b>	Psycho-m.sante@univ-lyon2.fr





# PROJET INDIRA



## 1<sup>ST</sup> REFUNDING

### ACTIVITE 08-3 – STUDY HUMAN AND SOCIAL SCIENCES

**BUT :** The aim of this workpackage was to develop and carry out an SHS study on healthy donors from the INDIRA cohort.

**SUMMARY:** The INDIRA results show that it is now possible to predict the level of individual sensitivity after exposure to ionizing radiation, for common medical exposures. This work raises questions about the possible reactions of patients after this type of predictive announcement. To investigate this question, the theoretical framework offered by the sociogenetic approach to social representations seems most appropriate. This perspective on social representations makes it possible to highlight, on the one hand, the genesis of collective thought in social discourse and, on the other hand, its practical and useful purpose in behaviors. This work aims to study the representations of ionizing radiation and health prediction and through it, the possible impact of such a prediction. Given the lack of prior work on this subject, this study will begin with exploratory interviews in order to refine the main data collection. Based on the analysis of the interviews, a questionnaire will be constructed to investigate, on the one hand, the social representations of ionizing radiation and, on the other hand, the question of disease prediction. The qualitative data will be subject to a thematic content analysis and descriptive statistics. As for the quantitative data, they will be described statistically before looking for possible correlations between socio-demographic data and the answers to the questions. The analysis of the results should highlight the motivations and obstacles to carrying out this type of predictive tests, but also to understand how ionizing radiation is viewed by the general public.

#### Research Questions and Objectives

By combining these various elements of the literature with the knowledge already identified by the INDIRA project, we formulated the following research questions :

- What are the social representations of ionizing radiation in the general population?
- What are the perceptions of the possible prediction of cancer?

**Main objective:** To study the representations of ionizing radiation and prediction in health.

**Secondary objective:** To study the impact of predicting individual radiosensitivity on health behaviors.

The study of the general public's perception and prediction of cancer involved a deeper exploration of social representations of radiation. The ambivalence surrounding the perception of risks and exposure



to ionizing radiation from the general public's perspective prompted us to study this issue from the following perspectives:

- Research on social representations from a sociogenetic perspective. In this way, it is possible to study group thinking around a complex subject in common-sense discourse.
- Research on disease prediction, as other diseases are already the subject of early genetic testing.
- Health norms that implicitly guide our thoughts and behaviors.

Our results showed that representations of radiation are part of a cautious dimension but they are immediately associated with nuclear power plants before thinking about the medical aspects of their uses. Considering the development of a disease remains worrying for everyone because people only feel reassured by the possible actions to delay or treat the disease. The health objective remains a priority and normative. Finally, the notion of increased risks of disease depending on radiation is rather known by respondents who are aware of the risks of radiation in general. As a reminder, 65.53% of participants responded that radiation is dangerous for health and 100% responded that radiation increases the risk of cancer (32.26% from a small exposure and 70.97% when exposure is repeated or intense).

**CONCLUSION:** This study highlights the need for multidisciplinary support for predictive testing. Concerns, even anxieties, associated with the results should be addressed by a psychologist. Support appears necessary whether the test results place patients in a group with normal responses to DNA double-strand break repair or a radiosensitive group. This point is a lesson learned from the work on individuals tested for Huntington's disease. Finally, support regarding possible preventive measures or tests, as well as possible treatments for the diseases, also appears essential and desired by respondents.

**APPENDIX:** The SHS study report file is attached with all the documents.



# RAPPORT - INDIRA-SHS

Date : 03.09.2024

Version 1

Auteur : Manon Britel, Ph.D.



## Table des matières

Table des tableaux .....	4
Table des figures .....	4
Résumé du projet .....	5
I. Introduction et rationnel.....	6
A. Les représentations sociales de la radiosensibilité individuelle.....	6
1. Les représentations sociales de la santé et du cancer.....	6
2. Les représentations sociales des rayonnements ionisants.....	7
B. La prédiction en santé.....	8
1. Le cas de la maladie de Huntington .....	8
2. La prédiction proposée par le projet INDIRA.....	9
II. Questions de recherche et objectifs.....	9
III. Matériel et méthodes .....	9
A. Des entretiens exploratoires.....	9
B. Questionnaire.....	10
IV. Population étudiée .....	10
V. Traitement des données et méthode d'analyse .....	10
A. Entretiens exploratoires.....	10
B. Le questionnaire.....	11
VI. Résultats des entretiens .....	11
A. Description de la population .....	11
B. Perception des radiations.....	11
1. <b>Question 1</b> : Pouvez-vous indiquer les 3 mots ou expressions qui vous viennent spontanément à l'esprit lorsque l'on vous dit : « <b>rayonnements ionisants</b> ».....	12
2. <b>Question 2</b> : Pour vous est-ce un mot positif, négatif ou neutre ? .....	12
3. <b>Question 3</b> : Y a-t-il des implications positives aux rayonnements ionisants ? Si oui lesquelles ? .....	12
4. <b>Question 4</b> : Pouvez-vous me parler des risques liés aux rayonnements ionisants ? Dans quels cas pouvez-vous y être exposé ? Niveau de gravité ? .....	13
5. <b>Question 5</b> : Avez-vous déjà entendu le terme « <b>radio-induit</b> » ? Si oui, pouvez-vous m'en parler ? .....	13
C. Perception de la prédiction des maladies.....	13
6. <b>Question 6</b> : Imaginez que demain il soit possible de prédire si vous allez développer un <b>cancer</b> dans votre vie, qu'en pensez-vous ? Qu'est ce qui pourrait vous motiver à savoir / vous freiner ? .....	13



7.	<b>Question 7 :</b> Imaginez que demain il soit possible de prédire si vous allez développer une maladie de maladie dégénérative (Alzheimer), comme dans votre vie, qu'en pensez-vous ? Qu'est ce qui pourrait vous motiver à savoir / vous freiner ? .....	14
8.	<b>Question 8 :</b> Pensez-vous que connaître ces risques futurs changeraient votre vie présente ? Comment ? Pourquoi ?.....	14
VII.	<b>Résultats du questionnaire</b> .....	15
A.	Description de la population .....	15
B.	Perception des radiations.....	16
1.	<b>Question 1 :</b> Pouvez-vous indiquer les 3 mots ou expressions qui vous viennent spontanément à l'esprit lorsque l'on vous dit : « radiation » .....	16
2.	<b>Question 2 :</b> Pour vous, ce terme « radiation » est : .....	16
3.	<b>Question 3 :</b> Selon-vous, dans votre vie, avez-vous déjà été exposé aux radiations ? .....	16
4.	<b>Question 3.2 :</b> Si oui : Dans quel contexte pensez-vous que vous avez été exposé aux radiations ? .....	17
5.	<b>Question 4 :</b> Selon vous, les radiations sont-elles .....	17
C.	Perception de la prédiction de maladie .....	18
6.	<b>Question 5 :</b> Imaginez que demain il soit possible de prédire si dans votre vie vous aurez un cancer, qu'en pensez-vous ? .....	18
7.	<b>Question 6 :</b> Est-ce que cette perspective (toujours imaginaire de prédire un cancer) changerait votre façon d'agir dans le présent ? .....	18
8.	<b>Question 7 :</b> Imaginez que demain il soit possible de prédire si dans votre vie vous aurez une maladie dégénérative comme la maladie d'Alzheimer, qu'en pensez-vous ? .....	18
9.	<b>Question 8 :</b> Est-ce que cette perspective (toujours imaginaire de prédire une maladie d'Alzheimer) changerait votre façon d'agir dans le présent ? .....	19
10.	<b>Question 9 :</b> Est-ce que connaître votre « avenir-santé » (cancer ou maladie d'Alzheimer) vous ferait envisager : (plusieurs réponses possibles) .....	19
D.	Perception des effets des radiation sur la santé .....	20
11.	<b>Question 10 :</b> Selon vous, l'exposition aux radiations augmente-t-elle le risque de développer un cancer ? .....	20
12.	<b>Question 11 :</b> Selon vous, l'exposition aux radiations est-elle bénéfique pour la santé ? 20	
VIII.	<b>Analyses croisées</b> .....	21
IX.	<b>Discussion</b> .....	22
A.	Représentations sociales des radiations .....	22
B.	Prédiction des maladies .....	23
C.	Taille de l'échantillon, une limite évidente. ....	24
X.	<b>Conclusion</b> .....	25
XI.	<b>Bibliographie</b> .....	26



XII.	Annexes .....	28
A.	Annexe 1 : grille d’entretien.....	28
B.	Annexe 2 : questionnaire .....	31



## Table des tableaux

Tableau 1. Résumé de la grille d'entretien exploratoire .....	10
Tableau 2. Résumé du questionnaire .....	10
Tableau 3. Caractéristiques sociodémographiques des participants aux entretiens exploratoires. N=5 .....	11
Tableau 4. Regroupement thématique des réponses de la question 3. N=5 .....	12
Tableau 5. Regroupement thématique des réponses à la question 4. N=5 .....	13
Tableau 6. Caractéristiques sociodémographiques des participants au questionnaire. N = 32 .....	15
Tableau 7. Régression logistique binaire sur les facteurs associés à la variable "Ce serait rassurant de pouvoir anticiper les choses ". N = 32 .....	21

## Table des figures

Figure 1. Thèmes évoqués par les participants aux entretiens à l'évocation du mot "Radiation". N=5	12
Figure 2. Représentation de la valence associée au terme "Rayonnements ionisants". N=5 .....	12
Figure 3. Regroupement thématique à l'association verbale "Radiation". N = 90 .....	16
Figure 4. Valence associée au terme "radiation" N = 32 .....	16
Figure 5. Pourcentage de personnes pensant avoir déjà été exposées aux radiations. N = 32 .....	16
Figure 6. Contexte dans lesquels les répondants pensent avoir été exposés aux radiations. N = 86...	17
Figure 7. Estimation du niveau de danger des radiations par les participants. N = 32 .....	17
Figure 8. Perception de la prédiction d'un cancer par les participants. N = 32 .....	18
Figure 9. Changement de comportement si la prédiction du cancer était possible. N = 32 .....	18
Figure 10. Prédiction de la perception possible d'une maladie dégénérative comme la maladie d'Alzheimer. N = 32 .....	18
Figure 11. Changement de comportement si la prédiction de maladie dégénératives était possible. N = 32 .....	19
Figure 12. Changements envisagés par les participants s'ils connaissaient leur "avenir santé". N = 32 .....	19
Figure 13. Perception de l'augmentation du risque de cancer en fonction de l'exposition aux radiations selon les participants. N = 32 .....	20
Figure 14. Perception du bénéfice des radiations selon les participants. N = 32 .....	20



## Résumé du projet

TITRE	Etudier la perception les représentations sociales et de la prédiction de la radiosensibilité individuelle du grand public	
PROMOTEUR	Nom	APHP
	Adresse	27 rue du faubourg Saint Jacques, 75014 Paris
	Téléphone	01 40 27 30 00
INVESTIGATEUR PRINCIPAL	Nom	Manon Britel, PhD.
	Adresse	39 rue Léon Weber, 69400 Villefranche sur Saône
	Téléphone	01 40 27 30 00
TYPE D'ETUDE	Psychologie sociale de la santé	
DUREE DU PROJET	6 mois	
NOMBRE DE PARTICIPANT	Phase 1	N = 8
	Phase 2	N= 32
ASSURANCE	Hiscox	
MOTS CLES :	Représentations sociales ; radiosensibilité individuelle ; rayonnements ionisants	

### Introduction :

Les résultats INDIRA montrent qu'il est aujourd'hui possible de prédire le niveau de sensibilité individuelle après exposition aux rayonnements ionisants, pour des expositions médicales courantes. Ce travail soulève des questions sur les possibles réactions de patients après ce type d'annonce prédictive. Pour investiguer cette question le cadre théorique que nous offre l'approche sociogénétiques des représentations sociales semble le plus appropriée. Cette perspective des représentations sociales permet de mettre en évidence d'une part la genèse de la pensée collective dans le discours social et, d'une autre part, sa visée pratique et utile dans les comportements.

### Objectif :

Ce travail a pour objectif d'étudier les représentations des rayonnements ionisants et de la prédiction en santé et à travers lui, l'impact possible d'une telle prédiction.

### Matériel et méthodes :

Compte tenu du manque de travaux préalables sur ce sujet, cette étude débutera par des entretiens exploratoires afin d'affiner le recueil de données principal. Fort de l'analyse des entretiens, un questionnaire sera construit pour investiguer d'une part les représentations sociales des rayonnements ionisants et, d'une autre part, la question de la prédiction de maladies.

### Analyse des données :

Les données qualitatives feront l'objet d'une analyse thématique de contenu et de statistiques descriptives. Quant aux données quantitatives, elles seront décrites statistiquement avant de chercher les possibles corrélations entre les données socio-démographiques et les réponses aux questions.

### Résultats attendus :

L'analyse des résultats devraient mettre en évidence les motivations et des freins aux fait de réaliser ce type de tests prédictifs, mais aussi de comprendre comment les rayonnements ionisants sont envisagés par le grand public.



## I. Introduction et rationnel

Le projet initial INDIA vise à mieux comprendre la notion de radiosensibilité individuelle et à en mesurer sa fréquence dans la population générale. Les deux livrables majeurs de ce projet sont :

- Objectif 1 : le développement de tests prédictifs de la radiosensibilité ;
- Objectif 2 : l'estimation des sous-populations radiosensibles dans la population générale.

**La radiosensibilité individuelle** peut se définir comme le niveau de susceptibilité d'une personne à l'exposition aux rayonnements ionisants. Les travaux de Foray et al. (2013) ont montré qu'environ 20 % de la population générale est plus sensible aux rayonnements ionisants que les autres. Ces personnes sont dites « radiosensibles ». Pour elles, une exposition entraîne une mauvaise réparation des cassures double brin de l'ADN causées par l'irradiation, ce qui peut avoir pour conséquence une augmentation du risque de développer un cancer.

Pour rappel, une personne peut être exposée à ce type de rayonnements lorsqu'elle passe un examen médical, comme une radiographie, un scanner, une mammographie, ou d'autres actes de médecine nucléaire. Elle peut également être exposée en radiothérapie, en curiethérapie, en prenant l'avion ou par exposition naturelle, etc. Autrement dit, les sources possibles d'exposition et les raisons d'être exposé au cours d'une vie sont nombreuses et peuvent être fréquentes. Il semble donc important de mieux comprendre ce risque biologique grâce au projet INDIRA.

Du point de vue des sciences humaines et sociales, nous invite à nous questionner sur la façon dont le grand public pense ces questions. Comment l'exposition aux radiations peut être perçue par le grand public et comment ils appréhendent la survenue d'un cancer. Pour comprendre cela, nous avons étudié la littérature scientifique, d'abord du point de vue des représentations sociales, afin de comprendre comment cet enjeu est perçu du point de vue de la pensée collective. Ensuite, nous investiguerons la littérature sur la prévention et la prédiction des risques en santé.

### A. Les représentations sociales de la radiosensibilité individuelle

Les travaux en sciences humaines et sociales ont depuis longtemps la volonté de cerner les phénomènes psychologiques dans leur dimension sociale. Partant de l'idée selon laquelle aucune connaissance ne peut exister sans que l'individu en ait des représentations mentales, Durkheim a développé le concept de représentations collectives (Durkheim, 1898). C'est en s'appuyant sur ses travaux que Moscovici a élaboré la théorie des représentations sociales (Moscovici, 1961). Les représentations sociales peuvent être définies comme une forme de connaissances partagées par un groupe social. Cette connaissance possède une fonction, une utilité pratique. Elle est un outil de communication et de transmission des connaissances (Jodelet, 1984, 1989). D'après Jodelet (1989), les représentations sociales, dans leurs perspectives sociogénétiques prennent leur source dans la communication au sein du groupe social. Le groupe social est une entité qui partage au moins une partie de leur identité sociale car, les membres d'un même groupe ont en commun des normes, des valeurs et une culture (Doise, Palmonari, 1986 ; Jodelet, 1989 ; Herzlich, 2015).

#### 1. Les représentations sociales de la santé et du cancer

Dans le champ de la santé, les représentations sociales ont largement été étudiées. En effet, d'après Apostolidis (2006, p212) « *l'approche représentationnelle permet une « compréhension de la dynamique psychosociale en jeu dans la construction du rapport à la maladie* ». Les travaux sur la maladie de Herzlich (1969) sont encore aujourd'hui une référence. L'auteur considère qu'il existe un



discours de sens commun au sujet de la maladie. Ce discours est différent du discours médical ou scientifique même s'il peut en être imprégné. L'auteur a ainsi pu mettre en évidence des théories profanes de la maladie. Ses analyses ont également montré le caractère indissociable du discours profane sur les maladies de la société qui l'a produit. Les travaux de Herzlich ont mis en évidence que, selon le groupe social d'appartenance et selon le contexte culturel ou familial, plusieurs conceptions de la maladie étaient alors possibles. Les individus malades ou en bonne santé ne se conforment pas à une pensée unique de concepts si complexes. Autrement dit, nous ne concevons pas la maladie de la même manière en fonction de notre culture, de notre groupe socio-culturel ou économique par exemple.

Les travaux représentationnels sur le cancer ont permis de montrer qu'il renvoie à une réalité complexe dans laquelle l'individu, la société et l'objet sont liés à travers l'histoire collective, individuelle et subjective de l'individu, mais aussi, à travers les normes sociales, les croyances ou encore les savoirs associés au cancer (Deschamps, Paez, 1999 ; Dany, Dudois, Favre, 2008). Le facteur temps joue également un rôle dans l'évolution des représentations. En effet, le cancer qui pouvait être associé directement à la mort et à la fatalité il y a encore quelques décennies, est aujourd'hui davantage perçu comme une maladie chronique qui implique un lourd parcours de soin (Moulin, 2005).

Les travaux de Soussan, (2004) montrent que le cancer est associé au champ lexical de la guerre. Cette représentation semble avoir comme visée pratique de favoriser les patients à la combativité. Néanmoins, il semble que le revers de la médaille de cette image soit de limiter l'expression de la détresse émotionnelle (Byrne, Ellershaw, Holcombe, Salmon, 2002).

## 2. Les représentations sociales des rayonnements ionisants

Concernant la question de l'exposition aux rayonnements ionisants la littérature n'est pas aussi riche que pour le cancer ou la santé. Quelques études abordent la question des « représentations » au sens commun du terme, ou bien, il est question des accidents nucléaires comme dans le cas de Tchernobyl. A titre d'exemple, l'IRSN publie chaque année un baromètre (IRSN, 2018) qui a pour objectif de mettre en avant la perception qu'ont les Français des principaux risques présents dans notre société. Les questions portent sur la leur perception de 14 risques (Le terrorisme, le chômage, l'insécurité, la misère et l'exclusion, les bouleversements climatiques, la dégradation de l'environnement, les conséquences de la crise financière, la qualité des soins médicaux, les risques nucléaires, les toxicomanies, les accidents de la route, les risques alimentaires, le SIDA, les risques chimiques ou ne se prononce pas). Pour cette question, les risques nucléaires sont mentionnés en premier par seulement 2,2 % des répondants. Cette question concerne davantage les risques liés aux centrales nucléaires que l'exposition médicale. La question de l'exposition médicale est abordée ensuite pour savoir si, les personnes interrogées pensent qu'il s'agit d'un risque élevé, moyen, ou faible. Les données montrent que 46 % des personnes interrogées déclarent penser qu'il s'agit d'un risque faible, 36 % d'un risque moyen et 16 % d'un risque élevé. Ce document offre à lire des résultats bruts sous forme de graphique, mais il n'en propose pas une analyse ancrée dans un champ disciplinaire.

L'étude de Galli et Nigro (1987), quant à elle, est ancrée dans l'approche sociogénétique des représentations sociales. Elle vise à investiguer les représentations sociales qu'ont les enfants de la radioactivité. Pour cela, ils demandaient aux enfants de dessiner la radioactivité et de commenter leur dessin. Cependant, ce travail s'inscrit dans le contexte particulier de la période immédiate après l'accident de Tchernobyl en avril 1986. Les résultats sont empreints



de cet évènement et les enfants décrivent dans leur dessin des nuages mortels en abordant la notion de contamination.

## B. La prédiction en santé.

De façon à réduire le risque de maladie, les politiques publiques ont mis en place des campagnes de prévention des cancers les plus fréquents. En effet, la prévention en santé réside dans l'anticipation visant à réduire la probabilité de survenue d'un événement indésirable (Arwidson, 2013). La prévention en santé regroupe à la fois les risques psychosociaux au travail, la lutte contre le tabagisme ou encore la prévention de maladie comme le sida ou le cancer (Peretti-Watel, 2002, 2013).

Concernant les risques de cancer, il semble que la meilleure chance de lutte contre cette maladie s'inscrive dans le principe de prévention. Autrement, plus un cancer est dépisté tôt et meilleur seront les chances de survie à cinq ans (Peretti - Watel, Vergely, 2012).

Cependant, l'anticipation à long terme d'une maladie, comme le propose la technologie du projet INDIRA entraîne des questions d'ordre psychologiques. En effet, proposer une estimation probabiliste de la survenue d'un cancer peut aisément être confondu d'un point de vue émotionnel avec une réalité avérée à venir (Gargiulo, Durr, 2014). Les personnes se retrouvent avec une épée de Damoclès pour un certain nombre d'années car, ce résultat impose quatre dimensions (Durr et al, 2009 ; Gargiulo, Durr, 2014) :

- La question de la perte de l'insouciance au sujet de l'idée de sa propre finitude.
- La question de la temporalité de la maladie : Combien d'année me reste-il en bonne santé ? Comment parvenir à profiter du moment présent en sachant cela ?
- La question des solutions : Y a-t-il une solution curative à cette maladie éventuelle à venir.
- La question de la transmission : ai-je transmis cela à mes enfants ?

Aujourd'hui dans la littérature scientifique, nous trouvons beaucoup de données sur la prédiction des risques pour la maladie de Huntington. Nous proposons donc un rapide détour par les connaissances de cette maladie pour mieux comprendre ce qui peut se rapprocher de la prédiction possible des cancers à long terme comme le propose le projet INDIRA :

### 1. Le cas de la maladie de Huntington

Les études montrent que, paradoxalement, concernant le dépistage de la maladie Huntington, les personnes n'étant pas porteuses du gène ont un risque de développer de l'anxiété et de la dépression allant jusqu'au passage à l'acte suicidaire significativement plus élevé que ceux étant porteur du gène. La notion d'identité vient expliquer ce résultat. En effet, les personnes ont construit une grande partie de leur identité sur le fait d'être potentiellement porteur et donc, malade de Huntington. L'éventualité d'être non-porteur et ainsi en bonne santé, est en général moins pensée, moins anticipée car cela paraît moins risqué. Cependant, quand le verdict tombe et que la personne apprend qu'elle n'est pas porteuse, le manque d'anticipation de sa nouvelle identité est extrêmement déstabilisant. A tout cela s'ajoute la culpabilité d'être non-malade dans une fratrie où d'autre peuvent l'être associé à un sentiment de trahison. Le résultat des tests brise un élément qui rassemblait la fratrie et leur permettaient de faire groupe, ensemble (Gargiulo et al, 2009 ; Gargiulo, Durr, 2014).



## 2. La prédiction proposée par le projet INDIRA

Dans le cas de la prédiction proposé par le projet INDIRA, comme dans le cas des maladies mentionnées ci-dessus, il s'agit d'un diagnostic pré-symptomatiques. La personne en bonne santé, on ne peut évidemment pas parler de patient pour le moment, se retrouve menacée par un mal qui lui arrivera peut-être un jour, ou peut-être jamais, sans savoir ni quand, ni comment. De plus, la connaissance de cette éventualité peut entraîner une peur que l'angoisse associée ne devienne elle-même un déclencheur, un révélateur de la maladie. Dans ce cas, pour la personne tout se passe comme si, le fait de savoir et donc d'avoir des émotions négatives associées, allait activer le gène menaçant et ainsi, la rendre malade. Ces personnes ont tendance à regretter de savoir, pensant alors qu'elles auraient été plus sereine et que cette sérénité aurait prolongé leur état de bonne santé (Durr et al, 2009).

Cette problématique nous invite à réfléchir à la façon de se projeter dans le futur. Pour Triandafilidis (1990), il existe deux modalités du rapport de l'homme au temps futur. D'une part, le fait de connaître dans le passé le « savoir de l'à venir » et d'une autre part, la prévision de la mort (comme avenir) dans la vie. Dans ce cas, et c'est ce qui semble correspondre aux tests génétiques, d'après Durr, et al, (2009), il s'agit d'avancer non plus « dans la vie » mais d'avancer vers la mort (Minkowski, 1933). Cette perspective est angoissante par elle dépasse la personne du caractère positif de la vie.

## II. Questions de recherche et objectifs

En articulant ces différents éléments de la littérature avec les connaissances déjà mises en évidence par le projet INDIRA, nous avons formulé les questions de recherche suivantes :

### Questions de recherches :

- Quelles sont les représentations sociales des rayonnements ionisants en population générale
- Quelles perceptions de la prédiction possible du cancer ?

**Objectif principal :** Etudier les représentations des rayonnements ionisants et de la prédiction en santé.

**Objectif secondaire :** Etudier l'impact de la prédiction de la radiosensibilité individuelle sur les comportements de santé.

## III. Matériel et méthodes

Afin d'investiguer les différents aspects de cette problématique, deux phases de recueils de données seront réalisées.

### A. Des entretiens exploratoires

Les entretiens semi-directifs permettent d'amener un sujet à discuter sans a priori. Cette méthode est suffisamment guidée pour que la discussion concerne le sujet de la recherche et suffisant libre à la fois pour ne pas influencer la personne interrogée. De cette manière, nous pouvons affiner le reste de la recherche et voir si vous avons pris en compte toutes les dimensions de l'objet que nous étions ou s'il y a des impensés (Barthélémy, Le Pennec, 2018 ; Sauvayre, 2013). La grille d'entretien est présentée dans son intégralité en annexe 1.



Tableau 1. Résumé de la grille d'entretien exploratoire

N° des questions	Questions de recherche
	Introduction
1 à 6	Représentations des rayonnements ionisants
7 et 10	Perception de la prédiction des maladies
11	Clôture
Fiche signalétique	Sexe ; âge ; métier ; statut marital ; nombre d'enfant ; classes sociales perçues

## B. Questionnaire

Le questionnaire est construit à partir de l'analyse des données de la méthode exploratoire. Il investiguera les mêmes axes de recherche. Cette façon de procéder permet d'ajouter des impensées par les chercheurs, si les participants soulèvent des points qui n'ont jamais été mentionnés dans de précédentes études ou d'enlever les questions qui ne semblent pas pertinentes. C'est d'ailleurs le cas de l'association verbale proposé en début d'étude. En effet, l'analyse des entretiens nous a permis de nous rendre compte que le terme « rayonnements ionisants » ne correspondait à rien pour le grand public. Nous avons alors opté pour le terme « radiation » dans le questionnaire.

Le questionnaire se compose de quatre parties décrites dans le tableau ci-dessous. Le questionnaire est présenté dans son entier en annexe 2.

Tableau 2. Résumé du questionnaire

N° des questions	Questions de recherche
1 à 4	Perception des radiations
5 à 9	Perception de la prédiction de maladie
10 et 11	Perception des effets des radiation sur la santé
Fiche signalétique	Sexe ; âge ; CSP ; statut marital ; nombre d'enfant ; classes sociales perçues

## IV. Population étudiée

Qu'il s'agisse des entretiens exploratoires ou du questionnaire la population sera recrutée sur les mêmes critères :

- Sexe : mixte
- Age : > 18ns
- Catégories socio-professionnelles : variées
- Classes sociales perçues : variées

## V. Traitement des données et méthode d'analyse

### A. Entretiens exploratoires

Les entretiens seront analysés avec la méthode de l'analyse thématique de contenu par analogie sémantique. Cette méthode permet de réaliser, *in fine*, des statistiques descriptives permettant de mieux comprendre les réponses des participants (Bardin, 1977 ; Lejeune, 2014). Les statistiques descriptives seront réalisées sur Excel version 2408.



## B. Le questionnaire

Le questionnaire se compose à la fois de questions fermées à réponses uniques et de questions pour lesquelles les répondants pourront choisir plusieurs réponses. Dans les deux cas, les données seront analysées grâce à des statistiques descriptives. Celles-ci seront réalisées sur Excel version 2408.

L'ensemble des données fera ensuite l'objet d'une analyse globale de façon à mettre en évidence d'éventuelles corrélations entre les données socio-démographiques et les réponses aux questionnaires. Pour cela, le logiciel utilisé sera SPSS 29.0.2.0. Enfin, l'ensemble des résultats sera interprété à la lumière du cadre théorique précédemment décrit de façon à apporter un éclairage rigoureux aux questions de recherche.

## VI. Résultats des entretiens

La présentation des résultats débutera par la description de la population interrogée dans les entretiens. Ensuite, nous présenterons les résultats pour chaque question de façon descriptive. L'analyse des retranscriptions des entretiens a permis de regrouper les réponses sous forme de tableaux ou de graphique pour avoir des résultats concis.

### A. Description de la population

Les participants aux entretiens exploratoires étaient au nombre de cinq, âgés de 34 ans à 57 ans. Le tableau ci-dessous regroupe les différentes caractéristiques de l'échantillon.

Tableau 3. Caractéristiques sociodémographiques des participants aux entretiens exploratoires. N=5

	Genre	Âge	CSP	Statut marital	Enfant	Classes sociale perçue
1	Femme	40	Profession intermédiaire	Mariée	Oui	Classes moyennes supérieures
2	Femme	34	Profession intermédiaire	Pacsée	Non	Classes moyennes supérieures
3	Femme	34	Employée	Mariée	Oui	Classes moyennes modeste
4	Homme	38	Cadre	Vivant en union libre	Non	Classes moyennes modeste
5	Homme	57	Cadre	Divorcé	Oui	Classes moyennes supérieures

### B. Perception des radiations

Dans cette partie, nous présenterons pour chaque question les résultats synthétisés sous forme de graphique en rappelant la question posée. Les graphiques ont tous une légende décrivant ce qu'ils représentent de façon à éviter un texte descriptif pour chacun d'eux.



1. **Question 1 :** Pouvez-vous indiquer les 3 mots ou expressions qui vous viennent spontanément à l'esprit lorsque l'on vous dit : « **rayonnements ionisants** »

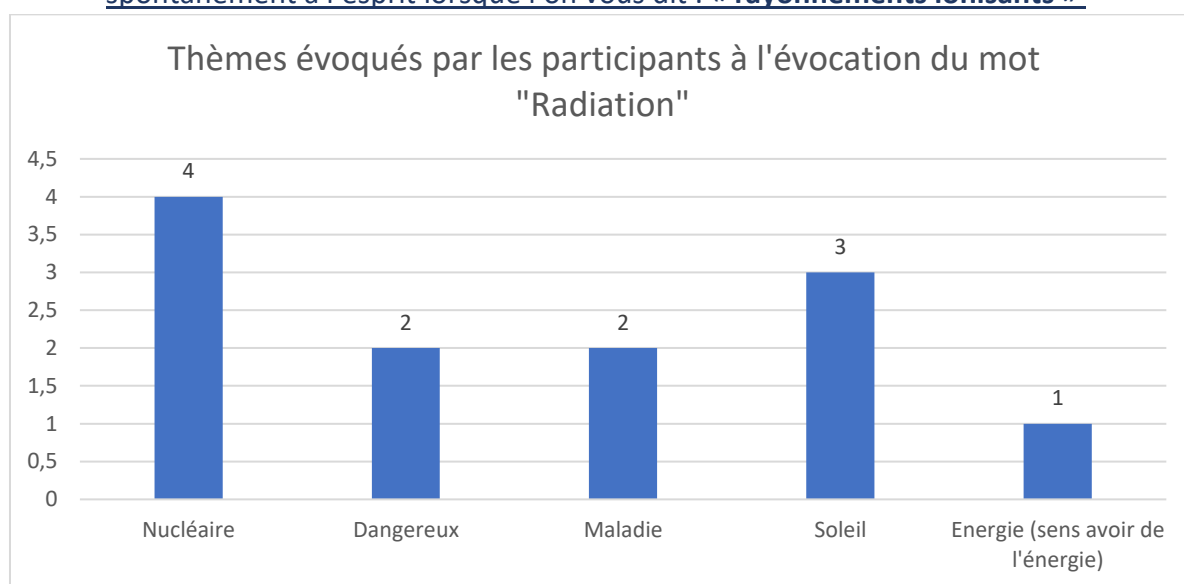


Figure 1. Thèmes évoqués par les participants aux entretiens à l'évocation du mot "Radiation". N=5

2. **Question 2 :** Pour vous est-ce un mot positif, négatif ou neutre ?

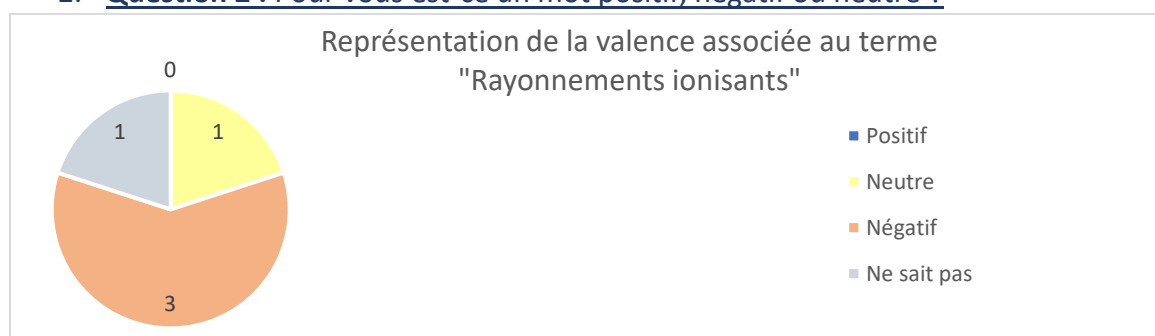


Figure 2. Représentation de la valence associée au terme "Rayonnements ionisants". N=5

3. **Question 3 :** Y a-t-il des implications positives aux rayonnements ionisants ? Si oui lesquelles ?

Tableau 4. Regroupement thématique des réponses de la question 3. N=5

Réponses	N
Radiothérapie	2
Traitement cancer	3
La recherche scientifique	1
Je ne sais pas	2



4. Question 4 : Pouvez-vous me parler des risques liés aux rayonnements ionisants ? Dans quels cas pouvez-vous y être exposé ? Niveau de gravité ?

Tableau 5. Regroupement thématique des réponses à la question 4. N=5

Items	N
Ne sait pas	2
Cancer	2
Problème de thyroïde	1
Maladies graves	1
Décès	1
Handicap	1
Accident de Tchernobyl	1

5. Question 5 : Avez-vous déjà entendu le terme « radio-induit » ? Si oui, pouvez-vous m'en parler ?

Parmi les 5 répondants aux entretiens aucun ne connaissait le terme « radio-induit »

### C. Perception de la prédiction des maladies

6. Question 6 : Imaginez que demain il soit possible de prédire si vous allez développer un cancer dans votre vie, qu'en pensez-vous ? Qu'est ce qui pourrait vous motiver à savoir / vous freiner ?

Les réponses à cette question ne sont pas tranchées car les participants exposent plusieurs arguments, parfois contradictoires qui leur permet de réfléchir à ce sujet. Les arguments développés par les répondants se divisent en trois groupes :

- Les conséquences négatives liées au fait de savoir : cela semble anxiogène pour certain et peut entrainer des conséquences négatives sur le quotidien.

P5 : « (...) ça fait un comme l'épée de Damoclès qui est au-dessus de ma tête et que plus l'échéance va arriver plus je vais savoir que je vais être malade. »

- Les conséquences positives liées au fait de savoir : les participants pensent que plus un cancer est diagnostiqué de façon précoce meilleurs sont les chances de guérison. Pour eux connaître ce statut permettrait de mettre en place un meilleur dépistage mais aussi de préparer leur entourage ou de mettre leurs papiers en règle.

P4 : « C'est plutôt une bonne chose, c'est intéressant. Au contraire même rassurant. Parce que ça permet de faire des actions préventives et donc justement d'y remédier. »

- Les nuances : la question de la fiabilité du test est évoquée par 2 participants ainsi que la question de la temporalité. Il faudrait pouvoir préciser une fourchette temporelle.

P5 « Etant scientifique et bah je me dis sur quelle base sont... se base les gens qui le prédisent...est-ce que c'est... sur quels critères. Moi je m'interrogerais sur la pertinence de la prédiction. »



Globalement, pour les répondants sont 4 à répondre qu'ils préféreraient savoir. Une seule personne ne souhaite pas connaître son avenir à ce sujet.

7. Question 7 : Imaginez que demain il soit possible de prédire si vous allez développer une maladie de maladie dégénérative (Alzheimer), comme dans votre vie, qu'en pensez-vous ? Qu'est ce qui pourrait vous motiver à savoir / vous freiner ?

De la même manière que pour le cancer, les réponses sur l'éventuelle prédiction d'une maladie dégénérative regroupent 3 types d'argument qui peuvent être évoqués par les mêmes participants au fur et à mesure de leur réflexion :

- Les conséquences négatives : connaître sont risques de maladies dégénératives seraient angoissant car, pour les participants, il n'existe pas de traitement pour ce type de maladie.

P2 : « *Je ne voudrais pas savoir (...) Euh... pour le moment ça ne se guérit et on ne sait pas trop quoi faire de ces gens.* »

- Les conséquences positives : le seul élément acceptable pour les répondants est qu'une solution leur soit proposé pour retarder le développement de la maladie.

P4 : « *Je m'intéresserais plus au traitement à ce qui peut être fait et je ferais plus d'actions pour prévenir ça. Donc oui de la même manière, ça me rassurerait qu'on puisse me diagnostiquer et me dire ou me dire non il n'y a pas de risques.* »

- Les nuances : Il s'agit dans ce cas d'une question de temporalité. Pour les répondants, il est beaucoup moins acceptable de savoir qu'une peuvent avoir une maladie dégénérative si elle intervient à un âge précoce par rapport à un âge plus avancé.

P2 : « *Après si c'est à 80 ans, j'ai envie de dire bon... à 80 ans, on a eu le temps de vivre pas mal quand même, même si ça serait pas mal que ça soit guérie maintenant. Mais si on m'annonçait qu'à 40 ans, c'est-à-dire dans 6 ans, je pourrais développer cette maladie, bah je crois que je préférerais vivre mes 6 dernières années de euh... naïveté une fois de plus peut être, assez tranquille, sans avoir à.. sans avoir à me poser la question de qu'est-ce que je dois mettre en place.* »

8. Question 8 : Pensez-vous que connaître ces risques futurs changeraient votre vie présente ? Comment ? Pourquoi ?

Pour les répondants connaître ces risques pourraient entraîner différents changements par rapport à leur vie actuelle. Un premier changement serait émotionnel car il entrainerait de l'anxiété. Néanmoins, on retrouve également des verbatims qui invitent à profiter davantage du moment présent avec l'évocation de plus de voyage pour 3 d'entre eux, de dépenser son argent pour 2 d'entre eux, de changer de regard sur la vie pour 3 répondants ou de réaliser des rêves pour 2 répondants. La notion de temporalité est également évoquée par un participant.

P1 : « *On va aller voyager parce qu'on ne pourra pas le faire quand je serais vieille parce que j'aurais Alzheimer, je pense oui que ça changera beaucoup de choses.* »



## VII. Résultats du questionnaire

Les données issues du questionnaire comprennent des données socio-démographiques qui nous permettent de débiter la présentation des résultats par la description de la population interrogée. Ensuite, nous présenterons les statistiques descriptives pour chaque question.

### A. Description de la population

Les participants aux questionnaires ont été 32 personnes entre 19 et 65 ans. Dans cette partie, nous présenterons la répartition de la population pour les variables choisies en amont du recueil : l'âge, la catégorie socio-professionnelle, le fait d'avoir des enfants ou d'en vouloir et enfin, le niveau de vie perçue.

Tableau 6. Caractéristiques sociodémographiques des participants au questionnaire. N = 32

<b>Variables</b>	<b>Modalités</b>	<b>N (%)</b>
<i>Genre</i>	Homme	13 (40,63)
	Femme	19 (59,38)
	Ni Homme ni femme	0 (0)
<i>Âge</i>	18 - 25 ans	5 (15,63)
	26 – 39 ans	9 (28,13)
	40 – 59 ans	17 (53,13)
	60 et plus	1 (3,13)
<i>Catégorie socio-professionnelles</i>	Agriculteurs exploitants	0 (0)
	Artisans, commerçants, chef d'entreprise	3 (9,38)
	Cadres et professions intellectuelles supérieures	14 (43,75)
	Professions intermédiaires	2 (6,25)
	Employés	7 (21,88)
	Ouvriers	0 (0)
	Retraités	1 (3,13)
	Autres personnes sans activités professionnelles	4 (12,50)
	Etudiants	1 (3,13)
<i>Statut marital</i>	Célibataire	10 (31,25)
	Vivant en union libre/ concubinage	7 (21,88)
	Marié.e	10 (31,25)
	Pacsé.e	3 (9,38)
	Veuf.veuve	0 (0)
	Divorcé.e	2 (6,25)
<i>Statut parental</i>	Ont des enfant	19 (59,38)
	N'ont pas d'enfant	13 (40,63)
<i>Classe sociale perçue</i>	Les classes privilégiées	1 (3,13)
	Les classes aisées	3 (9,38)
	Les classes moyennes supérieures	16 (50,00)
	Les classes moyennes modestes	8 (25,00)
	Les classes populaires	4 (12,50)
	Les classes défavorisées	0 (0)



## B. Perception des radiations

Afin de clarifier la présentation des résultats, nous présenterons les statistiques descriptives pour chaque question en rappelant la question en amont.

### 1. Question 1 : Pouvez-vous indiquer les 3 mots ou expressions qui vous viennent spontanément à l'esprit lorsque l'on vous dit : « radiation ».

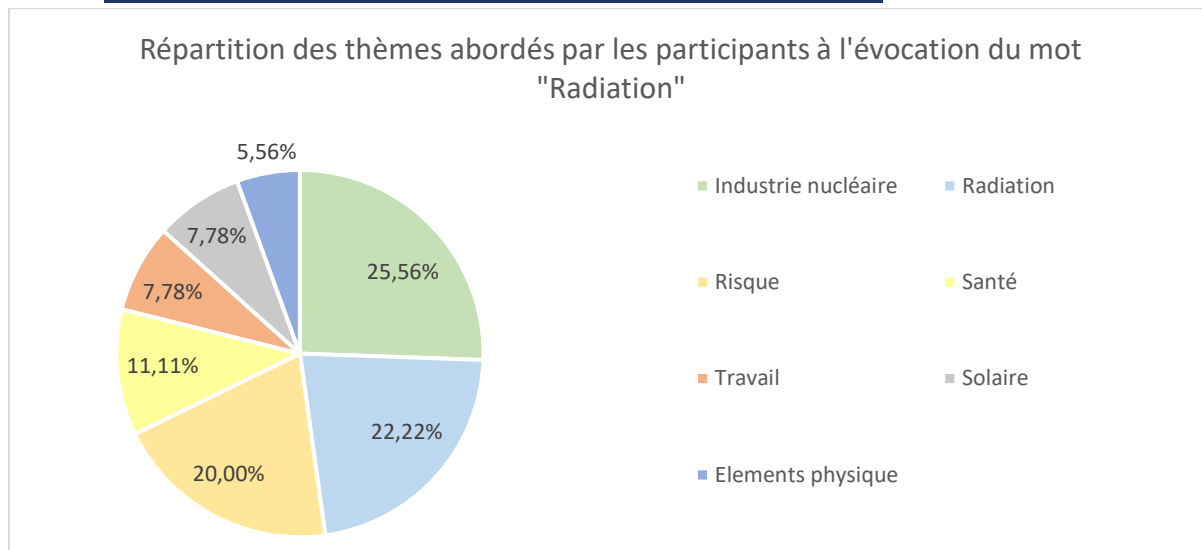


Figure 3. Regroupement thématique à l'association verbale "Radiation". N = 90

### 2. Question 2 : Pour vous, ce terme « radiation » est :

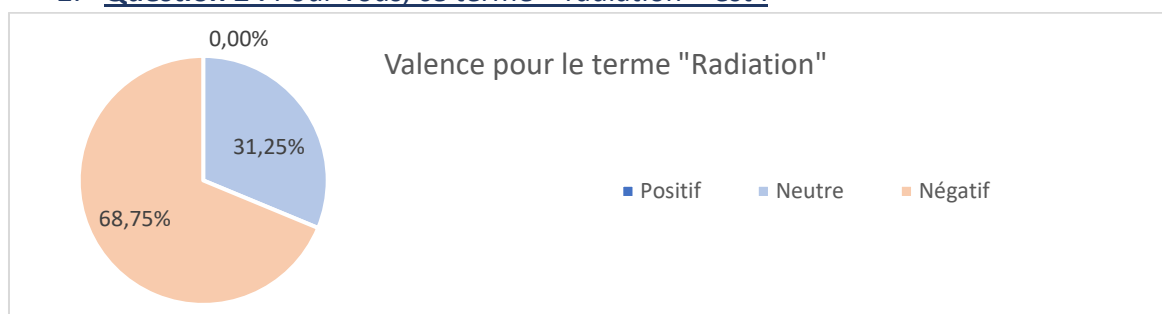


Figure 4. Valence associé au terme "radiation" N = 32

### 3. Question 3 : Selon-vous, dans votre vie, avez-vous déjà été exposé aux radiations ?

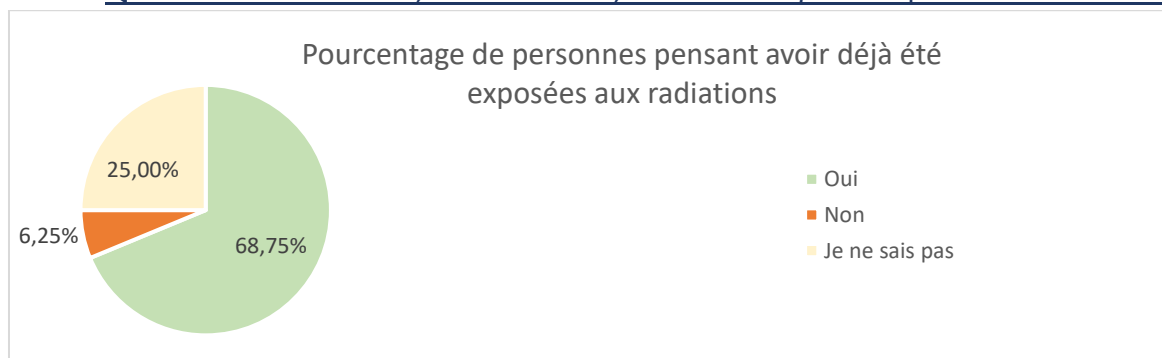


Figure 5. Pourcentage de personnes pensant avoir déjà été exposées aux radiations. N = 32



4. **Question 3.2 : Si oui : Dans quel contexte pensez-vous que vous avez été exposé aux radiations ?**

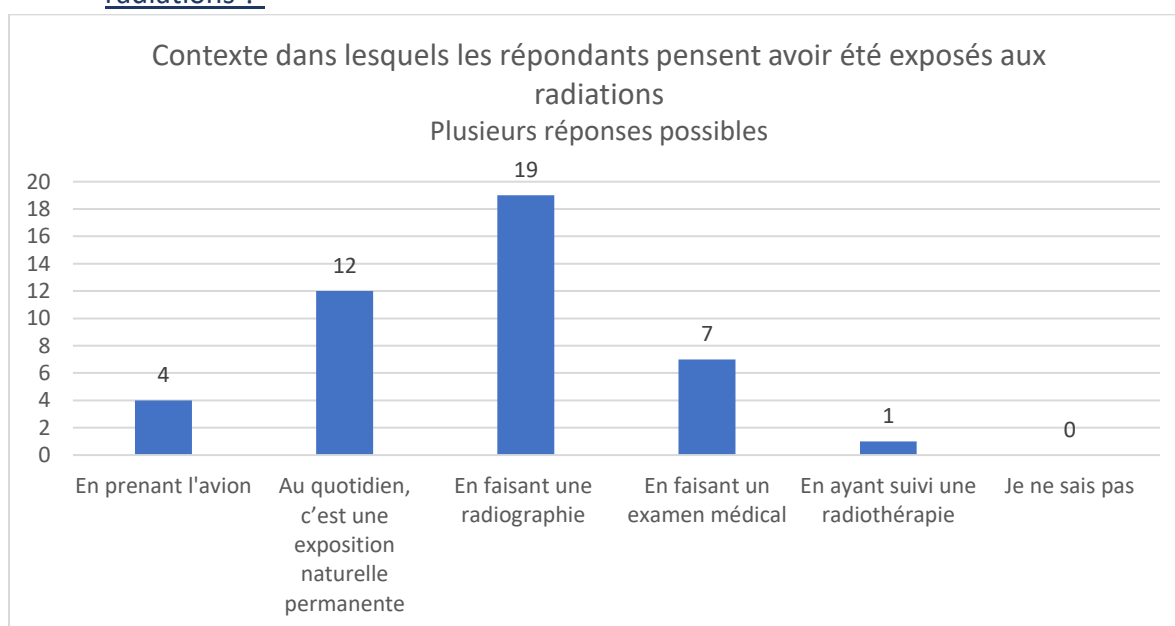


Figure 6. Contexte dans lesquels les répondants pensent avoir été exposés aux radiations. N = 86

5. **Question 4 : Selon vous, les radiations sont-elles**

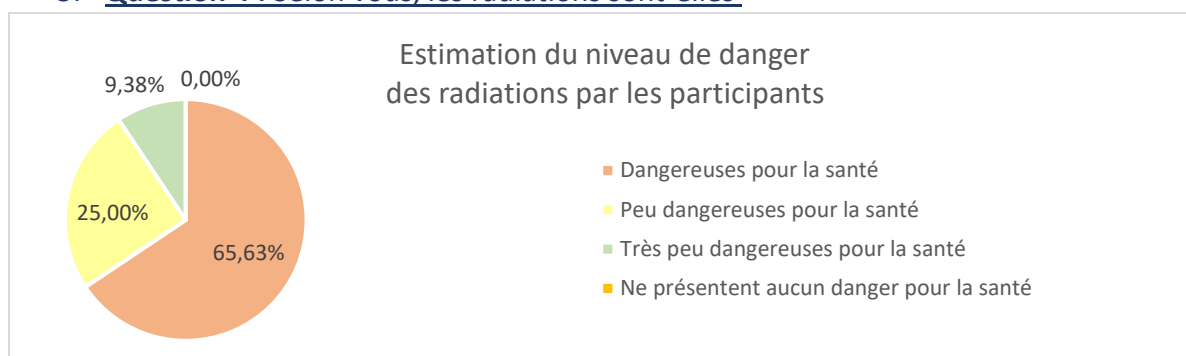


Figure 7. Estimation du niveau de danger des radiations par les participants. N = 32



## C. Perception de la prédiction de maladie

### 6. Question 5 : Imaginez que demain il soit possible de prédire si dans votre vie vous aurez un cancer, qu'en pensez-vous ?

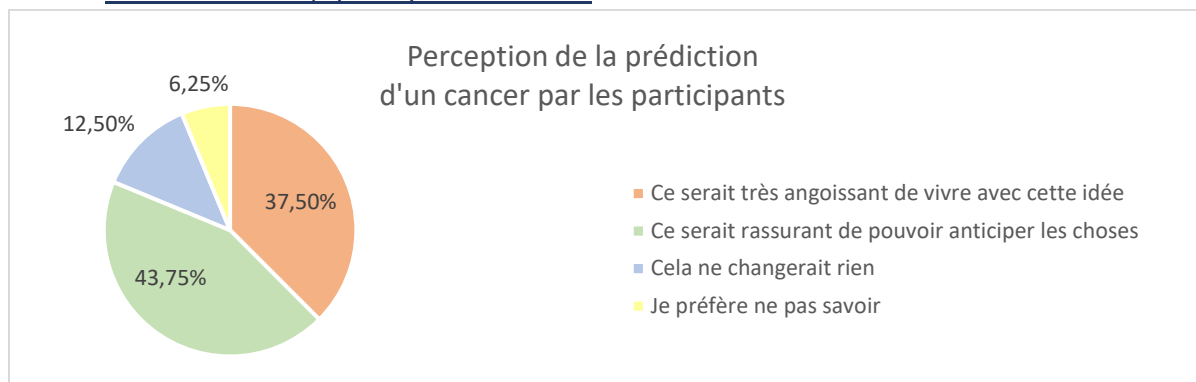


Figure 8. Perception de la prédiction d'un cancer par les participants. N = 32

### 7. Question 6 : Est-ce que cette perspective (toujours imaginaire de prédire un cancer) changerait votre façon d'agir dans le présent ?

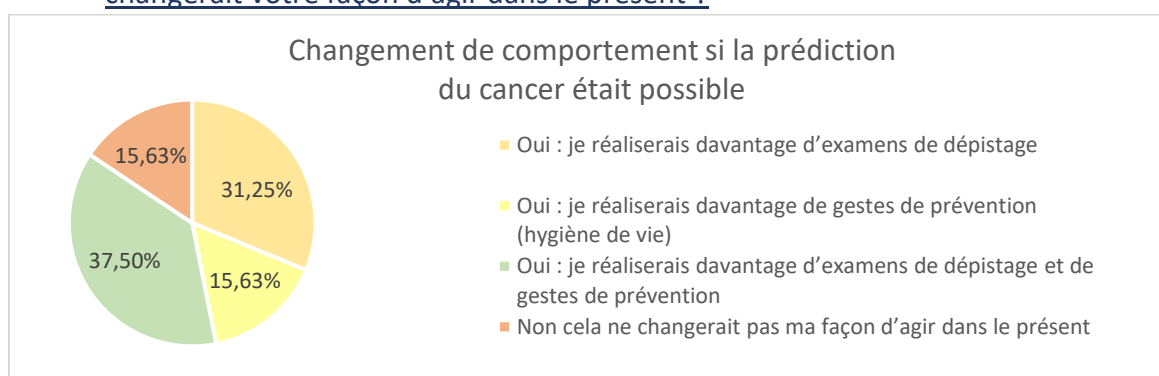


Figure 9. Changement de comportement si la prédiction du cancer était possible. N = 32

### 8. Question 7 : Imaginez que demain il soit possible de prédire si dans votre vie vous aurez une maladie dégénérative comme la maladie d'Alzheimer, qu'en pensez-vous ?

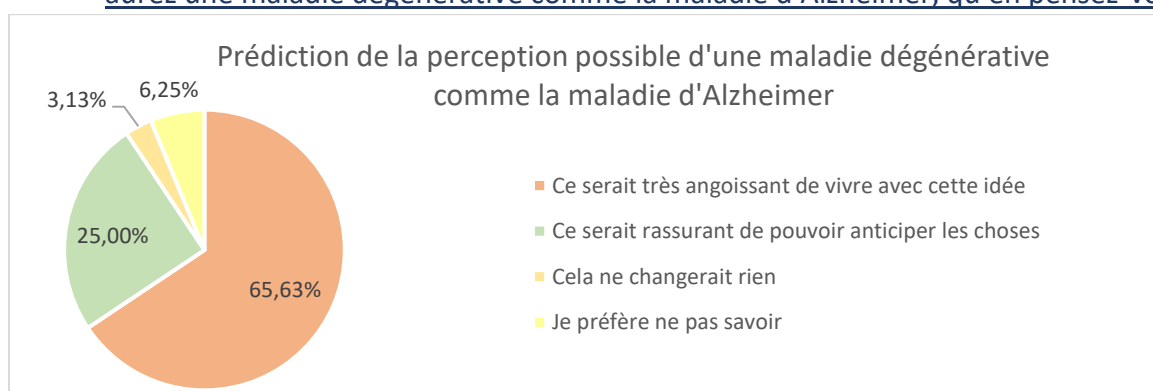


Figure 10. Prédiction de la perception possible d'une maladie dégénérative comme la maladie d'Alzheimer. N = 32



9. **Question 8 : Est-ce que cette perspective (toujours imaginaire de prédire une maladie d'Alzheimer) changerait votre façon d'agir dans le présent ?**

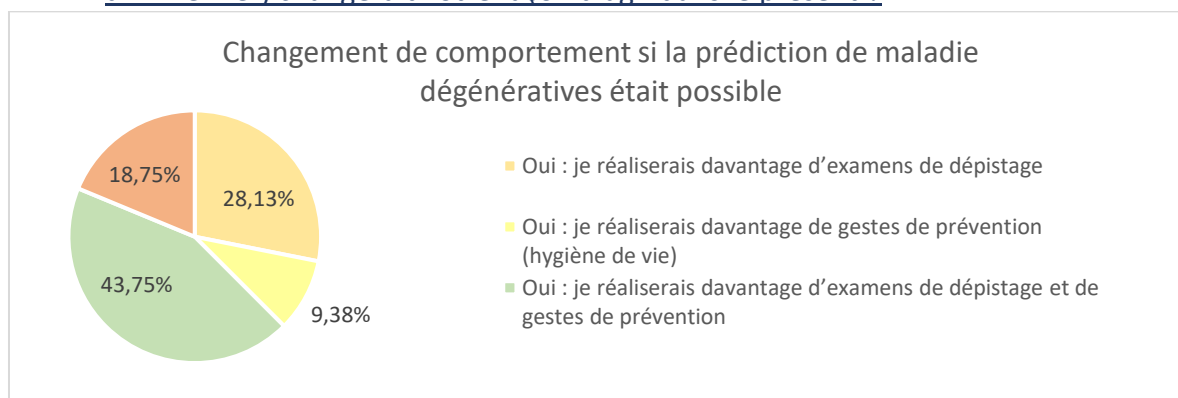


Figure 11. Changement de comportement si la prédiction de maladie dégénératives était possible. N = 32

10. **Question 9 : Est-ce que connaître votre « avenir-santé » (cancer ou maladie d'Alzheimer) vous ferait envisager : (plusieurs réponses possibles)**

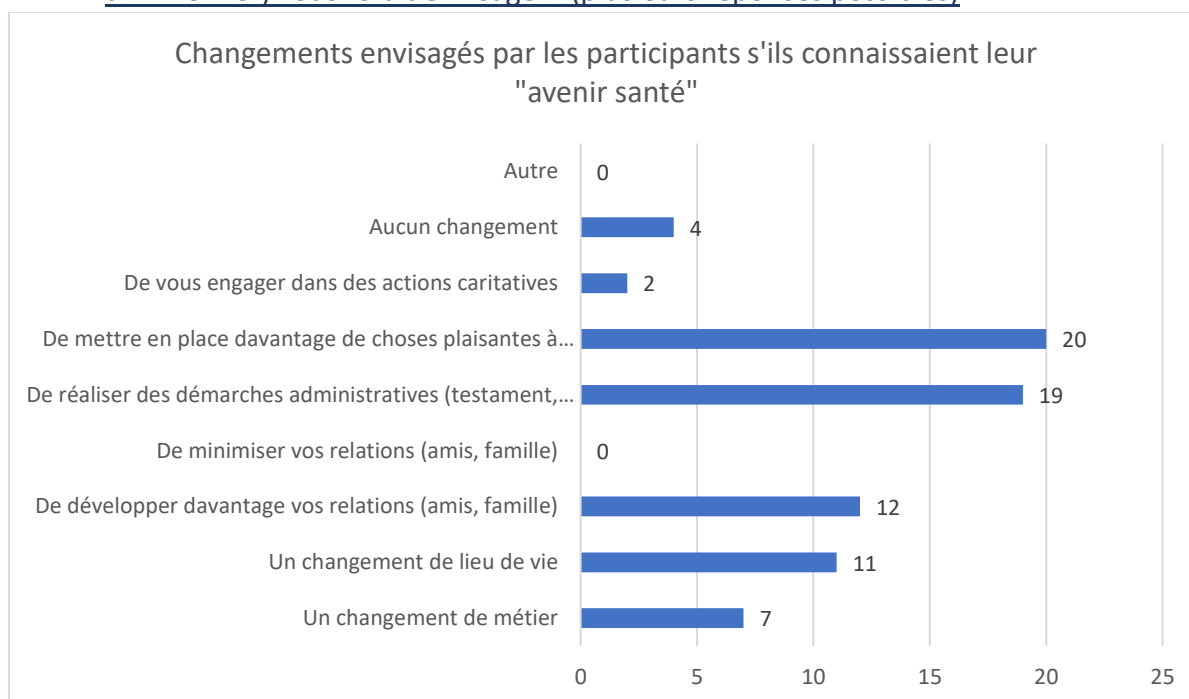


Figure 12. Changements envisagés par les participants s'ils connaissaient leur "avenir santé". N = 32



## D. Perception des effets des radiation sur la santé

### 11. Question 10 : Selon vous, l'exposition aux radiations augmente-t-elle le risque de développer un cancer ?

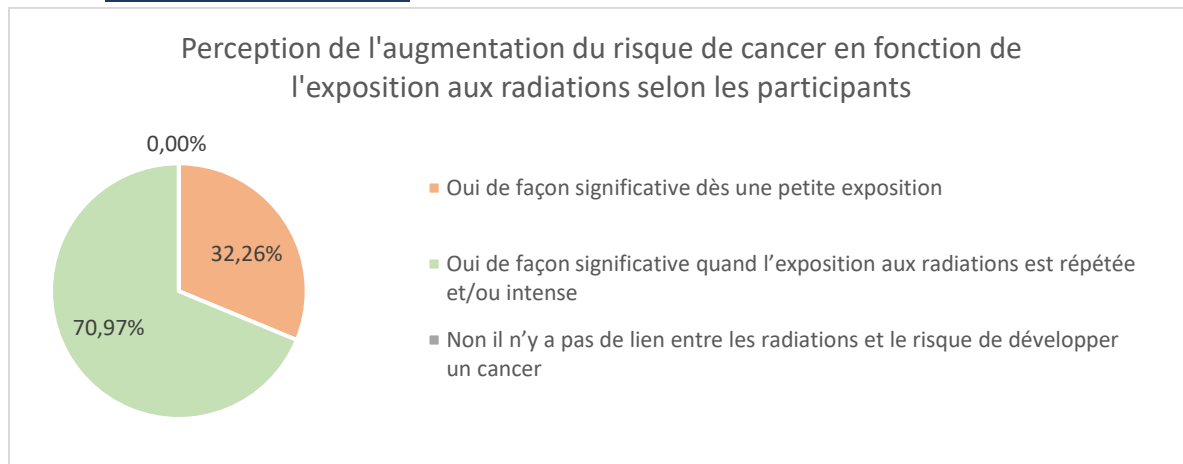


Figure 13. Perception de l'augmentation du risque de cancer en fonction de l'exposition aux radiations selon les participants. N = 32

### 12. Question 11 : Selon vous, l'exposition aux radiations est-elle bénéfique pour la santé ?

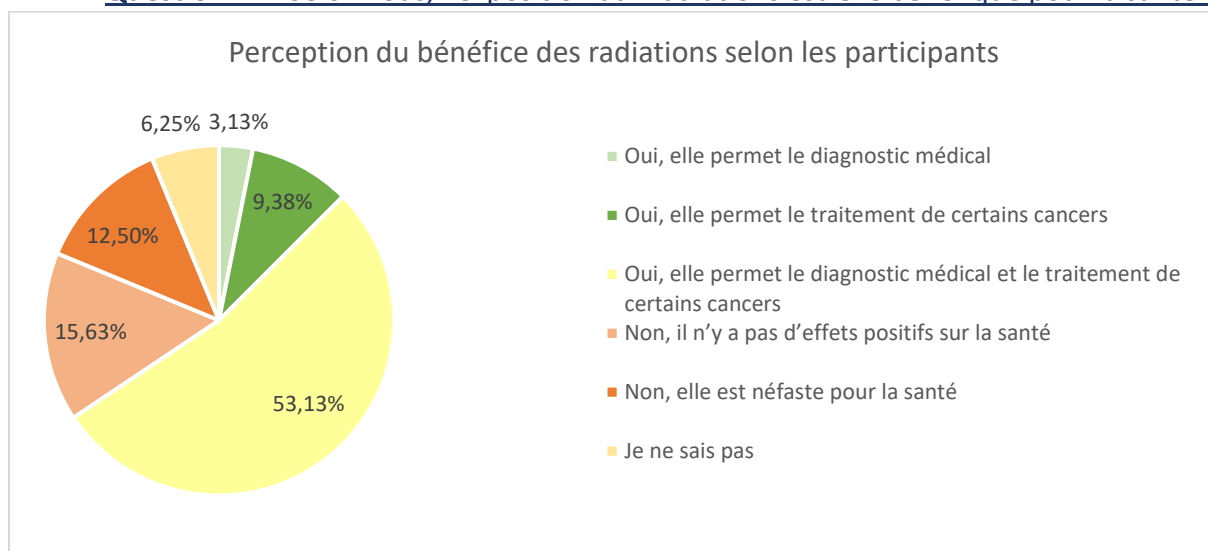


Figure 14. Perception du bénéfice des radiations selon les participants. N = 32



## VIII. Analyses croisées

Afin de donner du sens aux résultats, nous avons cherché à savoir s'il existait des groupes de répondants qui ont tendance à répondre que le fait de savoir si un cancer pourrait être prédit les rassure plutôt que leur fait peur. La variable dépendante utilisée est : « *Cela serait rassurant de pouvoir anticiper les choses face à la possible prédiction d'un cancer* ». Sur les 32 répondants, le premier groupe est constitué de personnes qui ont répondu que « cela serait angoissant » (N = 14). Compte tenu du peu de répondants, pour que les données aient plus de sens, nous avons regroupé les répondants « Ce serait très angoissant de vivre avec cette idée » N = 12 avant « Je préfère ne pas savoir » N = 2. De la même manière, pour le deuxième groupe, nous avons compté les répondants « Ce serait rassurant de pouvoir anticiper les choses » N = 14 avec « Cela ne changerait rien » N = 4. Ainsi le deuxième groupe compte N = 18. Le modèle le plus explicatif obtenu est décrit dans le tableau ci-dessous (tableau 7) avec un R<sup>2</sup> de Cox and Snell <sup>1</sup> de 0.523. En gris et en italique sont indiquées les variables de références. La colonne de la variable B indique le sens de lecture : si B est positive, et que la P valeur est <.05, la variable est associée au fait de trouver la possible prédiction du cancer angoissante. Si B est négatif, la variable est associée au groupe de référence, dans ce modèle, trouver la possible prédiction du cancer rassurante.

Tableau 7. Régression logistique binaire sur les facteurs associés à la variable "Ce serait rassurant de pouvoir anticiper les choses". N = 32

Variables	N (%)	P valeur	B	Exp(B)	Intervalle de confiance pour Exp(B) inf sup	
A quel sexe vous identifiez-vous						
Homme	13 (40,63)	,199	-1,603	,201	,017	2,324
<i>Femme</i>	<i>19 (59,38)</i>					
Quel est votre âge ?		1,000				
18 - 25 ans	5 (15,63)	,999	-16,471	,000	,000	.
26 - 39 ans	9 (28,13)	,999	-54,528	,000	,000	.
40 - 59 ans	17 (53,13)	1,000	-13,067	,000	,000	.
<i>Plus de 60 ans</i>	<i>1 (3,13)</i>					
Quelle est votre catégorie socioprofessionnelle ?		,999				
Agriculteurs exploitants	0 (0)	,999	17,671	47.10 <sup>6</sup>	,000	.
Artisans, commerçants, chef d'entreprise	3 (9,38)	1,000	-,593	,553	,000	.
Cadres et professions intellectuelles supérieures	14 (43,75)	,999	17,987	64.10 <sup>6</sup>	,000	.
Professions intermédiaires	2 (6,25)	,998	75,933	92.10 <sup>31</sup>	,000	.
Employés	7 (21,88)	,998	35,431	18.10 <sup>15</sup>	,000	.
Ouvriers	0 (0)	,999	17,671	47.10 <sup>6</sup>	,000	.
Retraités	1 (3,13)	1,000	-,599	,599	,000	.

<sup>1</sup> Le R<sup>2</sup> de Cox and Snell est un coefficient de détermination qui définit la proportion de la variance de la variable dépendante expliquée par les variables indépendantes du modèle. Plus le R<sup>2</sup> est élevé et plus le modèle multivarié explique une grande partie de la variance. Si R<sup>2</sup> = 0,523 cela signifie que 50,3 % de la variance est expliqué par ce modèle (Draper, Smith, 1998 ; Glantz, Slinker, Neiland, 1990). Les P valeurs sont considérées significatives si P < 0.05, soit si la probabilité est supérieure à 95 %.



Autres personnes sans activités professionnelles	4 (12,50)	1,000	-,613	,633	,000	
<i>Etudiants</i>	<i>1 (3,13)</i>					
Quel est votre statut marital ?		1,000				
Célibataire	10 (31,35)	,998	37,821	26.10 <sup>15</sup>	,000	.
Vivant en union libre/ concubinage	7 (21,88)	,998	37,431	18.10 <sup>15</sup>	,000	.
Marié.e	10 (31,25)	,998	77,807	61.10 <sup>32</sup>	,000	.
Pacsé.e	3 (9,38)	,998	75,923	93.10 <sup>31</sup>	,000	.
Veuf.veuve	0 (0)	,999	18,671	45.10 <sup>6</sup>	,000	
<i>Divorcé.e</i>	<i>2 (6,25)</i>					
Voici différents groupes de population. En fonction de votre situation personnelle, de celle de votre foyer et de votre manière de vivre, auquel de ces groupes pensez-vous appartenir ?		,800				
Les classes privilégiées	1 (3,13)	1,000	-19,666	,000	,000	.
Les classes aisées	3 (9,38)	1,000	-21,435	,000	,000	.
Les classes moyennes supérieures	16 (50,00)	1,000	-22,762	,000	,000	.
Les classes moyennes modestes	8 (25,00)	1,000	-22,349	,000	,000	.
Les classes populaires	4 (12,50)	,999	73,929	92.10 <sup>31</sup>	,000	
<i>Les classes défavorisées</i>	<i>0 (0,00)</i>					
Constante		1,000	21,203	16.10 <sup>8</sup>		

L'analyse multivariée ne montre pas d'association entre le fait d'être rassuré par la prédiction précoce d'un cancer et les différentes données sociodémographiques avec lesquelles nous les avons comparées. En effet, aucune P valeur n'est significative.

## IX. Discussion

Dans cette partie, nous nous attacherons à donner du sens aux résultats précédent grâce à la littérature scientifique. Nous débiterons par une interprétation des représentations sociales des radiations. Ensuite, nous développerons la question de la prédiction des maladies, notamment du cancer. Enfin dans une dernière partie, nous apporterons une explication à la taille réduite de l'échantillon que nous avons obtenu.

### A. Représentations sociales des radiations

Le questionnaire avait pour objectif d'étudier la perception de l'exposition aux radiations au sein de la population générale. Nos données ont permis de montrer que le terme « radiation » est principalement associé aux centrales nucléaires, aux radiations (exemple d'items : « rayons », « irradié », « radium ») et aux risques (exemple d'items : « brûlure », « danger », « mort »). La valence associée est à 65,63 % négative. Ce résultat va dans le sens de la littérature scientifique à ce sujet. Les représentations des radiations sont négatives et perçues comme dangereuses (Britel, et al 2020 ; Galli, Nigro, 1987). Ce résultat peut être lu à travers le niveau III d'analyse de Doise (Doise, 1982). Ancré dans l'approche des représentations sociales, Willem Doise a défini 4 niveaux d'analyse allant de l'interprétation la plus individuelle à la plus systémique. Cette approche permet d'affiner l'analyse



représentationnelle et d'en comprendre les différents niveaux d'implication. Il part de l'idée que l'expérience inter-individuel va alimenter la représentation au niveau du groupe, elle-même nourrit de la pensée systémique. Dans ce cas, la perception des radiations comme référent aux centrales nucléaires et aux dangers, voir même, à la souffrance physique, est probablement influencée par l'histoire collectif des accidents de Tchernobyl en 1986 ou de Fukushima en 2011. Cette représentation est alimentée par la peur des conséquences possibles des centrales. Dans ce cas, la visée pratique des représentations sociales est celle de la prudence (Jodelet, 1989, Moscovici 1961). A titre de comparaison, une autre visée pratique des représentations aurait pu être l'utilité des centrales nucléaires en faisant référence à la production d'électricité.

Ensuite, nos données montrent que les répondants ont majoritairement conscience d'être irradié car 68,75 % d'entre eux répondent : « oui » à la question « *Selon-vous, dans votre vie, avez-vous déjà été exposé aux radiations ?* ». Néanmoins, ils pensent que cette exposition est dangereuse à 70,97 % si celle-ci est répétée ou intense. De plus, 34,38 % des répondants pensent qu'il n'y a aucun effet positif pour la santé. Ce résultat étaye les éléments de représentations sociales que nous venons de proposer. La question 3.1 : « *Dans quel contexte pensez-vous que vous avez été exposé aux radiations ? (Plusieurs réponses possible)* », 19 personnes ont répondu « *En faisant une radiographie* » et/ou « *En faisant un examen médical* ». Ce résultat montre que malgré une représentation de radiation comme étant dangereuse et une certaine connaissance que les radiations sont utilisées en médecin, les répondants acceptent ce type d'irradiation. Cela peut s'expliquer par le fait qu'ils auraient également connaissance de la balance bénéfice / risque. En effet, si la balance bénéfice risque penche en faveur d'un bénéfice immédiate pour un risque seulement probable à long terme, il semble préférable de réaliser l'examen. Si le principe de précaution était appliqué *stricto sensu*, aucun examen utilisant les rayonnements ionisants ne pourrait être utilisé puisque ce principe revendique le risque zéro (David, 2009). Or, l'équilibre entre dans le calcul du bénéfice et du risque, le bénéfice immédiate (diagnostic urgent ou dépistage préventif) est souvent en faveur de la réalisation de l'examen. Cela est d'autant plus vrai que le niveau de radiosensibilité individuelle n'est généralement pas connu (Etner, 2011 ; Foray et al, 2013).

## B. Prédiction des maladies

La deuxième partie du questionnaire indique que 43,75 % des répondants pensent qu'il serait plus rassurant de pouvoir prédire la survenue d'un cancer. Ce chiffre tombe à 25 % quand il s'agit de la maladie d'Alzheimer. Pour mieux comprendre ce résultat, nous avons réalisé une régression logistique binaire dont le but était d'identifier d'éventuel groupes de répondants en fonction de leurs caractéristiques socio-démographiques. Néanmoins, le meilleur modèle que nous avons obtenu n'a un  $R^2$  de Cox and Snell que de 0.523 et aucune variable significative n'a pu être mise en évidence. De fait, l'interprétation que nous proposons dans ce paragraphe ne tient que sur les statistiques descriptives réalisées.

Le résultat montrant que 43,75 % des répondants pensent qu'il serait plus rassurant de connaître la survenue éventuelle d'un cancer longtemps à l'avance parce que cela leur permettrait de mettre en place des actions de prévention ou de dépistage. Ce point est étayé par la question sur la maladie d'Alzheimer pour laquelle les répondants pensent qu'il n'existe aucun traitement. P2 : « *je ne voudrais pas savoir (...) Euh... pour le moment ça ne se guérit et on ne sait pas trop quoi faire de ces gens* ». Ces résultats semblent aller dans le sens de la peur de la maladie. En effet, nos sociétés occidentales ont placé la santé au rang de norme. La norme « santé » implique qu'un individu tombant malade, *de facto* n'appartient plus au groupe socialement valorisé des personnes en bonne santé. Ce concept de l'*Homo medicus* (Peretti-Watel, Moatti, 2009) suggère une forme de responsabilité de la santé. L'*homo*



*medicus* est l'Homme qui sait protéger sa santé, il a les bons comportements de prévention, il consulte son médecin toujours au bon moment, sans tomber dans l'hypocondrie pour autant. Cette injonction de préserver la santé peut expliquer les réponses qui semblent guidées par la peur. En revanche, la différence entre ceux qui sont rassurés et ceux qui se sentent angoissés peut s'expliquer par leur perception de leur pouvoir d'agir sur la situation. En effet, pour le cancer, davantage de répondant se sentent rassurés, parce qu'ils perçoivent d'une part, des moyens de prévention et de dépistage et d'une autre part, des traitements efficaces. Nous rappelons que la représentation au cancer est aujourd'hui associée à une maladie chronique et non plus à une fatalité (Moulin, 2005).

Au-delà de la question de l'identité sociale d'être malade ou en bonne santé, il est également la question de la peur de la souffrance associée à la maladie et bien entendue de la mort prématurée. On retrouve ici des éléments de la représentation de la maladie comme « maladie destructrice » (Herzlich 1969). Pour rappel, l'auteur a défini 3 types de représentations de la maladie : la maladie libératrice (le patient construit une nouvelle identité grâce à la maladie), la maladie métier (dans laquelle le patient engage une lutte active et devient expert de sa maladie) et la maladie destructrice. Dans ce dernier cas, la maladie renvoie à la désocialisation de la personne. La personne se sentirait diminuée, anéantie mais pour autant, elle rejette l'idée de mort (Herzlich 1969). La perspective de notre propre finitude est difficile à envisager pour la majorité d'entre nous. C'est ce que questionne Gérard Apfeldorfer (2021) dans un ouvrage dans lequel il met en perspective les différents outils développés par les Hommes pour accepter cette idée : les religions, la philosophie comme alternative laïque ou encore le « bien mourir », la souffrance de fin de vie, etc. La conceptualisation de sa propre mort impose alors de trouver un sens spirituel pour quel celle-ci deviennent acceptable, (Apfeldorfer, 2021). Ainsi, le fait de connaître si longtemps à l'avance l'éventualité du développement d'un cancer ou d'une maladie dégénérative semble induire un questionnement profond sur notre propre finitude. Ce point paraît mieux accepté par les répondants qui se sont déjà confrontés à ce type de questionnement grâce leur métier ou leur histoire de vie, d'après l'analyse des entretiens.

### C. Taille de l'échantillon, une limite évidente.

Ce travail n'a pu interroger qu'un très petit nombre de personnes. Nous souhaitons dans ce paragraphe questionner ce point que nous considérons dans l'ensemble de l'interprétation des données comme la limite majeure de l'étude. En effet, le nombre total de répondant à l'étude n'a pu être que de 32 répondants. Pourtant, la diffusion du questionnaire a été la plus large possible sur les réseaux sociaux, via les réseaux personnels et professionnels et les relances ont été nombreuses. La première explication est que le questionnaire a été diffusé du 10 juillet au 21 août. Durant cette période de vacances estivales, il est possible que peu de personne n'ait pris le temps de réponse ou même de consulter les réseaux ou leurs emails. Ensuite, nous constatons que 11 personnes se sont connectées aux questionnaires et n'ont pas poursuivi au-delà de la question 1. Nous pouvons supposer que le sujet en lui-même est un frein car dans l'introduction du questionnaire il est expliqué que nous parlerons de santé à travers les radiations et le cancer. Dans ce cas, la peur de se confronter à un sujet délicat pourrait expliquer que 11 personnes ne sont pas allés au bout du questionnaire. Ce point renvoie à l'interprétation précédemment développé de la peur de la maladie et la mort.



## X. Conclusion

L'étude de la perception la prédiction du cancer envers le grand public a impliqué l'approfondissement des représentations sociales des radiations. L'ambivalence de la question de la perception des risques et de l'exposition aux rayonnements ionisants du point de vue du grand public nous a invité à étudier cette question sous l'angle :

- Des travaux sur les représentations sociales dans une perspective sociogénétique. De cette manière, il est possible d'étudier la pensée groupale autour d'un objet complexe dans le discours de sens commun.
- Des travaux sur la prédiction de maladie car d'autres maladies font d'ores et déjà l'objet de tests génétiques précoces.
- Des normes de santé qui guident nos pensées et comportements à tous de façon implicite.

Nos résultats ont montré que les représentations des radiations s'inscrivent dans une dimension de prudence mais elles sont immédiatement associées aux centrales nucléaires avant de penser aux aspects médicaux de leurs utilisations. Envisager le développement d'une maladie demeure inquiétant pour tout le monde car, les personnes ne se sentent rassurées que par les possibles actions pour repousser ou soigner la maladie. L'objectif santé reste prioritaire et normatif. Enfin, la notion d'augmentation des risques de maladie en fonction des radiations est plutôt connue par les répondants qui ont conscience des risques des radiations de façon globale. Pour rappel, les participants ont répondu à 65,53 % que les radiations sont dangereuses pour la santé et 100 % ont répondu que les radiations augmentent le risque de cancer (32,26 % dès une petite exposition et 70,97 % quand l'exposition est répétée ou intense).

Cette étude souligne alors la nécessité d'accompagner le test prédictif de façon pluridisciplinaire. Les inquiétudes, voir les angoisses, associées aux résultats doivent être accompagnées par un psychologue. L'accompagnement semble nécessaire que les résultats du test inscrivent les patients dans un groupe de réponses normales à la réparation des cassures doubles brins d'ADN ou à un groupe radiosensible. Ce point est un enseignement des travaux sur les personnes testées pour la maladie de Huntington. Enfin, un accompagnement sur les possibles gestes ou examens de prévention ainsi que les traitements envisageables pour les maladies semble également primordial et souhaité par les répondants.



## XI. Bibliographie

- Apfeldorfer, G. (2021). *Oser vivre, oser mourir*. Paris : Odile Jacob.
- Apostolidis, T. (2006). Représentations sociales et triangulation : une application en psychologie sociale de la santé. *Psicologia: Teoria e Pesquisa*, 22(2), 211-226.
- Arwidson, P. (2013). Développer en France une prévention à l'efficacité prouvée. *Actualité et Dossier de Santé Publique*, 83, 32-34.
- Bardin, L. (1977). *L'analyse de contenu*. Paris : Presses Universitaires de France.
- Barthelémy, M.-L., & Le Pennec, H. (2018). Outils 23. L'entretien exploratoire. In *L'accompagnement professionnel* (pp. 70-71). Paris : Dunod.
- Britel, M., Bourguignon, M., & Préau, M. (2020). How does radioprotection fit into the social representation of mammography in the mainstream press? *Public Health*.
- Byrne, A., Ellershaw, J., Holcombe, C., & Salmon, P. (2002). Patients' experience of cancer: Evidence of the role of 'fighting' in collusive clinical communication. *Patient Education and Counseling*, 48, 15-21.
- Coopman, A. L., & Janssen, C. (2006). La maladie génétique au cœur de la fratrie : « Tabou » et « Secret ». *Cahiers de Psychologie Clinique*, 2(27), 39-54.
- Dany, L., Dubois, E., & Favre, R. (2008). Analyse des représentations sociales du cancer et de la souffrance. *Psycho-Oncologie*, 2, 53-58. <https://doi.org/10.1007/s11839-007-0045-x>
- Deschamps, J.-C., & Paez, D. (1999). L'identité en psychologie sociale : Processus cognitifs, facteurs relationnels et représentations sociales. In J.-C. Deschamps, J.-F. Morales, D. Paez, & S. Worchel (Eds.), *L'identité sociale* (pp. 13-18). Grenoble : Presses Universitaires de Grenoble.
- Doise, W. (1982). *L'explication en psychologie sociale*. Paris : Presses Universitaires de France.
- Doise, W., & Palmonari, A. (1986). *Représentations sociales*. Paris : Delachaux et Niestlé.
- Draper, N., & Smith, H. (1998). *Applied Regression Analysis*. New York : Wiley-Interscience.
- Durkheim, E. (1898). *Représentations individuelles et collectives*. Paris : Presses Universitaires de France.
- Durr, A., et al. (2009). Les enjeux de la médecine prédictive en neurogénétique : Quelle place pour l'homme ? *Champ Psychosomatique*, 3(5), 83-95.
- Etner, J. (2011). Comment comprendre les comportements face à l'évolution des risques. *Humanisme et Entreprise*, 1(301), 13-28.
- Foray, N., Colin, C., & Bourguignon, M. (2013). Radiosensibilité : L'évidence d'un facteur individuel ? *Médecine Sciences*, 29, 397-403.
- Galli, I., & Nigro, G. (1987). The social representation of radioactivity among Italian children. *Social Science Information*, 26(3), 535-549.
- Gargiulo, M. (2009). Long-term outcome of presymptomatic testing in Huntington disease. *European Journal of Human Genetics*, 17, 165-171.



- Gargiulo, M., & Durr, A. (2014). Anticiper le handicap. Les risques psychologiques des tests génétiques. *Esprit*, 7, 52-65.
- Glantz, S., Slinker, B., & Neiland, T. (1990). *Primer of Applied Regression and Analysis of Variance*. New York : McGraw-Hill.
- Herzlich, C. (2015). *Représentations sociales et mondes de vie*. Suresnes : Archives Contemporaines.
- Institut de Radioprotection et de Sûreté Nucléaire (IRSN). (2018). *Baromètre 2018 – Essentiels*. Fontenay-aux-Roses : IRSN.
- Jodelet, D. (1984). Les représentations sociales : Phénomène et théorie. In S. Moscovici (Ed.), *Psychologie sociale* (pp. 357-378). Paris : Presses Universitaires de France.
- Jodelet, D. (1989). *Folie et représentations sociales*. Paris : Presses Universitaires de France.
- Lejeune, C. (2014). *Manuel d'analyse qualitative sans compter ni classer*. Paris : De Boeck.
- Minkowski, E. (1933). *Le temps vécu*. Paris : Presses Universitaires de France, 1995.
- Moscovici, S. (1961). *La psychanalyse, son image et son public*. Paris : Presses Universitaires de France.
- Moulin, P. (2005). Imaginaire social et cancer. *Revue Francophone de Psycho-Oncologie*, 4(4), 261-267.
- Moulin, P. (2005). Imaginaire social et cancer. *Revue Francophone de Psycho-Oncologie*, 4(4), 261-267.
- Peretti-Watel, P., & Moatti, J.-P. (2009). *Le principe de prévention*. Paris : République des Idées.
- Peretti-Watel, P. (2013). Principe et mise en œuvre de la prévention. *Actualité et Dossier de Santé Publique*, 83, 29-31.
- Peretti-Watel, P., & Vergely, C. (2012). Antenne relais et cancer : Évolutions et déterminants du risque perçu par le public, 2005-2010. *Santé Publique*, 3(24), 209-218.
- Peto, J. (2001). Cancer epidemiology in the last century and the next decade. *Nature*, 411, 390-395.
- Pinell, P. (1992). *Naissance d'un fléau : Histoire de la lutte contre le cancer en France (1890-1940)*. Paris : Éditions Métailié.
- Sauvayre, R. (2013). La préparation à l'entretien. In *Les méthodes de l'entretien en sciences sociales*. Paris : Dunod.
- Triandafillidis, A. (1990). Temps du savoir et temps de l'incertitude. *Psychanalyse à l'Université*, 60, 15-60. Paris : Presses Universitaires de France.



## XII. Annexes

### A. Annexe 1 : grille d'entretien



## Projet INDIRA

### Entretien de recherche

#### Contrat de communication

Nous vous proposons d'apporter votre contribution à une recherche scientifique dirigée par Dr Manon Britel, Ph.D., psychologue, docteur en psychologie. Ce projet de recherche s'inscrit dans la continuité du projet INDIRA.

Le **projet INDIRA** vise à mieux comprendre la notion de radiosensibilité individuelle et à en mesurer sa fréquence dans la population générale.

**Objectif de l'étude en sciences humaines et sociales :** Investiguer les représentations des rayonnements ionisants en population générale afin de compléter la compréhension du projet INDIRA.

#### Modalité de l'entretien :

- Il s'agit d'un entretien de recherche. En aucun cas, il ne sera question d'un entretien thérapeutique. Toutefois, si vous le souhaitez, les coordonnées de psychologues pourront vous être communiquées.
- Il n'y a ni bonne ni mauvaise réponse, seul votre avis nous intéresse.
- L'entretien sera **strictement anonyme et confidentiel**, conformément aux règles établis par la CNIL et à notre déontologie (code de déontologie des psychologues de France révisé en 2012). Seules les conclusions de l'étude feront l'objet d'une communication.

**Durée de l'entretien :** environ 30 minutes.

Dans le strict cadre de l'étude et selon le strict anonymat et la confidentialité de l'entretien autorisez-vous l'enregistrement de la rencontre ?

- ☐ Oui, je vous autorise à m'enregistrer
- ☐ Non, je ne vous autorise pas à m'enregistrer

Signature du participant à l'étude	Signature du responsable de l'étude
------------------------------------	-------------------------------------



Général	Pouvez-vous vous présenter ? - Métier - Loisirs
RI	1. Pouvez-vous indiquer les 3 mots ou expressions qui vous viennent spontanément à l'esprit lorsque l'on vous dit : « <b>rayonnements ionisants</b> » 2. Pour vous est-ce un mot positif, négatif ou neutre ? 3. Y a-t-il des implications positives aux rayonnements ionisants ? - Si oui lesquelles ? 4. Pouvez-vous me parler des risques liés aux rayonnements ionisants ? - Dans quels cas pouvez-vous y être exposé ? - Niveau de gravité ? 5. Avez-vous déjà entendu le terme « <b>radio-induit</b> » ? - Si oui, pouvez-vous m'en parler ?
Prédiction	6. Imaginez que demain il soit possible de prédire si vous allez développer un <b>cancer</b> dans votre vie, qu'en pensez-vous ? - Qu'est ce qui pourrait vous motiver à savoir / vous freiner ? 7. Imaginez que demain il soit possible de prédire si vous allez développer une maladie de <b>maladie dégénérative</b> (Alzheimer), comme dans votre vie, qu'en pensez-vous ? - Qu'est ce qui pourrait vous motiver à savoir / vous freiner ? 8. Pensez-vous que connaître ces risques futurs changeraient votre vie présente ? - Comment ? - Pourquoi ?
Clôture	9. Avez-vous quelque-chose à ajouter ?

#### Fiche signalétique :

Sexe :

- ☐ Homme  
☐ Femme

Age : .....ans

Métier : .....

Quel est votre statut marital

- ☐ Célibataire  
☐ Vivant en union libre/ concubinage  
☐ Marié.e  
☐ Pacs  
☐ Veuf.veuve  
☐ Divorcé.e

Avez-vous des enfants ?

- ☐ Oui  
☐ Non



Si non : est-ce un projet dans les 2 ans à venir ?

- ☐ Oui
- ☐ Non

Voici différents groupes de population. En fonction de votre situation personnelle, de celle de votre foyer et de votre manière de vivre, auquel de ces groupes pensez-vous appartenir ?

- ☐ Les classes privilégiées
- ☐ Les classes aisées
- ☐ Les classes moyennes supérieures
- ☐ Les classes moyennes modestes
- ☐ Les classes populaires
- ☐ Les classes populaires
- ☐ Les classes défavorisées



## B. Annexe 2 : questionnaire



### Projet INDIRA

### Questionnaire

#### Contrat de communication

Nous vous proposons d'apporter votre contribution à une recherche scientifique dirigée par Manon Britel psychologue Ph.D. Ce projet de recherche s'inscrit dans la continuité du projet INDIRA.

le **projet INDIRA** vise à mieux comprendre la notion de radiosensibilité individuelle et à en mesurer sa fréquence dans la population générale.

**Objectif de l'étude en sciences humaines et sociales :** Investiguer la perception des risques liés à l'exposition aux rayonnements ionisants auprès de la population générale.

#### Modalité du questionnaire :

- Il n'y a ni bonne ni mauvaise réponse, seul votre avis nous intéresse.
- Les réponses du questionnaire seront traitées de façon à préserver votre **anonymat et la confidentialité** des réponses, conformément aux règles établis par la CNIL et à notre déontologie (code de déontologie des psychologues de France révisé en 2012). Seules les conclusions de l'étude feront l'objet d'une communication

**Durée du questionnaire :** moins de 10 minutes.

1. Pouvez-vous indiquer les 3 mots ou expressions qui vous viennent spontanément à l'esprit lorsque l'on vous dit : « **radiation** ».

1.

2.

3.

2. Pour vous, ce terme « radiation » est :

- ☐ Positif
- ☐ Neutre
- ☐ Négatif

3. Selon-vous, dans votre vie, avez-vous déjà été exposé aux radiations ?

- ☐ Oui
- ☐ Non
- ☐ Je ne sais pas



3.1 Si oui : Dans quel contexte pensez-vous que vous avez été exposé aux radiations ? (plusieurs réponses possibles)

- ☐ En prenant l'avion
- ☐ Au quotidien, c'est une exposition naturelle permanente
- ☐ En faisant une radiographie
- ☐ En faisant un examen médical
- ☐ En ayant suivi une radiothérapie
- ☐ Je ne sais pas

4. Selon vous, les radiations sont-elles ?

- ☐ Dangereuses pour la santé
- ☐ Peu dangereuses pour la santé
- ☐ Très peu dangereuses pour la santé
- ☐ Ne représentent aucun danger pour la santé

5. Imaginez que demain il soit possible de prédire si dans votre vie vous aurez un cancer, qu'en pensez-vous ?

- ☐ Ce serait très angoissant de vivre avec cette idée
- ☐ Ce serait rassurant de pouvoir anticiper les choses
- ☐ Cela ne changerait rien
- ☐ Je préfère ne pas savoir

6. Est-ce que cette perspective (toujours imaginaire de prédire un cancer) changerait votre façon d'agir dans le présent ?

- ☐ Oui : je réaliserais davantage d'examens de dépistage
- ☐ Oui : je réaliserais davantage de gestes de prévention (hygiène de vie)
- ☐ Oui : je réaliserais davantage d'examens de dépistage et de gestes de prévention
- ☐ Non cela ne changerait pas ma façon d'agir dans le présent

7. Imaginez que demain il soit possible de prédire si dans votre vie vous aurez une maladie dégénérative comme la maladie d'Alzheimer, qu'en pensez-vous ?

- ☐ Ce serait très angoissant de vivre avec cette idée
- ☐ Ce serait rassurant de pouvoir anticiper les choses
- ☐ Cela ne changerait rien
- ☐ Je préfère ne pas savoir

8. Est-ce que cette perspective (toujours imaginaire de prédire une maladie d'Alzheimer) changerait votre façon d'agir dans le présent ?

- ☐ Oui : je réaliserais davantage d'examens de dépistage
- ☐ Oui : je réaliserais davantage de gestes de prévention (hygiène de vie)
- ☐ Oui : je réaliserais davantage d'examens de dépistage et de gestes de prévention
- ☐ Non cela ne changerait pas ma façon d'agir dans le présent



9. Est-ce que connaître votre « avenir-santé » (cancer ou maladie d'Alzheimer) vous ferait envisager : (plusieurs réponses possibles)

- ☐ Un changement de métier
- ☐ Un changement de lieu de vie
- ☐ De développer davantage vos relations (amis, famille)
- ☐ De minimiser vos relations (amis, famille)
- ☐ De réaliser des démarches administratives (testament, héritage, changement de gestion de voter épargne ou de votre patrimoine)
- ☐ De mettre en place davantage de choses plaisantes à court terme (voyage, loisirs, etc.)
- ☐ De vous engager dans des actions caritatives
- ☐ Aucun changement

10. Selon vous, l'exposition aux radiations augmente-t-elle le risque de développer un cancer ?

- ☐ Oui de façon significative dès une petite exposition
- ☐ Oui de façon significative quand l'exposition aux radiations est répétée et/ou intense
- ☐ Non il n'y a pas de lien entre les radiations et le risque de développer un cancer

11. Selon vous, l'exposition aux radiations est-elle bénéfique pour la santé ?

- ☐ Oui, elle permet le diagnostic médical
- ☐ Oui, elle permet le traitement de certains cancers
- ☐ Non, il n'y a pas d'effets positifs sur la santé
- ☐ Non, elle est néfaste pour la santé
- ☐ Je ne sais pas

12. Avez-vous quelque chose à ajouter ?

.....  
.....

#### Fiche signalétique :

Sexe :

- ☐ Homme
- ☐ Femme

Age : .....ans

Métier : .....

Quel est votre statut marital

- ☐ Célibataire
- ☐ Vivant en union libre/ concubinage
- ☐ Marié.e
- ☐ Pacsé.e
- ☐ Veuf.veuve
- ☐ Divorcé.e

Avez-vous des enfants ?

- ☐ Oui
- ☐ Non



Si non : est-ce un projet dans les 2 ans à venir ?

- ☐ Oui
- ☐ Non

Voici différents groupes de population. En fonction de votre situation personnelle, de celle de votre foyer et de votre manière de vivre, auquel de ces groupes pensez-vous appartenir ?

- ☐ Les classes privilégiées
- ☐ Les classes aisées
- ☐ Les classes moyennes supérieures
- ☐ Les classes moyennes modestes
- ☐ Les classes populaires
- ☐ Les classes défavorisées

Avez-vous été prélevé dans le cadre du projet INDIRA

- ☐ Oui
- ☐ Non
- ☐ Je ne sais pas de quoi il s'agit




# UP Valorization



Article

# Toward an Early Diagnosis for Alzheimer's Disease Based on the Perinuclear Localization of the ATM Protein

Elise Berthel <sup>1,2</sup> , Laurent Pujo-Menjouet <sup>3,†</sup> , Eymeric Le Reun <sup>1,†</sup>, Laurène Sonzogni <sup>1,†</sup>, Joëlle Al-Choboq <sup>1</sup> , Abdennasser Chekroun <sup>3</sup>, Adeline Granzotto <sup>1</sup>, Clément Devic <sup>1</sup>, Mélanie L. Ferlazzo <sup>1</sup>, Sandrine Pereira <sup>2</sup> , Michel Bourguignon <sup>1,4</sup>  and Nicolas Foray <sup>1,\*</sup> 

<sup>1</sup> Institut National de la Santé et de la Recherche Médicale, U1296 Research Unit «Radiation: Defense, Health, Environment», Centre Léon-Bérard, 28 Rue Laennec, 69008 Lyon, France; eberthel@neolys-diagnostics.fr (E.B.); eymeric.le-reun@inserm.fr (E.L.R.); laurene.sonzogni@inserm.fr (L.S.); joelle.al-choboq@inserm.fr (J.A.-C.); adeline.granzotto@inserm.fr (A.G.); ferlazzo@ansto.au (M.L.F.); michel.bourguignon@inserm.fr (M.B.)

<sup>2</sup> NEOLYS Diagnostics, 7 Allée de l'Europe, 67960 Entzheim, France; spereira@neolys-diagnostics.fr

<sup>3</sup> Université Claude-Bernard Lyon 1, CNRS UMR5208, INRIA, Institut Camille-Jordan, 21 Avenue Claude Bernard, 69603 Villeurbanne, France; pujo@maths.univ-lyon1.fr (L.P.-M.); checkroun@maths.univ-lyon1.fr (A.C.)

<sup>4</sup> Université Paris-Saclay, 78035 Versailles, France

\* Correspondence: nicolas.foray@inserm.fr; Tel.: +33-04-78-78-28-28

† These authors contributed equally to this work.

**Abstract:** Alzheimer's disease (AD) is the most common neurodegenerative dementia, for which the molecular origins, genetic predisposition and therapeutic approach are still debated. In the 1980s, cells from AD patients were reported to be sensitive to ionizing radiation. In order to examine the molecular basis of this radiosensitivity, the ATM-dependent DNA double-strand breaks (DSB) signaling and repair were investigated by applying an approach based on the radiation-induced ataxia telangiectasia-mutated (ATM) protein nucleoshuttling (RIANS) model. Early after irradiation, all ten AD fibroblast cell lines tested showed impaired DSB recognition and delayed RIANS. AD fibroblasts specifically showed spontaneous perinuclear localization of phosphorylated ATM (pATM) forms. To our knowledge, such observation has never been reported before, and by considering the role of the ATM kinase in the stress response, it may introduce a novel interpretation of accelerated aging. Our data and a mathematical approach through a brand-new model suggest that, in response to a progressive and cumulative stress, cytoplasmic ATM monomers phosphorylate the APOE protein (pAPOE) close to the nuclear membrane and aggregate around the nucleus, preventing their entry in the nucleus and thus the recognition and repair of spontaneous DSB, which contributes to the aging process. Our findings suggest that pATM and/or pAPOE may serve as biomarkers for an early reliable diagnosis of AD on any fibroblast sample.

**Keywords:** Alzheimer's disease; ATM; APOE; aging; fibroblasts; immunofluorescence; DNA double-strand breaks; irradiation



**Citation:** Berthel, E.; Pujo-Menjouet, L.; Le Reun, E.; Sonzogni, L.; Al-Choboq, J.; Chekroun, A.; Granzotto, A.; Devic, C.; Ferlazzo, M.L.; Pereira, S.; et al. Toward an Early Diagnosis for Alzheimer's Disease Based on the Perinuclear Localization of the ATM Protein. *Cells* **2023**, *12*, 1747. <https://doi.org/10.3390/cells12131747>

Academic Editor: Maurizio Romano

Received: 22 May 2023

Revised: 9 June 2023

Accepted: 26 June 2023

Published: 29 June 2023



**Copyright:** © 2023 by the authors. Licensee MDPI, Basel, Switzerland. This article is an open access article distributed under the terms and conditions of the Creative Commons Attribution (CC BY) license (<https://creativecommons.org/licenses/by/4.0/>).

## 1. Introduction

Alzheimer's disease (AD) is a progressive and devastating neurodegenerative disorder with a poor prognosis, and for which no efficient curative treatment is currently available [1,2]. AD has been shown to result in specific neurobiological events, such as extracellular deposits of  $\beta$ -amyloid (A $\beta$ ) plaques [3] and intracellular neurofibrillary tangles consisting in hyper-phosphorylated aggregates of the microtubule-associated tau protein [4]. Interestingly, cellular radiosensitivity was also reported in lymphocytes derived from AD patients [5–7]. However, to date, a mechanistic model linking the abnormal response to ionizing radiation (IR) and the accelerated neurodegeneration/aging observed in AD patients in response to oxidative stress, whether endogenous or exogenous, is still needed.



In 2016, from one of the largest collections of cutaneous fibroblasts derived from patients suffering from post-radiotherapy radiosensitivity, a unified mechanistic model of individual responses to IR was proposed [8,9]. This model was based on the radiation-induced (RI) nucleoshuttling of the ataxia telangiectasia-mutated (ATM) protein (RIANS) required for signaling and repair of DNA double-strand breaks (DSB), the key DNA damage in response to IR. The RIANS model has been shown to be the most reliable predictor of radiosensitivity [8,10–14], and to provide a molecular explanation of some low-dose-specific radiobiological phenomena [9,15–17]. It was also validated in non-radiative oxidative stress, such as contamination with metals and pesticides [18,19]. In the frame of the RIANS model, any oxidative stress induces DNA breaks and the monomerization of ATM dimers. Cytoplasmic ATM monomers diffuse thereafter in the nucleus and trigger the DSB recognition and repair via the non-homologous end-joining (NHEJ), the predominant DSB signaling and repair pathway in quiescent human cells [8,9]. Any delayed RIANS was shown to be associated with radiosensitivity (RI cell lethality), radio-susceptibility (RI cancers) and/or radio-degeneration (RI accelerated aging) [17,20]. Delayed RIANS is generally caused by the sequestration of cytoplasmic ATM monomers by overexpressed ATM substrate proteins, called X-proteins [17,21]. A number of X-proteins have already been identified in neurodegenerative/aging or cancer-prone diseases associated with radiosensitivity, therefore validating the RIANS model. This is notably the case of Huntington's disease [22], tuberous sclerosis complex [23], Xeroderma Pigmentosum D [24], retinoblastoma [25], neurofibromatosis type I [26] and Rothmund–Thomson syndromes [27]. It is noteworthy that the occurrence of cytoplasmic forms of ATM, the basis of the RIANS model, has been initially supported by several other research groups [28–32].

Here, the major steps of the ATM-dependent RI DSB signaling and repair pathway were investigated in cutaneous fibroblasts derived from 10 AD patients. The AD data were compared to those obtained from fibroblasts derived from 5 apparently healthy and radioresistant donors and 11 patients suffering from cancer or neurodegenerative diseases. During our investigations, a spontaneous perinuclear localization of the ATM protein was observed specifically in the AD fibroblasts, which prompted us to propose a mechanistic interpretation of AD deriving from the RIANS model and consolidated by a biomathematical approach.

## 2. Materials and Methods

### 2.1. Cell Culture

All the experiments were performed with human untransformed cutaneous fibroblasts that were routinely cultured as monolayers with Gibco modified Eagle's minimum medium (DMEM) (Thermo Fisher, Waltham, MA, USA), supplemented with 20% fetal calf serum, penicillin and streptomycin (Thermo Fisher). All the experiments were performed with cells in the plateau phase of growth to avoid any cell cycle effect [33]. The genetic and cellular features of the cutaneous fibroblasts tested are detailed in Table 1. The 10 untransformed AD fibroblasts were purchased from the Coriell Institute for Medical Research (Camden, NJ, USA). All the non-AD fibroblasts used in this study were purchased either from the European Collection of Authenticated Cell Cultures (ECACC, UK Health Security Agency, Salisbury, UK), the American Type Culture Collection (ATCC, Manassas, VA, USA), the Coriell Institute or from the COPERNIC collection of our lab that gathers primary fibroblasts of different origin and radiosensitivity. The COPERNIC collection was approved by a regional ethical committee, declared under the numbers DC2011-1437 and 2021-3957 to the Ministry of Research as required by the French regulations, and was already described elsewhere [8]. It obeys the French regulations about the anonymous sampling and the informed consent. Cell authentication and culture quality control were insured by commercial repositories. With regard to the cell lines isolated from the lab (COPERNIC collection), the respect of the good practices of the laboratory (GPL) was included in the declaration of the cell line collection to the French Ministry of Research.



**Table 1.** Major characteristics of the fibroblast cell lines used in this study.

Cell Lines	Gender	Associated Disease	Radiation Response	Age (at Sampling)	APOE Genotype	Origin
1BR3	Male	Apparently healthy	Radioresistant	3	nd	ECACC
149BR	Male	Apparently healthy	Radioresistant	51	nd	ECACC
HF19	Female	Apparently healthy	Radioresistant	fetus	nd	ECACC
Hs27	Male	Apparently healthy	Radioresistant	<1 month	$\epsilon 3/\epsilon 4$	ATCC
MRC5	Male	Apparently healthy	Radioresistant	children	$\epsilon 3/\epsilon 4$	ECACC
GM03399	Female	AT heterozygous mutation	Radioresistant	20	nd	Coriell Institute
AT2EM	nd	nd	Hyper-radiosensitive	nd	nd	COPERNIC
AT3BI	Male	nd	Hyper-radiosensitive	4	nd	COPERNIC
AT4BI	Male	nd	Hyper-radiosensitive	6	nd	COPERNIC
GM05823 (AT5BI)	Male	AT Compound heterozygous mutation	Hyper-radiosensitive	18	nd	Coriell Institute
Rackham 12	Male	Neurofibromatosis type I	Moderately radiosensitive	23	nd	COPERNIC
GM21756	Female	Huntington's disease	Moderately radiosensitive	nd	nd	Coriell Institute
XP26VI	nd	Xeroderma Pigmentosum D	Moderately radiosensitive	15	nd	COPERNIC
AG17524	Female	Rothmund–Thomson Syndrome	Moderately radiosensitive	4	nd	Coriell Institute
AG01972	Female	Hutchinson–Gilford syndrome	Hyper-radiosensitive	14	nd	Coriell Institute
AG06300	Male	Werner's syndrome	Hyper-radiosensitive	37	nd	Coriell Institute
AG11415	Male	AD	Moderately Radiosensitive	55	$\epsilon 3/\epsilon 3$	Coriell Institute
AG21158	Female	AD	Moderately Radiosensitive	69	$\epsilon 2/\epsilon 3$	Coriell Institute
AG06840	Male	AD <i>PSEN1</i> mutation	Moderately Radiosensitive	56	$\epsilon 3/\epsilon 3$	Coriell Institute
AG06844	Male	AD Family history early onset	Moderately Radiosensitive	59	$\epsilon 3/\epsilon 4$	Coriell Institute
AG06848	Female	AD <i>PSEN1</i> mutation	Moderately Radiosensitive	56	$\epsilon 3/\epsilon 4$	Coriell Institute
AG06869	Female	AD	Moderately Radiosensitive	60	$\epsilon 4/\epsilon 4$	Coriell Institute
AG07376	Male	AD	Moderately Radiosensitive	60	$\epsilon 3/\epsilon 3$	Coriell Institute
AG08170	Male	AD Family history early onset	Moderately Radiosensitive	56	$\epsilon 3/\epsilon 4$	Coriell Institute
AG08541	Female	AD	Moderately Radiosensitive	59	$\epsilon 3/\epsilon 3$	Coriell Institute
AG09908	Female	AD <i>PSEN2</i> mutation	Moderately Radiosensitive	81	$\epsilon 3/\epsilon 3$	Coriell Institute

Nd: not determined; ECACC: European Collection of Authenticated Cell Cultures; ATCC: American Type Culture Collection.

## 2.2. Treatment with Zoledronate and Pravastatine (ZOPRA)

The combination of zoledronate and pravastatin was called ZOPRA treatment, as described elsewhere [34], and it was applied to more than ten different genetic diseases associated with a delayed RIANs [35]. Briefly, cells were incubated with 1  $\mu$ M of pravastatin (Sigma-Aldrich, Saint-Quentin-Fallavier, France) in phosphate-buffered saline solution (PBS) for 24 h at 37 °C. Thereafter, 1  $\mu$ M of zoledronate (Sigma-Aldrich) in PBS was added into the culture medium and cells were incubated for 12 h at 37 °C. The culture medium was renewed immediately before irradiation.



### 2.3. Irradiation

All the irradiations were performed on a 6 MeV X-ray clinical irradiator (SL 15 Phillips) at the Anti-Cancer Centre Léon-Bérard (Lyon, France), at a dose of 2 Gy with a dose rate of 6 Gy min<sup>−1</sup>. Dosimetry was certified by the Radiophysics Department of Centre Léon-Bérard.

### 2.4. Clonogenic Cell Survival

The intrinsic cellular radiosensitivity was quantified by using the clonogenic cell survival assay, for which the protocol was detailed elsewhere [36]. Each survival data point is the mean of at least 3 replicates with 3 different dilutions tested per dose. The number of cells seeded ranged from 200 to 10,000 cells per 6 cm-diameter Petri dish [36]. The intrinsic radiosensitivity was quantified by the surviving fraction at 2 Gy (SF2) [9].

### 2.5. Phosphospecific APOE Antibodies

Two custom rabbit polyclonal phosphospecific APOE antibodies were developed against pAPOE<sup>ser72</sup> and pAPOE<sup>thr75</sup> residues at our request by the CliniSciences company (Nanterre, France) by following standard procedures developed by the manufacturer.

### 2.6. Immunofluorescence

Immunofluorescence and foci scoring procedures were described elsewhere [8,24,37]. Briefly, the anti- $\gamma$ -H2AX<sup>ser139</sup> antibody (clone JBW301; Merck, Millipore, Darmstadt, Germany) was applied at 1:800. Anti-pATM<sup>ser1981</sup> (clone 10H11.E12; Millipore, Germany) and anti-MRE11 (#56211; Abcys, Paris, France) were used at 1:100. Cells were counterstained with 4',6-diamidino-2-phenylindole, dihydrochloride (DAPI), which also permitted to score the micronuclei in the same conditions. The foci scoring procedure applied here has received the certification agreement of CE mark and ISO-13485 quality management norms and developed some features protected in the frame of the patents FR3017625 A1 and FR3045071 A1. The immunofluorescence data resulted in at least 3 independent replicates with 100 nuclei analyzed per experiment and per biomarker.

### 2.7. Micronuclei Assay

During each immunofluorescence experiment, the DAPI counterstaining permitted to quantify the micronuclei at magnification  $\times 100$  [14]. The micronuclei data resulted in at least 3 independent replicates with 100 nuclei analyzed per experiment and per biomarker.

### 2.8. Immunoprecipitation and Immunoblotting

Total extracts were obtained from 1 to 2  $\times 10^6$  cells collected by scraping and rinsed by centrifugation with cold phosphate-buffered saline (1500 rpm, 200  $\times g$ , 4  $^{\circ}\text{C}$ , 5 min), then lysed in lysis buffer A (50 mM Tris-HCl, pH 8, 150 mM NaCl, 2 mM EDTA, 0.2% NP40 nonidet and 10% glycerol) supplemented with protease and phosphatase inhibitors (#78442, Thermo Fisher, Waltham, MA, USA) and maintained in 4  $^{\circ}\text{C}$  for 15 min. Total extracts were finally obtained in the supernatant after centrifugation (1500 rpm, 200  $\times g$ , 4  $^{\circ}\text{C}$ , 5 min). Cytoplasmic extracts were obtained from 1 to 2  $\times 10^6$  rinsed cells using the buffer (10 mM Hepes pH 7.9, 1.5 mM MgCl<sub>2</sub>, 10 mM KCL, 2 mM ethylenediaminetetraacetic acid (EDTA) pH 8, 0.5 mM dithiothreitol (DTT), 0.2% Nonidet NP40, H<sub>2</sub>O), supplemented with protease and phosphatase inhibitors (#78442, Thermo Fisher, Waltham, MA, USA) and maintained in 4  $^{\circ}\text{C}$  for 15 min. Cytoplasmic extracts were finally obtained in the supernatant after centrifugation (5000 rpm, 800  $\times g$ , 4  $^{\circ}\text{C}$ , 5 min). After this procedure, nuclear extracts were obtained from the residual pellet lysed in the following buffer (10 mM Hepes pH 7.9, 1.5 mM MgCl<sub>2</sub>, 450 mM KCL, 2 mM EDTA, 1 mM ethyl-glycol-bis( $\beta$ -aminoethylether-tetraacetic acid) (EGTA) pH 8, 0.5 mM dithiothreitol (DTT), 0.25% glycerol, H<sub>2</sub>O), supplemented with protease and phosphatase inhibitors (#78442, Thermo Fisher, Waltham, MA, USA) applied for 1 h, at 4  $^{\circ}\text{C}$ . Nuclear extracts were finally obtained from the supernatant after centrifugation (5000 rpm, 800  $\times g$ , 4  $^{\circ}\text{C}$ , 5 min). Protein concentrations were determined by the Bradford procedure (Bio-Rad Laboratories, Hercules, CA, USA).



For immunoprecipitations, lysates containing 1.5 mg of protein were pre-cleared by stirring with 40  $\mu$ L of Protein G–Sepharose beads (GE Healthcare, Chicago, IL, USA) for 1 h, at 4 °C. After centrifugation, immunoprecipitation was performed with the pre-cleared lysate and 2  $\mu$ g of antibody for 3 h, at 4 °C. A 40  $\mu$ L volume of Protein G–Sepharose was added and incubated for 30 min at 4 °C. After centrifugation, beads were washed three times with lysis buffer A and proteins were eluted by heating at 95 °C for 5 min in SDS loading buffer and 100 mM of dithiothreitol (DTT) (Sigma-Aldrich). Proteins were subjected to SDS-PAGE and blotted onto PVDF membranes (Immobilon-P, Millipore, Burlington, MA, USA). Membranes were blocked in Tris-buffered saline (TBS) solution containing 0.05% Tween 20 and 5% (*w/v*) non-fat dried skimmed milk powder and incubated with primary antibodies. Horseradish peroxidase-conjugated secondary antibodies (Jackson ImmunoResearch-Europe, Ely, UK) were used for the detection of immunoreactive proteins via the ECL kit (Thermo Scientific, Waltham, MA, USA).

### 2.9. *In Situ Proximity Ligation Assay (PLA)*

The PLA technology allows the *in situ* detection of endogenous protein interactions by immunofluorescence microscopy [38]. This technique consists in recognition of two proteins of interest using secondary antibodies conjugated with DNA strands. When in close proximity ( $\leq 10$  nm), these strands form a template for rolling-circle amplification using fluorescent oligonucleotides. The interaction between the two proteins of interest is visible as a distinct fluorescent spot. Cells were fixed with 4% (*w/v*) paraformaldehyde for 15 min at room temperature and were permeabilized in 0.5% Triton X-100 solution (Sigma-Aldrich) for 3 min at 4 °C. Cells were then blocked for 2 h at room temperature using 30  $\mu$ L of blocking solution from the Duolink™ *In Situ* Orange Starter Kit Mouse/Rabbit (#DUO92102, Sigma-Aldrich) per coverslip. Mixtures of two primary antibodies' incubations were performed for 1 h at 37 °C (one raised in rabbit, the other one in mouse). The following antibodies were diluted in the Duolink antibody diluent 1X (#DUO82008-Sigma) at a ratio of 1:100: mouse monoclonal anti-ATM antibody (#2C1 (1A1); Abcam, Cambridge UK) and rabbit polyclonal anti-APOE antibody (#SAB2701971; Sigma-Aldrich). PLA probes (Duolink PLA Probe anti-mouse MINUS and Duolink PLA Probe anti-rabbit PLUS, Olink AB) were diluted the same as all Duolink reagents. After 1 h of incubation at 37 °C with the PLA probes, cells were washed in buffer A (10 mM Tris/HCl, pH 7.4, 150 mM NaCl and 0.05% Tween 20) and treated with the Duolink *In Situ* Detection Reagents Orange (Olink AB, Sigma-Aldrich). Cells were incubated with the ligation solution for 30 min at 37 °C in the humidified chamber. After washing in buffer A, cells were incubated with the amplification solution for 100 min at 37 °C in darkness in the humidified chamber. Cells were then washed with wash buffer B (DUO82048-1EA, Sigma-Aldrich), followed by a quick wash with 1/100 wash buffer B. Samples were mounted with Duolink *In Situ* Mounting Medium with DAPI (DUO82040; Sigma-Aldrich). Samples were analyzed under fluorescent microscopy. Fluorescent signals were viewed under an Olympus BX51 microscope ( $\times 100$  objective). Analysis and quantification of these samples were performed using the ImageJ 1.52g software. The PLA data resulted in at least 3 independent replicates with 100 nuclei analyzed per experiment and per biomarker couple.

### 2.10. *Statistical Analysis*

All data were obtained with the numbers of independent experiments indicated and each value was expressed as the mean and standard error of the mean (Poisson's law). The statistical analyses were performed either by PRISM software version 9.5.1 (GraphPad Software, San Diego, CA, USA) or by using Kaleidagraph version 4.5.4 (Synergy Software, Reading, PA, USA). One-way ANOVA tests were performed for point-to-point analysis.

### 2.11. *Mathematical Modeling*

A brand-new mathematical model was designed to unify all four patterns (no pATM crown, no pATM crown with foci, thin pATM crown with foci, thick pATM crown without



foci) in a single system of nonlinear differential equations, and based on the description of protein interactions, in six compartments: the ATM dimers in cytoplasm, the ATM monomers in cytoplasm, the ATM dimers inside the perinuclear crown, the APOE-ATM complexes, the APOE proteins, and finally, the ATM monomers in the nucleus. Each interaction from one compartment to another was represented by a term of the equation (interaction, nucleus passage, monomerization, dimerization, complex formation) with specific kinetics. Some of these kinetic parameters were protein-dependent (such as  $k_4$  depending on AM (that is the APOE-ATM complexes with saturation) and  $k_5$  depending inversely on  $D_A$  (that is the ATM dimers in the perinuclear crowns)). The simulation results led to one of the four patterns regarding the values of the parameters and/or initial conditions.

### 3. Results

#### 3.1. AD Fibroblasts Show Radiosensitivity Associated with a Delayed RIANS

Cellular radiosensitivity is currently quantified by the clonogenic cell survival fraction at 2 Gy (SF2) [39]. While the average SF2 values from the radioresistant controls ( $65.6 \pm 1.8\%$ ) were in good agreement with the literature [39–41], the AD fibroblasts tested showed significantly lower SF2 than controls (average SF2 =  $40.2 \pm 6.6\%$ ;  $p < 0.01$ ) (Figure 1A). The SF2 values of AD cells suggested a moderate but significant radiosensitivity, quantitatively similar to that of Werner's syndrome or Huntington's disease, but significantly lower than that observed in ataxia telangiectasia (AT), the human syndrome associated with the highest radiosensitivity (average SF2 =  $1.5 \pm 0.3\%$ ;  $p < 0.001$ ) [21,39–41] (Figure 1A). The SF2 values of AD fibroblasts were found in agreement with those from AD lymphocytes published in the 1980s [5–7].

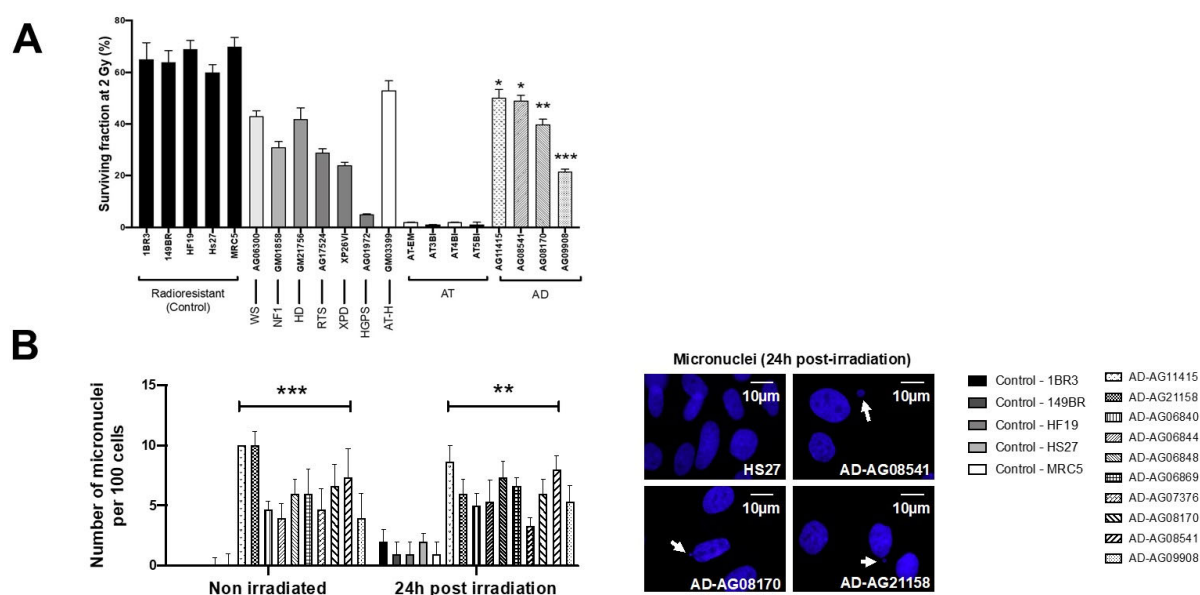


**Figure 1.** Cellular radiosensitivity and cytogenetic features of AD fibroblasts. (A) Surviving fraction at 2 Gy (SF2) of the indicated fibroblast cell lines from the indicated syndromes (WS: Werner's syndrome; NF1: neurofibromatosis type 1; HD: Huntington's disease; RTS: Rothmund–Thomson syndrome; XPD: Xeroderma Pigmentosum D; HGPS: Hutchinson–Gilford progeroid syndrome; ATH: ataxia telangiectasia heterozygous; AT ataxia telangiectasia; AD: Alzheimer's disease). Each bar represents the mean  $\pm$  standard error of the mean (SEM) of three replicates, at least. The asterisks are shown for AD cells vs. controls only. (B) Representative immunofluorescence images of micronuclei observed 24 h post-irradiation (2 Gy X-rays) in the indicated cells with DAPI staining. The arrows show isolated micronuclei during exonucleosis. Histogram showing the number of micronuclei per 100 cells assessed before irradiation or 24 h post-irradiation. Each bar represents the mean  $\pm$  SEM of three replicates, at least. \*\*,  $p < 0.01$  and \*\*\*,  $p < 0.001$ .



Micronuclei are cytogenetic endpoints resulting from the propagation of unrepaired DSB to G2/M phase and their transformation as chromosome fragments [14]. The yield of micronuclei has been shown to be quantitatively correlated with cellular radiosensitivity [14,20]. In the 10 AD fibroblasts tested, the yields of spontaneous and RI micronuclei were significantly higher than those of radioresistant controls ( $p < 0.01$  and  $p < 0.05$ , respectively) (Figure 1B). SF2 and micronuclei data from AD fibroblasts were found consistent with correlations with 200 different human cell lines, showing a large spectrum of radiosensitivity [14] (Figure S1).

Since the ATM phosphorylation of the X variant of the H2A histone ( $\gamma$ H2AX) was demonstrated to form nuclear foci at the RI DSB sites recognized by NHEJ [42], anti- $\gamma$ H2AX immunofluorescence was applied to AD fibroblasts. While no difference was observed at 4 and 24 h post-irradiation, the number of  $\gamma$ H2AX foci assessed 10 min and 1 h post-irradiation was found systematically lower in the AD fibroblasts than in the radioresistant controls ( $p < 0.01$  and  $p < 0.05$ , respectively) (Figure 2). These findings were found similar to those obtained from cells deriving from syndromes associated with moderate radiosensitivity, cancer proneness or accelerated aging [22–26]. It is noteworthy that the  $\gamma$ H2AX foci were either absent or impaired in AT cells, in agreement with the literature [8,27]. Again,  $\gamma$ H2AX data from AD data obeyed a correlation between  $\gamma$ H2AX and SF2 data established with 200 human fibroblast cell lines [14] (Figure S2).

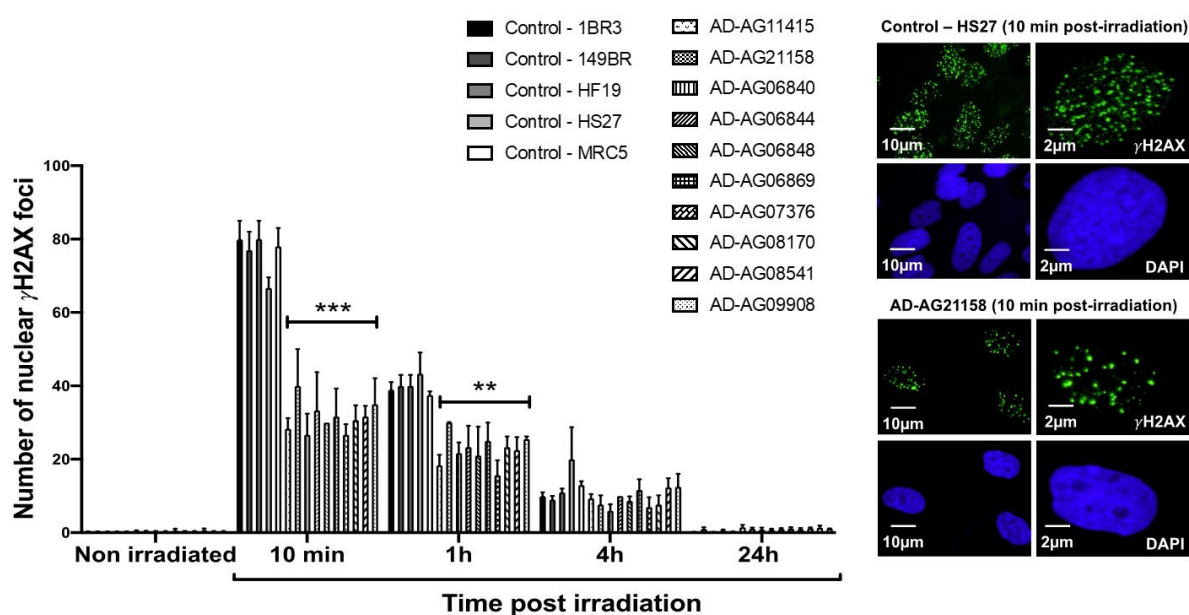


**Figure 2.**  $\gamma$ H2AX foci data from AD fibroblasts. Representative immunofluorescence images of nuclear  $\gamma$ H2AX foci observed 10 min after irradiation (2 Gy X-rays) in the indicated cells. The DAPI signal served as nuclear counterstaining. Histogram showing the number of nuclear  $\gamma$ H2AX foci per cell assessed before irradiation or at 10 min, 1 h, 4 h and 24 h post-irradiation. Each bar represents the mean  $\pm$  SEM of three replicates, at least. \*\*,  $p < 0.01$  and \*\*\*,  $p < 0.001$ .

In the frame of the RIANS model, the above data suggest a lack of ATM-dependent RI DSB recognition by NHEJ [8]. At the end of the repair process, trans-autophosphorylated ATM (pATM) monomers formed ATM dimers that were revealed by the formation of pATM foci in the nucleus and by a broader staining in the cytoplasm [17]. It is noted that pATM-positive signals indicate the presence of ATM dimers, while the anti-ATM antibody cannot discriminate ATM monomers and dimers [17,32]. By applying anti-pATM immunofluorescence, the number of RI pATM foci in AD fibroblasts at 10 min post-irradiation appeared significantly lower than in the radioresistant controls ( $p < 0.01$ ) (Figure 3). Such observation was consolidated by pATM immunoblots of nuclear extracts that showed a lower increase of the nuclear pATM molecules at 10 min post-irradiation in AD fibroblasts than in the



radioresistant controls (Figure 3). It is noteworthy that qPCR analysis of ATM synthesis did not reveal any difference between the radioresistant controls and the AD fibroblasts, suggesting that the RIANs is independent of the ATM protein synthesis. Besides, the pATM data observed at 10 min post-irradiation were unlikely due to any change of ATM expression that may generally occur some hours post-irradiation. Again, these findings were consistent with the pATM data observed in syndromes associated with moderate radiosensitivity, cancer proneness or accelerated aging [22–26]. Lastly, it must be stressed that AD data also obeyed a correlation between pATM and SF2 data that has been established with 200 other human fibroblast cell lines [14] (Figure S3).

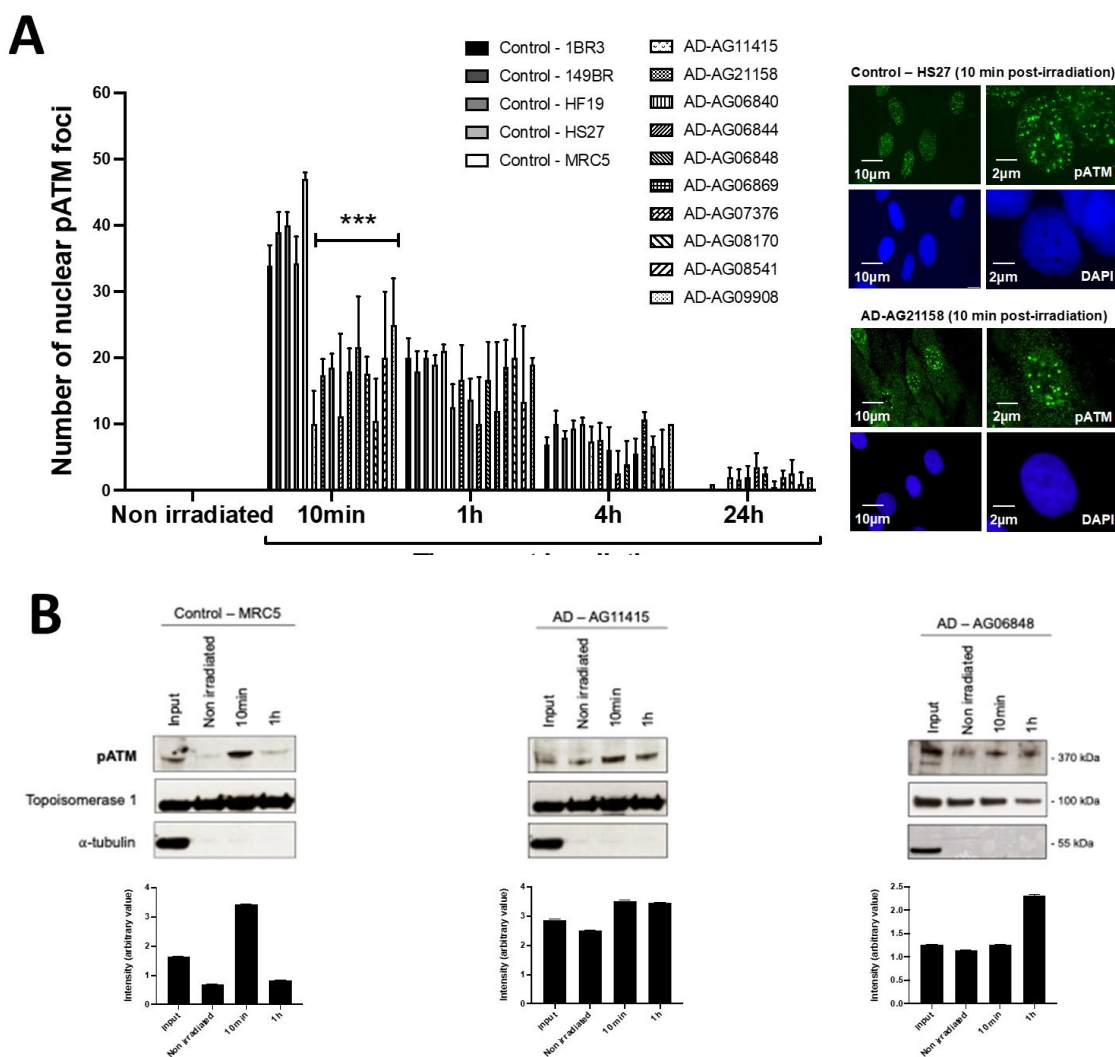


**Figure 3.** pATM foci and immunoblot data from AD fibroblasts. (A) Representative immunofluorescence images of nuclear pATM foci observed 10 min after irradiation (2 Gy X-rays) in the indicated cells. The DAPI signal served as nuclear counterstaining. Histogram showing the number of nuclear pATM foci per cell assessed before irradiation or at 10 min, 1, 4 and 24 h post-irradiation. Each bar represents the mean  $\pm$  SEM of three replicates, at least. \*\*\*,  $p < 0.001$ . (B) Immunoblots performed with anti-pATM antibodies in nuclear extracts from cells processed before irradiation or at 10 min and 1 h post-irradiation (2 Gy X-rays). Topoisomerase I and  $\alpha$ -tubulin served as cell fractionation and loading controls. The corresponding quantified Western blot bands were expressed as arbitrary units.

In our previous reports, a delayed RIANs was generally associated with abnormal radiation-induced re-localization of nuclear foci formed by the MRE11 nuclease. Particularly, cells from aging syndromes were found characterized by a delayed production of MRE11 foci, while cells from cancer syndromes generally showed early MRE11 foci [21]. By



applying anti-MRE11 immunofluorescence, all the AD fibroblasts tested elicited a number of nuclear MRE11 foci at 24 h post-irradiation, significantly higher than that of the controls ( $p < 0.01$ ), again supporting the relationship between late MRE11 foci and aging (Figure 4).

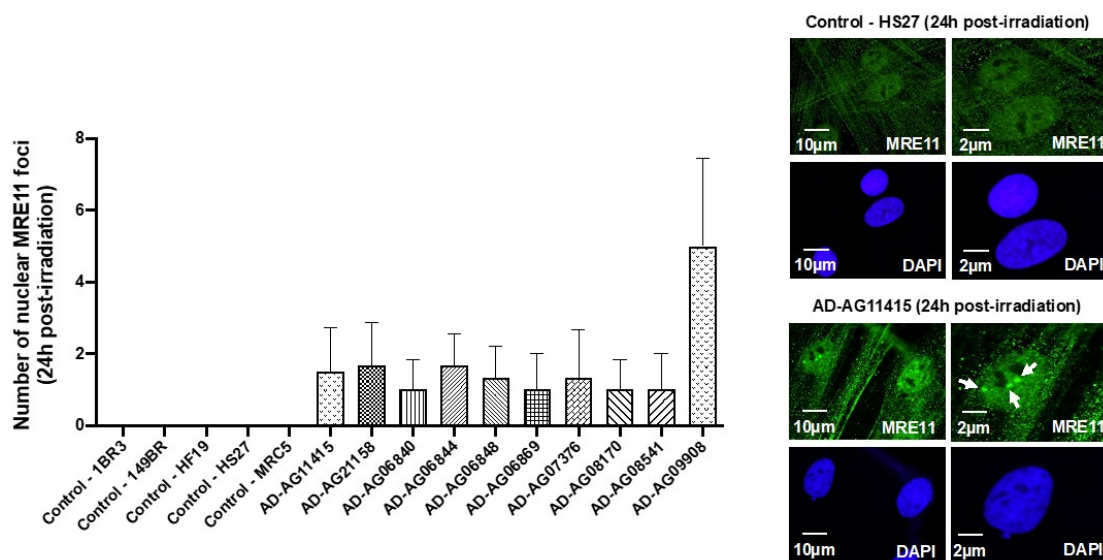


**Figure 4.** MRE11 foci from AD fibroblasts. Representative immunofluorescence images of nuclear MRE11 foci observed 24 h after irradiation (2 Gy X-rays) in the indicated cells. The DAPI signal served as nuclear counterstaining. Histogram showing the number of nuclear MRE11 foci per cell assessed before irradiation or at 24 h post-irradiation. Each bar represents the mean  $\pm$  SEM of three replicates, at least. White arrows indicate the nuclear MRE11 foci.

Altogether, our findings suggested that AD is associated with significant but moderate cellular radiosensitivity with impaired yields of micronuclei,  $\gamma$ H2AX, pATM and MRE11 foci, consistent with a delayed RIANs. It must be stressed here that the radiobiological features of the 10 AD fibroblast cell lines tested were not found to be dependent on age, gender or the genotype of the corresponding donors (Table 1 and Figure S4). Furthermore, all the relationships between the different RIANs biomarkers tested obeyed inter-correlations recently established with 200 fibroblast cell lines, showing a large spectrum of radiosensitivity [14] (see Supplementary Data), which suggests a strong quantitative relevance between the data assessed in AD cells.

### 3.2. Combination of Zoledronate and Pravastatin May Partially Protect Some AD Fibroblasts from IR

In the frame of the RIANs model, it was shown that bringing more ATM monomers into the nucleus significantly contributed to enhancing the radioresistance [17,35]. A radio-protective effect with the combination of bisphosphonates and statins, particularly with zoledronate and pravastatin (ZOPRA), was reported: the ZOPRA treatment accelerated the diffusion of the ATM monomers across the nuclear membrane in a number of genetic diseases [22–24,26,35]. Surprisingly, when applied to the 10 AD fibroblast cell lines, the ZOPRA treatment did not significantly change the yield of RI micronuclei (Figure 5A). It contributed to increase the number of  $\gamma$ H2AX (Figure 5B) and pATM foci assessed 10 min post-irradiation, but this trend was not significant for all the cell lines tested (Figure 5C). Regarding the MRE11 foci, the late MRE11 foci disappeared in only 4 of the 10 AD fibroblast cell lines (Figure 5D). Altogether, these findings suggest that the ZOPRA treatment may protect, at least partially, some AD fibroblasts from IR, while it has been applied more successfully in cancer syndromes with similar radiobiological features as AD cells [35]. It must be stressed that the ZOPRA treatment is not efficient in protecting the ATM-mutated cells since it cannot overcome the loss of the ATM protein function [35]. Besides, applying ATM inhibitors in our conditions would not help to understand the specificities of AD cells



since the activity of ATM kinase is required for the formation of ATM dimers, whether cytoplasmic or nuclear. The partial action of ZOPRA treatment in AD cells prompted us to hypothesize that ZOPRA molecules' diffusion in the nucleus was specifically prevented in AD cells, and we further investigated the cellular features of AD cells.

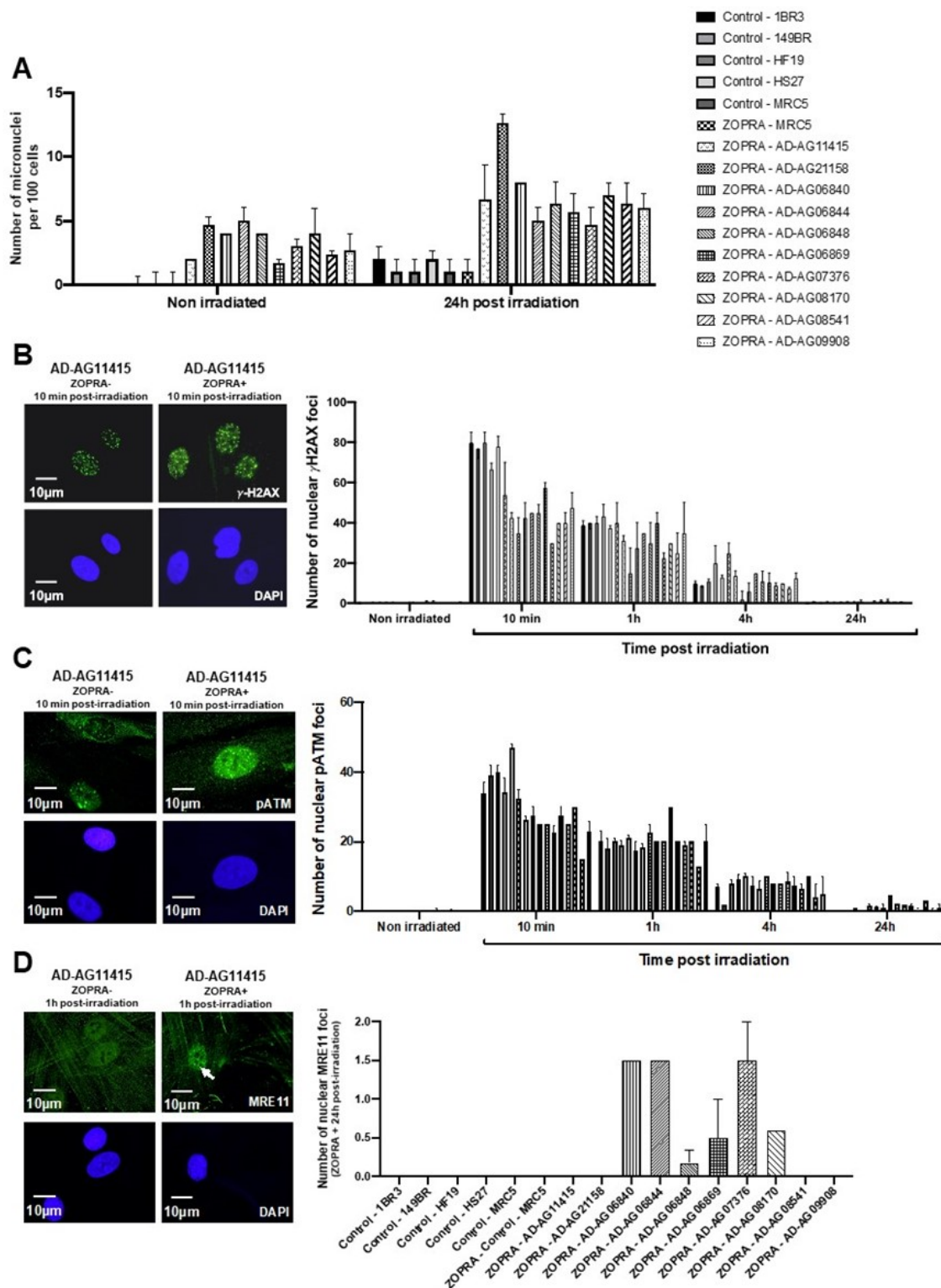


**Figure 5.** Effects of the ZOPRA treatment on AD fibroblasts. (A) Histogram showing the number of micronuclei per 100 cells in ZOPRA- and non-ZOPRA-treated cells, as indicated. After ZOPRA treatment, cells were exposed to 2 Gy X-rays, followed by 24 h for repair. The non-ZOPRA-treated.



cell data are those shown in Figure 1A. Each bar represents the mean  $\pm$  standard error of the mean (SEM) of three replicates, at least. (B) Representative immunofluorescence images of nuclear  $\gamma$ H2AX foci observed after or without ZOPRA treatment, followed by 2 Gy X-rays and 10 min for repair. The DAPI signal served as nuclear counterstaining. Histogram showing the number of nuclear  $\gamma$ H2AX foci per cell observed in ZOPRA-treated cells irradiated at 2 Gy, followed by the indicated times for repair. Each bar represents the mean  $\pm$  SEM of three replicates, at least. (C) Representative immunofluorescence images of nuclear pATM foci observed after or without ZOPRA treatment, followed by 2 Gy X-rays and 10 min for repair. The DAPI signal served as nuclear counterstaining. Histogram showing the number of nuclear pATM foci per cell observed in ZOPRA-treated cells irradiated at 2 Gy, followed by the indicated times for repair. Each bar represents the mean  $\pm$  SEM of three replicates, at least. (D) Representative immunofluorescence images of nuclear MRE11 foci observed after or without ZOPRA treatment, followed by 2 Gy X-rays and 24 h for repair. The DAPI signal served as nuclear counterstaining. Histogram showing the number of nuclear pATM foci per cell observed in ZOPRA-treated cells irradiated at 2 Gy, followed by 24 h for repair. Each bar represents the mean  $\pm$  SEM of three replicates, at least. White arrows indicate nuclear pATM foci.

### 3.3. AD Fibroblasts Spontaneously Show Specific Abnormal Perinuclear Localization of the ATM Protein

During the immunofluorescence experiments described above, a strong perinuclear pATM staining was noticed in non-irradiated AD fibroblasts, suggesting an abnormally high concentration of ATM dimers around the nuclear membrane. The percentage of cells with perinuclear pATM crowns varied from 7 to 44 at the lowest passages tested, among the AD cell lines tested (Figure 6A,B). No correlation was found between the percentage of cells with perinuclear pATM crowns and the age at the skin sampling gender or known mutation status of the AD donors, consistent with the fact that these last three endpoints are not necessarily linked to the AD progress (Figure S4). In contrast, the percentage of cells with perinuclear pATM crowns in AD cells progressively increased as a function of the cell culture passage and reached a plateau, suggesting a sigmoidal function of the passage with a threshold (ranging from passage 7 to 10) and a plateau (ranging from 20% to 40% of cells with perinuclear pATM crowns) (Figure 6C).

The perinuclear pATM crowns were totally absent in radioresistant controls cultured in the same passage range, whether irradiated or not (Figure 6B). Again, in the same passage range, no perinuclear pATM crown was observed in the non-AD fibroblasts derived from the other genetic syndromes described in Table 1, regardless of their radiosensitivity and whether they were irradiated or not (Figure 6B). It must be stressed that this statement is particularly true for fibroblasts from Huntington's disease (HD), Hutchinson–Gilford progeroid syndrome (HGPS), Xeroderma Pigmentosum D (XPB), Werner's syndrome (WS) and tuberous sclerosis complex syndrome (TSC), suggesting a strong specificity of this molecular feature for AD among the neurodegenerative or aging diseases tested (Figure 6B). Lastly, no perinuclear pATM crown was observed in the 200 radiosensitive skin fibroblasts of the COPERNIC collection derived from non-AD cancer patients treated by radiotherapy [8].

In each of the non-irradiated AD fibroblast cell lines tested, we identified four different patterns of pATM staining with different relative proportions, supporting a great heterogeneity in the AD fibroblast populations, but also an ordered temporal progression among the different patterns: (1) Cytoplasmic pATM broad staining without nuclear pATM foci, reflecting the absence of significant genotoxic stress, as observed in a number of non-AD fibroblasts and in radioresistant controls. (2) Cytoplasmic pATM broad staining with nuclear pATM foci, reflecting the presence of significant genotoxic stress, as observed in some cases of non-AD fibroblasts showing spontaneous DSB. (3) Perinuclear pATM crowns with nuclear pATM foci, suggesting that pATM molecules were still able to cross the nuclear membrane, as observed in AD fibroblasts only. (4) Perinuclear pATM crowns without pATM foci, suggesting that pATM molecules were unable to cross the nuclear membrane,



as observed in AD fibroblasts only. The ordered succession of these four patterns suggested a specific response to stress that may result in an agglutination or a “traffic-jam” of ATM molecules around the nuclear membrane, preventing the ATM nucleoshuttling and maybe the diffusion of ZOPRA molecules (Figure 6D).

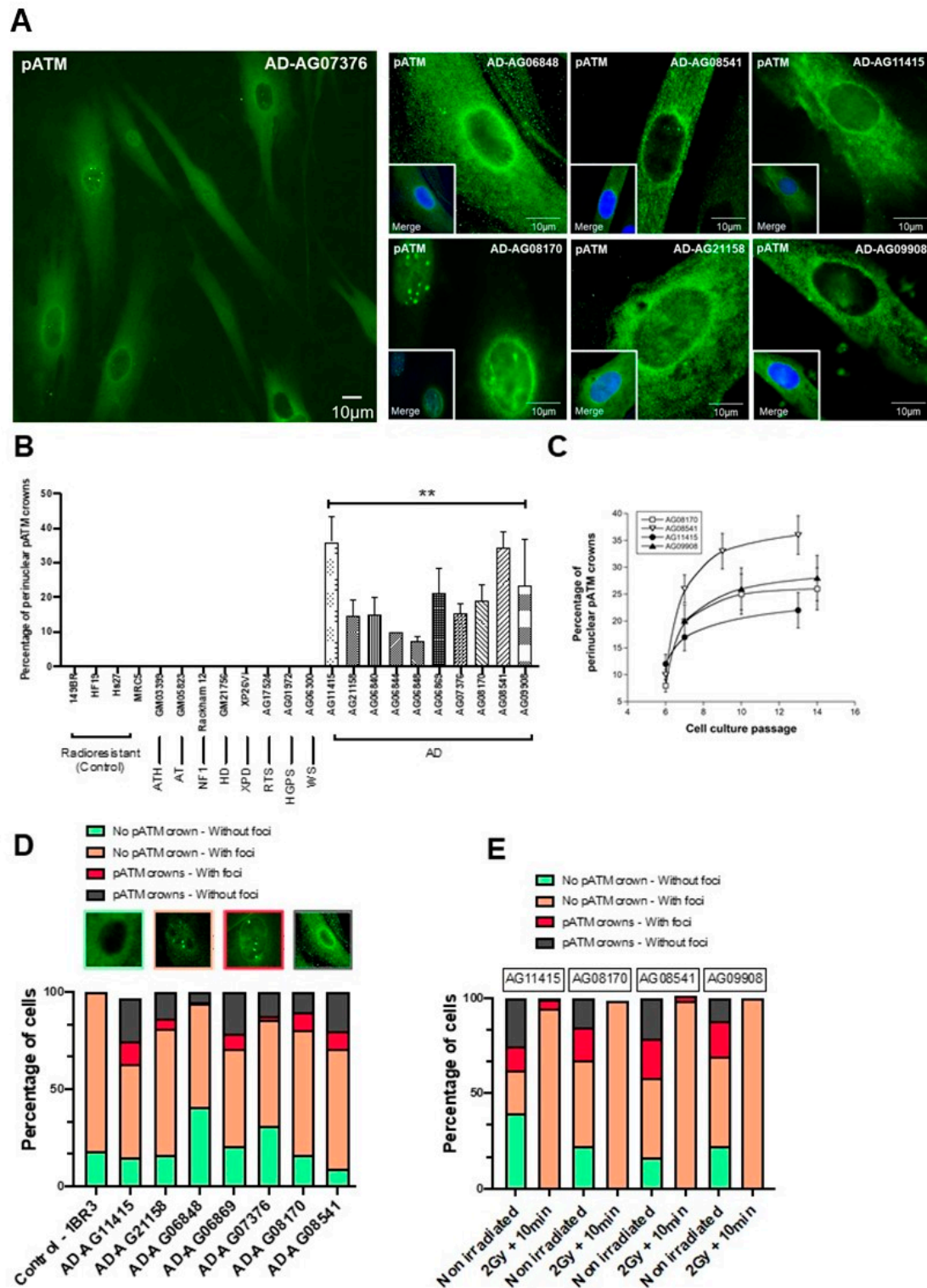


**Figure 6.** Specific spontaneous perinuclear localization of pATM in AD fibroblasts. (A) Representative immunofluorescence images of the perinuclear localization of pATM protein in AD cells. The DAPI signal served as nuclear counterstaining. (B) Histogram showing the percentage of spontaneous.



perinuclear pATM crowns observed in the indicated non-irradiated cells after an anti-pATM immunofluorescence. Each bar represents the mean  $\pm$  SEM of four replicates, at least. \*\*,  $p < 0.01$ . (C) Percentage of perinuclear pATM crowns as a function of cell culture passage in the indicated AD cells. Each point represents the mean  $\pm$  SEM of three replicates. (D) Relative proportions of four specific patterns of the perinuclear pATM crowns observed in the indicated cells after anti-pATM immunofluorescence. The data were obtained during the experiments that served for the quantification of the pATM crowns in cells (shown in panel B). (E) Relative proportions of four specific patterns of the perinuclear pATM crowns observed in the indicated cells after anti-pATM immunofluorescence, assessed before or after irradiation (2 Gy + 10 min).

After irradiation, the number of these perinuclear pATM crowns (patterns 3 and 4) drastically decreased 10 min after 2 Gy, regardless of the AD fibroblasts tested (Figure 6E). Since the pATM signals disappeared after irradiation, these findings suggest that the irradiation triggers the monomerization of ATM dimers, at least transiently.

### 3.4. AD Fibroblasts Show a Specific Protein Partnership between ATM and APOE Proteins

In the frame of the RIANs model, the ATM dimers dissociated in monomers in response to the oxidative stress [17], as already suggested [32]. Such monomers may be sequestered in the cytoplasm by overexpressed protein ATM substrates, called “X-proteins”: we have shown that each genetic disease associated with moderate radiosensitivity and delayed RIANs was characterized by one X-protein, at least [17]. We therefore examined which X-protein may be specifically both overexpressed in the cytoplasm and phosphorylated by ATM in AD fibroblasts. Among the potential X-protein candidates for AD, we quickly eliminated the  $\beta$ -amyloid peptides and the tau proteins since they did not show evident perinuclear staining in the 10 AD fibroblasts tested. In contrast, it appeared that the APOE protein, that is currently documented in AD research [43], showed: (1) Spontaneous cytoplasmic and perinuclear localization of APOE protein in the 10 AD fibroblasts tested, similar to fibroblasts provided from some other neurodegenerative or aging syndromes, when observed with anti-APOE immunofluorescence (Figure 7A). (2) Spontaneous cytoplasmic overexpression of APOE and pATM proteins, higher in all the AD fibroblasts tested than in controls, when observed by immunoblots with cytoplasmic extracts (Figure 7B). (3) A specific cytoplasmic interaction between ATM and APOE proteins in all the AD fibroblasts tested when observed with the proximity ligation assay (PLA) (Figure 7C).

Particularly, the PLA revealed dots (or foci) of interaction between ATM and APOE proteins that were found significantly more numerous in the cytoplasm of AD cells than in radioresistant controls. In fibroblasts derived from neurodegenerative or aging syndromes such as Werner’s syndrome, the PLA foci were either absent or much less numerous ( $p < 0.001$ ). Lastly, it is noteworthy that such PLA dots were also absent in ATM-mutated fibroblasts. It is also noteworthy that there is no human syndrome associated with null expression of APOE to serve as a negative control (Figure 7C).

Interestingly, the in silico analysis of the APOE sequence revealed the presence of two putative ATM phosphorylation SQ/TQ domains defined elsewhere [44]: the APOE<sup>ser72</sup> and the APOE<sup>thr75</sup>. In order to investigate whether these domains were involved in the interaction between ATM and APOE, we developed phosphospecific antibodies against both phosphorylated forms. Immunofluorescence analysis clearly showed that both spontaneous pAPOE signals were mainly localized in the cytoplasm and were stronger in the cytoplasm than in the nucleus. Furthermore, the pAPOE signals were also higher in AD fibroblasts than in controls. However, the conclusions reached with immunoblots were less clear: while both anti-pAPOE<sup>ser72</sup> and anti-pAPOE<sup>thr75</sup> antibodies revealed significant cytoplasmic forms of pAPOE, the anti-pAPOE<sup>thr75</sup> antibody did not provide reproducible and clear signals from nuclear extracts, suggesting a potential rarity and/or instability of the specific pAPOE<sup>thr75</sup> in the nucleus (Figure 7D,E).



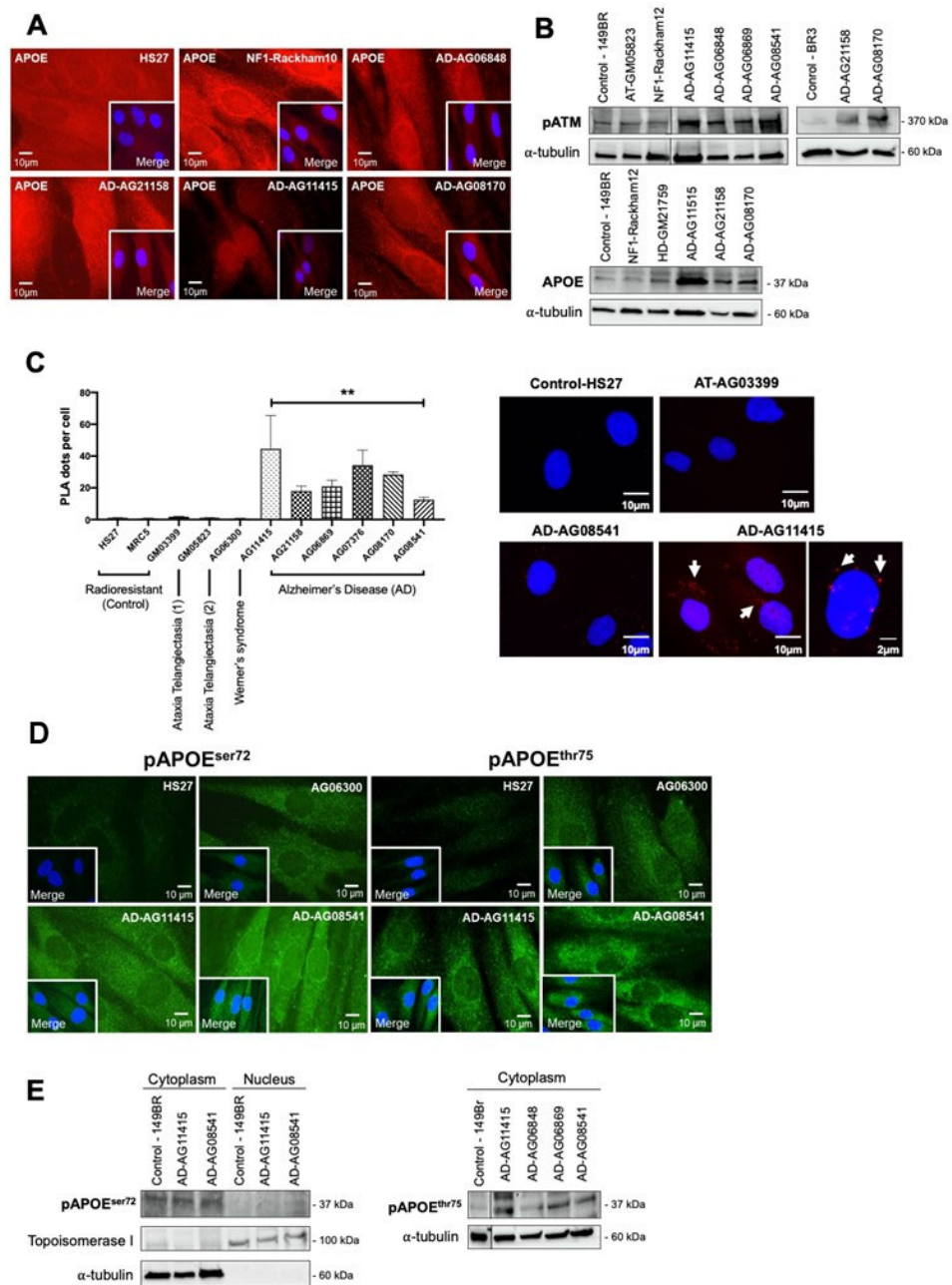


**Figure 7.** ATM and APOE interactions in AD fibroblasts. **(A)** Representative immunofluorescence images of the spontaneous APOE subcellular localization in the indicated non-irradiated cells. The DAPI signal served as nuclear counterstaining. **(B)** Immunoblots performed with anti-pATM and anti-APOE antibodies on cytoplasmic extracts from the indicated non-irradiated cells. Alpha-tubulin served as a cell fractionation and loading control. **(C)** The proximity ligation assay (PLA) with anti-ATM and anti-APOE antibodies was performed on the indicated non-irradiated cells. Histogram showing the PLA dots scored by immunofluorescence microscopy, that represent the detected ATM–APOE interaction. Each plot represents the mean ± SEM of three replicates. Representative PLA immunofluorescence images in the indicated non-irradiated cells. The DAPI signal served as nuclear counterstaining. \*\*,  $p < 0.01$ . **(D)** Representative immunofluorescence images of the spontaneous pAPOE<sup>ser72</sup> and pAPOE<sup>thr75</sup> subcellular localization in the indicated non-irradiated cells. The DAPI signal served as nuclear counterstaining. **(E)** Immunoblots performed with anti-pAPOE<sup>ser72</sup> and -pAPOE<sup>thr75</sup> antibodies in cytoplasmic or nuclear extracts from the indicated cells. Topoisomerase I and alpha-tubulin served as loading controls and as cytoplasmic and nuclear cell fractionation controls, respectively.



Altogether, these data were consistent with the formation of perinuclear pATM crowns in non-irradiated AD fibroblasts that may contain specific ATM-phosphorylated forms of APOE protein.

#### 4. Discussion

The initial goal of this study was to document, at the molecular level, the radiosensitivity of AD fibroblasts that was previously pointed out at the cellular scale [5–7]. To this aim, we deliberately chose to apply a routine approach based on the RIANs model. Such approach has been successfully applied to a number of genetic diseases, including aging syndromes [22–27]. During our investigations, a specific perinuclear localization of the pATM forms was noticed in all the non-irradiated AD fibroblast cell lines tested. This feature was not observed in any other fibroblast cell lines derived from the aging, cancer syndromes or apparently healthy donors tested at the same cell culture passages. In addition, the percentage of cells with perinuclear pATM crowns increased with the cell culture passage in AD fibroblasts, suggesting an age-dependent evolution. Such perinuclear pATM crowns disappeared, transiently at least, after an irradiation. We therefore hypothesized that these perinuclear crowns might be used as a specific biomarker of AD, for the early detection of AD, the progression of the disease, and potentially, for its treatment.

As described in Section 1, in the frame of the RIANs model, the RI oxidative stress causes the formation of ATM monomers from the cytoplasmic ATM dimers. The ATM monomers diffuse in the nucleus and participate to the recognition of DSB by NHEJ. A delayed RIANs caused by the sequestration of ATM monomers in the cytoplasm via overexpressed cytoplasmic ATM substrates (called X-proteins) provides moderate radiosensitivity associated with cancer proneness or accelerated aging [17]. Here, four molecular endpoints (micronuclei,  $\gamma$ H2AX, pATM and MRE11) converged to the same conclusions. Altogether, our data, through the RIANs model, provide the first molecular explanation of the radiosensitivity of cells derived from AD patients, in agreement with the historical observations at the cellular scale [5–7].

The spontaneous perinuclear localization of pATM forms prompted us to identify any X-protein candidate that would localize very close to the nuclear membrane in AD cells. Unlike  $\beta$ -amyloid peptides and tau proteins, the APOE protein reached the three major requirements: (1) APOE was found implicated in certain forms of AD, although there is still confusion between the roles of an overexpressed APOE protein in cells and the *APOE* $\epsilon$  polymorphism status [43]. (2) In silico studies showed that APOE holds putative ATM phosphorylation SQ/TQ domains [44]. (3) APOE, as an apolipoprotein, was found to be involved in the protein trafficking through cellular and nuclear membranes and the regulation to cholesterol [45–47]. Four observations consolidated our hypothesis: (1) APOE was found spontaneously more expressed in all the AD fibroblasts tested than in the controls (Figure 8B), (2) a partnership between ATM and APOE may occur through SQ/TQ phosphorylation (Figure 8), (3) PLA data suggested that some ATM-APOE complexes may be found close to the nuclear membrane (Figure 7C), and (4) the localization of the phosphospecific forms of the APOE (pAPOE) was consistent with the ATM-pAPOE interaction (Figure 7C,D). At this point, it is important to recall that the anti-pATM<sup>ser1981</sup> antibodies specifically reveal auto-phosphorylated dimers and not ATM monomers [17]. Hence, the presence of a perinuclear pATM crown revealed by anti-pATM immunofluorescence suggests a high concentration of ATM dimers close to the nuclear membrane.

What scenario may unify both the high accumulation of ATM dimers and ATM-pAPOE complexes? A permanent oxidative stress is responsible for the formation of spontaneous DNA breaks, but also for a continuous monomerization of the ATM dimers, as already suggested by treating cells with hydrogen peroxide [32]. Hence, some ATM monomers may be sequestered in the close vicinity of the nuclear membrane by APOE proteins, explaining the specific phosphorylated forms of APOE (pAPOE) revealed by the pAPOE<sup>ser72</sup> or pAPOE<sup>thr75</sup> immunofluorescence and the PLA data (Figure 7). Once the ATM-pAPOE complexes form, the stress-induced diffusion of ATM monomers may



progressively cause a highly localized concentration of ATM monomers, leading to ATM re-dimerization, and therefore producing a pATM perinuclear crown, easily visible with anti-pATM immunofluorescence. Hence, this model of accretion of ATM monomers strongly suggests that the perinuclear crowns of pATM are composed of an inner layer formed by ATM monomers, and that pAPOE forms and an outer layer formed by ATM dimers. In a cumulative and progressive process, this phenomenon may specifically contribute in AD cells to an increase of the number of cells with perinuclear pATM crowns and an increase of the crown “thickness”. Such model is, therefore, consistent with the patterns 1, 2, 3 and 4 described in Figure 8.

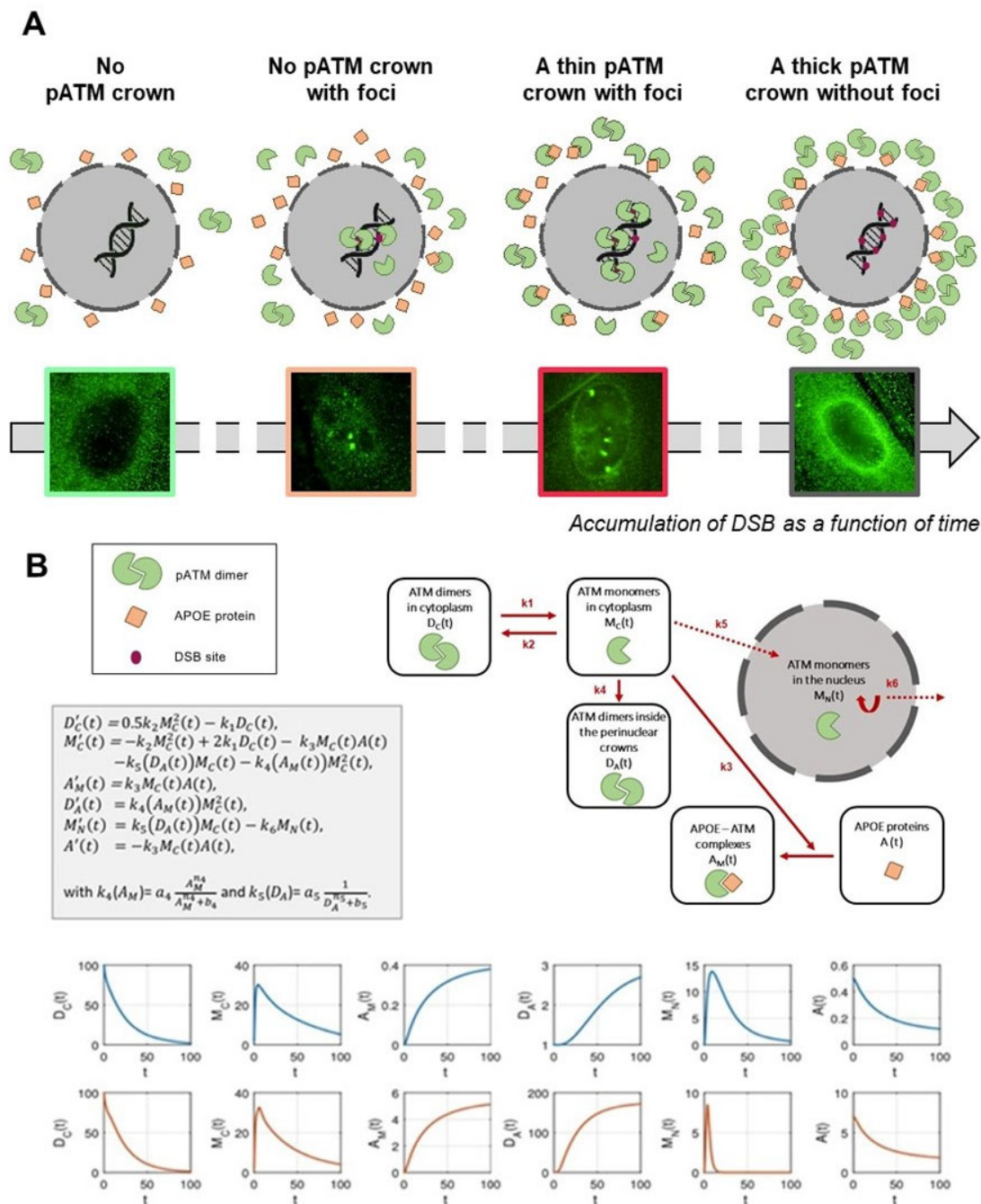


**Figure 8.** (A) Mechanistic model of the formation of the perinuclear pATM crowns in AD fibroblasts. The environmental stress, amplified by the potential predisposition to DNA damage impairment, produces oxidative stress, causing DNA strand breaks and monomerization of cytoplasmic ATM.



dimers, consistent with the RIANS model. In a context in which APOE, an ATM phosphorylation substrate, is overexpressed, the ATM monomers phosphorylate and preferentially bind to APOE by forming ATM-APOE complexes, instead of diffusing in the nucleus to recognized DSB, and trigger their repair by NHEJ. These complexes progressively prevent the ATM nucleoshuttling, which increases the concentration of ATM monomers around the nucleus. As a result, ATM monomers re-associate by forming ATM dimers around the nucleus, which prevents recognition of DSB that accumulate in nucleus. This re-dimerization of ATM monomers is easily visible by immunofluorescence as perinuclear pATM crowns. **(B)** Mathematical modeling of the formation of perinuclear pATM crowns. The first equation in  $D_c$  represents the variation of ATM dimers,  $D_c'(t)$ . The first term on the right side represents the formation of a dimer from two monomers, and the second term stands for the monomerization of an ATM dimer into two ATM monomers. Similarly, in the second equation, the right side describes, respectively, the dimerization, the monomerization, the APOE-ATM complex formation, the passage to the nucleus and the pATM crown, populated by dimerization in the crown. The third equation describes the formation of the APOE-ATM complex, and the fourth equation describes the crowding of the crown through dimerization of ATM monomers in the nucleus neighborhood. The fifth equation represents the passage to the nucleus with a degradation term, and the last equation stands for the loss of the free APOE protein to form a complex with ATM monomers. Representative examples of the variations of each parameter are shown in blue for non-AD radioresistant controls and in red for AD cells.

In order to support the above mechanistic model, and notably the occurrence of the different patterns of the pATM perinuclear crowns shown in Figure 3, we designed a brand-new mathematical approach consisting of six nonlinear differential equations. Each equation describes the kinetics of the concentrations of a specific protein form involved in the mechanistic model:  $D_C$  and  $M_C$ , time-dependent functions, reflect the ATM dimers and the ATM monomers in the cytoplasm, respectively.  $D_A$ ,  $A$  and  $A_M$ , time-dependent functions, reflect the dimers in the immediate vicinity of the nucleus, the free APOE monomers and the ATM-pAPOE complexes, respectively (Figure 8). Lastly,  $M_N$  reflects the nuclear ATM monomers varying with time. This mathematical approach was applied to simulate the consequences of a continuous oxidative stress induction with a low (such as in the controls) or a high cytoplasmic APOE protein level (such as in AD cells) (Figure 8). The resulting blue kinetics reflecting the control data clearly showed a slow production of ATM dimers, the absence of ATM-pAPOE complexation and a facilitated diffusion of ATM monomers in the nucleus (Figure 8). In contrast, in AD cells, the ATM-pAPOE complexation increased together with the formation of ATM dimers in the close vicinity of the nucleus. As a result, the function reflecting the ATM monomers in the nucleus rapidly decreased to zero. By further investigating this mathematical modeling, it was possible to explain the four perinuclear pATM crown patterns defined above. To this aim, initial  $A(0)$  parameter values were modified.

By considering both biological and mathematical models, the fact that the ZOPRA treatment did not fully correct the molecular AD phenotype with all four molecular endpoints tested (micronuclei,  $\gamma$ H2AX, pATM and MRE11) may be supported by the high concentration of ATM proteins cumulated in the close vicinity of the nucleus that did not help the statins and bisphosphonates to diffuse in the nucleus. In contrast, both models can also explain that a dose of IR, such as that mimicking a standard radiotherapy session, may cause a massive monomerization of ATM dimers early after irradiation, leading to the destruction of the perinuclear pATM crowns. Further investigations are, however, required to evaluate the benefit of a ZOPRA treatment in AD patients after radiotherapy, and to explore whether radiotherapy may influence the pattern and/or the number of perinuclear pATM crowns, as suggested in Figure 6D.

The spontaneous perinuclear pATM and pAPOE crowns found specifically in AD fibroblasts raised several questions about their potential role as specific biomarkers of AD: can they help in the detection of AD, the estimation of the disease progression and/or the definition of a possible predisposition to AD? Our experimental findings and the associated mathematical model were consistent with a progressive acceleration of aging due to non-



recognized DNA breaks that cumulate in the nucleus throughout life. Such statement is consistent with numerous studies suggesting that AD results from a cumulative oxidative stress [48,49]. Can our observations in AD fibroblasts reflect the same biological features in brain cells, notably in hippocampus cells? The relevance of the RIANS model has been verified in numerous tissues, including brain astrocytes [50]. Furthermore, cutaneous fibroblasts were shown to be the tissue model more representative of the individual response to IR than the other tissues [8]. Nevertheless, to sample brain cells would raise many more ethical and practical problems than skin biopsies. While brain cells are characterized by a low concentration of ATM protein [51] and most ATM molecules were found cytoplasmic [28–32], our findings may be consistent with a slower and less efficient ATM nucleoshuttling in brain cells, accompanied by a higher sensitivity to DNA breaks, with more significant clinical consequences than those observed in skin fibroblasts. Further investigations are needed to verify this hypothesis.

The cumulative nature of the perinuclear pATM and pAPOE crowns' formation also raised the question of a correlation between the yield or the pattern of the crowns and the disease progression. In this study, the clinical data about the progression of the disease in the 10 AD cell lines were not available. Besides, it must be stressed that post-mortem human brain data would not be useful to answer this question since they would not provide the threshold of perinuclear pATM crowns necessary for significant clinical features. Furthermore, the causes of cellular death and the progression of AD are not likely to be equally correlated with the perinuclear pATM crowns. Again, further clinical investigations will help document the AD progression and its associated clinical criteria.

Finally, our findings raised the question of a potential predisposition to AD that would be based on the existence of a significant amount of perinuclear pATM crowns at the earliest age. However, our experimental data and the mathematical model suggest that the environmental stress and the genetic factors may unequally contribute to increase or even accelerate the formation of perinuclear pATM crowns. Such hypothesis may explain the heterogeneity of the AD cases, notably vis-à-vis the age at diagnosis.

## 5. Conclusions

Altogether, our experimental findings and the mathematical model were consistent with the hypothesis that in the development of AD, there is a progressive accumulation of ATM-pAPOE and pATM-pATM dimeric complexes around the nuclear membrane in response to oxidative stress throughout life, facilitated by the predisposition of overexpressed APOE protein in the cytoplasm. Such specific subcellular localization of ATM may prevent the RIANS, i.e., the recognition and repair of DNA strand breaks by the ATM kinase. Irradiation may make the perinuclear pATM crowns disappear. For the first time, to our knowledge, the ATM kinase was shown to be involved in the pathology of AD, and its interaction with APOE may play a major role in aging, which may lead to a new approach in the understanding of AD. Particularly, with further investigations, our findings may help in the definition and the detection of individual predisposition to AD, helpful in the early diagnosis of AD.

**Supplementary Materials:** The following supporting information can be downloaded at: <https://www.mdpi.com/article/10.3390/cells12131747/s1>, Figure S1: Correlation between SF2 and residual micronuclei data. Figure S2: Correlation between SF2 and residual  $\gamma$ H2AX foci data. Figure S3: Correlation between SF2 and pATMmax data. Figure S4: The number of perinuclear pATM crowns per 100 cells vs. the age at skin sampling.

**Author Contributions:** Conceptualization, E.B., M.B. and N.F.; software, A.C. and L.P.-M.; data acquisition and methodology, E.B., L.P.-M., L.S., E.L.R., J.A.-C., A.G., A.C., M.L.F., C.D. and S.P.; validation and data analysis, E.B., L.P.-M., L.S., E.L.R., J.A.-C., A.G., A.C., M.L.F., C.D., S.P. and N.F.; writing and original draft preparation, E.B., M.B. and N.F.; review and editing, E.B., L.P.-M., L.S., E.L.R., J.A.-C., A.G., C.D., M.L.F., A.C., S.P., M.B. and N.F.; project administration and funding acquisition, N.F. All authors have read and agreed to the published version of the manuscript.



**Funding:** This research was funded by Commissariat General à l'Investissement (Programmes Investissement d'Avenir—INDIRA project, N.F.), Association Neurofibromatose et Recklinghausen (RACKHAM project, N.F.), National Space Agency (CNES) (ATHENA and BERNADOTTE projects, N.F.) and Inserm Transfert (TAG-MAAL Project).

**Institutional Review Board Statement:** Besides the notable exception of the cell lines belonging to the COPERNIC collection (see Table 1), all the fibroblast cell lines used in this study were purchased from commercial repositories (see the Materials and Methods Section). As already mentioned in the Materials and Methods Section, this study was performed with some fibroblast cell lines from the COPERNIC collection, which was approved by the regional Ethical Committee. Cell lines were declared under the numbers DC2008-585, DC2011-1437 and DC2021-3957 to the Ministry of Research. The database was declared under the reference number IDDN.FR.001.510017.000.D.P.2014.000.10300 to the Ministry of Research.

**Informed Consent Statement:** The commercial repositories that provided the fibroblast cell lines used in this study applied all the ethics and regulations related to human samplings. All the anonymous COPERNIC patients were informed and signed consent according to the ethics recommendations, notably for their consent to participate and for the publication of anonymous data (informed and written consent, anonymization and acceptance for publication).

**Data Availability Statement:** The data presented here are either present in a deposited database (see the Materials and Methods Section) or will be made available upon reasonable request.

**Acknowledgments:** We thank Sylvie Bouvier and Erick Mercier from CHU de Nîmes, France, for their technical assistance with the APOE genotyping.

**Conflicts of Interest:** A patent related to the early diagnosis of Alzheimer's disease from the perinuclear ATM crowns was deposited under the reference number 23305025.1 on 9 January 2023.

## References

1. Sery, O.; Povova, J.; Misek, I.; Pesak, L.; Janout, V. Molecular mechanisms of neuropathological changes in Alzheimer's disease: A review. *Folia Neuropathol.* **2013**, *51*, 1–9. [[CrossRef](#)] [[PubMed](#)]
2. Nikolac Perkovic, M.; Pivac, N. Genetic Markers of Alzheimer's Disease. *Adv. Exp. Med. Biol.* **2019**, *1192*, 27–52.
3. Glenner, G.G.; Wong, C.W.; Quaranta, V.; Eanes, E.D. The amyloid deposits in Alzheimer's disease: Their nature and pathogenesis. *Appl. Pathol.* **1984**, *2*, 357–369. [[PubMed](#)]
4. Grundke-Iqbal, I.; Iqbal, K.; Tung, Y.C.; Quinlan, M.; Wisniewski, H.M.; Binder, L.I. Abnormal phosphorylation of the microtubule-associated protein tau (tau) in Alzheimer cytoskeletal pathology. *Proc. Natl. Acad. Sci. USA* **1986**, *83*, 4913–4917. [[CrossRef](#)]
5. Tobi, S.E.; Moquet, J.E.; Edwards, A.A.; Lloyd, D.C.; Itzhaki, R.F. Chromosomal radiosensitivity of lymphocytes from Alzheimer's disease patients. *J. Med. Genet.* **1990**, *27*, 437–440. [[CrossRef](#)]
6. Robbins, J.H.; Otsuka, F.; Tarone, R.E.; Polinsky, R.J.; Brumback, R.A.; Nee, L.E. Parkinson's disease and Alzheimer's disease: Hypersensitivity to X rays in cultured cell lines. *J. Neurol. Neurosurg. Psychiatry* **1985**, *48*, 916–923. [[CrossRef](#)]
7. Smith, T.A.; Itzhaki, R.F. Radiosensitivity of lymphocytes from patients with Alzheimer's disease. *Mutat. Res.* **1989**, *217*, 11–17. [[CrossRef](#)] [[PubMed](#)]
8. Granzotto, A.; Benadjaoud, M.A.; Vogin, G.; Devic, C.; Ferlazzo, M.L.; Bodgi, L.; Pereira, S.; Sonzogni, L.; Forcheron, F.; Viau, M.; et al. Influence of Nucleoshuttling of the ATM Protein in the Healthy Tissues Response to Radiation Therapy: Toward a Molecular Classification of Human Radiosensitivity. *Int. J. Radiat. Oncol. Biol. Phys.* **2016**, *94*, 450–460. [[CrossRef](#)]
9. Bodgi, L.; Foray, N. The nucleo-shuttling of the ATM protein as a basis for a novel theory of radiation response: Resolution of the linear-quadratic model. *Int. J. Radiat. Biol.* **2016**, *92*, 117–131. [[CrossRef](#)]
10. Pereira, S.; Bodgi, L.; Duclos, M.; Canet, A.; Ferlazzo, M.L.; Devic, C.; Granzotto, A.; Deneuve, S.; Vogin, G.; Foray, N. Fast and binary assay for predicting radiosensitivity based on the nucleoshuttling of ATM protein: Development, validation and performances. *Int. J. Radiat. Oncol. Biol. Phys.* **2018**, *100*, 353–360. [[CrossRef](#)]
11. Belkacemi, Y.; Colson-Durand, L.; Granzotto, A.; Husheng, S.; To, N.H.; Majdoul, S.; Guet, S.; Herve, M.L.; Fonteneau, G.; Diana, C.; et al. The Henri Mondor Procedure of Morbidity and Mortality Review Meetings: Prospective Registration of Clinical, Dosimetric, and Individual Radiosensitivity Data of Patients with Severe Radiation Toxicity. *Int. J. Radiat. Oncol. Biol. Phys.* **2016**, *96*, 629–636. [[CrossRef](#)]
12. Vogin, G.; Bastogne, T.; Bodgi, L.; Gillet-Daubin, J.; Canet, A.; Pereira, S.; Foray, N. The Phosphorylated ATM Immunofluorescence Assay: A High-performance Radiosensitivity Assay to Predict Postradiation Therapy Overreactions. *Int. J. Radiat. Oncol. Biol. Phys.* **2018**, *101*, 690–693. [[CrossRef](#)]
13. Deneuve, S.; Mirjolet, C.; Bastogne, T.; Duclos, M.; Retif, P.; Zrounba, P.; Roux, P.-E.; Poupart, M.; Vogin, G.; Foray, N.; et al. Proof of Concept of a Binary Blood Assay for Predicting Radiosensitivity. *Cancers* **2021**, *13*, 2477. [[CrossRef](#)] [[PubMed](#)]



14. Le Reun, E.; Bodgi, L.; Granzotto, A.; Sonzogni, L.; Ferlazzo, M.L.; Al-Choboq, J.; El-Nachef, L.; Restier-Verlet, J.; Berthel, E.; Devic, C.; et al. Quantitative correlations between radiosensitivity biomarkers show that the ATM protein kinase is strongly involved in the radiotoxicities observed after radiotherapy. *Int. J. Mol. Sci.* **2022**, *23*, 10434. [\[CrossRef\]](#)
15. Devic, C.; Ferlazzo, M.L.; Berthel, E.; Foray, N. Influence of Individual Radiosensitivity on the Hormesis Phenomenon: Toward a Mechanistic Explanation Based on the Nucleoshuttling of ATM Protein. *Dose-Response A Publ. Int. Hormesis Soc.* **2020**, *18*, 1559325820913784. [\[CrossRef\]](#) [\[PubMed\]](#)
16. Devic, C.; Ferlazzo, M.L.; Foray, N. Influence of Individual Radiosensitivity on the Adaptive Response Phenomenon: Toward a Mechanistic Explanation Based on the Nucleo-Shuttling of ATM Protein. *Dose-Response A Publ. Int. Hormesis Soc.* **2018**, *16*, 1559325818789836. [\[CrossRef\]](#)
17. Berthel, E.; Foray, N.; Ferlazzo, M.L. The Nucleoshuttling of the ATM Protein: A Unified Model to Describe the Individual Response to High- and Low-Dose of Radiation? *Cancers* **2019**, *11*, 905. [\[CrossRef\]](#) [\[PubMed\]](#)
18. Viau, M.; Sonzogni, L.; Ferlazzo, M.L.; Berthel, E.; Pereira, S.; Bodgi, L.; Granzotto, A.; Devic, C.; Fervers, B.; Charlet, L.; et al. DNA Double-Strand Breaks Induced in Human Cells by Twelve Metallic Species: Quantitative Inter-Comparisons and Influence of the ATM Protein. *Biomolecules* **2021**, *11*, 1462. [\[CrossRef\]](#) [\[PubMed\]](#)
19. Sonzogni, L.; Ferlazzo, M.L.; Granzotto, A.; Fervers, B.; Charlet, L.; Foray, N. DNA Double-Strand Breaks Induced in Human Cells by 6 Current Pesticides: Intercomparisons and Influence of the ATM Protein. *Biomolecules* **2022**, *12*, 250. [\[CrossRef\]](#)
20. Foray, N.; Bourguignon, M.; Hamada, N. Individual response to ionizing radiation. *Mutat. Res. Rev.* **2016**, *770*, 369–386. [\[CrossRef\]](#)
21. El-Nachef, L.; Al-Choboq, J.; Restier-Verlet, J.; Granzotto, A.; Berthel, E.; Sonzogni, L.; Ferlazzo, M.L.; Bouchet, A.; Leblond, P.; Combemale, P.; et al. Human Radiosensitivity and Radiosusceptibility: What Are the Differences? *Int. J. Mol. Sci.* **2021**, *22*, 7158. [\[CrossRef\]](#) [\[PubMed\]](#)
22. Ferlazzo, M.L.; Sonzogni, L.; Granzotto, A.; Bodgi, L.; Lartin, O.; Devic, C.; Vogin, G.; Pereira, S.; Foray, N. Mutations of the Huntington's Disease Protein Impact on the ATM-Dependent Signaling and Repair Pathways of the Radiation-Induced DNA Double-Strand Breaks: Corrective Effect of Statins and Bisphosphonates. *Mol. Neurobiol.* **2014**, *49*, 1200–1211. [\[CrossRef\]](#) [\[PubMed\]](#)
23. Ferlazzo, M.L.; Bach-Tobdji, M.K.E.; Djerad, A.; Sonzogni, L.; Burlet, S.F.; Devic, C.; Granzotto, A.; Bodgi, L.; Djefal-Kerrar, A.; Foray, N. Radiobiological characterization of tuberous sclerosis: A delay in the nucleo-shuttling of ATM may be responsible for radiosensitivity. *Mol. Neurobiol.* **2017**, *55*, 4973–4983. [\[CrossRef\]](#) [\[PubMed\]](#)
24. Ferlazzo, M.; Berthel, E.; Granzotto, A.; Devic, C.; Sonzogni, L.; Bachelet, J.T.; Pereira, S.; Bourguignon, M.; Sarasin, A.; Mezzina, M.; et al. Some mutations in the xeroderma pigmentosum D gene may lead to moderate but significant radiosensitivity associated with a delayed radiation-induced ATM nuclear localization. *Int. J. Radiat. Biol.* **2019**, *96*, 394–410. [\[CrossRef\]](#)
25. Moulay Lakhdar, I.; Ferlazzo, M.L.; Al Choboq, J.; Berthel, E.; Sonzogni, L.; Devic, C.; Granzotto, A.; Thariat, J.; Foray, N. Fibroblasts from Retinoblastoma Patients Show Radiosensitivity Linked to Abnormal Localization of the ATM Protein. *Curr. Eye Res.* **2020**, *46*, 546–557. [\[CrossRef\]](#) [\[PubMed\]](#)
26. Combemale, P.; Sonzogni, L.; Devic, C.; Bencokova, Z.; Ferlazzo, M.L.; Granzotto, A.; Burlet, S.F.; Pinson, S.; Amini-Adle, M.; Al-Choboq, J.; et al. Individual Response to Radiation of Individuals with Neurofibromatosis Type I: Role of the ATM Protein and Influence of Statins and Bisphosphonates. *Mol. Neurobiol.* **2022**, *59*, 556–573. [\[CrossRef\]](#) [\[PubMed\]](#)
27. Al-Choboq, J.; Nehal, M.; Sonzogni, L.; Granzotto, A.; El Nachef, L.; Restier-Verlet, J.; Maalouf, M.; Berthel, E.; Aral, B.; Corradini, N.; et al. Molecular and Cellular Responses to Ionization Radiation in Untransformed Fibroblasts from the Rothmund–Thomson Syndrome: Influence of the Nucleo-Shuttling of the ATM Protein Kinase. *Radiation* **2023**, *3*, 21–38. [\[CrossRef\]](#)
28. Watters, D.; Khanna, K.K.; Beamish, H.; Birrell, G.; Spring, K.; Kedar, P.; Gatei, M.; Stenzel, D.; Hobson, K.; Kozlov, S.; et al. Cellular localisation of the ataxia-telangiectasia (ATM) gene product and discrimination between mutated and normal forms. *Oncogene* **1997**, *14*, 1911–1921. [\[CrossRef\]](#)
29. Alexander, A.; Cai, S.L.; Kim, J.; Nanez, A.; Sahin, M.; MacLean, K.H.; Inoki, K.; Guan, K.L.; Shen, J.; Person, M.D.; et al. ATM signals to TSC2 in the cytoplasm to regulate mTORC1 in response to ROS. *Proc. Natl. Acad. Sci. USA* **2010**, *107*, 4153–4158. [\[CrossRef\]](#)
30. Guo, Z.; Kozlov, S.; Lavin, M.F.; Person, M.D.; Paull, T.T. ATM activation by oxidative stress. *Science* **2010**, *330*, 517–521. [\[CrossRef\]](#)
31. Slonina, D.; Kowalczyk, A.; Janecka-Widla, A.; Kabat, D.; Szatkowski, W.; Biesaga, B. Low-Dose Hypersensitive Response for Residual pATM and gammaH2AX Foci in Normal Fibroblasts of Cancer Patients. *Int. J. Radiat. Oncol. Biol. Phys.* **2018**, *100*, 756–766. [\[CrossRef\]](#) [\[PubMed\]](#)
32. Paull, T.T. Mechanisms of ATM Activation. *Annu. Rev. Biochem.* **2015**, *84*, 711–738. [\[CrossRef\]](#)
33. Foray, N.; Priestley, A.; Alsbeih, G.; Badie, C.; Capulas, E.P.; Arlett, C.F.; Malaise, E.P. Hypersensitivity of ataxia telangiectasia fibroblasts to ionizing radiation is associated with a repair deficiency of DNA double-strand breaks. *Int. J. Radiat. Biol.* **1997**, *72*, 271–283. [\[PubMed\]](#)
34. Varela, I.; Pereira, S.; Ugalde, A.P.; Navarro, C.L.; Suarez, M.F.; Cau, P.; Cadinanos, J.; Osorio, F.G.; Foray, N.; Cobo, J.; et al. Combined treatment with statins and aminobisphosphonates extends longevity in a mouse model of human premature aging. *Nat. Med.* **2008**, *14*, 767–772. [\[CrossRef\]](#) [\[PubMed\]](#)
35. Restier-Verlet, J.; Drouet, M.; Pras, P.; Ferlazzo, M.L.; Granzotto, A.; Sonzogni, L.; Al-Choboq, J.; El Nachef, L.; Francois, S.; Bourguignon, M.; et al. Molecular Influence of the ATM Protein in the Treatment of Human Cells with Different Radioprotective Drugs: Comparisons between Antioxidative and Pro-Episkevic Strategies. *Biomolecules* **2023**, *13*, 524. [\[CrossRef\]](#)



36. Fertil, B.; Malaise, E.P. Inherent cellular radiosensitivity as a basic concept for human tumor radiotherapy. *Int. J. Radiat. Oncol. Biol. Phys.* **1981**, *7*, 621–629. [[CrossRef](#)]
37. Foray, N.; Marot, D.; Gabriel, A.; Randrianarison, V.; Carr, A.M.; Perricaudet, M.; Ashworth, A.; Jeggo, P. A subset of ATM- and ATR-dependent phosphorylation events requires the BRCA1 protein. *EMBO J.* **2003**, *22*, 2860–2871. [[CrossRef](#)]
38. Ristic, M.; Brockly, F.; Piechaczyk, M.; Bossis, G. Detection of Protein-Protein Interactions and Posttranslational Modifications Using the Proximity Ligation Assay: Application to the Study of the SUMO Pathway. *Methods Mol. Biol.* **2016**, *1449*, 279–290.
39. Deschavanne, P.J.; Fertil, B. A review of human cell radiosensitivity in vitro. *Int. J. Radiat. Oncol. Biol. Phys.* **1996**, *34*, 251–266. [[CrossRef](#)]
40. Weichselbaum, R.R.; Nove, J.; Little, J.B. X-ray sensitivity of fifty-three human diploid fibroblast cell strains from patients with characterized genetic disorders. *Cancer Res.* **1980**, *40*, 920–925.
41. Arlett, C.F.; Harcourt, S.A. Survey of radiosensitivity in a variety of human cell strains. *Cancer Res.* **1980**, *40*, 926–932.
42. Rothkamm, K.; Lobrich, M. Evidence for a lack of DNA double-strand break repair in human cells exposed to very low X-ray doses. *Proc. Natl. Acad. Sci. USA* **2003**, *100*, 5057–5062. [[CrossRef](#)] [[PubMed](#)]
43. Serrano-Pozo, A.; Das, S.; Hyman, B.T. APOE and Alzheimer’s disease: Advances in genetics, pathophysiology, and therapeutic approaches. *Lancet Neurol.* **2021**, *20*, 68–80. [[CrossRef](#)] [[PubMed](#)]
44. Kim, S.T.; Lim, D.S.; Canman, C.E.; Kastan, M.B. Substrate specificities and identification of putative substrates of ATM kinase family members. *J. Biol. Chem.* **1999**, *274*, 37538–37543. [[CrossRef](#)] [[PubMed](#)]
45. Fenili, D.; McLaurin, J. Cholesterol and apoe: A target for Alzheimer’s disease therapeutics. *Curr. Drug Targets CNS Neurol. Disord.* **2005**, *4*, 553–567. [[CrossRef](#)] [[PubMed](#)]
46. Getz, G.S.; Reardon, C.A. Apoprotein E and Reverse Cholesterol Transport. *Int. J. Mol. Sci.* **2018**, *19*, 3479. [[CrossRef](#)]
47. Dong, H.K.; Gim, J.A.; Yeo, S.H.; Kim, H.S. Integrated late onset Alzheimer’s disease (LOAD) susceptibility genes: Cholesterol metabolism and trafficking perspectives. *Gene* **2017**, *597*, 10–16. [[CrossRef](#)]
48. Angelova, P.R.; Abramov, A.Y. Role of mitochondrial ROS in the brain: From physiology to neurodegeneration. *FEBS Lett.* **2018**, *592*, 692–702. [[CrossRef](#)]
49. Collin, F. Chemical Basis of Reactive Oxygen Species Reactivity and Involvement in Neurodegenerative Diseases. *Int. J. Mol. Sci.* **2019**, *20*, 2407. [[CrossRef](#)] [[PubMed](#)]
50. Granzotto, A.; Bencokova1, Z.; Vogin, G.; Devic, C.; Joubert, A.; Balosso, J.; Foray, N. DNA double-strand breaks repair and signaling of human gliomas and normal brain cells in response to radiation: Potential impact of the ATM- and BRCA1-dependent pathways. In *Brain Tumors/Book 3*; Abujamra, A.L., Ed.; Intechweb: Rijeka, Croatia, 2011.
51. Soares, H.D.; Morgan, J.I.; McKinnon, P.J. Atm expression patterns suggest a contribution from the peripheral nervous system to the phenotype of ataxia-telangiectasia. *Neuroscience* **1998**, *86*, 1045–1054. [[CrossRef](#)] [[PubMed](#)]

**Disclaimer/Publisher’s Note:** The statements, opinions and data contained in all publications are solely those of the individual author(s) and contributor(s) and not of MDPI and/or the editor(s). MDPI and/or the editor(s) disclaim responsibility for any injury to people or property resulting from any ideas, methods, instructions or products referred to in the content.



# **UP Dissemination and Communication**



## Pioneers of radiation in Lyon



The life of the pioneers of radiation : Claudius Regaud  
Claudius Regaud (1870-1940)

[Read more >](#)



The life of the pioneers of radiation : Victor Despeignes  
Victor Despeignes (1868-1937)

[Read more >](#)



The life of the pioneers of radiation : Léon Bouchacourt  
Léon Bouchacourt (1865-1949)

[Read more >](#)



The life of the pioneers of radiation : Etienne Destot  
Etienne Destot (1864-1918)

[Read more >](#)



The life of the pioneers of radiation : Fabien Arcelin  
Fabien Arcelin (1876-1942)

[Read more >](#)

<https://www.radiobiologie.fr/videos>



- **Victor DESPEIGNES** : Between the 4th and 23rd July 1896, Victor Despeignes has performed the first anticancer radiotherapy that has been validated by undeniable publications and practical facts. However, the events and the intellectual approach that led him to perform this unique treatment are unknown. This unpublished biography endeavours to better understand the work of Victor Despeignes who was, first of all, an hygienist physician. The conjunction of Pasteur's ideas, the discovery of X-rays and a probable technical help of the Lumière brothers led him to irradiate a cancerous tumour. The life of Victor Despeignes can be divided in three parts; the Lyon period (1866-1894) during which he became physician and researcher in parasitology, working on the quality of tap water and tuberculosis; the period spent between 1894 and 1907 in Buis-les-Baronnies (Drôme) and thereafter in Les Échelles (Savoie) during which he was a simple district physician and performed the first radiotherapy; the Chambéry period (1907-1937) during which he was the Director of the Town Hygiene and provided a major action for public health.
- **Claudius REGAUD** : Born in 1870, Claudius Regaud was a pioneer of radiobiology and radiotherapy. As histologist, he developed a new : staining technique that allowed him to describe in detail all the reproduction system of a number of animal models. As radiobiologist, he contradicted the interpretations of Tribondeau and Bergonié about relationships between cell proliferation and radiosensitivity. In 1908, he suggested that chromatin was the main target of radiation. As physician, he defined the first bases of anti-cancer radiation treatments and treated patients suffering from incurable cancer from 1911. As military doctor, he organized war hospitals by creating multidisciplinary teams for the surgery of hurts. Organizer, he was one of the founders of the League against Cancer. As radiotherapist and brachytherapist, he contributed to make Institut Curie an international reference center for research and teaching, with nearly a thousand treated patients. As globe-trotter, he was at the origin of the creation of numerous worldwide radiotherapy and radiobiology centers. He died in December 1940 and left an impressive but still unknown scientific heritage. A re-reading of the familial archives and the Regaud Fund of Institut Curie is the occasion to remind the contribution of Regaud.
- **Etienne DESTOT** : Étienne Destot is a French physician from Burgundy who benefited, during his studies in Lyon, from the quality of teaching of the best specialists of the time: Augagneur for hygiene, Testut for anatomy, Ollier for surgery, Lépine for the medical applications of electricity and the Lumière brothers for the technological development. During its experiments, he met Despeignes, the first radiation oncologist, Regaud pioneer of radiobiology and Bouchacourt who pointed out individual radiosensitivity. Less than two months after the X-rays discovery by Roentgen, he produced one of the first French radiographic views that were at the origin of our current knowledge in bone and cartilage anatomy and traumatology. He funded the first department of radiology in France in a former library of the major hospital of Lyon, where he made a number of original advances. It appears obvious that, while Antoine Beclère was the great organizer of the French radiology, Destot was its pathfinder. Destot was at the origin of several technological advances that gave stereoscopy, internal organs imaging and quantification of the heart-thorax ratio. By contrast, he was not convinced of the



therapeutic properties of X-rays even if he contributed to the technological development of X-ray tubes. Victim of radiations, exhausted, Destot died on December 1918, by helping the Great War victims. His name is written in a war tribute monument in Arc-et-Senans (Burgundy).

- **Léon BOUCHACOURT** : Léon Bouchacourt (1865-1949) was a misknown pioneer of radiology and radiotherapy from Lyon, France. While he was resident in obstetrics in Hôpitaux de Paris from 1892 to 1898, he met Charcot, the future polar explorer, and wrote the first thesis dissertation about X-rays. He invented a new radiology technique for cavitary organs such as vagina, rectum and mouth, the endodiascopy, which permitted him to perform the first pelvimetry and dental radiographies in France. While he undertook the first trials of contact-radiotherapy, he was confronted with radiation-induced reactions. In 1911, he wrote the first paper about individual radiosensitivity. During the First World War, he commanded one of the radiology vehicles, he met Irène Curie and developed his « radiological helmet », which will hold his name and became essential for interventional radiology. After the war, with Béclère and ten others, Léon Bouchacourt funded the French Radiology Society. He ended his career by thinking about public health and the different aspects of the duties of radiologists.
- **Fabien ARCELIN** : Fabien Arcelin, physician working in Lyon, pioneer of radiology and radiotherapy, was both mentored by Destot (one of the fathers of the French radiology for his thesis of medicine) and by his own father Adrien Arcelin (one of the two codiscoverers of the prehistorical site of the Roche-de-Solutré in Burgundy) for archeological works. Hence, radiologist in Lyon during the week and archeologist during the weekend, Fabien Arcelin made significant advances in both radiation research and archeology. He was notably the discoverer of the first tombs of Aurignacian men. In radiology, he examined about 2000 radiographic heart views with the Destot's orthodiagraph to assess the cardiothoracic ratio and wrote a reference book about the use of X-rays to detect kidney stones. He made the first survey about the secondary effects of radiotherapy, important database for pointing out individual radiosensitivity. In parallel to the radiotherapy trials of Regaud at Curie institute (Paris), he performed the first series of anticancer treatments in Lyon.





Unité U1296 : Radiations  
Défense, Santé, Environnement  
Lyon & Brétigny-sur-Orge, France

# The tree of the projects of the Unit

2021-2024



**Inserm**  
La science pour la santé  
From science to health



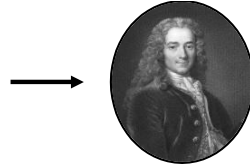


## Fondamental Radiobiology



Head : Dr. Nicolas Foray

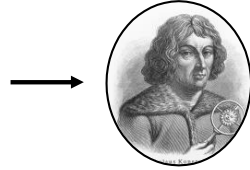
### Maths



#### MICROMEGAS

Mathematical modelling of radiobiological phenomena

### Genetics



#### COPENIC



##### INDIRA

Prediction of radiosensitivity – Healthy donors



##### COPENIC

Prediction of radiosensitivity – Radiotherapy patients



##### CELLINE

Prediction of radiosensitivity – Genetic syndromes

### Tumor Radioresistance



#### GLUTEN



##### GLUTEN

Modulation of tumor radioresistance via glucocorticoid receptors



##### METEOR

Modulation of tumor radioresistance via protein methyltransferase

### Aging / Cancer



#### CARAVAGE



##### TAG MAAL

ATM nucleoshuttling and Alzheimer's disease



##### PANDA

ATM nucleoshuttling and Parkinson's disease



##### CROCUS

Radiosensitivity of ocular system



##### HERA

Radiosensitivity of heart tissue



##### TOPAZE

Cellular transformation, cancer proneness and ZEB1 expression





Unité U1296 : Radiations  
Défense, Santé, Environnement  
Lyon & Brétigny-sur-Orge, France

## Defense



Head:  
Brigadier-General  
Dr. Michel Drouet



### AGENOR

New agents of radiation protection



### INDIRA

Prediction of radiosensitivity – Healthy donors



### PHIDIAS

ATM nucleoshuttling and High dose and Acute Irradiation syndrome



### DEMETER

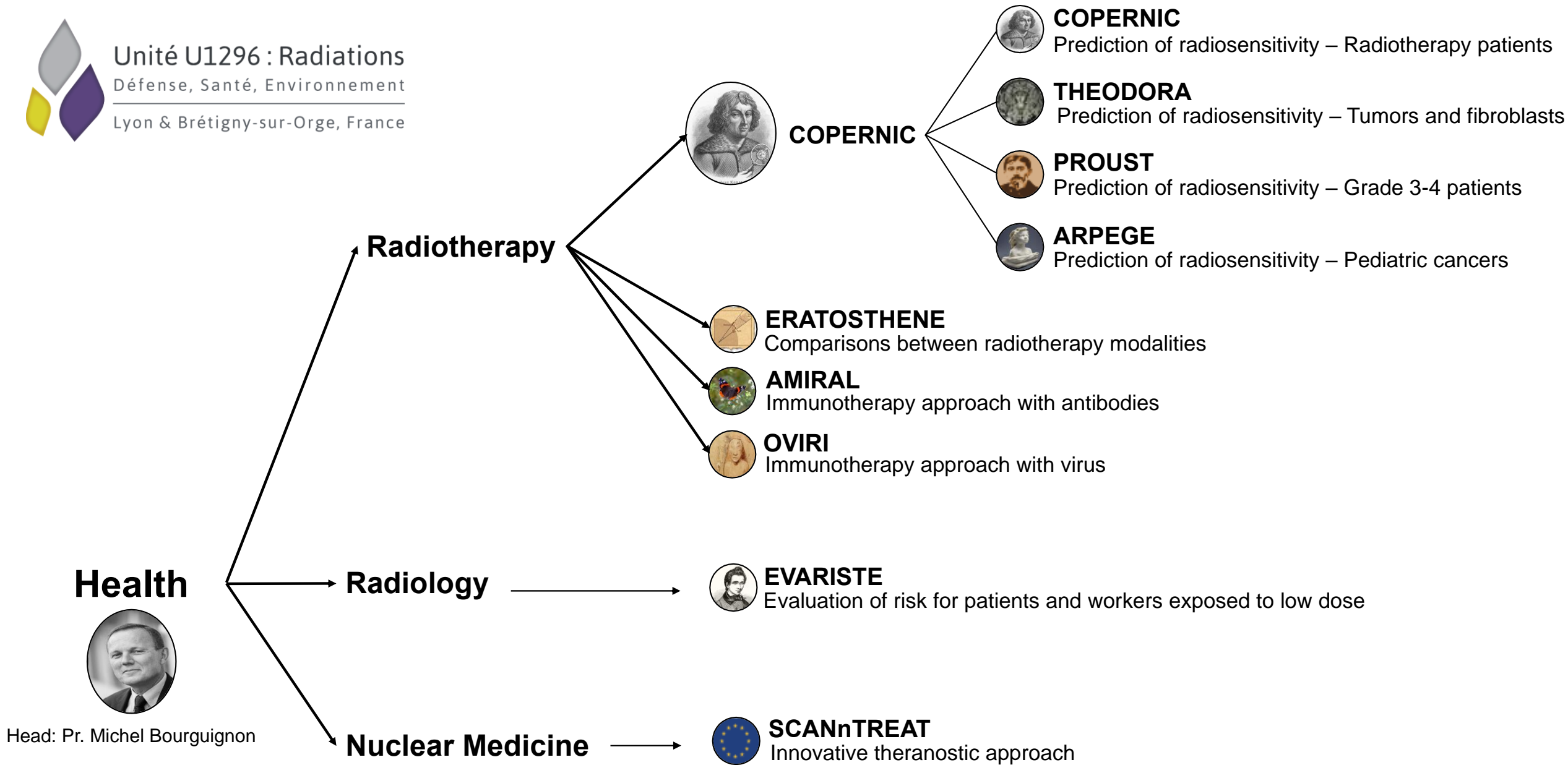
Molecular definition of the electrosensitivity to electromagnetic fields



### ANNONE

ATM nucleoshuttling and nanoparticles









Unité U1296 : Radiations  
Défense, Santé, Environnement  
Lyon & Brétigny-sur-Orge, France

## Environment and Space



Head: Pr. Béatrice Fervers

### Environmental Biology

### Environmental Epidemiology

### Space



### ICARE



#### HEMI-BREAKS

ATM nucleoshuttling and metals



#### EURIPIDE

ATM nucleoshuttling and pesticides



#### BACCHUS

ATM nucleoshuttling and Cu-pesticides of wine interest



#### G3M

Air pollution and breast cancer



#### TESTIS

Air pollution and testis cancer



#### COPERNIC - SPACE

Prediction of radiosensitivity of astronauts



#### PRAXITELE

ATM nucleoshuttling and particles



#### RAFFAEL

ATM nucleoshuttling and low dose rate



#### EROS - SPACE

ATM nucleoshuttling and bone radiosensitivity



#### AGENOR - SPACE

New agents of radiation protection



#### BERNADOTTE

Stratospheric balloons



#### CARAVAGE - SPACE

ATM nucleoshuttling and cellular aging





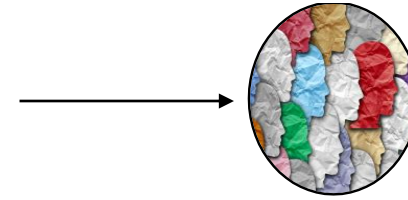
Unité U1296 : Radiations  
Défense, Santé, Environnement  
Lyon & Brétigny-sur-Orge, France

# Human Social Sciences



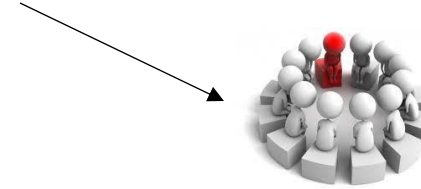
Head: Pr. Marie Préau

→ **Social Psychology**



**CLEPSYDRE**

Perception of risks related to radiation



**SOCIAL PSYCHOLOGY**

(non related to radiation)

→ **Laws and Regulations**



**JURA**

Laws and regulations related to radiation

→ **History of Sciences**



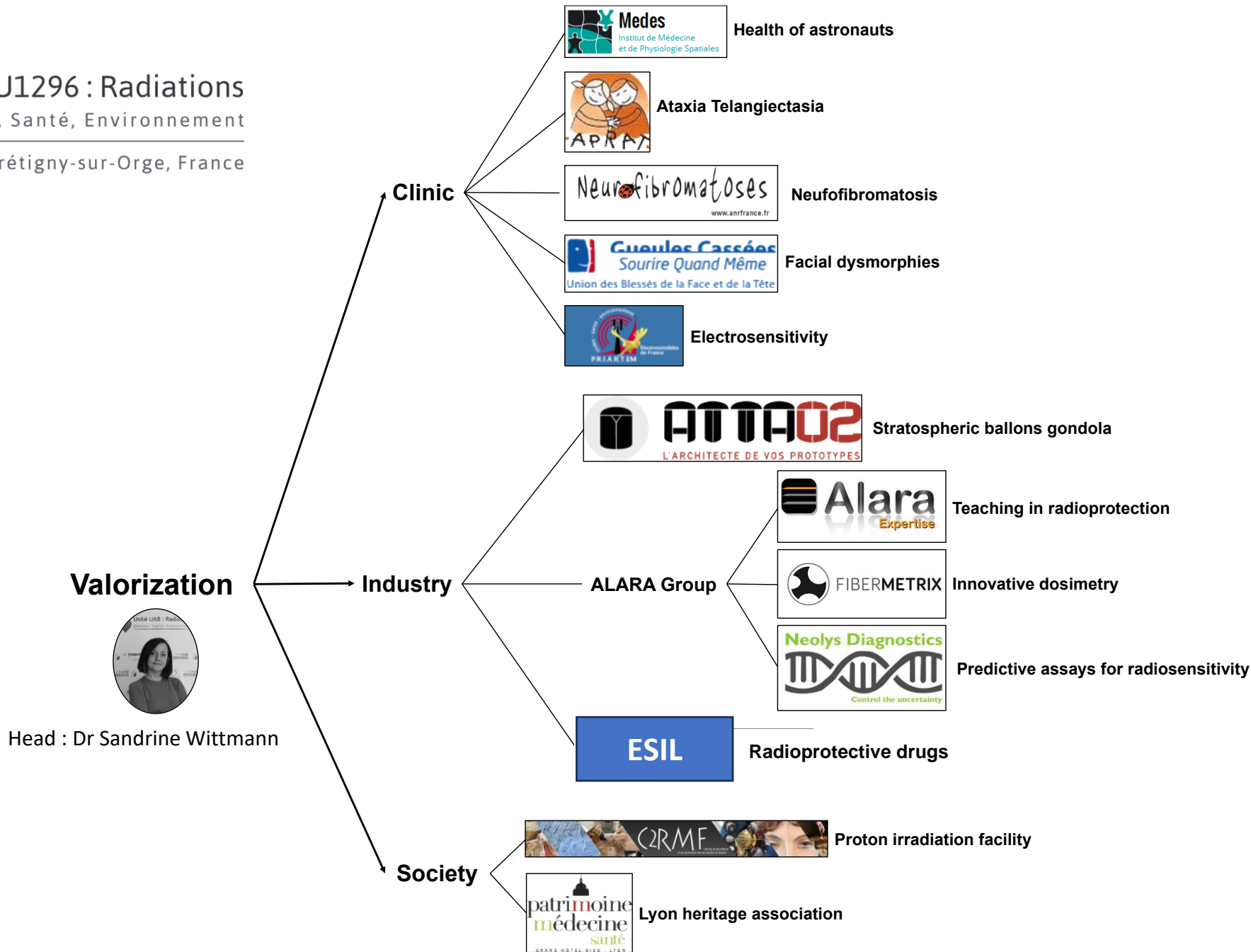
**BIBRACTE**

Bios of the pioneers of radiation





Unité U1296 : Radiations  
Défense, Santé, Environnement  
Lyon & Brétigny-sur-Orge, France







Unité U1296 : Radiations  
Défense, Santé, Environnement  
Lyon & Brétigny-sur-Orge, France

## Teaching and Dissemination



Heads : Drs. Audrey Bouchet  
and Fabien Forcheron

